frontiers | Research Topics

Women in breast cancer, volume III: 2023

Edited by
Francesca Bianchi, Rachel Wuerstlein and Anika Nagelkerke

Published in
Frontiers in Oncology

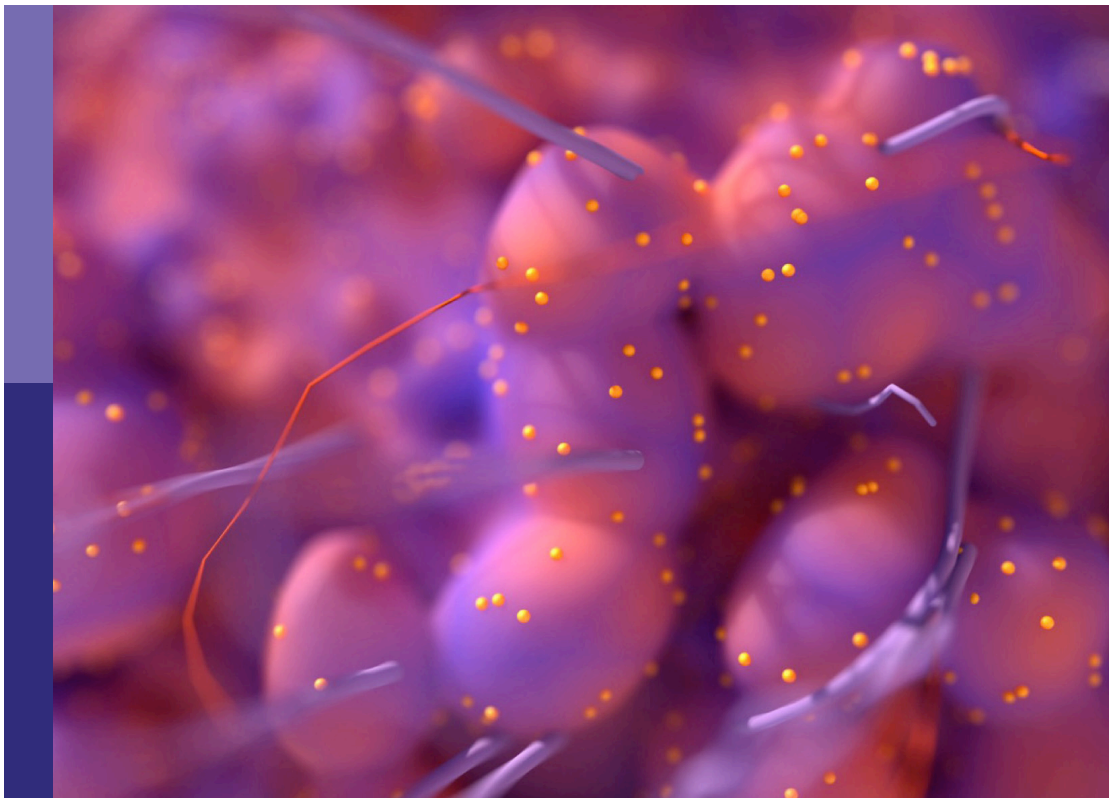

ISSN 1664-8714
ISBN 978-2-8325-5787-7
DOI 10.3389/978-2-8325-5787-7

About Frontiers

Frontiers is more than just an open access publisher of scholarly articles: it is a pioneering approach to the world of academia, radically improving the way scholarly research is managed. The grand vision of Frontiers is a world where all people have an equal opportunity to seek, share and generate knowledge. Frontiers provides immediate and permanent online open access to all its publications, but this alone is not enough to realize our grand goals.

Frontiers journal series

The Frontiers journal series is a multi-tier and interdisciplinary set of open-access, online journals, promising a paradigm shift from the current review, selection and dissemination processes in academic publishing. All Frontiers journals are driven by researchers for researchers; therefore, they constitute a service to the scholarly community. At the same time, the *Frontiers journal series* operates on a revolutionary invention, the tiered publishing system, initially addressing specific communities of scholars, and gradually climbing up to broader public understanding, thus serving the interests of the lay society, too.

Dedication to quality

Each Frontiers article is a landmark of the highest quality, thanks to genuinely collaborative interactions between authors and review editors, who include some of the world's best academicians. Research must be certified by peers before entering a stream of knowledge that may eventually reach the public - and shape society; therefore, Frontiers only applies the most rigorous and unbiased reviews. Frontiers revolutionizes research publishing by freely delivering the most outstanding research, evaluated with no bias from both the academic and social point of view. By applying the most advanced information technologies, Frontiers is catapulting scholarly publishing into a new generation.

What are Frontiers Research Topics?

Frontiers Research Topics are very popular trademarks of the *Frontiers journals series*: they are collections of at least ten articles, all centered on a particular subject. With their unique mix of varied contributions from Original Research to Review Articles, Frontiers Research Topics unify the most influential researchers, the latest key findings and historical advances in a hot research area.

Find out more on how to host your own Frontiers Research Topic or contribute to one as an author by contacting the Frontiers editorial office: frontiersin.org/about/contact

Women in breast cancer, volume III: 2023

Topic editors

Francesca Bianchi — University of Milan, Italy

Rachel Wuerstlein — Ludwig Maximilian University of Munich, Germany

Anika Nagelkerke — University of Groningen, Netherlands

Citation

Bianchi, F., Wuerstlein, R., Nagelkerke, A., eds. (2024). *Women in breast cancer, volume III: 2023*. Lausanne: Frontiers Media SA. doi: 10.3389/978-2-8325-5787-7

Table of contents

frontiers | Frontiers in Oncology

TYPE Editorial
PUBLISHED 03 December 2024
DOI 10.3389/fonc.2024.1515282

OPEN ACCESS

EDITED AND REVIEWED BY
Assia Konsoulova,
National Cancer Hospital, Bulgaria

*CORRESPONDENCE
Francesca Bianchi
francesca.bianchi1@unimi.it

†These authors have contributed equally to this work

RECEIVED 22 October 2024
ACCEPTED 18 November 2024
PUBLISHED 03 December 2024

CITATION
Bianchi F and Nagelkerke A (2024) Editorial: Women in breast cancer, volume III: 2023. *Front. Oncol.* 14:1515282. doi: 10.3389/fonc.2024.1515282

Editorial: Women in breast cancer, volume III: 2023

Francesca Bianchi[1,2*†] and Anika Nagelkerke[3†]

[1]Department of Biomedical Health Sciences, University of Milan, Milan, Italy, [2]Laboratorio di Morfologia Umana Applicata, IRCCS Policlinico San Donato, Milan, Italy, [3]Department of Pharmaceutical Analysis, Groningen Research Institute of Pharmacy, University of Groningen, Groningen, Netherlands

KEYWORDS

breast cancer, personalized medicine, quality of life, gender equality, prevention, leadership, fertility

Editorial on the Research Topic
Women in breast cancer, volume III: 2023

Introduction

Breast cancer is still the most common cancer among women worldwide, causing a heavy burden of disease, mortality and long-term survival. In this context, women's participation in breast cancer research, especially in the leadership process, is important for increasing knowledge and developing health policy. However, gender gaps in leadership still exist. According to the 2023 OCSE report, women make up less than 30% of scientists worldwide, and their representation in senior positions and as decision-makers is even lower, especially in programs such as medical and experimental oncology. This under-representation not only hinders development of new ideas to solve complex diseases, such as breast cancer, but also impedes the progress needed to solve the specific health problems faced by women.

Negative factors such as research funding bias, organizational bias, and lack of continuing education risk hindering women's advancement in scientific research. Furthermore, as a result of their significant contributions to research, female researchers should be recognized more for their contributions, leadership, and talent in relevant publications. The COVID-19 pandemic has further exacerbated inequality, negatively impacting female researchers who face greater supervisory responsibilities, thereby reducing research output. As we strive for a more social environment, it is even more important to provide platforms that support and promote the work of female scientists.

The Frontiers in Oncology's Women in Breast Cancer series provides one such platform to share the diverse, valuable latest contributions of female researchers to breast cancer research. Volume III contains 21 articles covering a wide range of topics from

molecular analysis and new diagnostics to clinical and patient care. These projects are all led by women and include a large number of female scientists, at various stages in their careers. Collectively, this series provides insight into the evolution of breast cancer research, providing a deeper understanding of early treatment and the biological, psychological, and treatment of the disease.

Innovations in non-invasive diagnostics

Advances in breast cancer diagnostics are critical to improving early diagnosis and ensuring that patients receive the best possible treatment and personalized care. A key study in this volume investigates the ability of ultrasound-based radiography to estimate the expression of important markers such as oestrogen receptor (ER), progesterone receptor (PR), HER2, and Ki-67 in breast cancer patients (Xu et al.). This new approach aims to eliminate molecular testing, reduces the need for biopsies, and offers a more efficient, patient-friendly alternative to traditional diagnostics. These advances are particularly important for improving diagnostic accuracy and guiding treatment in different types of breast cancer.

This research is complemented by another study on breast calcification, which is often an early sign of malignancy. A new machine learning algorithm was developed to improve the segmentation and quantification of calcium in mammograms (Tong et al.). The algorithm is superior in identifying microcalcifications compared to existing models, improving the diagnostic process by helping radiologists distinguish malignant diseases. This AI-powered innovation holds great promise for improving early detection and reducing misdiagnosis, especially in difficult-to-find early-stage breast tissue.

Personalized therapy and radiotherapy

Advances in decisive oncology continue to improve breast cancer treatment. Much of the research in this Research Topic focuses on personalized treatment strategies to improve outcomes based on the patient's molecular profile. A key example is the study of the Lem-D protein in triple-negative breast cancer (TNBC) (Rose et al.). Because TNBC lacks hormone receptors that are frequently targeted by other types of breast cancer, treatments are often limited. The researchers in this volume describe the role of nuclear envelope proteins, such as Ankle2, TMPO, and Emerin in TNBC cell growth, providing compelling evidence that these proteins may serve as a new treatment plan. This opens the door to more effective, targeted interventions for one of the most serious and difficult-to-treat breast cancers.

Improving of personalized therapy also include traditional treatment such as radiotherapy. Comparative studies of conventional and hypofractionated radiation therapy using the Halcyon system highlight the importance of radiation therapy to stabilize the tumour with reduced side effects (Tai et al.). The hypofractionation approach, which delivers more radiation in fewer sessions, has been shown to be better minimizing side effects, even if not as effective in controlling tumours, as than conventional ones.

Quality of life impact

Breast cancer, irrespective of its extent and treatment, has negative impacts on several aspects of women's lives. This Research Topic includes several studies that highlight the importance of health-related quality of life (HR-QoL) and patient outcomes, particularly in light of the COVID-19 pandemic. One study examined how the COVID-19 vaccine impacted HR-QoL in patients with breast and gynaecological cancer (Forster et al.). Findings suggest that vaccination helps improve patients' overall health, reduces stress, and improves their ability to participate in daily life. Given cancer patients' vulnerability to infection, these results highlight the important role of vaccination in reducing further health risks and improving mental health during a global health crisis.

A common complication after breast cancer surgery that also affects patients' quality of life is lymphedema. A study of clinical decongestant therapy (CDT) in women with postmastectomy lymphedema showed that the treatment resulted in significant improvements in physical health and pain intensity (Kavak and Ünver). Patients had increased mobility, reduced limb size, and improved health through exercise and education services. These findings emphasize the importance of incorporating rehabilitation into breast cancer treatment plans to ensure that holistic care continues beyond the postoperative period.

Fertility preservation is another important issue, especially for young women diagnosed with breast cancer. The reviews and assessments in this volume highlight the concerns related to pregnancy in young cancer patients, with over 50% of patients reporting serious concerns about becoming pregnant after treatment (Chen et al.). Factors such as education level, reproductive stress, and depression have been found to be important contributors to these stressors, while having a partner or having children has been shown to be protective. This study shows the need for counselling and support that not only affects the physical health of the patient, but also the patient's mental and emotional health among young women with cancer. In addition, data on pregnancy-associated cancer (PABC) highlight the unique challenges in cancer management during pregnancy (Innocenti et al.). The case describes the success of a patient who underwent breast-sparing mastectomy and immediate breast reconstruction. This multifaceted exercise emphasizes the importance of clinical strategies that define maternal and foetal health to ensure that breast cancer care is appropriate for reproductive outcomes.

Cancer prevention

The relationship between genes and breast cancer has been an important topic of research. The main report in this volume is about inflammatory breast cancer (IBC), a rare and serious disease

(Qinet al.). Through genetic analysis, researchers have identified the most important mutations, such as PIK3CA, and the mechanisms that can affect the recurrence of the disease. These data demonstrate the benefits of genetic analysis in guiding treatment strategies and identifying therapeutic targets, particularly in complex, recurrent cases.

In addition, research on the immune system and their association with cancer risk provides new insights into the possibility of immunotherapy. A Mendelian randomization study showed how immunosuppressants can increase or decrease the risk of cancer, especially in ER-positive and ER-negative subtypes (Wang et al.). These findings provide the basis for further research on immunotherapy, which can provide more personalized and effective treatments for patients with the disease.

Conclusion

The material collected in "Women with Breast Cancer Vol III: 2023" shows the depth of breast cancer research led and performed by women. From innovations in research and genetic information to the development of personalized treatment strategies and a focus on mental health, these studies are pushing the boundaries of our understanding and approach to breast cancer. In addition, this book shows the importance of addressing the specific problems of young patients, especially reproductive and health problems, while strengthening our understanding of the genetics and immune system involved in the disease.

As the work continues, the role of women in leading and improving breast cancer research cannot be overestimated. By providing a forum for female researchers, Frontiers in Oncology not only amplifies their voice, but also ensures that their contributions are recognized and included in the general discussion. The findings and research presented in this Research Topic provide important guidance to clinicians, researchers, and policy makers.

Author contributions

FB: Conceptualization, Investigation, Writing – original draft, Writing – review & editing. AN: Conceptualization, Investigation, Writing – review & editing.

Funding

The author(s) declare financial support was received for the research, authorship, and/or publication of this article. Funded by the European Union - Next Generation EU, Mission 4 Component 1 CUP G53D23000420006.

Conflict of interest

The authors declare that the research was conducted in the absence of any commercial or financial relationships that could be construed as a potential conflict of interest.

Publisher's note

frontiers | Frontiers in Oncology

TYPE Clinical Trial
PUBLISHED 31 July 2023
DOI 10.3389/fonc.2023.1216446

OPEN ACCESS

EDITED BY
Francesca Bianchi,
University of Milan, Italy

REVIEWED BY
Chen Li,
Free University of Berlin, Germany
Bilgin Kadri Aribas,
Bülent Ecevit University, Türkiye

*CORRESPONDENCE
Leilei Liu
bill_boss@sina.com
Qiufang Ouyang
torrent_100@163.com

RECEIVED 03 May 2023
ACCEPTED 11 July 2023
PUBLISHED 31 July 2023

CITATION
Xu R, You T, Liu C, Lin Q, Guo Q, Zhong G, Liu L and Ouyang Q (2023) Ultrasound-based radiomics model for predicting molecular biomarkers in breast cancer. *Front. Oncol.* 13:1216446. doi: 10.3389/fonc.2023.1216446

Ultrasound-based radiomics model for predicting molecular biomarkers in breast cancer

Rong Xu[1], Tao You[1], Chen Liu[2], Qing Lin[1], Quehui Guo[1], Guodong Zhong[3], Leilei Liu[1]* and Qiufang Ouyang[1]*

[1]Department of Ultrasound, The Second Affiliated Hospital of Fujian University of Traditional Chinese Medicine, Fuzhou, Fujian, China, [2]Department of Breast, The Second Affiliated Hospital of Fujian University of Traditional Chinese Medicine, Fuzhou, Fujian, China, [3]Department of Pathology, The Second Affiliated Hospital of Fujian University of Traditional Chinese Medicine, Fuzhou, Fujian, China

Background: Breast cancer (BC) is the most common cancer in women and is highly heterogeneous. BC can be classified into four molecular subtypes based on the status of estrogen receptor (ER), progesterone receptor (PR), human epidermal growth factor receptor 2 (HER2) and proliferation marker protein Ki-67. However, they can only be obtained by biopsy or surgery, which is invasive. Radiomics can noninvasively predict molecular expression *via* extracting the image features. Nevertheless, there is a scarcity of data available regarding the prediction of molecular biomarker expression using ultrasound (US) images in BC.

Objectives: To investigate the prediction performance of US radiomics for the assessment of molecular profiling in BC.

Methods: A total of 342 patients with BC who underwent preoperative US examination between January 2013 and December 2021 were retrospectively included. They were confirmed by pathology and molecular subtype analysis of ER, PR, HER2 and Ki-67. The radiomics features were extracted and four molecular models were constructed through support vector machine (SVM). Pearson correlation coefficient heatmaps are employed to analyze the relationship between selected features and their predictive power on molecular expression. The receiver operating characteristic curve was used for the prediction performance of US radiomics in the assessment of molecular profiling.

Results: 359 lesions with 129 ER- and 230 ER+, 163 PR- and 196 PR+, 265 HER2- and 94 HER2+, 114 Ki-67- and 245 Ki-67+ expression were included. 1314 features were extracted from each ultrasound image. And there was a significant difference of some specific radiomics features between the molecule positive and negative groups. Multiple features demonstrated significant association with molecular biomarkers. The area under curves (AUCs) were 0.917, 0.835, 0.771,

and 0.896 in the training set, while 0.868, 0.811, 0.722, and 0.706 in the validation set to predict ER, PR, HER2, and Ki-67 expression respectively.

Conclusion: Ultrasound-based radiomics provides a promising method for predicting molecular biomarker expression of ER, PR, HER2, and Ki-67 in BC.

KEYWORDS

radiomics, biomarker, breast cancer, ultrasonography, support vector machine

Introduction

Breast cancer (BC) is currently the most prevalent form of cancer and is also the leading cause of cancer-related deaths among women, according to the International Agency for Research on Cancer (1). The four molecular biomarkers, namely estrogen receptor (ER), progesterone receptor (PR), human epidermal growth factor receptor 2 (HER2), and proliferation marker protein Ki-67, garner significant clinical attention in the clinical practice (2). These four molecular biomarkers play a crucial role in diagnosing BC. Based on the expression levels of these four molecular profiles (3), BC is classified into four distinct subtypes: luminal A, luminal B (including luminal B/HER2-negative and luminal B/HER2-positive), HER2-positive, and triple-negative BC (TNBC). In particular, the treatment protocols, prognosis, and metastatic potential of BC can vary significantly among these different molecular subtypes (4). Therefore, accurate prediction of the molecular profiles holds immense significance in guiding appropriate treatment strategies.

Currently, the assessment of molecular subtypes of BC before surgery typically relies on the results of immunohistochemistry (IHC) obtained through needle biopsy (5). However, this biopsy procedure is invasive and time-consuming. Additionally, a single local biopsy specimen may not always capture the complete molecular characteristics of the whole cancer, because of the high heterogeneity of BC (6). The tumor heterogeneity is an independent factor linked to the insufficient response to neoadjuvant chemotherapy (7). As a result, there is an urgent need for an alternative method that can accurately and non-invasively assess the expression of molecular biomarkers in BC.

With the rapid advancements in computer technology, the field of radiomics has emerged as a cutting-edge approach that harnesses high-throughput capabilities and mathematical algorithms to extract a wide range of quantitative features from medical images (8). This innovative technique not only overcomes the subjective limitations inherent in traditional imaging diagnosis but also enables a more comprehensive assessment of the overall characteristics of lesions and the surrounding tissue. Numerous studies have shown the effectiveness of radiomics based on X-ray, magnetic resonance imaging (MRI), ultrasound and positron emission tomography-computed tomography (PET-CT) for the evaluation of malignancy, differentiation of molecular subtype, and response to neoadjuvant therapy in BC (9). Ultrasound has unique advantages for clinical applications due to its real-time capabilities, frequent examination, and large data size. In particular, the US-radiomics model has demonstrated exceptional performance in distinguishing between benign and malignant breast lesions (10). However, despite these advantages, far few studies have investigated the application of ultrasound radiomics for predicting molecular biomarker expression (11). Furthermore, the number of studies exploring the specific radiomics features that hold great importance in predicting the molecular subtype of BC has been relatively limited.

In the present study, we investigated whether ultrasound radiomics features could be adopted as a predictive biomarker for discriminating the molecular biomarker profiling (ER, PR, HER2, and Ki-67). The purpose of this study was to explore the potential of radiomics features, and to provide complementary information to aid in the diagnostic molecular biomarker expression in BC.

Methods

Study design and cohort of the study

This study was approved by the Ethics Committee of the Second Affiliated Hospital of Fujian University of Traditional Chinese Medicine (SPHFJP-T2022007-01), and informed consent was waived due to the retrospective nature of this study. We retrieved 466 consecutive patients with BC who underwent breast US examination and following treatment in our hospital from January 2013 to December 2021. Inclusion criteria were as follows: (1) Breast US was performed before the operation, and patients did not receive neoadjuvant chemotherapy (NAC) or biopsy prior to US examination; (2) Primary BC was confirmed by pathology; (3) Molecular subtype data (ER, PR, Ki-67, and HER2) were complete; (4) The US image quality met the diagnostic requirements. Exclusion criteria were as follows: (1) Patients without US examination; (2) Cases with incomplete pathological data; (3) Patients who had undergone local or systemic treatment such as puncture biopsy, chemotherapy, radiotherapy, ablation, or resection before breast US examination; (4) Cases with poor imaging quality. Finally, a total of 342 patients with invasive BC were included in this study. Among them, 341 were female and 1 was male. Their mean age was 54.5 years

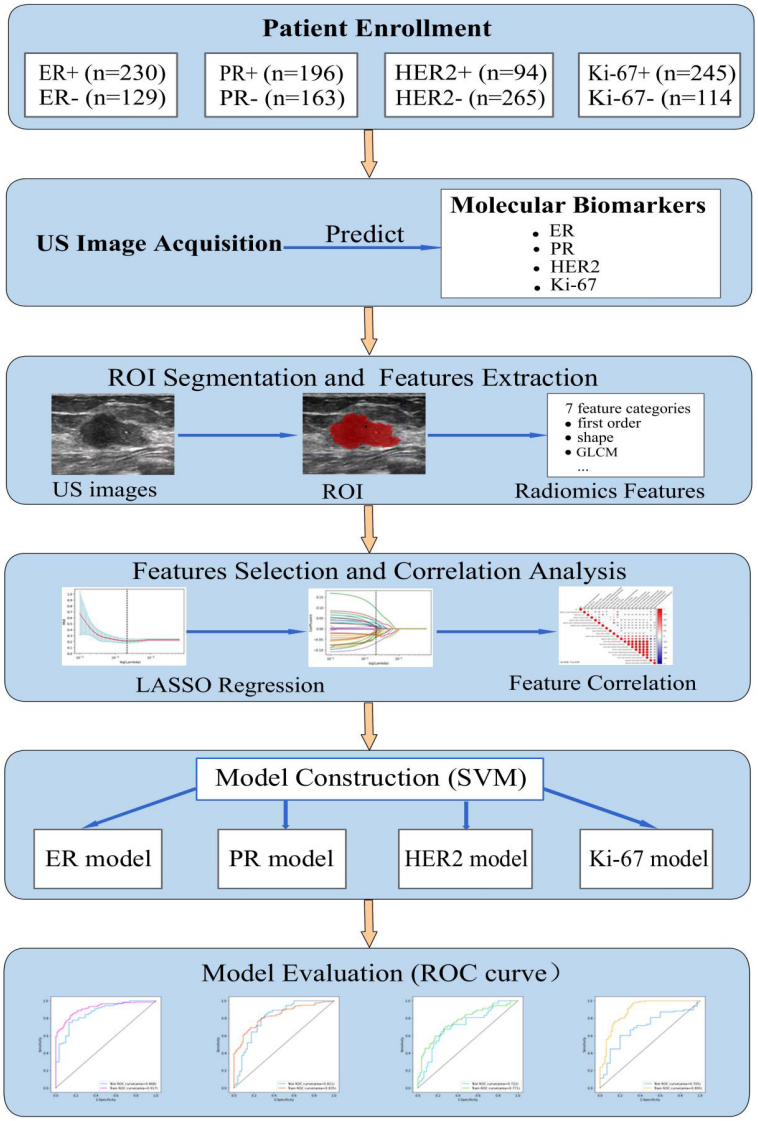

FIGURE 1
The workflow of this study. HER2, human epidermal growth factor receptor 2; TNBC, triple-negative breast cance; US, ultrasound; ER, estrogen receptor; PR, progesterone receptor; Ki-67, proliferating cell nuclear antigen; ROI, the region of interest; GLCM, gray level co-occurrence matrix; LASSO, least absolute shrinkage and selection operator; SVM, support vector machine; ROC, receiver operating characteristic.

(range from 25 to 90 years old). The workflow of this work shown in Figure 1 mainly includes six steps: patient enrollment, ultrasound image acquisition, features extraction, features selection, model construction and model evaluation.

Breast ultrasonography

Breast ultrasound scanning was performed using Philips, GE, or Siemens color Doppler ultrasound equipment. The patients were positioned in a supine or lateral recumbent position with their hands raised to expose both breasts and axillae, allowing for a multi-angle scan to be performed. The lesions were scanned from multiple angles. And the largest section of ultrasound in each lesion was selected for analysis. The ultrasonic characteristics of the lesions were recorded, including their BI-RADS classification, location, size, shape, boundary, internal echo, calcification, posterior echo changes, blood flow, and axillary lymph nodes. The images were stored in DICOM format. The quality control of the images was carried out by two experienced radiologists, namely, Qing Lin and Quehui Guo. Both these experts possess proficiency in image analysis and worked in consensus to ensure the accuracy and reliability of this work.

Pathology analysis

All primary breast lesions of the participants were pathologically confirmed by either biopsy or resection. Their expression levels of ER, PR, HER2, and Ki-67 were determined by IHC or fluorescence *in situ* hybridization. ER and PR positive is defined as more than 1%. For HER2, a score of 3+ indicated positive; + or no expression is negative;

a score of 2+ requires FISH to determine the amplification status (12). The cutoff threshold for the Ki-67 is 20%. If Ki-67 is greater than or equal to 20%, it indicates highly proliferative and defines as positive (13). Based on the expression of ER, PR, HER2, and Ki-67, BC is divided into four molecular subtypes, i.e. luminal A, luminal B (including luminal B/HER2-negative and luminal B/HER2-positive), HER2-positive, and triple-negative.

Segmentation of tumor and extraction of radiomics features

The breast lesion region of interest (ROI) was manually designated on a grayscale ultrasound image by two sonographers. Those sonographers had no prior knowledge of the histopathological results. An open-source imaging platform, ITK-SNAP (http://www.itksnap.org), was utilized. To demonstrate the effectiveness of the ROI selection method, Figure 2 displayed the original ultrasound image and the ROIs for four patients with breast carcinoma, each exhibiting different expression levels of molecular marker profile.

The extraction of lesion features was performed using Pyradiomics version 3.0 software. A total of 1314 radiomics features was extracted from each ultrasound image. Among these features, 7 categories of features were extracted: first order features (n = 252), shape features (n = 12), Gray Level Co-occurrence Matrix (GLCM, n = 336), Gray Level Run Length Matrix (GLRLM, n = 224), Gray Level Size Zone Matrix (GLSZM, n = 224), Gray Level Dependence Matrix (GLDM, n = 196), Neighboring Gray Tone Difference Matrix (NGTDM, n = 70).

Features selection

The consistency of the extracted radiomics features was assessed with the inter- and intra-class correlation coefficient (ICC). Forty cases of ultrasound images, comprising 20 positive and 20 negative cases for each of the molecular biomarkers (ER, PR, HER2, and Ki-67), were randomly selected for analysis. To assess the reproducibility of the radiomics features, two experienced sonographers independently performed the ROI segmentation. Additionally, in order to evaluate inter-class reproducibility, sonographer 1 repeated the segmentation process one month after the initial ROI segmentation. Radiomics features with inter- and intra-class correlation coefficients (ICCs) greater than 0.75 were considered to demonstrate good reproducibility and were selected for model construction. Pearson's coefficients matrix heatmaps were calculated to analyze the relationship between the radiomics features. And the most optimal features were selected.

Construction of the radiomics model

Before proceeding with the modeling process, several data pre-processing steps were undertaken. These steps involved manual elimination of duplicate information, unpacking the multidimensional array into one-dimensional data by column, and filtering out features with zero variance using ANOVA. After standardizing the data, the least absolute shrinkage and selection operator (LASSO) logistic regression algorithm was used to select molecular-related features with non-zero coefficients, and the penalty parameters were tuned by 10-fold cross-validation. The mean and standard deviation of the selected features were calculated for both the negative and positive groups. The *t*-values and *P*-values were calculated to determine whether the features differed significantly between the two groups. The selected features were saved as radiomics labels for subsequent model construction.

The data were divided into a training set (70%) and a validation set (30%), with 251 and 108 lesions in the training and validation sets, respectively. Four support vector machine (SVM) models were created using the radiomics labels and the binary targets for ER, PR, HER2, and Ki-67. To optimize the performance of those models, the tree-structured Parzen Estimator (TPE), a hyperparameter optimization algorithm, was used.

Evaluation of the model

To evaluate the diagnostic performance of the model on the training and validation sets, the receiver operating characteristic (ROC) curve was plotted, and the area under the curve (AUC) was calculated. Additionally, a confusion matrix was created to calculate the sensitivity, specificity, accuracy, and F1 score of the model.

Statistical analysis

Python was used for statistical analysis (version 3.8.2). The normality and homogeneity of variance of the numeric data were assessed using the Kolmogorov-Smirnov test and F-test, respectively. The baseline characteristics for numeric variables was evaluated with the t-test, Fisher's exact test, and MannWhitney U test. The Chi-square test was applied for categorical variables. A two-sided $p< 0.05$ was considered a significant difference. The statistical analysis packages include Levene, test, StandardScaler, MinMaxScaler, VarianceThreshold, train_test_split, cross_validate, cross_val_score, RepeatedKFold, confusion_matrix, accuracy_score, precision_score, recall_score, f1_score, roc_auc_score, roc_curve, LassoCV, SVC, and TPE. The Pearson's coefficient was calculated using origin software.

Results

Clinicopathological characters

A total of 359 lesions were confirmed by pathology, with 326 cases (95.3%) having a single lesion, 15 cases (4.4%) two lesions, and 1 case (0.3%) three lesions. In terms of the histologic types, the most common type was invasive ductal carcinoma, accounting for approximately 70.5% (253 lesions), followed by the carcinoma in situ, accounting for 14.2% (51 lesions) and by the special types of invasive carcinoma, accounting for 13.1% (47 lesions). The clinicopathological characteristics of the patients were presented in Table 1; Supplementary Table 2. The distribution of molecular subtype was as

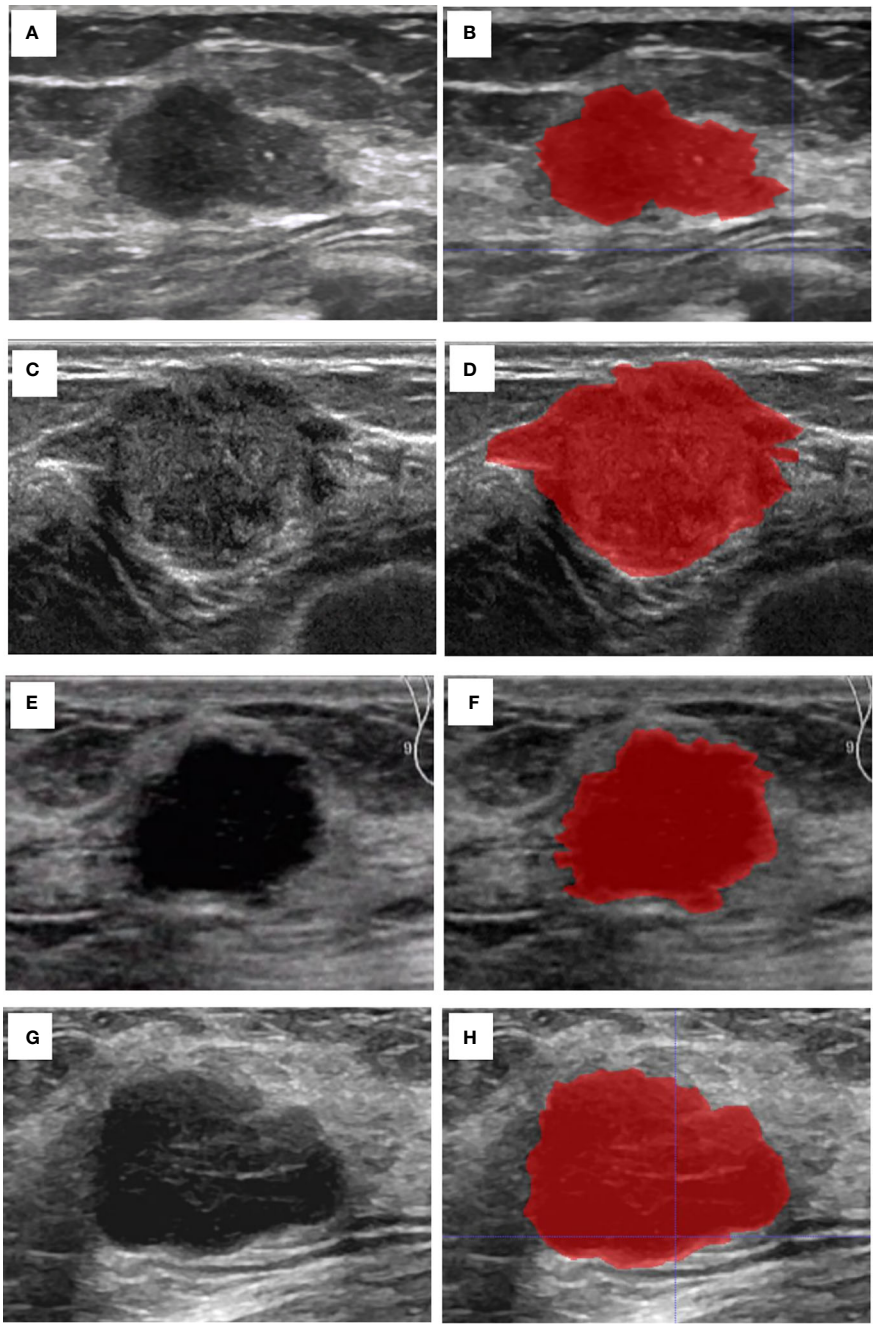

FIGURE 2
Cases of the original US image and the ROI. **(A)** The original US image of case 1 with invasive BC, Ki67 (5%+), ER (90%+), PR (60%+), and HER2 (-). **(B)** The ROI of case 1. **(C)** The original US image of case 2 with invasive BC, Ki-67 (30%+), ER (95%+), PR (95%+), and HER2 (-). **(D)** The ROI of case 2. **(E)** The original US image of case 3 shows a patient with invasive BC with myeloid characteristics, Ki67 (50%+), ER (-), PR (-), and HER2 (+). **(F)** The ROI of case 3. **(G)** The original US image of case 4 with invasive BC, Ki-67 (85%+), ER (-), PR (-), and HER2 (-). **(H)** The ROI of case 4.

follows: 86 were luminal A (24.0%), 146 were luminal B (40.7%), 63 were HER2+ (17.5%) and 64 were TNBC (17.8%). The baseline characteristics and clinicopathological information of both the training set and test set are summarized in Table 2. There were no significant differences in tumor size, age, gender, menopausal status, clinical staging, tumor types, molecular subtypes between the two groups. As demonstrated in Figure 3, the expression of ER, PR, HER2, and Ki-67 was as follows: 129 lesions were ER-negative and 230 were ER-positive. Similarly, 163 lesions were PR-negative while 196 were PR-positive. HER2 expression was negative in 265 lesions, while positive in 94 lesions. Moreover, Ki-67 expression was negative in 114 lesions, but positive in 245 lesions.

Radiomics signature building

The study extracted 1314 features from each ultrasound image, and 1205 features were retained after processing. Supplementary Table 1

TABLE 1 Characteristics of the molecular biomarkers of patients.

Characteristics	All lesions	ER			PR			HER-2			Ki-67		
		(+)	(-)	*P*-value	(+)	(-)	*P*-value	(+)	(-)	*P*-value	(+)	(-)	*P*-value
age	54.5	53.9	54.9	0.484	53.7	55.0	0.305	53.0	54.7	0.228	53.8	55.4	0.231
Menopausal status				0.040			0.005`			0.783			0.826
Premenopausal	156	112	44		100	56		40	116		106	50	
Perimenopausal	7	5	2		5	2		1	6		4	3	
Postmenopausal	192	113	79		91	101		50	142		131	61	
Not available	4	0	4		0	4		3	1		4	0	
Tumor types				0.032			0.076			`0.005			0.015
Invasive ductal carcinoma	253	151	102		129	124		73	180		185	68	
Invasive lobular carcinoma	8	5	3		3	5		0	8		4	4	
The specific type of IC	47	38	9		30	17		4	43		29	18	
Carcinoma in situ	51	36	15		34	17		17	34		27	24	
*Histologic grade of IC				0.000			0.000			0.000			0.000
Grade I	23	22	1		19	4		1	22		8	15	
Grade II	122	97	25		82	40		20	102		71	51	
Grade III	133	59	74		47	86		49	84		120	13	
Grade X	30	16	14		14	16		7	23		19	11	
#Tumor classification of CIS				0.001			0.000			0.000			0.001
Group 1	8	8	0		8	0		0	8		1	7	
Group 2	19	17	2		17	2		2	17		7	12	
Group 3	24	11	13		9	15		15	9		19	5	

*Tumor grade of invasive cancer was divided into grade I (well differentiated), grade II (moderately differentiated), or grade III (poorly differentiated) according to the Scarff-Bloom-Richardson System. Grade X was defined as the grade that cannot be assessed or is unavailable. #Carcinoma in situ (CIS) cases were classified as group 1 (nonhigh grade CIS without comedo-type necrosis), group 2 (nonhigh grade CIS with comedo-type necrosis), or group 3 (high-grade CIS with or without comedo-type necrosis) according to the Van Nuys Classification. ER, estrogen receptor; PR, progesterone receptor; HER2, human epidermal growth factor receptor 2; Ki-67, proliferating cell nuclear antigen.IC, invasive carcinoma.

shows the number of retained features after each step of feature selection. And the irrelevant features were removed. To select the relevant features, a LASSO logistic regression model was employed, then 39 and 20 signatures with non-zero coefficients were selected with the target of ER (Figures 4A, E) and PR (Figures 4B, F), respectively, in the primary cohort, after standardization. Normalization was applied before LASSO to choose the HER2-targeted signatures. And 14 signatures were selected by the LASSO algorithm (Figures 4C, G). Interestingly, no high-performance features were selected to classify Ki-67 binary data by 20% cutoff points, regardless of whether standardization or normalization was used before LASSO. Therefore, standardization was implemented, and LASSO was conducted on the Ki-67 target using continuous variables, specifically the exact values of the proliferation index, and 16 signatures were chosen (Figures 4D, H). The selected signatures were saved as radiomics labels for subsequent modeling.

Correlation between the radiomics signature and molecular biomarkers

The radiomics heatmap showcases a matrix of correlation coefficients among the features (Figure 5). The Pearson correlation coefficient was computed to evaluate the relationships among these features. The resulting heatmaps represents these associations, with the color red denoting positive correlations and the color blue indicating negative correlations.

To ensure the accuracy of the radiomics analysis, features with high correlation coefficients ($r \geq 0.9$) were removed from the initial pool of 1205 radiomics features. Only the features that exhibited a significant inter-group distribution difference were retained for further analysis. As a result, a total of 39 features were identified as essential for predicting ER expression, while 20 features for PR, 14 features for HER2, and 16 features for Ki-67. Notably, significant correlations are observed between the four molecular biomarkers and various radiomics features, including morphological features, grayscale features, texture features, and laws features.

Radiomic features to predict molecular profiles

Table 3 summarized the top five most significant features selected by the LASSO model, along with their corresponding *t*-values and *P*-values for the *t*-test. These values demonstrated a significant difference between

TABLE 2 Baseline characteristics comparison between the training set and test set.

Characteristics	Training set (n=251)	Test set (n=108)	*P*-value
Clinical tumor size (cm)			0.141
cT1 (≤ 2.0 cm)	128 (51.0%)	45 (41.7%)	
cT2 (2.1–5.0 cm)	109 (43.4%)	59 (54.6%)	
cT3 (> 5.0 cm)	14 (5.6%)	4 (3.7%)	
Age (years)	53.7	54.5	0.556
Gender			0.301
Female	251 (100%)	107 (99.1%)	
Male	0 (0%)	1 (0.09%)	
Menopausal status			0.397
Premenopausal	107 (42.6%)	49 (45.4%)	
Perimenopausal	138 (55.0%)	54 (50.0%)	
Postmenopausal	3 (1.2%)	4 (3.7%)	
Not available	3 (1.2%)	1 (0.9%)	
Clinical staging			0.092
Phase I	112 (44.6%)	35 (32.4%)	
Phase II	106 (42.2%)	58 (53.7%)	
Phase III	30 (12.0%)	15 (13.9%)	
Phase IV	3 (1.2%)	0 (0%)	
Tumor types			0.634
Invasive ductal carcinoma	172 (68.5%)	81 (75.0%)	
Invasive lobular carcinoma	6 (2.4%)	2 (1.9%)	
The specific type of IC	36 (14.3%)	11 (10.2%)	
Carcinoma in situ	37 (14.7%)	14 (13.0%)	
Molecular subtypes			0.391
Luminal A	58 (23.1%)	28 (25.9%)	
Luminal B	102 (40.6%)	44 (40.7%)	
HER2+	41 (16.3%)	22 (20.4%)	
Triple-negative	50 (19.9%)	14 (13.0%)	

TNM, Tumor node metastasis. IC, invasive carcinoma. DCIS, ductal carcinoma in situ. HER2, human epidermal growth factor receptor 2.

the positive and negative groups ($P<0.05$). As compared to ER-negative cancer, ER-postive tumors had higher values of ShortRunEmphasis (SRE), Complexity, and ShortRunHighGrayLevelEmphasis (SRHGLE), while lower values of Imc1 and SizeZoneNonUniformity Normalized (SZNUN). Alternatively, PR-positive lesions showed higher values of SmallDependenceHighGrayLevelEmphasis (SDHGLE), while lower values of Maximum, SZNUN, BoundingBox5 and Imc1. HER2-postive cancers displayed significantly higher GrayLevelNonUniformityNormalized (GLNUN), SizeZone NonUniformityNormalized (SZNUN), InverseVariance, ZonePercentage and Imc1, as compared with HER2-negative cancers. Ki-67-postive lesions showed higher BoundingBox5, SmallAreaEmphasis (SAE), while lower Coarseness, Short RunLowGrayLevelEmphasis (SRLGLE) than Ki-67-negative cancers. Notably, SRE, Imc1, SZNUN, Complexity, Maximum, SDHGLE, BoundingBox5, GLNU, SRLGLE, and SAE were the most frequently selected signatures with significantly high weights (all $p<0.005$), indicating their importance in distinguishing between the positive and negative groups. They mainly belong to glcm, glrlm, glszm, ngtdm.

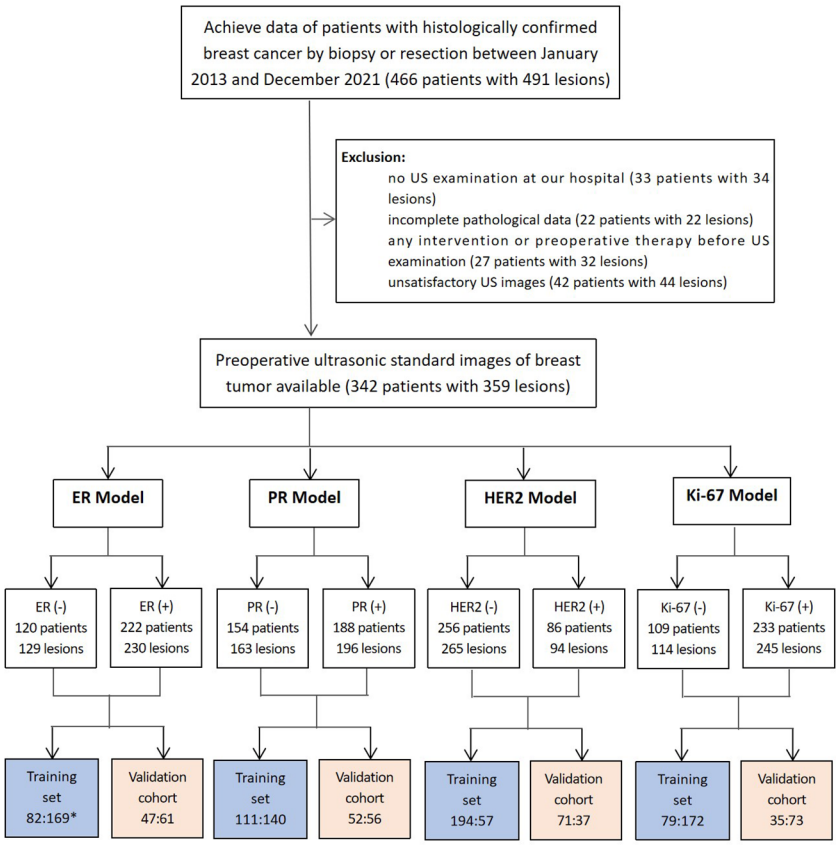

FIGURE 3
Patients included in this study (*comparison of the number of lesions in the negative and positive groups). 129 lesions were ER-negative and 230 were ER-positive. Similarly, 163 lesions were PR-negative while 196 were PR-positive. HER2 expression was negative in 265 lesions, while 94 lesions showed HER2-positive expression.

SVM model construction and validation of the model

Four models for predicting the molecular biomarkers of ER, PR, HER2, and Ki-67 were created using the features selected by LASSO and the parameters optimized by TPE. Subsequently, four ROC curves were plotted to evaluate the diagnostic efficacy of the models. The AUCs for the training and validation cohorts were presented in Figure 6. The diagnostic efficacy of the four ROC curves was ranked that ER model being the most effective, followed by the PR model, HER2 model, and lastly the Ki-67 model.

The performance of the four models namely the ER model, PR model, HER2 model, and Ki-67 model, were evaluated. Those assessment parameters, including sensitivity, specificity, accuracy, and F1 score are presented in Table 4. The ultrasound-based radiomics model displayed the highest discriminatory power for ER, achieving an AUC of 0.917 in the training set and 0.868 in the validation cohort (Figure 6A). For PR, the radiomics model achieved an AUC of 0.835 in the training set and 0.811 in the validation cohort (Figure 6B). The radiomics model generated an AUC of 0.722 (Figure 6C) and 0.706 (Figure 6D) for HER2 and Ki-67 in the validation cohort, respectively, which was slightly lower than those for ER and PR. Those results suggest that all four models are effective in predicting the molecular expression of BC. Notably, the degree of model fitting for ER, PR, and HER2 exhibited remarkable performance, with no significant signs of overfitting. Conversely, overfitting was evident for Ki-67.

Discussion

Molecular subtyping plays a vital role in tailoring treatment approaches to individual patients. However, it requires biopsy or surgery which is invasive, time-consuming, and sometimes prone to inaccurate due to the heterogeneity. In recent studies, radiomics shows good performance for predicting molecular subtypes of BC (14). In our study, we extracted ultrasound radiomics features to build the prediction models for the expression of ER, PR, HER2, and Ki-67 in BC. Our results indicate that the ultrasound-based radiomics models show excellent performance in predicting molecular biomarkers in BC. Additionally, our research identified several critical radiomics features that play a substantial role in distinguishing between positive and negative expressions of molecular biomarkers. These features, namely SRE, Imc1, SZNUN, Complexity, Maximum, SDHGLE, BoundingBox5, GLNU, SRLGLE, and SAE are highly associated with the expression of ER, PR, HER2, and Ki-67. It is noteworthy that, to the best of our knowledge, our study is the first to establish a relationship between ultrasound-based radiomics features and

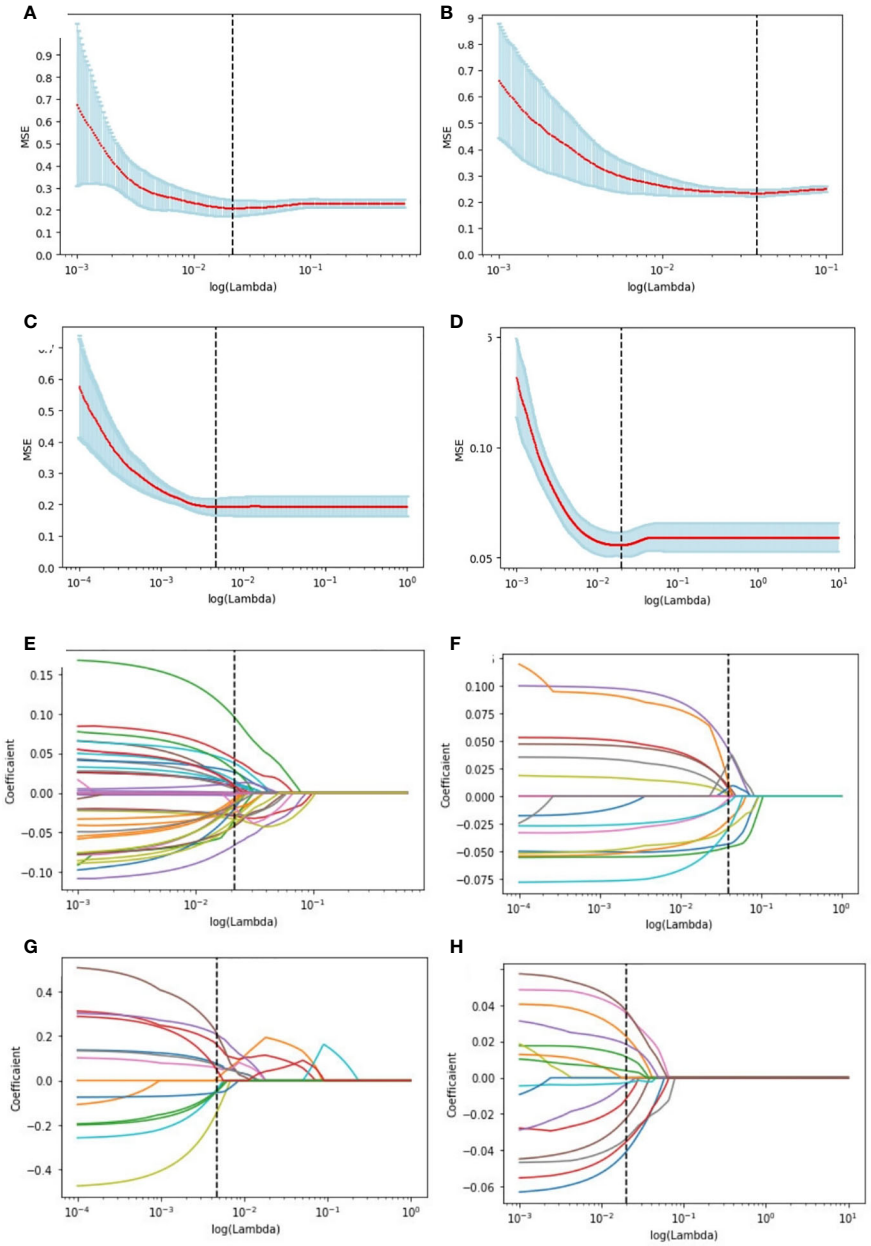

FIGURE 4
Radiomics feature selection using LASSO logistic regression in the primary cohort. Selection of the tuning parameter (λ) in the LASSO model of the ER **(A)**, PR **(B)**, HER2 **(C)**, and Ki-67 **(D)** *via* 10-fold cross-validation based on the mean standard error (MSE) of the minimum criteria. The value of Λ give the minimum average binominal deviance was used to select features. LASSO coefficient profiles of the selected radiomics features of the ER model **(E)**, PR model **(F)**, HER2 model **(G)**, and Ki-67 model **(H)**. Dotted vertical lines were drawn at the optimal values using the minimum criteria and the MSE criteria.

molecular profiles. Our study offers a non-invasive, cost-effective, and time-efficient alternative for BR molecular classification. And the identification of these specific features provides valuable insights for further research and potential development of diagnostic tools.

It is well-known that the aggressiveness of BC is closely related to its heterogeneity (15, 16), which sometimes is challenging to assess fully when using histopathological tissue samples obtained from needle biopsies (17, 18). The accuracy of molecule profiling diagnosis can be impacted by the size and number of samples obtained (19). Radiomics is a powerful tool that enables the non-invasive assessment of whole-tumor heterogeneity by extracting quantitative features based on texture, shape, and intensity (20). These features provide valuable insights into the underlying biological processes of the imaged tissue, including tumor heterogeneity, microenvironmental characteristics, and etc. There is a growing literature that has reported to predict molecular profiling in BC, but mostly based on MRI and X-ray analysis (21, 22). However, there has been a limited number of studies conducted thus far that utilize ultrasound imaging as the primary modality for investigation (23).

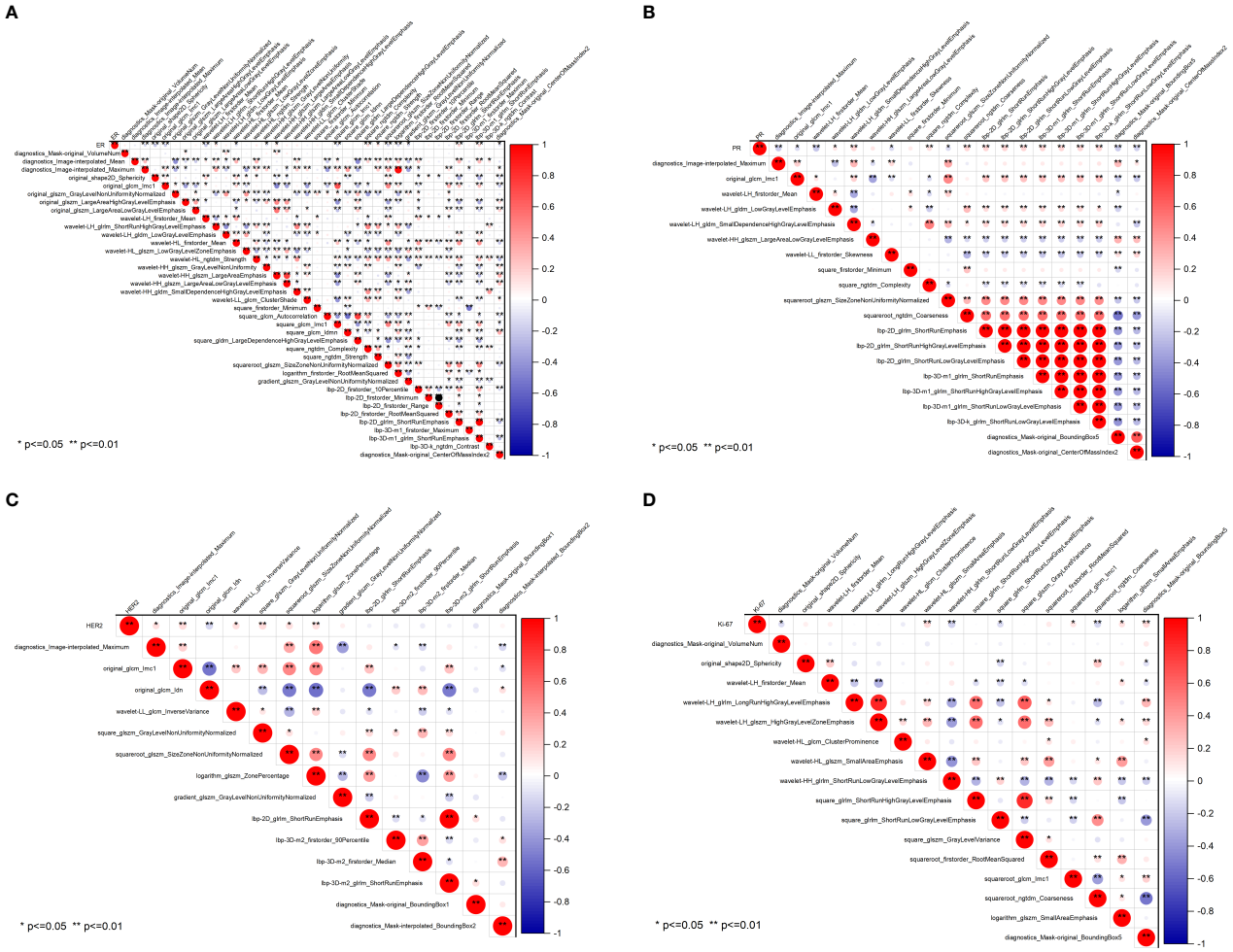

FIGURE 5
Pearson correlation coefficient heatmaps of selected features on predicting molecular expression of ER **(A)**, PR **(B)**, HER2 **(C)**, and Ki-67 **(D)**. Red represents positive correlations and blue indicates negative correlations. ER, estrogen receptor; PR, progesterone receptor; HER2, human epidermal growth factor 2; Ki-67, proliferating cell nuclear antigen.

TABLE 3 The top five signatures were selected by Lasso and the *t*-test values.

Target	Top five features selected by Lasso	Features	Filter	$\bar{x} \pm s$		*t*-value	*P*-value
				Positive	Negative		
ER	ShortRunEmphasis	glrlm	lbp-2D	0.109 ± 0.069	0.086 ± 0.052	3.341	0.0009
	Imc1	glcm	original	-0.198 ± 0.089	-0.164 ± 0.075	3.660	0.0003
	SizeZoneNonUniformityNormalized	glszm	squareroot	0.466 ± 0.107	0.502 ± 0.113	3.003	0.0029
	Complexity	ngtdm	square	3.261 ± 5.484	1.735 ± 3.168	2.900	0.0040
	ShortRunHighGrayLevelEmphasis	glrlm	wavelet-LH	59.517 ± 60.040	44.905 ± 32.122	2.565	0.0107
PR	Maximum	Image-interpolated	diagnostics	387.129 ± 124.209	438.003 ± 142.456	3.614	0.0003
	SmallDependenceHighGrayLevelEmphasis	gldm	wavelet-LH	22.668 ± 26.959	15.418 ± 12.397	3.165	0.0017
	SizeZoneNonUniformityNormalized	glszm	squareroot	0.461 ± 0.125	0.494 ± 0.112	2.485	0.0134
	BoundingBox5	Mask-original	diagnostics	172.755 ± 87.278	204.883 ± 82.722	3.556	0.0004
	Imc1	glcm	original	-0.196 ± 0.089	-0.173 ± 0.079	2.561	0.0109

(Continued)

TABLE 3 Continued

Target	Top five features selected by Lasso	Features	Filter	$\bar{x} \pm s$		*t*-value	*P*-value
				Positive	Negative		
HER2	GrayLevelNonUniformityNormalized	glszm	square	0.493 ± 0.206	0.429 ± 0.179	2.878	0.0042
	SizeZoneNonUniformityNormalized	glszm	squareroot	0.503 ± 0.109	0.470 ± 0.109	2.524	0.0120
	InverseVariance	glcm	wavelet-LL	0.418 ± 0.052	0.399 ± 0.065	2.467	0.0140
	ZonePercentage	glszm	logarithm	0.484 ± 0.167	0.429 ± 0.176	2.654	0.0083
	Imc1	glcm	original	-0.163 ± 0.075	-0.193 ± 0.088	2.996	0.0029
Ki-67	Coarseness	ngtdm	squareroot	0.021 ± 0.022	0.029 ± 0.032	2.802	0.0054
	BoundingBox5	Mask-original	diagnostics	195.792 ± 86.362	169.184 ± 84.711	2.734	0.0066
	ShortRunLowGrayLevelEmphasis	glrlm	wavelet-HH	0.088 ± 0.062	0.115 ± 0.091	3.213	0.0014
	SmallAreaEmphasis	glszm	wavelet-HL	0.604 ± 0.078	0.575 ± 0.106	2.911	0.0038
	ShortRunLowGrayLevelEmphasis	glrlm	square	0.154 ± 0.061	0.172 ± 0.067	2.490	0.0132

ER, estrogen receptor; PR, progesterone receptor; HER2, human epidermal growth factor receptor 2; Ki-67, proliferating cell nuclear antigen.

Radiomics features are quantitative descriptors that encompass various aspects of a medical image, including intensity, shape, volume, texture, and etc. They are usually difficult to be interpreted and analyzed intuitively. In our study, 7 categories of image features were extracted from the 1314 radiomics features. We have innovatively developed four molecular prediction models based on ultrastructural features. In the ER-positive model, higher values were observed for SRE, Complexity, and SRHGLE, while lower values were found for Imc1 and SZNUN. Similarly, in the PR-positive model, higher values were observed for SDHGLE, while lower values were

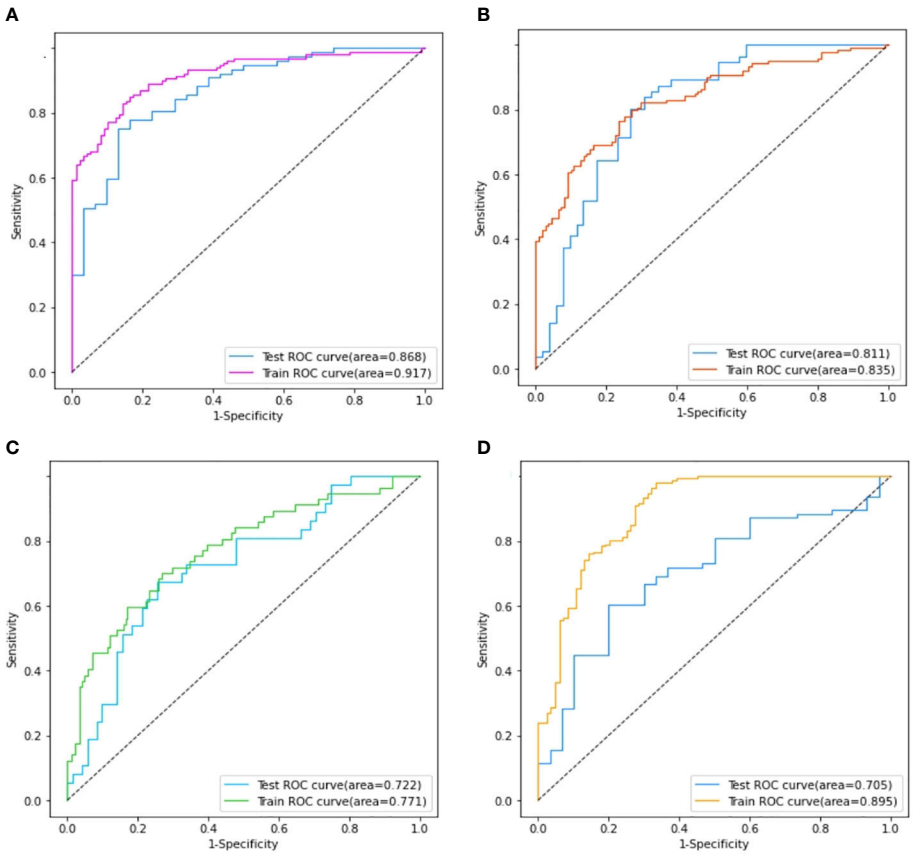

FIGURE 6
Comparison of the area under the ROC curves on the training set and validation cohort of ER model **(A)**, PR model **(B)**, HER2 model **(C)**, and Ki-67 model **(D)**.

TABLE 4 Diagnostic Performances of the SVM model.

target	cohort	AUC	%Sn	%Sp	%Acc	F1 score
ER	train	0.917	77.1	89.8	82.1	0.840
	validate	0.868	75.3	87.1	78.7	0.835
PR	train	0.835	69.3	81.1	74.5	0.752
	validate	0.810	78.6	73.1	75.9	0.772
HER2	train	0.771	71.9	70.1	70.5	0.526
	validate	0.722	73.0	66.2	68.5	0.614
Ki-67	train	0.896	73.3	83.5	76.5	0.810
	validate	0.706	61.6	77.1	66.7	0.714

support vector machine, SVM; area under the curve, AUC; sensitivity, Sn; specificity, Sp; accuracy, ACC; ER, estrogen receptor; PR, progesterone receptor; HER2, human epidermal growth factor receptor 2; Ki-67, proliferating cell nuclear antigen.

found for Maximum, SZNUN, BoundingBox5, and Imc1. The HER2-positive model displayed significantly higher values for GLNUN, SZNUN, InverseVariance, ZonePercentage, and Imc1 compared to HER2-negative BC. In the Ki-67-positive model, higher values were observed for BoundingBox5 and SAE, while lower values were found for Coarseness and SRLGLE, compared to Ki-67-negative lesions. The features of SRE, Imc1, SZNUN, Complexity, Maximum, SDHGLE, BoundingBox5, GLNU, SRLGLE, and SAE are heavily weighted (all $P<0.005$), indicating their pivotal role in discerning the negative or positive expression of ER, PR, HER2, and Ki-67 molecules. SRE can assess the distribution of short runs of similar intensity values within an image, which can characterize the texture of BC. Its higher values mean a greater proportion of short runs of similar intensity values in the image. Imc1 can characterizes the similarity of gray-level intensity values between adjacent pixels, taking into account their relative positions. SZNUN can determine the degree of heterogeneity in the sizes of homogeneous regions within an image. Its higher values indicate greater variability in the sizes of homogeneous regions across the image. Complexity characterizes the heterogeneity and irregularity in the image intensity values. And the higher values indicating greater complexity and heterogeneity in the image. Maximum is to measure the maximum intensity value in the interpolated image. Complexity characterizes the heterogeneity and irregularity in the image intensity values. And the higher values indicating greater complexity and heterogeneity in the image. Maximum is to measure the maximum intensity value in the interpolated image. SDHGLE measures the joint probability of occurrence of small dependence gray level values with high gray-level values. It can characterize the heterogeneity of a tumor. BoundingBox5 characterizes the compactness of ROI in an image, with higher values indicating that the ROI is more compact. GLNU quantifies the degree of variation in gray-level intensity. A higher value of GLNU indicates that the intensity values within the ROI are more widely distributed, suggesting higher degree of heterogeneity. SRLGLE quantifies the small runs of low gray-level values within an image. SAE measures the proportion of small homogeneous areas in the image, with a higher value indicating a greater proportion of small, homogeneous areas. To the best of our knowledge, this is the first study to investigate the correlation between the aforementioned radiomics features and molecular biomarkers. Their heavy weight emphasizes their importance as crucial markers in the assessment of molecular expression.

These features, including GLCM, GLRLM, GLSZM, and NGTDM, mainly belong to the categories of second-order statistics or higher-order statistics. They provide valuable insights into the irregular or heterogeneous texture of tumors that are not discernible to the naked eye. As far as we know, there are very few studies on the correlation between the aforementioned radiomics features and molecular biomarkers. Previous report indicated that higher Ki-67 expression was associated with posterior acoustic enhancement, and P53-positive cancer was associated with an absence of anecho halo, which was different from ours (24). This inconsistency may be due to the different feature extraction methods. The presence of irregular or heterogeneous tumor textures, as indicated by these features, holds significant clinical implications. It suggests the presence of diverse tissue components within the tumor, potentially reflecting variations in cellularity, vascularity, and spatial organization.

The SVM models created based on the LASSO-selected features and PET-optimized parameters can identify molecular indicators effectively. Our results indicate that US-based radiomics models show optimal performance to predict molecular profiling, with the best for ER, and followed by PR. Both of them had an AUC greater than 0.80 in the validation cohort, whereas they showed lower diagnostic efficacy for HER2 and Ki-67, with an AUC slightly higher than 0.70 in the validation cohort. The ER model performed well in the validated cohort with a high specificity of 87.1% and an F1 score of 0.835. Before modeling, the choice of normalization and the setting of LASSO parameters is crucial, as both will affect the quantity and quality of LASSO feature selection. Moreover, the effectiveness of features will greatly influence the model's validity. The AUCs for predicting molecular subtype we achieved are similar to the AUCs of 0.74–0.97 in the other literature (25, 26).

In recent years, deep learning techniques have been widely employed to investigate the molecular expression of BC (27, 28). Deep learning models have demonstrated superior diagnostic performance compared to traditional machine learning models.

However, deep learning models require a relatively larger sample size than traditional machine learning approaches. Additionally, the training process of deep learning models can be likened to a "blind box," making it challenging to discern which features are utilized in the modeling process and how they are interconnected. In contrast, machine learning models offer interpretability by enabling the analysis of specific features and their corresponding weights throughout the modeling process (29, 30).

Our study has certain limitations that should be acknowledged. Firstly, it is based on a retrospective, single-center design, and the sample size is relatively small. Therefore, caution should be exercised in generalizing the findings to larger populations. To validate and strengthen our results, further investigations using a larger, multi-center cohort are warranted. Another limitation of our study is the utilization of only two-dimensional grayscale data. The inclusion of additional imaging modalities or three-dimensional data could provide a more comprehensive assessment of the molecular profiling in BC. Additionally, research in the series including the prediction of molecular subtypes, clinical decision making or therapy response based on radiomics would enhance the reliability and value of the radiomics analysis. Despite these limitations, our findings hold significant value and contribute to the understanding of the potential of ultrasound radiomics in assessing the molecular characteristics of BC.

Conclusions

Our study provides evidence that some specific radiomics features extracted from ultrasound images can effectively predict molecular expression of ER, PR, HER2, and Ki-67 in BC. The radiomics models based on the selected radiomics features show good performance in non-invasively assessing the molecular subtypes. Our findings provide a promising method in assessing the molecular profile of breast cancer.

Data availability statement

The original contributions presented in the study are included in the article/Supplementary Material, Further inquiries can be directed to the corresponding authors.

Ethics statement

The studies involving human participants were reviewed and approved by the Ethics Committee of the Second Affiliated Hospital of Fujian University of Traditional Chinese Medicine (SPHFJP-T2022007-01). The ethics committee waived the requirement of written informed consent for participation. Ethical review and approval was not required for the animal study because There were no animal experiments in this study and no animal ethics is required. Written informed consent was obtained from the individual(s) for the publication of any potentially identifiable images or data included in this article.

Author contributions

RX contributed to concept development, literature searching, and writing original draft. TY contributed to the software using, and language editing. CL contributed to the patient enrollment. QL and QG contributed to the imaging processing, and methodology. GZ contributed to the analysis of pathology. LL contributed to study management, statistical analysis and methodology. QO contributed to the funding acquisition, and study management. All authors contributed to the article and approved the submitted version.

Funding

This work was funded by the National Natural Science Foundation of China (82174469, 81973916), Natural Science Foundation of Fujian Province (2023J01815) and the Fujian Science Association Science and Technology Innovation Think Tank Research Project (2022XKB037).

Acknowledgments

We thank Engineer Qiang Chen from Fujian Juvenile & Children's Library for his professional programming expertise. We express our gratitude to our colleague, Na Yang, for providing valuable insights and expertise. We also extend special appreciation to Liling Wang for her insightful comments and invaluable suggestions.

Conflict of interest

The authors declare that the research was conducted in the absence of any commercial or financial relationships that could be construed as a potential conflict of interest.

Publisher's note

Supplementary material

The Supplementary Material for this article can be found online at: https://www.frontiersin.org/articles/10.3389/fonc.2023.1216446/full#supplementary-material

References

1. Sung H, Ferlay J, Siegel RL, Laversanne M, Soerjomataram I, Jemal A, et al. Global cancer statistics 2020: GLOBOCAN estimates of incidence and mortality worldwide for 36 cancers in 185 countries. *CA Cancer J Clin* (2021) 71(3):209–49. doi: 10.3322/caac.21660

2. Perou CM, Sørlie T, Eisen MB, van de Rijn M, Jeffrey SS, Rees CA, et al. Molecular portraits of human breast tumours. *Nature* (2000) 406(6797):747–52. doi: 10.1038/35021093

3. Curigliano G, Burstein HJ, Winer EP, Gnant M, Dubsky P, Loibl S, et al. De-escalating and escalating treatments for early-stage BC: the St. Gallen International Expert Consensus Conference on the Primary Therapy of Early BC 2017. *Ann Oncol* (2017) 28(8):1700–12. doi: 10.1093/annonc/mdx308

4. Wu J, Ge L, Jin Y, Wang Y, Hu L, Xu D, et al. Development and validation of an ultrasound-based radiomics nomogram for predicting the luminal from non-luminal type in patients with breast carcinoma. *Front Oncol* (2022) 12:993466. doi: 10.3389/fonc.2022.993466

5. Wu L, Zhao Y, Lin P, Qin H, Liu Y, Wan D, et al. Preoperative ultrasound radiomics analysis for expression of multiple molecular biomarkers in mass type of breast ductal carcinoma in situ. *BMC Med Imaging* (2021) 21(1):84. doi: 10.1186/s12880-021-00610-7

6. Roulot A, Héquet D, Guinebretière JM, Vincent-Salomon A, Lerebours F, Dubot C, et al. Tumoral heterogeneity of BC. Hétérogénéité tumorale des cancers du sein. *Ann Biol Clin (Paris)* (2016) 74(6):653–60. doi: 10.1684/abc.2016.1192

7. Quan MY, Huang YX, Wang CY, Zhang Q, Chang C, Zhou SC. Deep learning radiomics model based on breast ultrasound video to predict HER2 expression status. *Front Endocrinol (Lausanne)* (2023) 14:1144812. doi: 10.3389/fendo.2023.1144812

8. Shi W, Chen Z, Liu H, Miao C, Feng R, Wang G, et al. COL11A1 as an novel biomarker for BC with machine learning and immunohistochemistry validation. *Front Immunol* (2022) 13:937125. doi: 10.3389/fimmu.2022.937125

9. Choudhery S, Gomez-Cardona D, Favazza CP, Hoskin TL, Haddad TC, Goetz MP, et al. MRI radiomics for assessment of molecular subtype, pathological complete response, and residual cancer burden in BC patients treated with neoadjuvant chemotherapy. *Acad Radiol* (2022) 29(Suppl 1):S145–54. doi: 10.1016/j.acra.2020.10.020

10. Lin F, Wang Z, Zhang K, Yang P, Ma H, Shi Y, et al. Contrast-enhanced spectral mammography-based radiomics nomogram for identifying benign and malignant breast lesions of sub-1 cm. *Front Oncol* (2020) 10:573630. doi: 10.3389/fonc.2020.573630

11. Conti A, Duggento A, Indovina I, Guerrisi M, Toschi N. Radiomics in BC classification and prediction. *Semin Cancer Biol* (2021) 72:238–50. doi: 10.1016/j.semcancer.2020.04.002

12. Gradishar WJ, Anderson BO, Abraham J, Aft R, Agnese D, Allison KH, et al. BC, version 3.2020, NCCN clinical practice guidelines in oncology. *J Natl Compr Canc Netw* (2020) 18(4):452–78. doi: 10.6004/jnccn.2020.0016

13. Jiang M, Zhang D, Tang SC, Luo XM, Chuan ZR, Lv WZ, et al. Deep learning with convolutional neural network in the assessment of BC molecular subtypes based on US images: a multicenter retrospective study. *Eur Radiol* (2021) 31(6):3673–82. doi: 10.1007/s00330-020-07544-8

14. Moyya PD, Asaithambi M. Radiomics - quantitative biomarker analysis for BC diagnosis and prediction: a review. *Curr Med Imaging* (2022) 18(1):3–17. doi: 10.2174/1573405617666210303102526

15. Pertschuk LP, Axiotis CA, Feldman JG, Kim YD, Karavattayhayyil SJ, Braithwaite L, et al. Marked intratumoral heterogeneity of the proto-oncogene her-2/neu determined by three different detection systems. *Breast J* (1999) 5(6):369–74. doi: 10.1046/j.1524-4741.1999.97088.x

16. Allison KH, Dintzis SM, Schmidt RA. Frequency of HER2 heterogeneity by fluorescence in *situ* hybridization according to CAP expert panel recommendations: time for a new look at how to report heterogeneity. *Am J Clin Pathol* (2011) 136(6):864–71. doi: 10.1309/AJCPXTZSKBRIP07W

17. Davis BW, Zava DT, Locher GW, Goldhirsch A, Hartmann WH. Receptor heterogeneity of human BC as measured by multiple intratumoral assays of estrogen and progesterone receptor. *Eur J Cancer Clin Oncol* (1984) 20(3):375–82. doi: 10.1016/0277-5379(84)90084-1

18. Nassar A, Radhakrishnan A, Cabrero IA, Cotsonis GA, Cohen C. Intratumoral heterogeneity of immunohistochemical marker expression in breast carcinoma: a tissue microarray-based study. *Appl Immunohistochem Mol Morphol* (2010) 18(5):433–41. doi: 10.1097/PAI.0b013e3181dddb20

19. Seol H, Lee HJ, Choi Y, Lee HE, Kim YJ, Kim JH, et al. Intratumoral heterogeneity of HER2 gene amplification in BC: its clinicopathological significance. *Mod Pathol* (2012) 25(7):938–48. doi: 10.1038/modpathol.2012.36

20. Wang X, Xie T, Luo J, Zhou Z, Yu X, Guo X. Radiomics predicts the prognosis of patients with locally advanced BC by reflecting the heterogeneity of tumor cells and the tumor microenvironment. *Breast Cancer Res* (2022) 24(1):20. doi: 10.1186/s13058-022-01516-0

21. Niu S, Jiang W, Zhao N, Jiang T, Dong Y, Luo Y, et al. Intra- and peritumoral radiomics on assessment of BC molecular subtypes based on mammography and MRI. *J Cancer Res Clin Oncol* (2022) 148(1):97–106. doi: 10.1007/s00432-021-03822-0

22. Huang Y, Wei L, Hu Y, Shao N, Lin Y, He S, et al. Multi-parametric MRI-based radiomics models for predicting molecular subtype and androgen receptor expression in BC. *Front Oncol* (2021) 11:706733. doi: 10.3389/fonc.2021.706733

23. Gu J, Jiang T. Ultrasound radiomics in personalized breast management: Current status and future prospects. *Front Oncol* (2022) 12:963612. doi: 10.3389/fonc.2022.963612

24. Cui H, Zhang D, Peng F, Kong H, Guo Q, Wu T, et al. Identifying ultrasound features of positive expression of Ki67 and P53 in BC using radiomics. *Asia Pac J Clin Oncol* (2021) 17(5):e176–84. doi: 10.1111/ajco.13397

25. Li JW, Cao YC, Zhao ZJ, Shi ZT, Duan XQ, Chang C, et al. Prediction for pathological and immunohistochemical characteristics of triple-negative invasive breast carcinomas: the performance comparison between quantitative and qualitative sonographic feature analysis. *Eur Radiol* (2022) 32(3):1590–600. doi: 10.1007/s00330-021-08224-x

26. Ferre R, Elst J, Senthilnathan S, Lagree A, Tabbarah S, Lu FI, et al. Machine learning analysis of breast ultrasound to classify triple negative and HER2+ BC subtypes. *Breast Dis* (2023) 42(1):59–66. doi: 10.3233/BD-220018

27. Boulenger A, Luo Y, Zhang C, Zhao C, Gao Y, Xiao M, et al. Deep learning-based system for automatic prediction of triple-negative BC from ultrasound images. *Med Biol Eng Comput* (2023) 61(2):567–78. doi: 10.1007/s11517-022-02728-4

28. Zhang T, Tan T, Han L, Appelman L, Veltman J, Wessels R, et al. Predicting BC types on and beyond molecular level in a multi-modal fashion. *NPJ BC* (2023) 9(1):16. doi: 10.1038/s41523-023-00517-2

29. Zhang X, Li H, Wang C, Cheng W, Zhu Y, Li D, et al. Evaluating the accuracy of BC and molecular subtype diagnosis by ultrasound image deep learning model. *Front Oncol* (2021) 11:623506. doi: 10.3389/fonc.2021.623506

30. Choi RY, Coyner AS, Kalpathy-Cramer J, Chiang MF, Campbell JP. Introduction to machine learning, neural networks, and deep learning. *Transl Vis Sci Technol* (2020) 9(2):14. doi: 10.1167/tvst.9.2.14

frontiers | Frontiers in Oncology

TYPE Original Research
PUBLISHED 01 August 2023
DOI 10.3389/fonc.2023.1230083

OPEN ACCESS

EDITED BY
Francesca Bianchi,
University of Milan, Italy

REVIEWED BY
Till Kaltofen,
University Medical Center Regensburg, Germany
Torill Sauer,
University of Oslo, Norway

*CORRESPONDENCE
Min Xiao
xiaomin@hrbmu.edu.cn

RECEIVED 28 May 2023
ACCEPTED 11 July 2023
PUBLISHED 01 August 2023

CITATION
Zhu Y, Chen X, Dou H, Liu Y, Li F, Wang Y and Xiao M (2023) Vacuum-assisted biopsy system for breast lesions: a potential therapeutic approach. *Front. Oncol.* 13:1230083. doi: 10.3389/fonc.2023.1230083

Vacuum-assisted biopsy system for breast lesions: a potential therapeutic approach

Yue Zhu, Xingyan Chen, He Dou, Yuqi Liu, Fucheng Li, Youyu Wang and Min Xiao*

Department of Breast Surgery, Harbin Medical University Cancer Hospital, Harbin, Heilongjiang, China

Purpose: The primary objective is to optimize the population eligible for Mammotome Minimally Invasive Surgery (MIS) by refining selection criteria. This involves maximizing procedure benefits, minimizing malignancy risk, and reducing the rate of malignant outcomes.

Patients and methods: A total of 1158 female patients who came to our hospital from November 2016 to August 2021 for the Mammotome MIS were analyzed retrospectively. Following $\chi 2$ tests to screen for risk variables, binary logistic regression analysis was used to determine the independent predictors of malignant lesions. In addition, the correlation between age and lesion diameter was investigated for BI-RADS ultrasound (US) category 4a lesions in order to better understand the relationship between these variables.

Results: The malignancy rates of BI-RADS US category 3, category 4a and category 4b patients who underwent the Mammotome MIS were 0.6% (9/1562), 6.4% (37/578) and 8.3% (2/24) respectively. Malignant lesions were more common in patients over the age of 40, have visible blood supply, and BI-RADS category 4 of mammography. In BI-RADS US category 4a lesions, the diameter of malignant tumor was highly correlated with age, and this correlation was strengthened in patients over the age of 40 and with BI-RADS category 4 of mammography.

Conclusion: The results of this study demonstrate that the clinical data and imaging results, particularly age, blood supply, and mammography classification, offer valuable insights to optimize patients' surgical options and decrease the incidence of malignant outcomes.

KEYWORDS

vacuum-assisted breast biopsy system, mammotome minimally invasive surgery, breast ultrasonography, breast imaging-reporting and data system (BI-RADS), mammography, malignant lesions

Introduction

Currently, breast cancer is the primary cause of cancer-related death in women and has the greatest incidence of malignant tumors worldwide (1). For breast imaging examinations, it is generally recommended that women initiate early screening for breast cancer at the age of 40 (2). Early screening is a cost-effective and straightforward approach to assess asymptomatic women for breast cancer (3). In addition to clinical and imaging examinations, breast cancer knowledge promotion and breast self-examination are also important components of comprehensive breast cancer care. With the pervasive publicity of the concept of early screening and the continuous change of people's lifestyle, the probability of women being detected with breast lesions has increased significantly. Therefore, the physical and mental health of patients who are diagnosed with breast lesions are extremely vulnerable to severe effects (4). Ultrasound is a non-radiation and non-invasive method commonly used for breast examination, but its primary limitation is its lower specificity and the potential for increased false positive results (5). The Breast Imaging-Reporting and Data System classifies breast tumors into six groups based on various ultrasound characteristics (BI-RADS US). Most BI-RADS US category 3 lesions are benign, while category 4 lesions suggest an increased risk of malignancy. For example, the malignant probability of category 4a is 2% to 10%, category 4b is 10% to 50%, and category 4c is 50% to 95% (6). The unnecessary invasive examination can be minimized by screening and observing category 3 and category 4a patients on a regular basis (7, 8). Surgical resection is typically advised if the patient's daily life, physical health, or mental health are affected by these low-risk breast lesions (9).

In comparison to other treatment modalities, surgical intervention has consistently held a pivotal role as the fundamental component of comprehensive breast tumor management throughout its history (10). Traditional breast surgery has lengthy preparation, surgical trauma, blood loss, and visible scars. With research advancements and patient preferences, breast surgeons' treatment approach has significantly evolved (11). Johnson & Johnson company of the United States launched the vacuum-assisted breast biopsy (VABB) system (The Mammotome System) in 1995, which was mainly used for the location and biopsy of suspicious breast lesions at the initial stage rather than treatment (12). However, the diagnostic advantage of Mammotome system is not particularly obvious, and few doctors only use it for breast tumor biopsy. Later, for small breast masses with negative palpation, clinicians removed the tumor completely while using this equipment for biopsy, so as to accomplish the goal of treatment, and obtained satisfactory results (13). Ultrasound-guided Mammotome Minimally Invasive Surgery (MIS) is a popular therapy option among patients due to the benefits of local anesthesia, tiny incisions, fewer scars, a low incidence of postoperative complications, and rapid wound healing (14, 15). The indications and contraindications of Mammotome MIS are more stringent than those of traditional surgery, but as instruments develop and experience accumulates, the scope of contraindications and indications for this procedure is changing slightly (16, 17).

Currently, the Mammotome system is extensively utilized for the removal of suspected benign breast tumors (18, 19). Breast biopsies are commonly performed using either 14-gauge core biopsy (CB) needles or the VABB technique. The VABB method employs larger gauge probes, ranging from 11 to 7-gauge, compared to CB (20). Unlike CB, the VABB technique offers the advantage of complete lesion removal while also providing histological verification (21). Typically, clinicians relied on chief complaints, medical history, and imaging reports to make an initial assessment of the patient's condition. Patients who suspected their lesion to be benign were advised to consider MIS as an option. It not only fulfills the patients' aesthetic concerns but also successfully achieves the therapeutic objective, thereby enhancing overall patient satisfaction (22, 23). This study conducted a comprehensive review and analysis of the clinical characteristics and imaging data of female patients with BI-RADS 3, 4a, and 4b lesions who underwent Mammotome MIS. The aim was to enhance the detection accuracy of malignant lesions and strengthen the intervention and treatment of benign lesions using Mammotome MIS. Due to the high malignancy rate (50%-95%) observed in category 4c lesions and the classification of category 5 for lesions with a malignancy rate exceeding 95%, MIS is generally not recommended as a preferred clinical option (24). In addition, given the increasing number of patients with BI-RADS 4a lesions opting for MIS and the relatively high malignancy rate associated with this category, our study also focused on investigating the relationship between age and lesion diameter, aiming to gain deeper insights into the correlation between these variables.

Methods

Patients

This retrospective study was approved by the Research Ethics Review Committee of the Harbin Medical University Cancer Hospital. Using the digital integrated management system of medical records from hospital, we collected 1188 female patients who underwent Mammotome MIS from November 2016 to August 2021. Screening based on the following inclusion criteria: (a) Aged 18 or older; (b) The results of conventional ultrasound examination were BI-RADS (BI-RADS US) category 3 or above; (c) Underwent Mammotome MIS for the first time; (d) Have a complete histopathological report. Finally, we decided to include 1158 patients with a total of 2164 breast lesions. The BI-RADS category of patient is defined according to the highest BI-RADS category of each patient's lesion. According to the results of ultrasound diagnosis, the patients and the lesions were separately divided into three groups: BI-RADS US category 3 (may be benign), category 4a (low grade suspected malignant) and category 4b (moderately suspected malignant) (Figure 1).

Variables

The basic clinical data included the patient's age (< 40 years/≥ 40 years), menarche age (< 15 years/≥ 15 years), the location of the

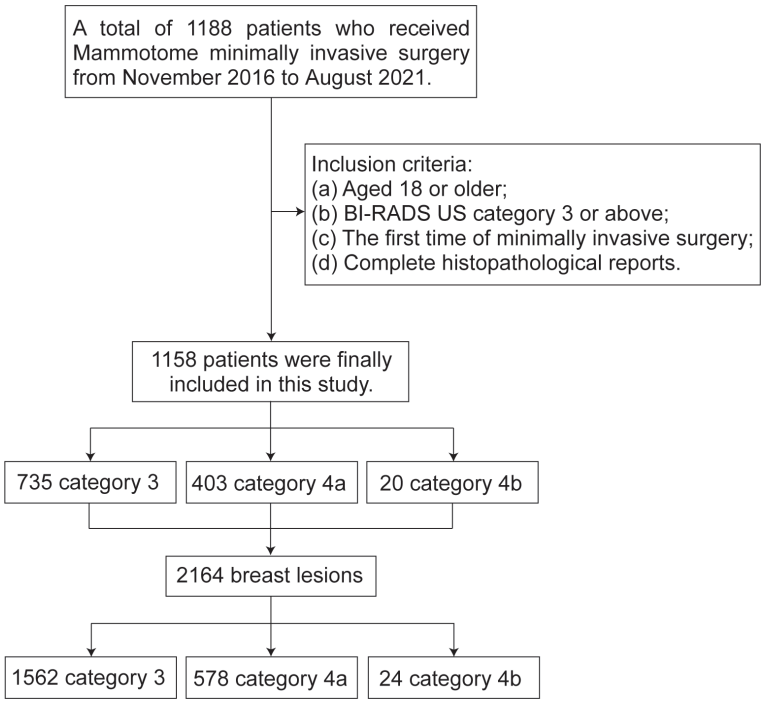

FIGURE 1
Flowchart of patient selection.

lesions (left/right) and quadrant position (UO/UI/LO/LI/CA) (Figure 2). The imaging results were jointly evaluated by both diagnostic doctors and audit doctors, including maximal lesion diameter (≥ 20 mm/< 20 mm), blood supply (invisible/visible), mammography BI-RADS category, calcification (invisible/single/multiple/unidentified). The ultrasound-guided biopsy device used in this study is Mammotome breast biopsy system (Tai Weikang Medical Devices (Shanghai) Co., Ltd.). The pathological results of all lesions were divided into benign and malignant. Malignant tumors included intraductal carcinoma in situ, invasive ductal carcinoma, solid papillary carcinoma and mucinous carcinoma. Patients with malignant diagnosis need to undergo a second operation, and the supplementary information includes the mode of operation, pathological results, histological grade, number of lymph nodes, immunohistochemical results, Ki-67 index value, accompanying with or without Intravascular tumor thrombus.

Statistical analysis

R software (V4.2.2) is used for all statistical analysis. The quantitative variables (patient's age, menarche age and maximal lesion diameter) were expressed as mean ± standard deviation. $\chi 2$ test or Fisher's exact test is used to analyze qualitative variables. Binary logistic regression analysis was used to find the potentially independent risk factors of benign and malignant tumors in BI-RADS category 4a. P values less than 0.05 are considered statistically significant.

Results

Baseline characteristics of patients and their lesions

The basic clinical data of 1158 patients with a total of 2164 breast lesions are summarized in Table 1. The patients ranged in age from 18 to 72 years (mean, 38.4 years). Comparatively, it has been shown that patients in BI-RADS US category 3 tend to be younger than patients in category 4a and category 4b, and that this difference is statistically significant (3 vs 4a, P<0.001; 3 vs 4b, P=0.006). However, the menarche age was comparable and unrelated to the BI-RADS US category. Based on our findings, a significant number of patients presented multiple lesions, with 1562 (72.2%) categorized as category 3, 578 (26.7%) as category 4a, and 24 (1.1%) as category 4b. Unsurprisingly, the UO quadrant (47%) had the highest incidence rate of lesions, followed by the UI quadrant (21.8%) and the LO quadrant (20.8%). The CA quadrant had the lowest incidence rate of lesions (0.9%). Furthermore, a consistent pattern was observed across the different types of lesions categorized by BI-RADS. The diameter of the lesion was primarily less than 20mm (12.9 ± 6.0, 85.9%) due to Mammotome equipment limitations. The visible blood supply increased as the BI-RADS category increased, and there were statistical differences (3 vs 4a, P<0.001; 3 vs 4b, P<0.001; 4a vs 4b, P<0.001). In the mammography BI-RADS category, we discovered that the category 3 and lower are more prevalent (58.3%). BI-RADS US category 4a of lesions have a higher prevalence BI-RADS

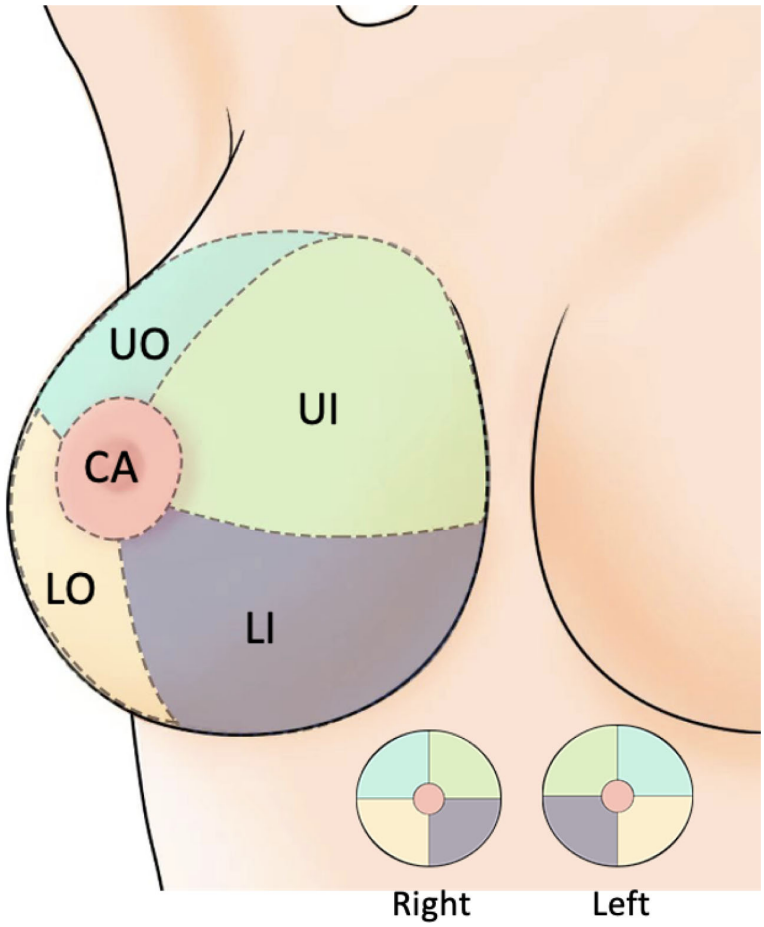

FIGURE 2
Breast quadrant division. UO, Upper Outer; LO, Lower Outer; LI, Lower Inner; UI, Upper Inner; CA, Central Area.

TABLE 1 Clinical data of patients and lesions based on BI-RADS US category and comparison of difference between categories.

Category	Total	BI-RADS US category			P-Value			
		3	4a	4b	3 vs 4a	3 vs 4b	4a vs 4b	All
Number of patients	1158 (100%)	735 (63.5%)	403 (34.8%)	20 (1.7%)				
Age (years)					<0.001	0.006	0.169	<0.001
< 40	636 (54.9%)	446 (60.7%)	184 (45.7%)	6 (30.0%)				
≥ 40	522 (45.1%)	289 (39.3%)	219 (54.3%)	14 (70.0%)				
Mean ± SD	38.4 ± 9.8	36.8 ± 9.6	41.0 ± 9.8	43.9 ± 7.7				
Range (min-max)	(18-72)	(18-66)	(18-72)	(30-58)				
Menarche age (years)					0.574	0.587	0.486	0.712
< 15	768 (66.3%)	484 (65.9%)	272 (67.5%)	12 (60.0%)				
≥ 15	390 (33.7%)	251 (34.1%)	131 (32.5%)	8 (40.0%)				
Mean ± SD	14.2 ± 1.4	14.2 ± 1.4	14.1 ± 1.4	14.4 ± 1.4				
Range (min-max)	(11-20)	(11-19)	(11-20)	(13-19)				
Number of lesions	2164 (100%)	1562 (72.2%)	578 (26.7%)	24 (1.1%)				
Location					0.731	0.312	0.359	0.577

(Continued)

TABLE 1 Continued

Category	Total	BI-RADS US category			P-Value			
		3	4a	4b	3 vs 4a	3 vs 4b	4a vs 4b	All
Left	1119 (51.7%)	813 (52.0%)	296 (51.2%)	10 (41.7%)				
Right	1045 (48.3%)	749 (48.0%)	282 (48.8%)	14 (58.3%)				
Quadrant					0.476	0.089	0.054	0.15
UO	1017 (47.0%)	739 (47.3%)	260 (45.0%)	18 (75%)				
LO	450 (20.8%)	324 (20.7%)	125 (21.6%)	1 (4.2%)				
LI	206 (9.5%)	152 (9.7%)	52 (9.0%)	2 (8.3%)				
UI	472 (21.8%)	336 (21.5%)	133 (23.0%)	3 (12.5%)				
CA	19 (0.9%)	11 (0.7%)	8 (1.4%)	0				
Maximal lesion diameter (mm)					0.092	0.409	0.193	0.154
< 20	1859 (85.9%)	1331 (85.2%)	509 (88.1%)	19 (79.2%)				
≥ 20	305 (14.1%)	231 (14.8%)	69 (11.9%)	5 (20.8%)				
Mean ± SD	12.9 ± 6.0	13.0 ± 6.0	12.5 ± 5.8	14.8 ± 6.7				
Range (min-max)	(2-43)	(2-43)	(3-38)	(6-29)				
Blood supply					<0.001	<0.001	<0.001	<0.001
Invisible	1738 (80.3%)	1310 (83.9%)	420 (72.7%)	8 (33.3%)				
Visible	426 (19.7%)	252 (16.1%)	158 (27.3%)	16 (66.7%)				
Mammography BI-RADS					<0.001	0.037	0.219	<0.001
0~3	1262 (58.3%)	887 (56.8%)	356 (61.6%)	19 (79.2%)				
4	292 (13.5%)	161 (10.3%)	128 (22.1%)	3 (12.5%)				
Unidentified	610 (28.2%)	514 (32.9%)	94 (16.3%)	2 (8.3%)				
Calcification					<0.001	<0.001	0.003	<0.001
Invisible	741 (34.2%)	518 (33.2%)	216 (37.3%)	7 (29.2%)				
Single	156 (7.2%)	105 (6.7%)	44 (7.6%)	7 (29.2%)				
Multiple	657 (30.4%)	425 (27.2%)	224 (38.8%)	8 (33.3%)				
Unidentified	610 (28.2%)	514 (32.9%)	94 (16.3%)	2 (8.3%)				
Diagnose					<0.001	<0.001	0.706	<0.001
Benign	2116 (97.8%)	1553 (99.4%)	541 (93.6%)	22 (91.7%)				
Malignant	48 (2.2%)	9 (0.6%)	37 (6.4%)	2 (8.3%)				

BI-RADS, Breast imaging-reporting and data system; US, Ultrasound; UO, Upper Outer; LO, Lower Outer; LI, Lower Inner; UI, Upper Inner; CA, Central Area; Unidentified denotes the absence of a mammography imaging report for the patient.

category 4 of mammography than BI-RADS US category 3 of lesions (P<0.001). Additionally, there were notable variations in calcification between the three types of BI-RADS (3 vs 4a, P<0.001; 3 vs 4b, P<0.001; 4a vs 4b, P=0.003), and category 4a had a considerably higher incidence of multiple calcifications (38.8%). Among the lesions analyzed, there were 2116 normal lesions and 48 malignant lesions. The malignancy rates varied across different BI-RADS US categories, with rates of 0.6% (9/1562) for category 3, 6.4% (37/578) for category 4a, and 8.3% (2/24) for category 4b.

Pathological type of breast lesions

Among benign lesions, fibroadenoma (853/2116, 40.3%) was the most common, followed by adenosis (594/2116, 28.1%) and fibroadenoma with adenosis (552/2116, 26.1%). Notably, the numbers of intraductal papilloma in BI-RADS US category 3 and category 4a were similar, but the incidence was different (31/1553 vs 33/541, 2.0% vs 6.1%). In malignant lesions, the main pathological type was invasive ductal carcinoma (IDC) (27/48, 56.3%), followed by ductal carcinoma *in situ* (DCIS) (19/48, 39.6%). The number of

malignant lesions diagnosed in category 4a was found to be the highest. In addition, two rare special type breast cancers were diagnosed, namely solid papillary carcinoma (SPC) and mucinous carcinoma (MC) (Table 2).

Comparison of characteristics between benign and malignant lesions

By comparing the basic data and imaging features of patients with benign and malignant lesions, it was found that negative results included factors such as menarche age, lesion location, quadrant division, and diameter size. Compared with benign lesions, patients older than 40 years old had a significantly higher probability of malignant lesions (P<0.001). There was a significant increase in malignant lesions with visible blood supply (P<0.001), BI-RADS category 4 of mammography (P<0.001), and multiple calcifications (P<0.001) (Table 3). We analyzed univariate and multivariate binary logistic regression analysis for these four significant risk variables. The results showed that aged 40 or above, visible blood supply, and BI-RADS category 4 of mammography were significant risk factors for breast cancer (Table 4).

Correlation analysis of BI-RADS US category 4a lesions

We compared the differences between patients of all ages and patients over the age of 40. In general, we discovered that the diameter of a malignant tumor was positively correlated with age (R=0.37, P=0.032), whereas benign lesions were the inverse (R=-0.19, P<0.001). However, this association was stronger in cancer patients over the age of 40 (R=0.48, P=0.0068) (Figure 3A). The association between malignant tumor and diameter of patients older than 40 years old was further reinforced when the menarche age was less than 15 years old (R=0.59, P=0.013) (Figure 3B). According to the analysis of left and right breast lesions, it was found that the correlation between malignant tumor diameter and age of left breast was slightly more obvious than that of right breast, but there was no statistical difference (Figures 3C, D). In contrast to BI-RADS 4a patients in all age groups, we discovered that there was a strong correlation between the malignant tumor diameter and age in patients older than 40 years old in all lesions in the UO quadrant (R=0.49, P=0.03) (Figure 3E). Similar phenomena were also found in the BI-RADS category 4 of mammography lesions (R=0.51, P=0.016) (Figure 3F). In patients without calcification, there was a substantial correlation

TABLE 2 Pathological types of benign and malignant lesions.

BI-RADS US category	3	4a	4b	Total
Benign lesions	1553	541	22	2116
Fibroadenoma	655	188	10	853
Adenosis	402	187	5	594
Fibroadenoma with adenosis	433	113	6	552
Intraductal papilloma	31	33	0	64
Benign lobular tumor	13	4	1	18
Benign breast tissue	9	6	0	15
Inflammation	3	3	0	6
Hamartoma	3	2	0	5
Atypical ductal hyperplasia	1	1	0	2
Breast Radial Scar	0	2	0	2
Cyst	1	1	0	2
Tubular adenoma	1	1	0	2
Borderline lobular tumor	1	0	0	1
Malignant lesions	9	37	2	48
Invasive ductal carcinoma	3	22	2	27
Ductal carcinoma in situ	5	14	0	19
Solid papillary carcinoma	1	0	0	1
Mucinous carcinoma	0	1	0	1

10.3389/fonc.2023.1230083

TABLE 3 Benign vs malignant in lesions.

Category	Benign	Malignant	χ2	P-Value
Age (years)			23.476	<0.001
< 40	1185 (99.2%)	10 (0.8%)		
≥ 40	931 (96.1%)	38 (3.9%)		
Menarche age (years)			0.043	0.835
< 15	1397 (97.8%)	31 (2.2%)		
≥ 15	719 (97.7%)	17 (2.3%)		
Location			0.119	0.73
Left	1093 (97.7%)	26 (2.3%)		
Right	1023 (97.9%)	22 (2.1%)		
Quadrant			5.107	0.276
UO	988 (97.1%)	29 (2.9%)		
LO	445 (98.9%)	5 (1.1%)		
LI	201 (97.6%)	5 (2.4%)		
UI	463 (98.1%)	9 (1.9%)		
CA	19 (100%)	0		
Maximal lesion diameter (mm)			0.879	0.349
< 20	1820 (97.9%)	39 (2.1%)		
≥ 20	296 (97.0%)	9 (3.0%)		
Blood supply			12.292	<0.001
Invisible	1709 (98.3%)	29 (1.7%)		
Visible	407 (95.5%)	19 (4.5%)		
Mammography BI-RADS			103.653	<0.001
0~3	1245 (98.7%)	17 (1.3%)		
4	262 (89.7%)	30 (10.3%)		
Unidentified	609 (99.8%)	1 (0.2%)		
Calcification			23.534	<0.001
Invisible	726 (98.0%)	15 (2.0%)		
Single	151 (96.8%)	5 (3.2%)		
Multiple	630 (95.9%)	27 (4.1%)		
Unidentified	609 (99.8%)	1 (0.2%)		

between the diameter of the malignant tumor and age (R=0.76, P=0.0039) (Figure 3G), but this phenomenon was not seen in patients with numerous calcifications (Figure 3H).

Secondary supplementary surgery for malignant lesions

Among these patients with malignant lesions, 31 of them underwent secondary supplementary surgery at our hospital, and a total of 38 tumors were identified. Table 5 shows the outcomes of secondary surgery for these malignant lesions. We observed that the second surgery had the highest proportion of breast-conserving surgery and sentinel lymph node biopsy (BCS+SLNB) (21/38, 55.3%). It was found that the pathological outcomes of the first Mammotome MIS and the second supplementary surgery were not exactly consistent. Among the IDC diagnosed by Mammotome MIS, the second pathological results were IDC, adenoid cystic carcinoma (ACC) and no evidence of disease (NED). Among the cases of DCIS, three cases were found to have transformed into IDC, while four cases showed NED. Furthermore, SPC transformed into DCIS, while MC showed NED (Figure 4). Based on the immunohistochemical findings, the vast majority of molecular subtypes were identified as Luminal A (33/38, 86.8%).

TABLE 4 Logistic regression analysis of the characteristics of benign and malignant lesions.

Category	Univariate		Multivariate	
	OR (95% CI)	P-Value	OR (95% CI)	P-Value
Age (years)	3.528 (1.653, 8.718)	0.003	3.008 (1.368, 7.591)	0.011
< 40				
≥ 40				
Blood supply	2.623 (1.342, 4.942)	0.003	2.28 (1.124, 4.478)	0.019
Invisible				
Visible				
Mammography BI-RADS	10.116 (5.291, 20.389)	<0.001	8.512 (4.397, 17.326)	<0.001
0~3				
4				
Calcification	2.074 (1.108, 4.029)	0.026	1.829 (0.950, 3.648)	0.077
Invisible				
Multiple				

OR, Odds ratio; 95% CI, 95% confidence interval.

Interestingly, low expression of Ki-67 was observed in 65.8% (25/38) of these malignant lesions.

Discussion

From traditional surgery to MIS, breast tumor surgery has been committed to the development of "reduction" and "precision". At the end of the 20th century, the theory of MIS progressively matured and endoscopic surgery developed rapidly (25). While it is true that MIS represents a relatively small portion of breast surgery procedures, it offers distinct advantages such as enhanced accuracy and minimal trauma (26). The maturity of these minimally invasive techniques and the success of clinical practice provide useful theories and techniques for the development of breast surgery. Ultrasound-guided Mammotome vacuum-assisted minimally invasive breast surgery, unlike laparoscopic surgery, does not involve the use of an endoscope. Currently, the indications for Mammotome MIS have been gradually expanded, allowing its application to the biopsy of various breast lesions. Under the guidance of imaging results and clinical experience, it may also be used to remove suspected benign lesions in addition to tissue biopsies.

In this study, we compare in detail the clinical basic data and imaging features of 1158 patients and 2164 lesions who underwent the Mammotome MIS. However, we discover that these patients still had a malignancy incidence of approximately 2.2%, with BI-RADS US category 4a lesions accounting for the highest proportion. Malignant lesions, as opposed to benign lesions, are more common in patients over the age of 40 and have visible blood supply, as well as BI-RADS category 4 of mammography. Usually, we recommend breast reexamination every six months for patients with BI-RADS US category 3 lesions (27). However, for patients with a psychological burden and a desire to maintain good breast appearance, we may recommend Mammotome MIS if the imaging findings show no obvious malignant features and the patients are willing to undergo lesion removal. The primary reason is that these patients have a very low malignancy rate, with the majority of them having carcinoma in situ. In the largest research to date, Berg et al. observe that the malignancy rate of BI-RADS US category 3 was 1.86% (28). This result is not in conflict with our data, as patients who have undergone Mammotome MIS have been preliminary screened. In a study to evaluate the accuracy of classification of category 3 lesions, computer-aided system also could reduce the misdiagnosis rate of malignant tumors (29).

The ultrasonic BI-RADS classification revised by the American College of Radiology (ACR) in 2013 defines category 4 lesions in more detail, and divides them into 4a, 4b and 4c (30). It has been argued that the subdivision of category 4 breast masses will not improve management, as all suspicious lesions still need to be clearly biopsied (31). In general, category 4a lesions require close observation for any changes, and biopsy should be performed when necessary to clarify the pathological nature. For category 4b lesions, patients are typically recommended to undergo biopsy in order to determine whether the lesion is benign or malignant. Our data reveals that patients with category 4b lesions represent a smaller subset in terms of the number of individuals who opted for Mammotome MIS, as compared to the other two categories. This is because category 4b lesions themselves have a 10% to 50% chance of developing malignancy, and our statistics also demonstrate a high incidence of malignancy. Therefore, most patients are advised to undergo core-needle biopsy rather than opting for Mammotome MIS.

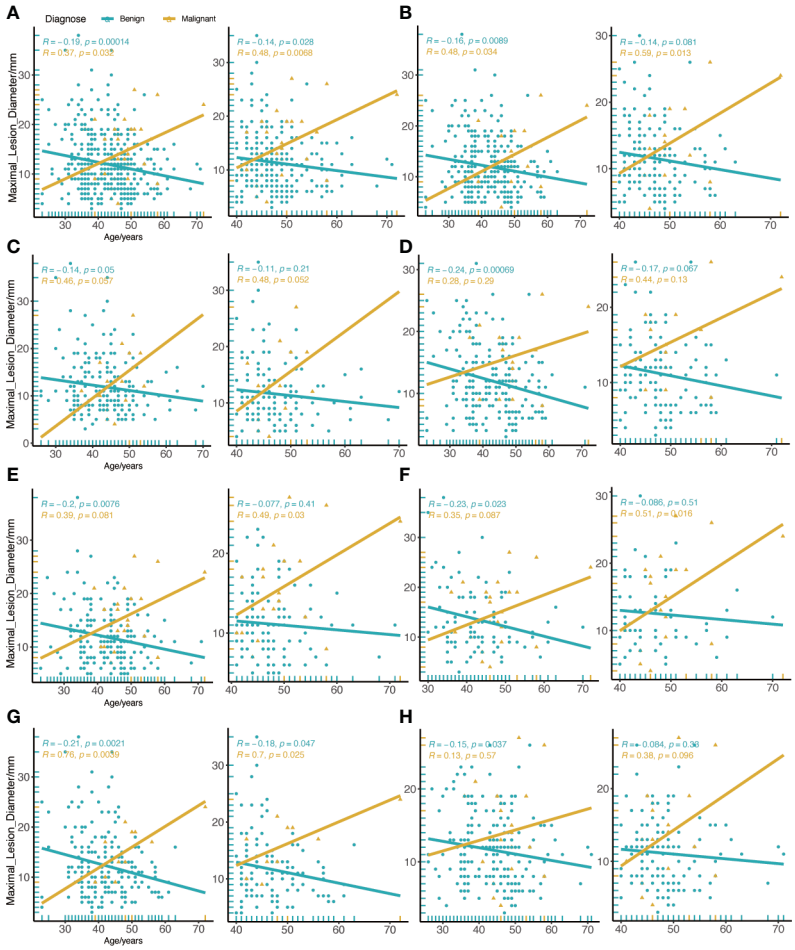

FIGURE 3
Correlation between age and maximal diameter of the lesion in all BI-RADS US category 4a. **(A)** All BI-RADS US category 4a patients. **(B)** Menarche age less than 15 years old. **(C)** Left breast lesions. **(D)** Right breast lesions. **(E)** Lesions in the UO quadrant. **(F)** the BI-RADS category 4 of mammography lesions. **(G)** Invisible calcification lesions. **(H)** Multiple calcification lesions. The left figure shows patients of all ages, and the right figure shows patients aged 40 or older.

TABLE 5 Pathological results of secondary supplementary surgery for malignant lesions.

Category	Total (n=38)	IDC (n=20)	DCIS (n=16)	SPC (n=1)	MC (n=1)
Second operation					
BCS+SLNB	21	6	14	1	0
M+SLNB	15	12	2	0	1
M+SLNB+ALND	1	1	0	0	0
MRM	1	1	0	0	0
Pathological types					
IDC	18	15	3	0	0
DCIS	10	0	9	1	0
ACC	2	2	0	0	0
NED	8	3	4	0	1

(Continued)

10.3389/fonc.2023.1230083

TABLE 5 Continued

Category	Total (n=38)	IDC (n=20)	DCIS (n=16)	SPC (n=1)	MC (n=1)
Grade					
I	3	3	0	0	0
II	11	9	2	0	0
III	4	3	1	0	0
None	20	5	13	1	1
Positive lymph nodes					
No	37	19	16	1	1
Yes	1	1	0	0	0
IHC					
Luminal A	33	18	13	1	1
Luminal B	1	1	0	0	0
TNBC	4	1	3	0	0
Ki-67					
≤10%	25	13	11	1	0
>10% and ≤25%	6	2	3	0	1
>25%	7	5	2	0	0
ITT					
No	37	19	16	1	1
Yes	1	1	0	0	0

BCS, Breast-conserving surgery; M, Mastectomy; MRM, Modified radical mastectomy; SLNB, Sentinel lymph node biopsy; ALND, Axillary lymph node dissection; IDC, Invasive ductal carcinoma; DCIS, Ductal carcinoma in situ; SPC, Solid papillary carcinoma; MC, Mucinous carcinoma; ACC, Adenoid cystic carcinoma; NED, No evidence of disease; IHC, Immunohistochemistry; ITT, Intravascular tumor thrombus.

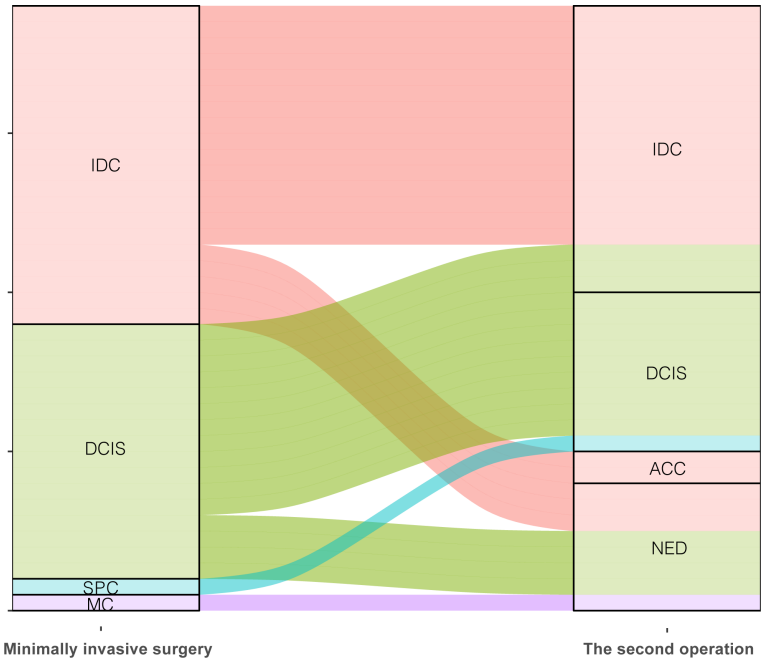

FIGURE 4
Comparison of pathological diagnosis results of two operations. IDC, Invasive ductal carcinoma; DCIS, Ductal carcinoma in situ; SPC, Solid papillary carcinoma; MC, Mucinous carcinoma; ACC, Adenoid cystic carcinoma; NED, No evidence of disease.

Our data reveal that 6.4% of malignant events occurred in BI-RADS US category 4a patients who underwent Mammotome MIS, despite their clinical screening. For category 4a lesions, there is still an urgent need to explore other potential high-risk factors to reduce the malignant possibility of patients underwent Mammotome MIS. So far, various studies have tried to overcome the limitations of breast ultrasound screening, including the application of risk assessment models (32) and the development of auxiliary systems (33). There are a variety of breast cancer risk assessment models, and Gail model is one of the most widely used standard breast cancer risk assessment methods (34). In addition, for category 4a lesion, artificial intelligence also shows high diagnostic efficiency (35). Our research reveals that the majority of patients with category 4a malignant lesions are over 40 years old, which matches the data collection included in a predictive model (36), and that age is positively correlated with tumor diameter. Menarche age is not a major risk factor for distinguishing benign from malignant lesions, but in patients with menarche age less than 15 years old, the relationship between age and tumor diameter is further strengthened. Simultaneously, identical findings are made in patients with malignant lesions that lacked calcification.

When considering the use of vacuum biopsy as a therapeutic approach in cancer, it is important to exercise caution and carefully evaluate its applicability. International guidelines recommend the use of vacuum-assisted excision for breast lesions with a maximum diameter of 25 mm (37). This technique is considered appropriate and effective for the removal of such lesions. In some cases of resected tumors with larger diameters, the presence of peri-interventional inflammation around the biopsy area can pose challenges to tumor resection. This inflammation can complicate the surgical procedure and potentially impact the effectiveness of the treatment. Antonio et al. discovered that post-biopsy peripheral inflammation can transmit growth signals to remaining cancer cells or precancerous cells, leading to a negative impact on disease progression (38). This inflammation can complicate the surgical procedure and potentially impact the effectiveness of the treatment. In order to fully ensure the negative histopathology of the incision margin during the resection of the lesion, a second supplementary operation is required. This is due to the limitations of the Mammotome MIS. Therefore, MIS should be cautiously chosen for patients with clearly malignant lesions in order to prevent needless medical disputes.

Conclusions

Patients in BI-RADS US category 3 who underwent Mammotome MIS tend to be younger compared to those in category 4a and 4b. Age, visible blood supply, and BI-RADS category 4 of mammography are potentially independent risk factors for breast malignancy. Additionally, we discovered a positive correlation between diameter size and age in malignant lesions by conducting a correlation analysis on BI-RADS US category 4a lesions. In patients with malignant lesions who are older than 40 years old, have an age of menarche younger than 15 years old, a mammography report greater than BI-RADS 4, and without calcifications, this positive correlation trend will further increase. High-risk groups with these factors should monitor lesion changes, undergo biopsy if need for pathology confirmation, and avoid using the vacuum biopsy system for treatment.

Data availability statement

The original contributions presented in the study are included in the article/supplementary material. Further inquiries can be directed to the corresponding author.

Ethics statement

The studies involving human participants were reviewed and approved by the institute research ethics committee of Harbin Medical University Cancer Hospital. The patients/participants provided their written informed consent to participate in this study.

Author contributions

We confirm that the manuscript is original. MX put forward the idea and supervised this project. YZ was responsible for analyzing data and writing manuscript. The authors read and approved the final manuscript.

Funding

This study was supported by the National Natural Science Foundation of China (81872145) and Heilongjiang Province Postdoctoral Science Foundation (LBH-Q18078).

Conflict of interest

The authors declare that the research was conducted in the absence of any commercial or financial relationships that could be construed as a potential conflict of interest.

Publisher's note

References

1. Giaquinto AN, Sung H, Miller KD, Kramer JL, Newman LA, Minihan A, et al. Breast Cancer Statistics, 2022. *CA A Cancer J Clin* (2022) 72(6):524–41. doi: 10.3322/caac.21754

2. Monticciolo DL, Newell MS, Moy L, Niell B, Monsees B, Sickles EA. Breast Cancer Screening in Women at Higher-Than-Average Risk: Recommendations From the ACR. *J Am Coll Radiol* (2018) 15(3):408–14. doi: 10.1016/j.jacr.2017.11.034

3. Ren W, Chen M, Qiao Y, Zhao F. Global guidelines for breast cancer screening: A systematic review. *Breast* (2022) 64:85–99. doi: 10.1016/j.breast.2022.04.003

4. Krasne M, Ruddy KJ, Poorvu PD, Gelber SI, Tamimi RM, Schapira L, et al. Coping strategies and anxiety in young breast cancer survivors. *Support Care Cancer* (2022) 30(11):9109–16. doi: 10.1007/s00520-022-07325-7

5. Lee JM, Arao RF, Sprague BL, Kerlikowske K, Lehman CD, Smith RA, et al. Performance of Screening Ultrasonography as an Adjunct to Screening Mammography in Women Across the Spectrum of Breast Cancer Risk. *JAMA Intern Med* (2019) 179 (5):658. doi: 10.1001/jamainternmed.2018.8372

6. Mercado CL. BI-RADS update. *Radiol Clin North Am* (2014) 52:481–7. doi: 10.1016/j.rcl.2014.02.008

7. Lee KA, Talati N, Oudsema R, Steinberger S, Margolies LR. BI-RADS 3: Current and Future Use of Probably Benign. *Curr Radiol Rep* (2018) 6:5. doi: 10.1007/s40134-018-0266-8

8. Strigel RM, Burnside ES, Elezaby M, Fowler AM, Kelcz F, Salkowski LR, et al. Utility of BI-RADS Assessment Category 4 Subdivisions for Screening Breast MRI. *AJR Am J Roentgenol* (2017) 208(6:1392–9. doi: 10.2214/AJR.16.16730

9. Hot S, Coşkun ZÜ, Akçakaya A, Bender Ö, Türkmen ÜA, Nayır PÖ, et al. The breast lesion excision system procedure: An optimal solution for the management of indeterminate BI-RADS category 3 breast lesions in women with severe anxiety. *Saudi Med J* (2018) 39(9):891–6. doi: 10.15537/smj.2018.9.22573

10. Jonczyk MM, Jean J, Graham R, Chatterjee A. Surgical trends in breast cancer: a rise in novel operative treatment options over a 12 year analysis. *Breast Cancer Res Treat* (2019) 173:267–74. doi: 10.1007/s10549-018-5018-1

11. Tea M-KM, Asseryanis E, Kroiss R, Kubista E, Wagner T. Surgical breast lesions in adolescent females. *Pediatr Surg Int* (2009) 25:73–5. doi: 10.1007/s00383-008-2285-7

12. Bozzini A, Cassano E, Raciti D, Disalvatore D, Pala O, Vingiani A, et al. Analysis of Efficacy and Accuracy of 2 Vacuum-Assisted Breast Biopsy Devices: Mammotome and Elite. *Clin Breast Cancer* (2018) 18(6):e1277–82. doi: 10.1016/j.clbc.2018.06.014

13. Nakano S, Sakamoto H, Ohtsuka M, Mibu A, Sakata H, Yamamoto M. Evaluation and indications of ultrasound-guided vacuum-assisted core needle breast biopsy. *Breast Cancer* (2007) 14(3):292–6. doi: 10.2325/jbcs.14.292

14. Jiang Y, Lan H, Ye Q, Jin K, Zhu M, Hu X, et al. Mammotome® biopsy system for the resection of breast lesions: Clinical experience in two high-volume teaching hospitals. *Exp Ther Med* (2013) 6(3):759–64. doi: 10.3892/etm.2013.1191

15. Pan S, Liu W, Jin K, Liu Y, Zhou Y. Ultrasound-guided vacuum-assisted breast biopsy using Mammotome biopsy system for detection of breast cancer: results from two high volume hospitals. *Int J Clin Exp Med* (2014) 7:239–46. eCollection 2014.

16. Kibil W, Hodorowicz-Zaniewska D, Kulig J. Mammotome biopsy under ultrasound control in the diagnostics and treatment of nodular breast lesions - own experience. *Pol Przegl Chir* (2012) 84:242–6. doi: 10.2478/v10035-012-0040-1

17. Kong Y, Lyu N, Wang J, Wang Y, Sun Y, Xie Z, et al. Does Mammotome biopsy affect surgery option and margin status of breast conserving surgery in breast cancer? *Gland Surg* (2021) 10(8):2428–37. doi: 10.21037/gs-20-701

18. Wang ZL. Percutaneous excisional biopsy of clinically benign breast lesions with vacuum-assisted system: Comparison of three devices. *Eur J Radiol* (2012) 81(4):725–30. doi: 10.1016/j.ejrad.2011.01.059

19. Baez E, Huber A, Vetter M. Minimal invasive complete excision of benign breast tumors using a three-dimensional ultrasound-guided mammotome vacuum device. *Ultrasound Obstet Gynecol* (2003) 21(3):267–72. doi: 10.1002/uog.74

20. Ames V, Britton PD. Stereotactically guided breast biopsy: a review. *Insights Imaging* (2011) 2(2):171–6. doi: 10.1007/s13244-010-0064-1

21. Bhatt AA, Whaley DH, Lee CU. Ultrasound-Guided Breast Biopsies. *J Ultrasound Med* (2021) 40(7):1427–43. doi: 10.1002/jum.15517

22. Zou S-F, Tao L, Feng ZC, Wang JY, Liu L, Liang WL, et al. A comparative study on ultrasound-guided elite, Mammotome, and core needle biopsy for diagnosing malignant breast masses. *Arch Med Sci* (2022) 18(2):422–31. doi: 10.5114/aoms.2019.87096

23. Guo R, Lu G, Qin B, Fei B. Ultrasound Imaging Technologies for Breast Cancer Detection and Management: A Review. *Ultrasound Med Biol* (2018) 44:37–70. doi: 10.1016/j.ultrasmedbio.2017.09.012

24. D'Orsi CJ, Sickles EA, Mendelson EB, Morris EA. *ACR BI-RADS Atlas, Breast Imaging Reporting and Data System, 5th ed*. American College of Radiology (2013).

25. Mok CW, Lai H-W. Endoscopic-assisted surgery in the management of breast cancer: 20 years review of trend, techniques and outcomes. *Breast* (2019) 46:144–56. doi: 10.1016/j.breast.2019.05.013

26. Lai H-W, Chen ST, Liao CY, Mok CW, Lin YJ, Chen DR, et al. Oncologic Outcome of Endoscopic Assisted Breast Surgery Compared with Conventional Approach in Breast Cancer: An Analysis of 3426 Primary Operable Breast Cancer Patients from Single Institute with and Without Propensity Score Matching. *Ann Surg Oncol* (2021) 28(12):7368–80. doi: 10.1245/s10434-021-09950-8

27. Moy L. BI-RADS Category 3 Is a Safe and Effective Alternative to Biopsy or Surgical Excision. *Radiology* (2020) 296:42–3. doi: 10.1148/radiol.2020201583

28. Berg WA, Berg JM, Sickles EA, Burnside ES, Zuley ML, Rosenberg RD, et al. Cancer Yield and Patterns of Follow-up for BI-RADS Category 3 after Screening Mammography Recall in the National Mammography Database. *Radiology* (2020) 296 (1):32–41. doi: 10.1148/radiol.2020192641

29. Moon WK, Lo CM, Chang JM, Huang CS, Chen JH, Chang RF. Quantitative ultrasound analysis for classification of BI-RADS category 3 breast masses. *J Digit Imaging* (2013) 26(6):1091–8. doi: 10.1007/s10278-013-9593-8

30. Spak DA, Plaxco JS, Santiago L, Dryden MJ, Dogan BE. BI-RADS® fifth edition: A summary of changes. *Diagn Interv Imaging* (2017) 98:179–90. doi: 10.1016/j.diii.2017.01.001

31. Spinelli Varella MA, Teixeira da Cruz J, Rauber A, Varella IS, Fleck JF, Moreira LF. Role of BI-RADS Ultrasound Subcategories 4A to 4C in Predicting Breast Cancer. *Clin Breast Cancer* (2018) 18(4):e507–11. doi: 10.1016/j.clbc.2017.09.002

32. Harkness EF, Astley SM, Evans DG. Risk-based breast cancer screening strategies in women. *Best Pract Res Clin Obstet Gynaecol* (2020) 65:3–17. doi: 10.1016/j.bpobgyn.2019.11.005

33. Xing J, Chen C, Lu Q, Cai X, Yu A, Xu Y, et al. Using BI-RADS Stratifications as Auxiliary Information for Breast Masses Classification in Ultrasound Images. *IEEE J BioMed Health Inform* (2021) 25(6):2058–70. doi: 10.1109/JBHI.2020.3034804

34. Wang X, Huang Y, Li L, Dai H, Song F, Chen K. Assessment of performance of the Gail model for predicting breast cancer risk: a systematic review and meta-analysis with trial sequential analysis. *Breast Cancer Res* (2018) 20(1):18. doi: 10.1186/s13058-018-0947-5

35. Huang Y, Han L, Dou H, Luo H, Yuan Z, Liu Q, et al. Two-stage CNNs for computerized BI-RADS categorization in breast ultrasound images. *BioMed Eng Online* (2019) 18(1):8. doi: 10.1186/s12938-019-0626-5

36. Luo W, Huang Q, Huang X, Hu H, Zeng F, Wang W. Predicting Breast Cancer in Breast Imaging Reporting and Data System (BI-RADS) Ultrasound Category 4 or 5 Lesions: A Nomogram Combining Radiomics and BI-RADS. *Sci Rep* (2019) 9(1):11921. doi: 10.1038/s41598-019-48488-4

37. Rageth CJ, O'Flynn EAM, Pinker K, Kubik-Huch RA, Mundinger A, Decker T, et al. Second International Consensus Conference on lesions of uncertain malignant potential in the breast (B3 lesions). *Breast Cancer Res Treat* (2019) 174(2):279–96. doi: 10.1007/s10549-018-05071-1

38. Antonio N, Bønnelykke-Behrndtz ML, Ward LC, Collin J, Christensen IJ, Steiniche T, et al. The wound inflammatory response exacerbates growth of pre-neoplastic cells and progression to cancer. *EMBO J* (2015) 34(17):2219–36. doi: 10.15252/embj.201490147

frontiers | Frontiers in Oncology

TYPE Original Research
PUBLISHED 11 August 2023
DOI 10.3389/fonc.2023.1198157

OPEN ACCESS

EDITED BY
Francesca Bianchi,
University of Milan, Italy

REVIEWED BY
Marcus Vetter,
University Hospital of Basel, Switzerland
Julio de la Torre,
Comillas Pontifical University, Spain

*CORRESPONDENCE
Carolin Müller
carolin.mueller@uks.eu

RECEIVED 31 March 2023
ACCEPTED 24 July 2023
PUBLISHED 11 August 2023

CITATION
Zemlin C, Schleicher JT, Altmayer L, Stuhlert C, Wörmann C, Lang M, Scherer L-S, Thul IC, Spenner LS, Simon JA, Wind A, Kaiser E, Weber R, Goedicke-Fritz S, Wagenpfeil G, Zemlin M, Steffgen G, Solomayer E-F and Müller C (2023) Improved awareness of physical activities is associated with a gain of fitness and a stable body weight in breast cancer patients during the first year of antineoplastic therapy: the BEGYN-1 study. *Front. Oncol.* 13:1198157. doi: 10.3389/fonc.2023.1198157

Improved awareness of physical activities is associated with a gain of fitness and a stable body weight in breast cancer patients during the first year of antineoplastic therapy: the BEGYN-1 study

Cosima Zemlin[1], Julia Theresa Schleicher[1], Laura Altmayer[1], Caroline Stuhlert[1], Carolin Wörmann[1], Marina Lang[1], Laura-Sophie Scherer[1], Ida Clara Thul[1], Lisanne Sophie Spenner[1], Jana Alisa Simon[1], Alina Wind[1], Elisabeth Kaiser[2], Regine Weber[2], Sybelle Goedicke-Fritz[2], Gudrun Wagenpfeil[3], Michael Zemlin[2], Georges Steffgen[4], Erich-Franz Solomayer[1] and Carolin Müller[1,5]*

[1]Department of Gynecology, Obstetrics, and Reproductive Medicine, Saarland University Medical Center, Homburg, Saar, Germany, [2]Department of General Pediatrics and Neonatology, Saarland University Medical Center, Homburg, Saar, Germany, [3]Institute for Medical Biometry, Epidemiology and Medical Informatics (IMBEI), Saarland University Campus Homburg, Homburg, Saar, Germany, [4]Department of Behavioural and Cognitive Sciences, Institute for Health and Behaviour, University of Luxembourg, Esch-sur-Alzette, Luxembourg, [5]Department of Outcomes Research, Anesthesiology Institute, Cleveland Clinic, Cleveland, OH, United States

Background: Breast cancer is the most frequent cancer in women. Reduced physical activity and overweight are associated with poor prognosis. Breast cancer patients have a high risk to gain weight, lose muscle mass and reduce physical activity during therapy. Concepts are urgently needed to motivate patients to engage in physical activity.

Methods: 110 non-metastatic breast cancer patients were included in the prospective observational BEGYN-1 study. Physiological parameters and body composition were measured before the start of therapy and then quarterly for one year. Patients used a fitness tracker and documented their physical activity in a diary throughout the study.

Results: Although the patients were not offered any guided exercise, and despite the restrictions during the COVID-19 pandemic, they increased their physical activity (metabolic equivalent of task (MET) -minutes): $p<0.001$), physical fitness

(decreasing resting heart rate: p=0.001) and did not gain weight (median - 0.4kg) over the course of the study.

Conclusion: Improved awareness of physical activity is associated with an increase in physical activity, fitness, and a stable weight during the first year of therapy in breast cancer patients. Counselling at diagnosis should motivate patients to engage in physical activity, wear a fitness tracker and document activities.

KEYWORDS

breast cancer, physical activity, resting heart rate, fitness tracker, MET, body composition, weight, COVID - 19

1 Introduction

The diagnosis of breast cancer often represents a traumatic event in patients that can result in reduced physical activity, weight gain and deteriorating physical fitness (1, 2). Especially weight gain during chemotherapy has already been recognized to be a problem in breast cancer patients (3). Weight gain, as well as reduction of physical activity and fitness are known to negatively influence the success of cancer therapy and overall outcome (4–7). In addition, obesity is a risk factor for the development of breast cancer in the first place. Especially occurrence of hormone-receptor positive breast cancer in postmenopausal women could be associated with obesity (8).

Physical activity is playing an important role in primary prevention of breast cancer, as physical activity is associated with a reduction of primary breast cancer and recurrent breast cancer (9). Based on a large population-based study among breast cancer patients, physical activity before and after chemotherapy was associated with significantly reduced hazard ratios of recurrence and mortality (10). However, in this study, physical activity was assessed using questionnaires (10). To better understand the consequences of physical activity during anticancer therapy on side effects, body composition and physiological parameters, we performed the prospective BEGYN-1 study (11, 12).

Van Gemert et al. showed that 5.5% of postmenopausal breast cancer cases are attributable to physical inactivity and 8.8% to overweight, making this together an even greater risk than smoking (4.6%) and alcohol (6.6%) (13). Healthcare professionals should counsel patients in ways that increase awareness of the importance of physical activity as well as a healthy lifestyle (14). But not only breast cancer patients can benefit from physical activities. The importance of physical activity and the positive influence on the quality of life in patients with other cancer entities, e.g., lung and colorectal cancer, has been shown previously (15, 16).

There is an urgent need to develop and implement novel strategies that motivate newly diagnosed breast cancer patients to engage in physical activity from diagnosis throughout the entire course of anticancer therapy. Several previous studies used an interventional approach to measure the influence of strength and/or endurance sports (7, 17–20). A meta-analysis found that supervised interventions regarding physical activity might be a greater independent motivator compared than partly supervised or unsupervised interventions (21). Supervised exercise showed a stronger effect on primary outcomes, quality of life, and physical function than the type or amount of recommended exercise (21). Recent systematic reviews demonstrated, that in combination with diet, exercise intervention led to improved cardiorespiratory fitness, muscular strength, body composition, quality of life, fatigue, anxiety, depression, and sleep compared to control groups (22–24). Furthermore, in long-term studies, healthy bodyweight resulting from regular physical exercise was associated with a better quality of life compared to overweight or obese women who gained body weight after diagnosis (25).

However, maintaining the level of physical activity is difficult after the completion of a short-term exercise intervention (26). It is important to provide patients with sustainable motivational concepts after an intervention (27). Activity diaries alone might offer some motivation, but there are considerable discrepancies between this form of self-assessment and other methods to quantify physical activity (28).

The use of fitness trackers has been recommended for a more objective assessment (29, 30). Fitness trackers have been successfully used to quantify physical activity by tracking step counts of patients undergoing oncological treatment (31). Furthermore, fitness trackers continuously measure the heart rate and determine the resting heart rate. The resting heart rate is an important marker not only for physical fitness but correlates with longevity and with the risk of all-cause mortality in breast cancer patients (32, 33). A systematic review showed that the use of a fitness tracker in combination with motivational interviews had the most consistent positive effect on adherence to physical activity (34). During the COVID-19 pandemic, an increased use of fitness trackers was observed that was positively associated with physical activity (35). However, multiple studies showed that physical activity decreased, and body weight increased during the Covid-19 pandemic in German and US-American population (36–38).The aim of the BEGYN-1 study was to assess the physical activity, resting heart rate and body weight, as well as body composition during the first year of newly diagnosed nonmetastatic breast cancer patients. We aimed to detect differences between the first and the

last three months during the first year after breast cancer diagnosis, thus after completion of most acute oncologic therapies (e.g., chemotherapy, radiotherapy, surgery). According to the national guideline for breast cancer, moderate physical activity was recommended to all patients (39, 40). Physical activity was measured by using a fitness tracker as well as a personal activity diary. Quarterly routine follow-up visits were used for monitoring physiological parameters and body composition and for evaluation of physical activity.

2 Patients and methods

2.1 Patients

Patients were enrolled in the BEGYN-1 study between September 2019 and January 2021 (11). The baseline study visit was scheduled before the start of any antineoplastic therapy or intervention (e.g., surgery, chemotherapy) but after information by a medical doctor about the diagnosis. The BEGYN-1 study lasted one year in total, and all patients presented themselves every three months for their follow-up visits. Clinical assessment was obtained at each visit, including anamnesis, measuring body weight, as well as blood pressure, resting heart rate, and bioelectrical impedance analysis. Therefore, nutritional and hydration deprivation (except water) was required prior to the measurements and patients presented themselves in sportswear.

The study was approved by the ethics committee of the Medical Association of Saarland (study # 229/18). Inclusion and exclusion criteria are presented in Figure 1. All patients provided written consent. Documentation of clinical characteristics (e.g., age, BMI, Karnofsky performance status scale), as well as histopathological parameters was performed.

2.2 Methods

All patients received their own fitness tracker (Fitbit charge 3™, Fitbit Inc., San Francisco) at the baseline visit. The fitness tracker was linked to a smartphone and patients were motivated to wear the fitness tracker during the whole day, ideally at any time (including nights) to measure steps, physical activity, and heart rate (29). Weekly fitness reports of the fitness tracker were read out during the follow-up visits.

Additionally, all patients documented their sporting activities and calorie consumption in their individual study diary. The diary included daily notes on the type and length of physical activities. The patients were asked to transfer the measurement results from the fitness tracker to the diary. They could add comments in a free text field. The diary was evaluated during the follow-up visits by study staff together with the patients.

METs (Metabolic Equivalents of Task) can be used to compare different activities regarding their energy consumption. One MET corresponds to the conversion of 3.15 ml oxygen per kilogram of

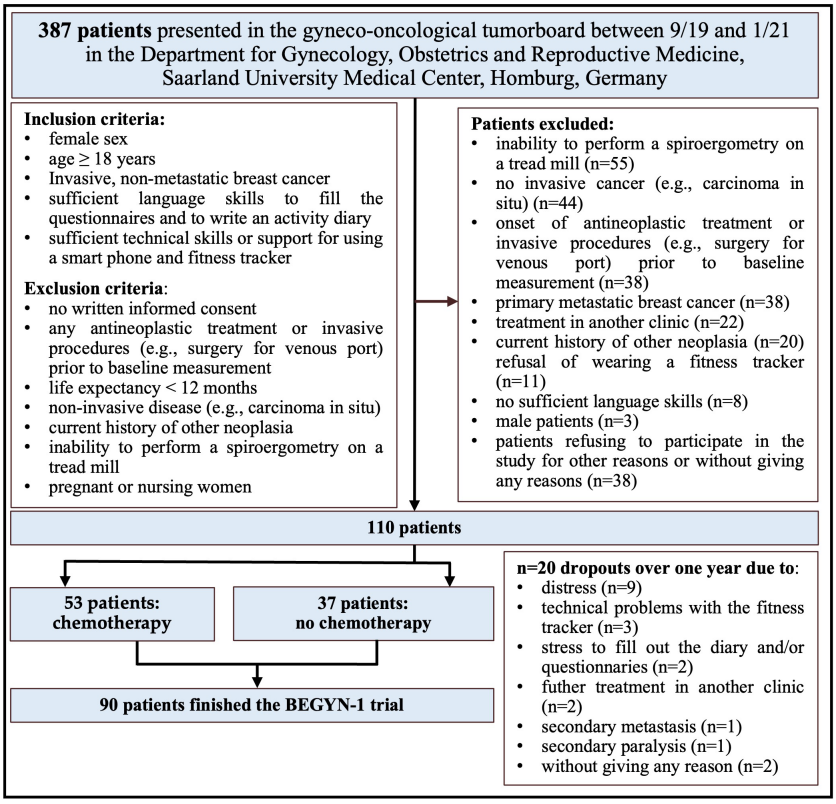

FIGURE 1
Recruitment and flow of participants in the BEGYN-1 trial.

body weight per minute in women. In the current study, METs were calculated using information from the fitness tracker, as well as the study diary. METs were calculated for all days throughout the year and mean values were calculated for individual days, weeks, and months. MET minutes (MET-min) were obtained by multiplying MET activity with duration of the activity ($MET\text{-}min_{activity} = MET_{activity} \times duration_{activity}$) (41, 42). When "MET-min" is mentioned in the following manuscript, this term refers to $MET\text{-}min_{activity}$. The energy expenditure (kcal) and the duration (minutes) of certain activities were documented from the fitness tracker's actigraphy. Body weight (kg) was measured weekly by the patients themselves. A distinction was made between total activity and workout. The daily calorie consumption, measured by the fitness tracker, was defined as the total activity. Periods of rest, or periods where the fitness tracker was not worn (e.g., nights) were included and the Fitbit app calculated the basal metabolic rate for these periods.

In the case of missing data imputation was carried out according to previously published methods by Stephens et al. (43). Missing values for the total activity occurred when the tracker was not worn or only partially worn during the day or when no value could be determined due to technical problems and/or lack of cooperation on the part of the patients. Where possible, the missing values were imputed according to standard procedures (43). Briefly, the requirement was that at least 50% of the data on daily calorie consumption was available in the relevant diary. At least three (if possible five) plausible references were used, and the arithmetic mean of the reference values was used as the estimated value for the missing value. Days with the same activities (e.g., walking and swimming or no sport) or with the same general condition (e.g., nausea or hospitalization) as on the day with the missing value were selected as references. To impute the activities as completely as possible, missing recordings were supplemented according to the following algorithm: If energy expenditure was not reported for an activity, an estimate was calculated based on other recorded exercises of the same type and intensity (at least three, if possible five references). For this purpose, an arithmetically averaged quotient was calculated with the duration or the route of the references. Implausible outlier values measured by the fitness tracker (e.g., an apparent extremely long walking distance), that were in conflict with the activity diary, were replaced by the patient's self-assessment in consultation with the patient, so that the energy consumption was estimated based on the patient information according to the above scheme. Consideration of both, fitness tracker measurements and activity diary thus lead to the most complete assessment of physical activity (43). In accordance with the published recommendations, we differentiated between data that was missing at random or systematically, e.g., when the patient only wore the fitness tracker during sporting activities but not during daily life (43).

Body composition was assessed using bioelectrical impedance analysis. For the bioelectrical impedance analysis (BIA) (TANITA 601 scale™, Tanita Europe BV, Stuttgart), the patients stood barefoot on a body scale and holding sensors in both hands. Based on a dual frequency bioelectrical impedance analysis at four measuring points, the scale yields information about the muscle, fat, bone, and water content of the whole body as well as individual compartments (44, 45).

2.3 Statistics

Statistical analyses were performed using SPSS as IBM Corp. Released 2021. IBM SPSS Statistics for Windows, Version 28.0. Armonk, NY: IBM Corp. Qualitative parameters (e.g., tumor stage) are presented as frequencies and quantitative parameters are given as mean with standard deviation or as median with range. Normal distribution was assessed by Shapiro-Wilk testing. Inter-group comparison was performed using the Mann-Whitney-U test. Assessments over time were compared with the Wilcoxon signed-rank test and repeated measures analysis of variance (Friedman test) combined with pair-wise comparisons adjusted for multiple testing according to the Bonferroni method. Correlations were analyzed using Spearman Rank correlation. Thus, ΔMET-min/week (ΔMET-min/week = MET-min/week [week 40-52] minus MET-min/week [week 1-13]) were used to correlate physical activity with weight, visceral fat, body fat, muscle mass and BMI between the first three months and the last three months within the first year after diagnosis.

3 Results

In total, 110 patients were included in the BEGYN-1 trial (Figure 1). In the period between September 2019 and January 2021, n=387 patients with high suspicion or newly diagnosed breast cancer were presented to the tumor board at the breast center of the Department of Gynecology, Obstetrics and Reproductive Medicine, Saarland University Medical Center, Homburg/Saar, Germany. Of these n=387 patients, n=181 met the inclusion criteria (Figure 1). N=110 patients signed the declaration of consent after being informed by a physician. N=20 patients dropped out of the study (Figure 1). The patients were 26 to 81 years old when included in the study.

Ninety patients completed the study until the final one year follow up assessment and were used for the analysis. Of these n=90 patients, n=53 patients received chemotherapy (CHT). N=37 patients did not receive chemotherapy (NCHT). Median length of chemotherapy was 147 days (min. 76, max. 189 days). All patients received surgical treatment and n=75 patients (83%) underwent radiotherapy. Median length of radiotherapy was 37 days (min. 18, max. 69 days). All patients received surgical treatment and n=72 patients (80%) endocrine therapy. Patients' characteristics regarding tumor entity, tumor subtype, and tumor stage, as well as age are listed in Table 1. Timing of oncological treatment throughout the year is illustrated in Table 2.

Overall, physical activity increased significantly from 16845 MET-min/week (median) in the first quarter of the study to 18114 MET-min/week in the last quarter of the study ($p<0.001$) (Figure 2). In the two subgroups, physical activity increased from 16804 MET-min/week to 17697 MET-min/week (CHT, $p<0.001$) and from 16973 MET-min/week to 18357 MET-min/week (NCHT,

Table 1 Patient characteristics including tumor entity (histology, grading), tumor stage (TNM-classification) and age in all patients/chemotherapy (CHT)/no chemotherapy (NCHT).

		CHT (n=53)	NCHT (n=37)	All patients (n=90)
Tumor entity	NST	44 (83.0%)	31 (83.8%)	75 (83.3%)
	invasive lobular	7 (13.2%)	2 (2.7%)	9 (10.0%)
	others	2 (3.8%)	4 (10.8%)	6 (6.7%)
cT	T0*	2 (3.8%)	1 (2.7%)	3 (3.3%)
	T1	29 (54.7%)	34 (91.8%)	63 (70.0%)
	T2	19 (35.8%)	2 (5.4%)	21 (23.3%)
	T3	1 (1.9%)	0 (0.0%)	1 (1.1%)
	T4	2 (3.8%)	0 (0.0%)	2 (2.2%)
cN	N0	38 (71.7%)	35 (94.6%)	73 (81.1%)
	N+	15 (28.3%)	2 (5.4%)	17 (18.9%)
cM	M0	53 (100%)	37 (100%)	90 (100%)
Grading**	G1	0 (0.0%)	10 (27.0%)	10 (11.1%)
	G2	19 (35.8%)	23 (62.2%)	42 (46.7%)
	G3	34 (64.2%)	3 (8.1%)	37 (41.1%)
Age	26-30 years	2 (3.8%)	1 (2.7%)	3 (3.3%)
	31-40 years	10 (18.9%)	3 (8.1%)	13 (14.4%)
	41-50 years	13 (24.5%)	9 (24.3%)	22 (24.4%)
	51-60 years	15 (28.3%)	10 (27.0%)	25 (27.8%)
	61-70 years	11 (20.8%)	10 (27.0%)	21 (23.3%)
	71-78 years	2 (3.8%)	4 (10.8%)	6 (6.7%)

*3 patients had a recurrent tumor in the lymph nodes without tumor manifestation in the breast, thus T0**Grading not available in one NCHT patient.

p=0.07), respectively. Furthermore, the ranges of activity increased over time in both therapy groups: 11860 to 22037 MET-min/week (CHT) and 13564 to 23443 MET-min/week (NCHT) in the first quarter of the study to 11093 to 24736 MET-min/week (CHT) and 12738 to 24300 MET-min/week (NCHT) in the last quarter of the study. There was no significant difference related to physical activity between the two therapy groups (Table 3).

The resting heart rate of all patients decreased significantly during the study period from 77/min at the baseline visit to 72/min at the final visit at the end of the study period (p<0.001) (Figure 3, Table 3). More precisely, the patients who received chemotherapy (CHT) as well as those who did not receive chemotherapy (NCHT) therefore also showed a significant reduction of the heart rate during the investigation period from 78/min to 72/min (median, CHT, p<0.001) and 74/min to 71/min (median, NCHT, p=0.037), respectively. Regarding the patients who received chemotherapy an additional increase in heart rate occurred from first week to week 13. This represents an increase in heart rate during chemotherapy (Figure 3).

The average weight of all patients decreased not significantly by 0.4 kg (p = 0.259) during the study period (Figure 4, Table 3). The weight changes of the patients receiving chemotherapy (CHT) and of those who did not receive chemotherapy (NCHT) also showed no significant differences over time (p = 0.145/p = 0.850) nor between

TABLE 2 Treatment (chemotherapy, radiotherapy, and surgery) according to time quartiles.

Therapy	0-3 months	3-6 months	6-9 months	9-12 months	Total therapy
Chemotherapy	53 (100%)	52 (98%)	15 (29%)	2 (4%)	53 (100%)
Surgery	55 (61%)	12 (13%)	22 (25%)	1 (1%)	90 (100%)
Radiotherapy	27 (36.5%)	7 (9.5%)	37 (50%)	3 (4%)	74 (100%)
Endocrine therapy	37 (41%)	46 (51%)	65 (72%)	72 (100%)	72 (100%)

All in all, n=53 patients underwent chemotherapy, all (n=90) patients had surgery, n=74 patients received radiotherapy, and n=72 patients received endocrine therapy. Values are given as n= number of patients and percentage (%).

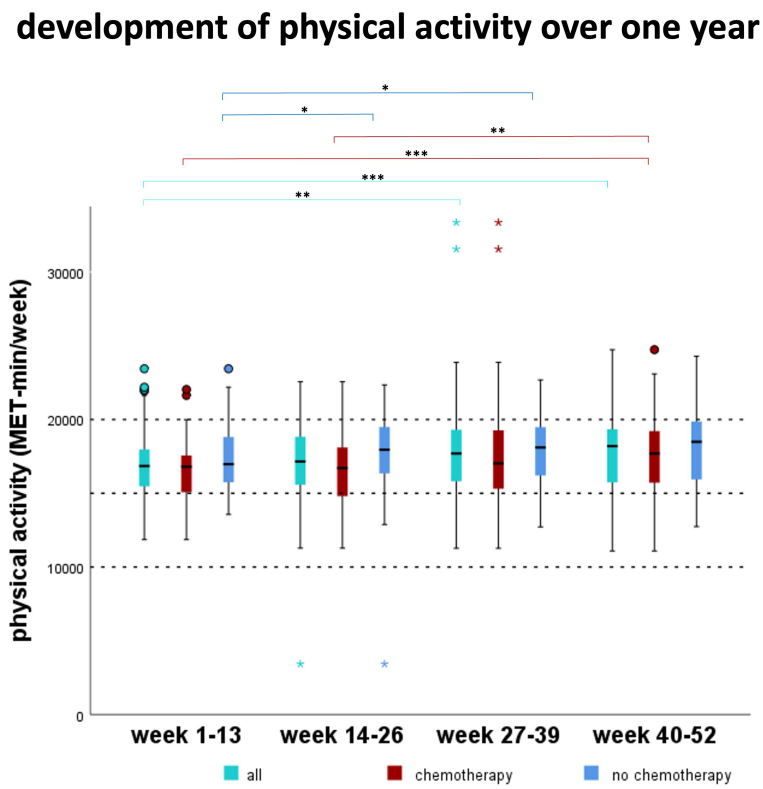

FIGURE 2
Development of the physical activity over one year. MET (Metabolic equivalents of task). Over all patients, the MET-mins significantly increased between week 1-13 compared to weeks 27-39 and 40-52 ($p<0.01$). In patients receiving chemotherapy, MET increased significantly between weeks 1-13 and 14-26 compared to week 40-52 ($p<0.01$). In patients who did not receive chemotherapy, MET increased significantly between week 1-13 compared to weeks 14-26 and 27-39 ($p<0.05$). *$p<0.05$, **$p<0.01$, ***$p<0.001$.

CHT and NCHT ($p = 0.650$). CHT- patients had no significant loss of weight (median -0.9kg), body fat (median -0.7kg), muscle mass (median -0,1kg) and reduction of their BMI (median -0.2kg/m²) (Table 3). There was no significant difference between the NCHT and CHT groups for the body composition (Table 3).

To test the hypothesis that the quantity of physical activity might influence physiological parameters, we studied the correlation between the physiological parameters with the deviation of physical activity during the study period.

Over the course of the study year, a significant correlation for the entire patient collective concerning weight, visceral fat, body fat, muscle mass and BMI was observed comparing week 1-13 to week 40-52. Correlating the examined variables with the ΔMET-min/week (ΔMET-min/week = MET-min/week [week 40-52] minus MET-min/week [week 1-13]) over the course of the study year yielded a significant correlation for the entire patient collective for weight, visceral fat, body fat, muscle mass and BMI (Figure 5). The heart rate did not correlate significantly with the ΔMET-min/week, neither when considering all patients nor when examining the different therapy groups. The muscle mass of the NCHT patients, as well as the body fat and the visceral fat of the CHT patients, did not correlate significantly with the ΔMET-min/week over the course of the study year.

4 Discussion

The BEGYN-1 study revealed that the use of a fitness tracker and an activity diary are associated with an increase in physical activity and physical fitness as well as a stable body weight in breast cancer patients after the first year of therapy. Moreover, we observed a negative correlation between the extent of physical activity and changes of body weight, BMI, body fat, and visceral fat over time.

The influence of physical activity during anticancer therapy on fitness, remains poorly understood (10). Thus, the aim of this study was to assess the physical activity, fitness, physiological parameters, and body composition in newly diagnosed non-metastatic breast cancer patients during the first year of treatment. Since other studies reported a decrease in physical activity and fitness and an increase in weight gain during anticancer therapy (1, 2), routine counselling appears to be insufficient to achieve a long-lasting effect on the patient's motivation. Guided successful short-term interventions were either not assessed with a long-term follow up (46) or they had little long-term effect on physical activity (26). Thus, we sought to identify factors that might motivate the patients to improve their lifestyle over the long term.

10.3389/fonc.2023.1198157

TABLE 3 Physical activity and body composition in all patients/chemotherapy (CHT)/no chemotherapy (NCHT) at two different time points (baseline visit/end of trial) and difference between baseline visit and end of the study (Δ).

	Median first visit	Range first visit	Median deviation after one year	First versus last visit*	CHT versus NCHT Δfinal-first visit*
MET-min/week					
All (n=90)	16845	11860 – 23443	+995	p < 0.001	
CHT (n=53) NCHT (n=37)	16804 16973	11860 – 22037 13564 – 23443	+1209 +709	p < 0.001 p = 0.07	p = 0.396
Resting heart rate [1/min]					
All (n=90)	77	58 - 138	-5	p < 0.001	
CHT (n=53) NCHT (n=37)	78 74	58 – 138 62 - 114	-5 -5	p < 0.001 p = 0.037	p = 0.625
Bodyweight [kg]					
All (n=90)	69.4	45.6 – 107.4	-0.4	p = 0.259	
CHT (n=53) NCHT (n=37)	70.2 69.3	51.0 – 107.4 45.6 – 92.8	-0.9 +0.6	p = 0.145 p = 0.850	p = 0.650
Visceral fat [absolute]					
All (n=90)	7	2 - 14	0	p = 0.509	
CHT (n=53) NCHT (n=37)	7 7	2 – 14 2 – 13	0 0	p = 0.943 p = 0.325	p = 0.281
Body fat [%]					
All (n=90)	34.8	16.9 – 48.5	+0.1	p = 0.936	
CHT (n=53) NCHT (n=37)	34.9 33.4	16.9 – 48.5 16.9 – 44.4	-0.7 +0.6	p = 0.247 p = 0.165	p = 0.800
Muscle mass [kg]					
All (n=90)	43.6	34.4 – 55.8	-0.2	p = 0.180	
CHT (n=53) NCHT (n=37)	44.4 42.3	34.4 – 55.8 35.2 – 51.2	-0.1 -0.6	p = 0.479 p = 0.216	p = 0.628
BMI [kg/m^2]					
All (n=90)	26	19 – 39	0	p = 0.250	
CHT (n=53) NCHT (n=37)	26 26	19 – 39 19 – 35	0 0	p = 0.148 p = 0.898	p = 0.256

MET, Metabolic equivalents of task. BMI, body mass index. *2-sided Mann Whitney-U test.

The BEGYN-1 study was designed as an observational study. All patients received a fitness tracker, were supposed to write an activity diary and were undergoing quarterly fitness assessments. While in intervention studies it is usually unclear how much the participants exercise outside of the interventions, the BEGYN study starts right here and aims to fully record physical activity throughout all days of the year. Although, patients did not receive guided exercise, we found evidence that the study participants were highly motivated to improve their lifestyle. Notably, 60% of the eligible patients agreed to participate in the BEGYN-1 study. This indicates that the majority of the newly diagnosed breast cancer patients were interested in actively addressing their physical condition even during the earliest stage of their disease and prior to the initiation of anticancer treatment. In agreement with this finding, the positive short-term and long-term effect of motivational interviews had been previously shown (34). We hypothesize that addressing the positive effects of physical activity during the initial disclosure of the diagnosis was perceived by the patients as a possibility to take control over the course of the disease and improve the feeling of self-efficiency. This has been shown to have a long-lasting positive effect on the psychological coping with the disease and to correlate with an improved outcome (47). The effect of higher self-efficiency and autonomy in cancer patients undergoing counseling for physical activity has been previously shown in different cancer entities (48).

In our cohort, a higher increase of weekly MET-min during the study period was associated with an improved physical status: We found a beneficial correlation between the extent of physical activity, bodyweight, BMI, and body fat mass. Thus, the BEGYN-1 study patients experienced similar benefits over a one-year period as interventional studies with supervised exercise (7, 17–20). Importantly, Zhou et al. have shown that a three-month wearable-based lifestyle intervention may help reduce weight and

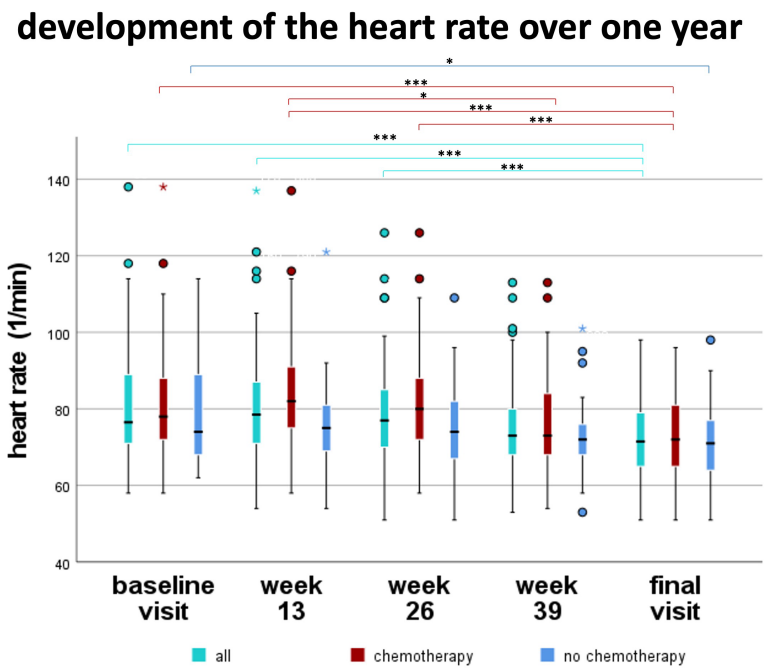

FIGURE 3
Development of the resting heart rate over one year. Over all patients, heart rate decreased significantly between baseline visit, week 13, and week 26 compared to final visit ($p<0.001$). In patients receiving chemotherapy, heart rate increased from week 1 to week 13. Afterwards, heart rate decreased significantly in chemotherapy patients comparing week 13 to 39 ($p<0.05$) and week 13 to final visit ($p<0.001$). *$p<0.05$, **$p<0.01$, ***$p<0.001$.

improve body composition in breast cancer survivors (20). Similar to our findings, Zhou et al. reported a decrease in overall muscle mass in patients with elevated physical activity. This apparent paradox might be due to suboptimal protein intake during antineoplastic therapy, due to the predominance of endurance sports overweight training- especially in patients that underwent surgery- and/or due to a loss of postural muscles as part of the weight loss (20).

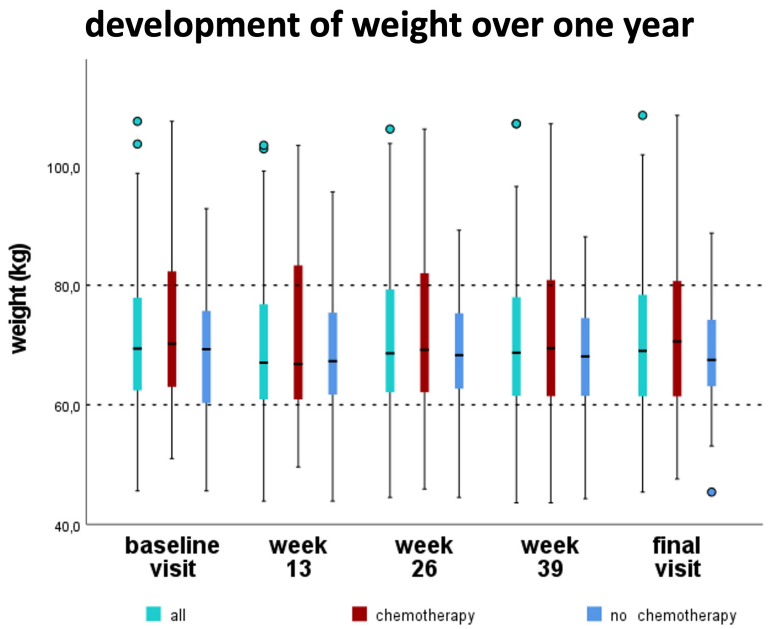

FIGURE 4
Development of the bodyweight over one year. Median body weight slightly decreased from 69.4kg (baseline visit) to 69.0kg (final visit) during the first year in newly diagnosed breast cancer patients, without reaching statistical significance.

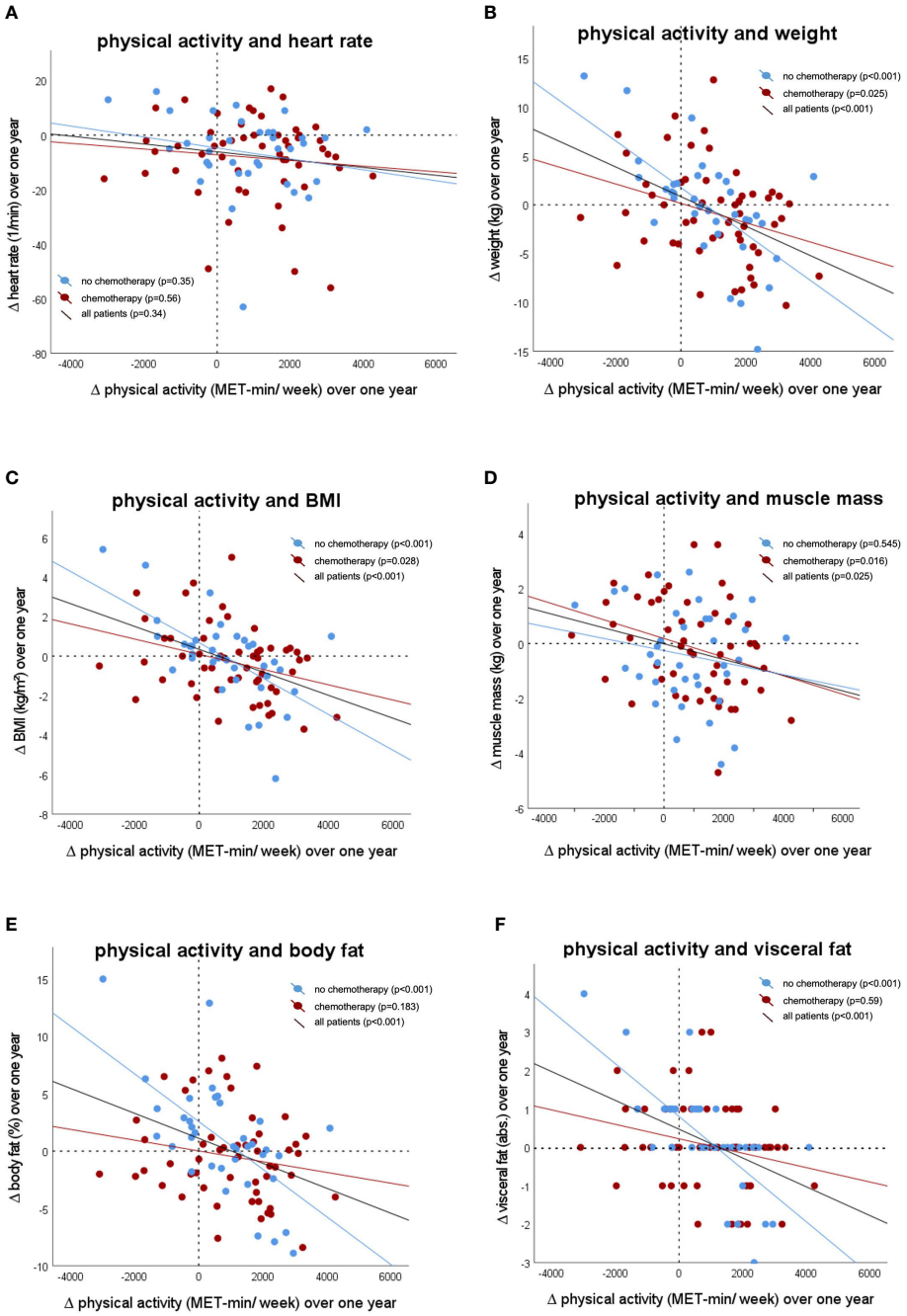

FIGURE 5
Correlation between the change of physical activity during the study period with **(A)** resting heart rate (correlation coefficient: -0.1; p=0.34), **(B)** body weight (correlation coefficient: -0.4; p<0.001), **(C)** Body mass index (BMI) (correlation coefficient: -0.4, p<0.001), **(D)** muscle mass (correlation coefficient: -0.2; p=0.03), **(E)** body fat (correlation coefficient: -0.4; p=0.001), **(F)** visceral fat (correlation coefficient: -0.5; p<0.001).

Recommendation of physical activity is already included in national and international guidelines (7, 39, 40, 49). However, optimal intensity and duration of physical activity is not clear (49). Thus, according to the guidelines (7, 39, 40), patients were advised to engage in moderate physical activity, but no upper limit was mentioned. Even though, none of the BEGYN-1 study patients showed any sign of overexertion or other negative side effects of too much physical activity, further research is needed to individualize recommendations for the level of physical activity to aim for (50, 51). The increased physical activity and fitness achieved in the BEGYN-1 study might have multiple other consequences that are known to be associated with increased physical activity in breast

cancer patients, e.g., increased bone health (52), reduced cancer related fatigue (53), and reduced cancer related cognitive impairment (54).

Strengths of our study are the high number of patients, the inclusion prior to therapy induction, the dual assessment of physical activities by using a fitness tracker and a diary, and the long follow up period of one year. METs are as a standardized quantification of physical activity, a validated method to summarize and compare differing physical activities (e.g., Nordic walking, swimming, cycling and weight training) (41, 42). This design allows to identify long-lasting effects on health parameters and minimizes potential transient confounders such as effects of perioperative immobility. Furthermore, improved physical activity was seen despite the Covid-19 pandemic. Previous studies revealed a reduction of physical activity during Covid-19 pandemic and especially during lockdowns (55). The biggest part of the BEGYN-1 study was carried out during Covid-19 pandemic, so patients were not able to participate in group sport or go to the gym, as most group activities were not allowed during Covid-19 pandemic.

The study results must be interpreted with caution due to some limitations: Due to ethical concerns, we did not include a control group that was deprived of counselling according to the guidelines (7, 39, 40). Thus, we can only hypothesize that the improvement of physical activity and fitness and the stability of body weight was a consequence of the motivation that was caused by participating in the study. Medical guidance, such as motivational interviews, using an activity diary or wearing a fitness tracker might contribute to additional motivation since patients knew, that corresponding data was evaluated. However, this hypothesis is strongly supported by other studies (20). Furthermore, physiological parameter (like heart rate) might be influenced due to higher level of function in some patients. These individuals might be more capable in participating in physical activity. Moreover, bioimpedance measurements and the use of fitness trackers are readily available, but they also have technical limitations (20) and missing values had to be calculated to approximate the total MET-mins (41, 42).

5 Conclusion

We conclude that prevention of decreased physical activity and fitness, as well as gain of weight during the first year after diagnosis of early breast cancer, even during the Covid-19 pandemic, is possible. Improved awareness of physical activity could lead to an increase in physical activity, fitness, and a stable body weight during the first year after diagnosis of early breast cancer. Patients should be encouraged to exercise, wear a fitness tracker, and/or document activities. By positively influencing their lifestyle, patients get back their self-control, increase their quality of life and long-term outcome.

Data availability statement

The datasets generated during the current study are available from the corresponding author on reasonable request.

Ethics statement

The studies involving humans were approved by ethics committee of the Medical Association of Saarland (study # 229/18). The studies were conducted in accordance with the local legislation and institutional requirements. The participants provided their written informed consent to participate in this study.

Author contributions

CZ wrote the study conception and design. CZ implemented the study in the clinic, recruited the patients and supervised the study. E-FS and MZ gave advice for the study design and supervised the study. Material preparation and data collection were performed by JTS, LA, CS, CW, ML, L-SS, IT, LS, JAS, AW, EK, RW, and SG-F. The data analysis was performed by CZ and GW. The first draft of the manuscript was written by CM and CZ. All authors commented on previous versions of the manuscript. All authors contributed to the article and approved the submitted version.

Funding

This work was supported by *miteinander gegen Krebs e.V. (to CZ)*, by a grant from the federal state of Saarland (to CM and CZ, grant number W/2 - LFFP 21/13) and by intramural funds of the Saarland University Medical Center.

Acknowledgments

The authors would like to thank Dr. Maria Cacacciola-Ketter, Cross against Cancer – *miteinander gegen Krebs e.V.*, Bernd Neuhardt (Laufschule Saarpfalz, Runners Gym Zweibrücken). Furthermore, we acknowledge support by the Deutsche Forschungsgemeinschaft (DFG, German Research Foundation) and Saarland University within the "Open Access Publication Funding" program.

Conflict of interest

The authors declare that the research was conducted in the absence of any commercial or financial relationships that could be construed as a potential conflict of interest.

Publisher's note

References

1. Cathcart-Rake EJ, Sanft T, Tevaarwerk AJ. Weight gain after breast cancer diagnosis: It's complicated. *Cancer* (2022) 128:3152–4. doi: 10.1002/cncr.34343

2. Makari-Judson G. Weight gain following breast cancer diagnosis: Implication and proposed mechanisms. *World J Clin Oncol* (2014) 5:272. doi: 10.5306/wjco.v5.i3.272

3. van den Berg MMGA, Winkels RM, de Kruif J, van Laarhoven HWM, Visser M, de Vries JHM, et al. Weight change during chemotherapy in breast cancer patients: a meta-analysis. *BMC Cancer* (2017) 17:259. doi: 10.1186/s12885-017-3242-4

4. Playdon MC, Bracken MB, Sanft TB, Ligibel JA, Harrigan M, Irwin ML. Weight gain after breast cancer diagnosis and all-cause mortality: systematic review and meta-analysis. *J Natl Cancer Inst* (2015) 107:djv275. doi: 10.1093/jnci/djv275

5. Lee K, Kruper L, Dieli-Conwright CM, Mortimer JE. The impact of obesity on breast cancer diagnosis and treatment. *Curr Oncol Rep* (2019) 21:41. doi: 10.1007/s11912-019-0787-1

6. Rose DP, Vona-Davis L. Influence of obesity on breast cancer receptor status and prognosis. *Expert Rev Anticancer Ther* (2009) 9:1091–101. doi: 10.1586/era.09.71

7. Ligibel JA, Bohlke K, May AM, Clinton SK, Demark-Wahnefried W, Gilchrist SC, et al. Exercise, diet, and weight management during cancer treatment: ASCO guideline. *J Clin Oncol* (2022) 40:2491–507. doi: 10.1200/JCO.22.00687

8. Picon-Ruiz M, Morata-Tarifa C, Valle-Goffin JJ, Friedman ER, Slingerland JM. Obesity and adverse breast cancer risk and outcome: Mechanistic insights and strategies for intervention. *CA Cancer J Clin* (2017) 67:378–97. doi: 10.3322/caac.21405

9. de Boer MC, Wörner EA, Verlaan D, van Leeuwen PAM. The mechanisms and effects of physical activity on breast cancer. *Clin Breast Cancer* (2017) 17:272–8. doi: 10.1016/j.clbc.2017.01.006

10. Cannioto RA, Hutson A, Dighe S, McCann W, McCann SE, Zirpoli GR, et al. Physical activity before, during, and after chemotherapy for high-risk breast cancer: relationships with survival. *JNCI: J Natl Cancer Institute* (2021) 113:54–63. doi: 10.1093/jnci/djaa046

11. Zemlin C, Stuhlert C, Schleicher JT, Wörmann C, Altmayer L, Lang M, et al. Longitudinal assessment of physical activity, fitness, body composition, immunological biomarkers, and psychological parameters during the first year after diagnosis in women with non-metastatic breast cancer: The BEGYN study protocol. *Front Oncol* (2021) 11:762709. doi: 10.3389/fonc.2021.762709

12. Zemlin C, Altmayer L, Stuhlert C, Schleicher JT, Wörmann C, Lang M, et al. Prevalence and relevance of vitamin D deficiency in newly diagnosed breast cancer patients: A pilot study. *Nutrients* (2023) 15:1450. doi: 10.3390/nu15061450

13. van Gemert WA, Lanting CI, Goldbohm RA, van den Brandt PA, Grooters HG, Kampman E, et al. The proportion of postmenopausal breast cancer cases in the Netherlands attributable to lifestyle-related risk factors. *Breast Cancer Res Treat* (2015) 152:155–62. doi: 10.1007/s10549-015-3447-7

14. Kraschnewski JL, Schmitz KH. Exercise in the prevention and treatment of breast cancer. *Curr Sports Med Rep* (2017) 16:263–7. doi: 10.1249/JSR.0000000000000388

15. Ho M, Ho JWC, Fong DYT, Lee CF, Macfarlane DJ, Cerin E, et al. Effects of dietary and physical activity interventions on generic and cancer-specific health-related quality of life, anxiety, and depression in colorectal cancer survivors: a randomized controlled trial. *J Cancer Survivorship* (2020) 14:424–33. doi: 10.1007/s11764-020-00864-0

16. Avancini A, Sartori G, Gkountakos A, Casali M, Trestini I, Tregnago D, et al. Physical activity and exercise in lung cancer care: will promises be fulfilled? *Oncologist* (2020) 25:e555–69. doi: 10.1634/theoncologist.2019-0463

17. An K, Morielli AR, Kang D, Friedenreich CM, McKenzie DC, Gelmon K, et al. Effects of exercise dose and type during breast cancer chemotherapy on longer-term patient-reported outcomes and health-related fitness: A randomized controlled trial. *Int J Cancer* (2020) 146:150–60. doi: 10.1002/ijc.32493

18. Carayol M, Ninot G, Senesse P, Bleuse J-P, Gourgou S, Sancho-Garnier H, et al. Short- and long-term impact of adapted physical activity and diet counseling during adjuvant breast cancer therapy: the "APAD1" randomized controlled trial. *BMC Cancer* (2019) 19:737. doi: 10.1186/s12885-019-5896-6

19. Leach HJ, Potter KB, Hidde MC. A group dynamics-based exercise intervention to improve physical activity maintenance in breast cancer survivors. *J Phys Act Health* (2019) 16:785–91. doi: 10.1123/jpah.2018-0667

20. Zhou C, Mo M, Wang Z, Shen J, Chen J, Tang L, et al. A short-term effect of wearable technology-based lifestyle intervention on body composition in stage I–III postoperative breast cancer survivors. *Front Oncol* (2020) 10:563566. doi: 10.3389/fonc.2020.563566

21. Andersen HH, Vinther A, Lund CM, Paludan C, Jørgensen CT, Nielsen D, et al. Effectiveness of different types, delivery modes and extensiveness of exercise in patients with breast cancer receiving systemic treatment – A systematic review and meta-analysis. *Crit Rev Oncol Hematol* (2022) 178:103802. doi: 10.1016/j.critrevonc.2022.103802

22. Pérez-Bilbao T, Alonso-Dueñas M, Peinado AB, San Juan AF. Effects of combined interventions of exercise and diet or exercise and supplementation on breast cancer patients: A systematic review. *Nutrients* (2023) 15:1013. doi: 10.3390/nu15041013

23. Joaquim A, Leão I, Antunes P, Capela A, Viamonte S, Alves AJ, et al. Impact of physical exercise programs in breast cancer survivors on health-related quality of life, physical fitness, and body composition: Evidence from systematic reviews and meta-analyses. *Front Oncol* (2022) 12:955505. doi: 10.3389/fonc.2022.955505

24. Li X, Wang J, Zhang J, Zhang N, Wu C, Geng Z, et al. The effect of exercise on weight and body composition of breast cancer patients undergoing chemotherapy. *Cancer Nurs* (2023) 1. doi: 10.1097/NCC.0000000000001196

25. Voskuil DW, van Nes JGH, Junggeburt JMC, van de Velde CJH, van Leeuwen FE, de Haes JCJM. Maintenance of physical activity and body weight in relation to subsequent quality of life in postmenopausal breast cancer patients. *Ann Oncol* (2010) 21:2094–101. doi: 10.1093/annonc/mdq151

26. Goldschmidt S, Schmidt ME, Steindorf K. Long-term effects of exercise interventions on physical activity in breast cancer patients: a systematic review and meta-analysis of randomized controlled trials. *Supportive Care Cancer* (2023) 31:130. doi: 10.1007/s00520-022-07485-6

27. Juvet LK, Thune I, Elvsaas IKØ, Fors EA, Lundgren S, Bertheussen G, et al. The effect of exercise on fatigue and physical functioning in breast cancer patients during and after treatment and at 6 months follow-up: A meta-analysis. *Breast* (2017) 33:166–77. doi: 10.1016/j.breast.2017.04.003

28. Helbrich H, Braun M, Hanusch C, Mueller G, Falk H, Flondor R, et al. Congruence and trajectories of device-measured and self-reported physical activity during therapy for early breast cancer. *Breast Cancer Res Treat* (2021) 188:351–9. doi: 10.1007/s10549-021-06195-7

29. Fuller D, Colwell E, Low J, Orychock K, Tobin MA, Simango B, et al. Reliability and validity of commercially available wearable devices for measuring steps, energy expenditure, and heart rate: systematic review. *JMIR Mhealth Uhealth* (2020) 8:e18694. doi: 10.2196/18694

30. Wagoner CW, Choi SK, Deal AM, Lee JT, Wood WA, Muss HB, et al. Establishing physical activity in breast cancer: self-report versus activity tracker. *Breast Cancer Res Treat* (2019) 176:395–400. doi: 10.1007/s10549-019-05263-3

31. Purswani JM, Ohri N, Champ C. Tracking steps in oncology: the time is now. *Cancer Manag Res* (2018) 10:2439–47. doi: 10.2147/CMAR.S148710

32. Jensen MT. Resting heart rate and relation to disease and longevity: past, present and future. *Scand J Clin Lab Invest* (2019) 79:108–16. doi: 10.1080/00365513.2019.1566567

33. Lee DH, Park S, Lim SM, Lee MK, Giovannucci EL, Kim JH, et al. Resting heart rate as a prognostic factor for mortality in patients with breast cancer. *Breast Cancer Res Treat* (2016) 159:375–84. doi: 10.1007/s10549-016-3938-1

34. Pudkasam S, Feehan J, Talevski J, Vingrys K, Polman R, Chinlumprasert N, et al. Motivational strategies to improve adherence to physical activity in breast cancer survivors: A systematic review and meta-analysis. *Maturitas* (2021) 152:32–47. doi: 10.1016/j.maturitas.2021.06.008

35. Tong HL, Maher C, Parker K, Pham TD, Neves AL, Riordan B, et al. The use of mobile apps and fitness trackers to promote healthy behaviors during COVID-19: A cross-sectional survey. *PloS Digital Health* (2022) 1:e0000087. doi: 10.1371/journal.pdig.0000087

36. Khubchandani J, Price JH, Sharma S, Wiblishauser MJ, Webb FJ. COVID-19 pandemic and weight gain in American adults: A nationwide population-based study. *Diabetes Metab Syndrome: Clin Res Rev* (2022) 16:102392. doi: 10.1016/j.dsx.2022.102392

37. Schienkiewitz A, Damerow S, Richter A, Mensink Gert BM. How has body weight changed since the beginning of the COVID-19 pandemic? *J Health Monit* (2022) 7:54–61. doi: 10.25646/10670

38. Beck F, Siefken K, Reimers A. Physical activity in the face of the COVID-19 pandemic: changes in physical activity prevalence in Germany. *Deutsche Z Für Sportmedizin/German J Sports Med* (2022) 73:175–83. doi: 10.5960/dzsm.2022.537

39. Wöckel A, Festl J, Stüber T, Brust K, Stangl S, Heuschmann P, et al. Interdisciplinary screening, diagnosis, therapy and follow-up of breast cancer. Guideline of the DGGG and the DKG (S3-level, AWMF registry number 032/045OL, december 2017) – part 1 with recommendations for the screening, diagnosis and therapy of breast cancer. *Geburtshilfe Frauenheilkd* (2018) 78:927–48. doi: 10.1055/a-0646-4522

40. Wöckel A, Festl J, Stüber T, Brust K, Krockenberger M, Heuschmann P, et al. Interdisciplinary screening, diagnosis, therapy and follow-up of breast cancer. Guideline of the DGGG and the DKG (S3-level, AWMF registry number 032/045OL, december 2017) – part 2 with recommendations for the therapy of primary, recurrent and advanced breast cancer. *Geburtshilfe Frauenheilkd* (2018) 78:1056–88. doi: 10.1055/a-0646-4630

41. Jetté M, Sidney K, Blümchen G. Metabolic equivalents (METS) in exercise testing, exercise prescription, and evaluation of functional capacity. *Clin Cardiol* (1990) 13:555–65. doi: 10.1002/clc.4960130809

42. Ainsworth BE, Haskell WL, Herrmann SD, Meckes N, Bassett DR, Tudor-Locke C, et al. Compendium of physical activities. *Med Sci Sports Exerc* (2011) 43:1575–81. doi: 10.1249/MSS.0b013e31821ece12

43. Stephens S, Beyene J, Tremblay MS, Faulkner G, Pullnayegum E, Feldman BM. Strategies for dealing with missing accelerometer data. *Rheumatic Dis Clinics North America* (2018) 44:317–26. doi: 10.1016/j.rdc.2018.01.012

44. Ward LC, Müller MJ. Bioelectrical impedance analysis. *Eur J Clin Nutr* (2013) 67:S1–1. doi: 10.1038/ejcn.2012.148

45. Ward LC. Bioelectrical impedance analysis for body composition assessment: reflections on accuracy, clinical utility, and standardisation. *Eur J Clin Nutr* (2019) 73:194–9. doi: 10.1038/s41430-018-0335-3

46. Zhu C, Lian Z, Chen Y, Wang J. Physical activity and cancer status among middle-aged and older chinese: A population-based, cross-sectional study. *Front Physiol* (2022) 12:812290. doi: 10.3389/fphys.2021.812290

47. Chen L, Ren T, Tan Y, Li H. Global trends of research on depression in breast cancer: A bibliometric study based on VOSviewer. *Front Psychol* (2022) 13:969679. doi: 10.3389/fpsyg.2022.969679

48. Huizinga F, Westerink N-DL, Berendsen AJ, Walenkamp AME, De Greef MHG, Oude Nijeweeme JK, et al. Home-based physical activity to alleviate fatigue in cancer survivors: A systematic review and meta-analysis. *Med Sci Sports Exerc* (2021) 53:2661–74. doi: 10.1249/MSS.0000000000002735

49. Pollán M, Casla-Barrio S, Alfaro J, Esteban C, Segui-Palmer MA, Lucia A, et al. Exercise and cancer: a position statement from the Spanish Society of Medical Oncology. *Clin Trans Oncol* (2020) 22:1710–29. doi: 10.1007/s12094-020-02312-y

50. Lavín-Pérez AM, Collado-Mateo D, Hinojo González C, de Juan Ferré A, Ruisánchez Villar C, Mayo X, et al. High-intensity exercise prescription guided by heart rate variability in breast cancer patients: a study protocol for a randomized controlled trial. *BMC Sports Sci Med Rehabil* (2023) 15:28. doi: 10.1186/s13102-023-00634-2

51. Ryu J, Lee E-Y, Min J, Yeon S, Lee J-W, Chu SH, et al. Effect of a 1-year tailored exercise program according to cancer trajectories in patients with breast cancer: study protocol for a randomized controlled trial. *BMC Cancer* (2023) 23:200. doi: 10.1186/s12885-023-10664-1

52. de Sire A, Lippi L, Marotta N, Folli A, Calafiore D, Moalli S, et al. Impact of physical rehabilitation on bone biomarkers in non-metastatic breast cancer women: A systematic review and meta-analysis. *Int J Mol Sci* (2023) 24:921. doi: 10.3390/ijms24020921

53. Liu Y-C, Hung T-T, Konara Mudiyanselage SP, Wang C-J, Lin M-F. Beneficial exercises for cancer-related fatigue among women with breast cancer: A systematic review and network meta-analysis. *Cancers (Basel)* (2022) 15:151. doi: 10.3390/cancers15010151

54. Liu Y, Liu J-E, Chen S, Zhao F, Chen L, Li R. Effectiveness of nonpharmacologic interventions for chemotherapy-related cognitive impairment in breast cancer patients. *Cancer Nurs* (2022) 1. doi: 10.1097/NCC.0000000000001152

55. Wilke J, Rahlf AL, Füzéki E, Groneberg DA, Hespanhol L, Mai P, et al. Physical activity during lockdowns associated with the COVID-19 pandemic: A systematic review and multilevel meta-analysis of 173 studies with 320,636 participants. *Sports Med Open* (2022) 8:1–9. doi: 10.1186/s40798-022-00515-x

frontiers | Frontiers in Oncology

TYPE Original Research
PUBLISHED 26 September 2023
DOI 10.3389/fonc.2023.1259416

OPEN ACCESS

EDITED BY
Francesca Bianchi,
University of Milan, Italy

REVIEWED BY
Patrizia Massaro,
IRCCS San Donato Polyclinic, Italy
Chenbin Liu,
Chinese Academy of Medical Sciences and Peking Union Medical College, China

*CORRESPONDENCE
Duong Thanh Tai
dttai@ntt.edu.vn
Nguyen Ngoc Anh
anh.nguyenngoc1@phenikaa-uni.edu.vn

RECEIVED 15 July 2023
ACCEPTED 07 September 2023
PUBLISHED 26 September 2023

CITATION
Tai DT, Phat LT, Ngoc Anh N, Sang HVT, Loc TM, Hai NX, Sandwall PA, Bradley D and Chow JCL (2023) Dosimetric and radiobiological comparison between conventional and hypofractionated breast treatment plans using the Halcyon system. *Front. Oncol.* 13:1259416. doi: 10.3389/fonc.2023.1259416

Dosimetric and radiobiological comparison between conventional and hypofractionated breast treatment plans using the Halcyon system

Duong Thanh Tai [1,2*], Luong Tien Phat [3], Nguyen Ngoc Anh [4,5*], Huynh Van Tran Sang [1], Tran Minh Loc [1], Nguyen Xuan Hai [6], Peter A. Sandwall [7], David Bradley [8,9] and James C. L. Chow [10,11]

[1]Department of Medical Physics, Faculty of Medicine, Nguyen Tat Thanh University, Ho Chi Minh, Vietnam, [2]Robarts Research Institute, University of Western Ontario, London, ON, Canada, [3]Department of Radiation Oncology, University Medical Shing Mark Hospital, Bien Hoa, Vietnam, [4]Faculty of Fundamental Science, PHENIKAA University, Hanoi, Vietnam, [5]PHENIKAA Research and Technology Institute (PRATI), A&A Green Phoenix Group JSC, Hanoi, Vietnam, [6]Dalat Nuclear Research Institute, Dalat, Vietnam, [7]Department of Radiation Oncology, OhioHealth, Mansfield Hospital, Mansfield, OH, United States, [8]Centre for Applied Physics and Radiation Technologies, Sunway University, Sunway, Malaysia, [9]School of Mathematics and Physics, University of Surrey, Guildford, United Kingdom, [10]Department of Radiation Oncology, University of Toronto, Toronto, ON, Canada, [11]Radiation Medicine Program, Princess Margaret Cancer Centre, University Health Network, ON, Canada

Purpose: The objective of this research is to compare the efficacy of conventional and hypofractionated radiotherapy treatment plans for breast cancer patients, with a specific focus on the unique features of the Halcyon system.

Methods and materials: The study collected and analyzed dose volume histogram (DVH) data for two groups of treatment plans implemented using the Halcyon system. The first group consisted of 19 patients who received conventional fractionated (CF) treatment with a total dose of 50 Gy in 25 fractions, while the second group comprised 9 patients who received hypofractionated (HF) treatment with a total dose of 42.56 Gy in 16 fractions. The DVH data was used to calculate various parameters, including tumor control probability (TCP), normal tissue complication probability (NTCP), and equivalent uniform dose (EUD), using radiobiological models.

Results: The results indicated that the CF plan resulted in higher TCP but lower NTCP for the lungs compared to the HF plan. The EUD for the HF plan was approximately 49 Gy (114% of its total dose) while that for the CF plan was around 53 Gy (107% of its total dose).

Conclusions: The analysis suggests that while the CF plan is better at controlling tumors, it is not as effective as the HF plan in minimizing side effects. Additionally, it is suggested that there may be an optimal configuration for the HF plan that can provide the same or higher EUD than the CF plan.

KEYWORDS

radiotherapy treatment plan, conventional fractionated (CF), hypofractionated (HF), breast cancer, radiobiology model, Halcyon, normal tissue complication probability (NTCP), tumor control probability (TCP)

1 Introduction

Breast cancer is a prevalent form of cancer and one of the leading causes of death among women worldwide. The World Health Organization (WHO) reports that breast cancer is the most commonly diagnosed cancer among women globally, with an estimated 2.3 million new cases in 2020. In the United States, breast cancer accounts for approximately 30% of all new female cancer diagnoses annually, and it is projected that 43,700 women will die from breast cancer in 20232. Despite advancements in diagnosis and treatment, breast cancer remains a significant public health concern. Breast cancer can be effectively treated with radiotherapy, which involves using high-energy radiation to destroy cancer cells and prevent their growth and spread. However, as radiation transmission in matter cannot be precisely controlled, it can affect healthy cells, particularly those near cancer cells. Therefore, an optimal treatment plan should aim to maximize the impact of radiation on the cancerous tissue while minimizing its effects on healthy tissues.

The radiotherapy technique is a critical factor in achieving an effective breast cancer treatment plan. Modern devices, such as the Halcyon system (1), that utilize intensity modulated radiation therapy (IMRT) and volumetric modulated arc therapy (VMAT), provide a simpler way to achieve this compared to less modern devices with fixed radiation beams. The Halcyon offers several advantages over a conventional LINAC in the context of treatment planning. With its single 6 MV flattening filter-free (FFF) X-ray, the Halcyon system delivers a higher dose rate, leading to faster treatment sessions and improved patient comfort. The double-layer multi-leaf collimator (MLC) enables precise beam shaping, enhancing target conformity and sparing surrounding healthy tissues. Additionally, the Halcyon's faster gantry rotation speed and maximum leaf speed contribute to reduced treatment times, increasing treatment efficiency and minimizing motion-related uncertainties. These combined features make the Halcyon LINAC a particularly choice for treatment planning, ensuring better dose delivery and overall treatment outcomes compared to conventional LINACs. However, given a specific radiotherapy technique, there are various treatment plans that can be constructed, with the total dose and number of treatment fractions being significant parameters. A conventional fractionated (CF) treatment plan for breast cancer typically involves a total dose of 50 Gy administered over 25 treatment fractions. The extended duration of the CF plan limits the capacity to treat a larger number of patients, particularly in developing countries such as Vietnam. Moreover, the cost and travel distance to the radio-therapy center for several weeks can cause financial difficulties for patients. There has been a trend towards using a hypo-fractionated (HF) plan, which has a shorter treatment duration than the CF plan. Although the total dose and number of treatment fractions are lower in an HF plan, the dosage per fraction is higher than that of the CF plan. This trend is evident in the review of Yasemin Bolukbasi and Ugur Selek (2), and studies have confirmed that the HF plan is safe and effective (3–6), yet some inconsistent results exist. For instance, Arezoo Kazemzadeh et al (7) used radiobiological models and found that the tumor control probability and equivalent uniform dose of the CF plan were better than those of the HF plan, contradicting the conclusion of Gloi (8). The review of Youssef and Stanford (9) added that *"breast fibrosis can be a potential side effect of hypofractionated radiotherapy"*. Additionally, there is no standard value for the HF treatment plan, necessitating further research to understand the differences in effectiveness between CF and HF treatment plans. The findings from these studies, as well as the dosimetric data collected, can help to explore more intensified hypofractionated treatment plans, with initial results indicating comparable effectiveness between the plan of 28.5 Gy in 5 fractions and the standard plan of 50 Gy in 25 fractions (10). While the Halcyon system is a state-of-the-art linear accelerator that provides high-quality IMRT and VMAT treatments, there are a limited number of studies on this specific machine. Therefore, the purpose of this study is to evaluate the efficacy of two breast cancer treatment plans based on the Halcyon system using two radiobiological models: the CF plan, which delivers a total dose of 50 Gy over 25 treatment fractions, and the HF plan, which delivers a total dose of 42.56 Gy over 16 treatment fractions.

It is worthy to note that at our hospital, we currently adhere to the National Comprehensive Cancer Network (NCCN) Guideline for treating breast cancer patients (11). In radiation therapy practice, we routinely accept both CF and HF plans according to the NRG Radiation Therapy Oncology Group (RTOG) Template for whole breast photon therapy (12–14). The final decision of which plan should be used in a given case is almost random. This is acceptable because both plans adapt the mandatory requirements of safety, nevertheless we aim to find out which plan.

2 Materials and methods

2.1 Data collection and manipulation

We collected IMRT treatment plan data for 28 breast cancer patients. Of these patients, 19 chose the CF plan, which consists of a total dose of 50-Gy in 25 fractions, and 9 chose the HF plan, whose total dose and number of treatment fractions are 42.56 Gy and 16, respectively. These IMRT plans were created to be used with the Halcyon system (Varian Medical Systems, Pal Alto, CA). The planning process has been carried out by Medical Physicists using the Eclipse 15.6 (15). All treatment plans considered in this work met the required dose constraints and were approved by physicians at the Hospital.

For each patient, we conducted a computed tomography (CT) scan that encompassed the area from the chin to below the breast crease, extending approximately 6 cm below, with the distance between two successive CT images being 1 mm. The resulting CT images were then input into the Eclipse 15.6 software for contouring and planning. For radiotherapy planning, all contouring of the planning treatment volume (PTV) and organs at risk (OARs), including the cancerous breast, contralateral breast, heart, ipsilateral and contralateral lungs, and spinal cord, was performed manually by a Radiation Oncologist. Contouring data is stored in radiotherapy structure (RT-structure) files, and dose data is stored in radiotherapy dose (RT-dose) files. From these two files, we used the dicompylercore python library (16) to extract the dose volume histogram data for various organs.

2.2 Dose volume histogram parameters and radiobiological models

2.2.1 Dosimetric parameters

In the field of radiotherapy modeling, the target volume, such as a tumor, is divided into a large number of voxels. Each voxel may receive a different amount of dose. While it is important to know the dose value of all the voxels to evaluate the treatment plan, storing this information would require a large amount of storage space. Therefore, a more efficient approach is to store the dose volume histogram (DVH), which provides information on the number of voxels that receive a given dose. From DVH data, it is possible to determine the maximum, minimum, and average dose that a voxel in the target volume receives. These parameters are denoted as D_{max}, D_{min}, and D_{mean}.

DVH analysis provides two additional important parameters: $D_{x\%}$ and V_{RI}. $D_{x\%}$ is the minimum dose value received by x% of the total voxels within the target volume, whereas V_{RI} is the relative number of voxels of the target volume that receives the dose of at least RI i.e., the reference isodose. It is noted that for different organs, the values of interest for x% and RI vary. Based on the DVH data and parameters mentioned above, one can deduce specific quantities that can be used to evaluate the effectiveness of a treatment plan. One of them is the homogeneity index (HI), which can be computed as (17)

$$\mathrm{HI} = \frac{D_{2\,\%} - D_{98\,\%}}{\text{total dose}} \tag{1}$$

with the total dose being 50 and 42.56 Gy for the CF and HF plans, respectively. Here, $D_{2\%}$ and $D_{98\%}$ are computed for the cancerous breast, i.e., the PTV. A HI value close to zero means that the dose is homogeneously distributed in the PTV. Another one is the conformity index (CI), which is calculated as

$$\mathrm{CI} = \frac{(V_{RI} \text{ for PTV})^2}{100 \times \sum_{\text{all organs}} (V_{RI} \text{ for the i}^{\text{th}} \text{ organ})} \tag{2}$$

where reference isodose RI = 40.43 and 47.5 Gy for HF and CF plans, respectively. Due to the difference in the definition of some quantities, Eq. 2 in the present work is not the same as the CI formula in the original work (18, 19), yet they are equivalent. In short, the ideal value of CI is 1, i.e., no region outside the PTV receives dose that is equal or more than the reference isodose.

2.2.2 Radiobiological models

In practice, it is difficult to deduce conclusions by comparing the dosimetric parameters of the CF and HF plans because the total doses of these plans are not the same. For instance, the D_{min}, D_{max}, and D_{mean} of the CF plan are always of greater value than those of the HF plans. Thus, one should use radiobiological models widely applied in the studies of radiotherapy treatment planning (20–22). In this work, we consider three important quantities, equivalent uniform dose (EUD), tumor control probability (TCP), and normal tissue complication probability (NTCP).

First, we determine the EUD based on Niemierko's phenomenological model (23) as

$$EUD = \left(\sum_{total \quad volume} \vartheta_i EQD_i^a\right)^{1/a} \tag{3}$$

where ϑ_i is the number of voxels that receive a dose of EQD_i and a is a model parameter that is specific to the organ considered. The EQD denotes the biologically equivalent physical dose of 2 Gy and is computed as

$$EQD = D \times \frac{\frac{\alpha}{\beta} + \frac{D}{n_f}}{\frac{\beta}{\alpha}} \tag{4}$$

with $\frac{\alpha}{\beta}$, D, and n_f being the tissue-specific linear-quadratic parameter of the organ being exposed, the total dose, and the number of fractions of the treatment plan, respectively.

For the TCP, we apply the Poisson linear quadratic (PoissonLQ) radiobiological model (24), namely

$$\mathrm{TCP(D)} = \prod_i^M \left[\exp\left(-\exp\left[e\gamma - \frac{EQD_i}{D_{50}}(e\gamma - \ln(\ln(2)))\right]\right)\right]^{\frac{v_i}{v_{\text{ref}}}} \tag{5}$$

here, e is the Euler's number, $\frac{v_i}{v_{\text{ref}}}$ is the relative volume of voxel i compared to the references volume, i.e., the total volume of the organ considered, and M is the total number of voxels. Whereas γ and D_{50} are the maximum normalized gradient of the dose response curve and dose giving a 50% response probability of the organ of interest, respectively.

For the NTCP, Lyman-Kutcher-Burman (LKB) model (24) is used. This model defines the NTCP as

$$\mathrm{NTCP(D)} = \frac{1}{\sqrt{2\pi}} \int_{\infty}^{t} e^{\frac{-x^2}{2}} dx \tag{6}$$

with

$$\mathrm{t} = \frac{\mathrm{D_{eff}} - \mathrm{D_{50}}}{\mathrm{m} \,.\, \mathrm{D_{50}}} \tag{7}$$

and

$$\mathrm{D_{eff}} = \sum_{i=1}^{M} \left(\frac{v_i}{v_{\mathrm{ref}}} \mathrm{EQD}_i^{1/\mathrm{n}} \right)^n \tag{8}$$

Within Eqs. 6, 7, and 8, m and n are the slope of the response curve and parameter reflecting the biological properties of the organ specifying volume dependence. TCP and NTCP are probability, thus their possible outcome of TCP and NTCP ranges from 0 to 1. The objective of a treatment plan is to simultaneously maximize TCP and EUD and minimize NTCP.

The radiobiology models described above are employed in the pyRadioBiology python package contributors (25), thus it is used to perform the calculation of TCP, NTCP, and EUD in the present work. The values of the parameters and their corresponding references are summarized in Table 1.

2.3 Plan evaluation

All the dosimetric parameters, including the CI and HI, and radiobiology model quantities presented in section 2.2 are determined for each patient. It is noted that the EUD and TCP are calculated for the PTV, namely the cancerous breast, whereas the NTCP is calculated for the heart and lung (ipsilateral and contralateral parts). The latter are important normal tissues that are in the vicinity of the PTV and thus need to be monitored.

To compare the effectiveness of the CF and HF plans, we compared CI, HI, EUD, TCP, and NTCP corresponding to these two groups of patients using the independent sample t-test. The significant level was considered at a p-value of 0.05, corresponding to the reliability of 95%.

In short, the ideal treatment plan should have:

- CI equal to 1,
- HI equal to 0,
- TCP equal to 1,
- NTCP equal to 0,
- and EUD is as high as possible.

3 Results and discussion

As described in section 2.1, CF and HF plans are applied to two separate groups of patients. To compare the effectiveness of the CF and HF plans, it is important to ensure that the two groups of patients have similar characteristics. However, in this study which only considered DVH data, it is only necessary to ensure that the organs being treated are anatomically comparable between the two groups. Other demographic factors, such as age and gender, do not affect the analysis. Figure 1 shows a boxplot to visually compare the size of organs of the two groups of patients. It is seen that the sizes of the organs of these two groups are comparable. This observation is confirmed with the t-test comparison given in Table 2. It is displayed that all the t-values are nearly zero except for the heart. The high t-value corresponding to the heart might be due to the bias of an outlier data point as can be seen in Figure 1. In fact, it may be preferable in a planning study to simulate both treatments in each patient, as this enables a paired comparison and even a voxel-by-voxel comparison of physical dose, and thus eliminates the need to determine whether the groups are comparable. However, a study based on actually delivered plans, such as the one presented here, has its own advantage in that it provides insight into the practical clinical experience, including the occurrence of any adverse effects. For this reason, a similar strategy was also carried out by many other works, see e.g., Refs (5, 7, 8, 21).

Table 3 presents a comparison of the CI, HI, EUD, TCP, and NTCP values of CF and HF plans using an independent sample t-test. The results show that both treatment plans have a high CI value (>0.95), indicating that they effectively concentrate radiation dose within the PTV, i.e., the cancerous breast, while

TABLE 1 Values of the parameters used within radiobiology model calculations.

Parameter	Organ	Value	Value References
$\frac{\alpha}{\beta}$ (unitless)	Breast (PTV), heart, and lung	4	Owen et al., 2006 (3)
a (unitless)	Breast (PTV)	-7.2	Okunieff et al., 1995; Horton et al., 2006 (26, 27)
γ (unitless)	Breast (PTV)	1.3	Okunieff et al., 1995; Horton et al., 2006 (26, 27)
D_{50} (Gy)	Breast (PTV)	30.89	Okunieff et al., 1995; Horton et al., 2006 (26, 27)
D_{50} (Gy)	Heart	48	Luxton et al., 2007; Oinam et al., 2011 (28, 29)
D_{50} (Gy)	Lung	37.6	Oinam et al., 2011; Semenenko VA, 2008 (29, 30)
M (unitless)	Heart	0.1	Luxton et al., 2007; Oinam et al., 2011 (28, 29)
n (unitless)	Heart	0.35	Luxton et al., 2007; Oinam et al., 2011 (28, 29)
M (unitless)	Lung	0.35	Oinam et al., 2011; Semenenko et al., 2008 (29, 30)
n (unitless)	Lung	0.87	Oinam et al., 2011; Semenenko et al., 2008 (29, 30)

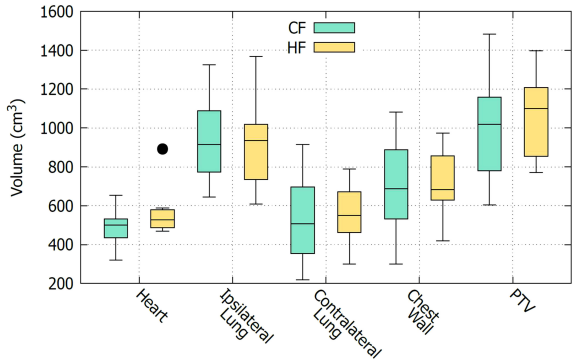

FIGURE 1
Comparison of the sizes of organs between two groups of patients.

minimizing exposure to healthy tissues. This is an important aspect of radiation therapy, as it reduces the likelihood of side effects and complications. The results suggest that both treatment plans are well-suited for treating breast cancer patients using the Halcyon system. A comparison with prior research demonstrates that the CI value is independent of the treatment plan, Refs (9, 10) also revealing nearly identical CI values for the CF and HF treatment plans. Indeed, a high value of CI can be attained through enhanced therapy methods. For example, the CF plan combined with the IMRT and VMAT treatment techniques in our work yields a CI value of 0.96, whereas the same treatment plan with the 3D-CRT technique in the work of Kazemzadeh A et al. (9) yields only 0.89.

When the HI values are compared, the CF plan does a little better than the HF plan. This means that the CF plan was able to spread the radiation dose more evenly across the PTV than the HF plan. A uniform distribution of radiation dose is essential, as an uneven dose distribution may cause certain parts of the cancerous organ to receive excessive radiation, while others receive insufficient radiation to effectively destroy the cancerous cells. This can result in incomplete treatment, allowing cancerous cells to survive and recover after the therapy. Therefore, a homogeneous distribution of radiation dose within the PTV is desirable in order to achieve optimal therapeutic outcomes. In general, the HI values of both the CF and HF plans in the present work are fairly good, as they are less than 0.10, indicating that the maximum discrepancy of the dose received at two random locations inside the PTV is less than 10%.

The TCP value of the CF plan, which is 96.0 ± 0.1%, is better than that of the HF, which is 94.0 ± 0.3%, as expressed by the large t-value of 23.67 together with a p-value of almost zero. This result for the TCP value is consistent with that reported in Ref (9). Yet inconsistent with that given in Ref (10), in which the TCP value of the CF plan is lower than the HF plan. We should note that the authors of Ref (10) reported their TCP values with extremely large uncertainty, in contrast to the small uncertainty reported in this study and Ref (9).

The NTCP values for the heart of both CF and HF plans are all extremely close to zero. For the lung, the NTCP values of the HF plan are better than those of the CF. In addition, the NTCP of the ipsilateral lung is 12 times larger than that of the contralateral lung for both treatment plans. It is evident because the ipsilateral lung is located on the same side as the PTV, so it receives a higher dose than the contralateral lung. In general, the CF plan is more effective at controlling tumor growth, as suggested by its better TCP values, yet the HF plan causes fewer side effects and complications for the patients, demonstrated by its better NTCP values, particularly the lung. We should note that this claim is only valid for treatments utilizing IMRT techniques on a Halcyon system, also noting that in the study of Kazemzadeh A et al. (9), in which the treatment were made on an ARTISTE radiation therapy system (SIEMENS) using 3D-CRT technique, the NTCP for the lung of the HF plan was reported to be worse than that of the CF.

For the EUD values, that of the CF plan is higher than that of the HF. This is expected because the total dose of the CF plan is greater than that of the HF case. However, there is an interesting observation that the relative ratio between the EUD and the total dose in the CF plan is lower than in the HF plan. In the CF plan, a total dose of 50 Gy results in a EUD of 52.39 Gy (107%), whereas a 42.56 Gy total dose in the HF plan causes a EUD of 49.14 (114%). A similar effect is seen when comparing V_{RI} of the CF and HF plans for the PTV and chest wall, as shown in Table 4. With the same relative reference isodose of 105% with respect to the total dose (i.e., 53.5 Gy versus 50 Gy and 45.53 Gy versus 42.56 Gy), the V_{RI} value of the CF plan is greater than that of the HF plan, whereas the V_{RI} values with the relative reference isodoses of 95% and 100% show the contrary. This observation suggests that the HF plan delivers

TABLE 2 Comparison of the size of organs of the CF and HF groups of patients using independent sample t-test.

Organ	CF (cm^3)	HF (cm^3)	t–value	p–value
Heart	490 ± 79	569 ± 129	−2.01	0.054
Ipsilateral Lung	928 ± 192	931 ± 234	−0.04	0.967
Contralateral Lung	1000 ± 268	1080 ± 220	−0.77	0.449
Chest Wall	515 ± 187	541 ± 164	−0.36	0.725
PTV	673 ± 206	706 ± 184	−0.40	0.691

Values corresponding to the CF and HF plans are presented as mean ± standard deviation.

TABLE 3 Comparison of the CI, HI, EUD, TCP, NTCP of CF and HF plans using independent sample t-test.

	CF	HF	*t*–value	*p*–value
CI	0.96 ± 0.01	0.95 ± 0.02	0.33	0.743
HI	0.08 ± 0.01	0.10 ± 0.02	−4.40	#
EUD (PTV)	52.39 ± 0.23	49.14 ± 1.27	11.00	#
TCP (PTV)	95.5 ± 0.1%	93.6 ± 0.3%	23.67	#
NTCP (Heart)	#	#	−0.76	0.453
NTCP (Ipsilateral Lung)	4.9 ± 0.6%	3.7 ± 0.3%	6.14	#
NTCP (Contralateral Lung)	0.38 ± # %	0.34 ± 0.04%	2.52	0.018

The symbol # indicates that the value is nearly equal to zero.
Values corresponding to the CF and HF plans are presented as mean ± standard deviation.

doses to the PTV more effectively than the CF plan. It also implies that the current configuration of the HF plan may not be optimal, and there may exist a treatment plan with a higher EUD, even greater than the EUD obtained from the CF plan. In addition, behaviour of the EUD observed in our work was not shown in Ref (9). Since both works considered the same CF and HF treatment plans but used different treatment techniques, namely IMRT and VMAT in this work versus 3D-CRT in Ref (7), it is possible that the choice of treatment plan varies with the treatment technique.

Overall, the results of the present work suggest that, for the Halcyon system with IMRT technique, the CF plan is better at controlling tumor growth than the HF plan, but the HF plan is better at keeping side effects and complications to a minimum. The HF plan has the additional advantage of a shorter treatment duration. In addition, the analysis of the EUD shows that there might exist a configuration of the HF plan that can provide the same or even a greater EUD value than that of the CF plan. In future studies, we intend to perform a search to find the optimal configuration of the HF plan. Moreover, although all the comparisons in this work are based on a *t*-test with a replication probability of more than 95%, recalling that we accept the hypothesis only if the *p*-value is less than 0.05. Further, it is to be acknowledged that the number of samples, 28 patients, is quite small. Therefore, the obtained results must be considered with caution until further studies with a larger sample size are conducted.

4 Conclusions

In conclusion, this study compared the effectiveness of conventional and hypofractionated radiotherapy treatment plans for breast cancer patients using radiobiological models and analyzed dosimetric parameters. The results suggest that while the CF plan is more effective in tumor control, the HF plan is better at minimizing side effects and complications and has the advantage of a shorter treatment duration. Additionally, the analysis of the EUD suggests that there might be an optimal configuration of the HF plan that can provide the same or even a higher EUD value than that of the CF plan.

Data availability statement

The raw data supporting the conclusions of this article will be made available by the authors, without undue reservation.

Author contributions

DT: Conceptualization, Data curation, Methodology, Project administration, Software, Supervision, Validation, Writing – original draft, Writing – review & editing. LT: Conceptualization, Data curation, Methodology, Software, Writing – original draft.

TABLE 4 Comparison between $V_{53.5}$ and $V_{45.53}$, V_{50} and $V_{42.56}$, and $V_{47.5}$ and $V_{40.43}$ of the CF and HF plans, for the PTV and chest wall.

Organ	Parameters	CF	HF	*t*–value	*p*–value
PTV	$V_{95\%}$	98.51 ± 1.33	93.69 ± 3.80	3.80	#
	$V_{100\%}$	99.96 ± 0.08	99.56 ± 0.08	3.10	0.005
	$V_{107\%}$	7.14 ± 4.62	11.00 ± 4.28	-2.11	0.045
Chest Wall	$V_{95\%}$	99.96 ± 0.07	99.50 ± 0.70	2.91	0.007
	$V_{100\%}$	98.48 ± 1.44	93.41 ± 4.30	4.70	#
	$V_{107\%}$	8.16 ± 4.99	12.25 ± 3.99	2.15	0.041

The values of 47.5, 50, and 53.5 correspond to 95%, 100%, and 107% of the total dose of the CF plan, whereas those of 40.43, 42.56, and 45.53 correspond to 95%, 100%, and 107% of the total dose of the HF plan.
Values corresponding to the CF and HF plans are presented as mean ± standard deviation.
The symbol # indicates that the value is almost equal to zero.

NN: Conceptualization, Methodology, Software, Writing – original draft. HS: Data curation, Writing – original draft. TL: Data curation, Writing – original draft. XN: Conceptualization, Investigation, Writing – original draft, Writing – review & editing. PS: Conceptualization, Writing – original draft, Writing – review & editing. DB: Investigation, Supervision, Writing – review & editing. JC: Conceptualization, Investigation, Project administration, Writing – original draft, Writing – review & editing.

Funding

The authors declare that no financial support was received for the research, authorship, and/or publication of this article.

Acknowledgments

We would like to acknowledge Ms. Sunny Chen, Deputy General Director of University Medical Shing Mark Hospital, and Dr. Tran Trung Kien, Head of the Department of Radiation Oncology at Shingmark Hospital, for their invaluable support and encouragement. The first author would like to express gratitude to Dr. Peter A. Sandwall for his exceptional guidance under the AAPM Mentorship program.

Conflict of interest

The authors declare that the research was conducted in the absence of any commercial or financial relationships that could be construed as a potential conflict of interest.

Publisher's note

References

1. Varian. *Halcyon treatment delivery system* (2023). Available at: https://www.varian.com/products/radiotherapy/treatment-delivery/halcyon (Accessed April 9, 2023).

2. Bolukbasi Y, Selek U. Modern radiotherapy era in breast cancer, in: *Breast cancer - from biology to medicine*. Available at: https://www.intechopen.com/chapters/53531 (Accessed April 9, 2023).

3. Owen JR, Ashton A, Bliss JM, Homewood J, Harper C, Hanson J, et al. Effect of radiotherapy fraction size on tumour control in patients with early-stage breast cancer after local tumour excision: long-term results of a randomised trial. *Lancet Oncol* (2006) 7(6):467–71. doi: 10.1016/S1470-2045(06)70699-4

4. Whelan TJ, Pignol JP, Levine MN, Julian JA, MacKenzie R, Parpia S, et al. Long-term results of hypofractionated radiation therapy for breast cancer. *N Engl J Med* (2010) 362(6):513–20. doi: 10.1056/NEJMoa0906260

5. Abram WP, Clarke J, McAleer JJ, Graham JD, Riddle P, Goodman S, et al. The UK Standardisation of Breast Radiotherapy (START) Trial A of radiotherapy hypofractionation for treatment of early breast cancer: a randomised trial. *Lancet Oncol* (2008) 9(4):331–41. doi: 10.1016/S1470-2045(08)70077-9

6. Haviland JS, Owen JR, Dewar JA, Agrawal RK, Barrett J, Barrett-Lee PJ, et al. The UK Standardisation of Breast Radiotherapy (START) trials of radiotherapy hypofractionation for treatment of early breast cancer: 10-year follow-up results of two randomised controlled trials. *Lancet Oncol* (2013) 14(11):1086–94. doi: 10.1016/S1470-2045(13)70386-3

7. Kazemzadeh A, Abedi I, Amouheidari A, Shirvany A. A radiobiological comparison of hypo-fractionation versus conventional fractionation for breast cancer 3D-conformal radiation therapy. *Rep Pract Oncol Radiother*. (2021) 26(1):86–92. doi: 10.5603/RPOR.a2021.0015

8. Gloi AM. A broad evaluation of left breast radiotherapy. *Am J Biomed Sci* (2019) 152:152–71. doi: 10.5099/aj190300153

9. Youssef A, Stanford J. Hypofractionation radiotherapy vs. Conventional fractionation for breast cancer: A comparative review of toxicity. *Cureus*. (2018) 10 (10):e3516. doi: 10.7759/cureus.3516

10. FAST Trialists group, Agrawal RK, Alhasso A, et al. First results of the randomised UK FAST Trial of radiotherapy hypofractionation for treatment of early breast cancer (CRUKE/04/015). *Radiother Oncol* (2011) 100(1):93–100. doi: 10.1016/j.radonc.2011.06.026

11. Goetz MP, Gradishar WJ, Anderson BO, Abraham J, Aft R, Allison KH, et al. NCCN guidelines insights: Breast cancer, version 3.2018: Featured updates to the NCCN guidelines. *J Natl Compr Cancer Network*. (2019) 17(2):118–26. doi: 10.6004/jnccn.2019.0009

12. Kainz K, Huang Mi, Xiao Y, Li XA, Moran. JM. *NRG protocol radiation therapy template*. Available at: https://www.nrgoncology.org/ciro-breast (Accessed August 25, 2023).

13. Freedman GM, White JR, Arthur DW, Allen Li X, Vicini FA. Accelerated fractionation with a concurrent boost for early stage breast cancer. *Radiotherapy Oncol* (2013) 106(1):15–20. doi: 10.1016/j.radonc.2012.12.001

14. Vicini FA, Winter K, Freedman GM, Arthur DW, Hayman JA, Rosenstein BS, et al. NRG RTOG 1005: A phase III trial of hypo fractionated whole breast irradiation with concurrent boost vs. Conventional whole breast irradiation plus sequential boost following lumpectomy for high risk early-stage breast cancer. *Int J Radiat Oncology Biology Physics*. (2022) 114(3):S1. doi: 10.1016/j.ijrobp.2022.07.2320

15. Eclipse. Eclipse treatment planning system, in: (2023). Available at: https://www.varian.com/products/radiotherapy/treatment-planning/eclipse (Accessed April 9, 2023).

16. Panchal A, Couture G, Galler N, Hall DC, Wakita A, et al. *dicompyler/dicompyler-core v0.5.5. Zenodo*. doi: 10.5281/zenodo.3236628

17. Wu Q, Mohan R, Morris M, Lauve A, Schmidt-Ullrich R. Simultaneous integrated boost intensity-modulated radiotherapy for locally advanced head-and-neck squamous cell carcinomas. I: dosimetric results. *Int J Radiat Oncol Biol Phys* (2003) 56(2):573–85. doi: 10.1016/s0360-3016(02)04617-5

18. Shaw E, Kline R, Gillin M, Souhami L, Hirschfeld A, Dinapoli R, et al. Radiation Therapy Oncology Group: radiosurgery quality assurance guidelines. *Int J Radiat Oncol Biol Phys* (1993) 27(5):1231–9. doi: 10.1016/0360-3016(93)90548-a

19. Wambersie A. *ICRU report 62, prescribing, recording and reporting photon beam therapy (Supplement to ICRU 50) – ICRU*. Available at: https://www.icru.org/report/prescribing-recording-and-reporting-photon-beam-therapy-report-62/ (Accessed April 9, 2023).

20. Chow JCL, Jiang R. Dose-volume and radiobiological dependence on the calculation grid size in prostate VMAT planning. *Med Dosim*. (2018) 43(4):383–9. doi: 10.1016/j.meddos.2017.12.002

21. Chow JCL, Jiang R, Xu L. Dosimetric and radiobiological comparison of prostate VMAT plans optimized using the photon and progressive resolution algorithm. *Med Dosim*. (2020) 45(1):14–8. doi: 10.1016/j.meddos.2019.04.004

22. Tai DT, Oanh LT, Phuong PH, Sulieman A, Abolaban FA, Omer H, et al. Dosimetric and radiobiological comparison in head-and-neck radiotherapy using JO-IMRT and 3D-CRT. *Saudi J Biol Sci* (2022) 29(8):103336. doi: 10.1016/j.sjbs.2022.103336

23. Niemierko A. Reporting and analyzing dose distributions: a concept of equivalent uniform dose. *Med Phys* (1997) 24(1):103–10. doi: 10.1118/1.598063

24. Laboratories R. *RayStation 6 reference manual, raySearch laboratories*. (2017).

25. Sachpazidis I. *pyradiobiology: pyradiobiology is a package for radiobiological modeling (TCP, NTCP, EUD, gEUD) with Python*. Available at: https://www.sachpazidis.com/pyRadioBiology/ (Accessed April 9, 2023).

26. Okunieff P, Morgan D, Niemierko A, Suit HD. Radiation dose-response of human tumors. *Int J Radiat Oncol Biol Phys* (1995) 32(4):1227–37. doi: 10.1016/0360-3016(94)00475-z

27. Horton JK, Halle JS, Chang SX, Sartor CI. Comparison of three concomitant boost techniques for early-stage breast cancer. *Int J Radiat OncologyBiologyPhysics.* (2006) 64(1):168–75. doi: 10.1016/j.ijrobp.2005.07.004

28. Luxton G, Keall PJ, King CR. A new formula for normal tissue complication probability (NTCP) as a function of equivalent uniform dose (EUD). *Phys Med Biol* (2008) 53(1):23–36. doi: 10.1088/0031-9155/53/1/002

29. Oinam AS, Singh L, Shukla A, Ghoshal S, Kapoor R, Sharma SC. Dose volume histogram analysis and comparison of different radiobiological models using in-house developed software. *J Med Phys* (2011) 36(4):220–9. doi: 10.4103/0971-6203.89971

30. Semenenko VA, Li XA. Lyman-Kutcher-Burman NTCP model parameters for radiation pneumonitis and xerostomia based on combined analysis of published clinical data. *Phys Med Biol* (2008) 53(3):737–55. doi: 10.1088/0031-9155/53/3/014

frontiers | Frontiers in Oncology

TYPE Original Research
PUBLISHED 12 October 2023
DOI 10.3389/fonc.2023.1217805

OPEN ACCESS

EDITED BY
Areerat Suputtitada,
Chulalongkorn University, Thailand

REVIEWED BY
Amina Aquil,
Hassan Premier University, Morocco
Shuzhao Chen,
First Affiliated Hospital of Shantou University Medical College, China

*CORRESPONDENCE
Anca Chelariu-Raicu
Anca.Chelariu-Raicu@med.uni-muenchen.de

RECEIVED 05 May 2023
ACCEPTED 28 September 2023
PUBLISHED 12 October 2023

CITATION
Forster M, Wuerstlein R, Koenig A, Stefan A, Wiegershausen E, Batz F, Trillsch F, Mahner S, Harbeck N and Chelariu-Raicu A (2023) Health-related quality of life and patient-centred outcomes with COVID-19 vaccination in patients with breast cancer and gynaecological malignancies. *Front. Oncol.* 13:1217805. doi: 10.3389/fonc.2023.1217805

Health-related quality of life and patient-centred outcomes with COVID-19 vaccination in patients with breast cancer and gynaecological malignancies

Marie Forster, Rachel Wuerstlein, Alexander Koenig, Alexandra Stefan, Elisa Wiegershausen, Falk Batz, Fabian Trillsch, Sven Mahner, Nadia Harbeck and Anca Chelariu-Raicu*

Department of Obstetrics and Gynecology, Breast Center, Gynecologic Oncology Center and CCC Munich, University Hospital, LMU Munich, Munich, Germany

Introduction: Safety and tolerability of COVID-19 vaccines were demonstrated by several clinical trials which led to the first FDA/EMA approvals in 2021. Because of mass immunizations, most social restrictions were waived with effects on quality of life. Therefore, our a-priori hypothesis was that COVID-19 vaccination impacted the health-related quality of life (HR-QoL) in patients with breast and gynecological cancer.

Methods: From March 15th until August 11th, 2022, fully vaccinated patients with breast and gynecological cancer treated in the oncological outpatient clinics of the Department of Obstetrics and Gynecology, LMU University Hospital, Munich, Germany filled out a vaccine related QoL survey. Patients were asked about demographics (age, comorbidities), clinical parameters related to previous COVID-19 infections, and HR-QoL related parameters (living situation, responsibilities in everyday life). Subsequently, a questionnaire with 12 items was designed using a 5-point Likert scale (0 – strongly disagree/4 – strongly agree), covering the aspects health and therapy, social environment, participation in everyday life and overall assessment.

Results: By August 11th, 2022, 108 out of 114 (94.7%) patients had received at least three doses of COVID-19 vaccine and six patients at least two doses. More than half of the surveyed patients were >55y (52.6%; mean: 55.1y, range 29-86y). Patients with breast cancer (n= 83) had early (59.0%) or metastatic cancer (41.0%); gynecological cancers (n=31) also included metastatic (54.8%) and non-metastatic cancer (45.2%). 83.3% of the patients stated that COVID-19 vaccination had a positive impact on their HR-QoL. Furthermore, 29 patients (25.4%) had undergone a COVID-19 infection. These patients reported self-limiting symptoms for a median duration of 5.9 days and no hospital admissions were registered.

Conclusions: Our study demonstrates that vaccination against COVID-19 was positively associated with HR-QoL in patients with breast and gynecological cancer. Furthermore, vaccinated patients who underwent COVID-19 disease experienced only self-limiting symptoms.

KEYWORDS

SARS-CoV-2 pandemic, COVID-19 vaccination, breast cancer, gynecological cancer, health-related quality of life

Introduction

The COVID-19 pandemic showed a meaningful impact on oncology care: Delays and interruptions of both diagnosis and therapy were reported (1, 2). In addition, after starting systemic treatment for cancer, many patients experience side-effects that lead to immunosuppression (3), which may favor a severe course of COVID-19 infection. Lastly, multiple psychological impacts on the quality of life have been demonstrated (4).

Safety and tolerability of Conmirnaty (BioNTech/Pfizer), Vaxzevria (Astra Zeneca), and COVID-19 vaccine Moderna was demonstrated by several clinical trials which resulted in the first FDA/EMEA approvals in 2021 (5). However, data on safety of vaccines and courses of COVID-19 infections in cancer patients remain limited (6).

Still, in order to demonstrate that the vaccination is worthwhile, its benefit should not only be limited to its safety and tolerability but also be associated with patients' satisfaction. Especially during a pandemic, factors such as social environment or regular participation in everyday life have a crucial influence on quality of life (QoL) (7). These aspects have been noticeably influenced by the COVID-19 pandemic since its beginnings in 2020 (8).

In particular, oncology patients restricted themselves to a greater extent than the rest of the population. Consequently, QoL in this group might have been affected even more than the general population, before and after vaccination. Importantly, studies on safety and tolerability of the COVID-19 vaccination did not include QoL data. However, this aspect is clinically especially meaningful when counselling oncologic patients regarding the clinical benefit of COVID-19 vaccination. Several side effects of systemic therapy such as neutropenia (increased possibility of infections), anemia, thrombocytopenia (increased possibility of bleeding), thromboembolic events, cardiac toxicity, fatigue, and chemotherapy-induced nausea/vomiting (CINV) could negatively influence health-related quality of life (HR-QoL) and these conditions could be additionally aggravated by COVID-19 (9–12).

The aim of this study is to evaluate the impact of COVID-19 vaccination on HR-QoL in patients with breast or gynecological cancer. We also aim to assess the clinical manifestation of COVID-19 disease in these vaccinated patients. The objectives of our study are to assess different quality of life aspects and investigate their impact on oncologic patients receiving COVID vaccine.

Methods

Study population and data collection

The study received ethics approval from the Ludwig-Maximilians-University (LMU) Munich Ethics Committee in February 2022 (number of ethical approval: 21-1237). Signed informed consent was obtained from all participants. From March 15th until August 11th, 2022, vaccinated patients with breast or gynecological cancer receiving oncological treatment in the oncological outpatient clinics of the LMU Department of Obstetrics and Gynecology were asked to fill out the quality of life (QoL) survey (consecutive sampling). The survey (Supplementary Figure 1) contained questions regarding demographics (age, comorbidities, current disease and treatment, COVID vaccination) and lifestyle parameters (working and living situation, responsibilities in everyday life, e.g., caring for children, grandchildren, or pets), as well as duration and symptoms in the case of a COVID-19 infection.

The above-mentioned questions were followed by a self-designed questionnaire with 12 items using a 5-point Likert scale (0 –not at all/4 –very much), covering the aspects health and therapy, social environment, participation in daily life, and overall assessment (Supplementary Figure 2). The collected data were analyzed anonymously.

Figure 1 describes the process of data collection: In total, 115 patients received the survey, of whom one was not vaccinated against COVID-19 and thus excluded from the study. All other patients had at least received two doses of vaccine. The remaining 114 patients were analyzed regarding their indicated demographic and clinical parameters as well as symptoms and their duration during COVID-19 infection, if applicable. Six patients had ≥50% of the requested data in the subsequent questionnaire missing and were thus not included in the evaluation of the vaccine-related HR-QoL questionnaire (Figure 1).

Study definitions

Patients with breast and gynecological cancer receiving oncological treatment in the oncological outpatient clinics of the LMU Department of Obstetrics and Gynecology were included in

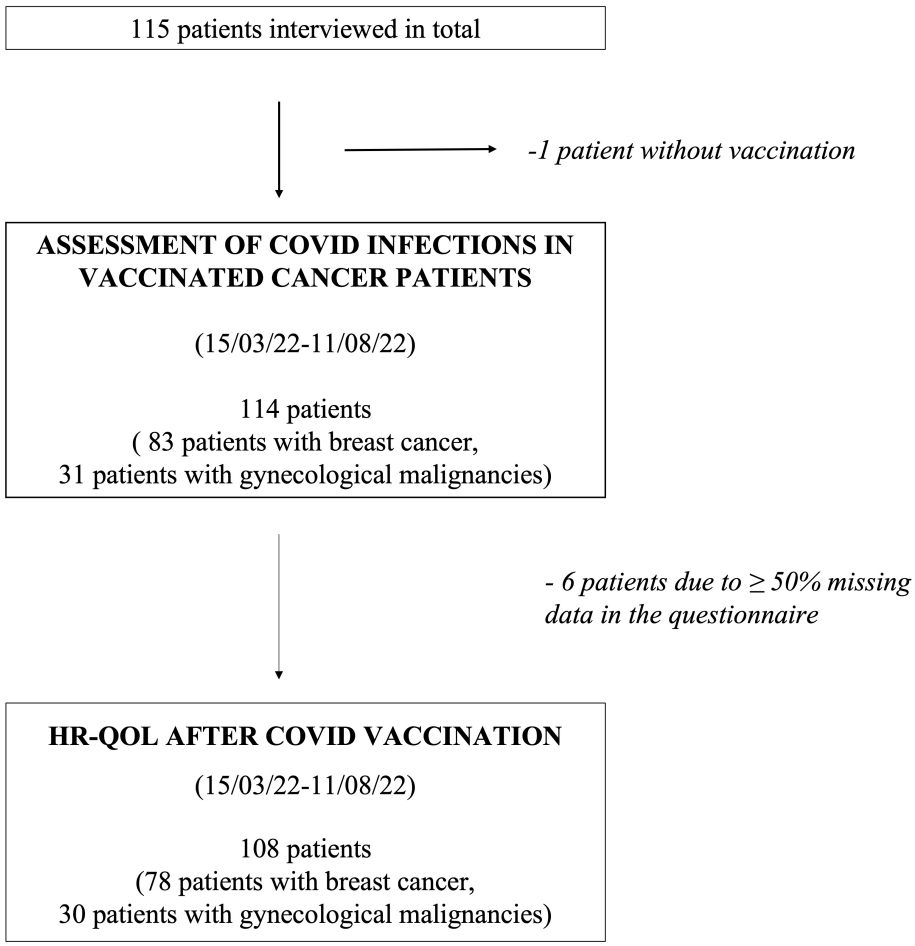

FIGURE 1
Study design and data collection.

the study. Types of anti-cancer therapy included neoadjuvant, adjuvant, and maintenance therapy as well as therapy for locally recurrent or metastatic disease. Therapy regimen consisted of chemotherapy +/- targeted therapy (e.g., taxane- or carboplatin-based, gemcitabine), targeted therapies (HER2-targeted therapies, bevacizumab, and PARP-inhibitors), immunotherapy +/- chemotherapy (PD-1 and PD-L1 inhibitors) as well as endocrine-based targeted therapy (CDK4/6-inhibitors or PIK3CA-inhibitors in combination with aromatase-inhibitors or Fulvestrant) and endocrine-based therapy.

Statistical analysis

Patient characteristics and endpoints were summarized. The scores according to the Likert scale of the QoL-questionnaire were added to a total score with only one item being reverse-scored (item 1.0 on negative influence of the vaccine on HR-QoL). Furthermore, basic questionnaire parameters such as floor and ceiling effects were assessed. 15% missing data were set as the acceptable threshold for individual items. Internal consistency was evaluated by calculating Cronbach's alpha, which was considered as indicating good internal consistency with a value more than 0.7.

Statistical analysis was performed using R Studio, Version 1.4.1103. Fisher's exact test was used to test for differences between specific groups. All statistical tests were performed two-sided. P-values of <0.05 were considered statistically significant. Power calculation and sample size justification were performed *a priori* using the program "G*Power". For the calculations performed using Fisher's exact test, a total sample size of 69 patients was required to achieve an actual power of 0.8 with a significance level of 0,05 (alpha error), reporting a medium effect size of 0.4 for calculations with up to three degrees of freedom.

Questionnaire construction

The vaccine related QoL- questionnaire consists of 12 items covering five superordinate topics:

item 1.1 assesses patients' HR-QoL with regard to side effects of the COVID-19 vaccine.

item 2.1 – 2.3 (subscale 2) cover the aspect "Health and therapy" since previously conducted studies showed that "concerns of contracting COVID-19 infection were correlated with lower scores of global QoL and the emotional functioning scale" (13).

item 3.1 – 3.3 (subscale 3) focus on the impact of the vaccination on social environment (mainly family and friends). Due to ongoing restrictions regarding social life during COVID-19 many patients lacked the support of family or friends (8), which is especially important during a cancer diagnosis and outcome of therapy (14, 15). Travelling and work precaution for caregivers raised concern among cancer patients (16), which might lead to inner-familiar conflicts (item 3.1).

item 4.1 – 4.4 (subscale 4) assess the impact of the vaccine on participation in everyday life in various aspects (socially, work-related, leisure activities, sports), which have a measurable impact on cancer patients' life (17–20).

item 5.1 examines the overall perception of the patients regarding a positive impact of COVID-19 vaccination on their HR-QoL.

We did not carry out a pilot study before using the questionnaire as the topic of COVID-19 was very current at that time and we wanted to collect results as up to date as possible. To still prove the scientific quality of the questionnaire used we assessed missing data rates, floor/ceiling effects as well as Cronbachs alpha prove internal consistency.

The missing data rate in the vaccine related QoL questionnaire was extremely low (1.6%), exclusive item 4.1, which could only be completed by those patients currently working (not those currently on sick leave/no longer working/already retired; item completed by 20 patients). Missing data were distributed across 9 of the 11 items with no item having more than 5 missing responses.

Total scores (n=108) ranged from 2 – 44 (possible range: 0 – 44), with mean 20.9, SD 10.0, and median 20. No participants had minimum scores. 2 participants (1.9%) had maximum scores (threshold for ceiling effects set at 15%).

Cronbachs alpha for the whole vaccine related QoL-questionnaire was 0.89. Furthermore, it was assessed for subscale 2, 3 and 4 (as "subscale" 1 and 5 only consisted of one item, respectively). Cronbach's α for "health and therapy" was 0.89 (n =108); for "social environment" 0.77 (n = 108) and for "participation in everyday life" 0.9 (n = 107).

Results

Demographic characteristics and clinical presentation

A total of 114 patients (83 patients with breast cancer and 31 with gynaecological malignancies) were interviewed, of whom 25.4% previously had a COVID-19 infection. Clinical characteristics of patients were stratified by COVID-19 infection (Table 1). Mean age in breast cancer and gynecological cancer patients was 55.1 years (Median 55y, range 29 – 86y). Patients who experienced a COVID-19 infection after vaccination were significantly younger than those with no COVID-19 (47.8y vs. 57.8y, $p < 0.01$).

72.8% of the surveyed patients were diagnosed with breast cancer and 27.2% with gynecological cancers such as ovarian carcinoma, endometrium carcinoma, cervix carcinoma and vaginal carcinoma (Table 1). 44.7% of the patients indicated at least one comorbidity, of these mostly thyroid (42.0%) or vascular pathologies (42.0%). No significant differences could be observed between cancer type or co-morbidities and COVID-19 infection.

94.7% of the patients had received at least three COVID-19 vaccinations. 62.5% received the vaccine Conmirnaty (by BioNTech/Pfizer) and 24.6% of the patients a combination of vaccines (35.7% of those were combinations of Conmirnaty/Vaxzevria by Astra Zeneca and 35.7% Conmirnaty/COVID-19 vaccine Moderna).

59.0% of the 83 breast cancer patients had early breast cancer and 41.0% metastatic disease; most of them were in the metastatic (41.0%) or neoadjuvant (32.5%) therapy setting. The majority received chemotherapy +/- targeted therapy (51.8%) (Table 2). In contrast, patients with gynecological cancer mostly had metastatic disease (54.8%). Gynaecological cancer patients were in the metastatic (41.9%) or adjuvant (25.8%) oncological therapy setting and also mostly received chemotherapy +/- targeted therapy (51.6%) (Table 3).

No significant differences could be observed regarding a potential influence of both, patient and therapy characteristics, on whether the patients got infected with COVID-19 or not (Tables 2, 3).

COVID-19 infections – clinical presentation

Figure 2 displays the symptoms of the vaccinated cancer-patients during COVID-19 infections (n=29). The most frequent symptoms during infection were cold symptoms such as coughing (51.7%), and rhinitis (51.7%) followed by flu symptoms fever (37.9%) and headache (34.5%). Median duration of symptoms was 5.9 days (median: 6d, range: 0-18d).

Supplementary Figure 3 presents the COVID-19 infections based on the date of the first positive PCR test. The majority of the patients (82.8%) got infected with COVID-19 in 2022, more specifically, in March 2022 (31.0%).

Lifestyle impact on acquiring of COVID-19 infections

Table 4 summarizes patient lifestyle parameters and COVID-19 infections. Patients who were employed got significantly more often infected ($p < 0.05$). If counted together, those who were still active at work (employed and self-employed) caught more infections than those unemployed, retired, housewives, or students ($p < 0.01$). The

TABLE 1 Clinical and COVID-19 vaccine-related characteristics of the surveyed patients.

Characteristics	All patients	Patients with COVID-19 infection	Patients without COVID-19 infection
In total (%)	114	29 (25.4)	85 (74.6)
Gender (♂ male, ♀ female)	2 ♂, 112 ♀	1 ♂, 28 ♀	1 ♂, 84 ♀
Age			
median/mean (y)	55/55.1	45/47.8*	59/57.8*
range (y)	29 - 86	29 – 74	30 – 86
Diagnosis			
Breast cancer (%)	83 (72.8)	22 (26.5)	61 (73.5)
Gynecological malignancies (%)	31 (27.2)	8 (25.8)	23 (74.2)
Ovarian carcinoma (%)	22 (19.3)	5	17
Endometrium carcinoma (%)	4 (3.5)	1	3
Cervix carcinoma (%)	4 (3.5)	2	2
Vaginal carcinoma (%)	1 (0.9)	0	1
Time since cancer diagnosis			
< 1 year (%)	45 (39.5)	11 (24.4)	34 (75.6)
1 -2 years (%)	21 (18.4)	11 (52.4)*	10 (47.6)
2– 5 years (%)	26 (22.8)	6 (23.1)	20 (76.9)
> 5 years (%)	22 (19.3)	2 (9.1)	20 (90.9)
Comorbidities			
None (%)	63 (55.3)	16 (25.4)	47 (74.6)
In total (%)	51 (44.7)	14 (27.5)	37 (72.5)
Vascular (%)	21 (42.0)	2 (9.5)	19 (90.5)
Respiratory (%)	5 (10.0)	1 (20.0)	4 (80.5)
Inflammatory bowel diseases (%)	2 (4.0)	1 (50.0)	1 (50.0)
Metabolic (%)	12 (24.0)	4 (33.3)	8 (66.7)
Thyroid (%)	21 (42.0)	7 (33.3)	14 (66.7)
Psychic (%)	3 (6.0)	1 (33.3)	2 (66.7)
Cancer (%)	5 (10.0)	0	5 (100)
Other (%)	10 (20.0)	4 (40.0)	6 (60.0)
Number of COVID-19 vaccinations received			
2 (%)	5 (4.4)	2	3
3 (%)	100 (87.7)	25	75
4 (%)	9 (7.9)	2	7
Vaccine			
Conmirnaty (BioNTech) (%)	80 (62.5)	24 (30.0)	56 (70.0)
COVID-19 vaccine Moderna (%)	1 (0.9)	0	1
Vaxzevria (Astra Zeneca) (%)	2 (1.8)	1 (50.0)	1
Combination of vaccines (%)	28 (24.6)	4 (15.4)	24 (84.6)
Conmirnaty/ Moderna (%)	10 (35.7)	0	10 (100)
Conmirnaty/ Vaxzevria (%)	10 (35.7)	0	10 (100)
Other (%)	8 (28.6)	4 (50.0)	4 (50.0)
NA (%)	3 (2.6)	1 (33.3)	2 (66.7)

Fisher's exact test was used to test for differences between specific groups; significant differences between groups are marked with a star.

TABLE 2 Clinical characteristics of the surveyed breast cancer patients.

Characteristic	All patients	Patients with COVID-19 infection	Patients without COVID-19 infection
In total (%)	83	23 (27.7)	60 (72.3)
Tumor stage			
Early breast cancer (%)	49 (59.0)	11 (22.4)	38 (77.6)
Metastatic breast cancer (%)	34 (41.0)	8 (23.5)	26 (76.5)
Therapy setting			
neoadjuvant therapy (%)	27 (32.5)	5 (18.5)	22 (81.5)
adjuvant therapy (%)	21 (25.3)	6 (28.6)	15 (71.4)
metastatic therapy (%)	34 (41.0)	8 (23.5)	26 (76.5)
local recurrence therapy (%)	1 (1.2)	0	1 (100)
Oncological therapy			
chemotherapy +/- targeted therapy (%)	43 (51.8)	9 (20.9)	34 (79.1)
targeted therapy (%)	17 (20.5)	3 (17.6)	14 (82.4)
immunotherapy + chemotherapy (%)	7 (8.4)	3 (42.9)	4 (57.1)
endocrine-based therapy (%)	16 (19.3)	4 (25.0)	12 (75.0)

infection rate was significantly lower in the retired patients ($p < 0.01$).

Moreover, patients living with their families reported more frequently (significant, $p < 0.01$) an infection with COVID-19 than those living alone or with their partner. Patients with responsibilities in their everyday life (n=62, of those 71.0% involved in childcare, 16.1% taking care of their parents, and 37.1% of their pets (multiple entries possible)) showed a higher proportion of COVID-19 infections than those without (32.3% vs. 19.2%, not significant, p=0.1).

Vaccine related QoL in patients with breast and gynecological cancer

Table 5 summarizes the mean total scores of the vaccine related QoL questionnaire of different groups of patients. Here, higher scores indicate a higher impact of COVID-19 vaccination on the patients' HR-QoL. Breast cancer patients showed a tendency towards a higher mean total score (22.5 vs. 17.1, not significant, p=0.07). Patients with comorbidities had significantly lower mean total scores than those without comorbidities (19.2 vs. 22.6, $p < 0.05$) and patients with metastatic disease reached significantly lower mean total scores than patients with non-metastatic cancers (20.3 vs. 21.6, $p<0.05$). However, this effect was only present in the breast

10.3389/fonc.2023.1217805

TABLE 3 Clinical characteristics of the surveyed patients with a gynecological malignancy.

Characteristics	All patients	Patients with COVID-19 infection	Patients without COVID-19 infection
In total	31	8 (25.8)	23 (74.2%)
Tumor stage			
non-metastatic (%)	14 (45.2)	3 (21.4)	11 (78.6%)
metastatic (%)	17 (54.8)	1 (5.9)	16 (94.1%)
Therapy modality			
adjuvant therapy (%)	8 (25.8)	3 (37.5)	5 (62.5)
metastatic therapy (%)	13 (41.9)	1 (7.6)	12 (92.3)
maintenance therapy (%)	5 (16.1)	0	5 (100)
local recurrence therapy (%)	5 (16.1)	0	5 (100)
Oncological therapy			
Chemotherapy +/- targeted therapy (%)	16 (51.6)	1 (6.2)	15 (93.8)
targeted therapy (%)	12 (38.8)	2 (16.7)	10 (83.3)
endocrine-based therapy (%)	1 (3.2)	1 (100)	0
immunotherapy +/- chemotherapy (%)	2 (6.4)	0	2 (100)

cancer cohort; the gynaecological cancer patients with metastatic disease and those with comorbidities reached higher scores compared to those with non-metastatic disease and no comorbidities (Tab. 5). No significant differences could be shown regarding the total scores of patients with different oncological therapies, although patients receiving endocrine-based therapy showed higher total scores (not significant, p>0.05, Table 5). Patients receiving oral therapies also tended to show higher scores than those with i.v. therapies (not significant, p >0.05). Age of the patients, their status of employment, living situation and their responsibilities in everyday life did not appear to significantly influence the impact of the vaccine on their HR-QoL.

Figure 3A presents the mean scores of the individual items of the vaccine related QoL questionnaire and Figure 3B displays the distribution of the scores for the individual items. The patients strongly denied the statement, that the COVID-19 vaccination had negative influence on their QoL (mean item score of item 1.1 = 3.6, Figure 3A). Reasons for stating "a bit" of negative influence on QoL (Figure 3B) were flu-like symptoms and local reactions at the vaccination site.

Regarding the items assessing "health and therapy" (items 2.1 – 2.3), more than a quarter of the patients agreed fairly or very much to the statement that due to vaccination they would worry less on developing COVID-19, interruption of treatment/therapy due to the COVID-19 pandemic, and seeking medical assistance for health problems (31%, 26%, 28%, respectively, Figure 3B).

Item 3.1 on less conflicts within the family due to complete vaccine protection in the third subscale 'social environment", received the lowest degree of agreement with a mean score of 1.2 (Figure 3A). 36% of the patients agreed fairly or very much on meeting more with friends since complete vaccine protection (Figure 3B).

Additionally, 30.8% of the surveyed patients indicated fairly or very much to further engage in leisure activities (item 4.2), 21.0% fairly or very much to do more sports (item 4.3) and 40.2% fairly or

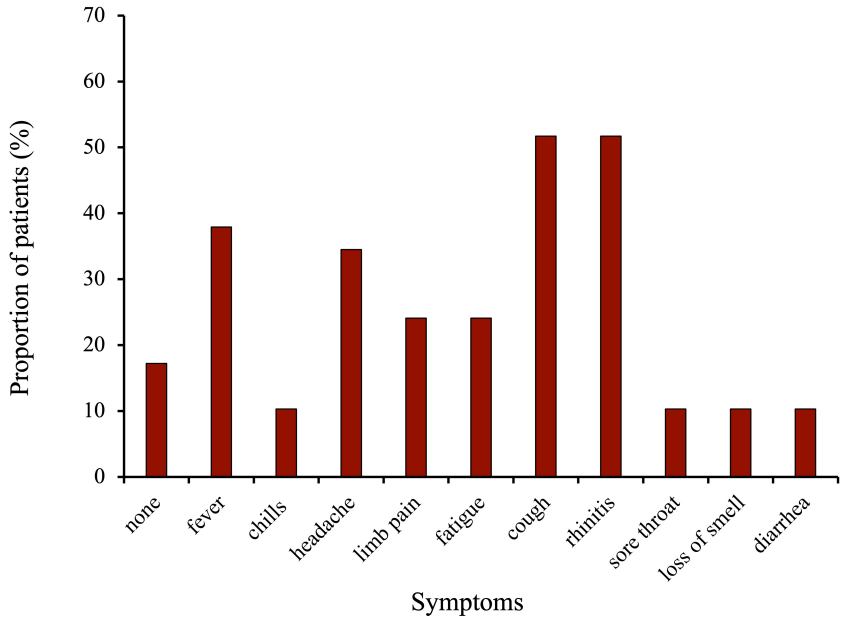

FIGURE 2
Symptoms during COVID-19 infection in the vaccinated breast and gynecological cancer patients.

TABLE 4 Lifestyle parameters that may potentially influence the probability of COVID-19 infection in the surveyed patients.

Characteristics	All patients	Patients with COVID-19 infection	Patients without COVID-19 infection
In total	114	29	85
Status of employment			
Employed (%)	53 (46.5)	20 (27.7)	33 (62.3)*
Self-employed (%)	13 (11.4)	4 (30.8)	9 (69.2)
Unemployed (%)	4 (3.5)	1 (25.0)	3 (75.0)
Retired (%)	39 (34.2)	4 (10.3)	35 (89.7)*
Housewife (%)	3 (2.6)	1 (33.3)	2 (66.7)
Student (%)	1 (0.8)	0	1 (100)
Living situation			
Living alone (%)	22	2 (9.1)	20 (90.9)
Living with partner (%)	44	7 (15.9)	37 (84.1)
Living with family (%)	48	21 (43.8)*	27 (56.3)
Responsibilities			
Yes (%)	62	20 (32.3)	42 (68.4)
None (%)	52	10 (19.2)	42 (80.8)

Fisher's exact test was used to test for differences between specific groups; significant differences between groups are marked with a star.

very much to participate more in everyday-life (item 4.4) due to vaccine protection (Figure 3B).

Overall, 60% of the patients stated fairly or very much that the COVID-19 vaccination had a positive impact on their QoL (item 5, mean 2.5), whereas only 16.8% indicated the vaccination did "not at all" have that positive impact (Figure 3B).

Discussion

The present study first evaluated to which extend COVID-19 vaccination might be associated with HR-QoL in patients with breast and gynecological cancer. Our data showed a noticeable although not statistically significant improvement of the patients' quality of life due to their COVID-19 vaccination: 78.5% participated more in their everyday life (38.3% a bit or rather more; 40.2% fairly or very much more), 77.8% of the patients spent more time with their friends (44.4% a bit or rather more; 33.4% fairly or very much more), and 64.8% of the patients spent more time practicing sports after receiving complete vaccine protection (43.8% a bit or rather more; 21.0% fairly or very much more). Furthermore, 83.3% of the surveyed patients reported a positive effect on their quality of life after receiving the vaccine. Second, we evaluated COVID-19 infections in fully vaccinated patients with breast and gynecological cancer. The symptoms of the surveyed patients were self-limiting, and no hospital admissions were reported.

Our questionnaire showed good psychometric results regarding acceptance and internal consistency. Our findings from the questionnaire might reassure undecided patients regarding COVID-19 vaccination: A previous study conducted one year ago at our gynecological outpatient clinic demonstrated a rate of only 61.1% of cancer patients willing to receive the vaccine (21). This study also showed no vaccine-related serious events and self-limiting vaccine-related adverse events of mostly short duration. This is in line with our data from item 1 of the questionnaire (Figures 3A, B), with 77% of the surveyed patients stating the vaccination did not at all negatively influence their QoL.

Approximately 25% of the patients in the present survey worried less about interruption of their oncological therapy and seeking medical help in the case of health-related problems. The reluctancy observed in the beginning of the pandemic (2) may have led to less diagnostic procedures and thus less treatment of non-COVID-19-related diseases (22).

A previously conducted study reported a positive influence on patients' global HR-QoL, physical, social, emotional, cognitive and role functioning if they had been working before diagnosis (17). 50% of our currently working patients agreed very strong that returning physically to work after vaccination positively impacted their HR-QoL. Besides working, according to the ESMO-ESO international consensus guidelines for advanced breast cancer as well as other studies physical exercise, sports, or yoga are suggested to further improve QoL, fitness and fatigue (18, 23). 64.8% of the surveyed patients reported to do more sports due to COVID-19 vaccination, which reveals another positive impact of the vaccine on their HR-QoL.

A study by Vuagnat et al. showed a higher impact of the presence of comorbidities on the course of the COVID-19 disease than the oncological therapy which patients were undergoing (24). Breast cancer patients with comorbidities significantly showed lower total scores than those without comorbidities in the vaccine-related QoL-questionnaire, indicating less of a positive influence of the vaccination on their QoL. This might be due to the fact, that these patients have a higher risk of having severe courses of COVID-19 (especially those with vascular, metabolic or respiratory comorbidities) (25, 26), and thus limit themselves, their social contacts and participation in everyday life more strictly – vaccinated or not. The same could apply for patients with metastatic disease, since according to the ACHOCC-19 Study metastatic disease is associated with a higher mortality due to COVID-19 (27). Compared to patients with non-metastatic cancer, patients with metastatic disease showed significantly lower total scores in our study implying less benefit of the vaccine for their HR-QoL. The fact, that the effect was not significant among gynecological cancer patients might be related to the time of diagnose and stage of disease in gynecological malignancies, which are more often diagnosed at an advanced stage. Therefore, patients with non-metastatic cancer are more likely to be impaired by their disease compared to (early) breast cancer patients with non-metastatic cancer.

Our results show a COVID-19 infection rate of 25.4% in patients having received at least two doses of vaccine (booster rate 95.6%) All of these patients reported self-limiting symptoms and no case of hospitalization was noted. Compared to the general population in Germany with an infection rate of 38.78% (proportion of fully vaccinated persons: 76.3%, 62.0% having

TABLE 5 Parameters that may influence the vaccine related HR-QoL in the surveyed patients and their corresponding mean total scores in the questionnaire.

Characteristics	All patients	Mean QoL score	Mean QoL score breast cancer patients (n=83)	Mean QoL score gyn. cancer patients (n=31)
In total	114	20.8	22.5	17.1
Age				
< 55 years (%)	54 (47.4)	23.3	23.5	22.2
> 55 years (%)	60 (52.6)	18.5	18.7	18.3
Time since cancer diagnosis				
< 1 year (%)	45 (39.5)	21.0	21.0	21.0
1 -2 years (%)	21 (18.4)	22.4	23.4	20.8
2– 5 years (%)	26 (22.8)	22.2	22.4	22.0
> 5 years (%)	22 (19.3)	17.7	18.4	16.4
Stage of carcinoma				
non-metastatic (%)	63 (55.3)	21.6*	23.0	18.7
metastatic (%)	51 (44.7)	19.9*	20.5	19.7
Oncological therapy				
Chemotherapy +/- targeted therapy (%)	59 (51.8)	20.7	21.5	17.6
targeted therapy (%)	29 (25.4)	19.2	19.4	18.0
immunotherapy +/- chemotherapy (%)	9 (7.9)	21.9	24.8	4.0
endocrine-based therapy (%)	17 (14.9)	23.1	23.5	21.5
Comorbidities				
None (%)	64 (56.1)	21.8*	22.0	20.6
Present (%)	50 (43.9)	19.6*	18.7	22.5
Status of employment				
Employed (%)	53 (46.5)	22.9	22.8	22.0
Self-employed (%)	13 (11.4)	24.5	24.2	26.0
Unemployed (%)	4 (3.5)	17.8	18.7	15.0
Retired (%)	39 (34.2)	17.1	18.7	14.6
Housewife (%)	3 (2.6)	18.7	20.0	16.0
Student (%)	1 (0.9)	20.0	-	20.0
Living situation				
Living alone (%)	22 (19.3)	19.6	23.2	13.2
Living with partner (%)	44 (38.6)	20.4	20.5	21.2
Living with family (%)	48 (42.1)	21.8	21.9	21.2
Responsibilities				
Yes (%)	62 (54.4)	22.4	23.5	18.3
None (%)	52 (45.6)	19.0	17.6	22.9

Fisher's exact test was used to test for differences between specific groups; significant differences between groups are marked with a star.

received a booster vaccine), the infection rate in the surveyed cohort of vaccinated patients with breast and gynecological cancer is considerably lower than in the general population (28).

The majority of the surveyed patients developed cold- or flu-like symptoms (Figure 2). A study by Rüthrich et al. which enrolled 435 cancer patients including 59% with solid tumors (18.5% with breast and gynecological cancer) and 54% with active malignancy observed a rate of 27.5% patients being admitted to ICU (29). Most common symptoms were fever (34%), coughing (24.5%) and excessive tiredness (18.9%). This is in line with our results which showed fever in 37.9%, coughing in 51.7%, and fatigue in 24.1% of the patients. Interestingly, we had a much a higher amount (51.7% vs 24.5%) of patients with coughing but no cases of admittance to ICU in the vaccinated cohort. The above-mentioned study was conducted in 2020, meaning the patients were not vaccinated and probably infected with the alpha variant, whereas 93.1% of the patients surveyed here got infected from October 2021 onwards (Supplementary Figure 3), when the predominant virus variant in Germany was Omikron, which is associated with a milder course of the disease than the variants before (30).

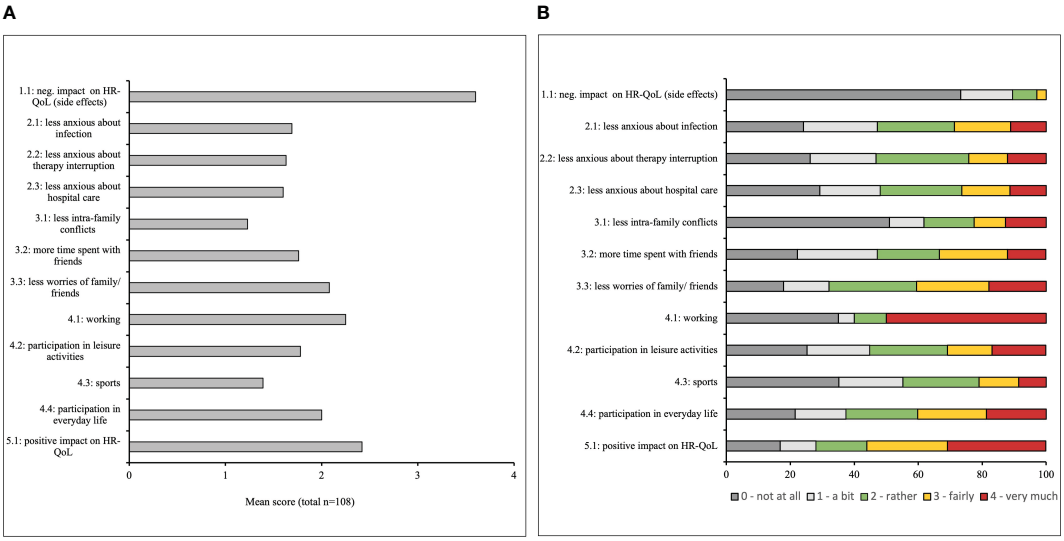

FIGURE 3
(A) Mean item score (possible range: 1 – 4) in the COVID-19 vaccine-related Health-related quality of life (HR-QoL) questionnaire. Higher scores indicate a higher impact of the vaccine on the HR-QoL in the surveyed breast and gynecological cancer patients. **(B)** Distribution of response options for all items in the COVID 19 vaccine-related HR-QoL questionnaire. The patients were asked to what extent the COVID-19 vaccine impacted their HR-QoL regarding different aspects, given the answer options "very much", "fairly", "rather", "a bit" and "not at all".

Interestingly, patients who received a combination of vaccines (Conmirnaty/Moderna, Conmirnaty/Vaxzevria) showed fewer infection rates than those who received only Conmirnaty. Due to the small cohort size, this difference is not significant. Two independent reviews reported good immunogenicity and a stronger T cellular immunity in patients with a combination of ChAdOx1 and Conmirnaty, which may be a reason for our clinical observation (31, 32).

A review performed by Lasagna et al. in 2020 explored the question, whether the gut microbiota and estrogen levels in breast cancer patients could influence the course of their COVID-19 infections (33). A possible conclusion of the data discussed in the paper was that breast cancer patients with hormone receptor positive breast cancer may be better protected against COVID-19 infections due to higher estrogen levels, which showed a negative correlation with severity of COVID-19 infection in a multi-center study performed in China in 2020 (34). By implication, this raises the question whether endocrine-based therapy increases the risk for more severe COVID-19 infections. Our results from Table 2 showed that 4/16 (25.0%) of the breast cancer patients treated with endocrine-based therapy had a COVID-19 infection. The mean duration of symptoms was 6.4 days (n=5) vs. 5.6 days in those patients not receiving endocrine based therapies (n=18), which would thus support this hypothesis (not significant due to the small number of patients).

Limitations of our study mostly consist of the small cohort included in the study. Second, the study had a monocentric design, and all patients were recruited from the two LMU gynecological outpatient clinics in Munich. In addition, we did not have a control group as almost all patients in the oncological outpatient clinics had received at least two vaccinations at the time of the survey. Further studies are thus required to validate our findings.

Conclusion

Overall, the conducted study pointed out that the COVID-19 vaccine had a positive impact on patients' HR-QoL. Moreover, in an ambulatory setting, fully vaccinated patients with breast and gynecological cancer showed predominantly mild courses of COVID-19 infection without hospital admissions. These results should be considered when consulting cancer patients regarding COVID-19 vaccination.

Data availability statement

The raw data supporting the conclusions of this article will be made available by the authors, without undue reservation.

Ethics statement

The study received ethics approval from the Ludwig-Maximilians-University (LMU) Munich Ethics Committee in February 2022 (number of ethical approval: 21-1237). Signed informed consent was obtained from all participants.

Author contributions

MF, RW, NH, and AC-R contributed to conception and design of the study. MF, AK, AS, EW and AC-R contributed to acquisition of data. MF performed the statistical analysis, FB, FT, SM and AC-R were engaged in analysis and interpretation of data. MF, RW, NH and AC-R drafted the article. All authors contributed to the article and approved the submitted version.

Conflict of interest

RW received honoraria from Agendia, Amgen, Aristo, Astra Zeneca, Boehringer Ingelheim, Carl Zeiss, Celgene, Daiichi-Sankyo, Eisai, Exact Sciences, Genomic Health, Gilead, Glaxo Smith Kline, Hexal, Lilly, Medstrom Medical, MSD, Mundipharma, Mylan, Nanostring, Novartis, Odonate, Paxman, Palleos, Pfizer, Pierre Fabre, PumaBiotechnolgogy, Riemser, Roche, Sandoz/Hexal, Sanofi Genzyme, Seattle Genetics/Seagen, Tesaro Bio, Teva, Veracyte, Viatris, FOMF, Aurikamed, Clinsol. FT reports grants and personal fees from AstraZeneca, Clovis, Eisai, Medac, MSD, PharmaMar, Roche, and Tesaro/GSK. SM reports research funding, advisory board, honorary or travel expenses: AbbVie, AstraZeneca, Clovis, Eisai, GlaxoSmithKline, Hubro, Medac, MSD, Novartis, Nykode, Olympus, PharmaMar, Pfizer, Roche, Sensor Kinesis, Teva, Tesaro NH reports honoraria for lectures and/or consulting from AstraZeneca, Daiichi-Sankyo, Gilead, Lilly, MSD, Novartis, Pierre-Fabre, Pfizer, Roche, Sanofi, Sandoz, Seagen.

The remaining authors declare that the research was conducted in the absence of any commercial or financial relationships that could be constructed as a potential conflict of interest.

Publisher's note

All claims expressed in this article are solely those of the authors and do not necessarily represent those of their affiliated organizations, or those of the publisher, the editors and the reviewers. Any product that may be evaluated in this article, or claim that may be made by its manufacturer, is not guaranteed or endorsed by the publisher.

Supplementary material

The Supplementary Material for this article can be found online at: https://www.frontiersin.org/articles/10.3389/fonc.2023.1217805/full#supplementary-material

References

1. Papautsky EL, Hamlish T. Patient-reported treatment delays in breast cancer care during the COVID-19 pandemic. *Breast Cancer Res Treat* (2020) 184(1):249–54. doi: 10.1007/s10549-020-05828-7

2. de Joode K, Dumoulin DW, Engelen V, Bloemendal HJ, Verhaij M, van Laarhoven HWM, et al. Impact of the coronavirus disease 2019 pandemic on cancer treatment: the patients' perspective. *Eur J Cancer* (2020) 136:132–9. doi: 10.1016/j.ejca.2020.06.019

3. Rolston KV. Infections in cancer patients with solid tumors: A review. *Infect Dis Ther* (2017) 6(1):69–83. doi: 10.1007/s40121-017-0146-1

4. Ciążyńska M, Pabianek M, Szczepaniak K, Ułańska M, Skibińska M, Owczarek W, et al. Quality of life of cancer patients during coronavirus disease (COVID-19) pandemic. *Psychooncology* (2020) 29(9):1377–9. doi: 10.1002/pon.5434

5. EMA EMA. COVID-19 vaccines: authorised(2021). Available at: https://www.ema.europa.eu/en/human-regulatory/overview/public-health-threats/coronavirus-disease-covid-19/treatments-vaccines/vaccines-covid-19/covid-19-vaccines-authorised#authorised-covid-19-vaccines-section.

6. Aboueshia M, Hussein MH, Attia AS, Swinford A, Miller P, Omar M, et al. Cancer and COVID-19: analysis of patient outcomes. *Future Oncol* (2021) 17(26):3499–510. doi: 10.2217/fon-2021-0121

7. Catt S, Starkings R, Shilling V, Fallowfield L. Patient-reported outcome measures of the impact of cancer on patients' everyday lives: a systematic review. *J Cancer Surviv* (2017) 11(2):211–32. doi: 10.1007/s11764-016-0580-1

8. Bargon CA, Batenburg MCT, van Stam LE, Mink van der Molen DR, van Dam IE, van der Leij F, et al. Impact of the COVID-19 pandemic on patient-reported outcomes of breast cancer patients and survivors. *JNCI Cancer Spectr* (2021) 5(1):pkaa104. doi: 10.1093/jncics/pkaa104

9. Hamer J, McDonald R, Zhang L, Verma S, Leahey A, Ecclestone C, et al. Quality of life (QOL) and symptom burden (SB) in patients with breast cancer. *Support Care Cancer* (2017) 25(2):409–19. doi: 10.1007/s00520-016-3417-6

10. Aapro M, Lyman GH, Bokemayer C, Rapoport BL, Mathieson N, Koptelova N, et al. Supportive care in patients with cancer during the COVID-19 pandemic. *ESMO Open* (2021) 6(1):100038. doi: 10.1016/j.esmoop.2020.100038

11. Johnston SR. The role of chemotherapy and targeted agents in patients with metastatic breast cancer. *Eur J Cancer* (2011) 47 Suppl 3:S38–47. doi: 10.1016/S0959-8049(11)70145-9

12. Westin SN, Labrie M, Litton JK, Blucher A, Fang Y, Vellano CP, et al. Phase ib dose expansion and translational analyses of olaparib in combination with capivasertib in recurrent endometrial, triple-negative breast, and ovarian cancer. *Clin Cancer Res* (2021) 27(23):6354–65. doi: 10.1158/1078-0432.CCR-21-1656

13. Jeppesen SS, Bentsen KK, Jørgensen TL, Holm HS, Holst-Christensen L, Tarpgaard LS, et al. Quality of life in patients with cancer during the COVID-19 pandemic - a Danish cross-sectional study (COPICADS). *Acta Oncol* (2021) 60(1):4–12. doi: 10.1080/0284186X.2020.1830169

14. Nausheen B, Gidron Y, Peveler R, Moss-Morris R. Social support and cancer progression: a systematic review. *J Psychosom Res* (2009) 67(5):403–15. doi: 10.1016/j.jpsychores.2008.12.012

15. Usta YY. Importance of social support in cancer patients. *Asian Pac J Cancer Prev* (2012) 13(8):3569–72. doi: 10.7314/APJCP.2012.13.8.3569

16. Moraliyage H, De Silva D, Ranasinghe W, Adikari A, Alahakoon D, Prasad R, et al. Cancer in lockdown: impact of the COVID-19 pandemic on patients with cancer. *Oncologist* (2021) 26(2):e342–4. doi: 10.1002/onco.13604

17. Schmidt ME, Scherer S, Wiskemann J, Steindorf K. Return to work after breast cancer: The role of treatment-related side effects and potential impact on quality of life. *Eur J Cancer Care (Engl)* (2019) 28(4):e13051. doi: 10.1111/ecc.13051

18. Dieli-Conwright CM, Courneya KS, Demark-Wahnefried W, Sami N, Lee K, Sweeney FC, et al. Aerobic and resistance exercise improves physical fitness, bone health, and quality of life in overweight and obese breast cancer survivors: a randomized controlled trial. *Breast Cancer Res* (2018) 20(1):124. doi: 10.1186/s13058-018-1051-6

19. Leclerc AF, Foidart-Dessalle M, Tomasella M, Coucke P, Devos M, Bruyère O, et al. Multidisciplinary rehabilitation program after breast cancer: benefits on physical function, anthropometry and quality of life. *Eur J Phys Rehabil Med* (2017) 53(5):633–42. doi: 10.23736/S1973-9087.17.04551-8

20. Hinzey A, Gaudier-Diaz MM, Lustberg MB, DeVries AC. Breast cancer and social environment: getting by with a little help from our friends. *Breast Cancer Res* (2016) 18(1):54. doi: 10.1186/s13058-016-0700-x

21. Forster M, Wuerstlein R, Koenig A, Amann N, Beyer S, Kaltofen T, et al. COVID-19 vaccination in patients with breast cancer and gynecological Malignancies: A German perspective. *Breast* (2021) 60:214–22. doi: 10.1016/j.breast.2021.10.012

22. Figueroa JD, Gray E, Pashayan N, Deandrea S, Karch A, Vale DB, et al. The impact of the Covid-19 pandemic on breast cancer early detection and screening. *Prev Med* (2021) 151:106585. doi: 10.1016/j.ypmed.2021.106585

23. Cardoso F, Paluch-Shimon S, Senkus E, Curigliano G, Aapro MS, André F, et al. 5th ESO-ESMO international consensus guidelines for advanced breast cancer (ABC 5). *Ann Oncol* (2020) 31(12):1623–49. doi: 10.1016/j.annonc.2020.09.010

24. Vuagnat P, Frelaut M, Ramtohul T, Basse C, Diakite S, Noret A, et al. COVID-19 in breast cancer patients: a cohort at the Institut Curie hospitals in the Paris area. *Breast Cancer Res* (2020) 22(1):55. doi: 10.1186/s13058-020-01293-8

25. Ejaz H, Alsrhani A, Zafar A, Javed H, Junaid K, Abdalla AE, et al. COVID-19 and comorbidities: Deleterious impact on infected patients. *J Infect Public Health* (2020) 13(12):1833–9. doi: 10.1016/j.jiph.2020.07.014

26. Müller-Wieland D, Marx N, Dreher M, Schnell O. COVID-19 and cardiovascular comorbidities. *Exp Clin Endocrinol Diabetes* (2022) 130(3):178–89. doi: 10.1055/a-1269-1405

27. Ospina AV, Bruges R, Mantilla W, Triana I, Ramos P, Aruachan S, et al. Impact of COVID-19 infection on patients with cancer: experience in a latin american country: the ACHOCC-19 study. *Oncologist* (2021) 26(10):e1761–73. doi: 10.1002/onco.13861

28. R.K.I. *COVID-19: Number of cases in Germany* (2022). Available at: https://www.rki.de/DE/Content/InfAZ/N/Neuartiges_Coronavirus/Fallzahlen.html/.

29. Rüthrich MM, Giessen-Jung C, Borgmann S, Classen AY, Dolff S, Grüner B, et al. COVID-19 in cancer patients: clinical characteristics and outcome-an analysis of the LEOSS registry. *Ann Hematol* (2021) 100(2):383–93. doi: 10.1007/s00277-020-04328-4

30. Meo SA, Meo AS, Al-Jassir FF, Klonoff DC. Omicron SARS-CoV-2 new variant: global prevalence and biological and clinical characteristics. *Eur Rev Med Pharmacol Sci* (2021) 25(24):8012–8. doi: 10.26355/eurrev_202112_27652

31. Chiu NC, Chi H, Tu YK, Huang YN, Tai YL, Weng SL, et al. To mix or not to mix? A rapid systematic review of heterologous prime-boost covid-19 vaccination. *Expert Rev Vaccines* (2021) 20(10):1211–20. doi: 10.1080/14760584.2021.1971522

32. Fiolet T, Kherabi T, MacDonald C-J, Ghosn J, Peiffer-Smadja N. Comparing COVID-19 vaccines for their characteristics, efficacy and effectiveness against SARS-CoV-2 and variants of concern: a narrative review. *Clin Microbiol Infect* (2022) 28 (2):202–21. doi: 10.1016/j.cmi.2021.10.005

33. Lasagna A, Zuccaro V, Ferraris E, Corbella M, Bruno R, Pedrazzoli P. COVID-19 and breast cancer: may the microbiome be the issue? *Future Oncol* (2021) 17(2):123–6. doi: 10.2217/fon-2020-0764

34. Ding T, Zhang J, Wang T, Cui P, Chen Z, Jiang J, et al. Potential influence of menstrual status and sex hormones on female severe acute respiratory syndrome coronavirus 2 infection: A cross-sectional multicenter study in Wuhan, China. *Clin Infect Dis* (2021) 72(9):e240–8. doi: 10.1093/cid/ciaa1022

frontiers | Frontiers in Oncology

TYPE Original Research
PUBLISHED 17 November 2023
DOI 10.3389/fonc.2023.1243126

OPEN ACCESS

EDITED BY
Anika Nagelkerke,
University of Groningen, Netherlands

REVIEWED BY
Sven Kurbel,
Josip Juraj Strossmayer University of Osijek, Croatia
Bilgin Kadri Aribas,
Bülent Ecevit University, Türkiye

*CORRESPONDENCE
Guang Zhang
zhangguanglaoshi@yeah.net

†These authors have contributed equally to this work

RECEIVED 20 June 2023
ACCEPTED 06 November 2023
PUBLISHED 17 November 2023

CITATION
Liu M, Zhang S, Du Y, Zhang X, Wang D, Ren W, Sun J, Yang S and Zhang G (2023) Identification of Luminal A breast cancer by using deep learning analysis based on multi-modal images.
Front. Oncol. 13:1243126.
doi: 10.3389/fonc.2023.1243126

Identification of Luminal A breast cancer by using deep learning analysis based on multi-modal images

Menghan Liu[1†], Shuai Zhang[2,3†], Yanan Du[1], Xiaodong Zhang[3], Dawei Wang[4], Wanqing Ren[3], Jingxiang Sun[3], Shiwei Yang[5] and Guang Zhang[1*]

[1]Department of Health Management, The First Affiliated Hospital of Shandong First Medical University & Shandong Engineering Laboratory for Health Management, Shandong Medicine and Health Key Laboratory of Laboratory Medicine, Shandong Provincial Qianfoshan Hospital, Jinan, China, [2]Department of Radiology, Shandong Provincial Hospital Affiliated to Shandong First Medical University, Jinan, China, [3]Postgraduate Department, Shandong First Medical University (Shandong Academy of Medical Sciences), Jinan, China, [4]Department of Radiology, The First Affiliated Hospital of Shandong First Medical University, Jinan, China, [5]Department of Anorectal Surgery, The First Affiliated Hospital of Shandong First Medical University, Jinan, China

Purpose: To evaluate the diagnostic performance of a deep learning model based on multi-modal images in identifying molecular subtype of breast cancer.

Materials and methods: A total of 158 breast cancer patients (170 lesions, median age, 50.8 ± 11.0 years), including 78 Luminal A subtype and 92 non-Luminal A subtype lesions, were retrospectively analyzed and divided into a training set (n = 100), test set (n = 45), and validation set (n = 25). Mammography (MG) and magnetic resonance imaging (MRI) images were used. Five single-mode models, i.e., MG, T2-weighted imaging (T2WI), diffusion weighting imaging (DWI), axial apparent dispersion coefficient (ADC), and dynamic contrast-enhanced MRI (DCE-MRI), were selected. The deep learning network ResNet50 was used as the basic feature extraction and classification network to construct the molecular subtype identification model. The receiver operating characteristic curve were used to evaluate the prediction efficiency of each model.

Results: The accuracy, sensitivity and specificity of a multi-modal tool for identifying Luminal A subtype were 0.711, 0.889, and 0.593, respectively, and the area under the curve (AUC) was 0.802 (95% CI, 0.657- 0.906); the accuracy, sensitivity, and AUC were higher than those of any single-modal model, but the specificity was slightly lower than that of DCE-MRI model. The AUC value of MG, T2WI, DWI, ADC, and DCE-MRI model was 0.593 (95%CI, 0.436-0.737), 0.700 (95%CI, 0.545-0.827), 0.564 (95%CI, 0.408-0.711), 0.679 (95%CI, 0.523-0.810), and 0.553 (95%CI, 0.398-0.702), respectively.

Conclusion: The combination of deep learning and multi-modal imaging is of great significance for diagnosing breast cancer subtypes and selecting personalized treatment plans for doctors.

KEYWORDS

molecular subtype, breast cancer, multi-modality, deep learning, mammography, MRI

1 Introduction

Breast cancer is the most common cancer in women and the second cause of death after cardiovascular diseases (1). In 2020, more than 2.2 million new breast cancer cases were diagnosed in women worldwide. In recent years, due to increased awareness of early breast cancer screening and the development of effective targeted therapy techniques, the overall mortality rate of breast cancer has decreased; however, the incidence rate continues to rise, especially in the younger population (1). Breast cancer can be classified into four molecular subtypes, i.e., Luminal A, Luminal B, human epidermal growth factor, and triple-negative breast cancer (2). Patients with different subtypes require different treatment plans and have different prognoses. The Luminal A subtype, also known as estrogen receptor-positive and progesterone receptor-positive cancer, accounts for about 40% of all breast cancers and is the most common subtype, more common in postmenopausal women with low histological grades (3). Luminal A subtype is early-stage breast cancer, less aggressive and more sensitive to endocrine therapy than Luminal B, and less sensitive to chemotherapy, with the lowest recurrence rate and the best prognosis among the four subtypes (4). Therefore, early and accurate identification of Luminal A breast cancer patients is of utmost importance.

Currently, imaging and pathological examination are the major means for diagnosing breast cancer. The most common imaging tool is mammography imaging; yet, its sensitivity tends to decrease when screening middle-aged people with higher mass density (5). Conventional magnetic resonance imaging (MRI) is also often applied; although highly sensitive, this method can potentially detect false positives (6). Pathological examinations are mainly based on examination on direct examination of breast cancer tissue collected by biopsy. Yet, the major drawbacks of this method are its invasive and limited sample collection. Thus, searching for a more accurate and less invasive breast cancer subtype screening tool is urgently needed.

In recent years, with the rapid development of artificial intelligence, deep learning has also been used to identify breast cancer molecular subtypes. Zhang et al. (7) and Sun et al. (8) used deep learning models based on breast ultrasound images and three dynamic contrast-enhanced magnetic resonance imaging (DCE-MRI) sequences to identify molecular subtypes obtaining good results. Yet, these studies were based on a single model of breast imaging.

Multi-modal imaging is a comparative analysis method that can simultaneously produce signals for more than one imaging technique, thus increasing accuracy and qualitative diagnosis of tumors through complementary and cross-validation. Recently, few studies have applied machine learning or deep learning to determine benign and malignant breast tumors based on breast multi-modal images. Li et al. (9) used a combination of digital breast tomosynthesis and mammography (MG) to improve the accuracy of the deep learning-based classification model of benign and malignant breast tumors. Hadad et al. (10) used the transfer learning method to classify benign and malignant lesions on breast MRI images with the pre-trained network based on MG images, achieving cross-modal effects. However, there is still a lack of research on deep learning in identifying breast cancer molecular subtypes based on breast multi-modal images.

The present study analyzed the value of deep learning methods in identifying molecular subtypes of breast cancer by combining X-ray and magnetic resonance multimodal images of breast cancer with AI.

2 Materials and methods

2.1 Patients

Institutional Review Board approved this study. Informed consent was waived because of the retrospective nature of the study. Anonymous clinical data were used in the analysis.

A total of 158 breast cancer patients (170 lesions) were enrolled from the First Affiliated Hospital of Shandong First Medical University. Inclusion criteria were the following (1): patients who underwent mammography and MRI scan for suspected breast cancer; (2) breast cancer confirmed by surgical pathology; (3) complete pathologic examination immunohistochemistry results. Exclusion criteria were the following: (1) those who received biopsy or neoadjuvant chemotherapy before the examination; (2) poor image quality, where condition and position were not up to standard, or there was a lack of part of the sequence; (3) imaging of lesions without one-to-one correspondence with postoperative pathologic results (Figure 1).

2.2 Mammography

MG examination was performed with digital mammography (Hologic Selenia Dimensions). During the examination, the breast was placed on the detector and flattened by the compressor. The bilateral breast's medial and lateral-oblique and cranial-caudal images were collected. If the observation was not satisfactory, other positions, such as lateral or cleavage, were added.

2.3 MRI examination

Breast MRI was performed using a 3.0T MRI scanner (Magnetom Skyra) from Siemens, Germany, and a 1.5T MRI scanner (Signa Explorer) from GE, USA, with the dedicated breast coil. The patient was placed in a prone position. The following four sequences were collected by the two instruments: axial T2-weighted image (T2WI), diffusion weighting imaging (DWI), apparent diffusion coefficient (ADC) images, and DCE-MRI sequences. The parameters of T2WI sequence in 3.0T MRI scanner are as follows: repetition time (TR) = 7600 ms, echo time (TE) = 102 ms, inverse Angle = 120°, slice gap = 0.8 mm, layer thickness = 4mm, field of view (FOV) = 34 cm × 34 cm, matrix = 576 × 576. The parameters of DWI in 3.0T MRI scanner are as follows: TR = 5030 ms, TE = 56 ms, reverse Angle = 180°, slice gap = 1.1 mm, slice thickness = 5.5 mm, FOV = 13.6 cm × 5.5 cm,

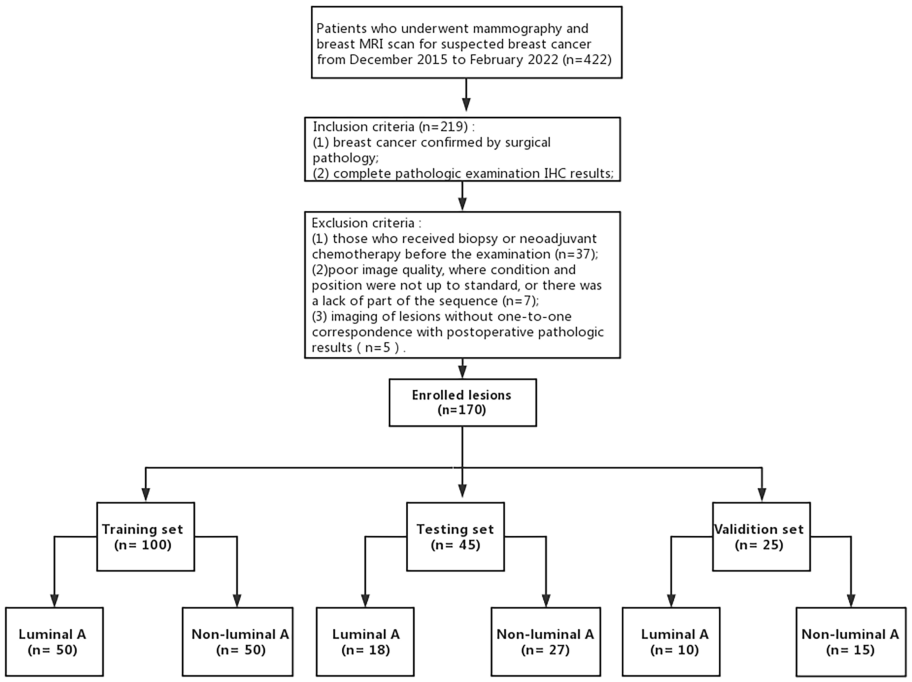

FIGURE 1
Process of enrolling patients with inclusion and exclusion criteria.

matrix = 224 × 224, DWI b value = 50/1000 s/mm^2. The parameters of DCE in 3.0T are as follows: TR = 5.6 ms, TE = 1.7 ms, reverse Angle = 10°, layer thickness = 1.5 mm, FOV = 17.3cm × 8.8 cm, matrix = 512 × 512. The parameters of T2WI sequence in 1.5T MRI scanner are as follows: TR = 5269 ms, TE = 79.7 ms, inverse Angle = 160°, slice gap = 1.0 mm, layer thickness = 5 mm, FOV = 32 cm × 32 cm, matrix = 288 × 224; The parameters of DWI sequence in 1.5T MRI scanner are as follows: TR = 5722 ms, TE = 98.4 ms, slice gap = 1.0 mm, layer thickness = 5.0 mm, FOV = 32 cm × 32 cm, matrix = 128 × 128, b value of DWI = 50/800 s/mm^2. The parameters of DCE sequence parameters in 1.5T MRI scanner are as follows: TR = 4.6 ms, TE = 2.1 ms, inverse Angle = 15°, layer thickness = 2.2 mm, FOV = 32 cm × 32 cm, matrix = 114 × 224. DCE-MRI sequence imaging was obtained after injecting 20 ml gadolinium contrast medium (Magnevist, Bayer Schering, Germany) at a rate of 4.0 ml/s. The 3.0T MRI machine had a duration of 5 minutes and 10 seconds with a total of 10 phases, and the 1.5T MRI machine had a duration of 6 minutes and 37 seconds with 10 phases.

2.4 Breast image analysis and region of interest (ROI) labeling

Two physicians specializing in breast imaging diagnosis with 7 years of experience who were blinded to the clinical and pathological data analyzed the breast MRI and MG images of 170 lesions, determined the location, size and boundary of tumors, evaluated the imaging characteristics of tumors, and recorded key signs. In case of disagreements, a senior doctor with 15 years of experience was invited. For breast MRI, T2WI, DWI, ADC and DCE-MRI were selected, and the sequence with the most obvious lesion enhancement contrast was selected for the DCE-MRI sequence. All lesion images were included.

ROI segmentation was performed in raw images of enrolled breast cancer lesions using the software Matlab-R2018b (Math works, Massachusetts, USA). First, the smallest square bounding box covering the tumors was determined as the input ROI for deep learning, as indicated by the radiologist analysis, as shown in Figure 2. Then, all the segmented ROI images were unified into a 224×224 size. Finally, the image was normalized by formula (1) so that the pixel value falls in the interval [0,1].

$$Norm = \frac{xi - min(x)}{max(x) - min(x)} \quad (1)$$

where xi represents the image pixel value, while $max(x)$ and $min(x)$ represent the maximum and minimum values of the image pixels, respectively.

2.5 Construction of deep learning model and training

Python and the open-source deep learning library torch and math were used to construct the deep residual network (ResNet). ResNet50 architecture and specific structure are shown in Figure 3. The training and testing were carried out on a Windows image workstation using NVIDIA GeForce GTX 2080ti GPU for parallel computing, as follows: (1) image preprocessing was completed on Matlab_R2018b (Mathworks, Massachusetts, USA), and the annotated image input

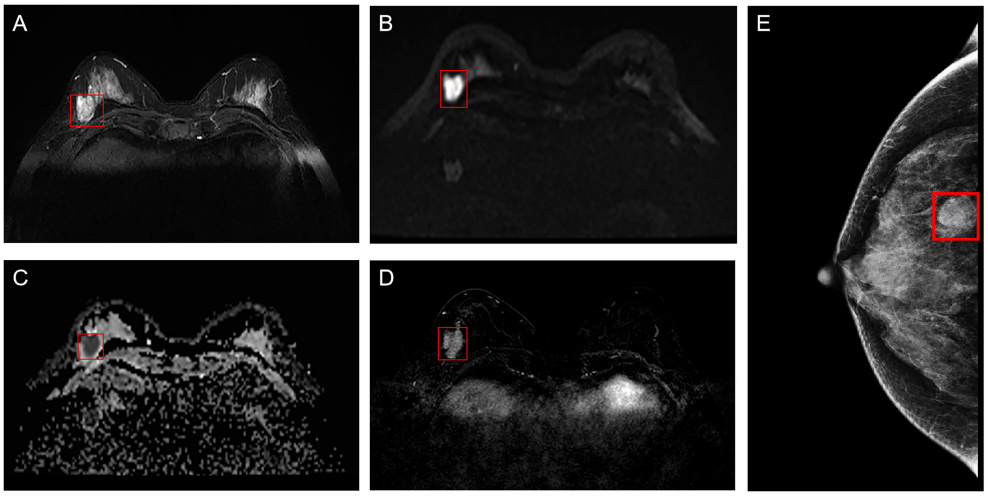

FIGURE 2
Example of ROI segmentation from raw MRI and MG images of breast cancer. **(A)** T2WI of the breast; **(B)** DWI of the breast; **(C)** ADC of the breast; **(D)** Period with the most significant enhancement in DCE-MRI of the breast; **(E)** MG of the breast. ROI, region of interest; MG, mammography; T2WI, T2-weighted imaging; DWI, diffusion weighting imaging; ADC, Apparent dispersion coefficient; DCE-MRI, dynamic contrast-enhanced magnetic resonance imaging.

was used to extract ROI; (2) the ROI images were randomly divided into a training set (n = 100), a testing set (n = 45), and a validation set (n = 25). The training set contained 50 lesions of Luminal A and 50 lesions of non-luminal A, the testing set contained 18 lesions of Luminal A and 27 lesions of non-luminal A, and the validation set contained 10 lesions of Luminal A and 15 lesions of non-luminal A. The validation set in our study belongs to an internal validation set, in order to choose the appropriate parameters for the deep learning model. The training times epoch was set to 300 times, and the size of the training set batch_size was set to 64 frames each time. The learning rate was between 0.001 and 0.0001. (3) Data augmentation was performed on the dataset, and only the training set data was expanded, mainly by performing random geometric image transformation on the original ROI image, to expand the training samples of deep learning, which is conducive to better model generalization and prevention of overfitting. (4) Under the guidance

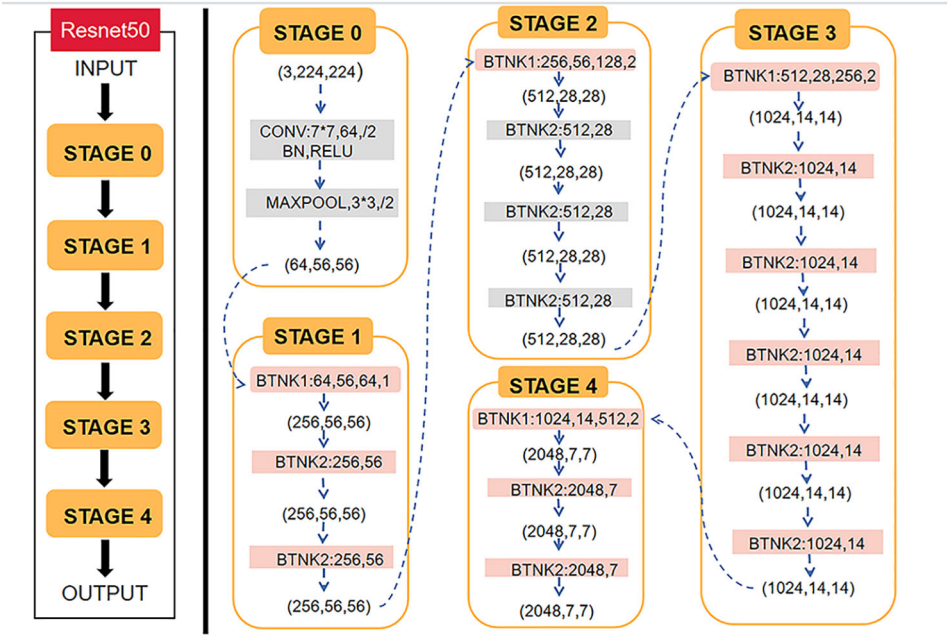

FIGURE 3
ResNet50 architecture and specific structure of each stage of ResNet50.

of the theory of residual learning, the alternate connection of the residual network structure Conv Block and Identity Block not only increases the depth of the network but also solves the degradation problem of deep learning caused by the deepening of the network. Finally, the average pooling layer and the full connection layer were used to integrate the category discriminative information extracted by the previous layer. The data were input into the feature classifier Softmax for classification, and five classification models based on MG, T2WI, DWI, ADC and DCE-MRI images of the same lesion were constructed. The classifier finally outputs the predicted probability values of the image for the Luminal A subtype. When the predicted probability value of Luminal A was > 0.5, it was classified as a Luminal A subtype; when the probability value of Luminal A was< 0.5, it was judged as a non-Luminal A subtype. (5) The classification results of the five modalities were fused by the majority voting method of the idea in ensemble learning, i.e., the category with more classification results in the five modalities is output as the final classification result of the multimodal model (Figure 4). The multi-modal model fusion process is shown in Figure 5.

2.6 Statistical analysis

SPSS 22.0 and MedCalc 15.2.2 software were used for statistical analysis. Kolmogorov-Smirnov test was used to evaluate the normality. Quantitative data conforming to normal distribution were expressed as mean ± standard deviation, while qualitative data were expressed as frequency. An independent sample t-test was used to compare age and maximum lesion diameter differences between Luminal A and non-Luminal A lesions. χ^2 test was used to compare the pathological grade, lesion margin, calcification, lymph node metastasis and time-signal intensity curve (TIC) types between Luminal A and non-Luminal A patients. P< 0.05 was considered statistically significant. Confusion matrix and receiver operating characteristic (ROC) curve analysis were used to evaluate the efficiency of single - and multimodal molecular typing. DeLong test was used to evaluate the ROC curve and area under the curve (AUC) between different models, and P< 0.05 was considered statistically significant.

3 Results

3.1 General information

A total of 422 patients who underwent mammography, breast MRI scan and enhancement examination for suspected breast cancer between December 2015 and February 2022 were included in the study. Among these, the breast cancer patients confirmed by surgical pathology and who completed pathologic examination IHC results (n = 219) were included in the study. Moreover, 49 patients were excluded because of the following reasons: receiving biopsy or neoadjuvant chemotherapy before the examination (n = 37), poor image quality, condition, and position were not up to standard, lack

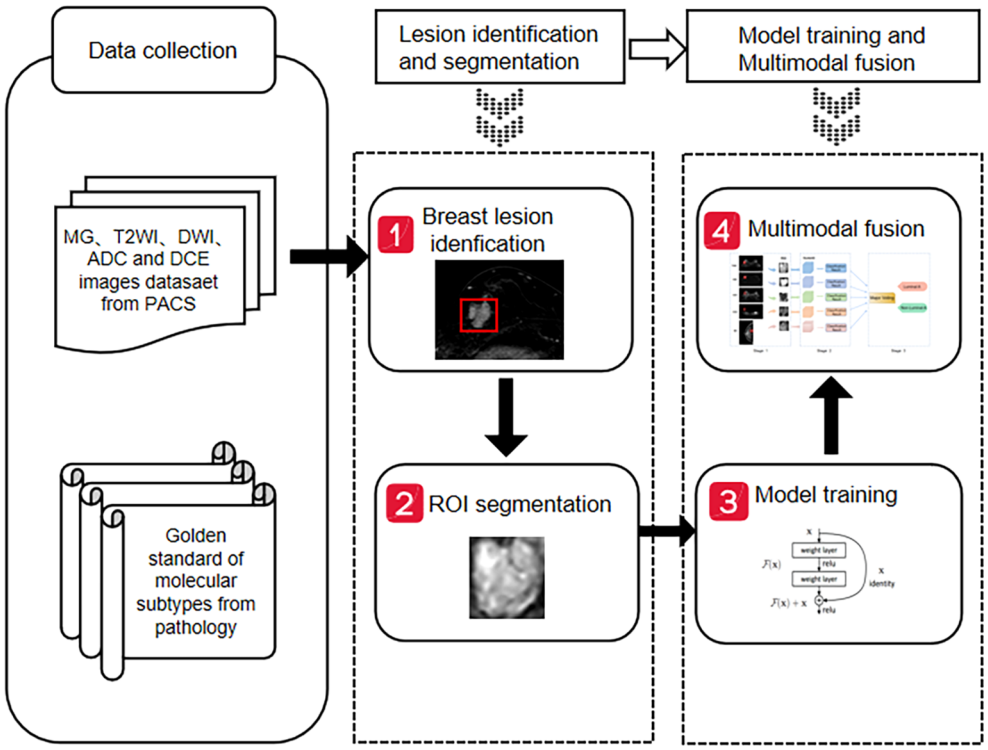

FIGURE 4
Workflow of breast cancer molecular subtypes classification.

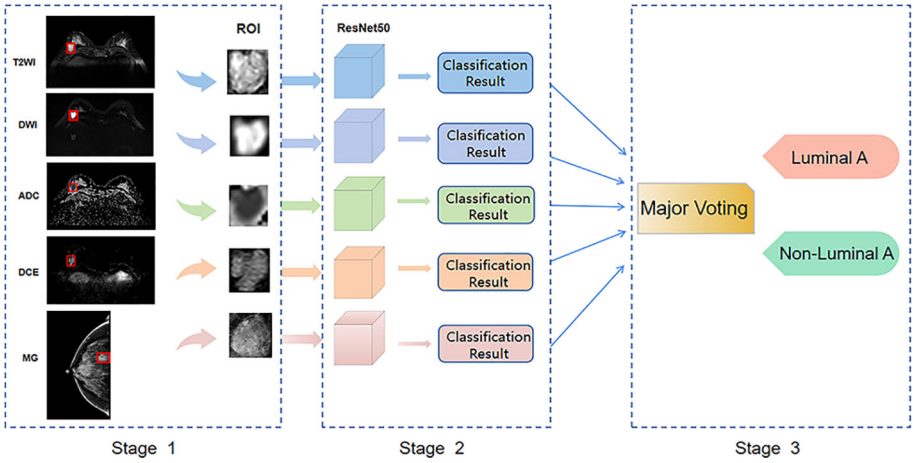

FIGURE 5
Workflow of breast cancer multi-modal fusion.

of part of the sequence (n = 7), imaging of lesions without one-to-one correspondence with postoperative pathologic results (n = 5). Finally, a total of 158 breast cancer patients (170 lesions, median age, 50.8 ± 11.0 years), among which 12 females had 2 lesions, were included in the final analysis. Pathological types included 146 lesions of invasive breast cancer, 12 of ductal carcinoma in situ, 5 of papillary carcinoma, 4 of non-invasive lobular tumor, and 3 of mucoepidermoid carcinoma. After the immunohistochemistry examination, patients were divided into 78 Luminal A subtype cases and 92 non-Luminal A subtype cases (including the 60 Luminal B lesions, 11 HER-2 lesions, and 21 triple-negative lesions). Compared with non-Luminal A subtype, Luminal A subtype lesions had a smaller tumor size (2.0 ± 0.8 cm versus 2.5 ± 1.4 cm; p = 0.007), a higher prevalence of old age (53.0 ± 11.7 years versus 48.9 ± 10.0 years; p = 0.015), a lower prevalence of axillary lymph node metastasis (ALMN) (21.8% versus 42.4%; p = 0.001), a lower pathological grade (I 39.7% versus 12.0%, II 56.4% versus 63.0%, III 3.8% versus 25.0%; p< 0.001).There were statistically significant differences in the age of breast cancer onset, the maximum diameter of the lesion, pathological grade and lymph node metastasis between the two groups (all P< 0.05), while the margin of the lesion, calcification, and TIC type were similar (all P > 0.05) (Table 1).

TABLE 1 Population characteristics.

Characteristics	Total n = 170	Luminal A n = 78	Non-Luminal A n = 92	P
Age, years	50.8 ± 11.0	53.0 ± 11.7	48.9 ± 10.0	0.015
Tumor size, cm	2.2 ± 1.2	2.0 ± 0.8	2.5 ± 1.4	0.007
Calcification	95 (55.9)	42 (53.8)	53 (57.6)	0.622
ALNM	56 (32.9)	17 (21.8)	39 (42.4)	0.004
Tumor margin				0.929
Regular	66 (38.8)	30 (38.5)	36 (39.1)	
Irregular	104 (61.2)	48 (61.5)	56 (60.9)	
TIC curve type				0.939
II	91 (53.5)	42 (53.8)	49 (53.3)	
III	79 (46.5)	36 (46.2)	43 (46.7)	
Pathological grade				<0.001
I	42 (24.7)	31 (39.7)	11 (12.0)	
II	102 (60.0)	44 (56.4)	58 (63.0)	
III	26 (15.3)	3 (3.8)	23 (25.0)	

Continuous variables are described as mean ± standard deviation (SD), and categorical variables are presented as numbers (%). ALMN, axillary lymph node metastasis; TIC, time-intensity curve.

3.2 Diagnostic efficacy of single-mode and multi-mode models in identifying molecular subtypes of breast cancer

Five models, i.e., MG, T2WI, DWI, ADC, and DCE-MRI, were applied for each patient. The accuracy, sensitivity, specificity, and AUC value of the model based on MG images were 0.533, 0.667, 0.444, and 0.593 (95%CI, 0.436-0.737), respectively; the accuracy, sensitivity, specificity, and AUC value of T2WI models were 0.667, 0.833, 0.556, and 0.700 (95%CI, 0.545-0.827), respectively; the accuracy, sensitivity, specificity, and AUC value of DWI image prediction were 0.060, 0.722, 0.519, and 0.564 (95%CI, 0.408-0.711), respectively; the accuracy, sensitivity, specificity and AUC value of ADC image prediction were 0.622, 0.722, 0.556, and 0.679 (95% CI, 0.523-0.810), respectively; the accuracy, sensitivity, specificity, and AUC value of DCE-MRI images were 0.667, 0.556, 0.741, and 0.553 (95%CI, 0.398-0.702), respectively; the accuracy, sensitivity, specificity, and AUC value of the multimodal fusion model were 0.711, 0.889, 0.593, and 0.802 (95%CI, 0.657-0.906), respectively.

Among the five single-mode models, the accuracy, sensitivity, specificity and AUC values of T2WI models were optimal, with an accuracy of 0.667 and an AUC of 0.700 (95%CI, 0.545-0.827). Yet, the multi-modal model had the best diagnostic performance in discriminating Luminal A and non-Luminal A breast cancer, with higher accuracy and sensitivity than any single-modal model but slightly lower specificity than the DCE-MRI model, as shown in Table 2; the AUC value obtained by the five single- modalities (MG, T2WI, DWI, ADC, and DCE-MRI) and multi-mode model was (0.593, 0.700, 0.564, 0.679, and 0.553) and 0.802, respectively, as shown in Table 2. The results showed that the AUC value of the multi-modal model was higher than that of any of the five single modalities, and the differences between the AUC values of a multi-modal model with MG, DWI, and DCE-MRI were statistically significant ($P< 0.05$). However, the differences between the AUC values of the multimodal model, the T2WI model, and the ADC model were not obvious ($P > 0.05$), as shown in Figure 6.

4 Discussion

In the present study, we found significant differences in the treatment and prognosis of patients with different molecular subtypes of breast cancer. Differentiating Luminal A breast cancer from non-Luminal A molecular subtype is very important to guide clinical treatment and improve prognosis. Although several diagnostic methods have been developed, the accuracy and sensitivity of those tools for differentiating breast cancer subtypes need to be further improved. This study used a deep learning model based on multimodal imaging (mammography plus MRI) to distinguish Luminal A from non-Luminal A molecular subtypes, and good diagnostic efficacy was achieved, which was superior to MG and MRI modality alone. Therefore, the deep learning method has a certain value in the differential diagnosis of molecular subtypes of breast cancer, and multimodal image information can complement each other, providing a new idea for predicting molecular subtypes of breast cancer.

The general clinical data of breast cancer have a certain role in the differentiation of molecular subtypes of breast cancer. In this study, patients with Luminal A breast cancer showed smaller maximum diameter, lower pathological grade, and fewer axillary lymph-node metastasis than non-A breast cancer, suggesting a less aggressive type of tumor, which is consistent with the results of Szep et al. (11). However, no differences in imaging features such as tumor margin, calcification and TIC type were found, which may be related to the non-A type, including the other three subtypes and the unbalanced distribution of molecular subtypes in the enrolled patients. MG and MRI features of breast cancer with different molecular subtypes are different, which is helpful for the preliminary prediction and analysis of molecular subtypes. Other studies have found that Luminal A subtype patients' tumor margins are more irregular than those of triple-negative breast cancers, with MG presenting stellar-shaped edges (12) and MRI presenting burr edges and unclear boundaries. Also, intralesional dark internal septation and no edema around the lesion were observed in patients with the Luminal A subtype, while type II TIC was more common (13, 14). However, these methods rely on limited human-extracted clinical and imaging features. More studies on deeper imaging features invisible to the naked eye are necessary.

Computer-aided diagnosis based on artificial intelligence has become a hot field in medical imaging research. At present, the reports on the identification of molecular subtypes of breast cancer based on artificial intelligence have mainly focused on radiomics. For example, machine learning technology has been used to extract radiomics features from MG, ultrasound, and DCE-MRI to

TABLE 2 Diagnostic performance of the single models and multimodal.

Modality	ACC	SEN	SPE	AUC (95%CI)	P Value*
MG	0.533	0.667	0.444	0.593 (0.436-0.737)	<0.05
T2WI	0.667	0.833	0.556	0.700 (0.545-0.827)	0.2882
DWI	0.060	0.722	0.519	0.597 (0.440-0.740)	<0.05
ADC	0.622	0.722	0.556	0.679 (0.523-0.810)	0.2778
DCE-MRI	0.667	0.556	0.741	0.553 (0.398-0.702)	<0.05
Multi-modal	0.711	0.889	0.593	0.802 (0.657-0.906)	–

MG, mammography; T2WI, T2-weighted imaging; DWI, diffusion weighting imaging; ADC, apparent dispersion coefficient; DCE-MRI, dynamic contrast-enhanced magnetic resonance imaging; ACC, accuracy; SEN, sensitivity; SPE, specificity; AUC, area under the receiver operating characteristic curve; CI, confidence interval.
*The P-value is the result meaning of comparing the AUC of each single modal and multi-modal according to the Delong's test.

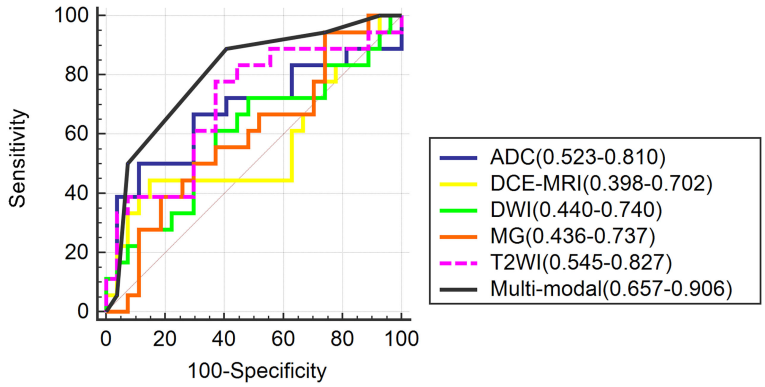

FIGURE 6
The receiver operating characteristic curves of the single models and multi-modal.

establish a model that can non-invasively and quantitatively predict molecular subtypes, but the accuracy must be improved (15–18). Deep learning is a feature learning method in machine learning, which simulates the mechanism of the human brain neural network and converts input data into multiple abstract layers in the deep neural network that can automatically learn the required abstract deep features (19). It does not require the feature extraction steps of traditional machine learning, thus reducing the dependence on the artificial selection of key features. It can also directly achieve the end-to-end effect and may improve the accurate discrimination ability of breast cancer subtypes.

So far, a few studies have reported on molecular typing based on deep learning methods using MRI data sets (20–24). For example, a previous study (25) found that MRI-enhanced features and textures contribute to identifying molecular types of breast cancer. Ha et al. (21) demonstrated that combining deep learning-enhanced MRI images and immunohistochemical indicators is useful for identifying breast cancer subtypes, as it provides a reliable basis for the treatment, management, follow-up and prognosis of breast cancer patients. Zhang et al. (22) designed a hierarchical learning structure based on convolutional neural network, which achieved a sensitivity of 0.750 and a positive prediction rate of 0.773 in tumor segmentation. This model can be used for molecular typing of breast cancer to distinguish Luminal A breast cancer from the other three subtypes at the same time. Also, the study compared the diagnostic performance of the model with the reading results of four radiologists and concluded that the performance of the model was equal or even better than that of the radiologists. Moreover, Zhu and colleagues (23) used the transfer learning method in their study to identify Luminal A type and non-Luminal A with the pre-trained VGGNet on ImageNet, and the AUC was 0.64. Zhang et al. (24) used the DCE-MRI sequence, and based on traditional convolutional neural network and convolutional long short-term memory network, the accuracy of the deep learning model was significantly improved by the transfer learning method. Yet, the above studies only used MRI images as the research object, while the deep learning model of multi-modal images is still lacking.

In the present study, a deep learning network based on ResNet50 was used to combine the multi-modal images of MG and MRI. The accuracy, sensitivity, and AUC value of the multi-modal model were higher than those of any single-modal model, but the specificity was slightly lower than that of the DCE-MRI model. Sensitivity refers to the accuracy of the true-positive prediction of the Luminal A type, while specificity refers to the accuracy of the true-negative prediction of the non-Luminal A type. The purpose of this study was to identify Luminal A breast cancer, and non-Luminal A breast cancer includes three molecular subtypes. Therefore, as an evaluation index of diagnostic ability, sensitivity was of great significance in this study, while the evaluation of specificity was limited. Meanwhile, we found that in the five single models, the AUC of the T2WI model was relatively high, almost close to the result of the multi-modal model, which indicates that the T2WI model is relatively effective in identifying Luminal A subtype breast cancer among the deep learning models based on single-mode images. The reasons may be as follows: first, the T2WI sequence is sensitive to identifying Luminal A subtype breast cancer. T2WI images can clearly show the necrosis and low signal separation in breast cancer lesions and determine whether there is peritumoral edema (14), which is consistent with the results of Gao et al. (26). Second, the Resnet50 neural network used in this study may be more suitable for T2WI images and can extract more in-depth features. In our previous study (27), T2WI combined with the Resnet50 network model also showed superior performance in predicting breast cancer lymph node metastasis. While T2WI model showed good perfomance in the single models, the accuracy, sensitivity, and specificity of the multi-modal model were higher than that of the T2WI model. In comprehensive evaluation, the multi-modal model was still a better performing model. On the other hand, and our study also found that the specificity of the DCE-MRI model showed comparative advantages in the five single models, which also suggests the potential of the DCE-MRI model in differentiating three types of non-Luminal A breast cancer, and will be the focus of our further research. Compared with the practical application of radiologists, the

diagnostic efficacy of DWI, ADC and DCE-MRI models was relatively low. This may be related to the low spatial resolution and signal-to-noise ratio of DWI and ADC images and the fact that the DCE-MRI model only selects one phase image with enhancement. The Resnet50 network may have difficulty extracting enough information from these three modalities.

Convolutional neural network (CNN) is currently the most commonly used network for deep learning in image analysis applications. In 1993, CNN was firstly introduced for medical image analysis (28). Early CNNs were relatively shallow, but demonstrated the feasibility of their ability to analyze medical images. In 2012, Hinton et al. (29) designed a CNN with five convolutional layers (also known as the "AlexNet") that won the ImageNet Large-scale Visual Recognition Challenge with a far higher accuracy rate. Due to the breakthrough performance of AlexNet, a wide upsurge of deep learning has been set off in the academic community. VGG (Visual Geometry Group) network is a pre-trained CNN model proposed by Simonyan of Oxford University in 2014 (30). VGG pre-trained on the ImageNet dataset, which contains 1.3 million images across 1,000 categories, 100,000 for training and 50,000 for validation. The structure of VGGNet is very simple. The model consists of highly connected convolutional and fully-connected layers which enables better feature extraction and, the use of Maxpooling (in the place of average pooling) for downsampling prior classification using SoftMax activation function. But the disadvantage is that it consumes more computing resources and uses more parameters, which leads to more memory usage.

In this study, we selected ResNet50 as the basic network to conduct the deep learning model. ResNet50 is a 50-layer deep convolutional neural network. Generally, deep networks can extract more abstract information from low-level feature maps, which enables them to perform better than shallow networks (31). The residue strategy of ResNet provides a skip connection to solve the degradation problem, making it possible to train a very deep network (31). Meanwhile, ResNet has smaller parameters, faster speed and higher accuracy, which provides more feasibility for advanced feature extraction and classification. To make full use of the multi-modal image features, ResNet50 was used as the basic network for feature extraction in our method. At present, it has been used in many breast cancer image classifications. Al-Tam (32) et al. utilized the ResNet50 to identify benign and malignant breast issue. In our latest work (27), Resnet50 network model also got good result in predicting breast cancer lymph node metastasis. Therefore, we chose 50-layer ResNet for this deep learning multi-modal imaging.

In this study, we adopted the idea of ensemble learning and performed multi-modal fusion on the diagnostic results of five single modalities, i.e., MG, T2WI, DWI, ADC and DCE-MRI, which were constructed using a deep learning network. Ensemble learning requires training multiple individual learners and combining multiple individual learners to form a powerful learner through a certain combination strategy. Its advantage is that the classification results of different models are independent and do not affect each other, and the judgment errors of a single model do not cause further accumulation of errors. The majority voting method in the ensemble learning strategy adopted in this study was based on the results of five single-mode classification models and adopted the principle of the obedience of the minority to the majority to determine the category label predicted by the model. In this study, the ensemble learning method was used to combine the five modalities, which made full use of the image information of each sequence and complemented and verified the information of different modalities. It improved the accuracy of identifying breast cancer molecular subtypes and was more in line with the clinical application of radiologists.

The present study has some limitations: (1) the classification proposed in this paper only focused on Luminal A and non-Luminal A breast cancer; thus, it cannot accurately distinguish the four subtypes, which is also the common limitation of most of the studies based on deep learning in breast cancer molecular typing mentioned above; (2) This was a retrospective analysis with a relatively small sample size. For our next work, we plan to use a multi-center external validation dataset and prospective validation to further confirm these findings.

These data suggest that the deep learning method has a certain value in the differential diagnosis of molecular subtypes of breast cancer, and multimodal image information can complement each other, providing a new idea for predicting molecular subtypes of breast cancer.

Data availability statement

The raw data supporting the conclusions of this article will be made available by the authors, without undue reservation.

Ethics statement

The studies involving humans were approved by the ethics committee and institutional review of Shandong Qianfoshan Hospital. The studies were conducted in accordance with the local legislation and institutional requirements. The ethics committee/institutional review board waived the requirement of written informed consent for participation from the participants or the participants' legal guardians/next of kin because of the retrospective nature of the study.

Author contributions

ML: Conceptualization, Writing-Original Draft, Writing-Review & Editing; SZ: Conceptualization, Writing-Original Draft; YD: Investigation, Data Curation, Project administration; XZ: Formal analysis, Funding acquisition; DW: Data Curation, Project administration; WR: Resources, Investigation; JS: Validation; SY: Methodology, Software; GZ: Resources, Visualization, Supervision, Funding acquisition. All authors contributed to the article and approved the submitted version.

Funding

The author(s) declare financial support was received for the research, authorship, and/or publication of this article. This study was supported by the Natural Science Foundation of Shandong Province (ZR2020MF026), Qianfoshan Hospital Nurturing Fund of NSFC (QYPY2020NSFC0603) and Health Science and Technology Development Program of Shandong Province (2019WS505).

Acknowledgments

The authors thank Mr. Kesong Wang and Mr. Xiaoming Xi from the School of Computer Science and Technology of Shandong Jianzhu University for providing us with software support and post-processing guidance.

Conflict of interest

The authors declare that the research was conducted in the absence of any commercial or financial relationships that could be construed as a potential conflict of interest.

Publisher's note

References

1. Sung H, Ferlay J, Siegel RL, Laversanne M, Soerjomataram I, Jemal A, et al. Global cancer statistics 2020: GLOBOCAN estimates of incidence and mortality worldwide for 36 cancers in 185 countries. *CA Cancer J Clin* (2021) 71:209–49. doi: 10.3322/caac.21660

2. Goldhirsch A, Winer EP, Coates AS, Gelber RD, Piccart-Gebhart M, Thürlimann B, et al. Personalizing the treatment of women with early breast cancer: Highlights of the st gallen international expert consensus on the primary therapy of early breast cancer 2013. *Ann Oncol* (2013) 24:2206–23. doi: 10.1093/annonc/mdt303

3. Sotiriou C, Neo SY, McShane LM, Korn EL, Long PM, Jazaeri A, et al. Breast cancer classification and prognosis based on gene expression profiles from a population-based study. *Proc Natl Acad Sci U S A* (2003) 100:10393–8. doi: 10.1073/pnas.1732912100

4. Voduc KD, Cheang MC, Tyldesley S, Gelmon K, Nielsen TO, Kennecke H. Breast cancer subtypes and the risk of local and regional relapse. *J Clin Oncol* (2010) 28:1684–91. doi: 10.1200/JCO.2009.24.9284

5. Autier P, Boniol M. Mammography screening: A major issue in medicine. *Eur J Cancer* (2018) 90:34–62. doi: 10.1016/j.ejca.2017.11.002

6. Morrow M, Waters J, Morris E. MRI for breast cancer screening, diagnosis, and treatment. *Lancet* (2011) 378:1804–11. doi: 10.1016/S0140-6736(11)61350-0

7. Zhang X, Li H, Wang C, Cheng W, Zhu Y, Li D, et al. Evaluating the accuracy of breast cancer and molecular subtype diagnosis by ultrasound image deep learning model. *Front Oncol* (2021) 11:623506. doi: 10.3389/fonc.2021.623506

8. Sun R, Meng Z, Hou X, Chen Y, Yang Y, Huang G, et al. Prediction of breast cancer molecular subtypes using DCE-MRI based on CNNs combined with ensemble learning. *Phys Med Biol* (2021) 66:17. doi: 10.1088/1361-6560/ac195a

9. Li X, Qin G, He Q, Sun L, Zeng H, He Z, et al. Digital breast tomosynthesis versus digital mammography: integration of image modalities enhances deep learning-based breast mass classification. *Eur Radiol* (2020) 30:778–88. doi: 10.1007/s00330-019-06457-5

10. Hadad O, Bakalo R, Ben-Ari R, Hashoul and G. Amit S. (2017). Classification of breast lesions using cross-modal deep learning, in: *2017 IEEE 14th International Symposium on Biomedical Imaging (ISBI 2017)*, Melbourne, VIC, Australia. pp. 109–12. doi: 10.1155/2022/4609625

11. Szep M, Pintican R, Boca B, Perja A, Duma M, Feier D, et al. Multiparametric MRI features of breast cancer molecular subtypes. *Medicina (Kaunas)* (2022) 58:1716. doi: 10.3390/medicina58121716

12. Taneja S, Evans AJ, Rakha EA, Green AR, Ball G, Ellis IO. The mammographic correlations of a new immunohistochemical classification of invasive breast cancer. *Clin Radiol* (2008) 63:1228–35. doi: 10.1016/j.crad.2008.06.006

13. Net JM, Whitman GJ, Morris E, Brandt KR, Burnside ES, Giger ML, et al. Relationships between human-extracted MRI tumor phenotypes of breast cancer and clinical prognostic indicators including receptor status and molecular subtype. *Curr Probl Diagn Radiol* (2019) 48:467–72. doi: 10.1067/j.cpradiol.2018.08.003

14. Navarro Vilar L, Alandete Germán SP, Medina García R, Blanc García E, Camarasa Lillo N, Vilar Samper J. MR imaging findings in molecular subtypes of breast cancer according to BIRADS system. *Breast J* (2017) 23:421–8. doi: 10.1111/tbj.12756

15. Niu S, Jiang W, Zhao N, Jiang T, Dong Y, Luo Y, et al. Intra- and peritumoral radiomics on assessment of breast cancer molecular subtypes based on mammography and MRI. *J Cancer Res Clin Oncol* (2022) 148:97–106. doi: 10.1007/s00432-021-03822-0

16. Liang X, Li Z, Zhang L, Wang D, Tian J. Application of contrast-enhanced ultrasound in the differential diagnosis of different molecular subtypes of breast cancer. *Ultrason Imaging* (2020) 42:261–70. doi: 10.1177/0161734620959780

17. Whitney HM, Taylor NS, Drukker K, Edwards AV, Papaioannou J, Schacht D, et al. Additive benefit of radiomics over size alone in the distinction between benign lesions and luminal A cancers on a large clinical breast MRI dataset. *Acad Radiol* (2019) 26:202–9. doi: 10.1016/j.acra.2018.04.019

18. Huang Y, Wei L, Hu Y, Shao N, Lin Y, He S, et al. Multi-parametric MRI-based radiomics models for predicting molecular subtype and androgen receptor expression in breast cancer. *Front Oncol* (2021) 11:706733. doi: 10.3389/fonc.2021.706733

19. Lecun Y, Bengio Y, Hinton G. Deep learning. *Nature* (2015) 521:436–44. doi: 10.1038/nature14539

20. Sun R, Meng Z, Hou X, Chen Y, Yang Y, Huang G, et al. Prediction of breast cancer molecular subtypes using DCE-MRI based on CNNs combined with ensemble learning[J]. *Phys Med Biol* (2021) 66:17. doi: 10.1088/1361-6560/ac195a

21. Ha R, Mutasa S, Karcich J, Gupta N, Pascual Van Sant E, Nemer J, et al. Predicting breast cancer molecular subtype with MRI dataset utilizing convolutional neural network algorithm. *J Digit Imaging* (2019) 32:276–82. doi: 10.1007/s10278-019-00179-2

22. Zhang J, Saha A, Zhu Z, Mazurowski MA. Hierarchical convolutional neural networks for segmentation of breast tumors in MRI with application to radiogenomics. *IEEE Trans Med Imaging* (2019) 38:435–47. doi: 10.1109/TMI.2018.2865671

23. Zhu Z, Albadawy E, Saha A, Zhang J, Harowicz MR, Mazurowski MA. Deep learning for identifying radiogenomic associations in breast cancer. *Comput Biol Med* (2019) 109:85–90. doi: 10.1016/j.compbiomed.2019.04.018

24. Zhang Y, Chen JH, Lin Y, Chan S, Zhou J, Chow D, et al. Prediction of breast cancer molecular subtypes on DCE-MRI using convolutional neural network with transfer learning between two centers. *Eur Radiol* (2021) 31:2559–67. doi: 10.1007/s00330-020-07274-x

25. Ab Mumin N, Ramli Hamid MT, Wong JHD, Rahmat K, Ng KH. Magnetic resonance imaging phenotypes of breast cancer molecular subtypes: A systematic review. *Acad Radiol* (2022) Suppl 1:S89–S106. doi: 10.1016/j.acra.2021.07.017

26. Gao W, Yang Q, Li X, Chen X, Wei X, Diao Y, et al. Synthetic MRI with quantitative mappings for identifying receptor status, proliferation rate, and molecular subtypes of breast cancer. *Eur J Radiol* (2022) 148:110168. doi: 10.1016/j.ejrad.2022.110168

27. Zhang X, Liu M, Ren W, Sun J, Wang K, Xi X, et al. Predicting of axillary lymph node metastasis in invasive breast cancer using multiparametric MRI dataset based on CNN model. *Front Oncol* (2022) 12:1069733. doi: 10.3389/fonc.2022.1069733

28. Lo SCB, Chan HP, Lin JS, Li H, Freedman MT, Mun SK. Artificial convolution neural network for medical image pattern recognition. *Neural Networks* (1995) 8:1201–14. doi: 10.1016/0893-6080(95)00061-5

29. Krizhevsky A, Sutskever I, Hinton GE. Imagenet classification with deep convolutional neural networks. *Adv Inneural Info Process Syst* (2012) 25:1097–105. doi: 10.1145/3065386

30. Simonyan K, Zisserman A. Very deep convolutional networks for large scale image recognition, *arXiv [preprint]*. (2014). Available at: https://doi.org/10.48550/arXiv.1409.1556 (Accessed Sep 4, 2014).

31. He K, Zhang X, Ren S, Sun J. (2016). Deep residual learning for image recog nition, in: *Proceedings of the IEEE Conference on Computer Vision and Pattern Recognition*, . pp. 770–8. Available at: https://doi.org/10.48550/arXiv.1512.03385 (Accessed Dec 10, 2015).

32. Al-Tam RM, Al-Hejri AM, Narangale SM, Samee NA, Mahmoud NF, Al-Masni MA, et al. A hybrid workflow of residual convolutional transformer encoder for breast cancer classification using digital X-ray mammograms. *Biomedicines* (2022) 10:2971. doi: 10.3390/biomedicines10112971

frontiers | Frontiers in Oncology

TYPE Review
PUBLISHED 19 December 2023
DOI 10.3389/fonc.2023.1273529

OPEN ACCESS

EDITED BY
Anika Nagelkerke,
University of Groningen, Netherlands

REVIEWED BY
Eva Nagele,
University Hospital Graz, Austria
Regina Barragán Carrillo,
National Institute of Medical Sciences and Nutrition Salvador Zubirán, Mexico

*CORRESPONDENCE
Lijuan Chen
xmetchenlijuan@163.com

†These authors have contributed equally to this work

RECEIVED 06 August 2023
ACCEPTED 04 December 2023
PUBLISHED 19 December 2023

CITATION
Chen L, Shen J, Jiang H, Lin H, He J, Fan S, Yang L, Yu D, Qiu R and Lin E (2023) Incidence and influencing factors of fertility concerns in breast cancer in young women: a systematic review and meta-analysis. *Front. Oncol.* 13:1273529. doi: 10.3389/fonc.2023.1273529

Incidence and influencing factors of fertility concerns in breast cancer in young women: a systematic review and meta-analysis

Lijuan Chen[1*†], Jiali Shen[2†], Hongzhan Jiang[2†], Huihui Lin[2†], Jiaxi He[3], Siyue Fan[2], Liping Yang[2], Doudou Yu[2], Rongliang Qiu[4] and Ende Lin[1]

[1]Department of General Surgery, Zhongshan Hospital of Xiamen University, School of Medicine, Xiamen, China, [2]School of Nursing, Fujian University of Traditional Chinese Medicine, Fuzhou, China, [3]School of Medicine, Xiamen University, Xiamen, China, [4]The Third Clinical Medical College of Fujian Medical University, Fuzhou, China

Objective: This systematic review and meta-analysis aimed to evaluate the prevalence and influencing factors of fertility concerns in breast cancer in young women.

Methods: A literature search on PubMed, Embase, Web of Science, and Cochrane Library databases was conducted up to February 2023 and was analyzed (Revman 5.4 software) in this study. The papers were chosen based on inclusion standards, and two researchers independently extracted the data. The included studies' quality was evaluated using criteria set out by the Agency for Healthcare Research and Quality. To identify significant variations among the risk factors, odds ratios (ORs) and the corresponding 95% confidence intervals (CIs) were utilized.

Results: A total of 7 studies that included 1579 breast cancer in young women were enrolled in the study. The results showed that for breast cancer in young women, the incidence of fertility concerns 53%(95%*CI* [0.45,0.58]). The results showed that education (2.65, 95% *CI* 1.65–5.63), full-time work (0.12, 95% *CI* 1.03–1.93), fertility intentions (7.84, 95% *CI* 1.50–37.4), depression level (1.25, 95% *CI* 1.03–1.5), and endocrine therapy (1.32, 95% *CI* 1.08–1.62) were risk factors for fertility concerns in young women with BC. Having a partner (0.41, 95% *CI* 0.33–0.5), ≥1 child (0.3, 95% *CI* 0.22–0.4) were identified as protective factors against fertility concerns in young women with BC.

Conclusions: The incidence of fertility concerns in breast cancer in young women is at a moderately high level. We should pay more attention to the risk factors of fertility concerns to help breast cancer in young women cope with their fertility concerns and promote their psychological well-being.

KEYWORDS

breast cancer, fertility concerns, women, meta-analysis, systematic review

1 Introduction

Breast cancer (BC) has the highest frequency of occurrence among global malignancies and stands as the leading cause of death in young women aged ≤40 years (1, 2). BC rates continue to rise in younger women, with an estimated 12,000 cases diagnosed annually in the United States (3). In other advanced nations, the prevalence of BC, specifically among women below the age of 40 years, is estimated to be 5–7% of all BC cases (4). BC therapies have both immediate and enduring detrimental effects on fertility, primarily stemming from the harm inflicted upon ovarian function. This harm results in conditions such as amenorrhea, premature menopause, and diminished fecundity. Therefore, young patients with BC who desire to pursue conception may face challenges because these consequences can contribute to fertility concerns (5). Consequently, patients worry about disease progression, lifespan expectations, communication with partners, emotional adaptation to potential infertility, and fertility well-being (6).

In recent years, increasing attention has been paid to oncofertility care in young adult patients with cancer (7). According to previous studies, nearly half of young individuals seeking medical care for cancer treatment also experience fertility issues (8). Additionally, >80% of young patients with cancer express a desire for spontaneous conception (9). Fertility concerns may impact patients more than the cancer itself, because they last longer and significantly reduce the quality of life of young women with BC (10). In accordance with all guidelines, patients diagnosed with any malignancy and stage at a reproductive age must receive adequate counseling on the dangers of gonadotoxicity caused by anticancer treatment at the time of diagnosis (11, 12). The management of oncofertility treatment in young women with breast cancer requires unique considerations (13). Fertility preservation and the desire for pregnancy should be pivotal in addressing fertility concerns in young women with BC (14). Despite being a major concern for patients, the adoption of fertility preservation options has been limited (15).

Therefore, determining the factors that influence fertility concerns in young women with BC is important to alleviate such concerns. Established risk factors for BC include aging, education, depression, and fertility. However, recent studies have introduced some controversies. For instance, a study by Villarreal Garza et al. reported that age is an influential factor in fertility concerns among patients with BC (9). In contrast, research conducted by Gorman et al. showed that fertility concerns among patients receiving chemotherapy are unrelated to their age (16). The present study aimed to investigate the frequency and factors contributing to fertility concerns in patients with BC through a systematic review and meta-analysis. By analyzing existing literature, the goal was to identify factors influencing fertility concerns and offer evidence-based recommendations to clinicians regarding fertility preservation and posttreatment pregnancies.

2 Materials and methods

This systematic review was conducted according to the recommendations of the Preferred Reporting Items for Systematic Reviews and Meta-analyses (PRISMA) (17). The study protocol has been registered in PROSPERO (ID: CRD42023412503).

2.1 Search strategy

Databases such as PubMed, Embase, Cochrane Library, and Web of Science were used for literature searches up to February 2023, using the following keywords: ("breast neoplasm*" OR "breast tumor*" OR "breast cancer*" OR "breast carcinoma*" OR "mammary cancer*" OR "mammary neoplasm*" OR "mammary carcinoma*") AND ("fertility concerns" OR "fertility-related concerns" OR "reproductive concerns" OR "childbearing concerns " OR "pregnancy concerns").

2.2 Selection of studies

To be included in this systematic review and meta-analysis, eligible studies had to meet the following inclusion criteria: (i) the study was conducted on female patients aged 18–40 years; (ii) patients were diagnosed with BC through pathological examination; (iii) a scale assessed the level of fertility concerns in patients; (iv) the type of study was observational; and (v) the studies were in the English language.

The exclusion criteria were: (i) conference abstracts, (ii) literature for which full text was not available or duplicate publications, (iii) literature from which data could not be extracted, and (iv) literature with a quality evaluation of <3 points.

2.3 Data extraction and quality assessment

Two researchers (Jiali Shen and HongZhan Jiang) independently screened the literature according to the inclusion standards. They excluded the literature that was irrelevant to the topic or appeared repeatedly. Subsequently, they read the remaining literature in full to determine the final selection for this study, and finally extracted and cross-checked the data. In case of disagreement or other issues, a third party (Huihui Lin) made the final decision. The first author, title, publication date, sample size, measurement tools, and patient age were extracted from all included studies.

The evaluation of literature quality was independently conducted by two researchers using the evaluation criteria recommended by the Agency for Healthcare Research and Quality (18). The evaluation comprised 11 items, which were answered with "Yes," "No," or "Unclear." Each answer of "Yes" was scored as one point, while the opposite was scored as zero points, out of a total of 11 points. A score of ≥8 indicated high quality, 4–7 denoted medium quality, and ≤3 indicated low quality. In cases of disagreement, an agreement was reached through discussion.

2.4 Data analysis

Statistical analyses were performed using RevMan 5.4 software (https://revman.cochrane.org). The odds ratio (OR) or relative risk (RR) values (95% confidence interval [CI]) for factors influencing fertility concerns in young female patients with cancer were extracted as effect sizes. Heterogeneity was assessed using the Q

test. If P >0.1 and I^2 <50%, it indicated no significant heterogeneity among the studies, and a fixed-effect model was selected; conversely, if P <0.05, it indicated a significant difference, and a random-effect model was selected. To assess the reliability of the meta-analysis, random- and fixed-effect models were analyzed separately, and the robustness of the meta-analysis results was calculated.

3 Results

3.1 Study selection

Following an initial literature search across PubMed, Embase, Cochrane Library, and Web of Science databases, 2041 articles were identified. After excluding duplicates and irrelevant studies (Endnote X 9.1), 1343 potentially relevant articles remained. Among these, 1334articles were excluded after reviewing titles or abstracts. After thoroughly reading the full texts of the remaining nine articles, two studies were excluded due to the unavailability of data. Finally, seven studies were included in this meta-analysis (Figure 1).

3.2 Characteristics of the included studies

Seven studies included a total of 1579 patients, including five cross-sectional studies (9, 16, 19–21) and two prospective cohort studies (22, 23). Five studies (9, 16, 19, 22, 23) were of high quality, and two (20, 21) were of moderate quality, resulting in an overall moderate to high quality. The basic characteristics and quality evaluation scores of the included studies are listed in Table 1.

3.3 Prevalence of fertility concerns among breast cancer patients

The prevalence of fertility concerns in young women with BC ranged from 36% to 64%, and heterogeneity was observed after combination treatment (I^2 = 100%, P <0.00001). Therefore, using a random-effect model, the prevalence of fertility concerns in young women with BC after combination therapy was 53% (95% *CI* 0.45–0.58).

3.4 Factors affecting fertility concerns

Two studies revealed depression, four reported ≥1 child, three reported endocrine therapy, and four reported genetic factors (cancer in the immediate family) as influencing factors of fertility concerns in young women with BC, which showed less heterogeneity (I^2 ≤50%, P >0.1). Therefore, a fixed-effect model was used. Four studies revealed age, four reported education, three reported having a partner, three reported economic level, three reported fertility intention, three reported surgery, four reported

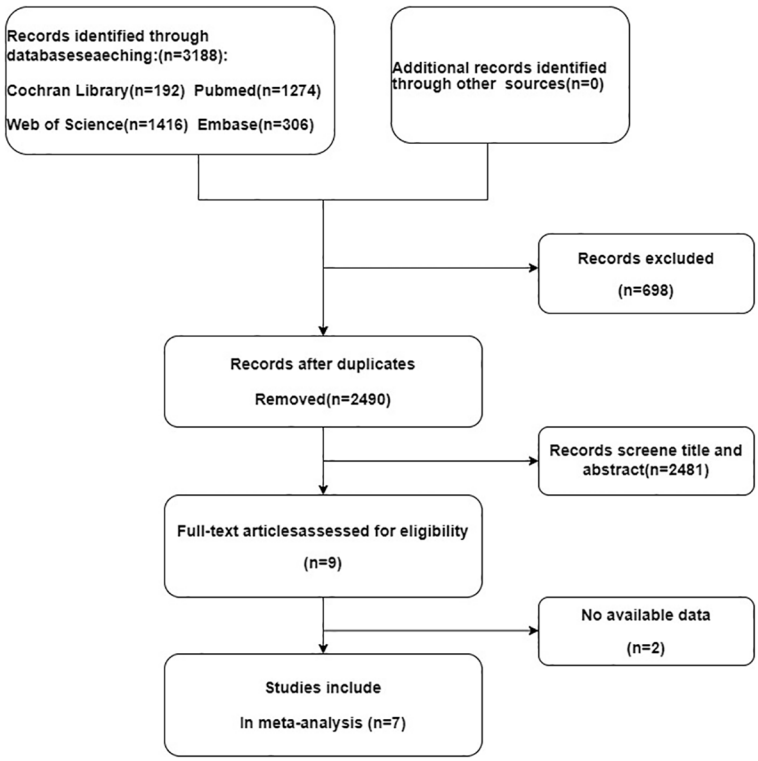

FIGURE 1
Study flow diagram.

TABLE 1 The characteristics of the included studies.

Author	Year	Country	Instrument	Sample size	Aged (Years)	Type of Study	Prevalence	Influence factor	Quality assessment
Villarreal Garza C et al. (12)	2017	Mexico	FIS	134	34.6	Cross-sectional	44%	CDFGHIJ	8
Gorman JR et al. (13)	2010	USA	RCS	131	36.7	Cross-sectional	64%	AFG	8
Ba´rtolo A et al. (16)	2019	Portuguesa	RACA	104	36.1 ± 3.03	Cross-sectional	36%	K	6
LjungmanL et al. (17)	2018	Sweden	RACA	181	34.6 ± 4.1	Cross-sectional	56%	BFIJ	9
Ruggeria M et al. (18)	2014	Switzerland Italy	RACA	297	18-40	Cohort study	58%	ABCDEGHIJL	8
Ruddy KJ et al. (19)	2014	USA	FIS	620	17-40	Cohort study	51%	ABCDEGHIJKL	8
Jiajia Qiu et al. (20)	2022	China	RACA	112	21-40	Cross-sectional	–	ABG	6

A, age; B, education; C, With partner; D, economic; E, genetic; F, desire to have children; G, >1 child; H, surgery; I, chemotherapy; J, endocrine therapy; K, depression; L, full-time job FIS, Fertility Issues and Outcomes Scale; RCAC, Reproductive Concerns After Cancer Scale; RCS, reproductive concerns scale.
"–", No data available.

chemotherapy, and two reported full-time work as factors influencing fertility concerns in young women with BC, and these were found to be heterogeneous (I^2 ≥50%, P <0.1). Thus, a random-effect model was used.

The results showed that education (2.65, 95% *CI* 1.65–5.63), full-time work (0.12, 95% *CI* 1.03–1.93), fertility intentions (7.84, 95% *CI* 1.50–37.4), depression level (1.25, 95% *CI* 1.03–1.5), and endocrine therapy (1.32, 95% *CI* 1.08–1.62) were risk factors for fertility concerns in young women with BC. Having a partner (0.41, 95% *CI* 0.33–0.5), ≥1 child (0.3, 95% *CI* 0.22–0.4) were identified as protective factors against fertility concerns in young women with BC (Table 2; Figure 2).

3.5 Sensitivity analysis and publication bias

The sensitivity analysis of the seven studies was performed by excluding each study one by one, and the results did not change significantly, suggesting good stability of the results. Egger's test was conducted to evaluate potential publication bias. The results

TABLE 2 Meta-analysis of risk factors of fertility concerns in breast cancer patients.

Influencing factors	Combination studies	*Heterogeneity of study design*		Analysis model	OR (95%*CI*)	P_2	Egger's test
		I^2	P_1				
Full-time work	2	51%	0.15	Random	1.41[1.03,1.93]	**0.03**	NA
Age	4	97%	<0.00001	Random	0.63[0.14,2.85]	0.54	0.761
Education	4	82%	0.0007	Random	2.65[1.65,5.63]	**0.01**	0.075
Economic	3	55%	0.11	Random	0.89[0.63,1.26]	0.51	0.536
Fertility intentions	3	88%	0.0003	Random	7.84[1.50,37.40]	**0.01**	0.815
With partner	3	75%	0.02	Random	0.41[0.33,0.50]	**<0.00001**	0.374
Depression	2	0%	0.62	Fixed	1.25[1.03,1.52]	**0.02**	NA
≥1 child	4	19%	0.29	Fixed	0.3[0.22,0.40]	**<0.00001**	0.273
Surgery	3	71%	0.03	Random	0.72[0.47,1.11]	0.14	0.859
Chemotherapy	4	55%	0.08	Random	1.38[0.96,2.00]	0.08	0.433
Endocrine therapy	4	14%	0.32	Fixed	1.32[1.08,1.62]	**0.008**	0.225
Genetic	2	0%	0.92	Fixed	1.07[0.71,1.60]	0.74	NA

NA: Insufficient number for Egger's test.The bold values: Nominal p-value <0.05.

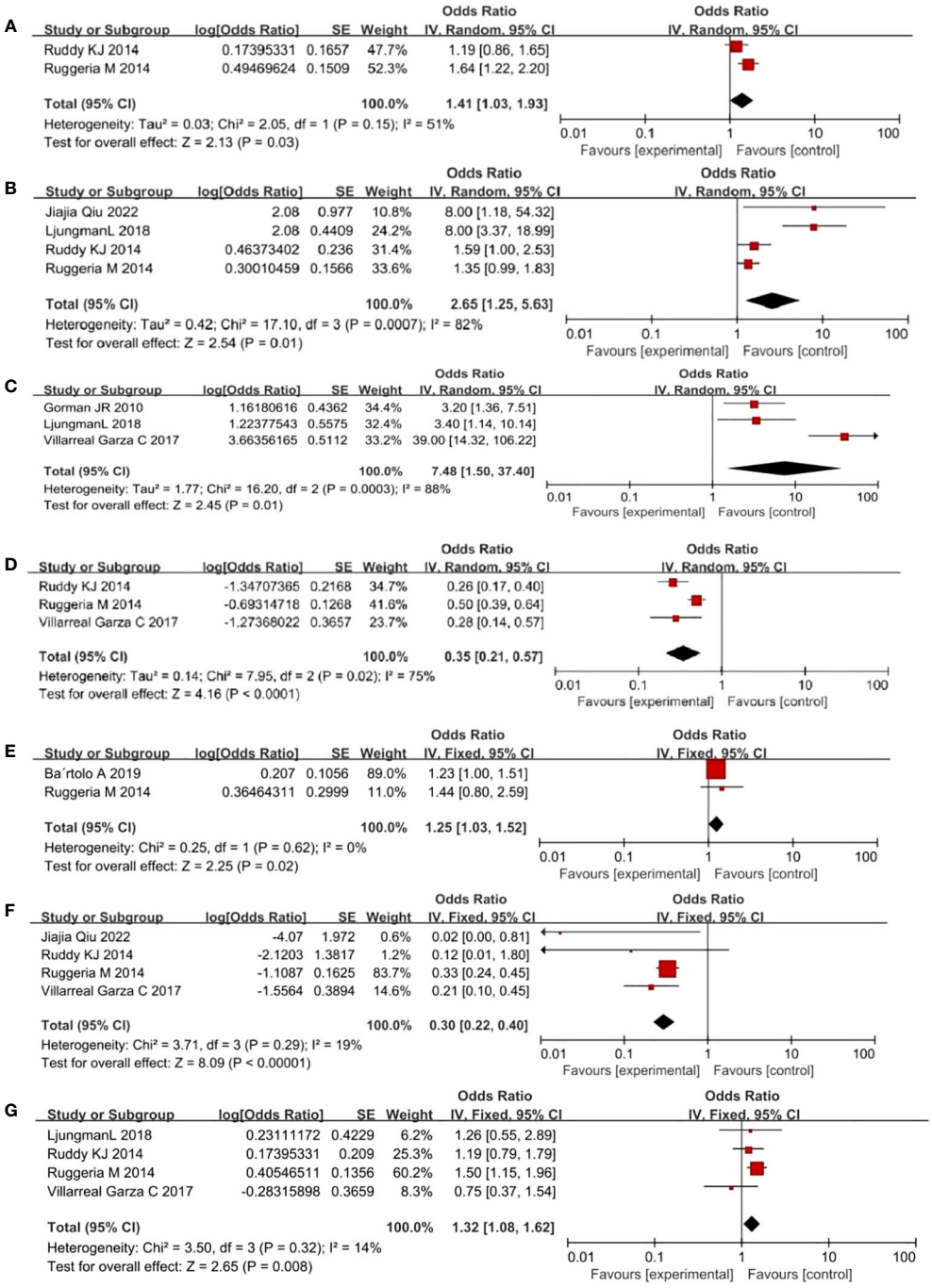

FIGURE 2
Forest plot of risk factors in breast cancer in young women. ((**A**) full-time work **(B)** education **(C)** desire to have children **(D)** with partner **(E)** depression **(F)** ≥ 1 child **(G)** endocrine therapy. Horizontal lines: 95% confidence intervals for study results, Square boxes: Effect quantity for a single study, Diamonds: Merged results, Vertical lines: Invalid line, determining whether the difference in results is statistically significant or not.).

revealed that most risk factors did not have publication bias (P >0.05; Table 2).

4 Discussion

The seven studies included in this systematic review and meta-analysis specified the inclusion and exclusion criteria of the study patients, assessment methods, and correct use of statistical methods. The quality of the literature met the requirements with high reliability. The prevalence of fertility concerns among young patients with BC in this study was 53%, which is relatively high. It is lower than the results of the high-concern group by Gorman JR et al. in the United States at 56% (16); however, it is higher than the results reported by Bartolo A et al., where 35.6% of this sample presented moderate-to-high overall reproductive concerns in

Portugal (20). This difference may be attributed to variations in countries, cultures, and ideologies. Nevertheless, our study shows that a significant proportion of patients with BC are already affected by fertility concerns or will be affected shortly. Therefore, more attention should be paid to helping these patients cope with their fertility concerns and promoting their psychological well-being.

Education was identified as a risk factor for the development of fertility concerns in young women with BC, likely related to the increased informational needs of more literate patients about the disease and fertility. Studies have indicated that highly educated BC patients require more information (24). Patients are more prone to experiencing emotional issues, such as despair and anxiety, when their information needs are not being satisfied. A foreign survey (25) revealed that only 30% of patients with cancer had received health guidance on fertility protection, and merely 23.4% of patients with BC received fertility counseling during treatment (26). In the United States and the United Kingdom, 30–60% of cancer survivors of reproductive age reported having no information on cancer fertility protection (27). Healthcare professionals should prioritize enhancing fertility-related information and education after BC diagnosis to provide patients with high-quality, credible, and evidence-based information about fertility through various channels, including the internet and social media. Thus, the fertility knowledge needs of patients with BC can be met.

Full-Time work increases the risk of reproductive issues in young women with BC, potentially due to concerns that their jobs might be negatively impacted by disease treatment (28). Patients whose work is affected may face a greater financial burden, including the cost of treatment, costs related to the risk of future pregnancy and potential health problems of their children. This situation can lead to difficulties in fertility decision-making and heightened levels of fertility concerns (29). Providing adequate information support, especially for patients working full-time, is important. Fertility education has a positive effect on improving disease-related knowledge and anxiety. Stark et al. (30) and Su et al. (31) developed an internet-based survivor reproductive healthcare program that provided online reproductive health and fertility education; it reduced the level of fertility concerns among BC survivors. Fertility counseling and educational intervention services are required to lessen the lack of knowledge that causes concerns about fertility.

Fertility intention was identified as a risk factor for fertility concerns, representing the subjective expectation of having children. This expectation involves considerations such as the number, sex, timing, spacing, and quality of children. Additionally, this expectation stems from a person's basic needs and is influenced by various circumstances (32). When their behavior does not meet their psychological expectations for various reasons, they experience different degrees of apprehension. Patients with strong fertility intentions are more concerned about the impact of tumors and related treatments on their reproductive function, and excessive attention to this aspect is likely to cause heightened worry. According to some studies, implementing fertility preservation can alleviate patients' concerns about fertility (33). Several nations have developed guidelines for fertility preservation in oncology that suggest providing patients fertility preservation counseling before treatment (11, 12). The guidelines and practicing physicians suggest the use of embryo cryopreservation, cryopreservation of unfertilized oocytes, ovarian transposition and suppression, and ovarian tissue cryopreservation and transplantation for fertility preservation (34). The implementation of fertility preservation still requires the joint efforts of the government and all medical personnel.

In this study, depression was found to be a risk factor for fertility concerns. The news of a tumor diagnosis is extremely upsetting for the patient and can result in decreased quality of life, fewer social opportunities, and increased financial burden—all of which can quickly lead to depression. Fertility concerns remain a contributor to depression risk, with each additional contributor increasing the likelihood of depression by 2.423 times (35). BC may impair the integrity of the secondary sexual characteristics in female patients, which may lead to long-term feelings of self-blame and inferiority, making it more likely to cause depression (36). Therefore, medical personnel should pay attention to patients' psychological states to identify and provide timely relief. According to practicing physicians' recommendations, positive stress-reduction therapy reduces depression levels. For example, encouraging an increase in physical activity (37), contemplation (38), and mindfulness-based stress reduction (39) can improve mental health and reduce depression levels.

Studies have shown that having ≥1 child and having a partner are protective factors against fertility concerns in patients with BC. As the basic unit of society, a sound family typically includes children; therefore, patients who already have children do not face the demands and pressure from their husbands and other family members to have more children (40). Children can also act as caregivers, sharing the emotional and psychological stresses that tumors bring to patients. Patients with partners tend to have more stable and intimate relationships. Moreover, good family intimacy can enhance the willingness and efficacy of self-expression between patients and their family members. Patients can actively and flexibly utilize the available resources around them, obtaining emotional and material support from their spouses, family members, and friends; the more tolerance and care patients feel, the better it helps them readjust to stressful events. Additionally, the patient's self-expression process helps family members or friends identify the patient's concerns and provide relief. This, in turn, stimulates the patient to express positive emotions, build positive cognition, and alleviate concerns due to fertility problems (41).

4.1 Study limits

This systematic review and meta-analysis had several limitations. First, we included only English-language literature from the four databases, which may have resulted in insufficient retrieval. Second, some risk factor indicators in this meta-analysis were not combined effectively because of the limited amount of available literature, which may have affected the results. Third, because the research methods, study populations, and observational periods varied among the included studies, the findings were dispersed and heterogeneous. Therefore, prospective cohort studies with multicenter approaches and larger sample sizes are required to increase the effect size and enrich the results.

5 Conclusion

Through this systematic review and meta-analysis, we examined the prevalence of and factors contributing to fertility concerns among young women with BC. The results revealed a high prevalence of concern about fertility in this population. Education, full-time work, fertility intentions, depression, and endocrine therapy were identified as risk factors for fertility concerns in young women with BC. Having partners and ≥1 child were protective factors against fertility concerns in young patients with BC. The results of the present study can be used as a basis for better planning to address fertility concerns and offer evidence-based recommendations for clinicians regarding fertility preservation and post-treatment pregnancies.

Author contributions

JS: Writing – original draft, Writing – review & editing. HJ: Data curation, Supervision, Validation, Writing – review & editing. HL: Supervision, Writing – review & editing. EL: Supervision, Validation, Writing – review & editing. JH: Conceptualization, Data curation, Supervision, Writing – review & editing. RQ: Conceptualization, Methodology, Supervision, Writing – review & editing. SF: Supervision, Validation, Writing – review & editing. DY: Data curation, Investigation, Supervision, Visualization, Writing – review & editing. LY: Data curation, Methodology, Supervision, Writing – review & editing. LC: Writing – review & editing.

Funding

The author(s) declare financial support was received for the research, authorship, and/or publication of this article. This study is supported by the nursing research project of Zhongshan Hospital affiliated with Xiamen University (2023zsyyhlky-002).

Acknowledgments

We thank the staff of the Zhongshan Hospital affiliated with Xiamen University for supporting the research.

Conflict of interest

The authors declare that the research was conducted in the absence of any commercial or financial relationships that could be construed as a potential conflict of interest.

Publisher's note

References

1. Miller KD, Fidler-Benaoudia M, Keegan TH, Hipp HS, Jemal A, Siegel RL. Cancer statistics for adolescents and young adults, 2020. *CA Cancer J Clin* (2020) 70:443–59. doi: 10.3322/caac.21637

2. You L, Lv Z, Li C, Ye W, Zhou Y, Jin J, et al. Worldwide cancer statistics of adolescents and young adults in 2019: a systematic analysis of the Global Burden of Disease Study 2019. *ESMO Open* (2021) 6:100255. doi: 10.1016/j.esmoop.2021.100255

3. Kim HJ, Kim S, Freedman RA, Partridge AH. The impact of young age at diagnosis (age <40 years) on prognosis varies by breast cancer subtype: A U.S. SEER database analysis. *Breast Edinb Scotl* (2022) 61:77–83. doi: 10.1016/j.breast.2021.12.006

4. Ellington TD, Miller JW, Henley SJ, Wilson RJ, Wu M, Richardson LC. Trends in breast cancer incidence, by race, ethnicity, and age among women aged ≥20 years - United States, 1999-2018. *MMWR Morb Mortal Wkly Rep* (2022) 71:43–7. doi: 10.15585/mmwr.mm7102a2

5. Murphy D, Klosky JL, Reed DR, Termuhlen AM, Shannon SV, Quinn GP. The importance of assessing priorities of reproductive health concerns among adolescent and young adult patients with cancer. *Cancer* (2015) 121:2529–36. doi: 10.1002/cncr.29466

6. Nair S, Raj A, Saggurti N, Naik DD, Dasgupta A, Balaiah D. Reproductive health concerns of women contending with spousal violence and husband's alcohol use in a Mumbai slum community. *Int J Gynaecol Obstet Off Organ Int Fed Gynaecol Obstet.* (2013) 122:268–9. doi: 10.1016/j.ijgo.2013.04.009

7. Lambertini M, Kim HJ, Poorvu P. Editorial: breast cancer in young women: dedicated research efforts are needed. *Front Oncol* (2022) 12:913167. doi: 10.3389/fonc.2022.913167

8. Lampic C, Ljungman L, Micaux Obol C, Eriksson LE, Wettergren L. A web-based psycho-educational intervention (Fex-Can) targeting sexual dysfunction and fertility-related distress in young adults with cancer: study protocol of a randomized controlled trial. *BMC Cancer.* (2019) 19:344. doi: 10.1186/s12885-019-5518-3

9. Villarreal-Garza C, Martinez-Cannon BA, Platas A, Mohar A, Partridge AH, Gil-Moran A, et al. Fertility concerns among breast cancer patients in Mexico. *Breast Edinb Scotl.* (2017) 33:71–5. doi: 10.1016/j.breast.2017.02.010

10. Ulrich ND, Raja NS, Moravek MB. A review of fertility preservation in patients with breast cancer. *Best Pract Res Clin Obstet Gynaecol.* (2022) 82:60–8. doi: 10.1016/j.bpobgyn.2022.01.004

11. Lambertini M, Peccatori FA, Demeestere I, Amant F, Wyns C, Stukenborg J-B, et al. Fertility preservation and post-treatment pregnancies in post-pubertal cancer patients: ESMO Clinical Practice Guidelines†. *Ann Oncol* (2020) 31:1664–78. doi: 10.1016/j.annonc.2020.09.006

12. Anderson RA, Amant F, Braat D, D'Angelo A, Chuva de Sousa Lopes SM, Demeestere I, et al. ESHRE guideline: female fertility preservation†. *Hum Reprod Open* (2020) 2020(4):hoaa052. doi: 10.1093/hropen/hoaa052

13. Carr AL, Roberts S, Bonnell LN, Kolva E. Existential distress and meaning-making among female breast cancer patients with cancer-related fertility concerns. *Palliat Support Care* (2022) 1–9. doi: 10.1017/S1478951522001675

14. Razeti MG, Soldato D, Arecco L, Levaggi A, Puglisi S, Solinas C, et al. Approaches to fertility preservation for young women with breast cancer. *Clin Breast Cancer.* (2023) 23:241–8. doi: 10.1016/j.clbc.2023.01.006

15. Wang SSY, Loong H, Chung JPW, Yeo W. Preservation of fertility in premenopausal patients with breast cancer. *Hong Kong Med J Xianggang Yi Xue Za Zhi.* (2020) 26:216–26. doi: 10.12809/hkmj198268

16. Gorman JR, Malcarne VL, Roesch SC, Madlensky L, Pierce JP. Depressive symptoms among young breast cancer survivors: the importance of reproductive concerns. *Breast Cancer Res Treat* (2010) 123:477–85. doi: 10.1007/s10549-010-0768-4

17. Page MJ, McKenzie JE, Bossuyt PM, Boutron I, Hoffmann TC, Mulrow CD, et al. The PRISMA 2020 statement: an updated guideline for reporting systematic reviews. *BMJ* (2021) 372:n71. doi: 10.1136/bmj.n71

18. Farquhar M. AHRQ quality indicators. In: Hughes RG, editor. *Patient Saf Qual Evid-Based Handb Nurses*. Rockville (MD: Agency for Healthcare Research and Quality (US (2008). Available at: http://www.ncbi.nlm.nih.gov/books/NBK2664/.

19. Ljungman L, Ahlgren J, Petersson L-M, Flynn KE, Weinfurt K, Gorman JR, et al. Sexual dysfunction and reproductive concerns in young women with breast cancer:

Type, prevalence, and predictors of problems. *Psychooncology* (2018) 27:2770–7. doi: 10.1002/pon.4886

20. Bártolo A, Santos IM, Valério E, Monteiro S. Depression and health-related quality of life among young adult breast cancer patients: the mediating role of reproductive concerns. *J Adolesc Young Adult Oncol* (2020) 9:431–5. doi: 10.1089/jayao.2019.0144

21. Qiu J, Tang L, Li P, Fu J. An investigation into the reproductive concerns of young women with breast cancer. *Asia-Pac J Oncol Nurs.* (2022) 9:100055. doi: 10.1016/j.apjon.2022.03.007

22. Ruddy KJ, Gelber SI, Tamimi RM, Ginsburg ES, Schapira L, Come SE, et al. Prospective study of fertility concerns and preservation strategies in young women with breast cancer. *J Clin Oncol Off J Am Soc Clin Oncol* (2014) 32:1151–6. doi: 10.1200/JCO.2013.52.8877

23. Ruggeri M, Pagan E, Bagnardi V, Bianco N, Gallerani E, Buser K, et al. Fertility concerns, preservation strategies and quality of life in young women with breast cancer: Baseline results from an ongoing prospective cohort study in selected European Centers. *Breast Edinb Scotl.* (2019) 47:85–92. doi: 10.1016/j.breast.2019.07.001

24. Albada A, van Dulmen S, Lindhout D, Bensing JM, Ausems MGEM. A pre-visit tailored website enhances counselees' realistic expectations and knowledge and fulfils information needs for breast cancer genetic counselling. *Fam Cancer.* (2012) 11:85–95. doi: 10.1007/s10689-011-9479-1

25. Gwede CK, Vadaparampil ST, Hoffe S, Quinn GP. The role of radiation oncologists and discussion of fertility preservation in young cancer patients. *Pract Radiat Oncol* (2012) 2:242–7. doi: 10.1016/j.prro.2011.12.001

26. Ju J, Zhang LX, Yue J, Zhu AJ, Wang JY, Luo Y, et al. [An investigation of the fertility needs of young patients with breast cancer]. *Zhonghua Zhong Liu Za Zhi.* (2020) 42(5):408–12. doi: 10.3760/cma.j.cn112152-112152-20191017-00672

27. Shnorhavorian M, Harlan LC, Smith AW, Keegan THM, Lynch CF, Prasad PK, et al. Fertility preservation knowledge, counseling, and actions among adolescent and young adult patients with cancer: A population-based study. *Cancer* (2015) 121:3499–506. doi: 10.1002/cncr.29328

28. Benedict C, Thom B, Kelvin JF. Fertility preservation and cancer: challenges for adolescent and young adult patients. *Curr Opin Support Palliat Care* (2016) 10:87–94. doi: 10.1097/SPC.0000000000000185

29. Maeda E, Nakamura F, Kobayashi Y, Boivin J, Sugimori H, Murata K, et al. Effects of fertility education on knowledge, desires and anxiety among the reproductive-aged population: findings from a randomized controlled trial. *Hum Reprod Oxf Engl* (2016) 31:2051–60. doi: 10.1093/humrep/dew133

30. Stark SS, Natarajan L, Chingos D, Ehren J, Gorman JR, Krychman M, et al. Design of a randomized controlled trial on the efficacy of a reproductive health survivorship care plan in young breast cancer survivors. *Contemp Clin Trials.* (2019) 77:27–36. doi: 10.1016/j.cct.2018.12.002

31. Irene Su H, Stark S, Kwan B, Boles S, Chingos D, Ehren J, et al. Efficacy of a web-based women's health survivorship care plan for young breast cancer survivors: a randomized controlled trial. *Breast Cancer Res Treat* (2019) 176:579–89. doi: 10.1007/s10549-019-05260-6

32. Yang Y, He R, Zhang N, Li L. Second-child fertility intentions among urban women in China: A systematic review and meta-analysis. *Int J Environ Res Public Health* (2023) 20:3744. doi: 10.3390/ijerph20043744

33. Logan S, Perz J, Ussher J, Peate M, Anazodo A. Clinician provision of oncofertility support in cancer patients of a reproductive age: A systematic review. *Psychooncology* (2018) 27:748–56. doi: 10.1002/pon.4518

34. Oktay K, Harvey BE, Partridge AH, Quinn GP, Reinecke J, Taylor HS, et al. Fertility preservation in patients with cancer: ASCO clinical practice guideline update. *J Clin Oncol Off J Am Soc Clin Oncol* (2018) 36:1994–2001. doi: 10.1200/JCO.2018.78.1914

35. Gorman JR, Su HI, Roberts SC, Dominick SA, Malcarne VL. Experiencing reproductive concerns as a female cancer survivor is associated with depression. *Cancer* (2015) 121:935–42. doi: 10.1002/cncr.29133

36. Liang C, Chung H-F, Dobson AJ, Hayashi K, van der Schouw YT, Kuh D, et al. Infertility, recurrent pregnancy loss, and risk of stroke: pooled analysis of individual patient data of 618 851 women. *BMJ* (2022) 377:e070603. doi: 10.1136/bmj-2022-070603

37. Pearce M, Garcia L, Abbas A, Strain T, Schuch FB, Golubic R, et al. Association between physical activity and risk of depression: A systematic review and meta-analysis. *JAMA Psychiatry* (2022) 79:550–9. doi: 10.1001/jamapsychiatry.2022.0609

38. Wielgosz J, Goldberg SB, Kral TRA, Dunne JD, Davidson RJ. Mindfulness meditation and psychopathology. *Annu Rev Clin Psychol* (2019) 15:285–316. doi: 10.1146/annurev-clinpsy-021815-093423

39. Ladenbauer S, Singer J. Can mindfulness-based stress reduction influence the quality of life, anxiety, and depression of women diagnosed with breast cancer? -A review. *Curr Oncol Tor Ont.* (2022) 29:7779–93. doi: 10.3390/curroncol29100615

40. Yamashita A, Yoshioka S-I. Resilience associated with self-disclosure and relapse risks in patients with alcohol use disorders. *Yonago Acta Med* (2016) 59(4):279–87.

41. Naik H, Leung B, Laskin J, McDonald M, Srikanthan A, Wu J, et al. Emotional distress and psychosocial needs in patients with breast cancer in British Columbia: younger versus older adults. *Breast Cancer Res Treat* (2020) 179:471–7. doi: 10.1007/s10549-019-05468-6

frontiers | Frontiers in Oncology

TYPE Case Report
PUBLISHED 08 January 2024
DOI 10.3389/fonc.2023.1332862

OPEN ACCESS

EDITED BY
Francesca Bianchi,
University of Milan, Italy

REVIEWED BY
J. Guilherme Gonçalves - Nobre,
University of Lisbon, Portugal
Andrea Shields,
University of Connecticut Health Center,
United States

*CORRESPONDENCE
Tommaso Susini
tommaso.susini@unifi.it

RECEIVED 03 November 2023
ACCEPTED 08 December 2023
PUBLISHED 08 January 2024

CITATION
Innocenti A, Susini P, Grimaldi L and Susini T (2024) Breast cancer in pregnancy: concurrent cesarean section, nipple-sparing mastectomy, and immediate breast reconstruction—case report.
Front. Oncol. 13:1332862.
doi: 10.3389/fonc.2023.1332862

Breast cancer in pregnancy: concurrent cesarean section, nipple-sparing mastectomy, and immediate breast reconstruction—case report

Alessandro Innocenti[1], Pietro Susini[2], Luca Grimaldi[2] and Tommaso Susini[3]*

[1]Plastic and Reconstructive Microsurgery, Careggi University Hospital, Florence, Italy, [2]Plastic Surgery Unit, Department of Medicine, Surgery and Neuroscience, University of Siena, Siena, Italy, [3]Breast Unit, Gynecology Section, Department of Health Sciences, University of Florence, Florence, Italy

Background: Pregnancy-associated breast cancer (PABC), with an incidence rate from 1:3,000 to 1:10,000 deliveries, is the most frequent cancer during pregnancy. PABC appropriate management must take into consideration both the maternal oncological safety and the fetal health, thus posing a challenge for the mother, the baby, and the clinicians. The treatment should adhere as closely as possible to the breast cancer (BC) guidelines. Therefore, surgery is a mainstay, and, when mastectomy is required, breast reconstruction (BR) is a topic of debate. To minimize the risks to the baby, most surgeons postpone BR to delivery. However, a delayed breast reconstruction (DBR) could affect the outcome. In the present case, we report cesarean section concurrent with mastectomy and immediate breast reconstruction (IBR).

Methods: A 37-year-old patient, at the 36th week of pregnancy with PABC, underwent simultaneous cesarean delivery, nipple-sparing mastectomy, and IBR. To minimize risks for the newborn, cesarean was firstly performed under spinal anesthesia. Immediately after, breast surgery, including mastectomy and IBR, was performed under general anesthesia. Partial submuscular IBR with an acellular porcine dermal matrix concluded the surgical procedure. Lactation was inhibited, and adjuvant chemotherapy and hormone therapy were administered to the patient.

Results: In a single surgical session, cesarean delivery, subcutaneous mastectomy, axillary dissection, and IBR were successfully carried out. No early or late postoperative complications were reported for both the patient and the newborn. Histopathological investigation reported a multifocal and multicentric infiltrating ductal carcinoma. After a 6-year follow-up, the patient is alive and well.

Conclusion: To the best of our knowledge, this is the first reported case of concomitant cesarean delivery, PABC mastectomy, axillary dissection, and IBR. This surgical strategy allowed PABC treatment by the BC guideline, minimizing the newborn's disadvantage and permitting, at the same time, the best final BR outcome.

KEYWORDS

pregnancy-associated breast cancer, breast cancer, nipple-sparing mastectomy, immediate breast reconstruction, case report

Introduction

Pregnancy-associated breast cancer (PABC) is defined as breast cancer (BC) diagnosed during pregnancy or up to 1 year after delivery (1). Despite its relatively low incidence, ranging from 1:3,000 to 1:10,000 pregnancies, it represents the most common cancer in pregnancy (2, 3). Due to the breast physiological changes occurring in pregnancy, PABC could pose a severe diagnostic challenge (3, 4). Moreover, psychological and ethical aspects play a crucial role in PABC because the appropriate management must fulfill both the oncological threat and the pregnancy (5–7).

According to the most accredited guidelines, BC surgical treatment during pregnancy should be as close as possible to the standard treatment of non-pregnant patients. Because immediate breast reconstruction (IBR) currently represents one of the most popular reconstructive methods, when possible, it should be considered even in PABC (8–10).

Although BC surgery is commonly performed during all trimesters of pregnancy (11), timing and method for BR are largely debated in the literature. With the aim to minimize the newborn risks, delayed breast reconstruction (DBR) is frequently preferable. However, IBR has other advantages, such as the avoidance of a secondary surgical procedure, the reduction of patient's distress, and, possibly, more favorable outcomes (12–14).

Although mastectomy and IBR during pregnancy have been already reported (12, 15), to the best of our knowledge, this is the first paper to report concurrent cesarean delivery, PABC mastectomy, axillary dissection, and IBR. Hereby, our team will present the case report, at every stage, and will discuss the potential risks and benefits of this PABC approach pathway.

Case report

Clinical case and preoperative evaluation

The presence of a 7-cm firm mass in the right breast of a 37-year-old patient was confirmed by the ultrasound investigation at the 34th week of pregnancy (Figure 1). The patient had no previous

FIGURE 1
(A) Pre-operative frontal view of 37-year-old, 36-week pregnant woman, presenting with a right breast PABC. **(B)** Post-operative frontal view showing the result after 1 year from the right IBR.

relevant medical, family, or psycho-social history. Physical examinations showed a firm nodule in the upper lateral pole of the right breast. Palpation of the axillary lymph nodes was negative for lymphadenopathy. A 14-gauge semi-automated core biopsy (Precisa®) allowed the diagnosis of an invasive carcinoma: ER+, 90%; PgR+, 70%; Ki67 index, 25%; and Human epidermal growth factor receptor 2 (HER2)-positive, score 3+.

From the discussion with the patient, her perspective was to protect the fetus, even at the expense of her own health. Following a multidisciplinary approach including breast surgeon, gynecologist, plastic surgeon, oncologist, psychologist, and neonatologist, concomitant cesarean delivery, subcutaneous nipple-sparing mastectomy, sentinel lymph node biopsy, and IBR were planned at 36th week, after induction of fetal lung maturation. The surgical timing considered both the mother and the ongoing pregnancy, avoiding general anesthesia for the fetus, limiting the risks of an excessively premature birth, allowing adequate fetal lung maturation, and ensuring appropriate management of the oncological threat.

Surgical procedure

On the second day of the 36th week, cesarean delivery was firstly performed under spinal anesthesia as usual. Fetal monitoring prior to the cesarean delivery was routinely performed by cardiotocography. As soon as extracted, the newborn was taken care of by the neonatologists and was in good health (APGAR index, 9/9/10). Immediately after, general anesthesia was induced, and the patient underwent nipple-sparing mastectomy, sentinel lymph node biopsy with intraoperative frozen section examination, and IBR. In fact, after cesarean section, there were no longer contraindications for general anesthesia, which is routinely adopted for breast oncological procedures. Due to the presence of sentinel lymph node macro-metastases on frozen-section, radical ipsilateral axillary dissection was performed. IBR consisted of partial submuscular coverage of the breast implant by the pectoral major muscle, covering the inferior part of the prosthesis with an acellular porcine dermal matrix. Drains were applied as in routinely authors' practice (Figure 2).

Results

The whole surgical sequence, including anesthesia times, lasted 240 min. Specifically, the surgical time for cesarean section was 25 min and that of nipple-sparing mastectomy, axillary lymph node dissection, and IBR was 140 min.

The patient was discharged on the fourth postoperative day. Breast drain were removed on the sixth postoperative day when drainage was less than 20 cc, whereas axillary drain on the fourth post-op. No major or minor complications were reported during recovery for both the mother and the newborn.

Pathology report showed a multifocal and multicentric no–special type G3-infiltrating ductal carcinoma with vascular and lymphatic infiltration. Four out of the 18 lymph nodes removed were involved. According to TNM 2017 VIII edition classification, the oncological staging reported the following: pT2 (m) (50mm) and pN2a (4/18). According to American Joint Commettee on Cancer (AJCC) TNM eighth edition stage IIIA, immunohistochemical staining was ER+ of 90%, PgR+ of 90%, Ki67 index of 50%, and HER2-positive score of 3+. No pathologic BRCA1 and BRCA2 mutations or additional abnormal findings were detected at genetic study. No distant metastases were found by skeletal scintigraphy and total body CT investigation.

Lactation inhibition was obtained by oral administration of a single dose of 1 mg of cabergoline, because adjuvant chemotherapy

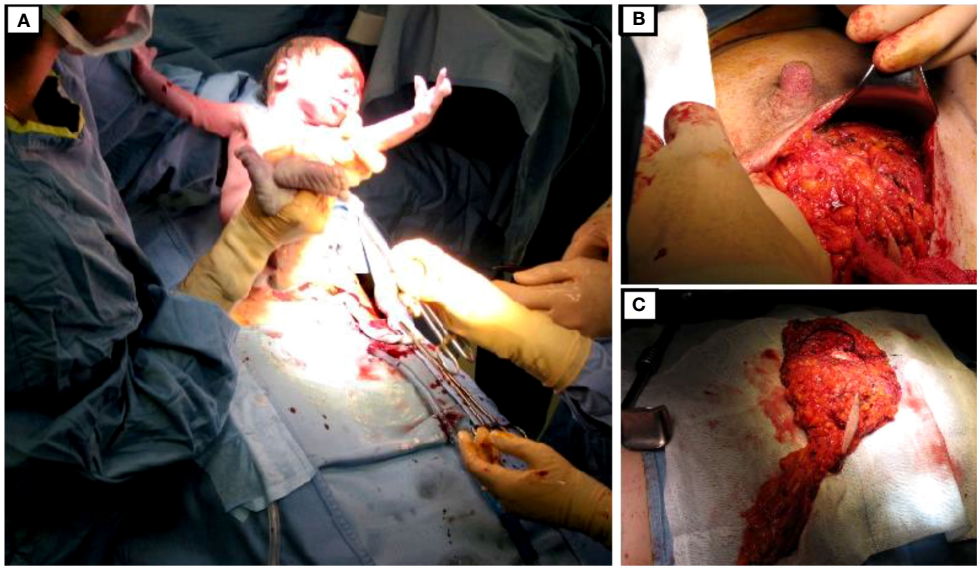

FIGURE 2
(A) The newborn. **(B, C)** Nipple-sparing mastectomy with *en bloc* axillary dissection.

was necessary to be administered. The following treatment was started 4 weeks later: four cycles of intravenous AC (doxorubicin and cyclophosphamide) every 3 weeks, followed by 12 taxol weekly administration; trastuzumab every 21 days for 18 months; and hormonal therapy with 3.75 mg of triptorelin 1 fl every 28 days for 3 years and 20 mg of tamoxifen one tablet per day for 2 years, later replaced with 25 mg of exemestane one tablet per day. Radiotherapy (40 + 15 Gy) was administered to the operated breast/chest wall. The follow-up consisted of clinical examination with testing for Ca-15.3 and Carcinoembryonic antigen (CEA) every 6 months and breast ultrasound, mammography, and total body CT scan every year. After a 6-year follow-up, the patient is alive and disease-free (Figure 3).

Discussion

Although 80% of breast lesions during pregnancy are benign (16), PABC occurs in between 1:3,000 and 1:10,000 pregnancies, representing 0.2%–3.8% of all BC (2, 3). Despite its current low incidence, the burden of PABC will probably increase in the next years due to the trend to postpone pregnancy after 40 years that is taking place in many developed countries. In fact, as reported by Robertson et al., older-age pregnancy represents a sensitive risk with an increment of 5.3% per year beyond 25 years (17–19).

Breast modifications that occur during pregnancy and lactation, including hormonal changes, or increased levels of insulin-like growth factor–1, may be related to the enhanced incidence of PABC (20, 21). In addition, pregnancy-related immunological changes such as cellular immunosuppression and immune tolerance may also play a role (22).

Indeed, breast hypertrophy, increase in gland density, and nipple changes typically occur during pregnancy. In addition, the attention of patients and clinicians is more focused on the pregnancy issues. Therefore, PABC diagnosis is often delayed, resulting in many instances in a more advanced and aggressive disease (3, 4).

Although the prognosis of PABC is similar to that of non-pregnant BC of the same stage (3, 23, 24), delayed diagnosis and, consequently, more advanced stage at the onset as well as unfavorable histological features including higher rates of hormone-receptor negative tumors, HER2 overexpression, and lower prevalence of tumor-infiltrating lymphocytes typically occur in PABC. These features account for the worse prognosis of PABC (9, 25–27).

When technically feasible, breast conserving treatment should be considered in the second and third trimester of pregnancy, followed by post-delivery radiotherapy and systemic treatment as appropriate (28, 29). However, mastectomy is always indicated in the first trimester and often required also in the second and third trimester because of multicentric or locally advanced disease. Therefore, BR should be considered in a majority of these cases.

To minimize fetal risks, the 2010 European consensus suggested DBR versus IBR (30). Nevertheless, IBR offers considerable advantages such as a single-step surgical procedure for mastectomy and BR, reduced patients' distress, minor costs, and shorter waiting lists for the healthcare system. Moreover, due to an easier placement of the breast implant, IBR, respecting the infra mammary fold, optimizes the aesthetical outcome and reduces the need of contra-lateral breast symmetrization procedures.

Lohsiriwat et al. (12) in 2013 firstly proposed IBR during pregnancy, whereas Caragacianu et al. (15) reported the onset of intraoperative uterine contraction requiring tocolysis in one of the 10 patients undergoing IBR. Despite their favorable results, IBR during pregnancy could increase risks including preterm delivery, miscarriage, and fetal distress (31).

In the current case, taking advantage of a diagnosis in the third trimester of pregnancy, the cesarean delivery performed as usual

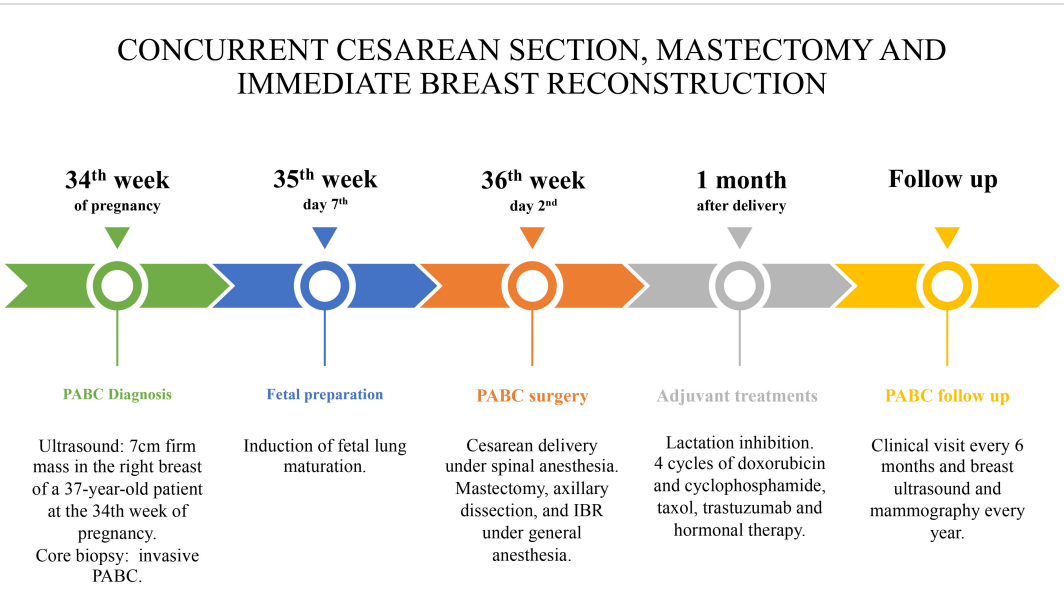

FIGURE 3
Timeline. PABC, pregnancy-associated breast cancer; IBR, immediate breast reconstruction.

under spinal anesthesia allowed avoidance of the surgical risks for the fetus associated with the breast procedure, including general anesthesia. The planned surgical sequence allowed, at the same time, a single-step procedure, ensuring patients' comfort, reducing psychological distress and allowing a satisfactory final IBR. Indeed, this approach was made possible by a strong collaboration within the multidisciplinary team of the Breast Unit, including breast surgeon, gynecologist, and plastic surgeon, and especially favored by the setting that, in our hospital, put together the Breast Unit and the Obstetrics and Gynecology Department. In addition, the breast surgeon in this case was also a gynecologist, thus further ensuring the appropriate consideration of both oncologic and obstetric issues.

The main drawback of this surgical strategy is that its applicability is limited to PABC diagnosed in the late third trimester. Indeed, an excessively anticipated preterm cesarean section may expose the fetus to the well-known risks of prematurity, including respiratory distress or even intraventricular hemorrhage. Future research is warranted to confirm the feasibility and safety of this surgical sequence and its appropriate timing.

Conclusions

PABC poses complex challenges that require a careful balance between appropriate cancer treatment and well-being of the fetus. In the current case, concomitant cesarean delivery, nipple-sparing mastectomy, axillary dissection, and IBR were successfully carried out, without complications for the mother and the baby and with no disease recurrence after a 6-year follow-up. This approach may be considered a suitable treatment for selected PABC cases in the third trimester. Further investigations are necessary to validate this surgical approach.

Data availability statement

The raw data supporting the conclusions of this article will be made available by the authors, without undue reservation.

Ethics statement

Ethical approval was not required for the studies involving humans because no experimental practices were performed. The studies were conducted in accordance with the local legislation and institutional requirements. The participants provided their written informed consent to participate in this study. Written informed consent was obtained from the individual(s) for the publication of any potentially identifiable images or data included in this article.

Author contributions

AI: Conceptualization, Data curation, Formal Analysis, Investigation, Methodology, Supervision, Validation, Visualization, Writing – original draft, Writing – review & editing. PS: Data curation, Formal Analysis, Investigation, Methodology, Validation, Visualization, Writing – original draft, Writing – review & editing. LG: Validation, Visualization, Writing – review & editing. TS: Conceptualization, Data curation, Formal Analysis, Investigation, Methodology, Resources, Supervision, Validation, Visualization, Writing – original draft, Writing – review & editing.

Funding

The author(s) declare financial support was received for the research, authorship, and/or publication of this article.

Conflict of interest

The authors declare that the research was conducted in the absence of any commercial or financial relationships that could be construed as a potential conflict of interest.

The author(s) declared that they were an editorial board member of Frontiers, at the time of submission. This had no impact on the peer review process and the final decision.

Publisher's note

References

1. Prosperi Porta R, Montruccoli-Salmi D, Lalle M, La Torre R, Coppola S, Patella A, et al. Pregnancy-associated breast cancer. *Eur J Gynaecol Oncol* (1998) 19(4):401–4.

2. Becker S. Breast cancer in pregnancy: A brief clinical review. *Best Pract Res Clin Obstet Gynaecol* (2016) 33:79–85. doi: 10.1016/j.bpobgyn.2015.10.013

3. Loibl S, Schmidt A, Gentilini O, Kaufman B, Kuhl C, Denkert C, et al. Breast cancer diagnosed during pregnancy: adapting recent advances in breast cancer care for pregnant patients. *JAMA Oncol* (2015) 1(8):1145–53. doi: 10.1001/jamaoncol.2015.2413

4. Woo JC, Yu T, Hurd TC. Breast cancer in pregnancy: a literature review. *Arch Surg* (2003) 138(1):91–8; discussion 99. doi: 10.1001/archsurg.138.1.91

5. Polivka J Jr., Altun I, Golubnitschaja O. Pregnancy-associated breast cancer: the risky status quo and new concepts of predictive medicine. *EPMA J* (2018) 9(1):1–13. doi: 10.1007/s13167-018-0129-7

6. Alpuim Costa D, Nobre JG, de Almeida SB, Ferreira MH, Gonçalves I, Braga S, et al. Cancer during pregnancy: how to handle the bioethical dilemmas?-A scoping

review with paradigmatic cases-based analysis. *Front Oncol* (2020) 10:598508. doi: 10.3389/fonc.2020.598508

7. Harris J, Ream E, Armes J, Gibson F, Marcu A, Parsons CT, et al. What do we know about the psychosocial issues associated with cancer during pregnancy? A scoping review and gap analysis. *BMJ Open* (2023) 13(3):e063283. doi: 10.1136/bmjopen-2022-063283

8. Rojas KE, Bilbro N, Manasseh DM, Borgen PI. A review of pregnancy-associated breast cancer: diagnosis, local and systemic treatment, and prognosis. *J Womens Health (Larchmt)* (2019) 28(6):778–84. doi: 10.1089/jwh.2018.7264

9. Rodriguez AO, Chew H, Cress R, Xing G, McElvy S, Danielsen B, et al. Evidence of poorer survival in pregnancy-associated breast cancer. *Obstet Gynecol* (2008) 112 (1):71–8. doi: 10.1097/AOG.0b013e31817c4ebc

10. Susini T, Renda I, Giani M, Vallario A, Nori J, Vanzi E, et al. Changing trends in mastectomy and breast reconstruction. Analysis of a single-institution experience between 2004-2016. *Anticancer Res* (2019) 39(10):5709–14. doi: 10.21873/anticanres.13770

11. Amant F, Loibl S, Neven P, Van Calsteren K. Breast cancer in pregnancy. *Lancet* (2012) 379(9815):570–9. doi: 10.1016/S0140-6736(11)61092-1

12. Lohsiriwat V, Peccatori FA, Martella S, Azim HA Jr, Sarno MA, Galimberti V, et al. Immediate breast reconstruction with expander in pregnant breast cancer patients. *Breast* (2013) 22(5):657–60. doi: 10.1016/j.breast.2013.06.005

13. Innocenti A, Melita D, Affortunati M, Susini T, Innocenti M. Immediate-implant-based-breast-reconstruction with two-stage expander-implant reconstruction versus one-stage-reconstruction with acellular dermal matrix: analysis of patients' satisfaction. *Acta BioMed* (2021) 92(3):e2021228. doi: 10.23750/abm.v92i3.9916

14. Ciancio F, Innocenti A, Cagiano L, Portincasa A, Parisi D. Skin-reducing mastectomy and direct-to-implant reconstruction in giant phyllodes tumour of breast: case report. *Int J Surg Case Rep* (2017) 41:356–9. doi: 10.1016/j.ijscr.2017.11.009

15. Caragacianu DL, Mayer EL, Chun YS, Caterson S, Bellon JR, Wong JS, et al. Immediate breast reconstruction following mastectomy in pregnant women with breast cancer. *J Surg Oncol* (2016) 114(2):140–3. doi: 10.1002/jso.24308

16. Collins JC, Liao S, Wile AG. Surgical management of breast masses in pregnant women. *J Reprod Med* (1995) 40(11):785–8.

17. Hou N, Ogundiran T, Ojengbede O, Morhason-Bello I, Zheng Y, Fackenthal J, et al. Risk factors for pregnancy-associated breast cancer: a report from the Nigerian Breast Cancer Study. *Ann Epidemiol* (2013) 23(9):551–7. doi: 10.1016/j.annepidem.2013.06.008

18. Jernstrom H, Lerman C, Ghadirian P, Lynch HT, Weber B, Garber J, et al. Pregnancy and risk of early breast cancer in carriers of BRCA1 and BRCA2. *Lancet* (1999) 354(9193):1846–50. doi: 10.1016/S0140-6736(99)04336-6

19. Kim YG, Jeon YW, Ko BK, Sohn G, Kim EK, Moon BI, et al. Clinicopathologic characteristics of pregnancy-associated breast cancer: results of analysis of a nationwide breast cancer registry database. *J Breast Cancer* (2017) 20(3):264–9. doi: 10.4048/jbc.2017.20.3.264

20. Lyons TR, Schedin PJ, Borges VF. Pregnancy and breast cancer: when they collide. *J Mammary Gland Biol Neoplasia* (2009) 14(2):87–98. doi: 10.1007/s10911-009-9119-7

21. Schedin P. Pregnancy-associated breast cancer and metastasis. *Nat Rev Cancer* (2006) 6(4):281–91. doi: 10.1038/nrc1839

22. Shakhar K, Valdimarsdottir HB, Bovbjerg DH. Heightened risk of breast cancer following pregnancy: could lasting systemic immune alterations contribute? *Cancer Epidemiol Biomarkers Prev* (2007) 16(6):1082–6. doi: 10.1158/1055-9965.EPI-07-0014

23. Ploquin A, Pistilli B, Tresch E, Frenel JS, Lerebours F, Lesur A, et al. 5-year overall survival after early breast cancer diagnosed during pregnancy: A retrospective case-control multicentre French study. *Eur J Cancer* (2018) 95:30–7. doi: 10.1016/j.ejca.2018.02.030

24. Guinee VF, Olsson H, Möller T, Hess KR, Taylor SH, Fahey T, et al. Effect of pregnancy on prognosis for young women with breast cancer. *Lancet* (1994) 343 (8913):1587–9. doi: 10.1016/S0140-6736(94)93054-6

25. Fajdic J, Gotovac N, Hrgović Z, Fassbender WJ. Diagnosis and therapy of gestational breast cancer: a review. *Adv Med Sci* (2008) 53(2):167–71. doi: 10.2478/v10039-008-0037-5

26. Azim HA Jr., Vingiani A, Peccatori F, Viale G, Loi S, Pruneri G. Tumour infiltrating lymphocytes (TILs) in breast cancer during pregnancy. *Breast* (2015) 24 (3):290–3. doi: 10.1016/j.breast.2015.01.009

27. Anderson BO, Petrek JA, Byrd DR, Senie RT, Borgen PI. Pregnancy influences breast cancer stage at diagnosis in women 30 years of age and younger. *Ann Surg Oncol* (1996) 3(2):204–11. doi: 10.1007/BF02305802

28. Toesca A, Gentilini O, Peccatori F, Azim HA Jr, Amant F. Locoregional treatment of breast cancer during pregnancy. *Gynecol Surg* (2014) 11(4):279–84. doi: 10.1007/s10397-014-0860-6

29. Martinez MT, Bermejo B, Hernando C, Gambardella V, Cejalvo JM, Lluch A. Breast cancer in pregnant patients: A review of the literature. *Eur J Obstet Gynecol Reprod Biol* (2018) 230:222–7. doi: 10.1016/j.ejogrb.2018.04.029

30. Amant F, Berveiller P, Boere IA, Cardonick E, Fruscio R, Fumagalli M, et al. Breast cancer in pregnancy: recommendations of an international consensus meeting. *Eur J Cancer* (2010) 46(18):3158–68. doi: 10.1016/j.ejca.2010.09.010

31. Evans SR, Sarani B, Bhanot P, Feldman E. Surgery in pregnancy. *Curr Probl Surg* (2012) 49(6):333–88. doi: 10.1067/j.cpsurg.2012.02.003

frontiers | Frontiers in Oncology

TYPE Case Report
PUBLISHED 12 January 2024
DOI 10.3389/fonc.2024.1276637

OPEN ACCESS

EDITED BY
Anika Nagelkerke,
University of Groningen, Netherlands

REVIEWED BY
Hossam Taha Mohamed,
October University for Modern Sciences and Arts, Egypt
Meera Srivastava,
Uniformed Services University of the Health Sciences, United States
John Maringa Githaka,
University of Alberta, Canada

*CORRESPONDENCE
Liang Yin
justinfly2080@gmail.com

†These authors have contributed equally to this work and share first authorship

RECEIVED 12 August 2023
ACCEPTED 08 January 2024
PUBLISHED 12 January 2024

CITATION
Qin R, Wang X, Fan T, Wu T, Lu C, Shao X and Yin L (2024) Bilateral inflammatory recurrence of HER-2 positive breast cancer: a unique case report and literature review.
Front. Oncol. 13:1276637.
doi: 10.3389/fonc.2024.1276637

Bilateral inflammatory recurrence of HER-2 positive breast cancer: a unique case report and literature review

Rong Qin[1†], Xiangyang Wang[2†], Tingting Fan[1], Ting Wu[3], Chao Lu[4], Xun Shao[5] and Liang Yin[6*]

[1]Department of Medical Oncology, Jiangsu University Affiliated People's Hospital, Zhenjiang Clinical Medical College of Nanjing Medical University, Zhenjiang, China, [2]Department of Traditional Chinese Medicine, Jiangsu University Affiliated People's Hospital, Clinical Medical College, Nanjing University of Chinese Medicine, Zhenjiang, China, [3]Department of Pathology, Jiangsu University Affiliated People's Hospital, Zhenjiang, China, [4]Department of Medical Iconography, Jiangsu University Affiliated People's Hospital, Zhenjiang, China, [5]Department of Nuclear Medicine, Jiangsu University Affiliated People's Hospital, Zhenjiang, China, [6]Department of Breast Surgery, Jiangsu University Affiliated People's Hospital, Zhenjiang, China

Inflammatory breast cancer (IBC) is an aggressive and rare form of breast cancer with a poor prognosis. The occurrence of bilateral IBC in a short period of time is extremely rare. In this case report, a 54-year-old woman diagnosed with invasive ductal carcinoma of the left breast underwent lumpectomy, lymph node dissection, chemotherapy, and radiotherapy but opted against trastuzumab treatment. Four years later, she experienced bilateral breast inflammation, skin changes, edema, and heat (calor). Biopsies confirmed breast cancer metastasis to both breasts. Whole-Exome Sequencing revealed genetic mutations, including PIK3CA and C4orf54, in both primary and recurrent tumors, with significant downregulation in the recurrent tumors. KEGG analysis suggested potential enrichment of axon guidance signal pathways in both tumors. The patient showed a partial response after treatment with liposome paclitaxel, along with targeted therapy using trastuzumab and pertuzumab. This case report sheds light on the rare occurrence of bilateral inflammatory breast cancer post-HER-2 treatment and highlights the importance of genetic profiling in understanding the disease. Further research on clinical targets for breast cancer management is warranted.

KEYWORDS

inflammatory breast cancer, bilateral recurrence, HER-2 positive breast cancer, case report, whole-exome sequencing

Introduction

Inflammatory breast cancer (IBC) represents a rare and highly aggressive type of invasive breast cancer, constituting just 2.5% of all breast cancer cases. Historically, its prognosis has been notably poor (1, 2). Among all molecular subtypes, triple-negative IBC patients experience the worst prognosis, with a 10-year overall survival rate of merely 17.8% (3). Typical clinical characteristics of IBC include involvement of ≥30% of the affected breast and/or skin, along with erythema, skin changes like peau d'orange, nipple inversion, edema, and warmth, often without an underlying palpable mass (2). Although IBC cells exhibit histopathological similarities with non-IBC breast cancer cells, they are usually distributed in clusters throughout the breast and skin, leading to common false negative imaging results. To distinguish IBC from non-IBC, pathological confirmation of invasive carcinoma is essential. When a patient presents with a strong suspicion of IBC on the basis of medical history and clinical signs, it is highly recommended to conduct breast imaging (e.g., mammography or ultrasound) and perform a tissue biopsy for definitive pathological confirmation (1, 4).

Breast cancer is classified into different molecular subtypes, namely hormone receptor (HR)-positive (defined by estrogen receptor-positive and/or progesterone receptor-positive), HER2-positive (also known as ERBB2), and triple-negative breast cancer (TNBC) (5). These subtypes are present not only in non-IBC but also in IBC, albeit with varying proportions (6). The occurrence of HER2-positive and triple-negative breast cancer is more frequent in IBC cases than in non-IBC cases. HER2-positive breast cancer accounts for up to 50% of IBC cases, while in non-IBC, it constitutes 20-25% of cases. Similarly, TNBC accounts for 10-15% of IBC cases, compared to 30% in non-IBC (7, 8). Therefore, HER2-positive breast cancer exhibits the highest incidence among IBC cases. As a result of these more aggressive phenotypes, distant metastasis often arises, impacting various locations such as the bone, lung, and liver. Patients with HER2-positive IBC frequently encounter relapse in the central nervous system (CNS) as their initial site of recurrence (9). It is worth mentioning that there is a scarcity of literature documenting instances of bilateral recurrence of IBC in patients with HER2-positive breast cancer.

Case report

A 58-year-old woman with a history of left-sided breast cancer (BC) diagnosed at age 54 in May 2018 underwent left-breast lumpectomy and axillary lymph node dissection. The postoperative pathology confirmed a grade 2 infiltrating ductal carcinoma (Figure 1A). Lymph nodes analysis showed no signs of metastasis, resulting in a TNM staging of pT2N0M0, Stage IIA. Immunohistochemical staining indicated negative results for estrogen receptor (ER) and progesterone receptor (PR), while being positive for human epidermal growth factor receptor 2 (c-erbB2) and Ki 67 (40%+) (Figures 1B–E). From May 2018 to October 2018, the patient received adjuvant chemotherapy with four cycles of Epirubicin and Cyclophosphamide followed by four cycles of docetaxel. However, for economic reasons, she declined targeted anti-HER-2 treatment with trastuzumab. Subsequently, she underwent postoperative adjuvant local radiotherapy, with a total dose of 50 Gy at 2 Gy/day × 25 fractions to the whole left breast, completing the radiotherapy in January 2019. Following treatment, the patient was under surveillance with clinic follow-ups every 3-6 months, focusing on tumor biomarkers and imaging monitoring in the local hospital. Notably, there had been no evidence of loco-regional or distant recurrence.

In September 2022, the patient presented at the hospital with vague breast pain. Physical examination revealed erythema, peau d'orange with skin thickening, inflammation, and edema of both breasts, along with left breast nipple retraction, and no palpable axillary nodes (Figures 2A–C). A chest computed tomography (CT) scan showed thickening skin of both breasts, multiple small nodules in the left breast, and multiple lung metastases (Figure 3A). Ultrasound scanning detected a suspicious node in her left breast (Figure 3B). Magnetic resonance imaging (MRI) of the breasts indicated the presence of a node in the center and upper external region of the left breast with BI-RADs:4a-4c (Figure 3C). A biopsy of the inflamed skin in both breasts confirmed breast cancer metastasis (Figure 1F). Immunohistochemistry results showed negative estrogen receptor (ER) and progesterone receptor (PR) status, c-erbB2 2+ expression, and positive Ki 67 (30%) (Figures 1G–J). Additionally, the fluorescence *in situ* hybridization (FISH) test confirmed c-erbB2 amplification.

Further metastatic surveys, including CT scans of the abdomen, pelvis, brain, and whole-body bone scanning, yielded negative results. Blood analysis and tumor markers like carbohydrate antigen 153 (CA 15-3) were within normal ranges. A multi-disciplinary review led to the decision for rescue treatment of advanced breast cancer. The patient received six cycles of liposome paclitaxel and targeted therapy with trastuzumab (initially 8 mg/kg followed by 6 mg/kg every 3 weeks) and pertuzumab (initially 840mg followed by 420mg every 3 weeks). During treatment, inflammation and erythema of the breast skin gradually decreased, and bilateral lung metastases showed improvement (Figures 2D–F). Follow-up CT, ultrasound, and MRI scans following liposome paclitaxel demonstrated excellent response (Figures 3D–F). At the end of treatment, positron emission tomography/computed tomography (PET/CT) did not show pulmonary or other visceral organ metastasis (Figure 4). The patient continued targeted treatment with trastuzumab and pertuzumab every 3 weeks, along with oral capecitabine for maintenance chemotherapy.

In this study, we present the diagnosis and treatment of a patient with inflammatory recurrence of breast cancer. To further investigate genetic alterations, particularly variants of unknown significance (VUS), we employed Whole Exome Sequencing (WES). The primary tumor (P) and skin recurrence (R) of the patient exhibited a Tumor Mutation Burden (TMB) of 0.12 and 0.81 mut/Mb, respectively. Through WES analysis (10), a total of 111 gene variants were identified in the primary tumor (P) and 28 gene variants in the recurrent tumor (R). Interestingly, two variants (PIK3CA and C4orf54) were found to be present in both samples. The abundance of PIK3CA was found to be 22.22% in the primary tumor (P) and 2.99% in the recurrent tumor (R), while the

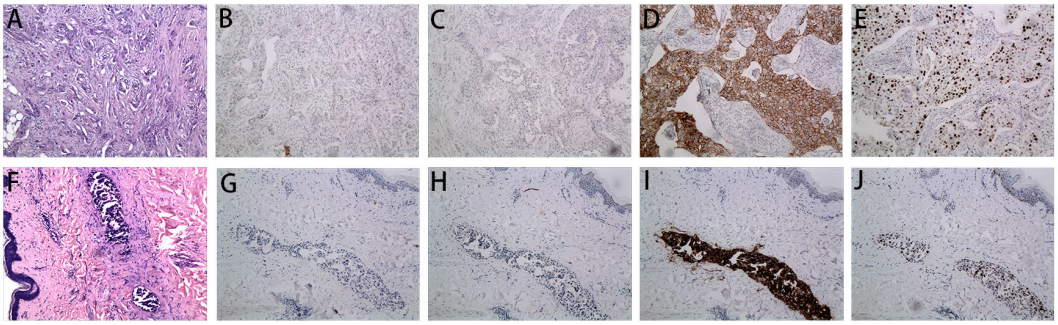

FIGURE 1
Microscopy examination of the breast specimen. **(A)** Postoperative HE staining suggested invasive ductal carcinoma of breast in 2018 (original magnification, 100 ×); The immunohistochemical staining of ER (negative, **B**), PR (negative, **C**), c-erbB2 (positive, **D**) and Ki 67 (40% positive, **E**) in 2018 (100 ×); **(F)** HE staining of the skin biopsy from the recurrent inflammation site showed lymphovascular tumor emboli and lymphatic dilatation in the superficial dermis. (original magnification, 100 ×); The immunohistochemical staining of skin biopsy at the site of inflammatory recurrence of ER (negative, **G**), PR (negative, **H**), c-erbB2 (positive, **I**) and Ki 67 (30% positive, **J**) in 2022 (original magnification, 100 ×).

abundance of C4orf54 was 30.95% in P and 4.01% in R (Table 1). KEGG analysis revealed potential enrichment of axon guidance signal pathways in both the primary tumor (P) and recurrent tumor (R) (Supplementary Figure S1). Molecular function analysis indicated that P may show changes in the activity of G protein-coupled neurotransmitter receptors, while R may exhibit changes in the activity of PI3 kinase (Supplementary Figure S2). Moreover, cellular component analysis revealed the detection of changes in the semaphorin receptor complex in both P and R (Supplementary Figure S3). These findings shed light on the genetic alterations and potential signaling pathways involved in the recurrence of inflammatory breast cancer in this patient.

Discussion

Only few cases of bilateral IBC have been reported in the past. One case report describes a patient with contralateral recurrence of IBC less than a year after the initial diagnosis (11). In the context of IBC, the incidence rate of HER2 positive breast cancer is as high as 50%, whereas in non-IBC, it ranges from 20-25%. Over the past decade, there have been significant advancements in improving the overall survival (OS) of HER2 positive metastatic breast cancer (MBC). However, despite these improvements, the survival rate for *de novo* MBC remains considerably higher than that of recurrent disease (12).

FIGURE 2
Photographic evidence showing the improvement of the disease (all provided by the patient for literature and education). **(A-C)** indicates the skin presented with erythema, peau d'orange, inflamed and oedematous of the bilateral breast and a nipple retraction of left breast (taken in September 2022). **(D-F)** indicates significant improvement in the presentation of skin with inflammatory recurrence after six cycles of chemotherapy and targeted therapy (taken in December 2022).

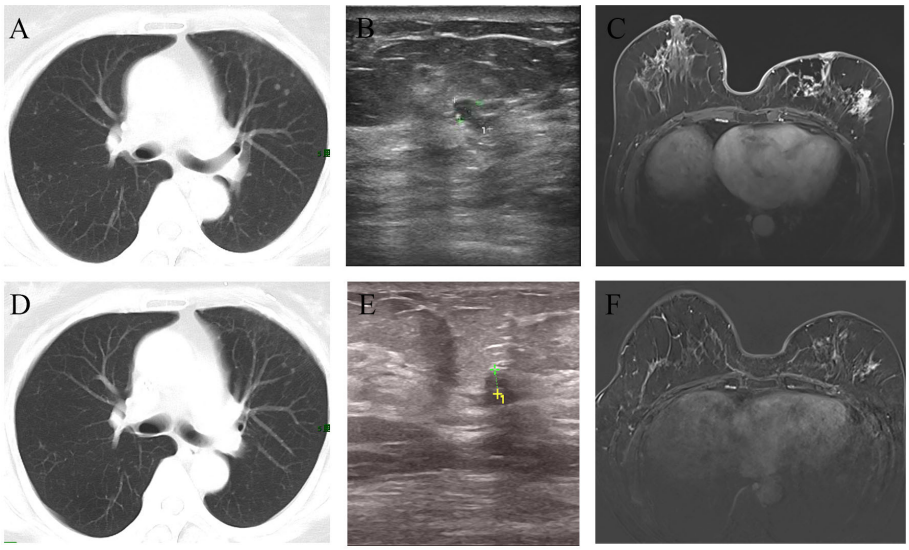

FIGURE 3
Imaging changes before and after treatment. The CT scan suggested multiple metastases in both lungs **(A)**. After chemotherapy combined with targeted therapy, the pulmonary metastatic lesions have significantly decreased compared to before **(D)**. Ultrasound revealed an irregular hypoechoic area measuring approximately 7*4mm adjacent to the left nipple in the 3 o'clock direction of the breast, with indistinct borders **(B)**. After treatment, the ultrasound indicated that the hypoechoic area has reduced in size to approximately 3.5*3.3mm compared to before **(E)**. MRI showed the presence of an irregular ring-enhancing lesion measuring approximately 11*11mm in the central region of the left breast. Additionally, there is thickening of the skin overlying the left breast with thickened skin **(C)**. After treatment, MRI indicated the absence of the previously visible nodule in the central region of the left breast **(F)**.

At present, there are many anti-HER2 therapies approved by the Food and Drug Administration (FDA), mainly including monoclonal antibodies (MAbs), the most representative of which are trastuzumab and pertuzumab, and small-molecule tyrosine kinase inhibitors (TKIs), such as lapatinib, tukatinib, and neratinib (13, 14). In recent years, antibody drug conjugates (ADC), such as ado-trastuzumab emtansine (T-DM1) and trastuzumab deruxtecan (T-DXd), also have good effects in HER2 positive patients with advanced breast cancer (15, 16). These different types of anti-HER2 drugs target anti-HER2 treatment through different mechanisms. According to the guidelines, THP regimen (paclitaxel, trastuzumab and pertuzumab) is recommended as the first-line treatment regimen for patients with HER-2 positive advanced breast cancer who were previously sensitive to trastuzumab treatment. The large, randomized, phase III CLEOPATRA clinical trial indicated that the median OS was 56.5 months in the group receiving the pertuzumab, trastuzumab and docetaxel, as compared with 40.8 months in the group receiving the trastuzumab, docetaxel and placebo. The study established the standard of care for treatment of patients with HER2-positive breast cancer in the front-line setting (17). In a Korean real-world study, the clinical outcomes of metastatic HER2-positive breast cancer patients treated with THP regime further proved the authenticity of the CLEOPATRA trial (18). Similarly, the study of weekly paclitaxel combined with trastuzumab and pertuzumab showed a longer follow-up of nearly 5 years and the median PFS was 24.2 months whereas the median OS was not reached for the overall group (19). Despite the fact that weekly paclitaxel has been demonstrated to have better tolerance compared to every-3-week docetaxel, a larger number of patients opt for the three-week regimen due to its convenience in daily life (20).

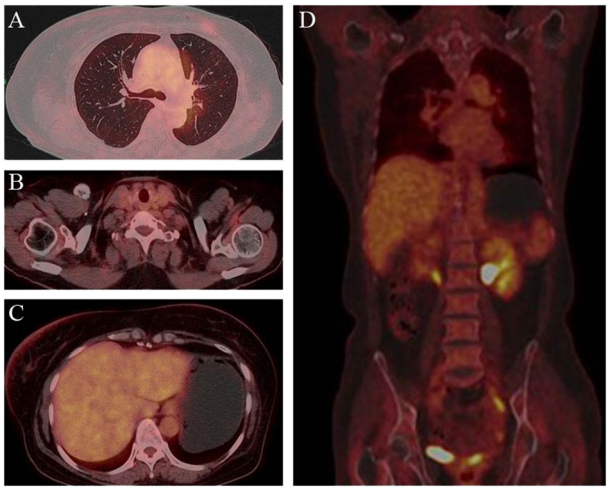

FIGURE 4
Post-treatment PET/CT findings. PET demonstrated clearcut accumulation of 18F fluorodeoxyglucose in lung **(A)**, lymph nodes in the clavicular region **(B)**, liver **(C)** and whole body **(D)**.

IBC and non-IBC are mainly differentiated by their clinical manifestations, but pathological confirmation is also essential to confirm the diagnosis of invasive cancer, which involves numerous dermal tumor emboli in the dermis overlying the breast (21). Among the four molecular types of breast cancer, the most prominent distinction between IBC and non-IBC lies in the overexpression of HER2-positive and triple-negative subtypes (22). Long-term survival rates for IBC patients are reported to be

TABLE 1 WES was used to analyze gene point mutations, deletions, insertions, and other genetic alterations in both the primary tumor (P) and skin recurrence (R) in breast cancer.

Gene	Mutant	Abundance (P)	Abundance (R)
PIK3CA	c.3140A>G (p.H1047R)	22.22%	2.99%
TP53	c.991C>T(p.Q331*)	–	3.57%
ASB11	c.623A>G (p.D208G)	9.23%	2.59%
C4orf54	c.4966G>T (p.A1656S)	30.95%	4.01%
CMYA5	c.2611C>T (p.P871S)	–	3.94%
EIF4G1	c.1428_1429del (p.S476Rfs*43)	–	3.27%
GOT1	c.277A>G (p.S93G)	–	2.34%
GPR156	c.852G>A (p.W284*)	–	2.77%
HIST1H4K	c.128G>A (p.G43D)	–	3.68%
HTR1F	c.470C>G (p.P157R)	–	2.39%
HYI	c.272A>C (p.E91A)	–	3.49%
KIF1A	c.3442C>G (p.L1148V)	–	2.38%
KLHL33	c.89T>C (p.F30S)	–	3.56%
KRT19	c.905_912delinsA (p.T302Kfs*11)	–	3.29%
LRP1	c.7370G>A (p.R2457H)	–	2.93%
MCC	c.578C>A (p.P193R)	–	3.04%
MUC16	c.5621G>A (p.R1874K)	–	2.88%
NAT10	c.2781G>T (p.E927D)	–	2.74%
PLEKHG2	c.146C>T (p.S49F)	–	2.19%
PLXNA3	c.4718T>G (p.V1573G)	–	4.27%
PLXNB3	c.1256C>T (p.P419L)	23.08%	3.07%
POLE2	c.852T>G (p.D284E)	–	2.69%
PTPRJ	c.2954T>C (p.L985P)	–	4.69%
RBMXL3	c.734C>T (p.P245L)	–	2.83%
TXNDC17	c.206G>A (p.C69Y)	–	2.50%
YTHDF1	c.1495A>C (p.N499H)	–	2.27%
ZSCAN12	c.452G>A (p.R151H)	–	3.38%

(*Tumor-specific mutations).

around 40%, and even with targeted treatment for HER2-positive IBC patients, resistance to HER2 targeted therapy often develops within two years, highlighting the urgency to explore disease pathogenesis and provide more treatment options (23, 24). Notably, IBC cases typically lack a single dominant tumor mass. Instead, tumor cells infiltrate loosely in the form of cell groups, clustering in both the matrix and lymphatic vessels (25). To identify potential therapeutic targets, Ross et al. employed next-generation sequencing technology to study metastatic parts of 53 IBC patients. The study identified TP53 and MYC as the most frequently altered genes, along with components of signaling pathways such as the RAS and phosphoinositide 3-kinase (PI3K) pathways. Within the RAS pathway, mutations were predominantly found in genes encoding ERBB2, KRAS, BRAF, and EGFR, while the PI3K pathway exhibited mutations in PIK3CA, PTEN, AKT1, and AKT3 (26). These findings provide crucial insights into potential avenues for targeted therapy in IBC.

In this patient, we adopted the classic three-week THP regime. Following the first cycle of chemotherapy and targeted therapy, the skin manifestations of metastatic inflammatory breast cancer showed progressive improvement without any safety issues. After completing the entire chemotherapy cycle, a comprehensive PET/CT evaluation revealed increased FDG uptake in the bilateral nipples and surrounding skin, with multiple small lung nodules significantly improved compared to before. Based on RECIST 1.1 criteria, the patient achieved partial response (PR). Moving forward, we are now considering the next step of treatment, which involves choosing between targeted maintenance therapy alone or combining targeted therapy with other drugs. Capecitabine, a well-established oral chemotherapy drug, has demonstrated positive maintenance treatment effects in numerous studies when combined with other therapies (27–29). For the follow-up maintenance treatment, we decided to use capecitabine in combination with trastuzumab and pertuzumab. This approach aims to provide the patient with the most effective and personalized treatment to further manage the disease.

At present, the patient's condition remains stable and well-tolerated. Given the frequent relapse and distant metastasis observed in HER-2 positive breast cancer, we conducted WES to further investigate gene and pathway changes, aiming to understand the mechanisms driving metastasis and lay the groundwork for future treatments. We found alterations in G protein-coupled receptor activity (molecular function) in pre-treatment inflammatory breast cancer (IBC) tumors. Cellular component analysis revealed the presence of the "semaphorin receptor complex." These findings align with Zare et al's research, identifying G protein-coupled receptors as the primary pathway in pre-treatment IBC samples. Notably, the Semaphorin-3E gene contributes to a molecular signature distinguishing IBC from non-IBC samples (30). We aslo managed to identified several mutations in the primary lesion and numerous other gene mutations in the recurrent tissue, with the most significant being TP53. TP53, as a tumor suppressor gene, is commonly mutated in various tumors, including breast cancer, and patients with TP53 gene mutations are more susceptible to developing various malignant tumors (31, 32). In this study, we detected a nonsense mutation in exon 9 (p.Q331*) of the TP53 gene in the recurrent tissues, potentially leading to the inactivation of P53's anti-tumor function, promoting tumor cell proliferation, migration, and anti-apoptosis, and contributing to tumor development. Moreover, it may result in resistance to chemotherapy drugs like platinum and fluorouracil. Several molecules targeting P53/TP53 have been developed, such as nutilins, MI-series analogs, PRIMA-1, and RITA, although only APR-246 and COTI-2 have progressed to clinical trials, while most others are still in the preclinical stage (33).

We also noted significantly higher abundances of PIK3CA and C4orf54 in the primary tumor compared to the skin recurrence

tissues. PIK3CA mutations in breast cancer are diverse, with varying proportions in different breast cancer subtypes, being highest in HR+/HER2- disease, followed by HER2+ disease and TNBC (34). The FDA-approved α-selective PI3K inhibitor, Alpelisib, has demonstrated efficacy in treating patients with advanced PIK3CA-mutated HR+/HER2- breast cancer, based on positive results from the SOLAR-1 phase III randomized trial, which evaluated the combination of alpelisib and fulvestrant in multiple countries with PIK3CA-mutated, HR+/HER2- advanced breast cancer following progression on or after endocrine therapy (35). Moreover, although the frequency of PIK3CA mutations is low in HER2+ and TNBC, research interest in this pathway is growing, with ongoing studies exploring its significance in these two breast cancer subtypes (36, 37). As for C4orf54 (chromosome 4 open reading frame 54), it remains relatively understudied, yet it shows potential as a meaningful treatment target for breast cancer, underscoring the need for further research to better understand its role in breast cancer development and progression.

Conclusion

The occurrence of bilateral inflammatory breast cancer, four years post-HER-2 positive breast cancer treatment, is exceptionally rare. We applied the standard rescue protocol for advanced HER-2 positive breast cancer. Our case underscores the vital role of consistent imaging and physical examinations in post-inflammatory breast cancer management, emphasizing patient compliance in battling this aggressive disease. Whole Exome Sequencing (WES) results provide promising insights for advancing breast cancer clinical target research. Our findings stress the need for ongoing research and targeted strategies to enhance the management and outcomes of this intricate condition.

Data availability statement

Data supporting the findings of this study are available in the in the Genome Sequence Archive (Genomics, Proteomics & Bioinformatics 2021) in National Genomics Data Center (Nucleic Acids Res 2022), China National Center for Bioinformation / Beijing Institute of Genomics, Chinese Academy of Sciences (GSA-Human: HRA006283) that are publicly accessible at https://ngdc.cncb.ac.cn/gsa-human.

Ethics statement

The studies involving humans were approved by Ethical Committee of Jiangsu University Affiliated People' Hospital. The studies were conducted in accordance with the local legislation and institutional requirements. The participants provided their written informed consent to participate in this study. Written informed consent was obtained from the individual(s) for the publication of any potentially identifiable images or data included in this article.

Author contributions

RQ: Writing – original draft. XW: Writing – original draft. TF: Data curation, Writing – review & editing. TW: Resources, Writing – review & editing. CL: Writing – review & editing. XS: Methodology, Writing – review & editing. LY: Writing – review & editing.

Funding

The author(s) declare financial support was received for the research, authorship, and/or publication of this article. This study was financially supported by the Research Project of Jiangsu University Affiliated People's Hospital (Y2020010, Y2002019), Project of Zhenjiang Ctiy Social Development (SH2023046), Clinical Research Project of the Jiangsu University Affiliated People's Hospital [Y2022019, JC-2023-004], Jiangsu Province Maternal and Child Health Research Project (F202322) and Medical Education Collaborative Innovation Fund of Jiangsu University (JDYY2023016, JDYY2023017, JDYY2023018).

Conflict of interest

The authors declare that the research was conducted in the absence of any commercial or financial relationships that could be construed as a potential conflict of interest.

Publisher's note

Supplementary material

The Supplementary Material for this article can be found online at: https://www.frontiersin.org/articles/10.3389/fonc.2024.1276637/full#supplementary-material

SUPPLEMENTARY FIGURE 1
KEGG analysis presented that both primary tumor (P) and skin recurrence (R) might be enriched in axon guidance signal pathways.

SUPPLEMENTARY FIGURE 2
Molecular function analysis showed that P and R may have changes in semaphorin receptor activity.

SUPPLEMENTARY FIGURE 3
Cellular component analysis indicated that the change of semaphorin receptor complex is detected in both P and R.

References

1. Hester RH, Hortobagyi GN, Lim B. Inflammatory breast cancer: early recognition and diagnosis is critical. *Am J Obstet Gynecol* (2021) 225(4):392–6. doi: 10.1016/j.ajog.2021.04.217

2. Hance KW, Anderson WF, Devesa SS, Young HA, Levine PH. Trends in inflammatory breast carcinoma incidence and survival: the surveillance, epidemiology, and end results program at the National Cancer Institute. *J Natl Cancer Inst* (2005) 97(13):966–75. doi: 10.1093/jnci/dji172

3. Masuda H, Brewer TM, Liu DD, Iwamoto T, Shen Y, Hsu L, et al. Long-term treatment efficacy in primary inflammatory breast cancer by hormonal receptor- and HER2-defined subtypes. *Ann Oncol* (2014) 25(2):384–91. doi: 10.1093/annonc/mdt525

4. Bonnier P, Charpin C, Lejeune C, Romain S, Tubiana N, Beedassy B, et al. Inflammatory carcinomas of the breast: a clinical, pathological, or a clinical and pathological definition? *Int J Cancer* (1995) 62(4):382–5. doi: 10.1002/ijc.2910620404

5. Sørlie T, Perou CM, Tibshirani R, Aas T, Geisler S, Johnsen H, et al. Gene expression patterns of breast carcinomas distinguish tumor subclasses with clinical implications. *Proc Natl Acad Sci U.S.A.* (2001) 98(19):10869–74. doi: 10.1073/pnas.191367098

6. Li J, Gonzalez-Angulo AM, Allen PK, Yu TK, Woodward WA, Ueno NT, et al. Triple-negative subtype predicts poor overall survival and high locoregional relapse in inflammatory breast cancer. *Oncologist* (2011) 16(12):1675–83. doi: 10.1634/theoncologist.2011-0196

7. Kertmen N, Babacan T, Keskin O, Solak M, Sarici F, Akin S, et al. Molecular subtypes in patients with inflammatory breast cancer; a single center experience. *J buon* (2015) 20(1):35–9.

8. Parton M, Dowsett M, Ashley S, Hills M, Lowe F. Smith IE: High incidence of HER-2 positivity in inflammatory breast cancer. *Breast* (2004) 13(2):97–103. doi: 10.1016/j.breast.2003.08.004

9. Matro JM, Li T, Cristofanilli M, Hughes ME, Ottesen RA, Weeks JC, et al. Inflammatory breast cancer management in the national comprehensive cancer network: the disease, recurrence pattern, and outcome. *Clin Breast Cancer* (2015) 15(1):1–7. doi: 10.1016/j.clbc.2014.05.005

10. Ng PC, Kirkness EF. Whole genome sequencing. *Genet variation: Methods Protoc* (2010) 215–26. doi: 10.1007/978-1-60327-367-1_12

11. Levy S, Hanna M. A case of bilateral inflammatory breast cancer. *Cureus* (2023) 15(6). doi: 10.7759/cureus.40101

12. Yardley DA, Kaufman PA, Brufsky A, Yood MU, Rugo H, Mayer M, et al. Treatment patterns and clinical outcomes for patients with *de novo* versus recurrent HER2-positive metastatic breast cancer. *Breast Cancer Res Treat* (2014) 145(3):725–34. doi: 10.1007/s10549-014-2916-8

13. Kunte S, Abraham J, Montero AJ. Novel HER2-targeted therapies for HER2-positive metastatic breast cancer. *Cancer* (2020) 126(19):4278–88. doi: 10.1002/cncr.33102

14. Gámez-Chiachio M, Sarrió D, Moreno-Bueno G. Novel therapies and strategies to overcome resistance to anti-HER2-targeted drugs. *Cancers (Basel)* (2022) 14(18):4543. doi: 10.3390/cancers14184543

15. Verma S, Miles D, Gianni L, Krop IE, Welslau M, Baselga J, et al. Trastuzumab emtansine for HER2-positive advanced breast cancer. *New Engl J Med* (2012) 367(19):1783–91. doi: 10.1056/NEJMoa1209124

16. Modi S, Saura C, Yamashita T, Park YH, Kim S-B, Tamura K, et al. Trastuzumab deruxtecan in previously treated HER2-positive breast cancer. *New Engl J Med* (2020) 382(7):610–21. doi: 10.1056/NEJMoa1914510

17. Swain SM, Baselga J, Kim SB, Ro J, Semiglazov V, Campone M, et al. Pertuzumab, trastuzumab, and docetaxel in HER2-positive metastatic breast cancer. *N Engl J Med* (2015) 372(8):724–34. doi: 10.1056/NEJMoa1413513

18. Lee YP, Lee MS, Kim H, Kim JY, Ahn JS, Im YH, et al. Real-world evidence of trastuzumab, pertuzumab, and docetaxel combination as a first-line treatment for Korean patients with HER2-positive metastatic breast cancer. *Cancer Res Treat* (2022) 54(4):1130–7. doi: 10.4143/crt.2021.1103

19. Wang R, Smyth LM, Iyengar N, Chandarlapaty S, Modi S, Jochelson M, et al. Phase II study of weekly paclitaxel with trastuzumab and pertuzumab in patients with human epidermal growth receptor 2 overexpressing metastatic breast cancer: 5-year follow-up. *Oncologist* (2019) 24(8):e646–52. doi: 10.1634/theoncologist.2018-0512

20. Tsubokura M, Kami M, Komatsu T. Weekly paclitaxel in the adjuvant treatment of breast cancer. *N Engl J Med* (2008) 359(3):310. doi: 10.1056/NEJMc081136

21. Morrow RJ, Etemadi N, Yeo B, Ernst M. Challenging a misnomer? The role of inflammatory pathways in inflammatory breast cancer. *Mediators Inflammation* (2017) 2017:4754827. doi: 10.1155/2017/4754827

22. Woodward WA, Cristofanilli M. Inflammatory breast cancer. *Semin Radiat Oncol* (2009) 19(4):256–65. doi: 10.1016/j.semradonc.2009.05.008

23. Mohamed MM, Al-Raawi D, Sabet SF, El-Shinawi M. Inflammatory breast cancer: New factors contribute to disease etiology: A review. *J Adv Res* (2014) 5(5):525–36. doi: 10.1016/j.jare.2013.06.004

24. Robertson FM, Bondy M, Yang W, Yamauchi H, Wiggins S, Kamrudin S, et al. Inflammatory breast cancer: the disease, the biology, the treatment. *CA Cancer J Clin* (2010) 60(6):351–75. doi: 10.3322/caac.20082

25. Jolly MK, Boareto M, Debeb BG, Aceto N, Farach-Carson MC, Woodward WA, et al. Inflammatory breast cancer: a model for investigating cluster-based dissemination. *NPJ Breast Cancer* (2017) 3:21. doi: 10.1038/s41523-017-0023-9

26. Ross JS, Ali SM, Wang K, Khaira D, Palma NA, Chmielecki J, et al. Comprehensive genomic profiling of inflammatory breast cancer cases reveals a high frequency of clinically relevant genomic alterations. *Breast Cancer Res Treat* (2015) 154(1):155–62. doi: 10.1007/s10549-015-3592-z

27. Chilà G, Guarini V, Galizia D, Geuna E, Montemurro F. The clinical efficacy and safety of neratinib in combination with capecitabine for the treatment of adult patients with advanced or metastatic HER2-positive breast cancer. *Drug Des Devel Ther* (2021) 15:2711–20. doi: 10.2147/dddt.S281599

28. Saura C, Oliveira M, Feng YH, Dai MS, Chen SW, Hurvitz SA, et al. Neratinib plus capecitabine versus lapatinib plus capecitabine in HER2-positive metastatic breast cancer previously treated with ≥ 2 HER2-directed regimens: phase III NALA trial. *J Clin Oncol* (2020) 38(27):3138–49. doi: 10.1200/jco.20.00147

29. Moy B, Oliveira M, Saura C, Gradishar W, Kim SB, Brufsky A, et al. Neratinib + capecitabine sustains health-related quality of life in patients with HER2-positive metastatic breast cancer and ≥ 2 prior HER2-directed regimens. *Breast Cancer Res Treat* (2021) 188(2):449–58. doi: 10.1007/s10549-021-06217-4

30. Zare A, Postovit LM, Githaka JM. Robust inflammatory breast cancer gene signature using nonparametric random forest analysis. *Breast Cancer Res* (2021) 23(1):92. doi: 10.1186/s13058-021-01467-y

31. Chompret A, Brugières L, Ronsin M, Gardes M, Dessarps-Freichey F, Abel A, et al. P53 germline mutations in childhood cancers and cancer risk for carrier individuals. *Br J Cancer* (2000) 82(12):1932–7. doi: 10.1054/bjoc.2000.1167

32. Marouf C, Tazzite A, Diakité B, Jouhadi H, Benider A, Nadifi S. Association of TP53 PIN3 polymorphism with breast cancer in Moroccan population. *Tumour Biol* (2014) 35(12):12403–8. doi: 10.1007/s13277-014-2556-y

33. Kaur RP, Vasudeva K, Kumar R, Munshi A. Role of p53 gene in breast cancer: focus on mutation spectrum and therapeutic strategies. *Curr Pharm Des* (2018) 24(30):3566–75. doi: 10.2174/1381612824666180926095709

34. Martínez-Sáez O, Chic N, Pascual T, Adamo B, Vidal M, González-Farré B, et al. Frequency and spectrum of PIK3CA somatic mutations in breast cancer. *Breast Cancer Res* (2020) 22(1):45. doi: 10.1186/s13058-020-01284-9

35. Rugo HS, André F, Yamashita T, Cerda H, Toledano I, Stemmer SM, et al. Time course and management of key adverse events during the randomized phase III SOLAR-1 study of PI3K inhibitor alpelisib plus fulvestrant in patients with HR-positive advanced breast cancer. *Ann Oncol* (2020) 31(8):1001–10. doi: 10.1016/j.annonc.2020.05.001

36. Sharma P, Abramson VG, O'Dea A, Nye L, Mayer I, Pathak HB, et al. Clinical and biomarker results from phase I/II study of PI3K inhibitor alpelisib plus nab-paclitaxel in HER2-negative metastatic breast cancer. *Clin Cancer Res* (2021) 27(14):3896–904. doi: 10.1158/1078-0432.Ccr-20-4879

37. Saura C, Bendell J, Jerusalem G, Su S, Ru Q, De Buck S, et al. Phase Ib study of Buparlisib plus Trastuzumab in patients with HER2-positive advanced or metastatic breast cancer that has progressed on Trastuzumab-based therapy. *Clin Cancer Res* (2014) 20(7):1935–45. doi: 10.1158/1078-0432.Ccr-13-1070

frontiers | Frontiers in Oncology

TYPE Original Research
PUBLISHED 24 January 2024
DOI 10.3389/fonc.2024.1341292

OPEN ACCESS

EDITED BY
Francesca Bianchi,
University of Milan, Italy

REVIEWED BY
Saeed Soleymanjahi,
Yale University, United States
Long Chen,
National Institutes of Health (NIH),
United States

*CORRESPONDENCE
Jie Chen
chenjiewestchina@163.com

†These authors have contributed equally to this work

RECEIVED 20 November 2023
ACCEPTED 09 January 2024
PUBLISHED 24 January 2024

CITATION
Wang X, Gao H, Zeng Y and Chen J (2024) A Mendelian analysis of the relationships between immune cells and breast cancer. *Front. Oncol.* 14:1341292. doi: 10.3389/fonc.2024.1341292

A Mendelian analysis of the relationships between immune cells and breast cancer

Xin Wang[1,2†], Haoyu Gao[3†], Yiyao Zeng[4] and Jie Chen[1,2*]

[1]Division of Breast Surgery, Department of General Surgery, West China Hospital, Sichuan University, Chengdu, China, [2]Breast Center, West China Hospital, Sichuan University, Chengdu, China, [3]Division of Cardiovascular Surgery, Department of General Surgery, West China Hospital, Sichuan University, Chengdu, China, [4]Department of Cardiology, Dushu Lake Hospital Affiliated to Soochow University, Medical Center of Soochow University, Suzhou Dushu Lake Hospital, Suzhou, Jiangsu, China

Background: Emerging evidence showed immune cells were associated with the development of breast cancer. Nonetheless, the causal link between them remains uncertain. Consequently, the objective of this study was to investigate the causal connection between immune traits and the likelihood of developing breast cancer.

Methods: A two-sample Mendelian randomization (MR) analysis was conducted to establish the causal relationship between immune cells and breast cancer in this study. Utilizing publicly accessible genetic data, we investigated causal connections between 731 immune cells and the occurrence of breast cancer. The primary approach for exploring this relationship was the application of the inverse-variance-weighted (IVW) method. Furthermore, sensitivity analyses, encompassing the leave-one-out analysis, Cochran Q test, and Egger intercept test were performed to validate the reliability of the Mendelian randomization results. Finally, we used Bayesian Weighted Mendelian Randomization (BWMR) approach to test the results of MR study.

Results: According to the Bonferroni correction, no immune trait was identified with a decreased or increased risk of overall breast cancer risk. As for the ER+ breast cancer, 6 immune trait was identified after the Bonferroni method. the IVW method results showed that CD45RA- CD4+ %CD4+ (p-value:1.37×10^{-6}), CD8dim %T cell (p-value:4.62×10^{-43}), BAFF-R on IgD+ CD38- unsw mem (p-value:6.93×10^{-5}), CD27 on PB/PC (p-value:2.72×10^{-18}) lowered the risk of breast cancer. However, CD19 on IgD- CD38br (p-value:1.64×10^{-6}), CD25 on IgD+ CD38dim (p-value: - ∞) were associated with a higher risk of developing breast cancer. As for the CX3CR1 on CD14+ CD16- monocyte (p-value: 1.15×10^{-166}), the IVW method clearly demonstrated a protective effect against ER- breast cancer. For the above positive results, BAFF-R on IgD+ CD38- unsw mem was the sole association linked to reduced breast cancer risk using the BWMR method. The intercept terms' p-values in MR-Egger regression all exceeded 0.05, indicating the absence of potential horizontal pleiotropy.

10.3389/fonc.2024.1341292

Conclusion: Through genetic approaches, our study has illustrated the distinct correlation between immune cells and breast cancer, potentially paving the way for earlier diagnosis and more efficient treatment alternatives.

KEYWORDS

immune cells, breast cancer, genetic approaches, Mendelian randomization, analysis

Introduction

Cancer has become a major problem worldwide, and despite medical advances, it remains the second leading cause of death. A study has suggested that the worldwide cancer burden is anticipated to increase by nearly 50% over the next two decades (1). As per the Cancer Statistics report for 2022, breast cancer makes up nearly one-third of diagnoses in women and prostate cancer constitutes 27% of male diagnoses (2). Considering the significant menace cancer poses to human health, early cancer screening and prevention hold paramount significance.

Immune cells increase the likelihood of cancer development and support all phases of tumorigenesis. Cancer cells, along with neighboring stromal and inflammatory cells, participate in coordinated interactions that lead to the creation of an inflamed tumor microenvironment (TME). Cells within the TME exhibit a high degree of flexibility, consistently altering their phenotypic and functional traits. Tumor-associated macrophages (TAMs) play a crucial role in the tumor microenvironment. High levels of TAM infiltration have been associated with poor prognosis in breast cancer. The balance between M1 (anti-tumor) and M2 (pro-tumor) macrophages is crucial in determining the impact on tumor progression (3). HER2-positive breast cancers often show distinct immune profiles. Studies have explored the interaction between HER2 status, TILs, and response to HER2-targeted therapies (4). In addition, Gaynor J Bates et al. explored the quantification of regulatory T cells in breast cancer patients and identified an association between increased Treg infiltration and high-risk disease and late relapse. Tregs were implicated in promoting immune evasion. Bell D, et al. examined the distribution of immature and mature dendritic cells in breast carcinoma tissue. Understanding the localization and function of dendritic cells contributes to our knowledge of antigen presentation and immune responses in breast cancer (5). But some immune cells help suppress the development of tumor cells. Tumor-infiltrating lymphocytes (TILs), particularly in triple-negative breast cancer (TNBC), have been associated with better prognosis. Higher levels of TILs have been linked to improved overall survival and response to certain therapies (6). These references provide a starting point for exploring the intricate relationship between immunophenotypes and breast cancer development or progression. It's important to note that the field is dynamic, and ongoing research continues to refine our understanding of the immune landscape in breast cancer. Always refer to the latest literature for the most up-to-date information.

Mendelian randomization (MR) is a primarily employed analytical technique in epidemiological investigations for inferring causality. It is crucial that the causal inference derived from MR is logically sound and substantiated (7, 8). This study conducted a thorough two-sample Mendelian randomization (MR) analysis to establish the causal link between immune cell signatures and breast cancer. Gaining insights into the risk factors linked to the progression of breast cancer will contribute to the development of innovative treatments for this aspect.

Method

Data sources for exposure data

We conducted an evaluation of the causal connection between 731 immune cell signatures and breast cancer using a Mendelian randomization analysis. The 731 immunophenotypes consist of median fluorescence intensities (MFI) (n=389), absolute cell (AC) counts (n=118), relative cell (RC) counts (n=192) and morphological parameters (MP) (n=32). The first three types include myeloid cells, B cells, mature stages of T cells, monocytes, TBNK (T cells, B cells, natural killer cells), CDCs and Treg panels, while the latter type comprises CDCs and TBNK panels. For the exposure instrument, we employed the summary statistics from a recent extensive genome-wide association study (GWAS) conducted on blood cell traits by the Blood Cell Consortium (BCX). This GWAS encompassed a vast cohort of 563,085 individuals of European descent (9). Around 22 million SNPs, genotyped using high-density arrays, underwent the process of imputation using a reference panel derived from Sardinian sequences (10). The associations were assessed while accounting for covariates, including sex, age, and age squared.

Data sources for outcome data

The overall breast cancer data (including 15680 cases and 167189 controls) used in this study were derived from the FinnGen database (https://finngen.gitbook.io/documentation/),

with the current version (release 11, data release date: May 8, 2023). In addition, the 69,501 ER-positive (ER+) breast cases and 21,468 ER-negative (ER-) breast cases were from the Breast Cancer Association Consortium (BCAC) in the GWAS database. Because it was based on publicly available aggregated data, no additional ethical approval or consent to participate was required.

Selection of genetic variants

The instrumental variables (IVs) at a P value less than 5×10^{-8} were selected, because of the available single nucleotide polymorphisms (SNPs) limited in number (11). To obtain IVs from independent loci, we used the "TwoSampleMR" software package to set the linkage disequilibrium threshold with $R^2<0.001$ and kb=10000. T Subsequently, essential details such as the effective allele and effective size (comprising β value, standard error, and P-value) of each SNP are extracted for the computation of the F-statistic to assess potential bias from weak instrumental variables (IVs). An F-statistic exceeding 10 is considered adequate for mitigating any bias arising from weak IVs. When no expose-related SNPs were present in the outcome data, we conducted a follow-up analysis by finding and selecting suitable proxy SNPs ($r^2>0.8$). Finally, SNPs with palindromic structures are automatically excluded during the analysis. More importantly, the selected genetic variances are significantly related to breast cancer only through immune cells, not associated with confounders. In addition, several potential confounding factors may influence the relationship between immune cells and breast cancer. We conducted additional queries for these SNPs in the PhenoScanner database (http://www.phenoscanner.medschl.cam.ac.uk/), excluding SNPs linked to alternative potential confounders like gender, educational attainment, smoking, body mass index, total cholesterol, Age at menarche, alcohol intake frequency, family history of cancer, other personal history of cancer. The following genetic variants, namely rs10758669, rs2049045, rs61739285, rs10146962, and rs7082470, were excluded from the analysis on account of age at menarche. Additionally, rs439401 and rs13344267 were omitted due to considerations related to total cholesterol levels. Variants rs10406080, rs6440013, rs754388, rs17437411, rs60699901, rs62501136, rs165944, rs880749, and rs2267373 were excluded from the study based on body mass index criteria. Similarly, rs63750417 and rs492602 were disregarded due to the frequency of alcohol intake. Lastly, rs17360661 was excluded from the analysis due to a family history of cancer.

Statistical analysis

Multiple statistical approaches were employed, encompassing the inverse-variance weighted (IVW) method, MR-Egger, weighted median, weighted mode, simple mode, and MR-Pleiotropy residual sum and outlier (MR-PRESSO) tests. The IVW model is the main analytical method to test causality by performing a meta-analysis of each Wald ratio of valid SNPs included, which yielded the most accurate effect estimates, and it served as the primary analysis in nearly all MR investigations (12). In contrast, the MR-Egger analysis can still work when all SNPS are invalid, which was evaluated as horizontal pleiotropy. The slope of MR-Egger shows the relationship between them when the intercept term has no statistical significance or zero. The Cochran Q test is employed to access heterogeneity among the selected SNPs, with heterogeneity indicated when the value falls below 0.05. Then, the MR-PRESSO test conducts a comprehensive assessment for heterogeneity to identify potential outliers within the SNP data, subsequently deriving an adjusted association outcome after eliminating these potential outliers. We utilized the odds ratio (OR) with its associated 95% confidence interval (CI) to gauge the causal relationship between the variables. To avoid horizontal pleiotropy caused by a single SNP, the "leave-one-out" analysis was performed. If the SNP in the analysis is less than 3, it will be excluded. Furthermore, scatter plots and funnel plots were employed. Scatter plots indicated that the outcomes remained unaffected by any outliers. Funnel plots confirmed the stability of the correlation and indicated the absence of heterogeneity.

Bonferroni method for correction

For a more robust elucidation of causality, we applied the Bonferroni method to set multiple test significance thresholds across various classification levels, considering the count numbers within each type (4.2×10^{-4} (0.05/118) for AC counts, 1.3×10^{-4} (0.05/389) for MFI counts, 1.6×10^{-3} (0.05/32) for MP counts, 2.6×10^{-4} (0.05/192) for RC type).

To tackle the complexities arising from the polygenic nature of complex immune traits and the widespread occurrence of pleiotropy, we applied a Bayesian Weighted Mendelian Randomization (BWMR) approach for causal inference (13). This method explicitly considers the uncertainty associated with weak effects stemming from polygenicity and addresses the violation of the Instrumental Variable (IV) assumption due to pleiotropy through outlier detection using Bayesian weighting. To enhance the computational stability and efficiency of causal inference with BWMR, they have developed a Variational Expectation-Maximization (VEM) algorithm, which shown to be statistically efficient and computationally stable. Thus, we used this method to test the results by the IVW method.

Our analysis was complied with a standard MR guideline (14) and our analysis was performed in the R program using the "TwoSampleMR", "ggplot2" and "MR-PRESSO" packages. Figure 1 shows the specific MR study design.

Results

To investigate the causal impacts of breast cancer on immune cells, an MR analysis was conducted, with the IVW method being the primary analytical approach employed. As for the overall breast cancer, no immune trait was identified after the Bonferroni method. With a significance level of 0.05, we detected 18 indicative immunophenotypes. IgD+%B cell (p-value=0.0066; B cell panel),

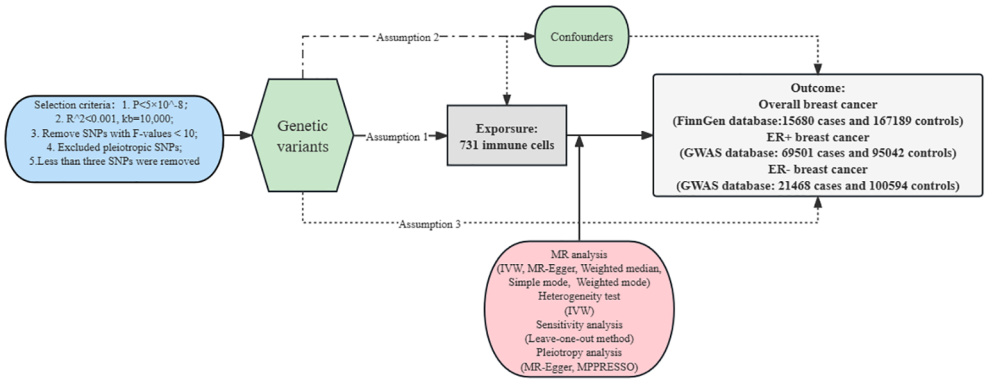

FIGURE 1
The design of Mendelian randomization analysis between immune cells and breast cancer. Assumption 1, the selected genetic variances are robustly associated with exposure; Assumption 2, the selected genetic variances are not associated with confounders; Assumption 3, the selected genetic variances are significantly related to breast cancer only through immune cells. SNPs, single-nucleotide polymorphisms. LD, linkage disequilibrium; IVW, inverse variance weighted; LOO, leave-one-out; MR, Mendelian randomization.

CD20-CD38-%B cell (p-value=0.0457; B cell panel), CD11c+ HLA DR++ monocyte %monocyte (p-value=0.0127; cDC panel), CD28- CD25++ CD8br %T cell (p-value=0.0339; Treg panel), Activated & resting Treg AC (p-value=0.0018; Treg panel), and T/B (p-value=0.0223; TBNK panel), DP (CD4+CD8+) %leukocyte (p-value=0.0087; TBNK panel), HLA DR+ CD8br AC (p-value=0.0386; TBNK panel), CD45 on CD4+ (p-value=0.0335; TBNK panel) had a positive correlation effect on the risk of breast cancer. While IgD+CD24+%B cell (p-value=0.0282; B cell panel), CD28+ CD45RA+ CD8dim AC (p-value=0.0284; Treg panel), CD28 + CD45RA+ CD8br %T cell (p-value=0.0013; Treg panel), CD3 on CD28+ DN (CD4-CD8-) (p-value=0.0322; Treg panel), Activated & secreting Treg %CD4+ (p-value=0.0456; Treg panel), CD33- HLA DR+ AC (p-value=0.0249; Myeloid cell panel), CD4/CD8br (p-value=0.0355; TBNK panel), HLA DR on CD14+ CD16- monocyte (p-value=0.0397; mature stages of T cells panel) and CCR2 on CD62L+ myeloid DC (p-value=0.0483; cDC panel) exhibited an elevated risk of breast cancer development. Among all these positive results, CD28+ CD45RA+ CD8br %T cell has been proven to have a positive negative effect by MR-Egger (p-value=0.0008), weighted median (p-value=0.0127), weighted mode methods (p-value=0.0324). The above analysis was shown in Supplementary Table 1. After Bayesian Weighted Mendelian Randomization (BWMR) approach testing, we found positive results for CD20- CD38- %B cell (p-value=0.0094), CD11c+ HLA DR++ monocyte %monocyte (p-value=0.0021), Activated & resting Treg AC (p-value=0.0130), Activated & secreting Treg %CD4+ (p-value=0.0041), T/B (p-value=0.0479), CD4/CD8br (p-value=0.0496), DP (CD4+CD8+) %leukocyte (p-value=0.0147), HLA DR+ CD8br AC (p-value=0.0369), CD28+ CD45RA+ CD8dim AC (p-value=0.0409), CD28- CD25++ CD8br %T cell (p-value=0.0335), CD28+ CD45RA+ CD8br %T cell (p-value=0.0061). The results were shown in Figure 2 and Supplementary Table 5.

In the context of ER+ breast cancer, we identified 27 suggestive immunophenotypes at a significance level of 0.05, which summarized in Supplementary Table 2. After employing the Bonferroni method through the IVW approach, six immune traits were discerned. Results from the IVW method indicated that CD45RA- CD4+ %CD4+ significantly decreased the risk of breast cancer (mature stages of T cells panel; Odds ratio: 0.9140, 95%CI: 0.8810 - 0.9480, p-value: 1.37×10−6), and this was corroborated by the weighted mode (Odds ratio: 0.9498, 95%CI: 0.9084 - 0.9931, p-value: 0.0471) and MR-Egger method (Odds ratio: 0.8747, 95%CI: 0.8114 - 0.9430, p-value: 0.0068). Furthermore, CD8dim %T cell was associated with a lowered risk of breast cancer as per the IVW method (TBNK panel; Odds ratio: 0.9663, 95%CI: 0.9616-0.9710, p-value: 4.62×10−43), and this was supported by the weighted mode (Odds ratio: 0.9681, 95%CI: 0.9533-0.9832, p-value: 0.0093) and weighted median (Odds ratio: 0.9671, 95%CI: 0.9474-0.9871, p-value: 0.0014). BAFF-R on IgD+ CD38- unsw mem (B cell panel; Odds ratio:0.9819, 95%CI:0.9731-0.9908, p-value:6.93×10^{-5}) and CD27 on PB/PC (B cell panel; Odds ratio:0.7162, 95%CI:0.7162-0.8093, p-value:2.72×10^{-18}) were both linked to a decreased risk of breast cancer according to the IVW method, and these findings were consistent with the results from the weighted mode and weighted median. Conversely, CD19 on IgD- CD38br (B cell panel; Odds ratio:1.1429, 95%CI:1.0821-1.2071, p-value:1.64×10^{-6}) was associated with an increased risk of breast cancer across the IVW method, weighted mode, and weighted median. Similarly, CD25 on IgD+ CD38dim (B cell panel; Odds ratio:1.0329, 95%CI:1.0326-1.0332, p-value: - ∞) was linked to a higher risk of breast cancer based on the IVW method, weighted median, and MR-Egger. The above analysis was shown in Table 1 and Figure 3. Following the Bonferroni method applied to the six aforementioned immune cells showing positive correlations, our analysis revealed that BAFF-R on IgD+ CD38- unsw mem was the sole association linked to reduced breast cancer risk using the BWMR method. The results were shown in Figure 2 and Supplementary Table 5.

Seven suggestive immunophenotypes were identified at the significance of 0.05, and only one immune trait was identified in ER- breast cancer after the Bonferroni method (see Supplementary Table 3). As for the CX3CR1 on CD14+ CD16- monocyte (Monocyte type, IVW: Odds ratio:0.7196, 95%CI:0.7029-0.7367, p-value: 1.15×10^{-166}), the IVW method and weighted median

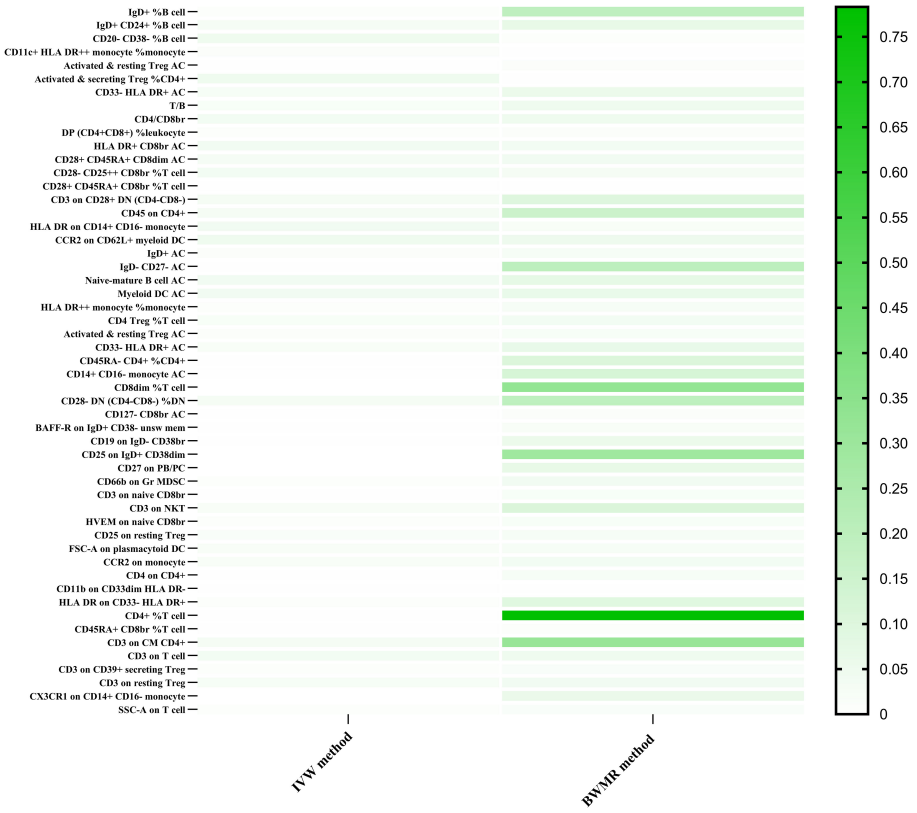

FIGURE 2
The Heatmap showed the Bayesian Weighted Mendelian Randomization (BWMR) approach to test the positive results between immune traits and breast cancers after the IVW method.

clearly demonstrated a protective effect against ER- breast cancer. But after the BWMR test, CX3CR1 on CD14+ CD16- monocyte did not show a positive result. The results were shown in Figure 2 and Supplementary Table 5.

We also plotted a schematic summary figure for the positive results in Figure 4. would be helpful for general audience to comprehend the results We employed Cochrane's Q test and MR Egger regression analysis to assess the extent of heterogeneity and horizontal pleiotropy (see Supplementary Table 4). Consistently across all reported outcomes, these tests consistently indicated an absence of heterogeneity ($p > 0.05$). Furthermore, both the intercept term in MR-Egger regression and MR-PRESSO analysis indicated the absence of significant overall horizontal pleiotropy. The Leave-one-out sensitivity analysis for the associations was shown in Supplementary Figure S1, while the scatter and funnel plots of each pair of associations were shown in Supplementary Figures S2, S3.

Discussion

Utilizing a substantial volume of publicly accessible genetic data, we investigated the causal association between 731 immune cell signatures and breast cancer. To the best of our knowledge, this study represents the inaugural Mendelian randomization (MR) analysis exploring the causal connection between numerous immunophenotypes and breast cancer. Our findings indicated that 53 immunophenotypes spanning four types of immune signatures (MFI, RC, AC, and MP) causally influences breast cancers. After the Bonferroni method, 7 immunophenotypes were found to be associated with breast cancer.

Ruffell et al. observed that breast cancer tissue contained infiltrates dominated by CD8+ and CD4+ lymphocytes, with fewer NK cells and B lymphocytes, while myeloid cells including macrophages, mast cells, and neutrophils were more pronounced in normal breast tissue (15). Among these immune phenotypes, the most significant reduction in breast cancer is CD4+ %T cell. CD4+ % cells are mainly considered as helper cells for activating CD8 +effector T cells, and there is evidence that CD4+% T cells also have independent functions in promoting anti-tumor immunity. Research has found that a subgroup of CD4+%T cells can produce a cytolytic effect on tumor cells expressing MHC II; Moreover, CD4+%T cells have demonstrated the capability to eradicate tumor cells lacking MHC-II expression through the mobilization of myeloid cells (16, 17). The Thomas Tüting team found that CD4+T cells could also independently eliminate formed tumors like CD8+cytolytic T cells, engage with CD11c+MHC-II +antigen presenting immune cells, and indirectly lead to the elimination of tumors. Meanwhile, it was further revealed that CD4+T cells, in conjunction with IFN-activated mononuclear phagocytes, collectively instigated an indirect inflammatory process resulting in tumor cell death (18).. In recent years, CAR-

TABLE 1 The Mendelian analysis showed the causal effect between immune cells and breast cancers after Bonferroni method.

Immune traits	Outcome	Inverse variance weighted		MR-Egger		Weighted median		Weighted mode		Simple mode	
		OR (95% CI)	P value	OR (95% CI)	P value	OR (95% CI)	P value	OR (95% CI)	P value	OR (95% CI)	P value
CD45RA- CD4+ %CD4+	ER (+) breast cancer	0.9140 (0.8812-0.9480)	$1.37*10^{-6}$	0.8747 (0.8114-0.9430)	0.0068	0.9422 (0.8876-1.0001)	0.0505	0.9498 (0.9084-0.9931)	0.0471	1.0010 (0.9379-1.0685)	0.9756
CD8dim %T cell	ER (+) breast cancer	0.9663 (0.9616-0.9710)	$4.63*10^{-43}$	0.8449 (0.6524-1.0940)	0.2702	0.9671 (0.9474-0.9871)	0.0014	0.9681 (0.9533-0.9832)	0.0093	1.0021 (0.8897-1.1286)	0.9741
BAFF-R on IgD+ CD38- unsw mem	ER (+) breast cancer	0.9819 (0.9731-0.9908)	$6.93*10^{-5}$	0.9805 (0.9596-1.0020)	0.1049	0.9879 (0.9740-1.0021)	0.0939	0.9884 (0.9793-0.9976)	0.0318	0.9833 (0.9608-1.0062)	0.1794
CD19 on IgD- CD38br	ER (+) breast cancer	1.1429 (1.0822-1.2071)	$1.64*10^{-6}$	1.3879 (1.0975-1.7550)	0.0715	1.1197 (1.0204-1.2287)	0.0171	1.1653 (1.0784-1.2591)	0.0180	0.9968 (0.7948-1.2502)	0.9794
CD25 on IgD + CD38dim	ER (+) breast cancer	1.0329 (1.0326-1.0332)	0	1.0613 (1.0466-1.0762)	$1.53*10^{-5}$	1.0233 (1.0058-1.0410)	0.0086	1.0259 (0.9938-1.0590)	0.1464	0.9861 (0.9188-1.0585)	0.7074
CD27 on PB/PC	ER (+) breast cancer	0.7614 (0.7162-0.8093)	$2.27*10^{-18}$	1.8823 (0.2686-13.1929)	0.5590	0.7851 (0.6721-0.9171)	0.7614	0.7510 (0.6562-0.8596)	0.0088	1.0144 (0.6697-1.5363)	0.9490
CX3CR1 on CD14 + CD16- monocyte	ER (-) breast cancer	0.7196 (0.7029-0.7367)	$1.15*10^{-166}$	0.6111 (0.2584-1.4450)	0.3437	0.7327 (0.6133-0.8754)	0.0006	0.7190 (0.6193-0.8348)	0.0123	1.1004 (0.6831-1.7726)	0.7143

T technology has been used to modify CD4+ T cells, and anti-tumor ability does not depend on cytotoxicity, but indirectly acts on tumor cells through the production of interferon-γ (IFN-γ), a large area and a long distance (19). In addition, the successful application of Adoptive cell transfer (ACT) immunotherapy with CD4+T cells in clinical research holds immense significance for the prospective treatment of cancer patients, undoubtedly paving the way for advancements in future therapies. By releasing the CD4+T cell effector function, it can immune escape the killing of tumors (20). In addition, CD45RA- CD4+ %CD4+ was also proven to be significantly linked with a decreased risk of breast cancer (21).

Monocytes, the main subpopulation of 'classical' $CD14^{+}CD16^{-}$ monocytes, can differentiate into dendritic cells and macrophages, which can participate in the host's anti-tumor response. In addition, CX3CL1 has antitumor effects by recruiting anti-tumor immune cells into the tumor microenvironment to control tumor growth (22). And we found that they could reduce the risk of ER breast cancer. Some results showed that CD14+CD16+ monocytes CD14+CD16+ monocytes could serve as a valuable indicator for the early detection of breast cancer, but our analysis found no evidence of this (23).

New research findings suggested that enhanced clinical outcomes may be linked to various facets of the humoral immune

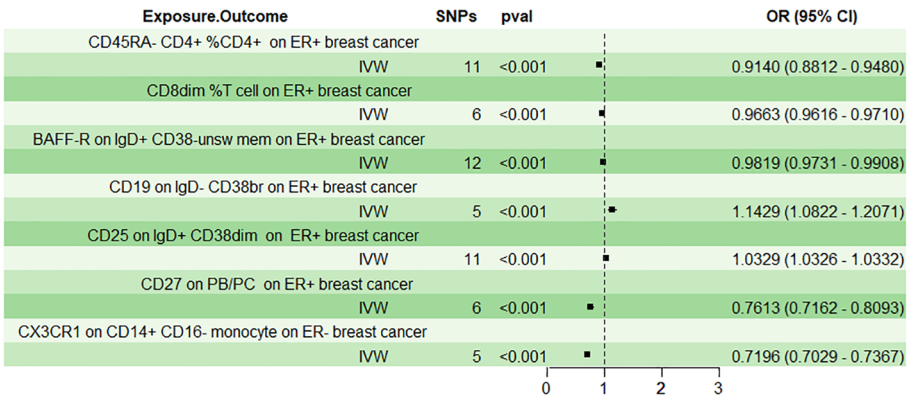

FIGURE 3
The effect of immune cells on breast cancer used the inverse-variance weighted (IVW) method after the Bonferroni method.

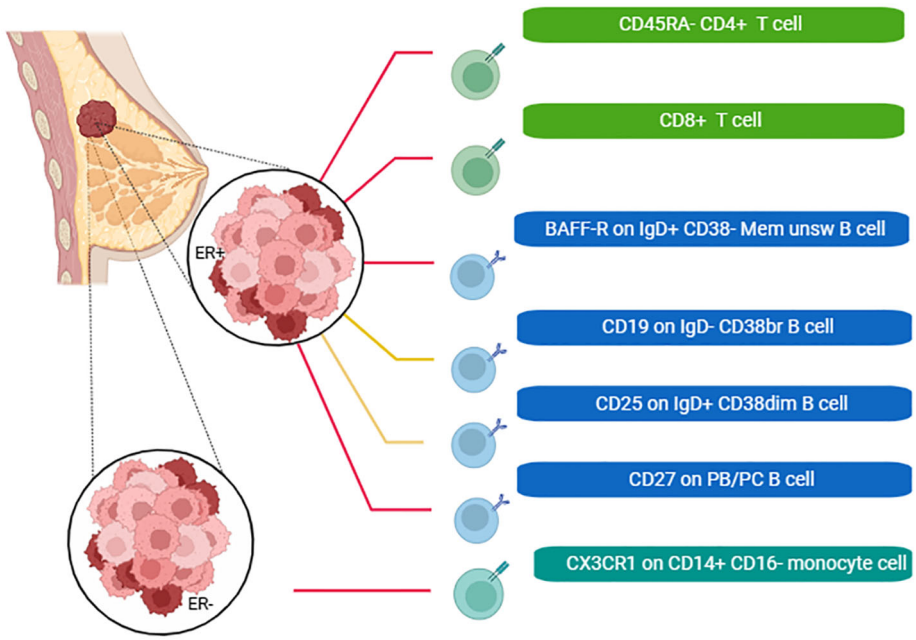

FIGURE 4
A schematic summary figure for the positive results after the Bonferroni method. The red line indicated that the immune cells could reduce the incidence of breast cancer, while the yellow line was the opposite (Created with BioRender.com).

response, characterized by B-lymphocyte infiltration into tumors and the expression of antibodies in lesions or circulation (24). Tumor-infiltrating B lymphocytes (TIL-B) clustered within the tertiary lymphoid structure may exhibit antigen-educing phenotypes, and autoantibodies are believed to trigger tumor cell clearance (25). Robert J. Harris et al. found a positive correlation between IgG+-based clonal expansion of B-lymphocyte immune system highly infiltrated response cells of breast cancer, and IgG-like regulatory signals and patient prognosis (26). Compared to $CD27^{+}IgG^{-}$ B cells, the $CD27^{+}IgG^{+}$ B cells markedly elevated expression of IFN-γ, which was consistent with our finding that CD27 on PB/PC reduces the risk of breast cancer.

The obtained results are robust and remained unaffected by horizontal pleiotropy and other potential confounding factors, ensuring the reliability and validity of the findings. However, our study also has limitations. Firstly, we didn't investigate the immune cell and other cancer phenotypes, such as lung cancer, thyroid cancer, colorectal cancer, etc. Secondly, the majority of our data pertains to individuals of European ancestry, so further research is necessary to ascertain whether our findings extend to Asian and other ancestral groups. Finally, despite conducting multiple sensitivity analyses to assess the assumptions of the Mendelian randomization study, it is not possible to entirely eliminate the potential for confounding bias and/or horizontal pleiotropy.

The implications of immune cells in breast cancer have significant implications for future studies and clinical practice. Further investigation into the role of immune cells can guide the development of targeted immunotherapies. Research focusing on harnessing the body's immune response to specifically target breast cancer cells may offer new treatment modalities. Identifying specific immune cell profiles, such as CD45RA- CD4+ %CD4+, CD8dim %T cell, BAFF-R on IgD+ CD38- unsw mem, CD27 on PB/PC, CD19 on IgD- CD38br, CD25 on IgD+ CD38dim, CX3CR1, as prognostic and predictive biomarkers is an ongoing area of research. Future studies may explore the dynamic changes in immune cell composition throughout the course of the disease and in response to different treatments. Stratifying patients based on their immune profiles may become essential for tailoring treatment strategies. Future studies could focus on refining subtyping based on the immune microenvironment, allowing for more precise treatment selection.

Conclusions

Through the application of Mendelian randomization analysis, we have effectively showcased the causal associations between multiple immunophenotypes and breast cancer. This underscores the intricate and multifaceted nature of interactions between the immune system and breast cancer within our findings. Our discoveries broaden the scope of immunological insights and offer valuable indications for breast cancer prevention, potentially facilitating earlier diagnosis and the development of more efficacious treatment alternatives.

Data availability statement

The original contributions presented in the study are included in the article/Supplementary Material. Further inquiries can be directed to the corresponding author.

Author contributions

XW: Conceptualization, Data curation, Formal analysis, Writing – original draft. HG: Formal analysis, Methodology, Validation, Writing – original draft. YZ: Investigation, Software, Supervision, Writing – original draft. JC: Supervision, Validation, Visualization, Writing – review & editing.

Funding

The author(s) declare financial support was received for the research, authorship, and/or publication of this article. This study was supported by the funding from the West China Hospital-Sichuan University(2022HXFH021) and Sichuan Science and Technology Program (2023YFG0125).

Conflict of interest

The authors declare that the research was conducted in the absence of any commercial or financial relationships that could be construed as a potential conflict of interest.

Publisher's note

Supplementary material

The Supplementary Material for this article can be found online at: https://www.frontiersin.org/articles/10.3389/fonc.2024.1341292/full#supplementary-material

SUPPLEMENTARY FIGURE 1
The sensitivity analysis of immune cells on overall breast cancer, ER+ breast cancer and ER- breast cancer.

SUPPLEMENTARY FIGURE 2
The scatter plots of the associations between immune cells on overall breast cancer, ER+ breast cancer and ER- breast cancer.

SUPPLEMENTARY FIGURE 3
Funnel plot to assess heterogeneity between immune cells on overall breast cancer, ER+ breast cancer and ER- breast cancer.

References

1. Kocarnik JM, Compton K, Dean FE, Fu W, Gaw BL, Harvey JD, et al. Cancer incidence, mortality, years of life lost, years lived with disability, and disability-adjusted life years for 29 cancer groups from 2010 to 2019: A systematic analysis for the global burden of disease study 2019. *JAMA Oncol* (2022) 8(3):420–44. doi: 10.1001/jamaoncol.2021.6987

2. Sung H, Ferlay J, Siegel RL, Laversanne M, Soerjomataram I, Jemal A, et al. Global cancer statistics 2020: GLOBOCAN estimates of incidence and mortality worldwide for 36 cancers in 185 countries. *CA Cancer J Clin* (2021) 71(3):209–49. doi: 10.3322/caac.21660

3. Qian BZ, Pollard JW. Macrophage diversity enhances tumor progression and metastasis. *Cell* (2010) 141(1):39–51. doi: 10.1016/j.cell.2010.03.014

4. Perez EA, Ballman KV, Tenner KS, Thompson EA, Badve SS, Bailey H, et al. Association of stromal tumor-infiltrating lymphocytes with recurrence-free survival in the N9831 adjuvant trial in patients with early-stage HER2-positive breast cancer. *JAMA Oncol* (2016) 2(1):56–64. doi: 10.1001/jamaoncol.2015.3239

5. Bell D, Chomarat P, Broyles D, Netto G, Harb GM, Lebecque S, et al. In breast carcinoma tissue, immature dendritic cells reside within the tumor, whereas mature dendritic cells are located in peritumoral areas. *J Exp Med* (1999) 190(10):1417–26. doi: 10.1084/jem.190.10.1417

6. Loi S, Michiels S, Salgado R, Sirtaine N, Jose V, Fumagalli D, et al. Tumor infiltrating lymphocytes are prognostic in triple negative breast cancer and predictive for trastuzumab benefit in early breast cancer: results from the FinHER trial. *Ann Oncol* (2014) 25(8):1544–50. doi: 10.1093/annonc/mdu112

7. Davey Smith G, Hemani G. Mendelian randomization: genetic anchors for causal inference in epidemiological studies. *Hum Mol Genet* (2014) 23(R1):R89–98. doi: 10.1093/hmg/ddu328

8. Timpson NJ, Wade KH, Smith GD. Mendelian randomization: application to cardiovascular disease. *Curr Hypertens Rep* (2012) 14(1):29–37. doi: 10.1007/s11906-011-0242-7

9. Orrù V, Steri M, Sidore C, Marongiu M, Serra V, Olla S, et al. Complex genetic signatures in immune cells underlie autoimmunity and inform therapy. *Nat Genet* (2020) 52(10):1036–45. doi: 10.1038/s41588-020-0684-4

10. Sidore C, Busonero F, Maschio A, Porcu E, Naitza S, Zoledziewska M, et al. Genome sequencing elucidates Sardinian genetic architecture and augments association analyses for lipid and blood inflammatory markers. *Nat Genet* (2015) 47(11):1272–81. doi: 10.1038/ng.3368

11. Yu XH, Yang YQ, Cao RR, Bo L, Lei SF. The causal role of gut microbiota in development of osteoarthritis. *Osteoarthritis Cartilage* (2021) 29(12):1741–50. doi: 10.1016/j.joca.2021.08.003

12. Hemani G, Zheng J, Elsworth B, Wade KH, Haberland V, Baird D, et al. The MR-Base platform supports systematic causal inference across the human phenome. *Elife* (2018) 7:e34408. doi: 10.7554/eLife.34408

13. Zhao J, Ming J, Hu X, Chen G, Liu J, Yang C. Bayesian weighted Mendelian randomization for causal inference based on summary statistics. *Bioinformatics* (2020) 36(5):1501–8. doi: 10.1093/bioinformatics/btz749

14. Burgess S, Davey Smith G, Davies NM, Dudbridge F, Gill D, Glymour MM, et al. Guidelines for performing Mendelian randomization investigations: update for summer 2023. *Wellcome Open Res* (2019) 4:186. doi: 10.12688/wellcomeopenres.15555.1

15. Ruffell B, Au A, Rugo HS, Esserman LJ, Hwang ES, Coussens LM. Leukocyte composition of human breast cancer. *Proc Natl Acad Sci U S A.* (2012) 109(8):2796–801. doi: 10.1073/pnas.1104303108

16. Śledzińska A, Vila de Mucha M, Bergerhoff K, Hotblack A, Demane DF, Ghorani E, et al. Regulatory T cells restrain interleukin-2- and blimp-1-dependent acquisition of cytotoxic function by CD4(+) T cells. *Immunity* (2020) 52(1):151–66.e6. doi: 10.1016/j.immuni.2019.12.007

17. Corthay A, Skovseth DK, Lundin KU, Røsjø E, Omholt H, Hofgaard PO, et al. Primary antitumor immune response mediated by CD4+ T cells. *Immunity* (2005) 22(3):371–83. doi: 10.1016/j.immuni.2005.02.003

18. Kruse B, Buzzai AC, Shridhar N, Braun AD, Gellert S, Knauth K, et al. CD4(+) T cell-induced inflammatory cell death controls immune-evasive tumours. *Nature* (2023) 618(7967):1033–40. doi: 10.1038/s41586-023-06199-x

19. Boulch M, Cazaux M, Cuffel A, Guerin MV, Garcia Z, Alonso R, et al. Tumor-intrinsic sensitivity to the pro-apoptotic effects of IFN-γ is a major determinant of CD4(+) CAR T-cell antitumor activity. *Nat Cancer* (2023) 4(7):968–83. doi: 10.1038/s43018-023-00570-7

20. Waldman AD, Fritz JM, Lenardo MJ. A guide to cancer immunotherapy: from T cell basic science to clinical practice. *Nat Rev Immunol* (2020) 20(11):651–68. doi: 10.1038/s41577-020-0306-5

21. Bailur JK, Gueckel B, Derhovanessian E, Pawelec G. Presence of circulating Her2-reactive CD8 + T-cells is associated with lower frequencies of myeloid-derived suppressor cells and regulatory T cells, and better survival in older breast cancer patients. *Breast Cancer Res* (2015) 17(1):34. doi: 10.1186/s13058-015-0541-z

22. Bronger H, Magdolen V, Goettig P, Dreyer T. Proteolytic chemokine cleavage as a regulator of lymphocytic infiltration in solid tumors. *Cancer Metastasis Rev* (2019) 38(3):417–30. doi: 10.1007/s10555-019-09807-3

23. Feng AL, Zhu JK, Sun JT, Yang MX, Neckenig MR, Wang XW, et al. CD16+ monocytes in breast cancer patients: expanded by monocyte chemoattractant protein-1

and may be useful for early diagnosis. *Clin Exp Immunol* (2011) 164(1):57–65. doi: 10.1111/j.1365-2249.2011.04321.x

24. Scott AM, Wolchok JD, Old LJ. Antibody therapy of cancer. *Nat Rev Cancer* (2012) 12(4):278–87. doi: 10.1038/nrc3236

25. Rossetti RAM, Lorenzi NPC, Yokochi K, Rosa M, Benevides L, Margarido PFR, et al. B lymphocytes can be activated to act as antigen presenting cells to promote anti-tumor responses. *PloS One* (2018) 13(7):e0199034. doi: 10.1371/journal.pone.0199034

26. Harris RJ, Cheung A, Ng JCF, Laddach R, Chenoweth AM, Crescioli S, et al. Tumor-infiltrating B lymphocyte profiling identifies igG-biased, clonally expanded prognostic phenotypes in triple-negative breast cancer. *Cancer Res* (2021) 81(16):4290–304. doi: 10.1158/0008-5472.CAN-20-3773

frontiers | Frontiers in Oncology

TYPE Original Research
PUBLISHED 06 February 2024
DOI 10.3389/fonc.2024.1349021

OPEN ACCESS

EDITED BY
Francesca Bianchi,
University of Milan, Italy

REVIEWED BY
Nan Wang,
First Affiliated Hospital of Zhengzhou University, China
Francesca Piccotti,
Scientific Clinical Institute Maugeri (ICS Maugeri), Italy

*CORRESPONDENCE
Min Xiao
xiaomin@hrbmu.edu.cn

†These authors have contributed equally to this work and share first authorship

RECEIVED 04 December 2023
ACCEPTED 22 January 2024
PUBLISHED 06 February 2024

CITATION
Li F, Wang Y, Dou H, Chen X, Wang J and Xiao M (2024) Association of immune inflammatory biomarkers with pathological complete response and clinical prognosis in young breast cancer patients undergoing neoadjuvant chemotherapy.
Front. Oncol. 14:1349021.
doi: 10.3389/fonc.2024.1349021

Association of immune inflammatory biomarkers with pathological complete response and clinical prognosis in young breast cancer patients undergoing neoadjuvant chemotherapy

Fucheng Li†, Youyu Wang†, He Dou†, Xingyan Chen, Jianan Wang and Min Xiao*

Department of Breast Surgery, Harbin Medical University Cancer Hospital, Harbin, China

Background: The persistence of inflammatory stimulus has a tight relationship with the development of age-related diseases, ultimately resulting in a gradual escalation in the prevalence of tumors, but this phenomenon is rare in young cancer patients. Breast cancer arising in young women is characterized by larger tumor diameters and more aggressive subtypes, so neoadjuvant chemotherapy (NACT) can be especially appropriate for this population. Immune inflammatory biomarkers have been reportedly linked to the prognosis of some malignant tumor types, with varying results. In this study, we investigated the possible predictive value of blood-based markers in young breast cancer patients undergoing NACT, in addition to the association between the clinicopathological features and prognosis.

Methods: From December 2011 to October 2018, a total of 215 young breast cancer patients referred to Harbin Medical University Cancer Hospital received NACT and surgery were registered in this retrospective study. The pretreatment complete blood counts were used to calculate the neutrophil-to-lymphocyte ratio (NLR), platelet-to-lymphocyte ratio (PLR), monocyte-to-lymphocyte ratio (MLR), and pan-immune-inflammation value (PIV).

Results: NLR, PLR, MLR, and PIV optimal cut-off values were 1.55, 130.66, 0.24, and 243.19, as determined by receiver operating characteristic analysis. Multivariate analysis revealed that PIV, HR status, HER-2 status, and Ki-67 index were all independent predictive factors for pathological complete response. Subgroup analysis revealed that young breast cancer patients in the population characterized by low PIV and HR negative group were more likely to get pCR (P=0.001). The five-year overall survival (OS) rate was 87.9%, and Cox regression models identified PIV as independently related to OS.

Conclusion: In the present study, the pretreatment PIV was found to be a useful prognostic indicator for pCR and long-term survival in young breast cancer patients undergoing NACT. High immune and inflammation levels, MLR and PIV were connected to poor clinical prognosis in young breast cancer patients. PIV is a promising biomarker to guide strategic decisions in treating young breast cancer.

KEYWORDS

immune inflammatory biomarker, young women, breast cancer, pathological complete response, neoadjuvant chemotherapy, pan-immune-inflammation value (PIV)

Highlights

- Immune inflammatory biomarkers are investigated solely in young patients with breast cancer.
- High immune and inflammation levels are connected to poor clinical prognosis in young breast cancer patients.
- The pretreatment pan-immune-inflammation value (PIV) is associated with pathological complete response and clinical prognosis.
- HR status, HER-2 status, and Ki-67 index are all independent predictive factors for pathological complete response in young breast cancer patients undergoing neoadjuvant chemotherapy.
- PIV is a promising biomarker to guide strategic decisions in treating young breast cancer.

1 Introduction

By 2020, breast cancer has overtaken lung cancer as the most common malignant tumor worldwide, with more than 600,000 deaths (1). Breast cancer in young females was defined as being diagnosed before the age of 40 (2), and about 16.4% of the females were diagnosed with young breast cancer in China, with a slight increase in the incidence over the past few years (3). Compared with elderly counterparts, young breast cancer patients have larger tumor diameters, more aggressive subtypes, and poorer biological behavior (4–6). Therefore, neoadjuvant chemotherapy (NACT) is especially suitable for this group of patients. Numerous NACT regimens have been used in the therapeutic management of breast cancer (7); nevertheless, no universally embraced international standard exists for evaluating the effectiveness of NACT in young patients with breast cancer.

The prognosis of breast cancer is closely related to some immunologic and histologic indicators. However, these biomarkers are arduous and expensive to obtain, commonly used in foundation research, greatly limiting their clinical application (8, 9). In contrast, peripheral blood counts are simpler to acquire and indicate systemic immune and inflammatory conditions. Immune inflammatory biomarkers (IIBs), encompassing the levels of neutrophil (N), platelet (P), monocyte (M), and lymphocyte (L), in conjunction with the neutrophil-to-lymphocyte ratio (NLR), platelet-to-lymphocyte ratio (PLR), and monocyte-to-lymphocyte ratio (MLR), have been emerged as prognostic factors for various malignant tumors (10–14). Pan-immune-inflammation value (PIV) is a new comprehensive biomarker calculated from neutrophil, monocyte, platelet, and lymphocyte counts (PIV=N × M ×P/L) that outperforms superior other separate indicators of immune-inflammatory in prognosticating clinical outcomes (15).

Older adults are often accompanied by dysfunction of the immune system, which is called immunosenescence (16). Immunosenescence is a typical physiological phenomenon linked to chronic low-grade inflammation (17, 18). During aging, organisms often showcase a distinct inflammatory state, characterized by a noteworthy expression of pro-inflammatory markers (17), which means lower levels of inflammation in healthy youngsters. At the same time, inflammation plays a beneficial role in removing harmful factors in early life and adulthood (19). However, studies related to immune and inflammation have not been widely investigated solely in young cancer patients.

Drawing upon previous investigations, we posit that IIBs could potentially assume a significant part in breast cancer prognosis. Consequently, we embarked upon this retrospective investigation to explore the prognostic role of IIBs exclusively in young breast cancer patients receiving NACT, to furnish a predictive and convenient indicator for pathological complete response (pCR) and survival outcomes.

2 Materials and methods

2.1 Patient selection and data collection

Before receiving treatment, each patient had duly endorsed the informed consent form regarding the subsequent utilization of their

medical information or biological specimens. Furthermore, all activities involving human subjects within the study complied with the standards set forth by the committee, in strict accordance with the Helsinki Declaration of 1964 and other amendments to ethical standards.

As a retrospective study, we enrolled 215 young breast cancer patients, aged 40 or below when diagnosed, who received NACT and surgery in this trial at Harbin Medical University Cancer Hospital from December 2011 to October 2018. From each patient's medical record, the specific treatment information, clinical data, and demographic information were retrieved. Patients' peripheral blood was drawn from their veins within one week before NACT, and lymphocyte (L), monocyte (M), platelet (P), and neutrophil (N) counts were collected retrospectively to calculate NLR, PLR, MLR, and PIV.

The following were the patients' inclusion criteria: 1) ≤ 40 years old; 2) pathological confirmation of invasive breast cancer diagnosis through core needle biopsy before undergoing NACT; 3) all patients received NACT and surgery in our hospital; 4) each patient's clinical records and follow-up data were full.

The following were the patients' exclusion criteria: 1) prior to receiving NACT, patients received chemotherapy, radiation, endocrine therapy, or targeted therapy; 2) patients with distant metastases; 3) patients with autoimmune or chronic inflammatory disease; 4) patients who started NACT within one month of receiving a blood transfusion.

2.2 Chemotherapy regimens

Following diagnosis, chemotherapy regimens were chosen for each patient based on immunohistochemical results, patient's preferences, and financial situation. Our study took anthracycline- (A-) based and/or taxane- (T-) based NACT regimens, and a limited cohort of patients exhibiting human epidermal growth factor receptor-2 (HER-2) positivity received anti-HER-2 therapy. Repeat the cycle every three weeks for the selected regimens. All patients underwent a minimum of four cycles of NACT, followed by 2-3 weeks of respite before proceeding to surgery. It should be mentioned that only a portion of the patients received trastuzumab and pertuzumab due to financial difficulties. The recommended duration of treatment with anti-HER-2 therapy is one year, and completion of separate anti-HER-2 therapy should be continued for a full year after surgery. In this study, anti-HER-2 drugs were used concomitantly with paclitaxel-based chemotherapeutic agents, and anthracyclines were not used concomitantly with trastuzumab due to cardiotoxicity.

Antracycline and taxane regimens include: AC-T regimen: anthracyclines 100mg/m^2, cyclophosphamide (C) 600mg/m^2, followed by docetaxel 80-100mg/m^2; TAC regimen: taxanes 75mg/m^2, anthracyclines 50mg/m^2, and cyclophosphamide 500mg/m^2; AT regimen: taxanes 75mg/m^2 and doxorubicin 60mg/m^2.

Chemotherapy and trastuzumab regimens include: AC-TH regimen: anthracyclines 100mg/m^2, cyclophosphamide 600mg/m^2, followed by docetaxel 80-100mg/m^2 and herceptin (H) 8mg/kg for the first time, then 6mg/kg; THP regimen: docetaxel 80-100mg/m^2, herceptin 8 mg/kg for the first time, then 6 mg/kg and pertuzumab (P) first dose 840 mg, then 420 mg. TH regimen: docetaxel 80-100mg/m^2, herceptin (H) 8 mg/kg for the first time, then 6 mg/kg.

Other regimens include: AC regimen: anthracyclines 90mg/m^2 and cyclophosphamide 600mg/m^2; TC regimen: docetaxel 80-100mg/m^2 and cyclophosphamide 600mg/m^2.

2.3 Classification criteria and response assessment

The eighth edition of the American Joint Committee on Cancer (AJCC) was used to assess the tumor clinical stage of each patient (20), which was the latest staging standard for breast cancer. The status of estrogen receptor positive (ER), progesterone receptor (PR), HER-2, Ki-67, and P53 were evaluated by immunohistochemistry (IHC) staining or *in situ* hybridization (ISH). Hormone receptor (HR) positive was defined as ER positive and/or PR positive. High expression of Ki-67, characterized by a nuclear positivity of >14%, was delineated, while low expression was classified as ≤14%, based on the St Gallen International Expert Consensus on the Primary Therapy of Early Breast Cancer 2013 (21). HER-2 status was divided into positive HER-2 and negative HER-2. IHC 0, IHC 1+, or IHC 2+ and ISH negative were defined as HER2 negative, and IHC 3+ or IHC 2+ and ISH positive were defined as HER-2 positive. In this study, the histological response was assessed using the Miller and Payne grade (MPG), and pCR was described as the absence of any residual invasive cancer cells within both the mammary and the lymph nodes (22).

2.4 Follow-up and endpoints

For the first two years post-surgery, outpatients checked on all patients every three months. Subsequently, follow-up appointments were scheduled biannually for the following three to five years, and then annual assessments were conducted every year until death. The deadline for this study's follow-up was September 1, 2023. Patients who were lost to follow-up were excluded from this study, and 215 patients who met the enrollment criteria were ultimately included. Overall survival (OS) was defined as the date from the initial diagnosis to death or the end of follow-up.

2.5 Statistical analysis

All statistical processing and analyses were conducted using the SPSS software (version 26.0) and GraphPad prism software (version 8.0). Frequencies and percentages were used to describe categorical variables, and the median (interquartile range) was used to describe continuous variables. Receiver operating characteristic (ROC) analysis assessed the optimal cut-off value for IIBs. The optimal metric cutoff in the ROC curve makes for the best classification, with the optimal metric cutoff at the maximum value of the Yoden

index. Univariate and multivariate analyses of the correlation between clinicopathological features and pCR were conducted by the logistic regression model. To avoid overfitting and underfitting, common important variables were included in the model. The associations between different PIV and HR subgroups were assessed by chi-square test. The cox proportional hazards regression model (univariate and multivariate) was used to examine the independent prognostic factors. OS associations were evaluated using the Kaplan–Meier methodology and log-rank test. The two-tailed $P<0.05$ was considered to be statistically significant.

3 Results

3.1 Young breast cancer patients' clinicopathological characteristics

A total of 215 eligible young patients with breast cancer (≤40 years of age) were enrolled in this study. The median age was 36 years at diagnosis, and 76 cases (35.3%) were in the high body mass index (BMI) group (BMI>24). Most of the patients were clinical T2 stage (68.3%) and node positive (cN+, 84.7%) cancers, and the number of patients with clinical TNM (cTNM) III stage was 112 (52.0%), occupying more than half of the whole population. All of the young patients with HR positive, HER-2 negative, and Ki-67>14 was 147 (68.4%), 144 (67.0%), and 164 (76.3%), respectively. In a previously conducted prognostic analysis of breast cancer after NACT, T2 stage, cN+, and HER-2 negative accounted for 63.8%, 49.1%, and 74.2% in the overall population, respectively (23). There were 179 patients (83.2%) treated with antracycline and taxane regimen, and 24 patients (11.2%) received chemotherapy and trastuzumab regimen. About sixty percent of patients received more than or equal to six cycles of NACT (n = 131), and nearly sixteen percent underwent breast-conserving surgery (n = 34). At final histology after surgery, 51 (23.7%) patients obtained pCR (Table 1).

3.2 Analysis of pCR by univariate and multivariate

The optimal cut-off values of IIBs for prediction of pCR were determined by receiver operating characteristic (ROC) analysis grouping by NLR (1.55), PLR (130.66), MLR (0.24), and PIV (243.19), with area under curve (AUC) values of 0.567, 0.608, 0.603, and 0.608, respectively (Table 2). From the ROC curve analysis, the AUC of PIV was the largest than NLR and MLR, indicating that PIV has a higher prognostic ability for pCR than NLR and MLR.

Univariate analysis showed that all low IIBs subgroups were more likely to achieve pCR than the high IIBs subgroups (NLR: OR = 0.485, 95% CI 0.241-0.975, P value = 0.042; PLR: OR = 0.396, 95% CI 0.206-0.761, P value = 0.005; MLR: OR = 0.374, 95% CI 0.183-0.766, P value = 0.007; PIV: OR=0.360, 95% CI 0.181-0.716, P value = 0.004). Young breast cancer patients who were HR negative, HER-2 positive, and Ki-67>14% were more likely to reach pCR. In the multivariate analysis, indexes exhibiting statistically significant differences in the univariate analysis were included. Logistic regression analysis indicated that compared with the high PIV group, the low PIV group was more likely to obtain pCR (OR = 0.349, 95% CI 0.147-0.828, P value = 0.017), and this finding had statistical significance. The rate of pCR was significantly associated with the HR subgroup (OR = 0.214, 95% CI 0.102-0.453, P value <0.001), HER-2 subgroup (OR = 2.155, 95% CI 1.013-4.586, P value = 0.046), and Ki-67 subgroup (OR = 2.918, 95% CI 1.013-8.410, P value = 0.047). Our results revealed that PIV, HR status, HER-2 status, and Ki-67 index were independent predictors for pCR (Table 3).

TABLE 1 Clinicopathological characteristics of young breast cancer patients.

Variable	N (n=215)	Variable	N (n=215)
Age (median)	36(23-40)	**Ki-67**	
BMI		≤14%	51(23.7%)
≤24	139(64.7%)	>14%	164(76.3%)
>24	76(35.3%)	**P53**	
cT stage		Negative	119(55.3%)
T1	25(11.6%)	Positive	96(44.7%)
T2	147(68.3%)	**Chemotherapy regimen**	
T3	34(15.8%)	Antracycline + Taxane	179(83.2%)
T4	9(4.1%)	Chemotherapy + Trastuzumab	24(11.2%)
cN stage		Other regimens	12(5.6%)
N0	33(15.3%)	**Chemotherapy Cycle**	
N1	82(38.1%)	<6	84(39.1%)
N2	65(30.2%)	≥6	131(60.9%)
N3	35(16.2%)	**Surgery**	
cTNM stage		Mastectomy	181(84.2%)
I	4(1.8%)	Conservative surgery	34(15.8%)
II	99(46.0%)	**pCR**	
III	112(52.0%)	No	164(76.3%)
HR		Yes	51(23.7%)
Negative	68(31.6%)	**NLR**	2.0(0.2-9.0)
Positive	147(68.4%)	**PLR**	134.2(51.5-401.9)
HER-2		**MLR**	0.2(0.1-0.7)
Negative	144(67.0%)	**PIV**	227.0 (24.5-1681.5)
Positive	71(33.0%)		

TABLE 2 Optimal cutoff values of NLR, PLR, MLR and PIV based on ROC curve analysis for prediction of pCR in patients.

Curve	Cut-off value	AUC	Sensitivity	Specificity	*P* value
NLR	1.55	0.567	0.333	0.805	0.149
PLR	130.66	0.608	0.647	0.579	**0.019**
MLR	0.24	0.603	0.765	0.451	**0.027**
PIV	243.19	0.608	0.725	0.512	**0.020**

Bold values indicate that they are statistically significant at P<0.05

TABLE 3 Univariate and multivariate analysis of clinical characteristics and IIBs in relation to pCR.

Variable	pCR(n=51)	Univariate analysis HR(95% CI)	*P* value	Multivariate analysis HR(95% CI)	*P* value
Age					
≤35	21(41.1%)	Ref.			
>35	30(58.8%)	1.175(0.621-2.221)	0.620		
BMI					
≤24	32(62.7%)	Ref.			
>24	19(37.2%)	1.115(0.581-2.140)	0.744		
cT stage					
T1+T2	44(86.2%)	Ref.			
T3+T4	7(13.7%)	0.566(0.235-1.363)	0.204		
cN stage					
N0	9(17.6%)	Ref.			
N+	42(82.3%)	0.800(0.345-1.853)	0.603		
cTNM stage					
I-II	27(52.9%)	Ref.			
III	24(47.0%)	0.768(0.409-1.441)	0.411		
HR					
Negative	29(56.8%)	Ref.		Ref.	
Positive	22(43.1%)	0.237(0.122-0.458)	**<0.001**	0.214(0.102-0.453)	**<0.001**
HER-2					
Negative	27(52.9%)	Ref.		Ref.	
Positive	24(47.0%)	2.213(1.160-4.220)	**0.016**	2.155(1.013-4.586)	**0.046**
Ki-67					
≤14%	5(9.8%)	Ref.		Ref.	
>14%	46(90.1%)	3.586(1.341-9.592)	**0.011**	2.918(1.013-8.410)	**0.047**
P53					
Negative	27(52.9%)	Ref.			
Positive	24(47.0%)	1.136(0.605-2.134)	0.692		
Chemotherapy regimen					
Antracycline + Taxane	40(78.4%)	Ref.			
Chemotherapy + Trastuzumab	9(17.6%)	2.085(0.849-5.119)	0.109		

(Continued)

TABLE 3 Continued

Variable	pCR(n=51)	Univariate analysis HR(95% CI)	*P* value	Multivariate analysis HR(95% CI)	*P* value
Other regimens	2(3.9%)	0.655(0.146-3.302)	0.647		
Chemotherapy Cycle					
<6	17(33.3%)	Ref.			
≥6	34(66.6%)	1.381(0.714-2.673)	0.337		
Surgery					
Mastectomy	40(78.4%)	Ref.			
Conservative surgery	11(21.5%)	1.686(0.758-3.751)	0.201		
NLR					
≤1.55	17(33.3%)	Ref.		Ref.	
>1.55	34(66.6%)	0.485(0.241-0.975)	**0.042**	0.746(0.302-1.842)	0.526
PLR					
≤130.66	33(64.7%)	Ref.		Ref.	
>130.66	18(35.2%)	0.396(0.206-0.761)	**0.005**	0.629(0.283-1.396)	0.254
MLR					
≤0.24	39(76.4%)	Ref.		Ref.	
>0.24	12(23.5%)	0.374(0.183-0.766)	**0.007**	0.649(0.270-1.562)	0.335
PIV					
≤243.19	37(72.5%)	Ref.		Ref.	
>243.19	14(27.4%)	0.360(0.181-0.716)	**0.004**	0.349(0.147-0.828)	**0.017**

Bold values indicate that they are statistically significant at P<0.05

3.3 Association between different PIV groups and clinicopathological characteristics

With the above findings, we have already known that PIV was particularly associated with pCR. We further explored the relationship between different PIV groups and clinicopathological features. Low PIV value was significantly associated with pCR (χ^2 = 8.860, P = 0.003) and has no statistical significance with other clinicopathological characteristics. It is worth noting that the difference between PIV and HER-2 subgroups was close to reach statistical significance (χ^2 = 3.735, P = 0.053) (Table 4).

3.4 Relationship between PIV and HR subgroups

Based on the above results, HR status and PIV were independent predictors for pCR in young breast cancer patients treated with NACT. Subgroup studies were conducted to examine the link between PIV and HR status in more detail. In the HR positive group (n = 147), the pCR rate of the low PIV group was 19.0% (16 cases), and that of the high PIV group was 9.5% (6 cases). There was no significant difference in the probability of pCR between different PIV subgroups (χ^2 = 2.566, P = 0.109). In the HR negative group (n = 68), the pCR rate of the low PIV subgroup was 63.6% (21 cases), and that of the high PIV subgroup was 22.9% (8 cases). The probability of pCR was significantly different between different PIV subgroups (χ^2 = 11.548, P = 0.001) (Table 5). Our results implied that the young breast cancer patients with HR negative status and low PIV level were easier to achieve pCR.

3.5 Survival analysis

There was a 3- to 140-month follow-up period, and the mean survival time from the start of follow-up for 215 young breast cancer patients was 75.8 months. High clinical T stage (P = 0.011), cTNM staging level III (P = 0.028), high MLR (P = 0.023), and high PIV (P = 0.005) were all associated with a higher risk of death in univariate analysis. Nevertheless, cox regression models revealed only PIV as independently correlated with OS in multivariable analysis, and the prolonged OS time was shown in the low PIV group (OR = 2.523, 95% CI 1.005-6.334, P value = 0.049) (Table 6).

Kaplan–Meier methodology and log-rank test showed that the OS time in young breast cancer patients with low MLR and low PIV before NACT was significantly longer than those with high MLR and high PIV (MLR: P = 0.018; PIV: P = 0.003). This trend persists in both short-term and long-term prognosis, suggesting the prognostic impact of MLR and PIV in young breast cancer

10.3389/fonc.2024.1349021

TABLE 4 Relationship between clinicopathological characteristics and different PIV groups.

Variable	N (n=215)	PIV ≤ 243.19 (n=117)	PIV>243.19 (n=98)	χ^2	*P* value
Age				0.553	0.457
≤35	95(44.2%)	49(41.9%)	46(46.9%)		
>35	120(55.8%)	68(58.1%)	52(53.1%)		
BMI				2.356	0.125
≤24	139(64.7%)	81(69.2%)	58(59.2%)		
>24	76(35.3%)	36(30.8%)	40(40.8%)		
cT stage				0.675	0.411
T1+T2	172(80.0%)	96(82.1%)	76(77.6%)		
T3+T4	43(20.0%)	21(17.9%)	22(22.4%)		
cN stage				2.358	0.125
N0	33(15.3%)	22(18.8%)	11(11.2%)		
N+	182(84.7%)	95(81.2%)	87(88.8%)		
cTNM stage				1.172	0.279
I-II	103(47.9%)	60(51.3%)	43(43.9%)		
III	112(52.1%)	57(48.7%)	55(56.1%)		
HR				1.391	0.238
Negative	68(31.6%)	33(28.2%)	35(35.7%)		
Positive	147(68.4%)	84(71.8%)	63(64.3%)		
HER-2				3.735	0.053
Negative	144(67.0%)	85(72.6%)	59(60.2%)		
Positive	71(33.0%)	32(27.4%)	39(39.8%)		
Ki-67					
≤14%	51(23.7%)	27(23.1%)	24(24.5%)		
>14%	164(76.3%)	90(76.9%)	74(75.5%)		
P53				1.718	0.190
Negative	119(55.3%)	60(51.3%)	59(60.2%)		
Positive	96(44.7%)	57(48.7%)	39(39.8%)		
Chemotherapy regimen				4.478	0.107
Antracycline + Taxane	179(83.2%)	101(86.3%)	78(79.6%)		
Chemotherapy + Trastuzumab	24(11.2%)	13(11.1%)	11(11.2%)		
Other regimens	12(5.6%)	3(2.6%)	9(9.2%)		
Chemotherapy Cycle				0.007	0.935
<6	84(39.1%)	46(39.3%)	38(38.8%)		
≥6	131(60.9%)	71(60.7%)	60(61.2%)		
Surgery				0.318	0.573
Mastectomy	181(84.2%)	100(85.5%)	81(82.7%)		
Conservative surgery	34(15.8%)	17(14.5%)	17(17.3%)		
pCR				8.860	**0.003**

(Continued)

TABLE 4 Continued

Variable	N (n=215)	PIV ≤ 243.19 (n=117)	PIV>243.19 (n=98)	χ^2	*P* value
No	164(76.3%)	80(68.4%)	84(85.7%)		
Yes	51(23.7%)	37(31.6%)	14(14.3%)		

Bold values indicate that they are statistically significant at P<0.05

TABLE 5 Relationship between PIV and HR subgroups.

Variable	HR- (n=68)				HR+ (n=147)			
	Non-pCR	pCR	χ^2	*P* value	Non-pCR	pCR	χ^2	*P* value
PIV ≤ 243.19	12	21(63.6%)	11.548	**0.001**	68	16(19.0%)	2.566	0.109
PIV>243.19	27	8(22.9%)			57	6(9.5%)		

TABLE 6 Univariate and multivariate analysis of clinicopathological characteristics and IIBs in relation to OS.

Variable	Univariate analysis HR(95% CI)	*P* value	Multivariate analysis HR(95% CI)	*P* value
Age				
≤35	Ref.			
>35	0.940(0.435-2.032)	0.874		
BMI				
≤24	Ref.			
>24	1.154(0.524-2.544)	0.722		
cT stage				
T1+T2	Ref.		Ref.	
T3+T4	2.788(1.265-6.145)	**0.011**	2.137(0.902-5.063)	0.085
cN stage				
N0	Ref.			
N+	4.794(0.650-35.384)	0.124		
cTNM stage				
I-II	Ref.		Ref.	
III	2.637(1.109-6.274)	**0.028**	1.931(0.749-4.973)	0.173
HR				
Negative	Ref.			
Positive	0.706(0.320-1.555)	0.387		
HER-2				
Negative	Ref.			
Positive	1.492(0.685-3.249)	0.313		
Ki-67				
≤14%	Ref.			
>14%	2.524(0.758-8.408)	0.131		
P53				

(Continued)

TABLE 6 Continued

Variable	Univariate analysis HR(95% CI)	*P* value	Multivariate analysis HR(95% CI)	*P* value
Negative	Ref.			
Positive	0.900(0.413-1.960)	0.791		
Chemotherapy regimen				
Antracycline + Taxane	Ref.			
Chemotherapy + Trastuzumab	0.299(0.040-2.209)	0.237		
Other regimens	0.634(0.086-4.686)	0.655		
Chemotherapy Cycle				
<6	Ref.			
≥6	1.764(0.742-4.197)	0.199		
Surgery				
Mastectomy	Ref.			
Conservative surgery	0.435(0.103-1.842)	0.258		
NLR				
≤1.55	Ref.			
>1.55	3.761(0.889-15.913)	0.072		
PLR				
≤130.66	Ref.			
>130.66	1.471(0.667-3.241)	0.339		
MLR				
≤0.24	Ref.		Ref.	
>0.24	2.502(1.135-5.515)	**0.023**	1.891(0.815-4.388)	0.138
PIV				
≤243.19	Ref.		Ref.	
>243.19	3.466(1.457-8.247)	**0.005**	2.523(1.005-6.334)	**0.049**

Bold values indicate that they are statistically significant at P<0.05

patients treated with NACT. By contrast, the other two IIBs, NLR and PLR, were not significantly related to OS (NLR: $P = 0.053$; PLR: $P = 0.335$) (Figure 1). As the follow-up period increased, the patients with low NLR and low PLR may be significantly longer than those with high NLR and high PLR.

4 Discussion

To our knowledge, this is the first study demonstrating PIV's prognostic significance in young breast cancer patients treated with NACT. This study first showed that PIV was an independent predictor of pCR and OS, whereas the patient's outcome was not substantially correlated with the NLR, PLR, and MLR. Since the majority of our patients had cT2 stage, node-positive, and cTNM III stage breast cancer, our cohort was typical of those young breast cancer patients undergoing NACT. One notable advantage of our series lay in its long clinical follow-up, spanning a median period exceeding six years, which was far longer than that of most comparable studies. It enabled a mature and pertinent evaluation of survival outcome.

This increased lifespan is linked to a progressive deterioration in immunological function and chronic inflammation (24). Immune aging is primarily manifested by these modifications in T- and B-cell composition and function (25). What's more, the defective immune response is mainly characterized by thymic involution (25), bone marrow degeneration (26), and aging lymph nodes (27). Compared to those who are older, youngsters experience fewer innate and adaptive immune response modification changes by aging (28). However, there are relatively few studies concerning immune and inflammation, solely in young cancer patients. Our research revealed that the low level of PIV group was more easily to achieve pCR and had longer OS in young patients with breast cancer. Inflammation has been widely recognized for becoming detrimental at some point in the elderly (28), and low levels of inflammation help the body neutralize foreign detrimental agents in

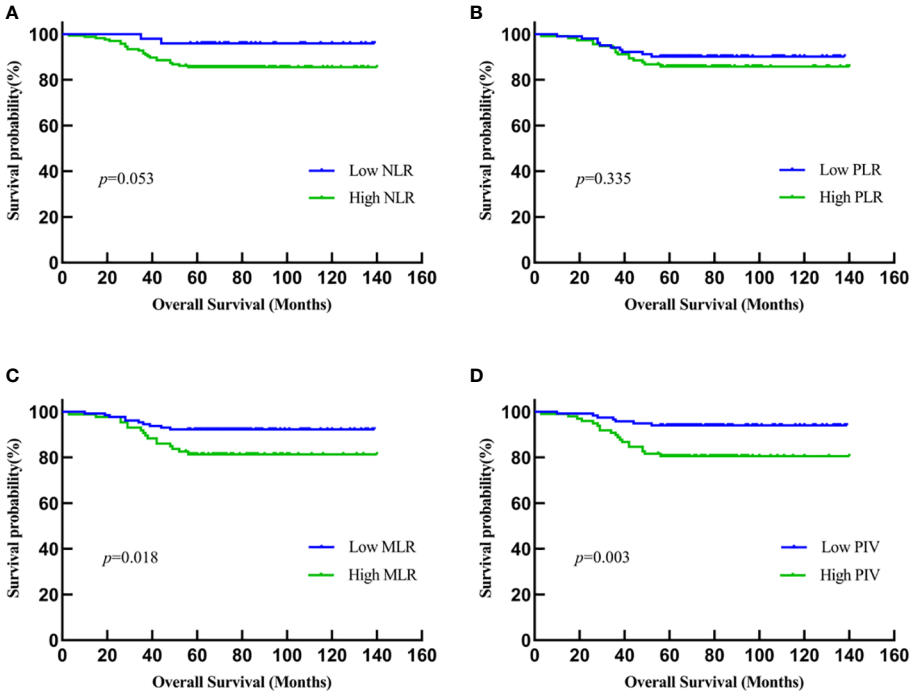

FIGURE 1
Kaplan-Meier analysis of the relationship between IIBs and OS. **(A)** NLR; **(B)** PLR; **(C)** MLR; **(D)** PIV.

healthy youngsters (17, 19). However, high inflammation level was intricately associated with poor prognosis in our study. It seems that when the tumor has not yet developed, the immune-inflammatory system assumes the role of a tumor suppressor, while in the presence of a fully formed tumor, the immune-inflammatory system acts as a tumor promoter in young breast cancer patients. It reflects that the immune-inflammatory system may affect a patient's prognosis through a local immune response and plays different roles in the different periods of tumor formation. In order to better understand its part in cancer formation and progression, more human studies are necessary in the future.

Various studies have demonstrated that the immune-inflammatory system plays a pivotal part in the proliferation, invasion, and metastasis of tumors (29–31). IIBs from peripheral venous blood can reflect the status of the whole immune-inflammatory system. Neutrophils participate in tumor invasion and metastasis by releasing inflammation intermediates, for instance, matrix metalloproteinase-9, neutrophil elastase, and interleukin-8 (32–34). Monocytes can alter the tumor microenvironment by inducing angiogenesis, immune tolerance, and cancer cell dissemination (35). Platelets promote the growth and metastasis of cancer through platelet-derived growth factors (36). In contrast, lymphocytes are essential to the anti-tumor immune response that prevents tumor growth and metastasis (37). PIV is based on the four types mentioned above of inflammatory cells; hence, it can sufficiently assess the state between host immunity and inflammatory status. Many academic works have discussed the prognostic value of PIV in various cancers. Feng et al. confirmed that PIV was associated with the tumor stage and prognosis in esophageal squamous cell carcinoma patients undergoing radical resection (38). Zhai et al. found that PIV can predict pCR of patients with non-small-cell lung cancer who received neoadjuvant immunochemotherapy (39). A meta-analysis demonstrated that colorectal tumor patients in the high pretreatment PIV group had poor OS and progression-free survival (40). Several researches supported the predictive role of PIV in breast cancer (15, 41). Among a population of patients with advanced triple-negative breast cancer undergoing platinum-based chemotherapy, Provenzano et al. found that both the baseline and initial on-treatment PIV correlate with OS (41). Our study also demonstrated that PIV was significantly related to pCR and OS in breast cancer patients undergoing NACT. More importantly, our population was entirely different from theirs since we only included young patients (≤ 40 years old).

Apart from PIV, our study's findings partially conflict with the already available literature, involving NLR, PLR, and MLR. An updated meta-analysis of 17079 breast cancer patients suggested that NLR and PLR were connected to a high risk of recurrence and poor OS, particularly in triple-negative breast cancer (12). Nevertheless, Suppan et al. could not show that NLR had predictive or prognostic significance in the group of patients with early-stage breast cancer receiving NACT (42). Similarly, Losada et al. found that PLR ≥150 was not associated with 5-year OS in elderly breast cancer patients (43). In this study, the high NLR and high PLR groups have lower pCR rates upon univariate analysis. Upon multivariable analysis, we did not find a significant relationship between NLR or PLR and pCR. We hypothesized that young women have a potential role in modulating systemic inflammation and can overcome the adverse prognostic effects of high baseline NLR and PLR. Another possible reason was that part

of the population used the herceptin and pertuzumab in this study. Meng et al. reported an association between MLR, chemotherapy response, and prognosis (44). However, we only found that a high MLR may have an adverse effect on OS by Kaplan–Meier methodology and log-rank test. In our study, PIV was not a predictive indicator for pCR. All these conflicting results may emanate from differences in the study cohorts and selection bias.

In this study, PIV was negatively correlated with pCR and lacked statistical significance with other clinicopathologic features. Patients with low PIV were more likely to get pCR than those with high PIV, suggesting that PIV has a potential predictive value for chemotherapeutic response. Since patients in the high PIV group may be in a tumor-immune-inflammatory state, it is difficult to correlate this state with separate clinicopathologic indicators.

Younger women with BC are a relatively small yet clinically extremely distinct subgroup who are unlikely to have a contraindication to undergoing NACT. About one-fifth of young breast cancer patients received NACT in China over the past two decades (23). There were two studies investigated young breast cancer patients undergoing NACT with anthracyclines/taxanes-based NACT regimens with or without targeted anti-HER-2 agents, pCR rate was 20.3% (7) and 20.9% (45), respectively, which were similar to our study data (23.7%). Li et al. found that molecular subtype and Ki-67 index were independently associated with pCR in young patients, which was consistent with our results (7). In addition to this, we further discovered that the pCR rate was significantly higher in the population of HR negative status and low PIV level. Wang et al. detected that the 5-year survival was 91.6% in young patients with breast cancer under 35 years old (23). In our study, the OS rate over five years was 87.9%. The reasons for this discrepancy in survival data may be disparate age ranges and pathological characteristics of the population.

We acknowledge that there are some limitations to this study. Firstly, it is a retrospective study with a monocentric design. More individuals should be included in future multicenter research. Secondly, systemic therapy approaches have evolved over this extensive study period, for instance, the large-scale use of targeted drugs for HER-2 positive breast cancer and neoadjuvant immunotherapy for triple-negative breast cancer (46). Thirdly, above one third of patients were in the high body mass index (BMI) group, given the potential fat mass effect on the immune system (47). Lastly, different cut-off points of IIBs may affect the prognostic value in different research.

5 Conclusion

Our research thoroughly explores the prognostic value of IIBs and finds that PIV is associated with pCR and OS in young breast cancer patients undergoing NACT. Besides, this research suggests that HR status, HER-2 status, and Ki-67 index are all independent predictive factors for pCR in young breast cancer patients, especially the patients with HR negative status and low PIV level, are easier to achieve pCR. In contrast to the NLR and PLR, which are not substantially associated with the young patient's prognosis, MLR is a good predictor of 5-year OS. Additional research is required to fully comprehend the different roles of the immune-inflammatory system between healthy young people and young cancer patients. Young patients with breast cancer have a worse prognosis; thus, we need to discover novel biomarkers and attempt to combine new biomarkers with PIV to improve clinical outcomes.

Data availability statement

The original contributions presented in the study are included in the article/supplementary material. Further inquiries can be directed to the corresponding author.

Ethics statement

The studies involving humans were approved by Harbin Medical University Cancer Hospital. The studies were conducted in accordance with the local legislation and institutional requirements. The participants provided their written informed consent to participate in this study. Written informed consent was obtained from the individual(s) for the publication of any potentially identifiable images or data included in this article.

Author contributions

FL: Conceptualization, Data curation, Investigation, Methodology, Software, Visualization, Writing – original draft, Writing – review & editing. YW: Conceptualization, Data curation, Formal analysis, Methodology, Project administration, Writing – review & editing. HD: Conceptualization, Formal analysis, Investigation, Software, Supervision, Validation, Writing – review & editing. XC: Data curation, Methodology, Supervision, Writing – review & editing. JW: Writing – review & editing. MX: Conceptualization, Formal analysis, Funding acquisition, Project administration, Resources, Supervision, Validation, Writing – review & editing.

Funding

The author(s) declare financial support was received for the research, authorship, and/or publication of this article. This study was approved by the National Natural Science Foundation of China (81872145).

Acknowledgments

We are grateful to all participants and coauthors in this study.

Conflict of interest

The authors declare that the research was conducted in the absence of any commercial or financial relationships that could be construed as a potential conflict of interest.

Publisher's note

References

1. Sung H, Ferlay J, Siegel RL, Laversanne M, Soerjomataram I, Jemal A, et al. Global cancer statistics 2020: GLOBOCAN estimates of incidence and mortality worldwide for 36 cancers in 185 countries. *CA: A Cancer J Clin* (2021) 71(3):209–49. doi: 10.3322/caac.21660

2. Paluch-Shimon S, Cardoso F, Partridge AH, Abulkhair O, Azim HA, Bianchi-Micheli G, et al. ESO-ESMO fifth international consensus guidelines for breast cancer in young women (BCY5). *Ann Oncol* (2022) 33(11):1097–118. doi: 10.1016/j.annonc.2022.07.007

3. Guo R, Si J, Xue J, Su Y, Mo M, Yang B, et al. Changing patterns and survival improvements of young breast cancer in China and SEER database, 1999-2017. *Chin J Cancer Res Chung-Kuo Yen Cheng Yen Chiu* (2019) 31(4):653–62. doi: 10.21147/j.issn.1000-9604.2019.04.09

4. Kim JK, Kwak BS, Lee JS, Hong SJ, Kim HJ, Son BH, et al. Do very young Korean breast cancer patients have worse outcomes? *Ann Surg Oncol* (2007) 14(12):3385–91. doi: 10.1245/s10434-006-9345-9

5. Yang Y, Wei W, Jin L, He H, Wei M, Shen S, et al. Comparison of the characteristics and prognosis between very young women and older women with breast cancer: A multi-institutional report from China. *Front Oncol* (2022) 12:783487. doi: 10.3389/fonc.2022.783487

6. Partridge AH, Hughes ME, Warner ET, Ottesen RA, Wong YN, Edge SB, et al. Subtype-dependent relationship between young age at diagnosis and breast cancer survival. *J Clin Oncol* (2016) 34(27):3308–14. doi: 10.1200/jco.2015.65.8013

7. Li Y, Chen H, He J, Fan Z, Zhang H. The outcome of neoadjuvant chemotherapy and the current trend of surgical treatment in young women with breast cancer: A multicenter real-world study (CSBrS-012). *Front Public Health* (2023) 11:1100421. doi: 10.3389/fpubh.2023.1100421

8. Bedognetti D, Hendrickx W, Marincola FM, Miller LD. Prognostic and predictive immune gene signatures in breast cancer. *Curr Opin Oncol* (2015) 27(6):433–44. doi: 10.1097/CCO.0000000000000234

9. Zheng T, Wang A, Hu D, Wang Y. Molecular mechanisms of breast cancer metastasis by gene expression profile analysis. *Mol Med Rep* (2017) 16(4):4671–77. doi: 10.3892/mmr.2017.7157

10. Mandaliya H, Jones M, Oldmeadow C, Nordman II. Prognostic biomarkers in stage IV non-small cell lung cancer (NSCLC): neutrophil to lymphocyte ratio (NLR), lymphocyte to monocyte ratio (LMR), platelet to lymphocyte ratio (PLR) and advanced lung cancer inflammation index (ALI). *Transl Lung Cancer r* (2019) 8(6):886–94. doi: 10.21037/tlcr.2019.11.16

11. Prabawa IPY, Bhargah A, Liwang F, Tandio DA, Tandio AL, Lestari AAW, et al. Pretreatment Neutrophil-to-Lymphocyte ratio (NLR) and Platelet-to-Lymphocyte Ratio (PLR) as a Predictive Value of. *Asian pac J Cancer p* (2019) 20(3):863–8. doi: 10.31557/APJCP.2019.20.3.863

12. Guo W, Lu X, Liu Q, Zhang T, Li P, Qiao W, et al. Prognostic value of neutrophil-to-lymphocyte ratio and platelet-to-lymphocyte ratio for breast cancer patients: An updated meta-analysis of 17079 individuals. *Cancer Med* (2019) 8 (9):4135–48. doi: 10.1002/cam4.2281

13. Kubota K, Shimizu A, Notake T, Masuo H, Hosoda K, Yasukawa K, et al. Preoperative peripheral blood lymphocyte-to-monocyte ratio predicts long-term outcome for patients with pancreatic ductal adenocarcinoma. *Ann Surg Oncol* (2022) 29(2):1437–48. doi: 10.1245/s10434-021-10848-8

14. Zhang X, Zhao W, Yu Y, Qi X, Song L, Zhang C, et al. Clinicopathological and prognostic significance of platelet-lymphocyte ratio (PLR) in gastric cancer: an updated meta-analysis. *World J Surg Oncol* (2020) 18(1):191. doi: 10.1186/s12957-020-01952-2

15. Şahin AB, Cubukcu E, Ocak B, Deligonul A, Oyucu Orhan S, Tolunay S, et al. Low pan-immune-inflammation-value predicts better chemotherapy response and survival in breast cancer patients treated with neoadjuvant chemotherapy. *Sci Rep* (2021) 11(1):14662. doi: 10.1038/s41598-021-94184-7

16. Bektas A, Schurman SH, Sen R, Ferrucci L. Human T cell immunosenescence and inflammation in aging. *J Leukocyte Biol* (2017) 102(4):977–88. doi: 10.1189/jlb.3RI0716-335R

17. Liu Z, Liang Q, Ren Y, Guo C, Ge X, Wang L, et al. Immunosenescence: molecular mechanisms and diseases. *Signal transduct tar* (2023) 8(1):200. doi: 10.1038/s41392-023-01451-2

18. Singh R, Mishra MK, Aggarwal H. Inflammation, immunity, and cancer. *Mediators Inflammation* (2017) 2017:6027305. doi: 10.1155/2017/6027305

19. Franceschi C, Bonafè M, Valensin S, Olivieri F, De Luca M, Ottaviani E, et al. Inflamm-aging. An evolutionary perspective on immunosenescence. *Ann ny Acad Sci* (2000) 908:244–54. doi: 10.1111/j.1749-6632.2000.tb06651.x

20. Abdel-Rahman O. Validation of the 8th AJCC prognostic staging system for breast cancer in a population-based setting. *Breast Cancer Res tr* (2018) 168(1):269–75. doi: 10.1007/s10549-017-4577-x

21. Goldhirsch A, Winer EP, Coates AS, Gelber RD, Piccart-Gebhart M, Thürlimann B, et al. Personalizing the treatment of women with early breast cancer: highlights of the st gallen international expert consensus on the primary therapy of early breast cancer 2013. *Ann Oncol* (2013) 24(9):2206–23. doi: 10.1093/annonc/mdt303

22. Nielsen TO, Leung SCY, Rimm DL, Dodson A, Acs B, Badve S, et al. Assessment of ki67 in breast cancer: updated recommendations from the international ki67 in breast cancer working group. *Jnci-j Natl Cancer i* (2021) 113(7):808–19. doi: 10.1093/jnci/djaa201

23. Loibl S, Jackisch C, Lederer B, Untch M, Paepke S, Kümmel S, et al. Outcome after neoadjuvant chemotherapy in young breast cancer patients: a pooled analysis of individual patient data from eight prospectively randomized controlled trials. *Breast Cancer Res tr* (2015) 152(2):377–87. doi: 10.1007/s10549-015-3479-z

24. Molony RD, Malawista A, Montgomery RR. Reduced dynamic range of antiviral innate immune responses in aging. *Exp Gerontol* (2018) 107:130–5. doi: 10.1016/j.exger.2017.08.019

25. Yanes RE, Gustafson CE, Weyand CM, Goronzy JJ. Lymphocyte generation and population homeostasis throughout life. *Semin Hematol* (2017) 54(1):33–8. doi: 10.1053/j.seminhematol.2016.10.003

26. Masters AR, Haynes L, Su DM, Palmer DB. Immune senescence: significance of the stromal microenvironment. *Clin Exp Immunol* (2017) 187(1):6–15. doi: 10.1111/cei.12851

27. Thompson HL, Smithey MJ, Surh CD, Nikolich-Žugich J. Functional and homeostatic impact of age-related changes in lymph node stroma. *Front Immunol* (2017) 8:706. doi: 10.3389/fimmu.2017.00706

28. Fulop T, Larbi A, Dupuis G, Le Page A, Frost EH, Cohen AA, et al. Immunosenescence and inflamm-aging as two sides of the same coin: friends or foes? *Front Immunol* (2017) 8:1960. doi: 10.3389/fimmu.2017.01960

29. Romero-Cordoba S, Meneghini E, Sant M, Iorio MV, Sfondrini L, Paolini B, et al. Decoding immune heterogeneity of triple negative breast cancer and its association with systemic inflammation. *Cancers* (2019) 11(7):911. doi: 10.3390/cancers11070911

30. Li L, Yu R, Cai T, Chen Z, Lan M, Zou T, et al. Effects of immune cells and cytokines on inflammation and immunosuppression in the tumor microenvironment. *Int Immunopharmacol* (2020) 88:106939. doi: 10.1016/j.intimp.2020.106939

31. Xie H, Ruan G, Ge Y, Zhang Q, Zhang H, Lin S, et al. Inflammatory burden as a prognostic biomarker for cancer. *Clin Nutr* (2022) 41(6):1236–43. doi: 10.1016/j.clnu.2022.04.019

32. Walz W, Cayabyab FS. Neutrophil infiltration and matrix metalloproteinase-9 in lacunar infarction. *Neurochemical Res* (2017) 42(9):2560–65. doi: 10.1007/s11064-017-2265-1

33. Cui C, Chakraborty K, Tang XA, Zhou G, Schoenfelt KQ, Becker KM, et al. Neutrophil elastase selectively kills cancer cells and attenuates tumorigenesis. *Cell* (2021) 184(12):3163–77.e3121. doi: 10.1016/j.cell.2021.04.016

34. Schimek V, Strasser K, Beer A, Göber S, Walterskirchen N, Brostjan C, et al. Tumour cell apoptosis modulates the colorectal cancer immune microenvironment via interleukin-8-dependent neutrophil recruitment. *Cell Death Dis* (2022) 13(2):113. doi: 10.1038/s41419-022-04585-3

35. Ugel S, Canè S, De Sanctis F, Bronte V. Monocytes in the tumor microenvironment. *Annu Rev pathol-mech* (2021) 16:93–122. doi: 10.1146/annurev-pathmechdis-012418-013058

36. Schlesinger M. Role of platelets and platelet receptors in cancer metastasis. *J Hematol Oncol* (2018) 11(1):125. doi: 10.1186/s13045-018-0669-2

37. Mohme M, Riethdorf S, Pantel K. Circulating and disseminated tumour cells - mechanisms of immune surveillance and escape. *Nat Rev Clin Oncol* (2017) 14(3):155–67. doi: 10.1038/nrclinonc.2016.144

38. Feng J, Wang L, Yang X, Chen Q, Cheng X. Clinical utility of preoperative pan-immune-inflammation value (PIV) for prognostication in patients with esophageal squamous cell carcinoma. *Int Immunopharmacol* (2023) 123:110805. doi: 10.1016/j.intimp.2023.110805

39. Zhai WY, Duan FF, Lin YB, Lin YB, Zhao ZR, Wang JY, et al. Pan-immune-inflammatory value in patients with non-small-cell lung cancer undergoing neoadjuvant immunochemotherapy. *J Inflammation Res* (2023) 16:3329–39. doi: 10.2147/JIR.S418276

40. Yang XC, Liu H, Liu DC, Tong C, Liang XW, Chen RH. Prognostic value of pan-immune-inflammation value in colorectal cancer patients: A systematic review and meta-analysis. *Front Oncol* (2022) 12:1036890. doi: 10.3389/fonc.2022.1036890

41. Provenzano L, Lobefaro R, Ligorio F, Zattarin E, Zambelli L, Sposetti C, et al. The pan-immune-inflammation value is associated with clinical outcomes in patients with advanced TNBC treated with first-line, platinum-based chemotherapy: an institutional retrospective analysis. *Ther Adv Med Oncol* (2023) 15:17588359231165978. doi: 10.1177/17588359231165978

42. Suppan C, Bjelic-Radisic V, La Garde M, Groselj-Strele A, Eberhard K, Samonigg H, et al. Neutrophil/Lymphocyte ratio has no predictive or prognostic value in breast cancer patients undergoing preoperative systemic therapy. *BMC Cancer* (2015) 15:1027. doi: 10.1186/s12885-015-2005-3

43. Losada B, Guerra JA, Malón D, Jara C, Rodriguez L, Del Barco S. Pretreatment neutrophil/lymphocyte, platelet/lymphocyte, lymphocyte/monocyte, and neutrophil/monocyte ratios and outcome in elderly breast cancer patients. *Clin Trans Oncol* (2019) 21(7):855–63. doi: 10.1007/s12094-018-1999-9

44. Meng X, Wang X, Jiang C, Zhang S, Cheng S. Correlation analysis of lymphocyte-monocyte ratio with pathological complete response and clinical prognosis of neoadjuvant chemotherapy in patients with breast cancer. *Trans Oncol* (2022) 18:101355. doi: 10.1016/j.tranon.2022.101355

45. Wang X, Xia C, Wang Y, Qi Y, Qi X, Zhao J, et al. Landscape of young breast cancer under 35 years in China over the past decades: a multicentre retrospective cohort study (YBCC-Catts study). *eClinicalMedicine* (2023) 64:102243 doi: 10.1016/j.eclinm.2023.102243

46. Korde LA, Somerfield MR, Carey LA, Crews JR, Denduluri N, Hwang ES, et al. Neoadjuvant chemotherapy, endocrine therapy, and targeted therapy for breast cancer: ASCO guideline. *J Clin Oncol* (2021) 39(13):1485–505. doi: 10.1200/JCO.20.03399

47. Prechtl P, Schmitz T, Pochert N, Traidl-Hoffmann C, Linseisen J, Meisinger C, et al. Association between body fat distribution and B-lymphocyte subsets in peripheral blood. *Immun Ageing* (2023) 20(1):47. doi: 10.1186/s12979-023-00372-6

frontiers | Frontiers in Oncology

TYPE Case Report
PUBLISHED 16 February 2024
DOI 10.3389/fonc.2024.1302196

OPEN ACCESS

EDITED BY
Anika Nagelkerke,
University of Groningen, Netherlands

REVIEWED BY
Nektarios Koufopoulos,
University General Hospital Attikon, Greece
Shahram Salek-Ardakani,
Inhibrx, United States
Isabella Castellano,
University of Turin, Italy

*CORRESPONDENCE
Cheng-gang Yang
2399853539@qq.com
Guo-Qing Pan
guoqing_pan@163.com

†These authors have contributed equally to this work

RECEIVED 26 September 2023
ACCEPTED 30 January 2024
PUBLISHED 16 February 2024

CITATION
Lei Z, Wang Y-X, Wang Z-Y, Yang C-g and Pan G-Q (2024) Case report: Tall cell carcinoma with reversed polarity of the breast: an additional case and review of the literature.
Front. Oncol. 14:1302196.
doi: 10.3389/fonc.2024.1302196

Case report: Tall cell carcinoma with reversed polarity of the breast: an additional case and review of the literature

Zi Lei[1†], Ying-Xia Wang[1†], Zhi-Yuan Wang[1], Cheng-gang Yang[2*] and Guo-Qing Pan[1*]

[1]Department of Pathology, First Affiliated Hospital of Kunming Medical University, Kunming, China, [2]Department of Pathology, Third Affiliated Hospital of Kunming Medical University, Kunming, China

Objective: The aim of this report was to comprehensively investigate the clinicopathological features, histological characteristics, and differential diagnosis of tall cell carcinoma with reversed polarity of the breast (TCCRP) to enhance the understanding of this tumour for precise therapeutic interventions.

Methods: The clinicopathological characteristics and differential diagnosis of a patient with TCCRP were retrospectively analysed, and a systematic literature review was extracted from relevant published studies on PubMed.

Results: All patients included in the study were female, with a median age of 51 years. Microscopically, the tumour cells exhibited a solid papillary growth pattern with tall columnar morphology and reversed nuclear polarity. Immunohistochemistry revealed that the tumours were triple-negative breast cancer (negative for ER, PR, and HER-2), with a low Ki-67 proliferation index. Different degrees of expression were observed for CK7, Calretinin, and S-100 markers; however, CK5/6 showed high expression levels.

Conclusions: TCCRP is an uncommon invasive carcinoma subtype found in the breast. Its histological morphology resembles that of tall cell subtype papillary thyroid carcinoma. Accurate diagnosis requires the integration of histomorphological assessment along with immunohistochemistry and molecular genetics analysis.

KEYWORDS

breast cancer, Tall cell carcinoma with reversed polarity of the breast, clinicopathological features, histological characteristics, differential diagnosis

Introduction

TCCRP is a rare type of invasive breast carcinoma. In 2003, Eusebi et al. reported five cases of breast tumours with histological features resembling those of tall cell variant papillary thyroid carcinoma (1). All patients were female, with an average age of 63 years, and no history of thyroid disease. The tumour cells exhibited solid or papillary growth patterns, with some areas showing a follicular structure reminiscent of the thyroid and containing eosinophilic glial material. These tumour cells displayed a columnar or cuboidal morphology, characterized by an eosinophilic cytoplasm due to abundant mitochondria. Most nuclei were oval-shaped with nuclear grooves observed in many instances. Some tumours exhibited intranuclear pseudoinclusions, psammoma bodies, and granular calcification. Immunohistochemical analysis revealed positive staining for CK7 and mitochondrial antibodies but negative staining for TG, TTF-1, oestrogen receptor (ER), and progesterone receptor (PR). Subsequent studies have contributed to our understanding of this tumour's morphology, immunophenotype, molecular genetic alterations, and biological behaviour (2–15). Notably, Chang et al. identified nuclear polarity inversion as a distinctive feature of these tumour cells (4). Chiang et al., through high-throughput whole-exome sequencing and targeted sequencing techniques, discovered an IDH2 R172 hotspot mutation in these tumors (8). Consequently, the name solid papillary carcinoma with reverse polarity (SPCRP) was coined, and the WHO (2019) designated this entity tall cell carcinoma with reversed polarity (TCCRP).

TCCRP is a rare disease that has been reported in only a limited number of studies, thus, it remains poorly understood by clinicians and pathologists. This study aimed to enhance the comprehension of this tumour and improve the accuracy of pathological diagnosis through an analysis of its clinicopathological features and a comprehensive literature review.

Materials and methods

Cases

One TCCRP case was obtained from the Pathology Consultation Center of Yunnan Province, and it met the diagnostic criteria for TCCRP as outlined in the WHO classification of breast tumours (2019).

A PubMed (http://www.ncbi.nlm.nih.gov/pubmed/) literature search was conducted using a combination of various keywords related to the title/abstract, such as "Breast tumor resembling the tall cell variant of papillary thyroid carcinoma," "Tall cell variant of papillary breast carcinoma," "Breast cancer with altered nuclear polarity," and "Solid papillary carcinoma with reverse polarity of the breast." Relevant published studies were reviewed, and necessary clinicopathological data were extracted. A total of 81 cases retrieved from the literature were included in our review.

Intraoperative pathological examination of frozen sections

Samples were obtained by surgical excision of breast tissue; immediately a thorough examination for the presence of nodules was performed. The nodule lesion was cut into a tissue block measuring approximately 1.5cm × 1.5cm × 0.2 cm, embedded it in a freezing agent, and placed in a -20°C frozen slicer. After embedding, the tissue was sliced into 5 mm sections, fixed them in alcohol ether for one minute, and subsequently stained with haematoxylin eosin (HE).

Paraffin pathological section examination

After sectioning the tissue, the remaining tissues were fixed in 10% neutral formaldehyde for 6-8 hours and dehydrated overnight. Subsequently, the wax blocks were cut into thin sections measuring 4 millimetres using a wax embedding machine. These sections underwent a baking process lasting for 30 minutes, followed by dewaxing and removal of benzenes through washing. Haematoxylin and eosin stains were applied prior to another round of washing, dehydration, transparentization, and sealing of the samples. Finally, morphological characteristics were observed under a light microscope.

Immunohistochemical staining

Immunohistochemical detection was performed using the optimized EnVision two-step method and DAB staining. The primary antibodies utilized for IHC were obtained from Fuzhou Maixin Biotechnology Development Co., LTD, except IDH2 R172S. The immunohistochemical analysis of IDH2 R172 was performed using a monoclonal antibody raised against IDH2 R172S (clone 11C8B1; NewEast Biosciences, Malvern, PA) (Table 1).

Results

Clinical presentation

The present case involved a 65-year-old woman who presented with a persistent left breast mass for over four months. Four months prior, the patient incidentally discovered a thumb-sized mass in her left breast accompanied by occasional tingling and no bloody nipple discharge. Physical examination revealed well-developed and symmetrical breasts without dimpling or skin changes resembling an orange peel. No bleeding or discharge was observed upon bilateral nipple compression. A large, hard-textured mass measuring less than 2 cm×2 cm was palpable in the inner upper quadrant of the left breast, displaying unclear boundaries and limited mobility. Mammography indicated an internal space-occupying lesion in the left breast suggestive of malignancy and

TABLE 1 Clones, and Dilution of primary antibodies for IHC.

Aigen	Clone	Dilution
Mammaglobin	MAB-0561	1:400
TTF-1	MAB-0677	1:400
p63	MAB-0694	1:400
TG	MAB0797	1:400
SMMHC	MAB0121	1:400
E-Cadherin	MAB0738	1:400
P120	MAB1077	1:400
ER	kit-0012	1:400
PR	kit-0013	1:400
AR	RMA-0807	1:400
HER-2	kit-0043	1:400
Ki-67	Ki-67	1:400
Syn	MAB-0742	1:400
CgA	MAB0707	1:400
CD56	MAB0743	1:400
CK5/6	MAB-0744	1:400
Calretinin	MX027	1:400
IDH2 R132	clone 11C8B1	1:2000

possible breast cancer (BI-RADS: 4C). B-ultrasound demonstrated a solid mass lesion of unknown nature in the left breast (BI-RADS: 4C), raising suspicion of breast cancer. Contrast-enhanced ultrasound showed no substantial lesions with an unknown nature in the left breast (BI-RADS: 5), further supporting consideration of breast cancer. Magnetic resonance imaging (MRI) confirmed a malignant-appearing medial mass on the left side highly indicative of breast cancer (BI-RADS: 5). The patient requested surgical removal of the mass directly, so a rapid intraoperative procedure was performed. Detailed clinical data from this case as well as previously reported cases are summarized in Table 2.

Intraoperative frozen section microscopic features

The intraoperative frozen sections revealed tumour cell nests exhibiting swelling and interstitial fibrosis (Figures 1A, B). In certain regions of the tumour, structures resembling intraductal papilloma were observed, accompanied by the accumulation of foam cells along the axis of the papilla (Figures 1C–E), making it challenging to differentiate them from intraductal papilloma using frozen section analysis. Some of these formations exhibited a sieve-like structure, with gum-like secretions visible within the cavity and sand bodies present in focal areas (Figures 1F–I). Notably, the columnar tumour cells appeared distant from the basement membrane (Figure 1G).

Postoperative paraffin section microscopic features

Macroscopically, the tumour presents as a solid nodular mass with grey-white areas, exhibiting a hard to firm consistency and indistinct margins from surrounding tissue. All reported tumors exhibited identical histological characteristics, with tumour cells forming round or ovoid nests of varying sizes and displaying expansive infiltrative growth (Figure 2A). Some of the tumour clusters exhibited irregular nests and twisted branches or structures, while the tumour stroma displayed hypocellular collagenized fibres or mild desmoplastic reactions (Figure 2B). The nests of tumour cells demonstrated three primary structures, including a solid papillary structure, an intraductal papilloma-like structure, and a papillocribriform structure. Specifically, the solid papillary structure revealed that the tumour cells proliferated around a fibrovascular axis with varying thickness (Figure 2C). Oedema, hyalinization, capillary congestion, and lymphocyte infiltration were observed in the stroma of the fibrovascular axis, while foam cells accumulated in the papillary axis (Figure 2D). In solid tumours, the cells surrounding the tumor nests and axis often exhibited a columnar morphology and were arranged in a palisade pattern perpendicular to the basement membrane (Figure 2E). The presence of an intraductal papilloma-like structure indicated the formation of a guideway-like arrangement around the tumour nests, with its inner wall lined with a single layer of columnar cells. Within the lumen, tall columnar and cuboid tumour cells covered the surface of the fibrovascular axis, forming intricate branching papillae (Figure 2F). Additionally, localized areas may exhibit hobnail changes. The proposed papillocribriform structure suggests fusion of neoplastic papillae, resulting in the formation of tension round/oval or irregular staghorn-shaped secondary gland cavities/sieves by tumour cells. Variable amounts of pink secretions were observed within the glandular cavities/ethmoid holes, some of which exhibited absorption vacuoles surrounding the secretions, resembling changes seen in thyroid follicles (Figure 2G). Some glandular cavities/ethmoids lacked secretion or showed calcifications. Additionally, focal nests of tubular and monofollicular tumour clusters were identified, predominantly composed of columnar (tall columnar, short columnar, or obese columnar) and polygonal tumour cells, characterized by abundant or moderate cytoplasm that appeared eosinophilic, reddish, or clear (Figure 2H). The nuclei of these tumour cells displayed a round, oval or irregular short rod-shaped morphology with finely granular chromatin and small- to medium-sized nucleoli that appeared reddish in colour. Mitotic figures were rare and conspicuous nuclear grooves were present; scattered intranuclear pseudoinclusion bodies were also observed. Reversal of nuclear polarity was noted in (tall) columnar cells lining the surface of glandular lumens or branching papillae where their nuclei resided close to the lumens but away from the basement membrane (Figure 2I).

Immunophenotypic characteristics

Immunohistochemical staining of tumour cells revealed positive expression of Mammoglobin (Figure 3A), and the absence of TTF-1 and Thyroglobin (TG) immunoreactivity

TABLE 2 Summary of clinical data in the TCCRP literature.

Literature	Cases	Age (The average)	Paimary site (cases)	Tumor size (cm)	Lymph node metastasis	Insitu/ infiltrated	Treatment	Follow-up (average month)
Present study	1	65	L	2.0	NA	CIS	Simple excision	48, NED
Eusebi et al.2003 (1)	5	56-74(63)	L (2) R (2) NA(1)	0.8~2.0	NA	CIS (1) MIC (2) IC (2)	Expanded resection	26-108(54)
Cameselle-Teijeiro et al 2006 (2).	1	64	R	4. 1	Yes (1)	IC	Single pure resection +C/XRT /HT	32 bone metastases
Tosi et al.2007 (3)	4	45-80	R(4)	2-5	Yes (1) No (3)	CIS (2) IC (1) NA (1)	Quadrantectomy (4)	5-120 (35. 8) NED (4)
Chang et al.2007 (4)	1	66	L	1.1	No	IC	Segmental resection	12, NED
Masood et al. 2012 (5)	1	57	L	3	No	IC	Simple excision	NA
Colella et al. 2015 (6)	1	79	R	8.5	No	MIC	Quadrantectomy	18, NED
Baohua Yu et al 2015 (7).	1	53	R	1.8	NA	IC	Lumpectomy	NA
Chiang, et al.2016 (8)	13	51-79 (65)	L (8) R (5)	0. 6-1. 8	No (8) NA (5)	IC (13)	S/XRT/C (1) S/XRT (2) S/C (1) S (1) NA (8)	12-77(33. 7) NED (7) NA (6)
Foschini* et al.2017 (9)	13	48-85 (63)	L (7) R (6)	0. 6- 2. 5	Yes (1) No (4) NA (8)	IC (13)	Mastectomy (12) Mastectomy + C /XRT (1)	24-132 (77), recurrence at 60 months with axillary lymph node metastasis (1) NED (10) NA (2)
Bhargava et al. 2016 (10)	3	48-77 (63)	L (2) R (1)	0. 9 -1. 7	NA (3)	IC (3)	NA (3)	19 NED (2) NA (1)
Pitino A et al.2017 (16)	1	65	R	0.7	No	IC	Quadrant resection	34 NED
Gai,L.et al.2018 (17)	1	55	R	NA	No	IC	Simple excision	NA
Alsodoun, N.et al.2018 (11)	9	52-75 (66)	L (5) R (4)	0.9-4	No (9)	IC (9)	segmental resection (9)	53 NED (1) NA (8)
Lozada,J.R.et al.2018 (12)*	6	58-85 (65)	NA (6)	0.6-2.1	No (2) NA (4)	IC (6)	NA (6)	NA(6)
Zhong,E.et al.2019 (13)※	9	63-79 (70)	L (5) R (4)	0.7-1. 8	NA (9) NA (9)	IC (9)	NA (9)	16-64 (32) NED (unknown)
Ding,L.M.et al.2019 (14)	1	70	L	1. 6	NA (1)	IC	Simple excision	9, NED
Pareja,F. et al.2020 (15)#	14	46-85(63)	NA (14)	0. 6-2. 6	NA (6) NA (8)	IC (14)	Partial resection (2) partial resection +XRT(3) mastectomy (1) NA(8)	NA (14)

(Continued)

TABLE 2 Continued

Literature	Cases	Age (The average)	Paimary site (cases)	Tumor size (cm)	Lymph node metastasis	Insitu/ infiltrated	Treatment	Follow-up (average month)
Haefliger, S. et al.2020 (18)	1	60	R	0.8	No	IC	Tumorectomy and sentinel lymph node excision	8, NED
Trihia HJ et al.2021 (19)	1	71	R	0.9	No	IC	Partial resection	18, NED
Zhang, X. et al. 2021 (20)	1	45	L	1.2	No	IC	Local excision sentinel and lymph node biopsy	NA
Cui LJ, et al. 2021 (21)	1	62	L	2.0	NA	IC	Mastectomy	6, NED
Jassim, M. et al.2021 (22)	1	40	R	5.5	No	IC	modified radical mastectomy with axillary clearance	6, NED

NA, no access to information; L, left; R, right; CIS, carcinoma in situ; IC, invasive carcinoma; MIC, minimally invasive carcinoma; NED, disease-free survival; C, chemotherapy; XRT, radiation therapy; HT, endocrine therapy; S, surgery. *Two cases in the Foschini group overlapped with those in the Eusebi and Tosi groups. ※One case in the Zhong group was duplicated with that in the Chiang group. # Five cases from Pareja's study were replicated in either Lozada's, Bhargava's, or Zhong's studies.

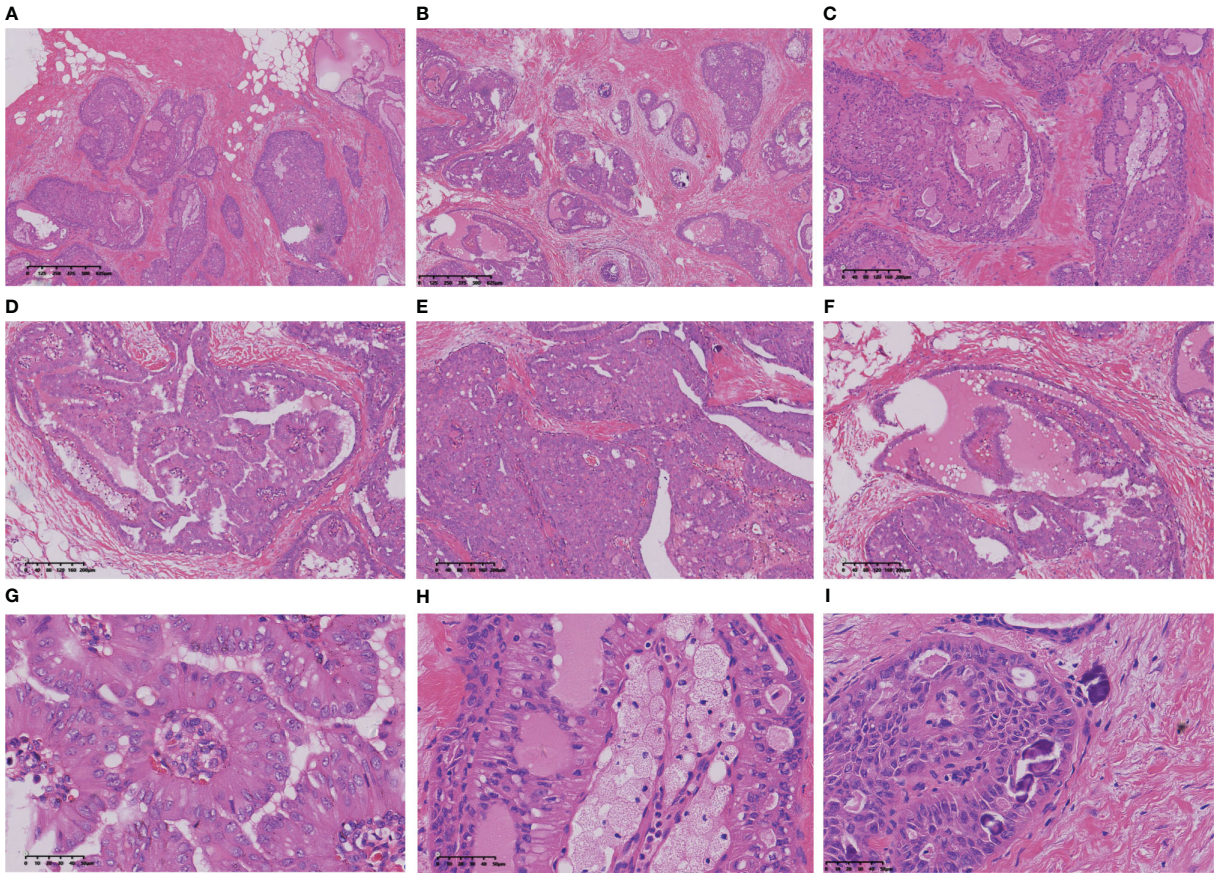

FIGURE 1
The nests of tumour cells showed expansion infiltrating growth **(A, B)**, interstitial collagenization **(C)**, intraductal papillomatous structures **(D)**, and solid papillomatous structures **(E)**. The tumour cells form a glandular cavity with glial secretions **(F)**. The tumour cells on the papillary surface are columnar, with the nucleus adjacent to the margin of the cavity and away from the basement membrane **(G)**. More foam cells were aggregated in the papillary axis **(H)**. Sand particles found in tumour nests and stroma **(I)**.

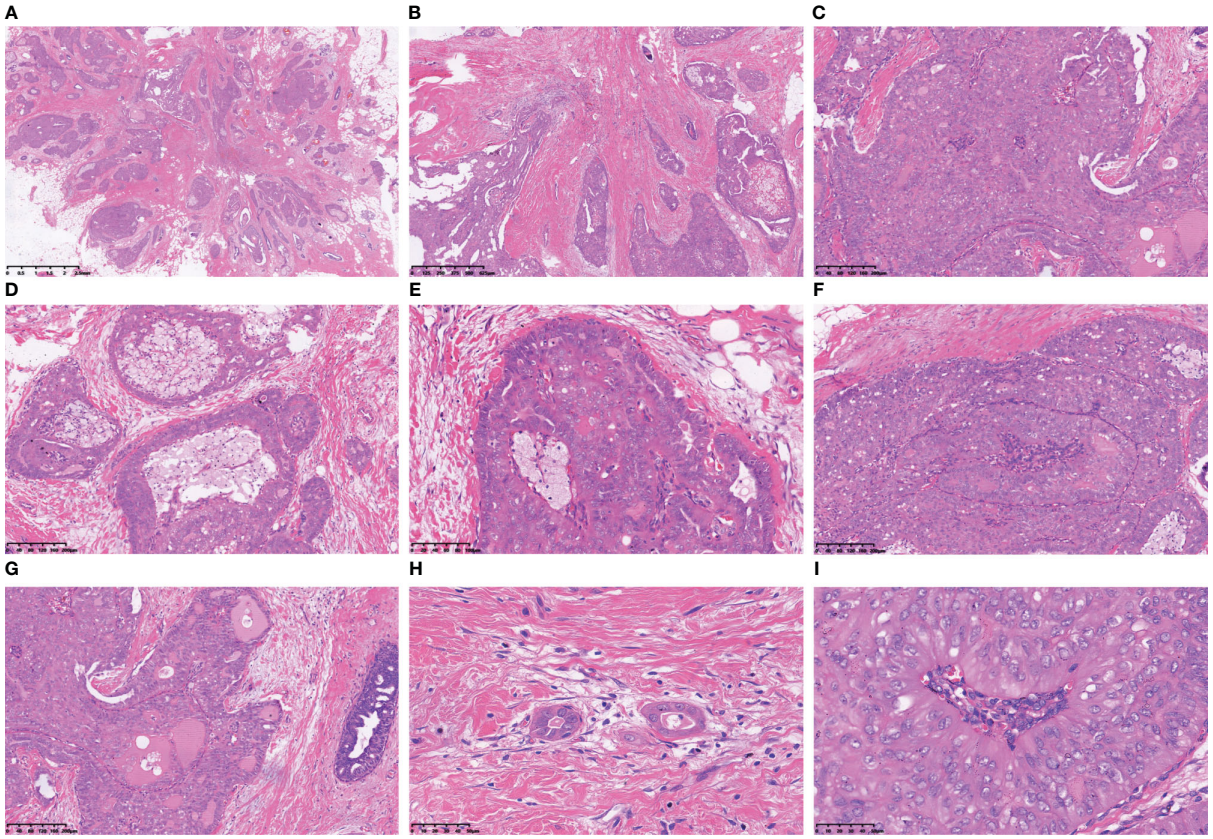

FIGURE 2
The tumour cells arrange themselves in nests and demonstrate infiltrative growth that expands extensively, accompanied by stromal collagenization **(A, B)**. The tumour cells exhibited a cohesive papillary architecture **(C)**, with an increased accumulation of foam cells within the central axis of the papillae **(D)**. The cells surrounding the tumour nest frequently exhibit a columnar morphology, being arranged in a perpendicular palisade orientation relative to the basement membrane **(E)**. The tumour cells form intraductal papillomatous structures characterized by intricate and heterogeneous papillary branching **(F)**. Tumour cells form secondary glandular cavities/ethmoids of varying sizes, and the quantity of glial secretions within these cavities varies **(G)**. Tubular-like and single follicular tumour clusters were observed within the fibrous interstitium **(H)**. The neoplastic cells lining the peri-lumen or papillary surface exhibited a columnar morphology, with their nuclei positioned adjacent to the lumen but distant from the basement membrane **(I)**.

suggested that the primary origin of the tumor cells is in the breast (Figures 3B, C). P63 and SMMHC exhibited negative staining patterns indicative of myoepithelial cell disappearance surrounding the tumor (Figures 3D, E). E-Cadherin and p120 protein were positively expressed and localized in the cell membrane (Figures 3F, G). The lack of ER, PR, AR and HER-2 indicated the tumour was triple-negative breast cancer (Figures 3H–K). A Ki-67 level of approximately 3% implied a low proliferation index for the tumour cells (Figure 3L). Additionally, varying degrees of positivity were observed with CD56 along with CK5/6 and Calretinin (Figures 3O-S), but Syn and CgA were negative (Figures 3M, N). IDH2 R172 positivity indicated IDH2 172 mutation (Figure 3T).

Discussion

TCCRP is a relatively rare subtype of breast cancer, with only 14 cases reported in the largest series (15). Due to its unique clinicopathological and molecular genetic characteristics, TCCRP has been classified as an independent subtype of "rare and salivary gland-type tumours" in the WHO (2019) classification of breast tumors to avoid confusion with breast papillary tumours and thyroid metastatic tumors (23).

A summary of the cases in this cohort and a literature review (Table 2) indicated that TCCRP is more prevalent among elderly females, with palpable breast masses as the primary clinical manifestation. TCCRP typically presents as small lesions (primarily T2), appearing as grey-white solid nodules with well-defined margins and a firm texture. The initial study conducted by Eusebi et al. strongly emphasized the histological similarities between TCCRP and papillary thyroid carcinoma, including the presence of papillary and follicular structures, columnar cells with nuclear grooves and intranuclear pseudoinclusion bodies, glial-like secretions, and calcification (1). In 2016, Chiang et al. identified a characteristic IDH2 R172 mutation in TCCRP and reported that the tumour exhibited distinct pathological features, including a solid papillary structure, reversal of nuclear polarity, accumulation of foam cells in the papillary axis, lack of myoepithelium and high expression of CK5/6 (8).

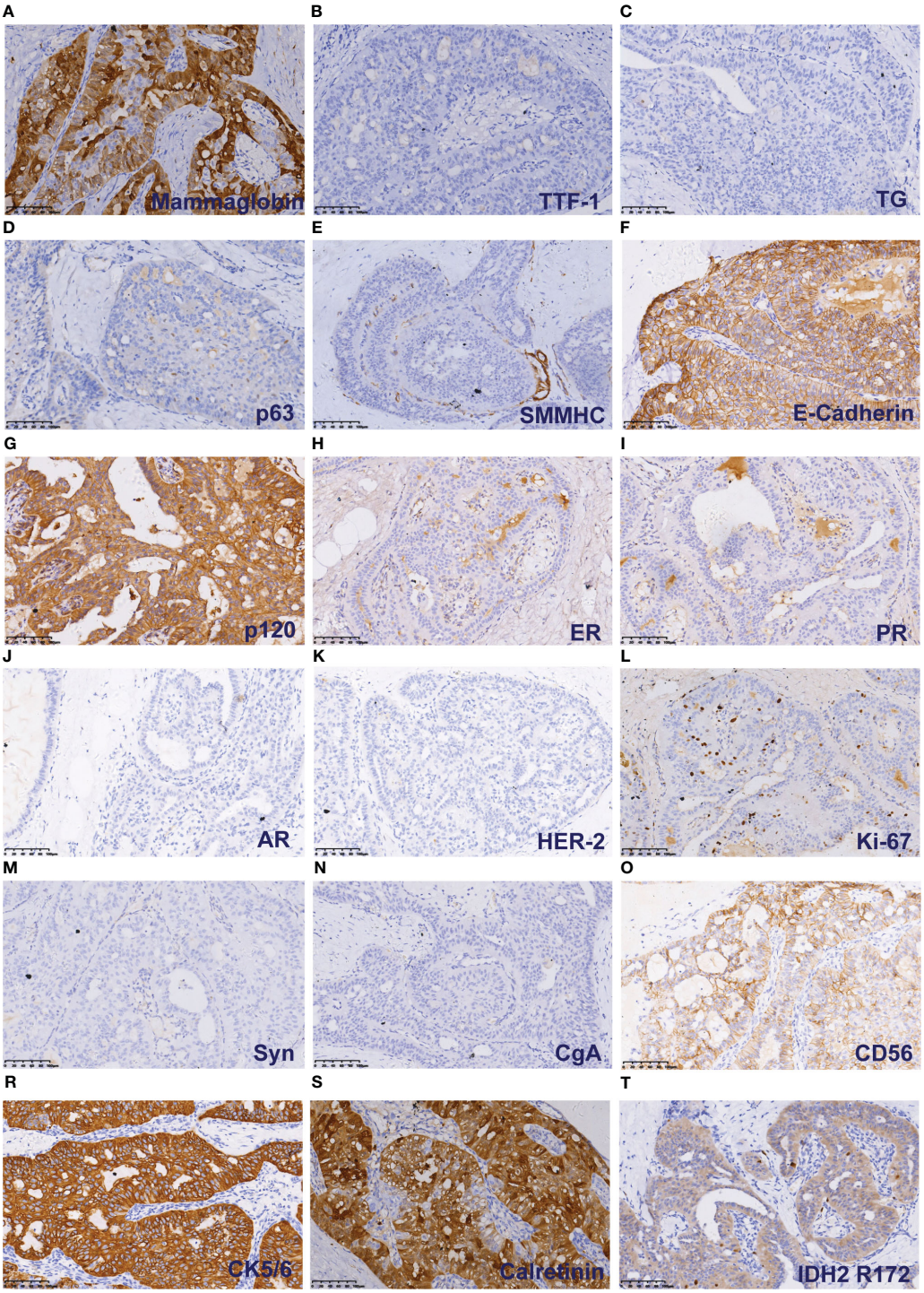

FIGURE 3
Immunohistochemical results of TCCRP. The cells were cytoplasmic positive for Mammaglobin **(A)**. The cells were negative for TTF-1 and TG **(B)**. The cells were negative for p63 and SMMHC **(D, E)**. The cells were membrane positive for E-Cadherin and p120 **(F, G)**. The cells were negative for ER, PR, AR and HER-2 **(H–K)**. The number of Ki-67 positive cells was <5% **(L)**. The cells were negative for Syn and CgA **(M, N)**. The cells were membrane positive for CD56, CK5/6, and Calretinin **(O-S)**. The cells were cytoplasmic positive for IDH2 R172 **(T)**.

This group of studies demonstrated that TCCRP exhibits three main structural patterns, including a solid mastoid head structure, a papilloma-like structure, and a papillocribriform structure. All tumours contain cribriform structures with varying proportions. While the solid papillary structure is the primary structural pattern in TCCRP, some tumours also exhibit morphological changes similar to thyroid papillary carcinoma. Familiarity with the diverse morphological changes in TCCRP can help prevent missed diagnoses when limited material is available, such as that obtained with biopsy. Notably, atypical lesions may occur in

TCCRP; for example, polygonal rather than columnar tumour cells may be present in some solid mastoid nests and nuclear polarity reversal may not always be significant or relatively limited (13), while complete lack of glial follicular changes and calcification are possible.

In the early literature, reported cases of TCCRP may solely represent *in situ* lesions; however, the 2019 Classification of Breast Tumours clearly categorizes TCCRP as a rare subtype of invasive breast adenocarcinoma. It is plausible that previously reported cases classified as *in situ* might have been misidentified. Nevertheless, if encountering hyperplastic breast lesions with an intact myoepithelial layer during routine practice, the likelihood of diagnosing TCCRP is diminished.

Several studies have shown that TCCRP stably expresses mitochondria (95%) due to the rich cytoplasm of mitochondria (1, 3, 9, 16). However, the infrequent use of this antibody in pathological laboratories poses a challenge to its accessibility. Recent studies conducted by Alsadoun et al. have demonstrated that TCCRP exhibits high expression of calretinin (clone number PAD: DC8), with only two cases of papilloma in the control group showing focal weak positive staining, indicating that calretinin is a useful marker for differential diagnosis (11). Pareja et al. reported that 10 tumours exhibited diffuse (5 cases) or focal (4 cases) positivity for calretinin (clone number SP65) (15). TCCRP demonstrated positive staining for GATA-3, GCDFP-15, MMT, and CK7 in this cohort; however, it was negative for TG, TTF-1, and PAX8 markers, providing support for its breast origin rather than originating from the thyroid gland.

The elevated expression levels of basal CK5/6 and CK34βE12 have diagnostic implications in TCCRP cases with histological grades 1 or 2. Analysis of tumour biomarkers demonstrated predominantly negative or low expression levels of hormone receptors and Her2 in TCCRP, where over half of the cases were categorized as triple-negative subtype. In published studies, the reported Ki67 proliferation index for TCCRP ranged from 1% to 31%, with a majority showing a positive index below 5%. Revised sentence: Early studies indicated that TCCRP lacks the typical molecular genetic alterations observed in papillary thyroid carcinoma, such as BRAF and RET gene mutations. Recently, Chiang et al. identified the IDH2 R172 mutation in TCCRP (10/13 cases) using high-throughput sequencing technology (8). Subsequent investigations and case reports by these researchers have confirmed that this gene mutation is a frequent occurrence in TCCRP (with R172S being the most common) (8, 10–15), which is not present in classic solid papillary carcinoma, intraductal papilloma with usual hyperplasia, encapsulated papillary carcinoma or invasive micropapillary carcinoma (11, 12, 15). Thus, this mutation holds significant diagnostic value.

TCCRP should be distinguished from other diseases, such as metastatic papillary thyroid carcinoma. A comparative study by Zhong et al. found that a solid structure, histiocyte aggregation, and nuclear polarity reversal were specific to the diagnosis of TCCRP (13).However, history, tissue origin, and IHC staining can aid in diagnosing metastatic carcinoma. Furthermore, reports of breast metastasis from classic or high cell subtype papillary thyroid carcinoma are limited to case studies (13). The intraductal papilloma with usual hyperplasia exhibited a papillary structure, accompanied by foam cell aggregation in the papillary axis. Additionally, it displayed features of usual hyperplasia, a solid growth pattern with nuclear groove formation, and intranuclear pseudoinclusion bodies. Immunohistochemical staining for CK5/6 showed positive results, while myoepithelial cells were identified to support the diagnosis of papilloma. The cells of classic solid papillary carcinoma exhibit polygonal or spindle-shaped morphology, accompanied by varying degrees of intracellular and extracellular mucus secretion. They demonstrate high expression levels of neuroendocrine markers and hormone receptors, while testing negative for CK5/6. The absence of nuclear polarity flip and glial follicle-like structures serve as distinguishing features from TCCRP. Secretory carcinoma, also observed in adults, may exhibit microcystic, solid, or even papillary structures. The content within the cystic cavity resembles thyroid follicular colloid secretion; however, the immunophenotype (e.g., triple negative or receptor low expression and CK5/6 positivity) is akin to TCCRP. Bhargava et al. employed FISH detection of the ETV-6 gene in one case of TCCRP and secretory carcinoma (yielding negative results) (10). A Solid mammary head, columnar cells, and reversal of nuclear polarity support the diagnosis of TRRCP while S-100 positivity is observed in TCCRP (10, 17). Cystic hypersecretory lesions/tumour: This group of diseases needs to be distinguished from TCCRP because of the prominent follicular changes in the thyroid. One case of TCCRP reported by Colella et al. showed a cystic cavity containing glia-like secretion, papillary hyperplasia of columnar cells in the local cystic cavity, nuclear sulcus and intranuclear pseudoinclusion bodies under the microscope, but IHC showed that the tumour was mainly in situ, so the possibility of cystic hypersecretory carcinoma *in situ* with microinvasion could not be excluded (6). Detection of IDH2 gene mutations plays an important role in differential diagnosis.

TCCRP exhibits unique clinicopathological characteristics and is a low-invasive tumour. Most patients experienced no tumour recurrence during the follow-up period. One patient in the literature had internal mammary lymph node metastasis but survived without tumour recurrence for 10 years. Another patient had local recurrence and axillary lymph node metastasis after 5 years of follow-up, but survived without tumor for 4 years after the second operation (9). Cameselle et al. reported a case of a stage IIIc (pT2N3bM0) tumour recurrence that developed bone metastasis after 32 months of follow-up (2). However, Bhargava et al. questioned that it might be a common ER-positive breast cancer (10). Due to its indolent biological behaviour and good prognosis, some scholars support no aggressive clinical management for TCCRP (9).

In summary, TCCRP is an uncommon invasive carcinoma subtype with indolent clinical behavior found in the breast. Its histological morphology resembles that of tall cell subtype papillary

thyroid carcinoma. Accurate diagnosis requires the integration of histomorphological assessment along with immunohistochemistry and molecular genetics analysis.

Data availability statement

The original contributions presented in the study are included in the article/supplementary material. Further inquiries can be directed to the corresponding author.

Ethics statement

The studies involving humans were approved by The Ethics Committee of the First Affiliated Hospital of Kunming Medical University. The studies were conducted in accordance with the local legislation and institutional requirements. The participants provided their written informed consent to participate in this study. The requirement of ethical approval was waived by Ethics Committee of the First Affiliated Hospital of Kunming Medical University for the studies involving animals because Subject information was recorded by means of identifiers. The studies were conducted in accordance with the local legislation and institutional requirements. Written informed consent was obtained from the individual(s) for the publication of any potentially identifiable images or data included in this article.

Author contributions

ZL: Writing – original draft. YW: Writing – review & editing. ZW: Data curation, Writing – review & editing. CY: Conceptualization, Methodology, Project administration, Writing – review & editing. GP: Funding acquisition, Supervision, Validation, Writing – review & editing.

Funding

The author(s) declare financial support was received for the research, authorship, and/or publication of this article. This study was supported by National Natural Science Foundation of China (82260512), Basic Research Project of Department of Science and Technology of Yunnan Province (202301AT070136), Basic Research Project of Department of Science and Technology of Yunnan Province (202201AS070076), Joint Projects of Applied Basic Research of Kunming Medical University and Yunnan Province Department of science and Technology (202101AY070001-016), Science and Technology Innovation team of Education Department of Yunnan Province (K1322121), and High-level personnel training program of Yunnan Province (RLMY20200016).

Acknowledgments

We thank all authors for their contributions.

Conflict of interest

The authors declare that the research was conducted in the absence of any commercial or financial relationships that could be construed as a potential conflict of interest.

Publisher's note

References

1. Eusebi V, Damiani S, Ellis IO, Azzopardi JG, Rosai J. Breast tumor resembling the tall cell variant of papillary thyroid carcinoma: report of 5 cases. *Am J Surg Pathol* (2003) 27:1114–8. doi: 10.1097/00000478-200308000-00008

2. Cameselle-Teijeiro J, Abdulkader I, Barreiro-Morandeira F, Ruiz-Ponte C, Reyes-Santías R, Chavez E, et al. Breast tumor resembling the tall cell variant of papillary thyroid carcinoma: a case report. *Int J Surg Pathol* (2006) 14:79–84. doi: 10.1177/106689690601400116

3. Tosi AL, Ragazzi M, Asioli S, Del Vecchio M, Cavalieri M, Eusebi LH, et al. Breast tumor resembling the tall cell variant of papillary thyroid carcinoma: report of 4 cases with evidence of Malignant potential. *Int J Surg Pathol* (2007) 15:14–9. doi: 10.1177/1066896906295689

4. Chang SY, Fleiszer DM, Mesurolle B, El Khoury M, Omeroglu A. Breast tumor resembling the tall cell variant of papillary thyroid carcinoma. *Breast J* (2009) 15:531–5. doi: 10.1111/j.1524-4741.2009.00773.x

5. Masood S, Davis C, Kubik MJ. Changing the term "breast tumor resembling the tall cell variant of papillary thyroid carcinoma" to "tall cell variant of papillary breast carcinoma". *Adv anatomic Pathol* (2012) 19:108–10. doi: 10.1097/PAP.0b013e318249d090

6. Colella R, Guerriero A, Giansanti M, Sidoni A, Bellezza G. An additional case of breast tumor resembling the tall cell variant of papillary thyroid carcinoma. *Int J Surg Pathol* (2015) 23:217–20. doi: 10.1177/1066896914536222

7. Yu B, Tu X, Yang W. [Tall cell variant of papillary breast carcinoma: report of a case]. *Zhonghua bing li xue za zhi = Chin J Pathol* (2015) 44:811–2.

8. Chiang S, Weigelt B, Wen HC, Pareja F, Raghavendra A, Martelotto LG, et al. IDH2 mutations define a unique subtype of breast cancer with altered nuclear polarity. *Cancer Res* (2016) 76:7118–29. doi: 10.1158/0008-5472.Can-16-0298

9. Foschini MP, Asioli S, Foreid S, Cserni G, Ellis IO, Eusebi V, et al. Solid papillary breast carcinomas resembling the tall cell variant of papillary thyroid neoplasms: A unique invasive tumor with indolent behavior. *Am J Surg Pathol* (2017) 41:887–95. doi: 10.1097/pas.0000000000000853

10. Bhargava R, Florea AV, Pelmus M, Jones MW, Bonaventura M, Wald A, et al. Breast tumor resembling tall cell variant of papillary thyroid carcinoma: A solid papillary neoplasm with characteristic immunohistochemical profile and few recurrent mutations. *Am J Clin Pathol* (2017) 147:399–410. doi: 10.1093/ajcp/aqx016

11. Alsadoun N, MacGrogan G, Truntzer C, Lacroix-Triki M, Bedgedjian I, Koeb MH, et al. Solid papillary carcinoma with reverse polarity of the breast harbors specific morphologic, immunohistochemical and molecular profile in comparison with other benign or Malignant papillary lesions of the breast: a comparative study of 9 additional cases. *Modern Pathol an Off J United States Can Acad Pathology Inc* (2018) 31:1367–80. doi: 10.1038/s41379-018-0047-1

12. Lozada JR, Basili T, Pareja F, Alemar B, Paula ADC, Gularte-Merida R, et al. Solid papillary breast carcinomas resembling the tall cell variant of papillary thyroid

neoplasms (solid papillary carcinomas with reverse polarity) harbour recurrent mutations affecting IDH2 and PIK3CA: a validation cohort. *Histopathology* (2018) 73:339–44. doi: 10.1111/his.13522

13. Zhong E, Scognamiglio T, D'Alfonso T, Song W, Tran H, Baek I, et al. Breast tumor resembling the tall cell variant of papillary thyroid carcinoma: molecular characterization by next-generation sequencing and histopathological comparison with tall cell papillary carcinoma of thyroid. *Int J Surg Pathol* (2019) 27:134–41. doi: 10.1177/1066896918800779

14. Ding LM, Hu HX, Wang YJ, Ji D, Ni LY, Sun ZH, et al. [Tall cell variant of papillary breast carcinoma: report of a case]. *Zhonghua bing li xue za zhi = Chin J Pathol* (2019) 48:815–7. doi: 10.3760/cma.j.issn.0529-5807.2019.10.015

15. Pareja F, da Silva EM, Frosina D, Geyer FC, Lozada JR, Basili T, et al. Immunohistochemical analysis of IDH2 R172 hotspot mutations in breast papillary neoplasms: applications in the diagnosis of tall cell carcinoma with reverse polarity. *Modern Pathol an Off J United States Can Acad Pathology Inc* (2020) 33:1056–64. doi: 10.1038/s41379-019-0442-2

16. Pitino A, Squillaci S, Spairani C, Rassu PC, Cosimi MF. Tall cell variant of papillary breast carcinoma: an additional case with review of the literature. *Pathologica* (2017) 109:162–7.

17. Gai L, Done SJ, Cook D, Denic N, Erivwo P, Voisey K, et al. Breast tumour resembling tall cell variant of papillary thyroid carcinoma: case presentation (in a patient with Lynch syndrome). *J Clin Pathol* (2018) 71:1031–2. doi: 10.1136/jclinpath-2018-205337

18. Haefliger S, Muenst S, Went P, Bihl M, Dellas S, Weber WP, et al. Tall cell carcinoma of the breast with reversed polarity (TCCRP) with mutations in the IDH2 and PIK3CA genes: a case report. *Mol Biol Rep* (2020) 47:4917–21. doi: 10.1007/s11033-020-05553-w

19. Trihia HJ, Lampropoulos P, Karelis L, Souka E, Galanopoulos G, Provatas I, et al. Tall cell carcinoma with reversed polarity: A case report of a very rare breast tumor entity and mini-review. *Breast J* (2021) 27:369–76. doi: 10.1111/tbj.14165

20. Zhang X, Wu H, Wang Z, Zhou Y, Mao F, Lin Y, et al. Tall cell carcinoma of the breast with reverse polarity: case report with gene sequencing and literature review. *Gland Surg* (2021) 10:837–43. doi: 10.21037/gs-20-695

21. Cui LJ, Zhao YF, He J, Lai BA, He ZZ. [Tall cell carcinoma with reverse polarity of breast with papillary thyroid carcinoma: report of a case]. *Zhonghua bing li xue za zhi = Chin J Pathol* (2021) 50:1299–301. doi: 10.3760/cma.j.cn112151-20210322-00222

22. Jassim M, Premalata CS, Okaly G, Srinivas C. Tall cell carcinoma with reverse polarity of breast: report of a case with unique morphologic and molecular features. *Turk patoloji dergisi* (2021) 37:183–8. doi: 10.5146/tjpath.2020.01511

23. Tan PH, Ellis I, Allison K, Brogi E, Fox SB, Lakhani S, et al. The 2019 World Health Organization classification of tumours of the breast. *Histopathology* (2020) 77:181–5. doi: 10.1111/his.14091

frontiers | Frontiers in Oncology

TYPE Original Research
PUBLISHED 07 March 2024
DOI 10.3389/fonc.2024.1346312

OPEN ACCESS

EDITED BY
Sharon R. Pine,
University of Colorado Anschutz Medical Campus, United States

REVIEWED BY
Ahmet Acar,
Middle East Technical University, Türkiye
Serena Lucotti,
NewYork-Presbyterian, United States

*CORRESPONDENCE
Osamu Ohneda
oohneda@md.tsukuba.ac.jp

RECEIVED 29 November 2023
ACCEPTED 22 February 2024
PUBLISHED 07 March 2024

CITATION
Nguyen H-NT, Vuong C-K, Fukushige M, Usuda M, Takagi LK, Yamashita T, Obata-Yasuoka M, Hamada H, Osaka M, Tsukada T, Hiramatsu Y and Ohneda O (2024) Extracellular vesicles derived from SARS-CoV-2 M-protein-induced triple negative breast cancer cells promoted the ability of tissue stem cells supporting cancer progression. *Front. Oncol.* 14:1346312. doi: 10.3389/fonc.2024.1346312

Extracellular vesicles derived from SARS-CoV-2 M-protein-induced triple negative breast cancer cells promoted the ability of tissue stem cells supporting cancer progression

Hoai-Nga Thi Nguyen[1], Cat-Khanh Vuong[1], Mizuho Fukushige[1], Momoko Usuda[1], Liora Kaho Takagi[1], Toshiharu Yamashita[1], Mana Obata-Yasuoka[2], Hiromi Hamada[2], Motoo Osaka[3], Toru Tsukada[3], Yuji Hiramatsu[3] and Osamu Ohneda[1]*

[1]Laboratory of Regenerative Medicine and Stem Cell Biology, Graduate School of Comprehensive Human Science, University of Tsukuba, Tsukuba, Japan, [2]Department of Obstetrics and Gynecology, University of Tsukuba, Tsukuba, Japan, [3]Department of Cardiovascular Surgery, University of Tsukuba, Tsukuba, Japan

Introduction: SARS-CoV-2 infection increases the risk of worse outcomes in cancer patients, including those with breast cancer. Our previous study reported that the SARS-CoV-2 membrane protein (M-protein) promotes the malignant transformation of triple-negative breast cancer cells (triple-negative BCC).

Methods: In the present study, the effects of M-protein on the ability of extracellular vesicles (EV) derived from triple-negative BCC to regulate the functions of tissue stem cells facilitating the tumor microenvironment were examined.

Results: Our results showed that EV derived from M-protein-induced triple-negative BCC (MpEV) significantly induced the paracrine effects of adipose tissue-derived mesenchymal stem cells (ATMSC) on non-aggressive BCC, promoting the migration, stemness phenotypes, and *in vivo* metastasis of BCC, which is related to PGE2/IL1 signaling pathways, in comparison to EV derived from normal triple-negative BCC (nEV). In addition to ATMSC, the effects of MpEV on endothelial progenitor cells (EPC), another type of tissue stem cells, were examined. Our data suggested that EPC uptaking MpEV acquired a tumor endothelial cell-like phenotype, with increasing angiogenesis and the ability to support the aggressiveness and metastasis of non-aggressive BCC.

Discussion: Taken together, our findings suggest the role of SARS-CoV-2 M-protein in altering the cellular communication between cancer cells and other non-cancer cells inside the tumor microenvironment via EV. Specifically, M-proteins induced the ability of EV derived from triple-negative BCC to promote the functions of non-cancer cells, such as tissue stem cells, in tumorigenesis.

KEYWORDS

SARS-CoV-2, breast cancer, extracellular vesicles, tissue stem cells, tumor microenvironment

Introduction

In the coronavirus disease 2019 (COVID-19) pandemic, cancer patients have the increased SARS-CoV-2 incidences and become more vulnerable to SARS-CoV-2 infection, according to previous pan-cancer studies (1, 2). Among cancer patients, those with breast cancer patients show high expression of TMPRSS2, a SARS-CoV-2 infection-associated gene and have poor prognosis prediction (3). In addition, breast cancer patients with COVID-19 have a significant increase in serum cancer biomarker levels, suggesting the influence of SARS-CoV-2 infection on tumorigenesis (4–6). Numerous studies suggested a high risk of worse outcomes in breast cancer patients with COVID-19 due to systemic inflammatory cytokine storms (7–11) and the increased malignancy of cancer cells, resulting in new metastasis, progress and death (5, 6, 12, 13).

Although the COVID-19 pandemic has been controlled, the long-term post-COVID-19 syndrome still causes many concerns for patients with cancer, including breast cancer. After recovery from COVID-19, SARS-CoV-2 viral proteins can be detected in patient sera (14–17); therefore, the effects of SARS-CoV-2 proteins on cancer cells and the tumor microenvironment (TME), which support the development of tumors, should be studied. We previously reported that the SARS-CoV-2 membrane protein (M-protein) promotes the malignancy of triple-negative BCC (6). However, whether M-protein-induced triple-negative BCC show altered behaviors in regulating non-cancer cells inside the TME remains obscure.

In the TME, cellular communication is performed by both direct cell-cell contact and classical paracrine signals, in which extracellular vesicles (EV) are a crucial means of communication (18). EV are lipid bilayer-bound vehicles secreted from the cell membrane, and their contents reflect the original cell, including signaling proteins, RNA, and DNA (18). Cancer cells constantly produce and release EV into the extracellular space, which transmits information to surrounding cells and even distant target cells (18, 19). EV facilitate specific cell-cell interactions and stimulate signaling pathways in their target cells (18) to support tumor development (20, 21). Notably, previous studies have suggested that the functions of cancer cell-derived EV in the TME are associated with the aggressiveness of parental cancer cells. For instance, breast cancer cells with oncogene overexpression altered their EV content toward a malignant phenotype (22, 23). Although many studies have reported the effects of SARS-CoV-2 proteins on cancer cells, its effects on EV derived from cancer cells remain obscure.

The TME consists of cancer and non-cancer cells, including fibroblast, immune cells, endothelial cells and tissue stem cells such as mesenchymal stem cells (MSC) and endothelial progenitor cells (EPC) (19, 24). We previously reported the abilities of MSC derived from adipose tissues to support the metastasis of triple negative BCC (25). In addition, previous studies reported that adapting to cancer signals in the TME, MSC change their behavior and synergize with cancer cells (26, 27). MSC can differentiate into cancer-associated fibroblasts or evolve into tumor-associated mesenchymal stem cells (TA-MSC) under the control of local factors in the TME (28, 29). However, up to date the effects of SARS-CoV-2 proteins on the breast cancer signals regulating MSC are still obscured.

Another type of tissue stem cells involved in tumor microenvironment besides MSC is EPC, which belong to endothelial lineage cells (30). EPC are recruited toward tumors from the blood by signals from cancer cells and contribute to tumor growth and angiogenesis, thereby transporting nutrients to the tumor core and maintaining metabolic homeostasis (31–33). In addition, the loose cell-cell connections inside blood vessels formed in the tumor facilitates the intravasation of circulating cancer cells, which initiates the process of metastasis (24). Moreover, in the TME, EPC differentiate into tumor endothelial cells (TEC) (34), which form new blood vessels and produce cytokines and growth factors for tumor growth and invasion (35). Notably, tumor angiogenesis in EPC and other endothelial lineage cells is strongly supported by MSC located inside the tumor microenvironment (26, 28).

In the present study, we examined the effects of the SARS-CoV-2 M-protein on the ability of EV derived from triple-negative BCC to regulate the characteristics and tumorigenic functions of tissue stem cells, including MSC and EPC.

Results

EV derived from M-protein-induced triple-negative BCC increased the cancer-supporting gene expression of ATMSC but did not alter their features

Breast tumors are mainly surrounded by mammary adipose tissue and merge with a repertoire of MSC, which interact mutually with cancer cells (36). In the TME, MSC derived from adipose tissues (ATMSC) receive stimulation signals from BCC to evolve into tumor-associated mesenchymal stem cells (TA-MSC) or to differentiate into cancer-associated fibroblasts (22, 28, 29). In addition, our previous study reported the ability of ATMSC inducing the metastasis of BCC. Therefore, we first examined the effects of M-protein on the ability of EV derived from triple-negative BCC to regulate ATMSC. EV were isolated from the conditioned medium of original triple-negative BCC, MDA-MB-231 cells, (nEV) and those induced with the SARS-CoV-2 M-protein (MpEV) by ultracentrifugation. The size of nEV and MpEV were measured by dynamic light scattering and the expression of markers were examined by Western Blotting. Both nEV and MpEV were nanosized, ranging from 60 to 500 nm (Supplementary Figure 1A) and showed the expression of CD63, TSG101, and the negative expression of APOA1 (Supplementary Figure 1B).

Next, ATMSC were incubated with PKH26-labeled nEV or MpEV to mediate the uptake. The percentage of ATMSC uptaking of PKH26-labeled nEV or MpEV was 90%, examined by flow cytometry (Supplementary Figure 1C). Characterization of ATMSC post-uptaking EV showed that the uptake of either nEV or MpEV to ATMSC did not affect their morphology (Figure 1A) and proliferation (Figure 1B). Meanwhile, in comparison to the original ATMSC, those uptaking nEV or MpEV showed the induced migratory ability (Figure 1C). However, no different effects between nEV and MpEV on the migratory ability of

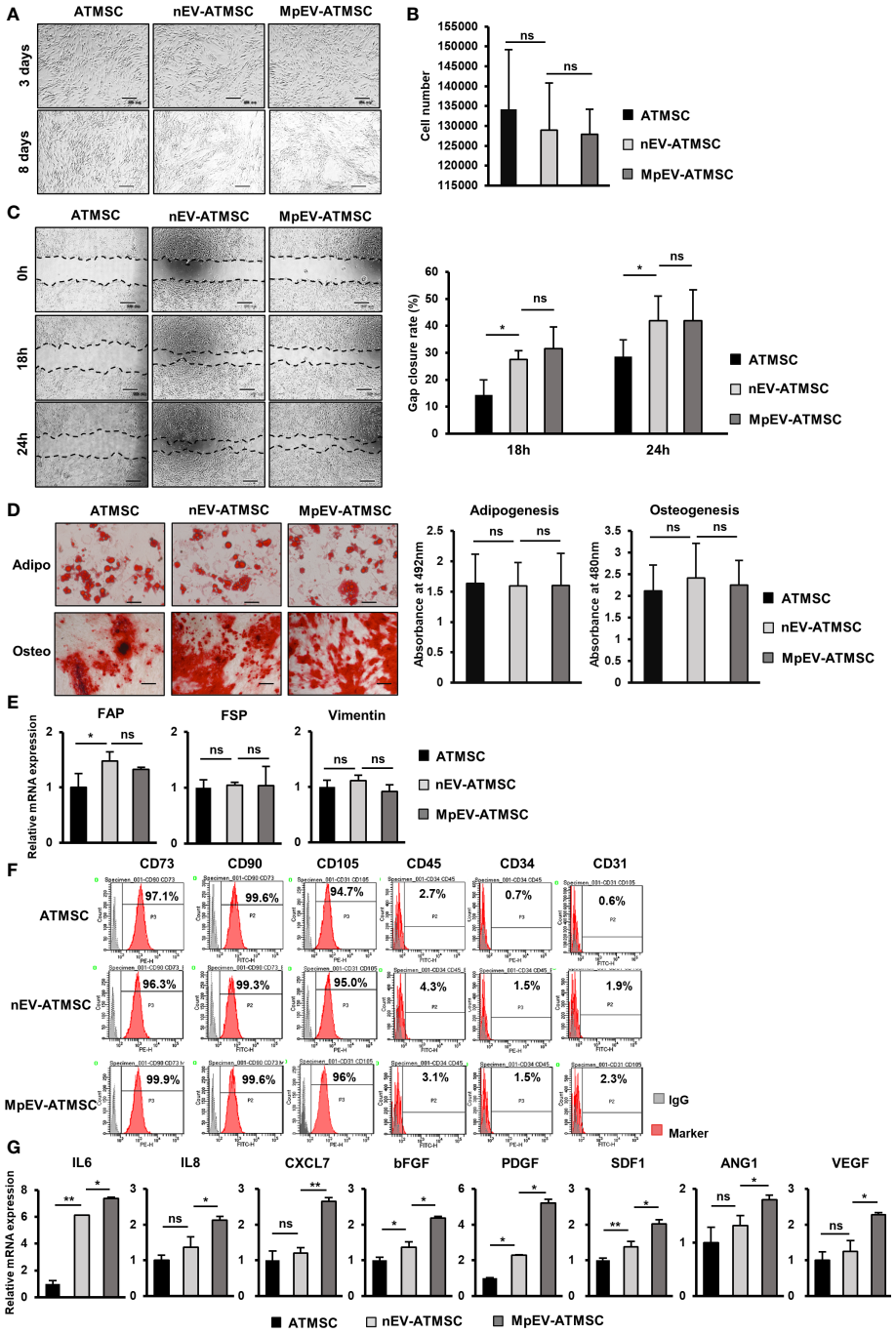

FIGURE 1
Effects of MpEV secreted from M-protein-induced triple negative BCC on ATMSC. **(A)** Morphology of ATMSC, nEV-ATMSC, MpEV-ATMSC (The scale bars indicate 500 μm). **(B)** Proliferation of ATMSC, nEV-ATMSC, MpEV-ATMSC. **(C)** Migration of ATMSC, nEV-ATMSC, MpEV-ATMSC (The scale bars indicate 500 μm). **(D)** Adipocyte and osteocyte differentiation of ATMSC, nEV-ATMSC, MpEV-ATMSC (The scale bars indicate 200 μm). **(E)** The cancer-associated fibroblasts marker expression of ATMSC, nEV-ATMSC, MpEV-ATMSC. **(F)** Characterized MSC markers of ATMSC, nEV-ATMSC, MpEV-ATMSC. **(G)** The cancer supporting gene expression of ATMSC, nEV-ATMSC, MpEV-ATMSC. The value represents the mean ± SD of triplicate experiments. (ns, no significance; $p > 0.05$; *$p \leq 0.05$; **$p \leq 0.01$).

ATMSC were observed (Figure 1C). In addition, the effects of nEV or MpEV on the abilities of ATMSC to differentiate to adipocytes and osteoblasts were assessed. The formation of adipocytes and osteoblasts was examined by staining with Oil red O and Alizarin red, respectively. As a result, the uptake of either nEV or MpEV to ATMSC did not affect their ability to differentiate into osteoblasts and adipocytes (Figure 1D). Next, the effects of MpEV on the cancer-associated fibroblast differentiation of ATMSC were examined by analyzing the gene expression of cancer-associated fibroblast markers in these cells. ATMSC which uptook either nEV (nEV-ATMSC) or MpEV (MpEV-ATMSC) showed no significant changes in the expression of cancer-associated fibroblast markers

(e.g., FAP, FSP, Vimentin) (Figure 1E). In addition, neither nEV nor MpEV affected the expression of MSC markers (Figure 1F).

In the breast TME, ATMSC support the progression of breast tumors via paracrine effects. The secretion of a spectrum of pro-tumorigenic factors from ATMSC promotes the growth and metastasis of cancer cells (37). Therefore, we next examined the effects of nEV and MpEV on the expression of growth factors and cytokines that support cancer. As shown in Figure 1G, in comparison to the original ATMSC and nEV-ATMSC, MpEV-ATMSC showed the significant upregulation of genes related to the invasion, metastasis, and drug resistance of breast cancer and angiogenesis, including IL6, IL8, bFGF, PDGF, SDF1, ANG1, VEGF, and CXCL7 (38–42).

Taken together, these results suggest that neither nEV nor MpEV altered the phenotypes of ATMSC, including their morphology, differentiation ability, and marker expression. However, MpEV-ATMSC showed the increased expression of cancer-related growth factors and cytokines, suggesting their ability to support tumor growth.

MpEV-ATMSC induced the metastasis of non-aggressive BCC via paracrine effects

We previously reported the induced metastasis of BCC treated with conditioned medium (CM) from ATMSC (25). Therefore, in order to examine the ability of MpEV-ATMSC to support breast cancer, CM from MpEV-ATMSC (MpEV-ATMSC-CM) was collected and used to culture non-aggressive BCC (MCF7). The results of a scratch assay showed that non-aggressive BCC treated with ATMSC-CM showed a significantly increased migratory ability in comparison to those cultured in normal medium (Figure 2A). Notably, non-aggressive BCC treated with MpEV-ATMSC-CM showed higher promotion of migration in comparison to those treated with CM derived from ATMSC or nEV-ATMSC (Figure 2A). Meanwhile, MpEV-ATMSC-CM reduced the proliferation of non-aggressive BCC after 48-hour treatment (Figure 2B) in comparison to those cultured under normal conditions. These data suggested that the higher percentage of gap closure in non-aggressive BCC treated with MpEV-ATMSC-

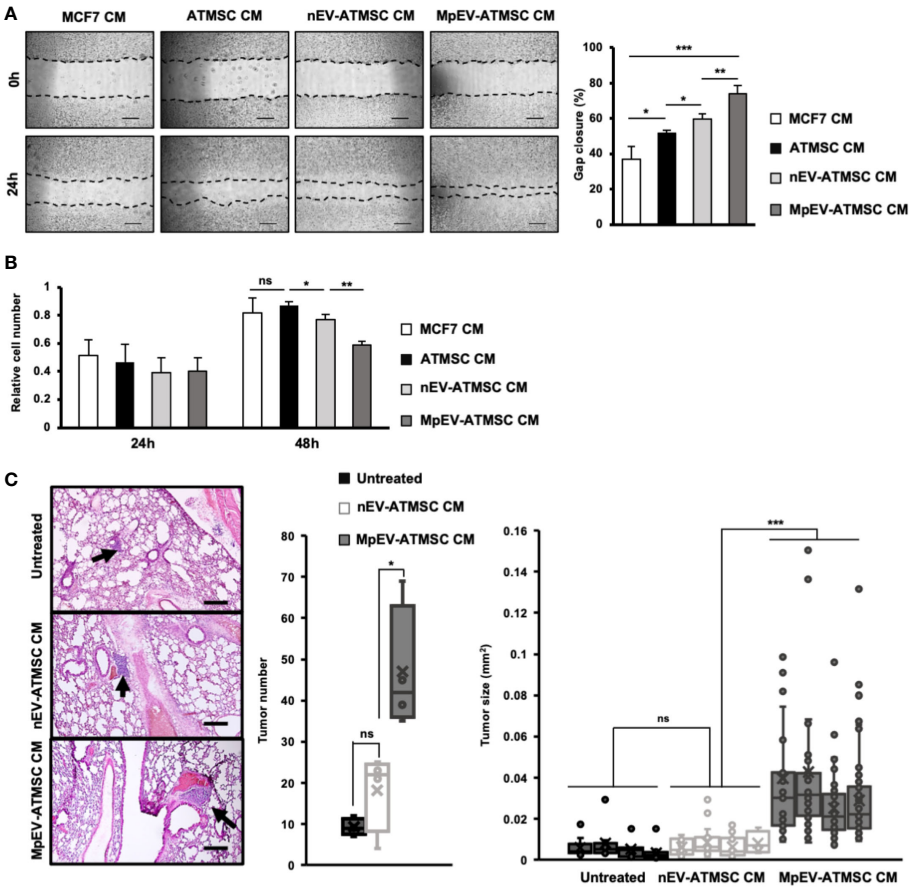

FIGURE 2
Paracrine effects of MpEV-ATMSC on BCC. **(A)** Migration of MCF7 cells treated with ATMSC, nEV-ATMSC, MpEV-ATMSC-derived CM (The scale bars indicate 500 μm). **(B)** Proliferation of MCF7 cells treated with ATMSC, nEV-ATMSC, MpEV-ATMSC-derived CM. **(C)** *In vivo* lung metastasis of MCF7 cells treated by CM derived from ATMSC, nEV-ATMSC, MpEV-ATMSC: HE staining of lung tissue (The arrows indicate tumors, the scale bars indicate 200 μm), number of tumor foci, and size of each tumor foci (each dot represents each tumor foci, each column represents each mouse). Each value represents the mean ± SD of triplicate experiments. (ns, no significance; $p > 0.05$; *$p \leq 0.05$; **$p \leq 0.01$; ***$p \leq 0.001$).

CM was not due to the increased proliferation of these cells (Figure 2A). A similar tendency was observed in MDA-MB-231 triple-negative BCC, in which the migratory ability of MDA-MB-231 cells was also promoted by MpEV-ATMSC-CM, whereas their proliferation was reduced (Supplementary Figures 2A, B).

Next, the effects of MpEV-ATMSC-CM on *in vivo* metastasis of non-aggressive BCC were examined using a lung metastatic mouse model, in which mice were injected with non-aggressive BCC treated with CM from different ATMSC via tail vein. Mice injected with non-aggressive BCC treated with MpEV-ATMSC-CM showed a significantly higher number of tumor foci in the lungs in comparison to those injected with non-aggressive BCC treated with nEV-ATMSC-CM (Figure 2C). In addition, non-aggressive BCC treated with MpEV-ATMSC-CM showed the ability to form larger tumors in mouse lungs in comparison to those treated with nEV-ATMSC-CM (Figure 2C).

Taken together, these results suggested that MpEV significantly induced the ability of ATMSC to promote the migration of non-aggressive BCC *in vitro* and metastasis *in vivo*.

PGE2/IL1 signaling pathway was involved in the induced tumorigenic ability of ATMSC by MpEV

Next, we examined the stemness potency of non-aggressive BCC in response to CM from ATMSC by colony formation and mammosphere formation assays. Sphere formation assay generates colony-forming units in 3D aggregates under a serum-free, nutritionally deficient and anchorage-independent culture conditions; therefore, cancer cells undergo apoptosis, while cancer stem cells still survive and proliferate. Meanwhile, colony formation assay examines the ability of single cells to initiate and growth into full colonies in very low density seeding in monolayer culture. The results showed that, in comparison to the original ATMSC-CM and nEV-ATMSC-CM, MpEV-ATMSC-CM significantly promoted colony formation (1.44 and 1.3 times, Figure 3A) and mammosphere formation (1.44 and 1.43 times, Figure 3B) of non-aggressive BCC, which implied their increased clonogenicity. The similar results, which the colony and mammosphere formation was induced in MDA-MB-231 triple-negative BCC-treated with MpEV-ATMSC-CM, were also observed (Supplementary Figures 2C, D).

Previous reports demonstrated that the interaction loop between MSC and cancer cells promoting cancer stemness is involved in the PGE2/IL1 signaling pathway (43). Therefore, we next examined the expression of PGE2 in MpEV-ATMSC. As shown in Figure 3C, in comparison to the control group without any treatment and the group treated with nEV, those treated with MpEV significantly increased the gene expression of PTGES2 and COX2, which are responsible for the production of PGE2 in ATMSC. Next the effects of MpEV on the secretion of PGE2 from ATMSC was examined by using an ELISA kit to measure the concentration of PGE2 in EV-free conditioned medium derived from ATMSC treated with MpEV. As a result, MpEV-ATMSC showed a higher secretion of PGE2, in comparison to nEV-ATMSC and the control ATMSC without any EV treatment (PGE2 concentration, Control ATMSC without any treatment: 40.85 ± 1.46 pg/mL, nEV-ATMSC: 46 ± 0.42 pg/mL, MpEV-ATMSC: 53.08 ± 0.05 pg/mL, Figure 3D).

PGE2 production was reported to be induced in ATMSC following their interaction with IL1 signaling in cancer cells. The secreted PGE2 and cytokines amplify the expression of cytokines (e.g., IL1, IL6, and IL8) in cancer cells, thereby activating their stemness (43). Therefore, we examined the expression of these cytokines in BCC. Consistent with the upregulation of PGE2 in MpEV-ATMSC, non-aggressive BCC treated with MpEV-ATMSC-CM showed the upregulation of IL1α, IL6, and IL8 in response to the stimulation signal from PGE2 in comparison to those treated with ATMSC-CM or nEV-ATMSC-CM (Figure 3E). This interaction was confirmed using the PGE2 inhibitor, pranoprofen. Non-aggressive BCC induced by CM from Pranoprofen-treated MpEV-ATMSC showed significantly reduced IL1, IL6, IL8 cytokine expression levels (Figure 3F), migratory ability (Figure 3G), and colony formation (Figure 3H), in comparison to non-aggressive BCC induced by CM from MpEV-ATMSC.

Taken together, these data suggest the role of the PGE2/IL1 signaling pathway in the interaction between MpEV-ATMSC and BCC to support the stemness of BCC.

MpEV altered the characteristics of EPC

We next examined whether MpEV show any effects on another type of tissue stem cells related to TME, in addition to ATMSC. In the breast TME, besides ATMSC, EPC is another type of tissue stem cells possessing the ability to differentiate into TEC, form new blood vessels, and secrete signals to promote cancer cells, thereby contributing to tumor growth (4). Therefore, we next incubated EPC with PKH-labeled nEV or MpEV to mediate the uptake of EV and examined the effects of MpEV on the functions of EPC in tumor development. The EV uptake by EPC was confirmed by a flow cytometry which showed that over 90% of EPC uptaking either nEV or MpEV (Supplementary Figure 3A). Next, the effects of MpEV on the proliferation of EPC were examined which showed that EPC uptaking MpEV (MpEV-EPC) exhibited a slightly reduced proliferation in comparison to the original EPC or those uptaking nEV (nEV-EPC) (Figure 4A). In addition, the results of the transwell migration assay showed a significantly increased migratory ability toward BCC in MpEV-EPC and nEV-EPC, in comparison to the original EPC (Figure 4B). Notably, MpEV-EPC showed a higher migratory ability toward BCC than nEV-EPC (Figure 4B).

Next, the effects of MpEV on the angiogenic ability of EPC were examined using a tube formation assay. EPC was seeded in the Matrigel-coated wells of a 24-well plate and the formation of tubes was observed and quantification after three and six hours. Intriguingly, the results showed that after 6 hours MpEV-EPC had an increased ability to form tubes, suggesting an increased angiogenetic ability, in comparison to nEV-EPC and the original EPC (1.18 and 1.07 times, respectively; Figure 4C). Moreover, in MpEV-EPC, the expression of genes related to angiogenesis (e.g., CXCR7, CXCR4, VEGF and IL8) was significantly induced in comparison to nEV-EPC and the original EPC (Figure 4D).

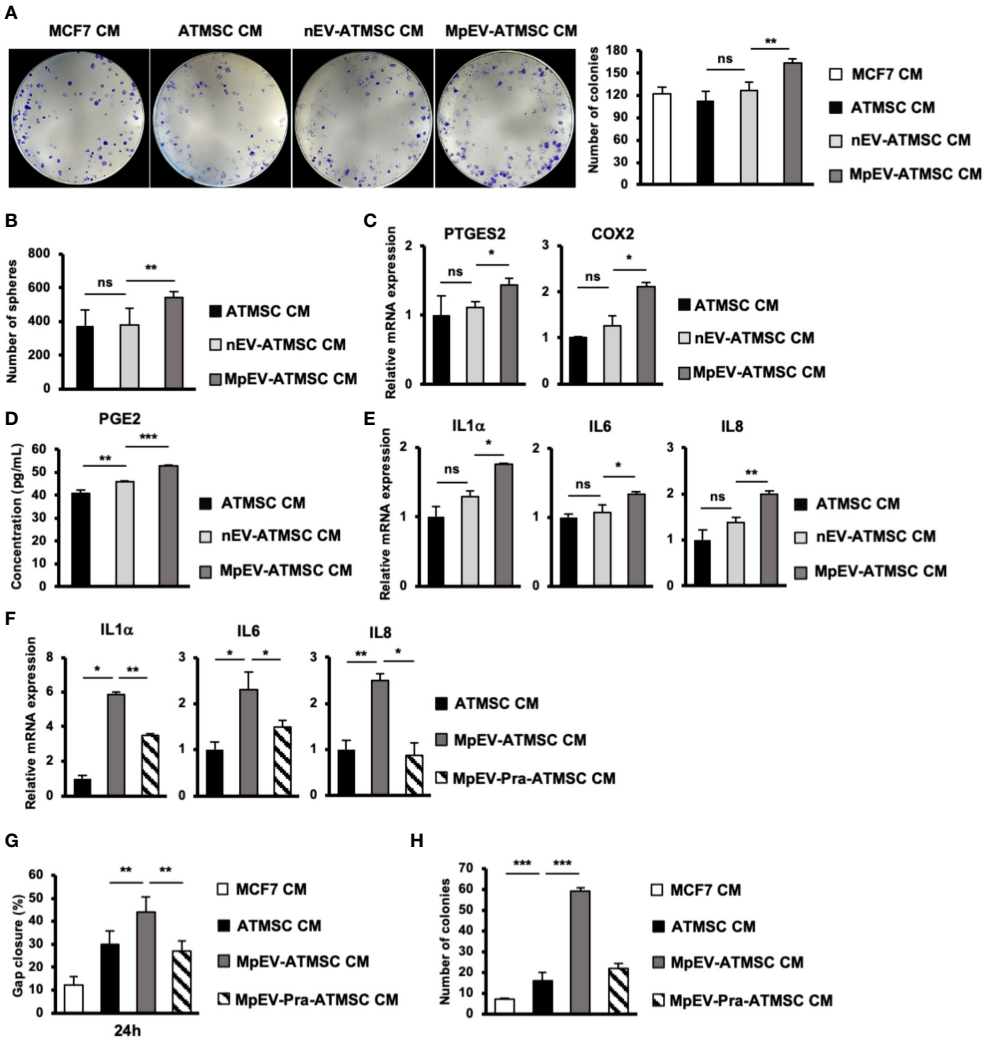

FIGURE 3
PGE2/IL1 signaling pathway was involved in the induced ability of MpEV-ATMSC to support cancer stemness. **(A)** Colony formation of MCF7 cells treated with CM derived from ATMSC, nEV-ATMSC, MpEV-ATMSC. **(B)** Mammosphere formation of MCF7 cells treated with CM derived from ATMSC, nEV-ATMSC, MpEV-ATMSC. **(C)** The expression of PTGES2 and COX2 in CM derived from ATMSC, nEV-ATMSC, MpEV-ATMSC. **(D)** Concentration of PGE2 in CM derived from ATMSC, nEV-ATMSC, MpEV-ATMSC measured by ELISA assay. **(E)** The expression of cytokines in MCF7 cells treated with CM derived from ATMSC, nEV-ATMSC, MpEV-ATMSC. **(F)** The expression of cytokines in MCF7 cells treated with CM derived from MpEV-ATMSC cultured in the presence of an inhibitor of PGE2 production. **(G)** Migration of MCF7 cells treated with CM derived from MpEV-ATMSC cultured in the presence of an inhibitor of PGE2 production. **(H)** Colony formation of MCF7 cells treated with CM derived from MpEV-ATMSC cultured in the presence of an inhibitor of PGE2 production. Each value represents the mean ± SD of triplicate experiments. (ns, no significance; $p > 0.05$; *$p \leq 0.05$; **$p \leq 0.01$; ***$p \leq 0.001$).

In addition, the effects of MpEV on endothelial cells (EC), the differentiated cells from EPC, were examined. After incubating with either nEV or MpEV and confirming the uptake of EV by EC (Supplementary Figure 3B), the migration, proliferation and tube formation ability of these EC were examined. Similar to the effects on EPC, MpEV promoted EC migration toward BCC signals in comparison to nEV (Supplementary Figure 3C). However, in contrast to the effects on EPC, MpEV promoted proliferation (Supplementary Figure 3C) and showed no effects on the angiogenic ability (Supplementary Figure 3D) of EC, in comparison to nEV. These results suggest different responses of stem cells and differentiated cells to MpEV signaling.

Taken together, these results suggest that the ability of EPC to migrate toward tumors and differentiate and incorporate themselves into newly formed blood vessels was strengthened by the induction of EV secreted from M-protein-induced triple-negative BCC.

MpEV-EPC acquired TEC-like characteristics

Among non-cancer cells in the TME, TEC—which originate from EC or EPC—show the notable capability of supporting cancer cells (8). Therefore, we next examined the effects of MpEV on the ability of EPC to acquire TEC-like phenotypes by checking the expression of TEC markers in MpEV-EPC. The results showed that MpEV-EPC exhibited the significantly upregulated expression of vWF, SNAIL, VE-Cadherin, FAP, and ALDH (TEC markers found in breast

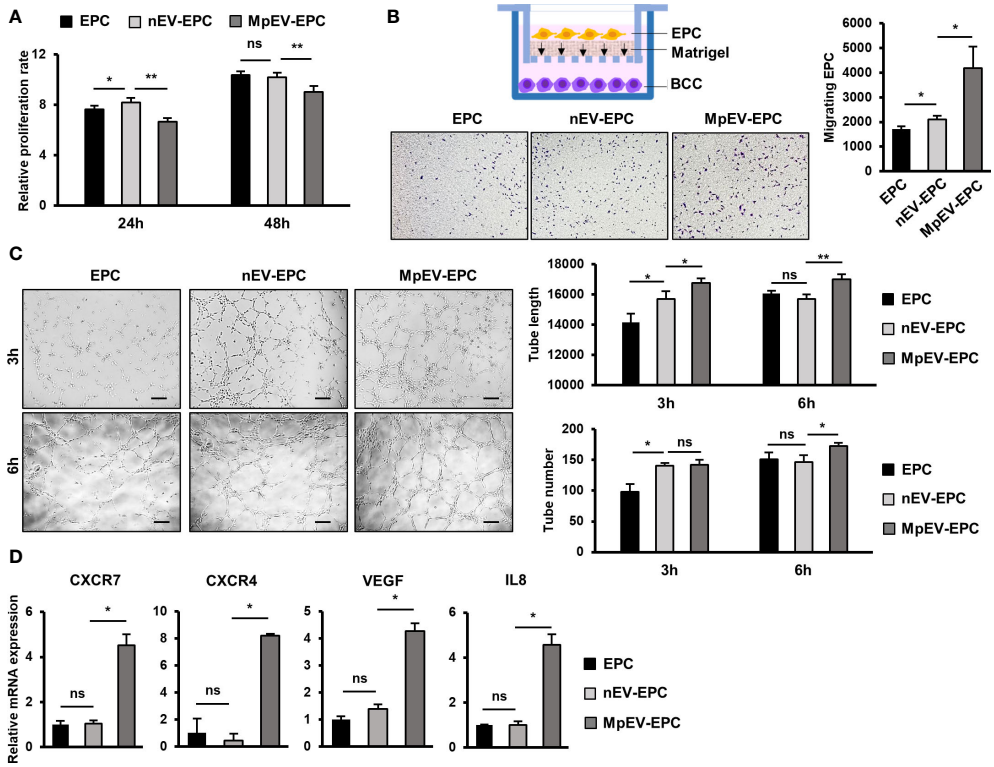

FIGURE 4
Effects of MpEV secreted from M-protein-induced triple negative BCC on EPC. **(A)** Proliferation of EPC, nEV-EPC, MpEV-EPC. **(B)** Transwell migration of EPC, nEV-EPC, MpEV-EPC. **(C)** Tube formation of EPC, nEV-EPC, MpEV-EPC. **(D)** The angiogenesis-related gene expression of EPC, nEV-EPC, MpEV-EPC. The scale bars indicate 200 μm. Each value represents the mean ± SD of triplicate experiments. (ns, no significance; $p > 0.05$; *$p \leq 0.05$; **$p \leq 0.01$).

tumors) (44–48) in comparison to nEV-EPC or the original EPC (Figure 5A). Next, the ability to form tubes without serum, a specific feature of TEC, was examined in MpEV-EPC. EPC was seeded in medium free serum in a Matrigel-coated well plate to induce the forming of capillary like structures (49). As shown in Figure 5B, while the control groups, including normal EC and EPC, hardly formed tubes, the uptake of nEV or MpEV induced tube formation in EPC under serum-depleted conditions. Notably, MpEV induced EPC tube formation in comparison to nEV (1.18 times, Figure 5B).

Next, to examine the characteristics of EPC under the effects of M-protein or MpEV in tumor microenvironment, we performed an *in vitro* 3D spheroid model which mimic the tumor microenvironment, reported by a recent study (50). Briefly, spheroids were developed by coculturing of PKH26-labeled BCC and CFSE-labeled EPC under the presence of M-protein for 5 days (Figure 5C). After that, the CFSE-labeled EPC was isolated by cell sorting, then the expression of TEC markers and the angiogenic ability in serum-free conditions of these EPC were accessed. The results showed that EPC isolated from spheroids with M-protein-treatment showed the induced gene expression of TEC markers (Figure 5D) and the promoted angiogenic ability under serum-depleted conditions (Figure 5E).

Next, the ability of MpEV-EPC to support non-aggressive BCC was examined by treating BCC with CM derived from EPC. As a result, non-aggressive BCC treated with CM derived from MpEV-EPC (MpEV-EPC-CM) showed significantly enhanced migratory ability (2.27-, 2.19 and 1.56 times, Figure 5E) and colony formation (3.04-, 2.03 and 1.38 times, Figure 5F), in comparison to the original non-aggressive BCC or non-aggressive BCC treated with CM derived from EPC or nEV-EPC. Furthermore, the effects of MpEV-EPC-CM on the *in vivo* metastasis of non-aggressive BCC were examined in lung metastatic mouse model. The results showed that non-aggressive BCC treated with MpEV-EPC-CM showed significantly enhanced metastatic ability to the lungs of mice in comparison to the original non-aggressive BCC or those treated with CM derived from nEV-EPC, as demonstrated by the increased number and size of tumor foci in the mouse lung tissues (Figure 5G).

In addition, the effects of MpEV-EPC-CM on MDA-MB-231 triple-negative BCC line were examined as a type of aggressive BCC. The results differed from the impact on non-aggressive BCC, in which MpEV-EPC-CM stimulated migration (Supplementary,32] ?> Figure 4A) but showed no effects on the proliferation (Supplementary Figure 4B) and colony formation (Supplementary Figure 4C) of MDA-MB-231 cells.

Taken together, EV derived from M-protein-induced triple-negative BCC altered the phenotypes of EPC, which acquired TEC-like characteristics, and induced the ability of EPC to promote metastasis of non-aggressive BCC.

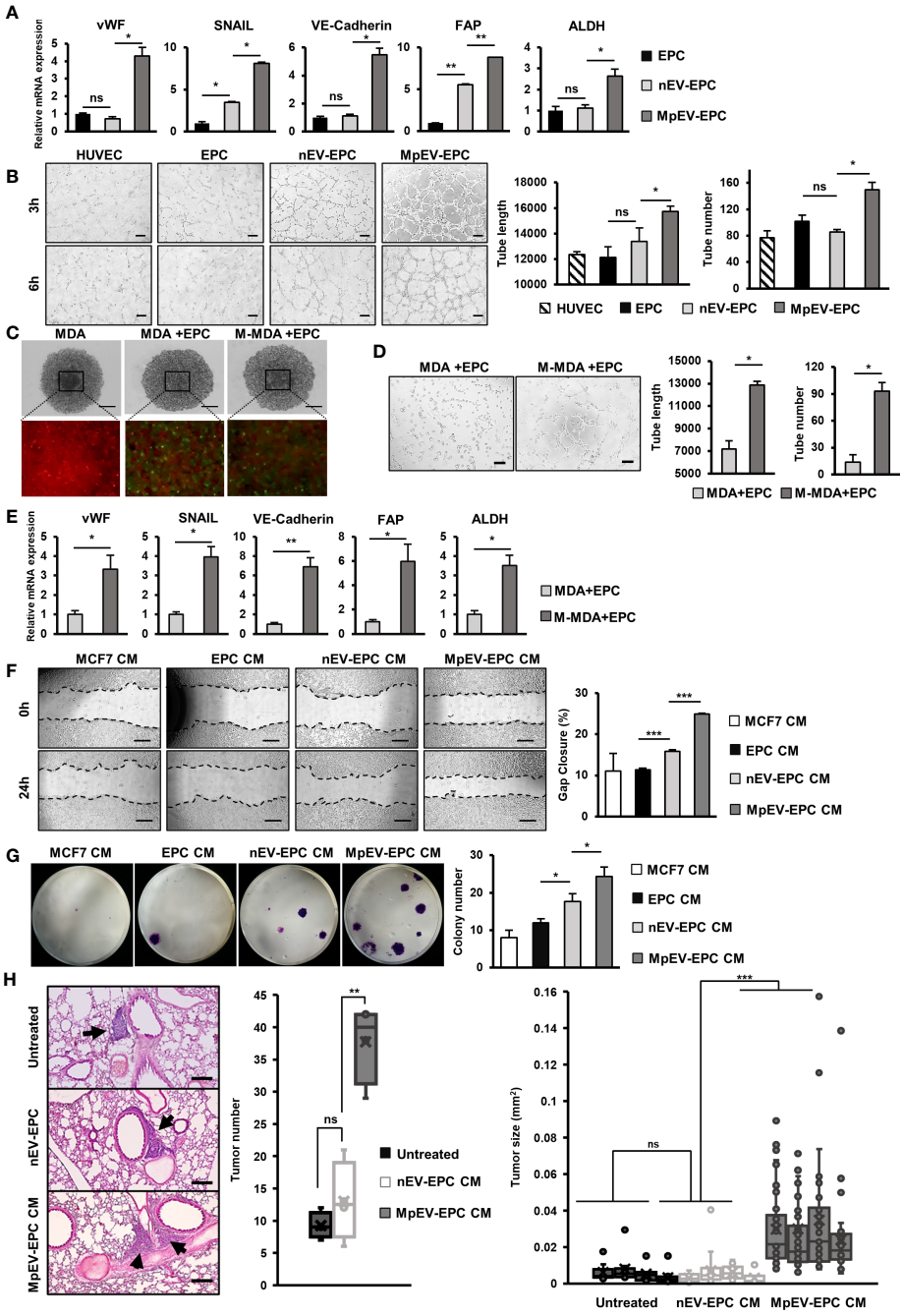

FIGURE 5
MpEV-EPC acquired TEC-like characteristics to support breast cancer cell progression. **(A)** The TEC-related gene expression of EPC, nEV-EPC, MpEV-EPC. **(B)** Tube formation in no-serum condition of EPC, nEV-EPC, MpEV-EPC (the scale bars indicate 200 μm). **(C)** 5-day spheroid culture of PKH26-labeled MDA-MB-231 cells and CFSE-labeled EPC (the scale bars indicate 500 μm, MDA: MDA-MB-231, M-MDA: M-protein-induced MDA-MB-231, Green: CFSE, Red: PHK26). **(D)** Tube formation of EPC isolated from spheroid (the scale bars indicate 200 μm, MDA: MDA-MB-231, M-MDA: M-protein-induced MDA-MB-231). **(E)** TEC-related gene expression of EPC isolated from spheroid (MDA: MDA-MB-231, M-MDA: M-protein-induced MDA-MB-231). **(F)** Migration of MCF7 treated with CM derived from EPC, nEV-EPC, MpEV-EPC (the scale bars indicate 500 μm). **(G)** Colony formation of MCF7 treated with CM derived from EPC, nEV-EPC, MpEV-EPC. **(H)** *In vivo* lung metastasis of MCF7 cells treated by CM derived from EPC, nEV-EPC, MpEV-EPC: HE staining of lung tissue (The arrows indicate tumors, the scale bars indicate 200 μm), number of tumor foci, and size of each tumor foci (each dot represents each tumor foci, each column represents each mouse). Each value represents the mean ± SD of triplicate experiments. (ns, no significance; $p > 0.05$; *$p \leq 0.05$; **$p \leq 0.01$; ***$p \leq 0.001$).

MpEV-ATMSC supported the angiogenesis of EPC

In addition to the ability to support cancer cells, ATMSC also have the ability to support the functions of EPC and TEC in a paracrine manner via their secreted factors (51–53). As MpEV-ATMSC showed the upregulation of angiogenic factors, such as bFGF, SDF1, PDGF, ANG1, VEGF, and CXCL7 (Figure 1G), we next investigated the ability of MpEV-ATMSC to support the angiogenic ability of EPC by a tube formation assay. EPC were treated with CM derived from MpEV-ATMSC (MpEV-ATMSC-CM) and their angiogenic abilities were examined by a tube formation assay using a Matrigel-coated 24-well plate. The results showed that EPC treated with MpEV-ATMSC-CM exhibited significantly increased tube formation ability in comparison to those treated with nEV-ATMSC-CM (1.59-fold increased, Figure 6A).

In addition, the effects of MpEV-ATMSC-CM on the migration of EPC toward signals from BCC were examined using a transwell insert system. Treatment with MpEV-ATMSC-CM significantly promoted the migration of EPC toward BCC, while ATMSC-CM and nEV-ATMSC-CM showed no effect (Figure 6B). Consistent with the induced angiogenic and migratory abilities, EPC treated with MpEV-ATMSC-CM showed a significant upregulation of genes related to angiogenesis and migration, such as CXCR7, CXCR4, and VEGF, in comparison to the original EPC and those treated with ATMSC-CM or nEV-ATMSC-CM (Figure 6C). Moreover, the effects of MpEV-ATMSC-CM on the gene expression of TEC markers and the tube formation of EPC under free serum condition were examined. The results showed that treatment with MpEV-ATMSC-CM showed no significant effects to induce the gene expression of TEC markers in EPC (Figure 6D) and the tube formation ability of EPC in serum-depleted condition, in comparison to nEV-ATMSC-CM (Figure 6E).

Moreover, to examine the contribution of ATMSC in the signaling network of BCC and EPC under the effects of M-protein, an *in vitro* 3D spheroid triculture of PKH26-labeled BCC, ATMSC and CFSE-labeled EPC was performed (Supplementary Figure 5). After 5 days, spheroids formed in the presence of ATMSC showed an increased condensation with smaller sizes than those without ATMSC, suggesting that ATMSC might promote the aggregation of cells inside the spheroids (Figure 6F). Next, the CFSE-labeled EPC was isolated from spheroids by cell sorting and the characteristics of TEC were accessed. As a result, compared to EPC isolated from spheroids without M-protein treatment, those isolated from spheroids with M-protein-treatment showed the induced gene expression of TEC markers (Figure 6G) and tube formation ability under serum-depleted conditions (Figure 6H). Notably, among the M-protein-treated groups, EPC isolated from spheroids with the presence of ATMSC showed the comparable gene expression of TEC markers (Figure 6G), but higher tube formation ability under serum-depleted condition, in comparison to those isolated from spheroids without ATMSC (Figure 6H). These data suggested that ATMSC did not change the phenotypes of EPC to TEC but supported the tube formation ability of EPC under a tumor microenvironment mimic condition.

Taken together, these results suggest that the uptake of MpEV induces the paracrine effects of ATMSC, supporting the migration of EPC toward tumor sites and the angiogenic ability of EPC.

Discussion

Our present study demonstrated that M-protein induced the ability of triple-negative BCC-derived EV promoting the functions of breast tissue stem cells including ATMSC and EPC in tumorigenesis. ATMSC uptaking of EV derived from M-protein-induced triple-negative BCC (MpEV) showed the induced paracrine effects on the malignancy of non-aggressive BCC, including migration, metastasis, and stemness potency, which was involved in the increased secretion of PGE2. Meanwhile, EPC uptaking of MpEV acquired tumor endothelial cell-like phenotype, with promoted abilities in angiogenesis and facilitating the metastasis and stemness characteristics of non-aggressive BCC (Figure 7).

Numerous studies have suggested that COVID19 increases the risk of accelerated cancer progression, metastasis, and death in cancer patients in general and in breast cancer patients in particular (5, 12, 13, 54, 55). Indeed, our previous study reported the induced effects of the SARS-CoV-2 M-protein on the migratory ability and metastasis of BCC, suggesting that it promoted aggressiveness in BCC (6). Several studies have reported the effects of SARS-CoV-2 infection on the TME, mainly focusing on acute inflammation and immune reactions. In addition, cancer cells have also been observed to be affected by the virus. In lung cancer, the abundant appearance of whole SARS-CoV-2 proteins has been shown to disrupt the immune system, cause cytokine storms, and alter metabolism in the TME, resulting in increased tumor growth (56). Moreover, a report on breast cancer and melanoma showed alterations in the immune response of the TME by direct injection of inactivated SARS-CoV-2 (57, 58). However, to date, the effects of SARS-CoV-2 infection and its proteins on the interactions between cancer cells and other cells in the TME after SARS-CoV-2 infection have not been discussed.

To gain and maintain a suitable surrounding environment, cancer cells actively contact and control the activities of neighboring cells in numerous ways, including the secretion of extracellular vesicles (EV) (30). EV derived from cancer cells were uptaken by the surrounding cells and regulate their behaviors to support tumor development. Although the effects of SARS-CoV-2 proteins on cancer cells have been widely reported, whether these proteins also affect EV derived from cancer cells are still obscured. Based on our previous findings of the induced malignancy of triple negative BCC by SARS-CoV-2 membrane protein (M-protein) (6), we expanded the study to examined the effects of M-protein on EV derived from triple negative BCC. We firstly isolated EV from the original triple negative BCC (nEV) and those with M-protein treatment (MpEV), then compared their effects on the triple negative BCC which received no treatment of M-protein. The results showed that in comparison to nEV, MpEV showed no different effects on the migration of BCC in a scratch assay (Supplementary Figure 6A) and the colony formation of BCC (Supplementary Figure 6B). However, MpEV induced a higher

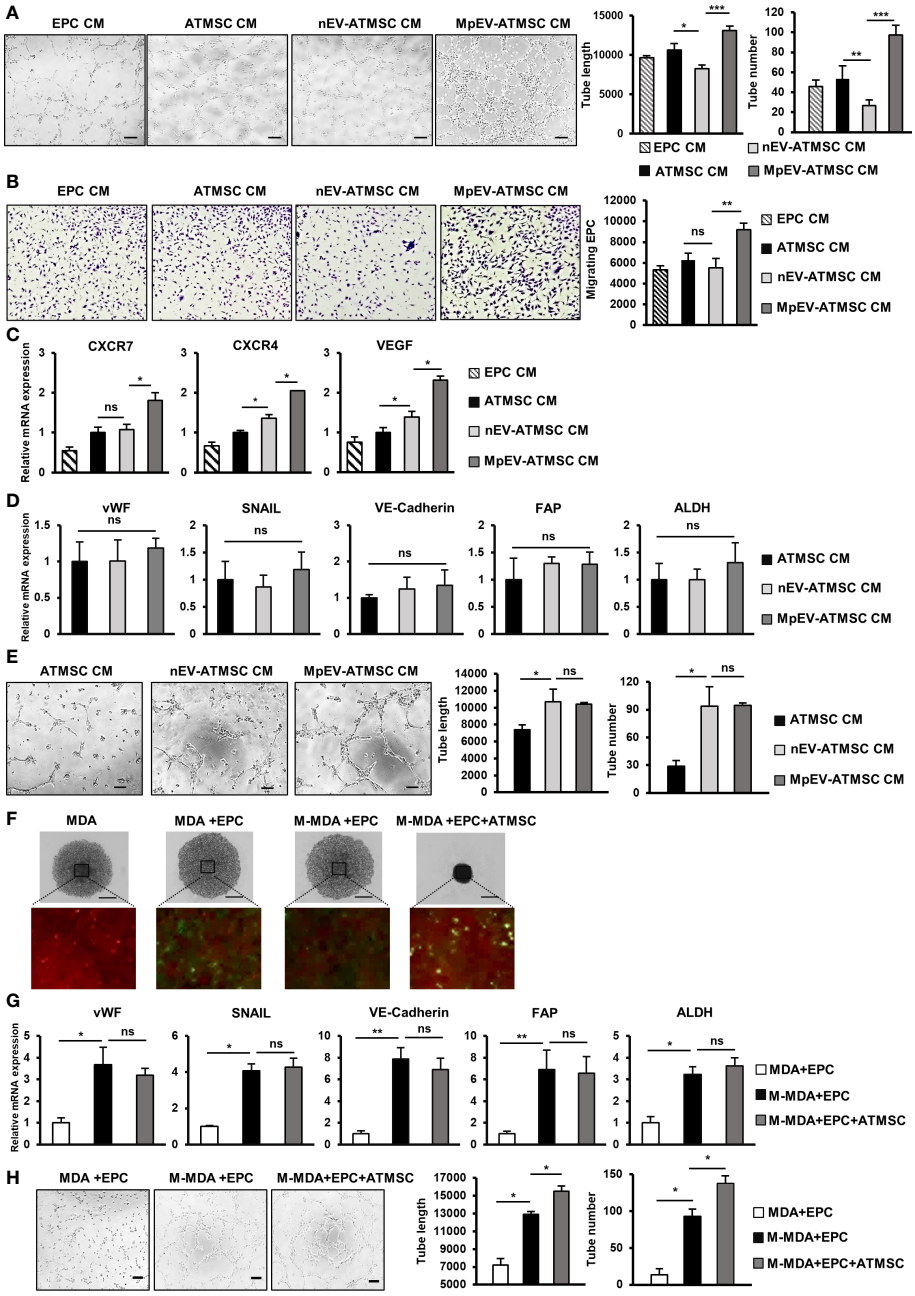

FIGURE 6
MpEV-ATMSC supported angiogenesis of EPC. **(A)** Tube formation of EPC treated by CM derived from ATMSC, nEV-ATMSC, MpEV-ATMSC (The scale bars indicate 200 μm). **(B)** Transwell migration of EPC treated by CM derived from ATMSC, nEV-ATMSC, MpEV-ATMSC. **(C)** Angiogenesis-related gene expression of EPC treated by CM derived from ATMSC, nEV-ATMSC, MpEV-ATMSC. **(D)** TEC-related gene expression of EPC treated by CM derived from ATMSC, nEV-ATMSC, MpEV-ATMSC. **(E)** Tube formation of EPC treated by CM derived from ATMSC, nEV-ATMSC, MpEV-ATMSC (The scale bars indicate 200 μm). **(F)** 5-day spheroid culture of PKH26-labeled MDA-MB-231 cells, CFSE-labeled EPC and ATMSC (the scale bars indicate 500 μm, MDA: MDA-MB-231, M-MDA: M-protein-induced MDA-MB-231, Green: CFSE, Red: PHK26). **(G)** TEC-related gene expression of EPC isolated from spheroid (MDA: MDA-MB-231, M-MDA: M-protein-induced MDA-MB-231). **(H)** Tube formation of EPC isolated from spheroid (The scale bars indicate 200 μm, MDA: MDA-MB-231, M-MDA: M-protein-induced MDA-MB-231). Each value represents the mean ± SD of triplicate experiments. (ns, no significance; $p > 0.05$; *$p \leq 0.05$; **$p \leq 0.01$; ***$p \leq 0.001$).

proliferation (Supplementary Figure 6C), cytokine gene expression such as IL6, IL8 and TNFα (Supplementary Figure 6D) and HIF1α (Supplementary Figure 6E) in BCC, in comparison to nEV. These data suggested the different effects of MpEV on the recipient cells in comparison to nEV, which confirmed the hypothesis that M-protein also affects the functions of EV derived from BCC.

TME consists of numerous types of cells including cancer cells, tissue stem cells and the other non-cancerous cells. We previously reported the ability of ATMSC, a type of tissue stem cells, supporting the metastasis of triple negative BCC via a paracrine effect. Therefore, in this study, we questioned whether MpEV affects the abilities of ATMSC supporting BCC. Although previous studies

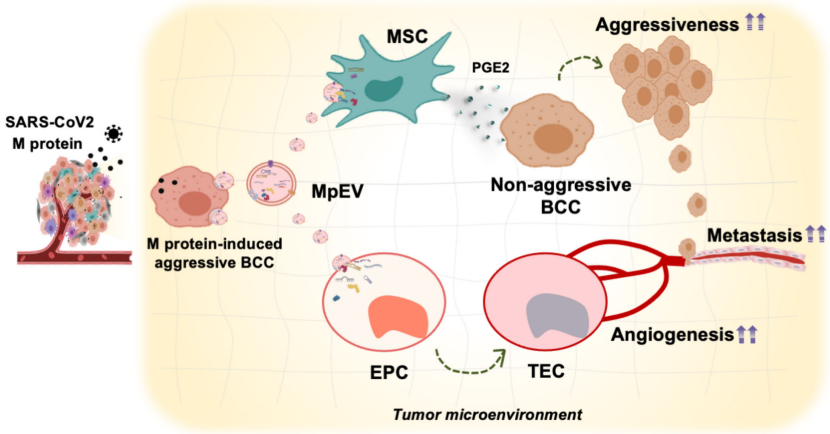

FIGURE 7
Proposed model: In TME, SARS-CoV-2 M-protein-induced BCC recruit and control the activity of ATMSC and EPC via EV which facilitate the development and metastasis of breast tumors.

have reported that human MSC lack ACE2 and TMPRSS2 expression and are resistant to SARS-CoV-2 infection (46, 47), in the present study, our data showed that the M-protein indirectly affected the gene expression of ATMSC via MpEV derived from M-protein-induced triple-negative BCC. The uptake of MpEV by ATMSC upregulated the expression of several genes involved in tumor development (Figure 1G). Consistently, nonaggressive BCC treated with conditioned medium derived from MpEV-ATMSC showed the induced migration (Figure 2A), *in vivo* metastasis (Figure 2C) and stemness potency (Figures 3A, B) while reduced the proliferation (Figure 2B). Although proliferation is necessary for the initiation of primary tumors, growth inhibition plays an important role for the survival of tumor cells in the circulation and invasion to secondary organs, resulting to a malignant phenotype (59, 60). Therefore, it is worthy for a further study to examine the correlation between the reduced proliferation and malignant phenotypes of non-aggressive BCC treated with conditioned medium from MpEV-ATMSC by clarifying the signaling pathways regulating proliferation of these cells.

Notably, MpEV-ATMSC showed the upregulation of PTGES2 and COX2 (Figure 3C), two factors responsible for PGE2 production, and the secretion of PGE2 (Figure 3D) which are known to be involved in the interaction between TA-MSC and cancer cells (59). A previous study reported that the PGE2/IL1 cytokine network mediates the interaction between TA-MSC and colon cancer cells, in which PGE2 and cytokines derived from cancer-educated MSC enhance IL1, IL6, and IL8 production in cancer cells, which in turn enriches the cancer stem cell population (43). In our study, the treatment of non-aggressive BCC with CM derived from MpEV-ATMSC induced the expression of IL6, IL8, and IL1α in these BCC (Figures 3E, F), suggesting the involvement of the PGE2 signaling pathway in the ability of MpEV-ATMSC to induce cancer stemness.

MSC have flexible fate determination controlled by cancer cells (26, 61). Previous studies reported that BCC recruits MSC to the TME and educates them to transform them into MSC (TA-MSC) or cancer-associated fibroblasts (CAF) (62–66). In our study, MpEV-ATMSC showed no upregulation of CAF markers, while expressed MSC typical markers and differentiation ability to adipocytes and fibroblast (Figures 1D, F). These data suggested that MpEV-ATMSC retained the phenotypes of MSC but exhibited a higher ability to induce tumorigenesis in non-aggressive BCC, in comparison to the original ATMSC or those internalized with nEV. Meanwhile, in comparison to naïve MSC, TA-MSC possess a higher ability to promote the development of tumors; for instance, a study reported that gastric TA-MSC co-injected with gastric cancer cells highly increased tumor growth (67) in comparison to non-cancerous MSC such as bone marrow MSC or MSC derived from adjacent tissues (68). In addition, previous studies have reported that TA-MSC secreted bFGF, PDGF, and SDF1 to recruit more naive MSC into the TME (69, 70); and IL6 to enhance tumor cell growth (71). In our study, MpEV-ATMSC showed the upregulation of IL6, bFGF, PDGF, and SDF1 (Figure 1G) and the induced abilities to promote the malignancy of BCC, suggesting that MpEV-ATMSC might acquire TA-MSC-like characteristics.

In addition to ATMSC, we also examined the effects of MpEV on the behaviors of EPC, another type of tissue stem cell involved in tumor tissues and angiogenesis (30, 72, 73). Angiogenesis of tumors can be initiated when EPC are recruited to the TME by signaling factors from cancer cells and educated to differentiate into TEC and form new blood vessels, which ultimately allow a better supply of nutrients to the tumor and promote its development (33). In our study, after uptake of MpEV, angiogenic ability and migration toward BCC was induced in EPC (Figures 4B, C). In contrast, MpEV did not affect the angiogenic ability of EC (Supplementary Figure 3C). These results suggest that the flexibility of stem cells to be educated by cancer cells is greater than that of their mature counterparts. In comparison to normal EC, TEC show the higher expression of several specific genes that are considered to be tumor endothelial markers (74). Interestingly, our data showed that MpEV-EPC showed the upregulation of vWF, SNAIL, VE-Cadherin, FAP, and ALDH

(Figure 5A), which are tumor endothelial markers associated with breast TEC (44–48). In addition, our data in Figure 5B show that MpEV-EPC exhibited breast TEC-like behavior with increased tube formation ability *in vitro* in the absence of serum, as reported in a previous study (47, 75). Notably, MpEV-EPC significantly induced aggressive phenotypes and *in vivo* metastasis of BCC (Figures 5F–H), which correlated with the increased expression of IL8, CXCR7, CXCR4, and VEGF (Figure 4D). IL8 from TEC was reported to play a mediating role in prostate cancer progression (76); meanwhile, CXCR7, CXCR4, and VEGF are angiocrine factors TEC stimulate angiogenesis and enhance survival of TEC in an autocrine manner (35, 77), thus supporting tumor progression and metastasis (78). Moreover, chemokine receptors CXCR7 and CXCR4 from TEC facilitate lymphoma and BCC transendothelial migration under the control of TEC (79).

In addition to signals from cancer cells, EPC and their angiogenesis in the TME are also affected by TA-MSC. TA-MSC in the TME have the ability to direct tumor angiogenesis by secreting angiogenic factors (26, 28, 80). In breast cancer, TA-MSC recruit EPC by secreting SDF1 and promoting the growth of tumor blood vessels (81). In our study, MpEV-ATMSC showed upregulation of growth factors and cytokines, including bFGF, PDGF, SDF1, and IL6 (Figure 1G), all of which contribute to the recruitment of EPC and driving angiogenesis (26, 40, 65). Consistently, conditioned medium derived from MpEV-ATMSC promoted tube formation, cancer-directed migration ability, and the expression of angiogenic genes in EPC, but showed no effects on the altered phenotypes of EPC to TEC-like cells (Figures 6A–E).

Of note, the contribution of ATMSC to the signaling network of M-protein-induced BCC and EPC was examined by a 3D spheroid triculture. After 5 days of triculture with M-protein-induced BCC, although EPC isolated from spheroids containing ATMSC showed no upregulation of TEC marker expression (Figure 6G), these cells exhibited the higher tube formation ability in serum free conditions (Figure 6H), in comparison to EPC isolated from spheroids without ATMSC. To directly examine the effects of MpEV under *in vitro* TME-mimic conditions, the spheroid triculture of BCC, EPC and ATMSC was performed with the addition of MpEV (Supplementary Figure 7A). Similarly, the results EPC isolated from spheroids with MpEV treatment showed the upregulation of TEC marker gene expression (Supplementary Figure 7B) and tube formation ability in serum free conditions (Supplementary Figure 7C), in comparison to those isolated from spheroids without MpEV treatment. Of note, the presence of ATMSC in the spheroid triculture did not induce the gene expression of TEC markers but promoted the tube formation ability of EPC in serum free conditions (Supplementary Figure 7). These data suggested that although showed no effects to alter EPC phenotype, ATMSC might contribute to promoting the angiogenic ability of EPC in the TME. In addition, MpEV induced the paracrine effects of ATMSC in both BCC and other non-cancer cells that are involved in facilitating the TME which is worthy for a further *in vivo* study.

In the TME, aside of tissue stem cells, cancer cells are supported by the other non-cancerous neighboring cells, such as cancer-associated fibroblasts (CAFs) and immune cells that supply nutrients, growth factors, cytokine signals, and blood vessel systems (26). In addition, a previous study showed that cancer cells with high malignancy tend to manipulate the surrounding cells more efficiently (27). Therefore, it is implied that BCC induced by the SARS-CoV-2 M-protein might possess a greater capability to regulate their TME. Indeed, our present study showed that MpEV derived from BCC induced by M-protein promoted the abilities of ATMSC and EPC to support cancer metastasis and malignancy. Therefore, it is worthy for a further study to examine the effects of MpEV on the other cell types in the TME such as CAFs and immune cells.

Conclusion

In this study, we examined how SARS-CoV-2 M-protein modulates the tissue stem cells involved in breast TME by altering the functions of EV derived from triple-negative BCC. Our findings suggest that triple-negative BCC induced by M-protein produced EV with a higher ability to promote the functions of tissue stem cells, such as ATMSC and EPC, supporting cancer growth and aggressiveness (Figure 7). Our study suggests that SARS-CoV-2 infection in breast cancer patients not only promotes the aggressiveness of BCC themselves, but also the ability of BCC to manipulate the surrounding TME. By understanding the specific interactions between BCC and non-cancer cells, as well as the underlying mechanisms governing these interactions that occur during COVID-19, appropriate management of both medical conditions can be addressed, as well as identifying possible ways to prevent the exacerbation of breast cancer cells and their metastasis. Targeting the TME, especially tissue stem cells such as ATMSC, EPC, and their derivatives, should be considered as cancer therapeutic agents for cancer patients with COVID-19 infection.

Materials and methods

Breast cancer cell culture and induction with SARS-CoV-2 M-protein

MDA-MB-231 (ATCC HTB-26) cells (a triple-negative BCC line) and MCF-7 cells (a Luminal A BCC line [ATCC HTB-22]) were cultured in a culture dish containing Iscove's modified Dulbecco's medium (IMDM) (Gibco, Waltham, MA, USA) with 1% penicillin/streptomycin (Thermo Fisher Scientific, Waltham, MA, USA) and 5% fetal bovine serum (FBS) (Sigma-Aldrich, St. Louis, MO, USA). The cell medium was changed every two days and the cells were kept in a humidified incubator at 37°C under 5% CO_2. The cells were subcultured to obtain 3.8×10^4 cells/ml of medium per dish via trypsinization upon reaching 80% confluence.

MDA-MB-231 cells (5×10^5 cells/ml) were treated with 60 pmol/ml SARS-CoV-2 M-protein (Miltenyi Biotec, Cologne, Germany) in EV-depleted FBS-containing medium for collecting EV in 5 days to collect CM and isolate EV. EV-depleted FBS-containing medium for collecting EV was prepared by ultracentrifugation using an Optima L-XP ultracentrifuge (Beckman Coulter, Inc. Brea, CA,

United States), as previously described (82). Briefly, 40 ml of IMDM containing 5% FBS and 1% penicillin/streptomycin was ultracentrifuged at 140,000×*g* for 18 h at 4°C using a Beckman Coulter Type 70 Ti Rotor. Then, 30 ml of supernatant was collected and used as the culture medium to collect EV.

Collection of EV

The CM of M-protein-treated and untreated BCC MDA-MB-231 cells was collected and centrifuged at 300×*g* for 5 min, followed by 1200×*g* for 20 min. The supernatant was ultracentrifuged at 140,000×*g* for 70 min at 4°C using an Optima XE-100 ultracentrifuge to collect the EV pellet. EV pellets were collected in 100 µL of PBS; these were considered to be isolated EV. The EV collected from the M-protein-treated BCC were called MpEV, and the EV collected from the untreated breast cancer cells were called nEV. For PKH26 labeling of EV, of 120 µg was resuspended in 250 µL of Diluent C (Sigma-Aldrich) and mixed with 250 µL of Diluent C containing 1 µL of PKH26 (Sigma-Aldrich). The mixture was then incubated in the dark for 5 min and neutralized by adding 40 ml of PBS containing 0.25% FBS. The solution was then ultracentrifuged at 140,000×*g* for 70 min at 4°C to collect stained EV pellet, then resuspended in 100 µL PBS and stored at -80°C. The protein concentration of EV was measured using a Bradford assay (Bio-Rad, Hercules, CA, USA) and was considered to be the EV concentration. The size of collected EV was measured by dynamic light scattering (Zetasizer Nano ZS, Melvern Instruments, United Kingdom). EV markers expression was characterized by Western Blotting.

Culturing of ATMSC, EPC, and EC

ATMSC were isolated from human adipose tissues with permission from the ethics authorities at the University of Tsukuba [previously described by Kimura et al. (83)] and cultured in a culture dish containing IMDM with 10% FBS, 2 mg/ml L-glutamine (Invitrogen, Waltham, MA, US), 100 units/ml penicillin, and 5 ng/ml bFGF (Peprotech, Rocky Hill, NJ, USA).

EPC were isolated from umbilical cord blood [previously described (84)] and cultured in a dish containing IMDM with 10% FBS, 2 mg/ml L-glutamine (Invitrogen, Waltham, MA, US), 100 units/ml penicillin, and 5 ng/ml bFGF (Peprotech, Rocky Hill, NJ, USA).

For EC culture, human umbilical vein endothelial cells (HUVEC) were purchased from ATCC and cultured in a culture dish containing IMDM with 10% FBS, 100 units/ml penicillin/streptomycin, 0.2 µl/ml bFGF, and 0.5 µl/ml VEGF (Peprotech, Rocky Hill, NJ, USA). All cells were maintained in the incubator, the medium was changed every 2 days, and the cells were subcultured upon reaching 80% confluence, to obtain 3.8×10^4 cells/ml of medium/dish.

EV treatment for ATMSC, EPC and EC

ATMSC were seeded at a density of 1×10^5 cells/ml in a 24-well culture plate, then treated with PKH26-labeled EV at an amount of 25 µg cultured for 4 days, followed by medium changing and another EV treatment for the next 4 days before examination. EPC or EC were seeded at a density of 1×10^5 cells/ml in a 24-well culture plate and then treated with 10 µg or 5 µg PKH26-labeled EV, respectively (which ensured over 90% uptake, Supplementary Figures 3A, B) cultured for 2 days before examination. The uptake of PKH26-labeled EV to target cells was examined by a flow cytometer (BD LSRFortessa X-20; BD Biosciences).

Collection of ATMSC- and EPC-derived CM

After EV treatment, ATMSC and EPC were washed with PBS before changing to a new corresponding medium without EV. After 48 h, the medium was collected and centrifuged at 300 g for 5 min, followed by 1200*xg* for 20 min (both at 4°C) to collect the supernatant. The collected CM was stored at -30°C.

CM treatment of MDA-MB-231 and MCF7 BCC

MDA-MB-231 and MCF7 cells were seeded at a density of 1×10^5 cells/ml in a 24-well culture plate for 2 h, and then the medium was replaced with ATMSC- or EPC-derived CM and cultured for 2 days before examination.

Differentiation of ATMSC to adipocytes and osteoblasts

ATMSC was seeded at a number of 1×10^5cells/well in a 4-well plate in MSC culture medium. After getting 100% confluency, the culture medium was changed to adipogenic or osteogenic differentiation medium. The culture medium was changed twice per week for 3 weeks. Adipogenic differentiation medium consisted of IMDM supplemented with 10% FBS, 0.1 mM dexamethasone (Sigma-Aldrich), 0.5 mM 3-isobutyl-1-methylxanthine (Sigma-Aldrich), 2 mg/mL insulin (Wako), and 0.1 mM indomethacine (Sigma-Aldrich). The formation of adipocytes was examined by staining with Oil Red O solution (Muto Pure Chemicals, Tokyo, Japan). For quantification, cells were dissolved with 4% IGPAL CA630 (Sigma-Aldrich) in isopropanol, and the absorbance at 492 nm was measured. Osteogenic differentiation medium consisted of IMDM supplemented with 1% FBS, 0.1 mM dexamethasone (Sigma-Aldrich), 10 mM β-glycerol-2-phosphate (Sigma-Aldrich), 0.2 mM ascorbic acid (Sigma-Aldrich), and 50 ng/mL human EGF (Wako). The formation of mineralized matrix was examined by staining with Alizarin Red S (Kodak,

Rochester, NY). For quantification, cells were dissolved with 0.2 N HCl (Wako) and 5% sodium dodecyl sulfate, then the absorbance at 480 nm was measured.

Analysis of MSC marker expression by flow cytometry

A number of 1×10^5 ATMSC was collected in 200 µL PBS containing 2% FBS. After that, ATMSC were incubated with antibodies for 30 minutes at 4°C, including FITC-labeled anti-CD90 (BioLegend, San Diego, CA; 328107), PE-labeled anti-CD105 (BioLegend; 323206), PE-labeled anti-CD73 (BD Biosciences, San Diego, CA, 550257), FITC-labeled anti-CD31 (BioLegend; 303103), FITC–labeled anti-CD45 (BD Biosciences; 560976) and PE-labeled anti-CD34 (BD Biosciences; 560941). Cells stained with PE-labeled anti-IgG1 (555749; BD Biosciences), and FITC-labeled anti-IgG1 (555748; BD Biosciences) were used as the isotype controls. After that, cells were washed with PBS and resuspended in 300 µL PBS containing 2% FBS. The expression of MSC markers was analyzed by a flow cytometer (BD LSRFortessa X-20; BD Biosciences).

ELISA for PGE2 quantification

CM from ATMSC was collected as described above. PGE2 concentration in CM was measured using ELISA kit Parameter Prostaglandin E2 assay (Biotechne R& D system, Mineapolis, USA). In short, CM and PGE2 standard with serial two-fold diluted concentration from 2500 pg/ml to 39 pg/ml were incubated in 96-well microplate together with primary antibody in 1 hour. The mixtures were then incubated with PGE2 conjugate in 2 hours and removed. After washing, the wells were incubated with substrate solution in 30 minutes, then reaction was stopped with acidic stop solution. Optical density at 450nm and 570nm (OD_{450nm} and OD_{570nm}) was measured using microplate reader. OD value of each sample was calculated as follows:

$$\text{OD sample} = \text{average}\,(OD_{450nm\ sample} - OD_{570nm\ sample}) - \text{average}\,(OD_{450nm\ blank} - OD_{570nm\ blank})$$

PGE2 concentration of each sample was calculated based on linear regression of OD value of standard curve in Microsoft Excel.

Migration assay

ATMSC, MDA-MB-231, or MCF7 cells (2×10^5 cells/400 µL/well) were seeded into 24-well plates in their respective culture medium and incubated for 24 h. Mitomycin C solution (Nacalai Tesque, Kyoto, Japan) was added at a concentration of 10 µg/ml and incubated for 1 h prior to creating a single scratch through the seeded cells using a 100 µl micropipette tip. The medium was removed and replaced with IMDM containing 0.25% FBS. Images of the scratch were taken immediately after the scratch and at 6-hour intervals up to 30 h or until closed using the Keyence BZ-XY710 microscope system (Keyence Corporation, Osaka, Japan). The gap closure percentage was analysis using ImageJ (NIH, Bethesda, MD).

Proliferation assay

After treatment, ATMSC, EPC, HUVEC, MDA-MB-231 cells, and MCF7 cells were seeded into a 96-well plate to obtain 1×10^4 cells/100 µl medium in each well. At 24 and 48 h, the absorbance at 450 nm (OD_{450nm}) was measured after an hour of adding Cell Counting Kit-8 (Dojindo Molecular Technologies, Kumamoto, Japan).

Transwell migration assay

MCF7 cells (5×10^4 cells/600 µL of medium) were seeded into the wells of a 24-well plate for 48 h. After treatment, EPC or HUVEC (2×10^5 cells/ml medium) were transferred into 8.0-µm pore cell transwell culture inserts (BD Falcon), which were then placed into the wells seeded with MCF7 cells. The cells were incubated for 6 h before staining. The cells were fixed with 4% paraformaldehyde before removing the cells on the membrane surface inside the transwells using a cotton swab. The remaining cells were permeabilized with methanol for 10 min, stained with a 2% crystal violet dye solution for 5 min, and then washed with distilled deionized water. Images of the transwell membrane were taken under a dissecting microscope, and the number of cells on the membrane was counted in 39 random areas on a created grid to calculate the estimated number of cells on the membrane.

Mammosphere formation assay

MDA-MB-231 and MCF7 cells pretreated with CM were mixed in MammoCult Basal medium (StemCell Technologies Inc., Vancouver, Canada) supplemented with heparin and hydrocortisone to obtain a ratio of 9.5×10^3 cells/2 ml. This suspension was cultured for 5 days on an ultra-low attachment surface in a 6-well plate (Corning, Corning, NY, USA). The mammosphere (diameter ≥100 µm) forming efficiency (MSFE) was calculated using the following equation:

MSFE (%) = number of mammospheres × 100/number of seeded cells.

Colony formation assay

MDA-MB-231 and MCF7 cells pretreated with CM were seeded in 6-well plates at a ratio of 100 cells/well. The cells were incubated for 1 week before being fixed with 4% paraformaldehyde and then stained with 5% w/v crystal violet. The colonies were analyzed and counted via macroscopic observations.

Spheroid culture

MDA-MB-231 cells were treated with M-protein (3 pmol/mL) 48 hours before being collected and stained with PKH26 (Sigma). EPC were collected and stained with CSFE (Dojindo, Japan). Spheroid culture was conducted based on the protocol of Dahndapani et al, 2023 (50), including monoculture, diculture and triculture. Briefly, 100 µL of a mixture of $6x10^4$ cells suspension were seeded into PrimeSurfaceU 96-well plate (Sumibe, Japan). Diculture spheroids consisted of a mixture of MDA-MB-231 cells and EPC with a ratio of $3x10^4$ cells:$3x10^4$ cells. Triculture spheroids consisted of a mixture of MDA-MB-231 cells, EPC and ATMSC with a ratio of $2x10^4$ cells:$2x10^4$cells:$2x10^4$ cells. After 1 week, spheroids were trypsinized to collected single cells. CFSE-labeled EPC were sorted using a flow cytometer (MoFlo XDP, Beckman Coulter) for a further analysis of TEC marker gene expression and tube formation.

Tube formation assay

EPC and HUVEC were treated for 48 h as described above. Matrigel (300 µL; Corning) was used to coat each well in the 4-well plates and incubated for 30 min before seeding $7.5×10^4$ cells/500 µl medium of the treated EPC and HUVEC. Images of tube formation were taken in nine random areas of the well at 3 h and 6 h after seeding. The lengths of the tubes formed were analyzed using the angiogenesis program in ImageJ.

Quantitative reverse transcription (qRT) PCR gene expression analyses

ATMSC, EPC, HUVEC, MDA-MB-231 cells, and MCF7 cells were treated with EV or CM as described above. Sepasol-RNA Super G (Nacalai Tesque) was added according to the manufacturer's instructions to isolate the total RNA, followed by reverse transcription into cDNA using a ReverTra Ace qPCR RT kit (Toyobo, Kita, Osaka, Japan). Two microliters of the cDNA were amplified with the THUNDERBIRD SYB qPCR Mix (Toyobo) via the Real-time PCR system QuantStudio 5 (Thermo Fisher Scientific). The samples were denatured for 10 min at 95°C followed by 15 s cycles of denaturation at 95°C. Finally, 30 s of annealing and extension was performed at 60°C. The level of gene expression in each sample was analyzed using the ΔΔCt method

TABLE 1 Primers used for quantitative polymerase chain reaction.

Gene	Forward sequence	Reverse sequence
β-Actin	CTCGCCTTTGCCGATCC	TCTCCATGTCGTCCCAGTTG
FAP	TGTCTGCCAGTCTTCCGTGAAG	GGAAGTGCCTGTTCCAGCAATG
FSP	CAGAACTAAAGGAGCTGCTGACC	CTTGGAAGTCCACCTCGTTGTC
Vimentin	AGGCAAAGCAGGAGTCCACTGA	ATCTGGCGTTCCAGGGACTCAT
IL6	ACAAGAGTAACATGTGTGAAAGCAG	TATACCTCAAACTCCAAAAGACCAG
IL8	GAGAGTGATTGAGAGTGGACCAC	CACAACCCTCTGCACCCAGTTT
CXCL7	CTGGCTTCCTCCACCAAAGG	GACTTGGTTGCAATGGGTTCC
bFGF	CAGAGTGTTGCTGTGACCAG	GATCGAGCTCACTGTGGAGT
PDGFa	ATCAATCAGCCCAGATGGAC	TTCACGGGCAGAAAGGTACT
SDF1	TGAGAGCTCGCTTTGAGTGA	CACCAGGACCTTCTGTGGAT
ANG1	GCCTGATCTTACACGGTGCT	GGCCACAAGCATCAAACCAC
VEGF	CAAGACAAGAAAATCCCTGTGG	CCTCGGCTTGTCACATCTG
IL1α	TGTGACTGCCCAAGATGAAG	AAGTTTGGATGGGCAACTGA
PTGES2	ACCTCTATGAGGCTGCTGACAAGT	CATACACCGCCAAATCAGCGAGAT
COX2	CCCTTGGGTGTCAAAGGTAA	GCCCTCGCTTATGATCTGTC
CXCR7	TCGGCAGCATTTTCTTCCTC	GCAGTCGGTCTCATTGTTGGAC
CXCR4	CCAAGGAAAGCATAGAGGATGGGGTTC	CTGTGACCGCTTCTACCCCAATGACTT
vWF	ATGCCCCTGGAGAAACAGTG	CCGAAAGGTCCCAGGGTTAC
SNAIL	AACTACAGCGAGCTGCAGGACTCTAA	CCTTTCCCACTGTCCTCATCTGACA
VE-Cadherin	CAGAGTACCACCTCACTGCTGTCATT	CCACTGCTGTCACAGAGATGACTGA
ALDH	GGAGTGTTGAGCGGGCTAAGAAGTA	CATTAGAGAACACTGTGGGCTGGAC

(formula $2^{-\Delta\Delta CT}$) and normalized to ACTB (β-actin) gene expression. The primers were listed in Table 1.

In vivo metastasis assay

All experimental procedures were approved by the University of Tsukuba Institute of Animal Care and Use Committee. Female C57BL/6J mice were bred under specific pathogen-free (SPF) conditions. MCF-7 cells after treatment with ATMSC- or EPC-derived CM were collected and resuspended in PBS. Cells with a density of 2×10^5 cells/300 µl were injected intravenously via the tail vein, followed by a daily injection of cyclosporin-A (Sigma – Aldrich) for the initial week. For the second week, cyclosporine was administered on alternating days. Mice were sacrificed by cervical dislocation after 14 days. The lungs were harvested, fixed with 4% paraformaldehyde (Wako Pure Chemical), frozen, and stained with hematoxylin and eosin. The cross-sections were observed under a microscope using 40x magnification to identify and capture tumor foci. The tumor foci areas are defined as the areas with high cell density, which are dense masses contains cells with epithelial morphology and high nuclear density (purple stained areas), while lung tissue areas have porous structure with low nuclear density (pink stained areas). All sections from one lung sample were observed in the order of cutting, so the tumor foci appeared at the same place in continuous sections would be considered as the same tumors. The size of a certain tumor was defined based on the largest focus of that tumor observed among continuous sections. Images were analyzed using the ImageJ software program.

Western blotting

Total protein was extracted from EV using RIPA buffer (Nacalai, Kyoto, Japan) and the concentration was measured by a Bradford assay (Bio-Rad). An amount of 50µg of extracted protein was separated by electrophoresis in 7.5% SDS-polyacrylamide gels. The proteins were transferred to a polyvinylidene difluoride membrane (Millipore). After that membranes were blocked with 5% skim milk in Tris-buffered saline containing 0.1% Tween 20 (TBST) for an hour at room temperature. Membranes were then incubated with primary antibodies, including rabbit anti-CD63 (GTX17441; GeneTex), rabbit anti-TSG101 (GTX118736; GeneTex), and rabbit apolipoprotein A1 (APOA1, GTX40453; GeneTex) at 1:1000 dilution overnight at 4°C. Membranes were washed with TBST, then incubated with HRP-conjugated goat anti-rabbit IgG (Thermo Fisher Scientific) at 1:10,000 dilution. The positive signals were analyzed by a luminescence imager (Image Quant LAS4000; GE Health Care, Little Chalfont, United Kingdom) using chemiluminescence reagents (Merck Millipore).

Statistical analyses

The results are presented as mean± standard deviation (SD). The t-test of the Microsoft Excel software program was used to calculate and analyze differences. P values of<0.05 were considered to indicate statistical significance.

Data availability statement

The original contributions presented in the study are included in the article/Supplementary Material. Further inquiries can be directed to the corresponding author.

Ethics statement

The studies involving humans were approved by The Ethics Committee of the University of Tsukuba. The studies were conducted in accordance with the local legislation and institutional requirements. The participants provided their written informed consent to participate in this study. The animal study was approved by University of Tsukuba Institute of Animal Care and Use Committee. The study was conducted in accordance with the local legislation and institutional requirements.

Author contributions

H-NN: Conceptualization, Data curation, Formal Analysis, Investigation, Methodology, Software, Writing – original draft. C-KV: Conceptualization, Data curation, Investigation, Methodology, Project administration, Supervision, Validation, Visualization, Writing – review & editing. MF: Data curation, Formal Analysis, Methodology, Software, Visualization, Writing – review & editing. MU: Data curation, Formal Analysis, Methodology, Validation, Writing – original draft. LT: Data curation, Formal Analysis, Methodology, Software, Writing – original draft. TY: Data curation, Formal Analysis, Methodology, Software, Writing – review & editing. MO-Y: Methodology, Writing – review & editing. HH: Methodology, Writing – review & editing. MO: Methodology, Writing – review & editing. TT: Methodology, Writing – review & editing. YH: Methodology, Project administration, Writing – review & editing. OO: Conceptualization, Data curation, Funding acquisition, Investigation, Project administration, Resources, Supervision, Validation, Visualization, Writing – review & editing.

Funding

The author(s) declare financial support was received for the research, authorship, and/or publication of this article. This work was supported by Grants-in-Aid from the Japan Society for the Promotion of Science and the Japanese Ministry of Education, Culture, Sports, Science and Technology.

Conflict of interest

The authors declare that the research was conducted in the absence of any commercial or financial relationships that could be construed as a potential conflict of interest.

Publisher's note

Supplementary material

The Supplementary Material for this article can be found online at: https://www.frontiersin.org/articles/10.3389/fonc.2024.1346312/full#supplementary-material

SUPPLEMENTARY FIGURE 1
Characteristics of EV derived from triple-negative BCC. **(A)** Size distribution of nEV and MpEV. **(B)** The marker expression of nEV and MpEV. **(C)** Uptake of PKH26-labeled EV by ATMSC, examined by flow cytometry.

SUPPLEMENTARY FIGURE 2
Response of MDA-MB-231 cells to CM derived from EV-ATMSC. **(A)** Migration of MDA-MB-231 cells treated with CM derived from ATMSC, nEV-ATMSC, MpEV-ATMSC. **(B)** Proliferation of MDA-MB-231 cells treated with CM derived from ATMSC, nEV-ATMSC, MpEV-ATMSC. **(C)** Colony formation of MDA-MB-231 cells treated with CM derived from ATMSC, nEV-ATMSC, MpEV-ATMSC. **(D)** Mammosphere formation of MDA-MB-231 cells treated with CM derived from ATMSC, nEV-ATMSC, MpEV-ATMSC.

SUPPLEMENTARY FIGURE 3
Uptake of nEV and MpEV by EPC, EC, and effects of MpEV secreted from M-protein-induced triple negative BCC on EC. **(A)** Uptake of PKH26-labeled EV by EPC, examined by flow cytometry. **(B)** Uptake of PKH26-labeled EV by EC, examined by flow cytometry. **(C)** Proliferation of HUVEC uptaking EV. **(D)** Transwell migration of HUVEC uptaking EV. **(E)** Tube formation of HUVEC uptaking EV.

SUPPLEMENTARY FIGURE 4
Response of MDA-MB-231 cells to CM derived from EPC, nEV- EPC, MpEV-EPC. **(A)** Migration of MDA-MB-231 cells treated with CM derived from EPC, nEV- EPC, MpEV-EPC (the scale bars indicate 500 μm). **(B)** Proliferation of MDA-MB-231 cells treated with CM derived from EPC, nEV- EPC, MpEV-EPC. **(C)** Colony formation of MDA-MB-231 cells treated with CM derived from EPC, nEV- EPC, MpEV-EPC. **(D)** Mammosphere formation of MDA-MB-231 cells treated with CM derived from EPC, nEV- EPC, MpEV-EPC.

SUPPLEMENTARY FIGURE 5
Spheroid culture of PKH26-labeled MDA-MB-231 cells, CFSE-labeled EPC and ATMSC (the scale bars indicate 500 μm, MDA: MDA-MB-231, M-MDA: M-protein-induced MDA-MB-231).

SUPPLEMENTARY FIGURE 6
Effects of MpEV and nEV on MDA-MB-231 cells. **(A)** Migration of MDA-MB-231 uptaking EV. **(B)** Proliferation of MDA-MB-231 uptaking EV. **(C)** Colony formation of MDA-MB-231 uptaking EV. **(D)** Cytokine gene expression of MDA-MB-231 uptaking EV. **(E)** EMT-related gene expression of MDA-MB-231 uptaking EV.

SUPPLEMENTARY FIGURE 7
Effects of MpEV on spheroid culture. **(A)** Spheroid culture of PKH26-labeled MDA-MB-231 cells, CFSE-labeled EPC and ATMSC (the scale bars indicate 500 μm). **(B)** TEC-related gene expression of EPC isolated from spheroid. **(C)** Tube formation of EPC isolated from spheroid (The scale bars indicate 500 μm).

References

1. Huang X, Liang H, Zhang H, Tian L, Cong P, Wu T, et al. The potential mechanism of cancer patients appearing more vulnerable to SARS-CoV-2 and poor outcomes: A pan-cancer bioinformatics analysis. *Front Immunol*. (2021) 12:804387. doi: 10.3389/fimmu.2021.804387

2. Temena MA, Acar A. Increased TRIM31 gene expression is positively correlated with SARS-CoV-2 associated genes TMPRSS2 and TMPRSS4 in gastrointestinal cancers. *Sci Rep*. (2022) 12:11763. doi: 10.1038/s41598-022-15911-2

3. Katopodis P, Anikin V, Randeva HS, Spandidos DA, Chatha K, Kyrou I, et al. Pan –cancer analysis of transmembrane protease serine 2 and cathepsin L that mediate cellular SARS–CoV–2 infection leading to COVID-19. *Int J Oncol*. 57(2):533–9. doi: 10.3892/ijo.2020.5071

4. Wei X, Su J, Yang K, Wei J, Wan H, Cao X, et al. Elevations of serum cancer biomarkers correlate with severity of COVID-19. *J Med Virol*. 92(10):2036–41. doi: 10.1002/jmv.25957

5. Saygideger Y, Sezan A, Candevir A, Saygıdeğer Demir B, Güzel E, Baydar O, et al. COVID-19 patients' sera induce epithelial mesenchymal transition in cancer cells. *Cancer Treat Res Commun*. (2021) 28:100406. doi: 10.1016/j.ctarc.2021.100406

6. Nguyen H-NT, Kawahara M, Vuong C-K, Fukushige M, Yamashita T, Ohneda O. SARS-CoV-2 M-protein facilitates Malignant transformation of breast cancer cells. *Front Oncol*. (2022) 12:923467. doi: 10.3389/fonc.2022.923467

7. Derosa L, Melenotte C, Griscelli F, Gachot B, Marabelle A, Kroemer G, et al. The immuno-oncological challenge of COVID-19. *Nat Cancer*. (2020) 1(10):946–64. doi: 10.1038/s43018-020-00122-3

8. Turnquist C, Ryan BM, Horikawa I, Harris BT, Harris CC. Cytokine storms in cancer and COVID-19. *Cancer Cell*. (2020) 38:598–601. doi: 10.1016/j.ccell.2020.09.019

9. Zanelli S, Fiorio E, Zampiva I, Zacchi F, Borghesani G, Giontella E, et al. Risk and severity of SARS-CoV-2 infection in breast cancer patients undergoing a structured infection screening program at the University and Hospital Trust of Verona. *Ann oncology : Off J Eur Soc Med Oncol*. (2022) 33:661–3. doi: 10.1016/j.annonc.2022.02.227

10. Li J, Bai H, Qiao H, Du C, Yao P, Zhang Y, et al. Causal effects of COVID-19 on cancer risk: A Mendelian randomization study. *J Med Virol*. (2023) 95:e28722. doi: 10.1002/jmv.28722

11. Vyshnavi AMH, Namboori PKK. Association of SARS-coV-2 infection and triple negative breast cancer (TNBC) A computational illustrative study. *Lett Drug Design Discovery*. (2023) 20:1107–16. doi: 10.2174/1570180819666220620101333

12. Marenco-Hillembrand L, Erben Y, Suarez-Meade P, Franco-Mesa C, Sherman W, Eidelman BH, et al. Outcomes and surgical considerations for neurosurgical patients hospitalized with COVID-19–A multicenter case series. *World Neurosurg*. (2021) 154:e118–29. doi: 10.1016/j.wneu.2021.06.147

13. Bilir C, Cakir E, Gülbagci B, Altindis M, Toptan H, Guclu E, et al. COVID-19 prevalence and oncologic outcomes of asymptomatic patients with active cancer who received chemotherapy. *Acta Med Mediterr*. (2021) 37:667–71. doi: 10.19193/0393-6384_2021_1_103

14. Li T, Wang L, Wang H, Li X, Zhang S, Xu Y, et al. Serum SARS-COV-2 nucleocapsid protein: A sensitivity and specificity early diagnostic marker for SARS-COV-2 infection. *Front Cell Infect Microbiol*. (2020) 10:470. doi: 10.3389/fcimb.2020.00470

15. Shan D, Johnson JM, Fernandes SC, Suib H, Hwang S, Wuelfing D, et al. N-protein presents early in blood, dried blood and saliva during asymptomatic and symptomatic SARS-CoV-2 infection. *Nat Commun*. (2021) 12(1):1931. doi: 10.1038/s41467-021-22072-9

16. Ogata AF, Maley AM, Wu C, Gilboa T, Norman M, Lazarovits R, et al. Ultra-sensitive serial profiling of SARS-coV-2 antigens and antibodies in plasma to understand disease progression in COVID-19 patients with severe disease. *Clin Chem*. (2020) 66(12):1562–72. doi: 10.1093/clinchem/hvaa213

17. Jana AK, Greenwood AB, Hansmann UHE. Presence of a SARS-COV-2 protein enhances Amyloid Formation of Serum Amyloid A. *bioRxiv*. (2021) 125(32):9155–9167. doi: 10.1101/2021.05.18.444723v2

18. Sullivan R, Maresh G, Zhang X, Salomon C, Hooper J, Margolin D, et al. The emerging roles of extracellular vesicles as communication vehicles within the tumor microenvironment and beyond. *Front Endocrinol*. (2017) 8:194. doi: 10.3389/fendo.2017.00194

19. Baghban R, Roshangar L, Jahanban-Esfahlan R, Seidi K, Ebrahimi-Kalan A, Jaymand M, et al. Tumor microenvironment complexity and therapeutic implications at a glance. *Cell Commun Signal*. (2020) 18(1):59. doi: 10.1186/s12964-020-0530-4

20. Wendler F, Favicchio R, Simon T, Alifrangis C, Stebbing J, Giamas G. Extracellular vesicles swarm the cancer microenvironment: from tumor–stroma communication to drug intervention. *Oncogene*. (2017) 36:877–84. doi: 10.1038/onc.2016.253

21. Cho JA, Park H, Lim EH, Lee KW. Exosomes from breast cancer cells can convert adipose tissue-derived mesenchymal stem cells into myofibroblast-like cells. *Int J Oncol*. (2012) 40:130–8. doi: 10.3892/ijo.2011.1193

22. Escobar P, Bouclier C, Serret J, Bièche I, Brigitte M, Caicedo A, et al. IL-1β produced by aggressive breast cancer cells is one of the factors that dictate their interactions with mesenchymal stem cells through chemokine production. *Oncotarget*. (2015) 6(30):29034–47. doi: 10.18632/oncotarget.4732

23. Amorim M, Fernandes G, Oliveira P, Martins-de-Souza D, Dias-Neto E, Nunes D. The overexpression of a single oncogene (ERBB2/HER2) alters the proteomic landscape of extracellular vesicles. *Proteomics*. (2014) 14(12):1472–9. doi: 10.1002/pmic.201300485

24. Anderson NM, Simon MC. The tumor microenvironment. *Curr Biol*. (2020) 30: R921–5. doi: 10.1016/j.cub.2020.06.081

25. Khanh VC, Fukushige M, Moriguchi K, Yamashita T, Osaka M, Hiramatsu Y, et al. Type 2 diabetes mellitus induced paracrine effects on breast cancer metastasis through extracellular vesicles derived from human mesenchymal stem cells. *Stem Cells Dev*. (2020) 29(21):1382–94. doi: 10.1089/scd.2020.0126

26. Hass R. Role of MSC in the tumor microenvironment. *Cancers (Basel)*. (2020) 12 (8):2107. doi: 10.3390/cancers12082107

27. Mandel K, Yang Y, Schambach A, Glage S, Otte A, Hass R. Mesenchymal stem cells directly interact with breast cancer cells and promote tumor cell growth *in vitro* and *in vivo*. *Stem Cells Dev*. (2013) 22:3114–27. doi: 10.1089/scd.2013.0249

28. Shi Y, Du L, Lin L, Wang Y. Tumour-associated mesenchymal stem/stromal cells: emerging therapeutic targets. *Nat Rev Drug Discovery*. (2017) 16:35–52. doi: 10.1038/nrd.2016.193

29. Hill BS, Pelagalli A, Passaro N, Zannetti A. Tumor-educated mesenchymal stem cells promote pro-metastatic phenotype. *Oncotarget*. (2017) 8:73296–311. doi: 10.18632/oncotarget.20265

30. Gehling UM, Ergün S, Schumacher U, Wagener C, Pantel K, Otte M, et al. *In vitro* differentiation of endothelial cells from AC133-positive progenitor cells. *Blood*. (2000) 95:3106–12. doi: 10.1182/blood.V95.10.3106

31. Zhao X, Liu H, Li J, Liu X. Endothelial progenitor cells promote tumor growth and progression by enhancing new vessel formation (Review). *Oncol Lett*. (2016) 12 (2):793–9. doi: 10.3892/ol.2016.4733

32. Nolan DJ, Ciarrocchi A, Mellick AS, Jaggi JS, Bambino K, Gupta S, et al. Bone marrow-derived endothelial progenitor cells are a major determinant of nascent tumor neovascularization. *Genes Dev*. (2007) 21:1546–58. doi: 10.1101/gad.436307

33. Zhang H, Chen FI, Xu CP, Ping YF, Wang QL, Liang ZQ, et al. Incorporation of endothelial progenitor cells into the neovasculature of Malignant glioma xenograft. *J Neurooncol*. (2009) 93(2):165–74. doi: 10.1007/s11060-008-9757-4

34. Annan DA-M, Kikuchi H, Maishi N, Hida Y, Hida K. Tumor endothelial cell-A biological tool for translational cancer research. *Int J Mol Sci*. (2020) 21(9):3238. doi: 10.3390/ijms21093238

35. Butler JM, Kobayashi H, Rafii S. Instructive role of the vascular niche in promoting tumour growth and tissue repair by angiocrine factors. *Nat Rev Cancer*. (2010) 10:138–46. doi: 10.1038/nrc2791

36. Ritter A, Kreis N-N, Hoock SC, Solbach C, Louwen F, Yuan J. Adipose tissue-derived mesenchymal stromal/stem cells, obesity and the tumor microenvironment of breast cancer. *Cancers (Basel)*. (2022) 14(16):3908. doi: 10.3390/cancers14163908

37. Gentile P. Breast cancer therapy: the potential role of mesenchymal stem cells in translational biomedical research. *Biomedicines*. (2022) 10(5):1179. doi: 10.3390/biomedicines10051179

38. Jansson S, Aaltonen K, Bendahl PO, Falck AK, Karlsson M, Pietras K, et al. The PDGF pathway in breast cancer is linked to tumour aggressiveness, triple-negative subtype and early recurrence. *Breast Cancer Res Treat*. (2018) 169(2):231–41. doi: 10.1007/s10549-018-4664-7

39. Johnston CL, Cox HC, Gomm JJ, Coombes RC. bFGF and aFGF induce membrane ruffling in breast cancer cells but not in normal breast epithelial cells: FGFR-4 involvement. *Biochem J*. (1995) 306:609–16. doi: 10.1042/bj3060609

40. Fenig E, Livnat T, Sharkon-Polak S, Wasserman L, Beery E, Lilling G, et al. Basic fibroblast growth factor potentiates cisplatinum-induced cytotoxicity in MCF-7 human breast cancer cells. *J Cancer Res Clin Oncol*. (1999) 125(10):556–62. doi: 10.1007/s004320050316

41. Ariad S, Seymour L, Bezwoda WR. Platelet-derived growth factor (PDGF) in plasma of breast cancer patients: Correlation with stage and rate of progression. *Breast Cancer Res Treat*. (1991) 20(1):11–7. doi: 10.1007/BF01833352

42. Kang H, Watkins G, Parr C, Douglas-Jones A, Mansel RE, Jiang WG. Stromal cell derived factor-1: its influence on invasiveness and migration of breast cancer cells *in vitro*, and its association with prognosis and survival in human breast cancer. *Breast Cancer Res*. (2005) 7(4):R402–10. doi: 10.1186/bcr1022

43. Li H-J, Reinhardt F, Herschman HR, Weinberg RA. Cancer-stimulated mesenchymal stem cells create a carcinoma stem cell niche via prostaglandin E2 signaling. *Cancer Discovery*. (2012) 2(9):840–55. doi: 10.1158/2159-8290.CD-12-0101

44. Parker BS, Argani P, Cook BP, Liangfeng H, Chartrand SD, Zhang M, et al. Alterations in vascular gene expression in invasive breast carcinoma. *Cancer Res*. (2004) 64:7857–66. doi: 10.1158/0008-5472.CAN-04-1976

45. Bhati R, Patterson C, Livasy CA, Fan C, Ketelsen D, Hu Z, et al. Molecular characterization of human breast tumor vascular cells. *Am J Pathol*. (2008) 172 (5):1381–90. doi: 10.2353/ajpath.2008.070988

46. Hida K, Maishi N, Akiyama K, Ohmura-Kakutani H, Torii C, Ohga N, et al. Tumor endothelial cells with high aldehyde dehydrogenase activity show drug resistance. *Cancer Sci*. (2017) 108(2):2195–203. doi: 10.1111/cas.13388

47. Grange C, Bussolati B, Bruno S, Fonsato V, Sapino A, Camussi G. Isolation and characterization of human breast tumor-derived endothelial cells. *Oncol Rep*. (2006) 15 (2):381–6. doi: 10.3892/or.15.2.381

48. Dhami SPS, Patmore S, Comerford C, Byrne CM, Cavanagh B, Castle J, et al. Breast cancer cells mediate endothelial cell activation, promoting von Willebrand factor release, tumor adhesion, and transendothelial migration. *J Thromb Haemost*. (2022) 20 (10):2350–65. doi: 10.1111/jth.15794

49. DeCicco-Skinner KL, Henry GH, Cataisson C, Tabib T, Gwilliam JC, Watson NJ, et al. Endothelial cell tube formation assay for the *in vitro* study of angiogenesis. *J Vis Exp: JoVE*. (2014) 91:e51312. doi: 10.3791/51312

50. Dhandapani H, Siddiqui A, Karadkar S, Tayalia P. *In vitro* 3D spheroid model preserves tumor microenvironment of hot and cold breast cancer subtypes. *Adv Healthc. Mater*. (2023) 12(21):e2300164. doi: 10.1002/adhm.202300164

51. Stavri GT, Zachary IC, Baskerville PA, Martin JF, Erusalimsky JD. Basic fibroblast growth factor upregulates the expression of vascular endothelial growth factor in vascular smooth muscle cells. Synergistic interaction with hypoxia. *Circulation*. (1995) 92(1):11–4. doi: 10.1161/01.cir.92.1.11

52. Mirshahi F, Pourtau J, Li H, Muraine M, Trochon V, Legrand E, et al. SDF-1 activity on microvascular endothelial cells: consequences on angiogenesis in *in vitro* and *in vivo* models. *Thromb Res*. (2000) 99(6):587–94. doi: 10.1016/s0049-3848(00)00292-9

53. Heidemann J, Ogawa H, Dwinell MB, Rafiee P, Maaser C, Gockel HR, et al. Angiogenic effects of interleukin 8 (CXCL8) in human intestinal microvascular endothelial cells are mediated by CXCR2. *J Biol Chem*. (2003) 278(10):8508–15. doi: 10.1074/jbc.M208231200

54. Bertuzzi AF, Marrari A, Gennaro N, Cariboni U, Ciccarelli M, Giordano L, et al. Low incidence of sars-cov-2 in patients with solid tumours on active treatment: An observational study at a tertiary cancer centre in lombardy, Italy. *Cancers (Basel)*. (2020) 12(9):1–9. doi: 10.3390/cancers12092352

55. de Joode K, Oostvogels AAM, GeurtsvanKessel CH, de Vries RD, Mathijssen RHJ, Debets R, et al. Case report: adequate T and B cell responses in a SARS-coV-2 infected patient after immune checkpoint inhibition. *Front Immunol*. (2021) 12:627186. doi: 10.3389/fimmu.2021.627186

56. Malkani N, Rashid MU. SARS-COV-2 infection and lung tumor microenvironment. *Mol Biol Rep*. (2021) 48(2):1925–34. doi: 10.1007/s11033-021-06149-8

57. Giurini EF, Williams M, Morin A, Zloza A, Gupta KH. Inactivated SARS-coV-2 reprograms the tumor immune microenvironment and improves murine cancer outcomes. *bioRxiv*. (2022) 2022.06.30.498305. doi: 10.1101/2022.06.30.498305

58. Zhang Z, Nomura N, Muramoto Y, Ekimoto T, Uemura T, Liu K, et al. Structure of SARS-CoV-2 membrane protein essential for virus assembly. *Nat Commun*. (2022) 13(1):4399. doi: 10.1038/s41467-022-32019-3

59. Evdokimova V, Tognon C, Ng T, Sorensen PHB. Reduced proliferation and enhanced migration: two sides of the same coin? Molecular mechanisms of metastatic progression by YB-1. *Cell Cycle*. (2009) 8:2901–6. doi: 10.4161/cc.8.18.9537

60. Zhan Q, Liu B, Situ X, Luo Y, Fu T, Wang Y, et al. New insights into the correlations between circulating tumor cells and target organ metastasis. *Signal Transduction Targeting Ther*. (2023) 8(1):465. doi: 10.1038/s41392-023-01725-9

61. Xuan X, Tian C, Zhao M, Sun Y, Huang C. Mesenchymal stem cells in cancer progression and anticancer therapeutic resistance. *Cancer Cell Int*. (2021) 21:595. doi: 10.1186/s12935-021-02300-4

62. Zhao W, Wang C, Liu R, Wei C, Duan J, Liu K, et al. Effect of TGF-β1 on the migration and recruitment of mesenchymal stem cells after vascular balloon injury: involvement of matrix metalloproteinase-14. *Sci Rep*. (2016) 6(1):21176. doi: 10.1038/srep21176

63. Ridge SM, Sullivan FJ, Glynn SA. Mesenchymal stem cells: key players in cancer progression. *Mol Cancer*. (2017) 16:31. doi: 10.1186/s12943-017-0597-8

64. Hossain A, Gumin J, Gao F, Figueroa J, Shinojima N, Takezaki T, et al. Mesenchymal stem cells isolated from human gliomas increase proliferation and

maintain stemness of glioma stem cells through the IL-6/gp130/STAT3 pathway. *Stem Cells*. (2015) 33(8):2400–15. doi: 10.1002/stem.2053

65. Kansy BA, Dißmann PA, Hemeda H, Bruderek K, Westerkamp AM, Jagalski V, et al. The bidirectional tumor–mesenchymal stromal cell interaction promotes the progression of head and neck cancer. *Stem Cell Res Ther*. (2014) 5(4):95. doi: 10.1186/scrt484

66. McLean K, Gong Y, Choi Y, Deng N, Yang K, Bai S, et al. Human ovarian carcinoma–associated mesenchymal stem cells regulate cancer stem cells and tumorigenesis via altered BMP production. *J Clin Invest*. (2011) 121:3206–19. doi: 10.1172/JCI45273

67. Kim E-K, Kim HJ, Yang YI, Kim JT, Choi MY, Choi CS, et al. Endogenous gastric-resident mesenchymal stem cells contribute to formation of cancer stroma and progression of gastric cancer. *Korean J Pathol*. (2013) 47(6):507–18. doi: 10.4132/KoreanJPathol.2013.47.6.507

68. Li W, Zhou Y, Yang J, Zhang X, Zhang H, Zhang T, et al. Gastric cancer-derived mesenchymal stem cells prompt gastric cancer progression through secretion of interleukin-8. *J Exp Clin Cancer Res*. (2015) 34(1):52. doi: 10.1186/s13046-015-0172-3

69. Langer HF, Stellos K, Steingen C, Froihofer A, Schönberger T, Krämer B, et al. Platelet derived bFGF mediates vascular integrative mechanisms of mesenchymal stem cells *in vitro*. *J Mol Cell Cardiol*. (2009) 47(2):315–25. doi: 10.1016/j.yjmcc.2009.03.011

70. Ball SG, Shuttleworth CA, Kielty CM. Mesenchymal stem cells and neovascularization: role of platelet-derived growth factor receptors. *J Cell Mol Med*. (2007) 11(5):1012–30. doi: 10.1111/j.1582-4934.2007.00120.x

71. Roccaro AM, Sacco A, Maiso P, Azab AK, Tai YT, Reagan M, et al. BM mesenchymal stromal cell-derived exosomes facilitate multiple myeloma progression. *J Clin Invest*. (2013) 123(4):1542–55. doi: 10.1172/JCI66517

72. Asahara T, Murohara T, Sullivan A, Silver M, van der Zee R, Li T, et al. Isolation of putative progenitor endothelial cells for angiogenesis. *Sci (80-.)*. (1997) 275 (5302):964–6. doi: 10.1126/science.275.5302.964

73. Peichev M, Naiyer AJ, Pereira D, Zhu Z, Lane WJ, Williams M, et al. Expression of VEGFR-2 and AC133 by circulating human CD34+ cells identifies a population of functional endothelial precursors. *Blood*. (2000) 95(3):952–8. doi: 10.1182/blood.V95.3.952.003k27_952_958

74. Bussolati B, Deregibus M, Camussi G. Characterization of molecular and functional alterations of tumor endothelial cells to design anti-angiogenic strategies. *Curr Vasc Pharmacol*. (2010) 8:220–32. doi: 10.2174/157016110790887036

75. Hida K, Ohga N, Akiyama K, Maishi N, Hida Y. Heterogeneity of tumor endothelial cells. *Cancer Sci*. (2013) 104(11):1391–5. doi: 10.1111/cas.12251

76. Pirtskhalaishvili G, Nelson JB. Endothelium-derived factors as paracrine mediators of prostate cancer progression. *Prostate*. (2000) 44(1):77–87. doi: 10.1002/1097-0045(20000615

77. Marçola M, Rodrigues CE. Endothelial progenitor cells in tumor angiogenesis: another brick in the wall. *Stem Cells Int*. (2015) 2015:832649. doi: 10.1155/2015/832649

78. Salazar N, Zabel BA. Support of tumor endothelial cells by chemokine receptors. *Front Immunol*. (2019) 10:147. doi: 10.3389/fimmu.2019.00147

79. Zabel BA, Wang Y, Lewén S, Berahovich RD, Penfold MET, Zhang P, et al. Elucidation of CXCR7-mediated signaling events and inhibition of CXCR4-mediated tumor cell transendothelial migration by CXCR7 ligands. *J Immunol*. (2009) 183 (5):3204–11. doi: 10.4049/jimmunol.0900269

80. Beckermann BM, Kallifatidis G, Groth A, Frommhold D, Apel A, Mattern J, et al. VEGF expression by mesenchymal stem cells contributes to angiogenesis in pancreatic carcinoma. *Br J Cancer*. (2008) 99(4):622–31. doi: 10.1038/sj.bjc.6604508

81. Orimo A, Gupta PB, Sgroi DC, Arenzana-Seisdedos F, Delaunay T, Naeem R, et al. Stromal fibroblasts present in invasive human breast carcinomas promote tumor growth and angiogenesis through elevated SDF-1/CXCL12 secretion. *Cell*. (2005) 121 (3):335–48. doi: 10.1016/j.cell.2005.02.034

82. Kornilov R, Puhka M, Mannerström B, Hiidenmaa H, Peltoniemi H, Siljander P, et al. Efficient ultrafiltration-based protocol to deplete extracellular vesicles from fetal bovine serum. *J Extracell. vesicles*. (2018) 7(1):1422674. doi: 10.1080/20013078.2017.1422674

83. Kimura K, Nagano M, Salazar G, Yamashita T, Tsuboi I, Mishima H, et al. The role of CCL5 in the ability of adipose tissue-derived mesenchymal stem cells to support repair of ischemic regions. *Stem Cells Dev*. (2014) 23(5):488–501. doi: 10.1089/scd.2013.0307

84. Nagano M, Yamashita T, Hamada H, Ohneda K, Kimura KI, Nakagawa T, et al. Identification of functional endothelial progenitor cells suitable for the treatment of ischemic tissue using human umbilical cord blood. *Blood*. (2007) 110(1):151–60. doi: 10.1182/blood-2006-10-047092

frontiers | Frontiers in Oncology

TYPE Original Research
PUBLISHED 04 April 2024
DOI 10.3389/fonc.2024.1281885

OPEN ACCESS

EDITED BY
Anika Nagelkerke,
University of Groningen, Netherlands

REVIEWED BY
Chin-Shiuh Shieh,
National Kaohsiung University of Science and Technology, Taiwan
Ramin Ranjbarzadeh,
Dublin City University, Ireland
Mehmet Dalmis,
Meta, Netherlands
Yogesh Kumar,
University Medical Center Hamburg-Eppendorf, Germany

*CORRESPONDENCE
Jianrong Jiang
13509572826@163.com

†These authors have contributed equally to this work

RECEIVED 23 August 2023
ACCEPTED 11 March 2024
PUBLISHED 04 April 2024

CITATION
Tong Y, Jiang J, Chen F, Guo G, Zhang C and Deng T (2024) A novel approach for segmentation and quantitative analysis of breast calcification in mammograms. *Front. Oncol.* 14:1281885. doi: 10.3389/fonc.2024.1281885

A novel approach for segmentation and quantitative analysis of breast calcification in mammograms

Yunfei Tong[1†], Jianrong Jiang[2*†], Fang Chen[2], Guanghua Guo[2], Chaoren Zhang[1] and Tiana Deng[1]

[1]Shanghai Yanghe Huajian Artificial Intelligence Technology Co., Ltd., Shanghai, China, [2]Mindong Hospital Affiliated to Fujian Medical University, Ningde, Fujian, China

Background: Breast cancer is a major threat to women's health globally. Early detection of breast cancer is crucial for saving lives. One important early sign is the appearance of breast calcification in mammograms. Accurate segmentation and analysis of calcification can improve diagnosis and prognosis. However, small size and diffuse distribution make calcification prone to oversight.

Purpose: This study aims to develop an efficient approach for segmenting and quantitatively analyzing breast calcification from mammograms. The goal is to assist radiologists in discerning benign versus malignant lesions to guide patient management.

Methods: This study develops a framework for breast calcification segmentation and analysis using mammograms. A Pro_UNeXt algorithm is proposed to accurately segment calcification lesions by enhancing the UNeXt architecture with a microcalcification detection block, fused-MBConv modules, multiple-loss-function training, and data augmentation. Quantitative features are then extracted from the segmented calcification, including morphology, size, density, and spatial distribution. These features are used to train machine learning classifiers to categorize lesions as malignant or benign.

Results: The proposed Pro_UNeXt algorithm achieved superior segmentation performance versus UNet and UNeXt models on both public and private mammogram datasets. It attained a Dice score of 0.823 for microcalcification detection on the public dataset, demonstrating its accuracy for small lesions. For quantitative analysis, the extracted calcification features enabled high malignant/benign classification, with AdaBoost reaching an AUC of 0.97 on the private dataset. The consistent results across datasets validate the representative and discerning capabilities of the proposed features.

Conclusion: This study develops an efficient framework integrating customized segmentation and quantitative analysis of breast calcification. Pro_UNeXt offers

precise localization of calcification lesions. Subsequent feature quantification and machine learning classification provide comprehensive malignant/benign assessment. This end-to-end solution can assist clinicians in early diagnosis, treatment planning, and follow-up for breast cancer patients.

KEYWORDS

breast cancer, breast calcification, segmentation, Pro_UNeXt, machine learning

1 Introduction

According to the latest global statistics, breast cancer incidence rates have risen over the last four decades. Breast cancer is the most common cancer (1) and the second leading cause of cancer death among women (2). Mammograms are one of the main methods for detecting and screening breast cancer at an early stage. Although there are many different types of breast lesions in mammograms, calcification cannot be ignored. Calcification refers to the accumulation of calcium deposits within female breast tissue and is an indicator that appears in the initial stages of breast cancer and is often associated with ductal carcinoma *in situ* and invasive cancer. In mammogram, calcification is considered a primary indication of malignancy. In screening programs, between 12.7% and 41.2% of women are recalled for further evaluation due to calcification lesions being the sole sign of potential breast cancer. Analyzing calcification aids in determining the most appropriate approach to patient management. Understanding the morphology, size, and distribution of calcification is crucial in determining whether they are MB (benign and malignant) and whether additional imaging or biopsies are warranted. Figure 1 shows the mammogram of a 57-year-old patient with breast cancer. In this

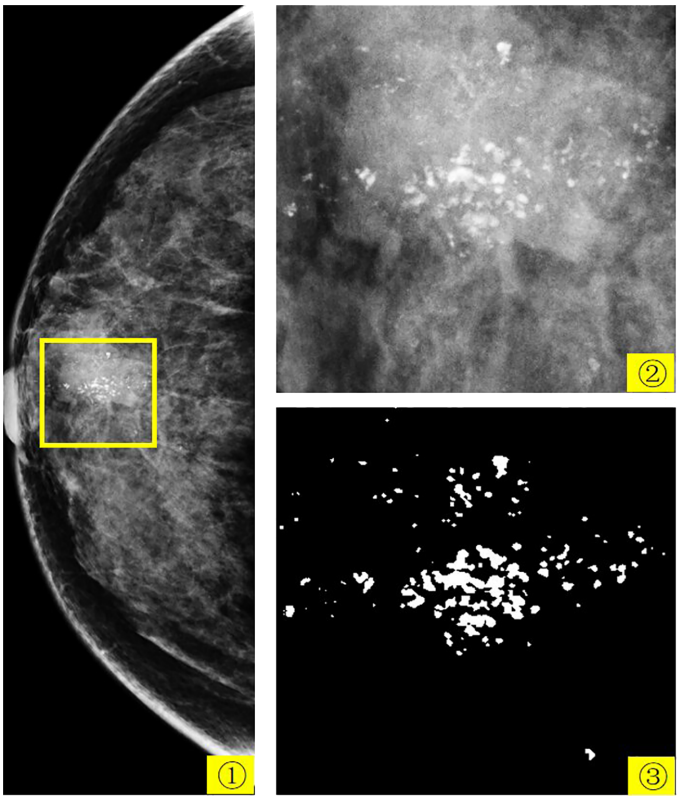

FIGURE 1
The mammogram of a 57-year-old patient with breast cancer. 1 is the patient's right CC view, 2 is the yellow box in 1, and 3 is the expert-labeled result of 2.

figure, 1 is the patient's right craniocaudal (CC) view, 2 is the yellow box within 1, and 3 is the expert-labeled result of 2, where calcification lesions are highlighted as white spots on the mammogram. In breast tissue, calcifications smaller than 0.5 mm are categorized as micro-calcification. While micro-calcification lesions do not always indicate malignancy, their presence often serves as an early warning sign of potential breast cancer.

In recent years, with the development of artificial intelligence technology, the application of artificial intelligence has achieved very good results in many fields (3–6). Computer-aided diagnosis (CAD) in the medical field has also made many breakthroughs based on artificial intelligence, including the brain (7–9), breast (10), thyroid (11), and other parts of the body. CAD algorithms have the potential to offer clinicians improved decision support for early segmentation and analysis of breast calcification. CAD algorithms founded on deep learning have demonstrated their effectiveness and robustness in automating breast cancer analysis. Image segmentation techniques are employed to segment calcification lesions, and among the deep learning-based methods, UNet (12) stands out as an efficient and robust medical image segmentation technique. In recent years, UNet has served as the cornerstone for nearly all leading medical image segmentation methods. Its extensions, such as UNet++(UNetPlus)Zhou et al. (13), V-Net (14), Y-Net (15), and TransUNet (16), have been at the forefront of medical image segmentation.

However, considering that mammograms are typically large-scale images whereas calcification lesions are notably small, especially micro-calcification, the aforementioned methods often face challenges, including an abundance of network parameters, complex computations, and slow processing speeds. In calcification process segmentation, issues like false positives and limited accuracy are prevalent. As a result, some scholars have proposed methods tailored to the unique characteristics of calcification (17–21). Wang and Yang (17) developed a context-sensitive deep neural network designed to simultaneously consider local image features of calcification and the surrounding tissue background for calcification detection. Marasinou et al. (19) proposed a deep learning method based on Hessian matrix Gaussian difference regression, a two-stage multiscale method for calcification segmentation. Valvano et al. (18) proposed a two-stage deep learning method: first, extract region proposals and then classify each region proposal. Hossain (21) proposed a method consisting of multiple preprocessing stages and then manually selected suspicious regions and fed them into a trained UNet network. Zamir et al. (20) developed a strategy to prioritize challenging pixels during the training phase to address the false-positive calcification issue. These methods are generally classified as CAD systems, which automatically flag suspicious calcification lesions in mammograms. While current CAD systems achieve high sensitivity, they also generate numerous false-positive markers, increasing radiologist interpretation time. Most breast calcification CAD systems primarily focus on segmentation or detection of calcification, lacking in-depth analysis of their features. They provide a visual observation but fail to comprehensively analyze and quantify calcification properties. To effectively assess the morphology, size, and distribution of calcification, it is necessary to accurately segment calcification from mammograms. Accurate segmentation allows for a more accurate quantitative description of the morphology, size, and distribution of calcification.

Based on the characteristics of calcification lesions in mammogram and the latest SOTA medical image segmentation algorithm UNeXt (22), this paper proposes a Pro_UNeXt algorithm. Based on the UNeXt algorithm, the Pro_UNeXt algorithm model first adds a micro-calcification learning block at the network input, which can effectively improve micro-calcification segmentation. The fused-MBConv (23) and Tok-MLP modules are used instead of the convolution module in the network, improving the model's ability to learn features and its operating speed. Based on the characteristics of calcification, the focal loss (24) and Dice loss (25) are used as the loss function in the first step of training, and then the Hausdorff distance (HD) loss (26) is used to fine-tune the model trained in the first step to improve the model's ability to segment micro-calcification. Due to the difficulty in labeling breast calcification data and that the image area occupied by calcification is very small, effective data augmentation (Aug) methods are used for the characteristics of calcification lesions. These methods include cropping, original image scaling, Gaussian blur, sharpening, grayscale transformation, affine transformation, grayscale histogram transformation (27), and calcification copy and paste (28).

As one of four common breast lesions, calcification is inseparable from breast cancer. To analyze the characteristics of calcification lesions, quantitative analysis is conducted on segmented calcification lesions. First, the quantitative characteristics of each mammogram is quantified. Including the number, density, size, area, distribution, calcification clusters, perimeter, roundness, long side, rectangularity, length–width ratio, and perimeter ratio. Then, the machine learning method is used to classify the MB.

In this paper, the problem of calcification segmentation and quantitative analysis is investigated. The proposed algorithm can not only reduce the calculation overhead and operation cost but also accurately segment micro-calcification. This paper presents a rapid calcification lesion segmentation algorithm that combines deep learning and breast calcification features. At the same time, machine learning methods were used to analyze the quantified calcification lesions. The method can help doctors conduct more effective analyses, assist doctors in film reading, and reduce errors.

2 Method

Based on the characteristics of calcification, this paper proposes a novel and comprehensive breast calcification lesion segmentation and analysis scheme. As shown in Figure 2, the scheme consists of three modules: segmentation, feature quantification, and feature analysis. The first is the calcification lesion segmentation module. The module designs a Pro_UNeXt algorithm with high accuracy and good performance based on the characteristics of calcification. Next is the calcification lesion feature quantification module and visualization. As one of the most common breast lesions, knowledge of the morphology, size, and distribution of calcification by the radiologist can help determine the extent of the lesion. According to the daily working habits of radiologists, we quantified the

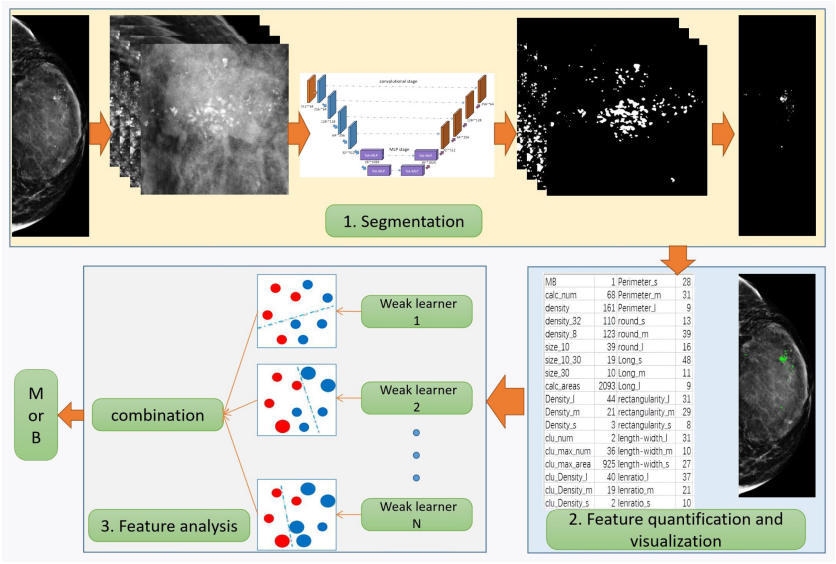

FIGURE 2
Segmentation and quantitative analysis flowchart of breast calcification in mammograms.

characteristics of the calcification segmented in the first step, including quantity, shape, size, density, peripheral density, cluster, and blurriness. The quantification results inform radiologists about various features, reducing the risk of oversight and facilitating analysis comparisons of feature changes. Finally, the calcification feature analysis module employs the machine learning algorithm to classify quantified features, providing a comprehensive assessment of lesion MB.

To obtain the first step of calcification lesion segmentation model, the calcification lesion processing process as shown in Figure 3 is designed. Mammograms with only calcification lesions were first collected and annotated by two junior radiologists. If the

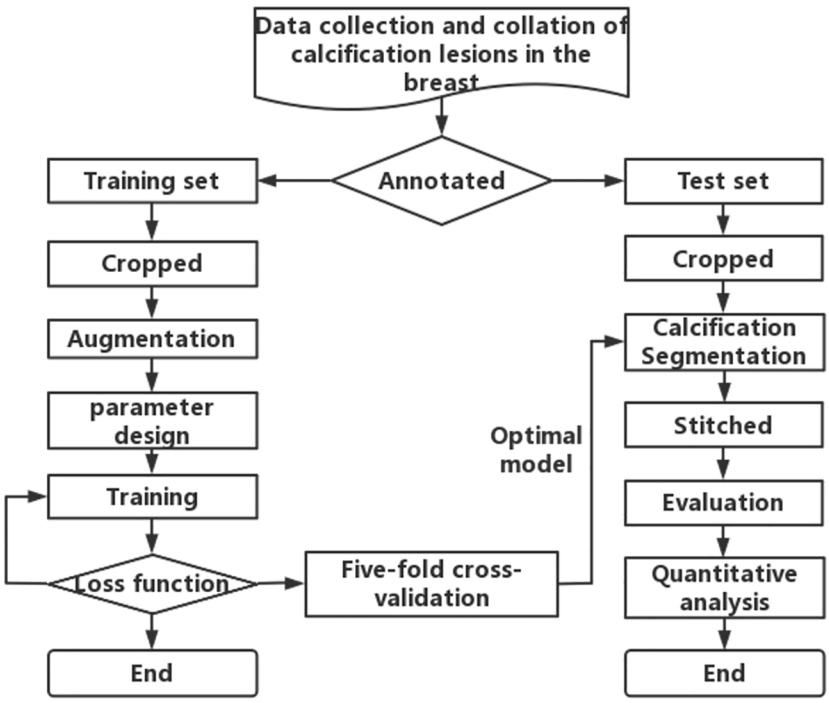

FIGURE 3
Flowchart for segmentation and quantitative analysis of mammographic calcification lesion.

Dice coefficient of the data annotated by junior radiologists was less than 95%, it was considered a discrepancy. If there was discrepancy between the two, it was corrected by a senior radiologist. The datasets involved in this article were all annotated and checked by radiologists. The annotated data were divided into a training set and a test set at the ratio of 4:1. Since breast calcification lesions are localized, the training and test sets were cropped to the size of 512 × 512 pixels. To reduce calcification on the edges of image, the overlap rate between cropped images was 20%. As shown on the left side of Figure 3, the model training process includes cropped, Aug, model parameter design, model training, loss function calculation, and fivefold cross-validation. The optimal models for the five validation sets were obtained through loop iterations, with each model being trained for 200 iterations. As shown on the right of Figure 3, the test set after cropping was segmented with five train models. The segmentation results were stitched together to obtain a map of calcification lesions for each mammogram. The Dice, specificity (SPE), recall, and intersection over union (IoU) (29) of the models were calculated to evaluate the segmentation models. Finally, the segmentation results were quantified and analyzed. To highlight the superior calcification segmentation performance of the algorithm in this study, comparable algorithms were employed using the same dataset and procedures. This was done to ensure the effectiveness of the algorithm. The annotation method employed in this article involves utilizing the labeling functions within the 3D Slicer software (30), specifically the level tracing feature found in the Segment Editor module. This entails setting constraints on the density range of calcifications and then clicking on the center of the calcification, thereby enabling the acquisition of the boundary of the calcified region.

2.1 Data Aug

According to the calcification characteristics, the Aug methods were as follows: cropping, original image scaling, Gaussian blurring, sharpening, grayscale transformation, affine transformation, grayscale histogram transformation, and copy and paste. In this paper, the original image was directly scaled and then cropped, which can improve the micro-calcification detection ability of the model. Image blurring and grayscale transformation can improve the segmentation of high fibrous density and fuzzy micro-calcification lesions. The copy and paste strategy is based on copying the calcification points in an image, counting the number of connected domains, selecting the connected domains using a random ratio (0 to 1), and then pasting them into other images. This method not only increases the number of annotated calcification points but also enhances the performance of model.

2.2 UNeXt algorithm

The UNeXt algorithm is a convolutional multilayer perceptron (MLP) (31)-based image segmentation network. It is designed with an early convolution stage and a latent-stage MLP stage. The early convolution stage is responsible for extracting low-level features from the input image, whereas the latent-stage MLP stage is used for modeling the representations.

One of the key components of UNeXt is the tokenized MLP (32) block. This block effectively tokenizes and projects the convolutional features and uses MLPs to model the representations. The tokenization process involves dividing the input into non-overlapping patches and flattening each patch into a 1D vector. These vectors are then projected into a higher dimensional space using a linear transformation. The projected vectors are then fed into the MLPs for further processing. UNeXt changes the channel of the input when entering the MLP to focus on learning local dependencies and improving the segmentation ability of object edges. Using tokenized MLP in the latent space not only reduces the number of parameters and computational complexity but also produces better representations to help segmentation. To further enhance the performance, channel shuffling is proposed before feeding the input into the MLPs. This allows the network to focus on learning local dependencies, which are crucial for image segmentation tasks.

Similar to UNet, the network also includes skip connections between the encoder and decoder at all levels. Compared with the current medical image segmentation architecture, UNeXt has 72 times fewer parameters, 68 times less computational complexity, and 10 times faster inference, while achieving better segmentation performance than state-of-the-art medical image segmentation architectures. This makes UNeXt a promising solution for real-time, fast image segmentation tasks in clinical applications.

2.3 Pro UNeXt algorithm

Combining the characteristics of breast calcification lesions, this paper proposes the Pro_UNeXt algorithm based on UNeXt. The Pro_UNeXt medical image segmentation is shown in Figure 4. Our algorithm adopts a UNet architecture consisting of an encoder and a decoder. The encoder comprises one convolutional block (orange), four fused-MBConv (23) blocks (blue), and two tokenized MLP blocks (purple). The decoder contains two tokenized MLP blocks (purple) and four convolutional blocks (orange).

In the encoder part, the first convolution block(orange) is not downsampled to achieve maximum retention of the micro-calcification features. To learn micro-calcification features, each image is fed into the first convolution block with 64 channels and a step of 1. After the first convolutional block (orange), the next 4 blocks of the network are fused-MBConv blocks (blue). To learn image features more accurately, the convolutional kernel in the encoding process is fused-MBConv. Fused-MBConv, compared with traditional convolutions, excels in parameter efficiency, feature adaptability with Squeeze-and-Excitation (SE) (33) blocks, reduced computational load, and suitability for resource-constrained environments. Its efficiency and versatility make it valuable in deep learning models, leading to improved accuracy in computer vision tasks, particularly in mobile and embedded applications. The last two blocks are tokenized MLP blocks (purple). The tokenized MLP block efficiently tokenizes and

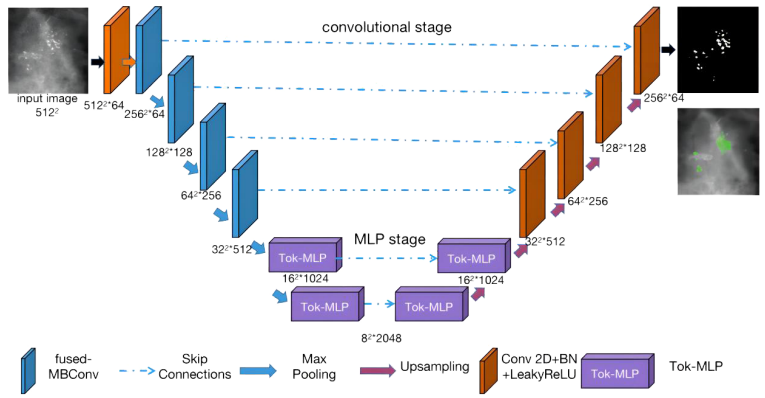

FIGURE 4
Image segmentation algorithm Pro_UNeXt network structure.

projects convolutional features into a higher-dimensional space, enabling the network to capture complex patterns. It focuses on local dependencies and reduces parameters and computational complexity, making the network more efficient for real-time applications.

The decoder part contains two tokenized MLP blocks (purple) and four convolutional blocks (orange) from bottom to top. In addition to the first micro-calcification convolutional block (orange), each other encoder block reduces the feature resolution by 1/2, and each decoder block increases the feature resolution by a factor of 2.

The other parameters of our algorithm are as follows: the input image size is fixed at 512 × 512, where the numbers of parameters in each channel layer of the encoding process are 64, 64, 128, 256, 512, 1,024, and 2,048 and the numbers of decoding parameters are 2,048, 1,024, 512, 256, 128, and 64. The network structure is an encoder–decoder architecture with two phases: (1) convolution phase and (2) tokenized MLP phase.

Convolution phase: This phase comprises both normal convolution blocks (orange) and fused-MBConv blocks (blue). Each normal convolution block includes a convolutional layer, a batch normalization layer, and a ReLU activation layer. The convolutional layers employ a kernel size of 3 × 3 with a stride of 1 and padding of 1. The fused-MBConv convolutional block comprises a 1 × 1 convolutional layer, a Squeeze-and-Excitation (SE) layer, and 3 × 3 convolutional layers. Within the encoder, the convolution block incorporates a maximum pooling layer with a pooling window of 2 × 2. Conversely, the convolution block within the decoder is composed of transposed convolutions. These convolutions act as learnable upsampling modules, enhancing the capacity for learnable parameters and improving boundary detection.

Tokenized MLP phase: First, the features are shifted and projected into tokens. Then, these tokenized blocks are passed to the shifted MLP (across the width). Next, the features are passed through the depthwise convolutional (DWConv) (34) layer. DWConv is used for two reasons: (1) It helps encode the positional information of the MLP features. (2) It uses fewer parameters compared with regular convolutions. The layer is then activated using the Gaussian Error Linear Unit (GELU) (35), which is a smoother alternative to the Rectified Linear Unit (ReLU) and has better performance. Afterward, the features are passed through another moving MLP (across height), and the original token blocks are connected using a residual structure. Finally, the application layer is normalized, and the output features are passed to the next block.

In summary, our Pro_UNeXt algorithm has three advantages: (1) The use of a micro-calcification learning block at the input to focus on detecting small lesions. (2) Replacing standard convolution blocks with fused-MBConv and Tok-MLP to improve feature learning and speed. (3) Increasing network channels for enhanced representation capacity.

2.4 Loss function

In deep learning, the loss function is used to measure the gap between the model's prediction results and the real results. Our goal is to minimize the loss so that the model's predictions become more accurate. In this paper, three loss functions are used to train the model: focal loss, Dice loss, and HD loss. The focal loss is a loss function that handles imbalanced sample issues. The Dice loss is a metric used to evaluate the similarity of two samples and is currently widely used in medical image segmentation. The HD loss is a boundary-based metric commonly used to segment small target. However, when the HD loss is used alone to train a neural network, training instability may occur. Therefore, in this paper, the focal loss + Dice loss combination is first used as the loss function for initial training, and then the HD loss is used to fine-tune the trained model to obtain better performance.

2.5 Statistical analysis method

For feature analysis of medical image segmentation, radiomics is most commonly used. However, radiomics is not applicable for

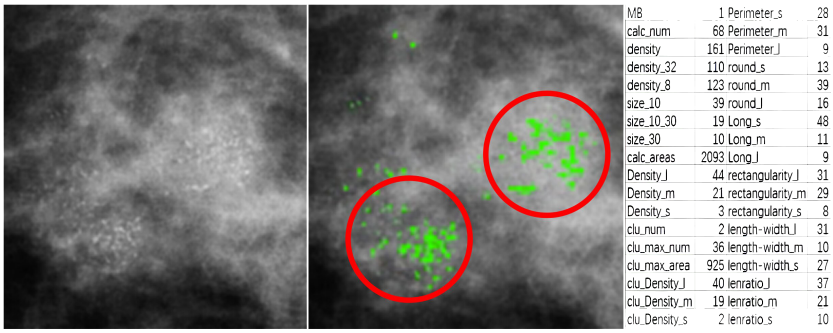

MB	1	Perimeter_s	28
calc_num	68	Perimeter_m	31
density	161	Perimeter_l	9
density_32	110	round_s	13
density_8	123	round_m	39
size_10	39	round_l	16
size_10_30	19	Long_s	48
size_30	10	Long_m	11
calc_areas	2093	Long_l	9
Density_l	44	rectangularity_l	31
Density_m	21	rectangularity_m	29
Density_s	3	rectangularity_s	8
clu_num	2	length-width_l	31
clu_max_num	36	length-width_m	10
clu_max_area	925	length-width_s	27
clu_Density_l	40	lenratio_l	37
clu_Density_m	19	lenratio_m	21
clu_Density_s	2	lenratio_s	10

FIGURE 5
A partial interception of mammographic calcification (left), calcification annotations (middle), and quantitative features table of calcification(right).

breast calcification lesions. Therefore, in this paper, other methods were used to learn the characteristics of calcification lesions. Figure 5 shows a partial interception of a mammographic calcification image (left), the calcification annotations (middle), and a table of quantitative features for the calcification (right). The MB in the statistical results is provided by pathological analyses. The calc_num indicates the number of calcification. The density represents the average density of calcification. The density_32 is the average density within a 32-pixel field surrounding each calcification. The density_8 is the average density within an 8-pixel field. The size_10 is the number of calcification less than 10 pixels. The size_10_30 is the number of calcification with sizes between 10 and 30 pixels. The size_30 is the number with sizes above 30 pixels. The calc_area indicates the total area of calcification. The suffixes _l, _m, and _s represent relative size categories. For example, density_l, density_m, and density_s indicate high-, medium-, and low-density calcification respectively. length_l, length_m, and length_s denote calcification with high, medium, and low aspect ratios. The clu_num, clu_max_num, and clu_max areas represent the number of clusters, number of calcification in the largest cluster, and area of the largest cluster. clu_Density_l, clu_Density_m, and clu_Density_s denote the number of high-, medium-, and low-density calcification within clusters. perimeter_s, perimeter_m, and perimeter_l indicate calcification with small, medium, and large perimeters. round_s, round_m, and round_l represent different roundness levels. long_l, long_m, and long_s denote different lengths of the long side of approximated rectangles. rectangularity_l, rectangularity_m, and rectangularity_s represent different rectangularity levels. lenratio_l, lenratio_m, and lenratio_s indicate different perimeter ratios. The statistical method for identifying calcification clusters is as follows: First, a dilation operator with a 16 × 16 all-one matrix is applied on the segmented image. This connects adjacent calcification points into connected domains. If the number of calcification points in a connected domain is greater than 5, it is considered a calcification cluster. As shown in Figure 5, two calcification clusters are highlighted within the red circles.

To help doctors accurately judge patients' MB, machine learning algorithms are used to analyze quantitative features, including decision tree (DTs) (36), logistic regression (LR) (37), support vector machines (SVMs) (38), K nearest neighbors (KNN) (39), random forests (RFs) (40), XGBoost (XGB) (41), and AdaBoost (42). The relationship between quantitative features and MB is established by the machine learning algorithm. It can provide more accurate digital services for clinics and help doctors make more accurate judgements. It is also of great significance for retrospective comparisons of patient follow-up.

2.6 Evaluation method

For the evaluation of calcification segmentation, the Dice (Equation 1), recall (Equation 3), SPE (Equation 2) and IoU (Equation 4) are used. These metrics are commonly employed in the evaluation of machine learning models, particularly in image segmentation. They provide valuable insights into different aspects of a model's performance, such as its ability to correctly identify positive and negative instances, and the degree of overlap between predicted and true positive regions. The formula is as follows:

$$\text{Dice} = 2\text{TP}/(2\text{TP} + \text{FP} + \text{FN}) \tag{1}$$

$$\text{SPE} = \text{TN}/(\text{TN} + \text{FP}) \tag{2}$$

$$\text{Recall} = \text{TP}/(\text{TP} + \text{FN}) \tag{3}$$

$$\text{IoU} = \frac{\text{TP}}{\text{TP} + \text{FP} + \text{FN}} \tag{4}$$

where TP is the true positive, TN is the true negative, FP is the false positive and FN is the false negative.

The 95% confidence interval provides a range of plausible values for a parameter estimate, conveying the level of uncertainty associated with the estimate. The p-value helps assess the strength of evidence against a null hypothesis in hypothesis testing, guiding the decision to accept or reject the null hypothesis based on a predetermined significance level (commonly 0.05). The ROC curve is a graphical representation used to evaluate the performance of a binary classifier. It is a plot of the TP rate against the FP rate at different classification thresholds. The AUC is the area under the ROC curve and is used as a metric to measure the performance of a

TABLE 1 General clinical characteristics of the private dataset.

Characteristics	Total	Malignant	Benign	P value
Mean age	49.0	50.5	47.9	
Age range	23-85	27-85	23-67	0.18
Breast density				0.27
Almost entirely fatty	8 (4.5%)	2 (2.6%)	6 (5.9%)	
Scattered densities	21 (11.2%)	7 (9.2%)	14 (13.7%)	
Heterogeneous dense	131 (73.6%)	56 (73.7%)	75 (73.5%)	
Extremely dense	18 (10.1%)	11 (14.5%)	7 (6.9%)	
BI-RADS classification				0.69
II	35 (19.7%)	0 (0%)	35 (34.3%)	
III	29 (16.3%)	5 (6.6%)	24 (23.5%)	
IVa	48 (27.0%)	11 (14.5%)	37 (36.3%)	
IVb	26 (14.6%)	20 (26.3%)	6 (5.9%)	
IVc	23 (12.9%)	23 (30.3%)	0(0%)	
V	17 (9.5%)	17 (22.4%)	0(0%)	
Total	178	76	102	

binary classifier. It ranges from 0 to 1. The higher the AUC is, the better the classifier performance.

3 Image segmentation results

3.1 Experimental conditions and the dataset

To train and test our model, we used one public dataset and one private dataset. The DDSM (43) is a public dataset created by medical institutions in the United States. We manually screen DDSM data with calcification lesions. A total of 401 benign and 358 malignant cases with calcification lesions were collected in the public dataset. The private dataset was provided by Mindong Hospital Affiliated with Fujian Medical University. As shown in Table 1, there were a total of 178 cases of mammograms, including 76 cases of malignant (average age 50.5) and 102 cases of benign (average age 47.9). The benign and malignant are generated by histopathology. The table includes age, breast density, and BI-RADS distribution. Their P values are 0.18, 0.27, and 0.69, respectively. It shows that there is no significant difference between benign and malignant data. Due to certain differences between the two datasets, both datasets were independently tested and trained, without cross-validation between them.

The parameters of our machine are Windows 10 Gen Intel(R) Core (TM) i7-11700K @ 3.60 GHz, 32 GB of memory, and 16 GB of graphics card A4000 memory. The private dataset acquisition machine is a GE full digital mammogram machine, which can display micro-calcification lesions less than 0.1 mm, and the single pixel is 0.068 mm. The data annotation software used was 3D slicer (30).

3.2 Image segmentation results

To verify the effectiveness of the segmentation algorithm, two datasets are used for testing: DDSM and a private dataset. Our algorithm is compared with classical algorithms: UNet, UNetPlus, and UNeXt, where UNet and UNetPlus use ResNet (44) and EfficientNet (45), respectively, as the backbone. The models of the comparison algorithm and Pro UNeXt+Aug+Loss are the result of optimization with Aug and loss functions.

3.2.1 DDSM dataset results

As shown in Figure 6, we selected the CC view image of the patient P-01108 in the DDSM, and the pathological result was malignant. The area in the light blue box is compared for different segmentation algorithms. Cut is the cropping image of the light blue box, and GT is the binary image of the cropping area marked by the imaging doctor. Others are segmentation results of different algorithms. the Dice scores of different segmentation algorithms in this image were as follows: UNet+ResNet: 0.77; UNet+EfficientNet: 0.80; UNetPlus+ResNet: 0.78; UNetPlus+EfficientNet: 0.76; UNeXt_S: 0.57; P UNeXt: 0.76; UNeXt_L: 0.75; Pro_UNeXt: 0.76; Pro_UNeXt+Aug: 0.82; and Pro_UNeXt+Aug+Loss: 0.94. GT is the ground truth of the manual annotation. By observing the red circles, we found that the UNeXt series of algorithms missed a lot of micro-calcification lesions. However, Pro_UNeXt, which adds a micro-calcification learning block, has a stronger detection ability for micro-calcification and muddy calcification. Compared with the UNet series algorithm, the Pro_UNeXt algorithm performs better in details.

As shown in Table 2, we tested different algorithms on the DDSM dataset. After the optimization with Aug and loss functions, Pro_UNeXt+Aug+Loss achieved the highest Dice score of 0.823

10.3389/fonc.2024.1281885

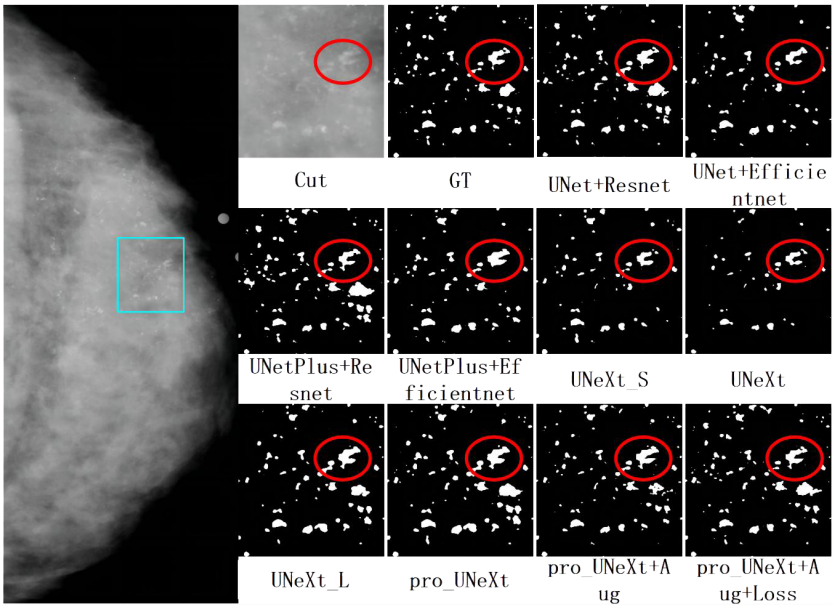

FIGURE 6
The first on the left is the CC view of the patient, where the area in the light blue box is compared for segmentation effect. Others are cut image, GT, and segmentation results of different algorithms.

(95% CI 0.747–0.901). Compared with the algorithm without Aug and loss function optimization, the Dice score increased from 0.794 (95% CI: 0.703–0.865) to 0.823 (95% CI: 0.747–0.901). The Dice score of Pro_UNeXt+Aug+Loss is 0.060 higher than that of the UNeXt series algorithms and 0.006 higher than that of the UNet series algorithms. Regarding other metrics, the Pro_UNeXt algorithms also showed excellent performance and obtained the optimal Dice of 0.823, IoU of 0.665, and SPE of 0.999. The recall is 0.01 lower than that of the best UNet+EfficientNet algorithm. The Pro_UNeXt algorithm only requires 7 ms to process a single 512 × 512 image, which is 3 ms slower than the original UNeXt. Compared with the speeds of the UNet and UNetPlus algorithms, the speed of Pro_UNeXt is more superior. Since the area occupied by calcification is very small relative to the entire image, the SPE of all algorithms is close to 1. After comparison, it is not difficult to see that our algorithm not only has better speed but also has the best performance in calcification segmentation.

3.2.2 Private dataset results

Figure 7 shows a malignant case in private dataset containing only calcification lesions with indistinct margins. The first on the left is the CC view of the patient, where the area in the light blue box is compared for segmentation. The second on the left is the result of the pro_UNeXt+Aug+Loss, where green is the segmented calcification point. Others are Cut image, GT, and segmentation results of different algorithms. As shown in Figure 7, our algorithm has better performance in terms of both missed segmentation and edges, especially micro-calcification. Figure 8 presents a benign case

TABLE 2 The segmentation results of different algorithms tested in the DDSM dataset.

Model	Dice (95%CI)	IoU	SPE	Recall	T(ms)
UNet+ResNet	0.786 (0.673-0.895)	0.597	0.998	0.809	14
UNet+EfficientNet	0.817 (0.706-0.892)	0.642	0.998	**0.837**	19
UNetPlus+ResNet	0.788 (0.687-0.861)	0.549	**0.999**	0.819	20
UNetPlus+EfficientNet	0.809 (0.734-0.866)	0.647	**0.999**	0.772	27
UNeXt_S	0.763 (0.699-0.841)	0.581	**0.999**	0.743	**3**
UNeXt	0.749 (0.657-0.817)	0.559	0.998	0.806	4
UNeXt_L	0.728 (0.603-0.811)	0.557	**0.999**	0.717	19
Pro_UNeXt	0.794 (0.703-0.865)	0.626	0.998	0.802	7
Pro_UNeXt+Aug	0.817 (0.723-0.896)	0.644	**0.999**	0.813	7
Pro_UNeXt+Aug+Loss	**0.823 (0.747-0.901)**	**0.665**	**0.999**	0.827	7

Bold numbers represent the optimal metric results.

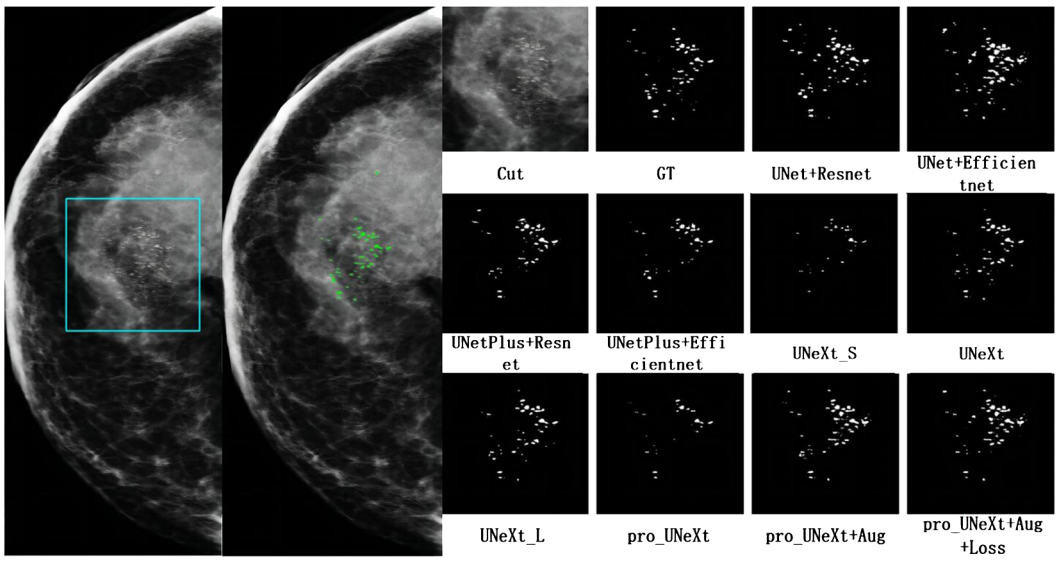

FIGURE 7
The mammogram of a breast cancer patient in the private dataset. The first on the left is the result of the pro_UNeXt+Aug+Loss, where green is the segmented calcification point. The second on the left is the CC view of the patient, where the area in the light blue box is compared for segmentation effect. Others are cut image, GT, and segmentation results of different algorithms.

in the Private dataset with macro-calcification. For this type of macro-calcification, our algorithm achieved the highest Dice score of 0.921, with most algorithms attaining Dice scores in the range of 0.88 to 0.91. From the two figures, we can see that in the private data set, our algorithm has better segmentation of muddy calcification, micro-calcification, and macro-calcification and has almost no false positives.

We conducted experiments on the test set in private dataset. Segmentation performance is presented in Table 3. The Pro UNeXt algorithm achieved a Dice score of 0.811 (95% CI 0.737–0.892), outperforming other methods. After optimization with Aug and loss functions, the Pro UNeXt+Aug+Loss model improved the Dice score to 0.838 (95% CI 0.769–0.911). The Pro_UNeXt algorithm was 0.057 better than the UNeXt series algorithm. It was also 0.028 better than the UNet series algorithm. Additionally, Pro_UNeXt demonstrated superior IoU, specificity, and recall versus all other segmentation algorithms.

In this section, we selected three typical case images from two data sets and compared the results of different segmentation algorithms. The Pro_UNeXt algorithm can accurately segment

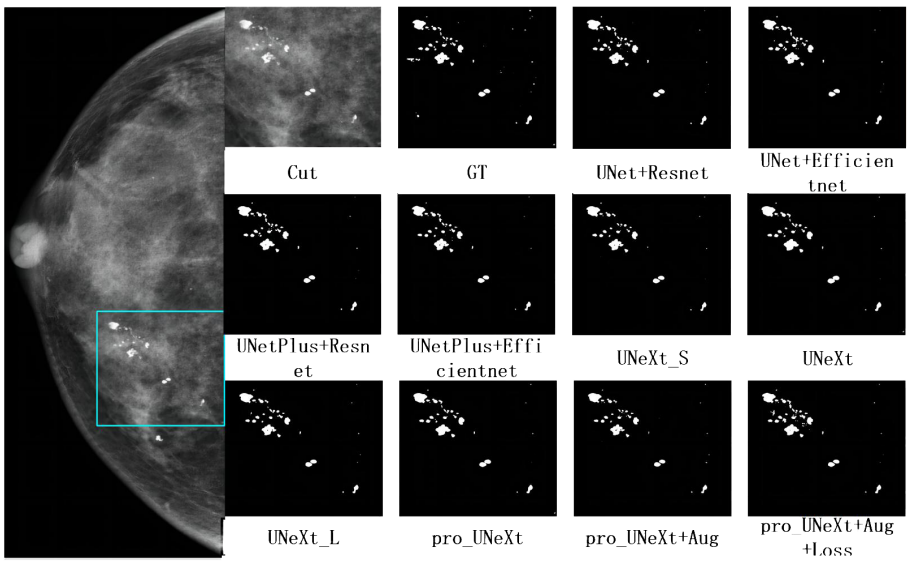

FIGURE 8
The mammogram of a patient with benign lesions. The first on the left is the CC view of the patient, where the area in the light blue box is compared for segmentation effect. Others are cut image, GT, and segmentation results of different algorithms.

TABLE 3 The segmentation results of different algorithms tested in private dataset.

Model	Dice (95%CI)	IoU	SPE	Recall
UNet+ResNet	0.779 (0.704-0.871)	0.603	**0.999**	0.747
UNet+EfficientNet	0.810 (0.736-0.878)	0.632	**0.999**	0.790
UNetPlus+ResNet	0.780 (0.702-0.834)	0.605	**0.999**	0.742
UNetPlus+EfficientNet	0.798 (0.718-0.877)	0.627	**0.999**	0.735
UNeXt_S	0.772 (0.710-0.852)	0.581	**0.999**	0.716
UNeXt	0.781 (0.715-0.876)	0.595	**0.999**	0.746
UNeXt_L	0.766 (0.709-0.834)	0.585	**0.999**	0.704
Pro_UNeXt	0.811 (0.737-0.892)	0.638	**0.999**	0.758
Pro_UNeXt+Aug	0.824 (0.753-0.910)	0.643	**0.999**	0.791
Pro_UNeXt+Aug+Loss	**0.838 (0.769-0.911)**	**0.670**	**0.999**	0.795

Bold numbers represent the optimal metric results.

both micro-calcification and macro-calcification. In terms of performance, the Pro_UNeXt algorithm of optimization with Aug and loss functions, customized for breast calcification lesions, attained the best results on both the DDSM and private datasets. This confirms its capability in detecting small lesions like micro-calcification. Despite the performance gains, Pro_UNeXt retained excellent computational efficiency. Relative to UNet+EfficientNet (19 ms), it reduced the runtime by over 60% to 7 ms per image.

4 Data analysis

Breast calcification segmentation can effectively solve the problem of difficulty in detecting calcification. However, breast calcification has the characteristics of diffuse distribution, small size, blurred edges, and uneven density. Therefore, imaging doctors still need to make subjective judgments after segmentation. This subjective and experience-dependent judgment method can easily lead to missed diagnosis and misdiagnosis. Therefore, this article will perform statistical analysis on two datasets after segmentation. To analyze the characteristics, the segmented images were divided into training and test sets at a 4:1 ratio. Then, quantitative features are calculated for each segmented image, and machine learning is used to classify the features into benign and malignant. The algorithms assessed were DT, LR, SVM, KNN, RF, XGB, and AdaBoost. After training, model performance was evaluated on the test set.

Figure 9 shows the ROC curves of different machine learning algorithms for MB classification in the private dataset. The AUC values, 95% CI, and accuracy rates of the algorithms were as follows: DT's AUC = 0.93 (95% CI: 0.90–0.97, accuracy rate of 90%), KNN's AUC = 0.92 (95% CI: 0.89–0.97, accuracy rate of 87%), LR's AUC = 0.95 (95% CI: 0.93–0.98, accuracy rate of 89%), SVM's AUC = .95 (95% CI: 0.92–0.98, accuracy rate of 91%), XGB's AUC = 0.96 (95% CI: 0.94–0.98, accuracy rate of 91%), RF's AUC = 0.95 (95% CI: 0.93–0.98, accuracy rate of 90%), and AdaBoost's AUC = 0.97 (95% CI: 0.96–0.99, accuracy rate of 93%). To further understand the importance of each feature, we performed feature importance analysis on the AdaBoost algorithm model. The results are shown in Figure 10, which indicates that the density of calcification clusters, calcification density, size, and the density around

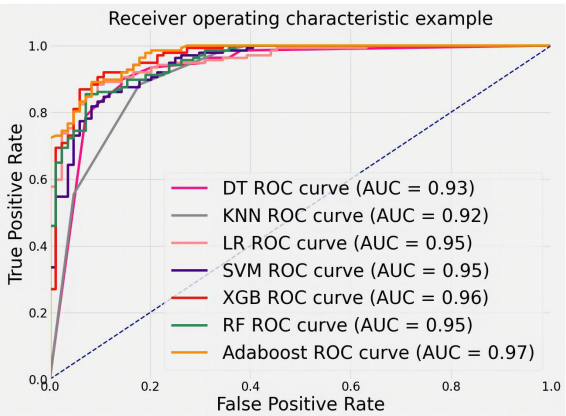

FIGURE 9
ROC curves for feature classification of private datasets by different machine learning algorithms.

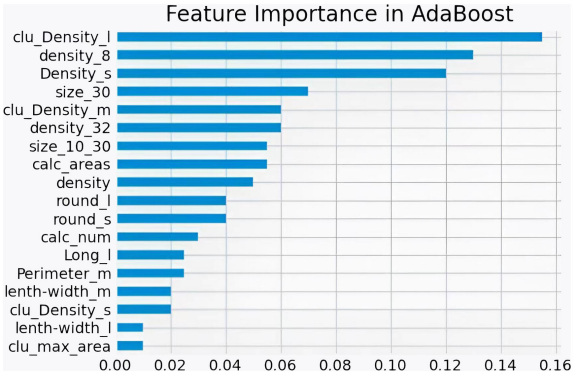

FIGURE 10
Feature Importance of AdaBoost in private datasets.

calcification lesions play a significant role in distinguishing between benign and malignant cases. This is consistent with radiologists' daily assessment of calcification. Combined with the algorithm's AUC of 0.97, it directly demonstrates the effectiveness of our quantified features in distinguishing MB cases.

To evaluate the ability of features to judge MB, we trained and tested with the public dataset DDSM. The results are shown in Figure 11. The AUCs values, 95% CI, and accuracy rates of the algorithms were as follows: DT's AUC = 0.83(95% CI: 0.73–0.90, accuracy rate of 78%), KNN's AUC = 0.82(95% CI: 0.74–0.90, accuracy rate of 79%), LR's AUC = 0.77(95% CI: 0.70–0.85, accuracy rate of 71%), SVM's AUC = 0.81(95% CI: 0.72–0.90, accuracy rate of 79%), XGB's AUC = 0.81(95% CI: 0.74–0.90, accuracy rate of 76%), RF's AUC = 0.82(95% CI: 0.75–0.91, accuracy rate of 78%), and AdaBoost's AUC = 0.84(95% CI: 0.76–0.91, accuracy rate of 79%). Most classifiers achieved AUCs above 0.80, with AdaBoost again showing the top performance. The consistent results validate that the proposed quantitative features are representative and highly useful for identifying MB.

In this section, our study statistically analyzes two datasets post-segmentation, dividing images into training and test sets (4:1 ratio). Quantitative features are calculated, and machine learning (DT, LR, SVM, KNN, RF, XGB, AdaBoost) classifies them as benign or malignant. AdaBoost exhibits superior performance (AUC = 0.97), emphasizing the importance of features like calcification cluster density and size in distinguishing cases. From Table 1, it can be seen that 21.1% of data in malignant cases are classified as below IVa, whereas 42.2% of data in benign cases are classified as above IVa. More than 33.1% cannot accurately determine the condition. Our algorithm's AUC is above 80%; evaluation on a public dataset (DDSM) and the private dataset confirms the accuracy of proposed features and the efficacy of quantified features in identifying malignant breast calcifications.

5 Summary

Breast cancer is the most prevalent malignancy in women globally. Assessing and quantifying breast calcification can inform optimal patient management, thereby improving survival and quality of life. However, the obscurity of calcification renders them prone to oversight, depriving patients of timely treatment. To address this, a technique for detecting breast calcification lesions is needed. Building on calcification characteristics and the state-of-the-art UNeXt segmentation algorithm, this study proposes the Pro UNeXt algorithm. The key innovation are: (1) an improved UNeXt

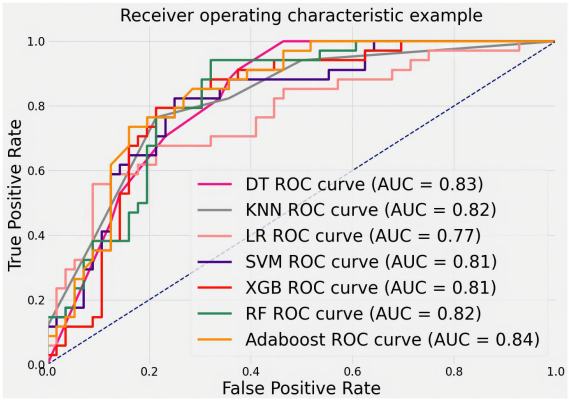

FIGURE 11
ROC curves for classifying features in the DDSM public dataset using various machine learning algorithms.

segmentation network using convolutional multilayer perceptron architecture. Pro_UNeXt first adds a micro-calcification learning block at input to improve segmentation performance. Fused-MBConv and Tok-MLP modules replace original convolution modules to boost feature learning and speed. (2) The Pro_UNeXt training process, with focal loss + Dice loss as the initial loss function, followed by fine-tuning with Hausdorff distance loss to refine microcalcification segmentation. (3) Effective data augmentation strategies to reinforce microcalcification segmentation. Experiments demonstrate Pro_UNeXt achieves superior performance on the DDSM and private datasets based on breast calcification lesions. It delivers highly accurate calcification segmentation result at 7 ms per image.

To analyze the characteristics of calcification, the characteristics were quantified for each calcification lesion after segmentation. MB classification of lesions was achieved using machine learning methods. The machine learning algorithms included DT, LR, SVM, KNN, RF, XGB, and AdaBoost. After training, different models were derived from these algorithms. With the private dataset, AdaBoost achieved an AUC of 0.97, demonstrating its superior analytical capability. For the public DDSM dataset, the AUC of AdaBoost was 0.84. Compared with other methods, AdaBoost consistently delivered the best classification accuracy on both datasets. These results validate that the quantitative features proposed in this study are representative and highly discerning for MB identification.

Although the Pro UNeXt algorithm conducts comprehensive analysis of calcification, the private dataset only contained 178 cases. The selective use of calcification lesions likely introduced biases, which may explain the lower accuracy on the private dataset. Additionally, calcification is just one of the four major breast lesions. The sole focus on calcification in this study presents limitations for real-world usage. Therefore, incorporating other types of lesions for holistic analysis will be necessary to better serve clinical needs and improve diagnostic performance. Next, we will carry out the following three tasks: 1. Combined with other lesion characteristics, further analyze the benign and malignant lesions, Bi-Rads grading and molecular classification. 2. Add multi-modal data for joint analysis, including DBT, MLO, and CC, clinical information, etc., to improve model performance. 3. Combined with the follow-up data, compare and analyze the changes in calcification to study the changing characteristics of different types of breast calcification.

In summary, this paper proposes a novel and comprehensive breast calcification lesion segmentation and analysis scheme, consisting of three modules: segmentation, feature quantification, and feature analysis. The first is the calcification lesion segmentation module. The module designs a Pro_UNeXt algorithm with high accuracy and good performance based on the characteristics of calcification. Compared with other calcification segmentation algorithms, the Pro_UNeXt algorithm can quickly and accurately segment calcification lesions, reduce false positives, improve diagnostic efficiency, and reduce the diagnostic time of radiologists. Next is the calcification lesion feature quantification module. To better describe breast calcification, this paper introduces a method for quantifying calcification features, including quantity, shape, size, density, peripheral density, cluster, and blurriness. The quantification results effectively inform radiologists about various features, reducing the risk of oversight and facilitating post-analysis comparisons of feature changes. Finally, the calcification feature analysis module employs the AdaBoost machine learning algorithm to classify quantified features, providing a comprehensive assessment of lesion MB. The algorithm exhibits excellent classification accuracy on two datasets, demonstrating the precision of our quantified calcification features in assessing calcification MB. This capability aids radiologists in making more informed decisions and planning for patient care. The proposed scheme offers a comprehensive solution for breast calcification segmentation and quantitative analysis. It enhances radiologists' ability to visually inspect lesions, perform more effective analyses, and efficiently interpret mammographic images, ultimately reducing diagnostic errors. Patients benefit from follow-up and retrospective comparisons of calcification lesions. The solution has the potential to alleviate radiologists' workload, decrease misdiagnosis rates, and improve the quality of life for breast cancer patients, with significant clinical application value.

Data availability statement

The data analyzed in this study are subject to the following license and access restrictions: Restriction: The datasets are proprietary and contain sensitive information, which necessitates controlled access to ensure confidentiality and compliance with privacy regulations. Researchers interested in accessing these datasets should submit a formal request outlining their research objectives, methodology, and intended use of the data. Requests must adhere to institutional review board (IRB) guidelines and any applicable data protection laws. Interested parties should direct their requests, along with the required documentation, to Dr. JJ at 13509572826@163.com.

Author contributions

YT: Writing – original draft, Writing – review & editing. JJ: Writing – original draft, Writing – review & editing. FC: Writing – review & editing. GG: Writing – review & editing. CZ: Writing – review & editing. TD: Writing – review & editing.

Funding

The author(s) declare that no financial support was received for the research, authorship, and/or publication of this article.

Conflict of interest

Authors YT, CZ, and TD were employed by the company Shanghai Yanghe Huajian Artificial Intelligence Technology Co., Ltd.

The remaining authors declare that the research was conducted in the absence of any commercial or financial relationships that could be construed as a potential conflict of interest.

Publisher's note

References

1. Giaquinto AN, Sung H, Miller KD, Kramer JL, Newman LA, Minihan A, et al. Breast cancer statistics 2022. *CA: A Cancer J Clin*. (2022) 72:524–41. doi: 10.3322/caac.21754

2. Bray F, Ferlay J, Soerjomataram I, Siegel R, Torre L, Jemal A, et al. Erratum: Global cancer statistics 2018: Globocan estimates of incidence and mortality worldwide for 36 cancers in 185 countries. *CA Cancer J Clin*. (2020) 70:313. doi: 10.3322/caac.21609

3. Fardad M, Mianji EM, Muntean G-M, Tal I. A fast and effective graph-based resource allocation and power control scheme in vehicular network slicing, in: *22022 IEEE International Symposium on Broadband Multimedia Systems and Broadcasting (BMSB) Proceedings*. Piscataway, NJ, USA: IEEE (2022), 1–6.

4. Ranjbarzadeh R, Jafarzadeh Ghoushchi S, Anari S, Safavi S, Tataei Sarshar N, Babaee Tirkolaee E, et al. A deep learning approach for robust, multi-oriented, and curved text detection. *Cogn Comput*. (2022), 1–13. doi: 10.1007/s12559-022-10072-w

5. Haseli G, Ranjbarzadeh R, Hajiaghaei-Keshteli M, Ghoushchi SJ, Hasani A, Deveci M, et al. Hecon: Weight assessment of the product loyalty criteria considering the customer decision's halo effect using the convolutional neural networks. *Inf Sci*. (2023) 623:184–205. doi: 10.1016/j.ins.2022.12.027

6. Kasgari AB, Safavi S, Nouri M, Hou J, Sarshar NT, Ranjbarzadeh R. Point-of-interest preference model using an attention mechanism in a convolutional neural network. *Bioengineering*. (2023) 10:495. doi: 10.3390/bioengineering10040495

7. Ranjbarzadeh R, Bagherian Kasgari A, Jafarzadeh Ghoushchi S, Anari S, Naseri M, Bendechache M. Brain tumor segmentation based on deep learning and an attention mechanism using mri multi-modalities brain images. *Sci Rep*. (2021) 11:10930. doi: 10.1038/s41598-021-90428-8

8. Tataei Sarshar N, Ranjbarzadeh R, Jafarzadeh Ghoushchi S, de Oliveira GG, Anari S, Parhizkar M, et al. Glioma brain tumor segmentation in four mri modalities using a convolutional neural network and based on a transfer learning method. In: *Brazilian Technology Symposium*. Springer (2021). p. 386–402.

9. Ranjbarzadeh R, Jafarzadeh Ghoushchi S, Tataei Sarshar N, Tirkolaee EB, Ali SS, Kumar T, et al. Me-ccnn: Multi-encoded images and a cascade convolutional neural network for breast tumor segmentation and recognition. *Artif Intell Rev*. (2023), 1–38. doi: 10.1007/s10462-023-10426-2

10. Shah SM, Khan RA, Arif S, Sajid U. Artificial intelligence for breast cancer analysis: Trends & directions. *Comput Biol Med*. (2022) 142:105221. doi: 10.1016/j.compbiomed.2022.105221

11. Anari S, Tataei Sarshar N, Mahjoori N, Dorosti S, Rezaie A. Review of deep learning approaches for thyroid cancer diagnosis. *Math Problems Eng*. (2022) 2022:1–8. doi: 10.1155/2022/5052435

12. Ronneberger O, Fischer P, Brox T. U-net: Convolutional networks for biomedical image segmentation, in: *Medical Image Computing and Computer-Assisted Intervention – MICCAI 2015: 18th International Conference, Munich, Germany, October 12-16, 2015, Proceedings, Part I*. Cham, Switzerland: Springer (2015), 234–41.

13. Zhou Z, Rahman Siddiquee MM, Tajbakhsh N, Liang J. Unet++: A nested u-net architecture for medical image segmentation, in: *Deep Learning in Medical Image Analysis and Multimodal Learning for Clinical Decision Support: 4th International Workshop, DLMIA 2018, and 8th International Workshop, ML-CDS 2018, Conjunction with MICCAI 2018, Granada, Spain, September 20, 2018, Proceedings, Part IV*. Cham, Switzerland: Springer (2018), 3–11.

14. Milletari F, Navab N, Ahmadi S-A. V-net: Fully convolutional neural networks for volumetric medical image segmentation, in: *2016 Fourth International Conference on 3D Vision (3DV), Proceedings*. Piscataway, NJ, USA: IEEE (Institute of Electrical and Electronics Engineers) (2016), 565–71.

15. Mehta S, Mercan E, Bartlett J, Weaver D, Elmore JG, Shapiro L. Y-net: joint segmentation and classification for diagnosis of breast biopsy images, in: *Medical Image Computing and Computer Assisted Intervention – MICCAI 2018: 21st International Conference, Granada, Spain, September 16-20, 2018, Proceedings, Part II*. Cham, Switzerland: Springer (2018), 893–901.

16. Chen J, Lu Y, Yu Q, Luo X, Adeli E, Wang Y, et al. Transunet: Transformers make strong encoders for medical image segmentation. *arXiv*. (2021). Available at: https://arxiv.org/abs/2102.04306.

17. Wang J, Yang Y. A context-sensitive deep learning approach for microcalcification detection in mammograms. *Pattern recognition*. (2018) 78:12–22. doi: 10.1016/j.patcog.2018.01.009

18. Valvano G, Santini G, Martini N, Ripoli A, Iacconi C, Chiappino D, et al. Convolutional neural networks for the segmentation of microcalcification in mammography imaging. *J healthcare Eng*. (2019) 2019. doi: 10.1155/2019/9360941

19. Marasinou C, Li B, Paige J, Omigbodun A, Nakhaei N, Hoyt A, et al. Segmentation of breast microcalcifications: a multi-scale approach. *arXiv*. (2021). Available at: https://arxiv.org/abs/2102.00754.

20. Zamir R, Bagon S, Samocha D, Yagil Y, Basri R, Sklair-Levy M, et al. Segmenting microcalcifications in mammograms and its applications. In: *Medical Imaging 2021: Image Processing*, vol. 11596. Bellingham, Washington, USA: SPIE (2021). p. 788–95.

21. Hossain MS. Microc alcification segmentation using modified u-net segmentation network from mammogram images. *J King Saud University-Computer Inf Sci*. (2022) 34:86–94. doi: 10.1016/j.jksuci.2019.10.014

22. Valanarasu JMJ, Patel VM. Unext: Mlp-based rapid medical image segmentation network, in: *International Conference on Medical Image Computing and Computer-Assisted Intervention – MICCAI 2022: Proceedings*. Cham, Switzerland: Springer (2022), 23–33.

23. Tan M, Le Q. Efficientnetv2: Smaller models and faster training, in: *Proceedings of the 38th International Conference on Machine Learning*. San Francisco, CA, USA: Proceedings of Machine Learning Research (PMLR) (2021), pp. 10096–106.

24. Lin T-Y, Goyal P, Girshick R, He K, Dollár P. Focal loss for dense object detection, in: *Proceedings of the IEEE International Conference on Computer Vision (ICCV)*. Piscataway, NJ, USA: IEEE (Institute of Electrical and Electronics Engineers) (2017), pp. 2980–8.

25. Zhao R, Qian B, Zhang X, Li Y, Wei R, Liu Y, et al. Rethinking dice loss for medical image segmentation, in: *2020 IEEE International Conference on Data Mining (ICDM) Proceedings*. Piscataway, NJ, USA: IEEE (Institute of Electrical and Electronics Engineers) (2020), pp. 851–60.

26. Karimi D, Salcudean SE. Reducing the hausdorff distance in medical image segmentation with convolutional neural networks. *IEEE Trans Med Imaging*. (2019) 39:499–513. doi: 10.1109/TMI.42

27. Jung AB, Wada K, Crall J, Tanaka S, Graving J, Reinders C, et al. imgaug (2020). Available online at: https://github.com/aleju/imgaug (Accessed 01-Feb-2020).

28. Bai Y, Chen D, Li Q, Shen W, Wang Y. Bidirectional copy-paste for semi-supervised medical image segmentation, in: *Proceedings of the IEEE/CVF Conference on Computer Vision and Pattern Recognition (CVPR)*. Los Alamitos, CA, USA, and New York, NY, USA: IEEE Computer Society and Computer Vision Foundation (CVF) (2023), pp. 11514–24.

29. Taha AA, Hanbury A. Metrics for evaluating 3d medical image segmentation: analysis, selection, and tool. *BMC Med Imaging*. (2015) 15:1–28. doi: 10.1186/s12880-015-0068-x

30. Pieper S, Halle M, Kikinis R. 3d slicer, in: *2004 2nd IEEE International Symposium on Biomedical Imaging: Nano to Macro Proceedings*. Piscataway, NJ, USA: IEEE (Institute of Electrical and Electronics Engineers (2004), pp. 632–5.

31. Taud H, Mas J. Multilayer perceptron (MLP). Geomatic approaches for modeling land change scenarios[J]. In *Lecture Notes in Geoinformation and Cartography, Mexico City*, Mexico. (2018) 451–455.

32. Tolstikhin IO, Houlsby N, Kolesnikov A, Beyer L, Zhai X, Unterthiner T, et al. Mlp-mixer: An all-mlp architecture for vision. *Adv Neural Inf Process Syst*. (2021) 34:24261–72.

33. Hu J, Shen L, Sun G. Squeeze-and-excitation networks, in: *Proceedings of the IEEE Conference on Computer Vision and Pattern Recognition (CVPR)*. Los Alamitos, CA, USA: IEEE Computer Society (2018) pp. 7132–41.

34. Chollet F. Xception: Deep learning with depthwise separable convolutions, in: *Proceedings of the IEEE Conference on Computer Vision and Pattern Recognition (CVPR)*. Los Alamitos, CA, USA: IEEE Computer Society. (2017) pp. 1251–8.

35. Hendrycks D, Gimpel K. Gaussian error linear units (gelus). *arXiv*. (2016). Available at: https://arxiv.org/abs/1606.08415

36. Song Y-Y, Ying L. Decision tree methods: applications for classification and prediction. *Shanghai Arch Psychiatry*. (2015) 27:130. doi: 10.11919/j.issn.1002-0829.215044

37. Kleinbaum DG, Dietz K, Gail M, Klein M, Klein M. *Logistic regression*. New York, Inc.: Springer (2002).

38. Huang S, Cai N, Pacheco PP, Narrandes S, Wang Y, Xu W. Applications of support vector machine (svm) learning in cancer genomics. *Cancer Genomics Proteomics*. (2018) 15:41–51. doi: 10.21873/cgp

39. Zhang M-L, Zhou Z-H. Ml-knn: A lazy learning approach to multi-label learning. *Pattern recognition*. (2007) 40:2038–48. doi: 10.1016/j.patcog.2006.12.019

40. Breiman L. Random forests. *Mach Learn*. (2001) 45:5–32. doi: 10.1023/A:1010933404324

41. Chen T, Guestrin C. Xgboost: A scalable tree boosting system, in: *Proceedings of the 22nd ACM SIGKDD International Conference on Knowledge Discovery and Data Mining (KDD '16)*. New York, NY, USA: Association for Computing Machinery (ACM). (2016) pp. 785–94.

42. Hastie T, Rosset S, Zhu J, Zou H. Multi-class adaboost. *Stat its Interface*. (2009) 2:349–60. doi: 10.4310/SII.2009.v2.n3.a8

43. Heath M, Bowyer K, Kopans D, Moore R, Jr PK. *The digital database for screening mammography*. Digital Mammography (2001).

44. He K, Zhang X, Ren S, Sun J. Deep residual learning for image recognition, in: *Proceedings of the IEEE Conference on Computer Vision and Pattern Recognition (CVPR)*. Los Alamitos, CA, USA: IEEE Computer Society (2016) pp. 770–8.

45. Tan M, Le Q. Efficientnet: Rethinking model scaling for convolutional neural networks, in: *Proceedings of the 36th International Conference on Machine Learning (ICML 2019)*. San Francisco, CA, USA: Proceedings of Machine Learning Research (PMLR) (2019) pp. 6105–14. PMLR.

frontiers | Frontiers in Oncology

TYPE Original Research
PUBLISHED 12 April 2024
DOI 10.3389/fonc.2024.1352191

OPEN ACCESS

EDITED BY
Sharon R. Pine,
University of Colorado Anschutz Medical Campus, United States

REVIEWED BY
Till Kaltofen,
University Medical Center Regensburg, Germany
Dinesh Pendharkar,
Sarvodaya Hospital and Research Centre, India

*CORRESPONDENCE
Selamawit Kebede
selamkebede70@gmail.com
Tsegaye Alemu
tsegayea49@gmail.com
Ashenafi Mekonnen
ashemw@gmail.com

RECEIVED 07 December 2023
ACCEPTED 25 March 2024
PUBLISHED 12 April 2024

CITATION
Kebede S, Alemu T and Mekonnen A (2024) Determinants of breast cancer among women attending oncology units in selected health facilities of Hawassa City, Sidama Region, Southern Ethiopia, 2023: case-control study.
Front. Oncol. 14:1352191.
doi: 10.3389/fonc.2024.1352191

Determinants of breast cancer among women attending oncology units in selected health facilities of Hawassa City, Sidama Region, Southern Ethiopia, 2023: case-control study

Selamawit Kebede [1*], Tsegaye Alemu [2*] and Ashenafi Mekonnen [1*]

[1]Public Health Department, Yanet-Liyana College of Health Sciences, Hawassa, Ethiopia, [2]School of Public Health, College of Medicine and Health Sciences, Hawassa University, Hawassa, Ethiopia

Background: The incidence of breast cancer (BC) is rampantly increasing in developing countries particularly Ethiopia. Unfortunately, the morbidity and mortality rates are sharply increasing, and because of this, families are suffering from socioeconomic crises. Despite this, there is limited evidence on the determinants of breast cancer in Ethiopia as well as in the study area.

Objective: To identify the determinants of BC among women attending oncology units in selected hospitals in Hawassa City, Ethiopia, in 2023.

Method: A hospital-based, case-control study with 300 patients (75 cases and 225 controls) was carried out in Hawassa from June to July 2023. A simple random sampling technique was used to select cases and controls. Data were collected via pretested and structured digitally installed questionnaires with Kobo collection/smartphones. The data were exported from the server to SPSS version 27 for analysis. Descriptive analysis of univariate, bivariate, and multivariable logistic regression data was conducted to determine the associations between breast cancer incidence and independent factors.

Results: A total of 300 women participated in this study for a response rate of 100%. The mean (± SD) ages of the respondents were 37.2 (± 14.8) and 36.6 (± 15.1) years for the cases and controls, respectively. According to the multivariate logistic regression model, postmenopausal status [AOR: 2.49; 95% CI (1.18, 5.23)], family history of cancer [AOR: 2.33; 95% CI (1.12, 4.82)], oral contraceptives [AOR: 2.74; 95% CI (1.34, 5.99)], overweight and/or obesity [AOR: 2.29; 95% CI: (1.14, 4.59)], and consumption of solid oil [AOR: 2.36; 95% CI (1.20, 4.67)] were independently associated with BC risk.

Conclusion: This study revealed important risk factors for BC. Therefore, women should adopt healthier lifestyles through healthy nutrition and regular exercise to reduce the risk of developing BC. In addition, early detection and regular screening are proactive approaches for detecting BC.

KEYWORDS

breast cancer, case–control, determinates, oncology units, Sidama Region Ethiopia

1 Introduction

Breast cancer (BC) is the most prevalent cancer in women globally accounting for 2.3 million new cases and one in six cancer deaths in 2020 (1). Globalization has led to a greater incidence of BC in high-income countries (571/100,000) than in low-income countries (95/10,000) (2). Due to globalization, risk factors for cancer are appearing with our modern diet, which emphasizes super grain and more processed food; the use of addictive substances, toxic and pharmaceutical products; and waste exposure. However, the prevention of cancer still depends on the recognition and elimination of risks from carcinogens (3). The five most prevalent nations were all in Europe. The number of new cases in Africa is estimated to have been 92,600 in 2008 and 133,900 in 2012 (1). In 2020, 2.3 million women were diagnosed with BC, and 685,000 women died from BC worldwide (4, 5).

In Africa, 8% of all BC cases are diagnosed, but the mortality rate is far higher than expected (1). Moreover, sub-Saharan Africa has the highest BC incidence and mortality rates attributed to Westernized lifestyles, food changes, and reduced physical activity among the African population (6). In 2020, there was significant geographical variation in the major cancers in sub-Saharan Africa (7).

In Ethiopia, BC is the most prevalent cancer accounting for 17.7% of cancer deaths and 22.6% of all cancer cases annually (8, 9). In addition, every year, approximately 60,000 new cases of BC are diagnosed. Similarly, evidence from the Addis Ababa cancer registry report shows that BC is responsible for 23% of all cancer cases and 33% of all cancer cases in women (10). Moreover, it is the most common malignancy in Ethiopia with increased rates of mortality and morbidity. For instance, of the 4,139 new cancer patients diagnosed between 2012 and 2013, 67% were female, and 31.5% had BC. The age-standardized incidence rate of BC was 43.3 per 100,000 (11) females, and a yearly average of 216 incident cases of BC were reported between 1997 and 2012 (11).

Multiple factors, such as alcohol consumption, tobacco use, obesity, inactivity, diet, family history, early menarche, late menopause, late age, null parity, and nonbreastfeeding practices, are known to increase the risk of BC (8). In contrast, lifestyle modifications, targeted prevention programs, and population-based screening can significantly reduce BC incidence (12).

Unfortunately, even if all of the potentially modifiable risk factors could be mitigated, this would only reduce the risk of developing BC by at most 30% (13). In addition, 20%–30% o BCs can be ascribed to controllable characteristics, and 5%–10% of BCs can be related to factors such as genetic mutations and family history (14). Thus, the healthcare system should be strengthened, and the gradual adoption of universal health coverage should be encouraged especially for low- and middle-income nations where cancer and noncommunicable disease programs are frequently inaccessible and limited-resource citizens are critical (10).

The World Health Organization launched the Global BC Initiative to address the increasing burden of BC, which is estimated to kill 685,000 women globally in 2020 (1). Similarly, the Federal Ministry of Health of Ethiopia (FMOHE) developed and amended a strategy to reduce risk factors and encourage a healthy lifestyle to prevent and control noncommunicable diseases (NCDs), including BC (15). On the other hand, the population of Ethiopia is diverse, representing a wide range of lifestyles, cultures, socioeconomic statuses, and breastfeeding practices. These elements may have an impact on overall health, which may include BC risk (15).

However, to the best of our knowledge, most of the existing studies are cross-sectional, and little is known about BC determination in Ethiopia or in the study area. Therefore, this study aimed to identify determinants of BC among women attending oncology units in the Sidama Region in selected hospitals.

2 Materials and methods

2.1 Study design

A hospital-based unmatched case-control study design was employed at Hawassa City from 1 June– to 30 July 2023.

2.2 Study area and period

The study was conducted in the public and private health facilities of Hawassa City. The Hawassa City Administration is located in Sidama Region, Ethiopia, approximately 275 km south of

Addis Ababa. The city had a total of 385,257 populations with male dominance in number. Of the total population, 89,765 were females of reproductive age.

Cities are administrative structures with dense grid populations of more than 1,500 people per km^2. Within a city, there are small units of administrative structure called subcities. Therefore, in Hawassa City, there are eight small administrative units composed of the smallest administrative units called kebeles. Based on the above explanation, Hawassa City had eight subcities (small administrative units), and each subcity had a different number of smallest administrative units called kebeles accounting for 32 kebeles. Of these smallest administrative units, 11 were rural and 21 were urban kebeles. Hawassa City also has 8 hospitals (3 public and 5 private), 12 public health centers, and 18 health posts. The three public hospitals are Hawassa University Comprehensive Specialized Hospital (HUCSH), Adare General Hospital (AGH), and Hawela Tula Primary Hospital (HTPH) (11). According to the 2022 Sidama Regional State Health Bureau report, a flow of approximately 177 patients per month is expected. The study was performed from 1 June to 30 July 2023.

2.3 Population

2.3.1 Source population and study population

All women who were more than 15 years old and who presented at Hawassa City health facilities were the source population. All women with confirmed BC visiting the selected health facilities for cases and all women without BC visiting the selected health facilities for other services during the study period composed the study population.

2.4 Inclusion and exclusion criteria

The patients were all women over the age of 15 years who had BC that had been confirmed and were receiving chemotherapy. The controls were all women over the age of 15 years who visited selected hospitals for other unrelated to cancer disease in the period of the study. However, women who were mentally incompetent or seriously ill during the course of data collection were excluded from both the case and control groups.

2.5 Sample size determination

Using the statistical software Epi-info version 7, the sample size for unmatched case-control studies was calculated. The following assumptions were used: 95% confidence level, 80% power, a case-to-control ratio of 1:3, a percentage of exposure among control-exposed women (i.e., the percentage of overweight and obese women without BC), and a percentage of exposure among cases (i.e., the percentage of obese women with BC).

The proportion of obese individuals among the controls was 25%, and the proportion of obese individuals among the patients was 31.9%, based on research performed in Addis Ababa, Ethiopia. Based on the above assumptions, the sample size was 272 (66 cases and 204 controls), and after adding a 10% nonresponse rate, the final sample size for the study was 300 (75 cases and 225 controls) (Table 1).

TABLE 1 Sociodemographic characteristics of the study participants in selected health facilities in Hawassa City, 2023.

Variables	Category	Case n (%)	Case n (%)	Total case n (%)	Pearson correlation (two tailed)	p-Value
Age in years	≤40	30 (40.0)	139 (61.8)	169 (56.3)	0.018	0.757
	40–49	18 (24.0)	33 (14.7)	51 (17.0)		
	50–59	12 (16.0)	23 (10.2)	35 (11.7)		
	≥60	15 (20.0)	30(13.3)	45 (15.0)		
Place of residence	Urban	47(62.7)	132 (58.7)	179 (59.7)	0.083	0.152
	Rural	28 (37.3)	93 (41.3)	121 (40.3)		
Educational status	No formal education	19 (25.3)	65 (28.8)	84 (28.0)	−0.035	0.548
	Primary	28 (37.3)	82 (36.4)	110 (36.6)		
	Secondary	11 (14.6)	37 (16.4)	48 (16.0)		
	College and above	17 (22.6)	41 (18.2)	58 (19.3)		
Marital status	Married	50 (66.6)	162 (72.0)	212 (70.6)	0.010	0.857
		25 (33.3)	63 (28.0)	88 (29.3)		

(Continued)

TABLE 1 Continued

Variables	Category	Case n (%)	Case n (%)	Total case n (%)	Pearson correlation (two tailed)	p-Value
	Currently unmarred¥					
Occupation	Housewife	26 (34.6)	79 (35.1)	105 (35.0)	0.068	0.239
	Employee	12 (16.0)	49 (21.7)	61 (20.3)		
	Merchant	21 (28.0)	46 (20.4)	67 (22.2)		
	Farmer	11 (14.6)	34 (15.1)	45 (15.0)		
	Others*	5 (6.6)	17 (7.5)	22 (7.3)		

¥Single, divorced, and widowed. *Students and daily laborer.

2.6 Sampling technique and procedures

The study was performed in two hospitals, namely, Hawassa University Comprehensive (HUCSH) and Specialized Hospital and Yanet Internal Medicine Specialized Center (YIMSC), which provide chemotherapy services. The final calculated sample size was proportionally allocated to each hospital based on the number of patients who received chemotherapy services for BC treatment within the last year's data from the health management information system (HMIS) report. Hence, 46 cases and 138 controls from HUCSH and 29 cases and 87 controls from YIMSC were included in the study. Since the cases are rare, we included all cases sequentially, but controls were included using a systematic random sampling technique. Therefore, once we included one patient, the next three controls were included in the study until the sample size was met.

2.7 Study variables

2.7.1 Dependent variable: breast cancer

Dependent variable is breast cancer.

2.7.2 Independent variables

Sociodemographic variables such as age, educational level, occupation, place of residence, and family history of cancer; behavior and/or alcohol intake, smoking status, fatty diet intake, and body mass index; reproductive variables such as age at first delivery, age at menarche, parity, breastfeeding practice, and use of hormonal contraceptives; diet and lifestyle variables such as vegetable intake, exercise, and fruit intake; and environmental and health-related variables such as pesticide contact, radiation exposure, breast trauma, and history of breast infection.

2.8 Data collection instruments and procedures

2.8.1 Data collection instruments

Primarily, the tool was developed in English after reviewing different literature from previous studies (16–18). Then, the questionnaire was translated into the local languages Sidamagna Afoo and Amharic by an expert and translated back to English by another expert to maintain consistency.

2.8.2 Data collection procedures

One day of training was given for two data collectors and one supervisor on the instrument. The interviewer administered a questionnaire supplemented with a checklist to collect data using the Kobo toolbox. Hence, during the interview, the data collector interviewed study participants about their sociodemographic, behavioral, clinical, and reproductive matters for both cases and controls. In addition, other pertinent determinant factors were identified from patients' medical records. Pretests were performed on 5% of the sample before the actual data collection, and the necessary amendments were made.

The patient's interview and the review of the patient's records were used to gather information about the patient's sociodemographic (age, residence, marital status, and level of education) and behavioral (smoking, BMI, alcohol consumption, and physical activity) BMI results. Patients were classified as underweight (<18.5), normal weight (18.5–24.9), overweight (25–29.9), or obese (>30). Reproductive (parity, OC use, menopausal status, breastfeeding practices) characteristics. Before the real data collection process, a pretest was conducted using the collected data.

2.9 Data quality assurance

To ensure data quality, first, the data collection tools were prepared in English, translated to Amharic, and then returned to English to ensure consistency. Appropriate training was given to the data collectors and supervisors. The training included a briefing on the general objectives of the study, approach to accessing study participants, clarity on each item in the instrument, data collection procedure, including or excluding the target data source, timeliness of data submission, data handling, and time management. Pretests were performed outside the study health institution on 5% of the sample before the actual data collection, and the necessary correction was made based on the pretest results to avoid any confusion and for better completion of the questions. Every day, the collected data were reviewed and cross-checked for completeness.

2.10 Data processing and analysis

The data were collected via Kobo data collection and exported to SPSS version 27 for analysis. Descriptive statistics, such as frequency and percent distribution, were used to present categorical variables. Means and standard deviations were used for continuous variables. We conducted an independent sample t test to evaluate the equality of variance and mean difference among cases and controls to exposure variables to evaluate the mean difference in exposure between cases and controls. To identify factors related to BC, a binary logistic regression analysis was performed. According to the bivariate analysis, variables with a p-value of 0.25 were candidates for multivariate analysis. To demonstrate the strength of the link, an adjusted odds ratio with a 95% confidence interval was calculated. The association of the dependent and independent variables was considered significant at a p-value of less than 0.05. The goodness of fit was checked by the Hosmer and Lemeshow test (p-value = 0.86). Moreover, multicollinearity was assessed for each variable considering variance inflation factor (VIF) values less than 10.

2.11 Operational definitions

BC: Women who had a confirmed BC diagnosis according to histological examination. Case: Women with BC and histologically confirmed cases (8). Controls: Women who visited gynecological OPD in selected hospitals for noncancer care. Cancer: This is a condition in which body cells multiply uncontrollably and become contagious to other parts of the body (19). BMI: Somebody's mass divided by the square of height in meters (20). For menopausal status, women who met any of the following criteria were classified as postmenopausal: 1) had menstruation for no less than 1 year (any age) and 2) had undergone bilateral oophorectomy or estrogen deprivation therapy (21). Active smoking is a condition in which people (including former smokers) have a history of smoking within 6 months (22). Passive smoking: People who are not smokers but are exposed to tobacco smoke for more than 15 min at least 1 day per week (22).

3 Results

3.1 Sociodemographic characteristics

A total of 300 women (75 cases and 225 controls) participated in the study for a response rate of 100%. Thirty (40%) of the cases and 139 (61.78%) of the controls were aged less than 40 years with the mean (± SD) age of the women being 37.2 (± 14.8) and 36.6 (± 15.1) for the cases and controls, respectively. More than half of the participants [47 (62.67%) cases and 132 (58.67%) controls] were urban dwellers. Seventeen (22.67%) patients and 41 (18.22%) controls had a college education or above. Regarding occupational status, 26 (34.67%) patients and 79 (35.11%) controls were housewives (1).

3.2 Reproductive health-related characteristics

Of the total respondents, 34.67% (n = 26) of the patients and 22.22% (n = 50) of the controls had experienced their first menstrual period before the age of 12 years, and the mean (± SD) ages of the women who experienced menarche were 13.5 (± 2.1) and 14 (± 1.92) years for the cases and controls, respectively. Approximately 10 (13.33%) patients and 8.44% (n = 19) of the controls had a history of abortion. Forty-two (56%) patients and 26.22% (n = 59) of the controls were premenopausal women. More than a quarter (29.33%) of the patients and 16.44% (n = 37) of the women had irregular menstrual periods. More than half (58.67%) of the patients and 36.89% (n = 83) of the controls used oral contraceptives. In the majority of the patients, 66.6% (n = 50) and 73% (n = 162) of the controls had never breastfed their infants. One-quarter 25.33%, n = 19) of the patients and 27.11% (n = 61) of the controls had a history of breast infection (Table 2).

3.3 Behavioral and biological-related characteristics

Among the patients, 30.67% (n = 23) and 16.00% (n = 36) of the controls had a family history of cancer. Forty percent (n = 30) of the patients and 25.33% (n = 57) of the controls were overweight and/or obese. In the majority of the patients, 77.33% (n = 58) and 70.22% (n = 158) of the controls did not participate in regular physical exercise. In the majority of the participants, 88% (n = 66) of the patients and 82.22% (n = 185) of the controls ate fewer than seven servings of fruit per week. Regarding exposure to smoking, 18.67% (n = 14) of the patients and 22.22% (n = 50) of the controls were exposed. Approximately 40% (n = 30) of the patients and 30.22% (n = 68) of the controls used packed food or drinks. Approximately 50.67% (n = 38) of the patients and 33.78% (n = 76) of the controls consumed solid oil. Among the participants, 9.33% (n = 7) of the patients and 8.8% (n = 8) of the controls had ever undergone a mammogram. Approximately 45.33% (n = 34) of the patients and 44.4% (n = 100) of the controls had practiced self-breast examinations (Table 3).

3.4 The mean difference in exposure between cases and controls

In this study, we conducted an independent-sample t-test to evaluate the equality of variance and mean difference among cases and controls to exposure variables. To check the similarity of variance among cases and controls, Levene's test for equality of variances was used (i.e., equal variances, $p > 0.05$, and unequal variances $p < 0.05$). Similarly, to identify the mean difference among cases and controls, a t-test for the equality of means with respective p-values was used [$p < 0.05$ indicates a significant difference in the means of the two sample populations tested (cases and controls)]. Since the variance is greater than 4 for almost all of the test

10.3389/fonc.2024.1352191

TABLE 2 Reproductive health-related characteristics of the women included in the study in selected health facilities in Hawassa City, 2023 (n = 300).

Variables	Category	Case n (%)	Control n (%)	Total Case in n (%)	Pearson correlation (two tailed)	p-Value
Menopausal status	Premenopausal	42 (56.0)	59 (26.2)	101 (33.6)	−0.040	0.714
	Menopausal	33 (44.0)	166 (73.7)	199 (66.3)		
History of abortion	Yes	10 (13.3)	19 (8.4)	29 (9.6)	0.095	0.165
	No	65 (86.6)	206 (91.5)	271 (90.3)		
Menstrual period regularity	Yes	53 (70.6)	188 (83.5)	241 (80.3)	−0.002	0.976
	No	22 (29.3)	37 (16.4)	59 (19.6)		
Age at menarche in years	≤12	26 (34.6)	50 (22.2)	76 (25.3)	0.011	0.856
	13-16	35 (46.6)	132 (58.6)	167 (55.6)		
	≥16	14 (18.6)	43 (19.1)	67 (19.0)		
Ever used an oral contraceptive	Yes	44 (58.6)	83 (36.8)	127 (42.3)	−0.152	0.008
	No	31 (41.3)	142(63.1)	173(57.6)		
Breastfeeding	Yes	50(66.6)	162 (72.0)	212 (70.6)	−0.051	0.381
	No	25 (33.3)	63 (28.0)	88 (29.3)		
Breast injury	Yes	2 (2.6)	12 (5.3)	14 (4.6)	−0.055	0.345
	No	73 (97.3)	213 (94.6)	286 (95.3)		
Breast infection	Yes	19 (25.3)	61 (27.1)	80 (26.6)	−0.017	0.764
	No	56 (74.6)	164 (72.8)	220 (73.3)		

TABLE 3 Behavioral and biological characteristics of the study participant women in selected health facilities in Hawassa City, 2023.

Variables	Category	Case n (%)	Control n (%)	Total case in n (%)	Pearson correlation (two tailed)	p-Value
Family history of cancers	Yes	23 (30.6)	36 (16.00)	59 (19.67)	0.16	0.006
	No	52 (69.3)	189 (84.00)	241 (80.33)		
BMI	Normal	35 (46.6)	142 (63.11)	177 (59.00)	0.122	0.035
	Underweight	10 (13.3)	26 (11.56)	36 (12.00)		
	Overweight and/ or Obesity	30 (40.0)	57 (25.33)	87 (29.00)		
Physical activity	Yes	17 (22.6)	67 (29.78)	84 (28.00)	0.085	0.144
	No	58 (77.3)	158 (70.22)	216 (72.00)		
Fruit intake per week	≤7	66 (88.0)	185 (82.22)	251 (83.67)	−0.141	0.014
	>7	9 (12.0)	40 (17.78)	49 (16.33)		
Exposure for smoking	Yes	14 (18.6)	50 (22.22)	64 (21.33)	−0.113	0.051
	No	61 (81.3)	175 (77.78)	236 (78.67)		
Use of packed food or drinks	Yes	30 (40.0)	68 (30.2)	98 (32.6)	0.126	0.029
	No	45 (60.0)	157 (69.7)	202 (67.3)		

(Continued)

TABLE 3 Continued

Variables	Category	Case n (%)	Control n (%)	Total case in n (%)	Pearson correlation (two tailed)	p-Value
Solid oil	Yes	38 (50.6)	76 (33.7)	114 (38.0)	0.05	0.0
	No	37 (49.3)	149 (66.2)	186 (62.0)		
Ever had a mammogram	Yes	7 (9.3)	18 (8.0)	25 (8.3)	0.021	0.719
	No	68 (92.0)	207 (90.6)	275 (91.6)		
Breast self-examination	Yes	34 (45.3)	100 (44.4)	134 (44.6)	−0.008	0.894
	No	41 (54.6)	125 (55.5)	166 (55.3)		

variables, we assumed unequal variance and used a one-sample t-test (23). The factors associated with an increased risk of BC among women were family history of cancer ($p < 0.014$), consumption of packed food ($p < 0.03$), BMI ($p < 0.04$), fruit consumption ($p < 0.03$), menopausal status ($p < 0.01$), and smoking status ($p < 0.01$) (Table 4).

3.5 Factors associated with BC

According to the bivariate logistic regression analysis, age, menopausal status, use of packed foods or drinks, history of abortion, regularity of menstruation, age at menarche, body mass index (BMI), family history of cancer, use of oral contraceptives, regular physical exercise, and consumption of solid oil were independently associated with BC. However, in the multivariate logistic regression analysis, menopausal status, overweight and obesity status, use of oral contraceptives, family history of cancer, and consumption of solid oil were independently associated with BC.

The odds of having BC were almost three times greater among postmenopausal women than among their male counterparts [adjusted odds ratio (AOR) = 2.5; 95% CI: 1.18–5.2, p = 0.01]. Women with a family history of cancer were 2.33 times more likely to develop BC than women without a family history of cancer (AOR = 2.33; 95% CI: 1.12–4.82, p = 0.02). The odds of developing BC were almost three times greater among oral contraceptive users than among their counterparts (AOR = 2.74; 95% CI: 1.34–5.99, p = 0.005). Similarly, the odds of having BC were almost two times greater among overweight women than among normal-weight women (AOR = 2.29; 95% CI: 1.14–4.59, p = 0.01). Finally, women who used palm/solid oil were 2.4 times more likely to have BC than were their male counterparts (AOR = 2.36; 95% CI: 1.20–4.67, p = 0.01) (Table 5).

4 Discussion

In this facility-based study, we evaluated the determinants of BC among women attending oncology health facilities in Hawassa City, Sidama Region, Ethiopia. Postmenopausal status ($p < 0.016$), BMI ($p < 0.020$), family history of cancer ($p < 0.023$), use of oral contraceptives ($p < 0.02$), and consumption of saturated fat ($p < 0.013$) were independently associated with BC.

Our study showed that menopausal status significantly increases BC risk with postmenopausal women having almost three times greater odds than premenopausal women. This finding is similar to that of a study in Addis Ababa (24). Another study from Malaysia showed that postmenopausal women had a 52% greater risk of BC (25). A meta-analysis from India comparable with this study showed that postmenopausal women have a 35% greater risk of developing BC than premenopausal women (26). A possible explanation could be that postmenopausal women face an increased risk of BC due to decreased estrogen levels, obesity, and a sedentary lifestyle, which can increase the risk of developing the disease. Thus, a systematic review and meta-analysis of evidence suggested that postmenopausal women should have regular physical activity and a healthy diet to prevent overweight and obesity to address BC (27).

Similarly, a family history of cancer significantly increases the risk of BC, and women with a history of BC are 2.3 times more likely to develop BC. This result is in line with research in Addis Ababa (8), which demonstrated that women with a family history of BC are substantially more likely to develop BC than other women. Early detection and screening could be key for BC progression. Families with a history of BC may also be more aware of the risks and symptoms leading them to seek regular screening and early detection. While this proactive approach to healthcare is important, it can create a perception of greater risk due to increased awareness and monitoring within the family.

The study revealed that oral contraceptives significantly increased BC risk with women using oral contraceptives having 2.74 times greater odds of developing BC than nonusers. This result is in line with a study conducted in Jordan and Ethiopia (28, 29). Naturally occurring estrogen and progesterone stimulate the development and growth of some cancers (e.g., cancers that express the receptor for these hormones, such as BC). Birth control pills contain synthetic versions of these female hormones. In contrast, oral contraceptives and BC were not significantly linked in a study in Ethiopia (24). The possible reason for this slight increase in risk could be related to the hormonal components of oral contraceptives. Oral contraceptives contain synthetic versions of the hormones estrogen and progestin, which are used to prevent pregnancy by suppressing ovulation and altering the cervical mucus and the lining of the uterus. Therefore, maintaining regular BC screenings and self-exams is crucial for the early detection

TABLE 4 Independent-sample t-test of respondents for determinants of BC among women attending oncology units at selected health facilities of Hawassa City, Sidama Region, Ethiopia, 2023 (n = 75 cases and n = 225 controls).

Independent-sample test		Levene's test for equality of variances		t-Test for equality of means						
		F	Sig.	t	df	Sig. (two tailed)	Mean difference	Std. error difference	95% Confidence interval of the difference	
									Lower	Upper
Place of residence	EVA	11.063	0.001	−1.435	298	0.152	−0.093	0.065	−0.221	0.035
	EVNA			−1.471	132.578	0.144	−0.093	0.063	−0.219	0.032
Family history	EVA	25.066	0.000	−2.794	298	0.006	−0.147	0.052	−0.250	−0.043
	EVNA			−2.489	106.597	**0.014***	−0.147	0.059	−0.264	−0.030
Physical activity	EVA	10.532	0.001	−1.465	298	0.144	−0.089	0.061	−0.208	0.031
	EVNA			−1.540	138.901	0.126	−0.089	0.058	−0.203	0.025
Packed food	EVA	10.998	0.001	−2.197	298	0.029	−0.138	0.063	−0.261	−0.014
	EVNA			−2.108	118.628	**0.037***	−0.138	0.065	−0.267	−0.008
BMI	EVA	2.861	0.092	−2.114	298	0.035	−0.249	0.118	−0.481	−0.017
	EVNA			−2.042	119.828	**0.043***	−0.249	0.122	−0.490	−0.008
Duration of household activities	EVA	16.478	0.000	−2.067	275	0.040	−2.009	0.972	−3.922	−0.096
	EVNA			−1.698	88.855	0.093	−2.009	1.183	−4.360	0.342
Fruit consumption	EVA	22.576	0.000	2.467	298	0.014	0.102	0.041	0.021	0.184
	EVNA			2.088	100.057	**0.039***	0.102	0.049	0.005	0.199
Ever used an oral contraceptive	EVA	3.642	0.057	2.659	298	0.008	0.173	0.065	0.045	0.302
	EVNA			2.615	123.390	**0.010***	0.173	0.066	0.042	0.305
Menopausal status	EVA	3.642	0.057	2.659	298	0.008	0.173	0.065	0.045	0.302
	EVNA			2.615	123.390	**0.010***	0.173	0.066	0.042	0.305
Passive smoker	EVA	19.012	0.000	1.959	298	0.051	0.107	0.054	0.000	0.214
	EVNA			2.188	157.178	**0.030***	0.107	0.049	0.010	0.203

BMI, body mass index; EVA, equal variances assumed; EVNA, equal variances not assumed; BC, Breast Cancer.
The bold value indicating statistically significant value.

10.3389/fonc.2024.1352191

TABLE 5 Bivariate and multivariate logistic regression analysis of factors associated with BC risk among women who attended selected health facilities in Hawassa City, 2023.

Variables	Category	Case	Control	COR (95% CI)	AOR (95% CI)	p-Value
Age in years	≤40	30	139	1		
	40–49	18	33	2.52 (1.25, 5.07)	1.03 (0.43, 2.47)	0.934
	50–59	12	23	2.41 (1.08, 5.38)	1.45 (0.52, 4.04)	0.477
	≥60	15	30	2.31(1.11, 4.83)	1.66 (0.61, 4.50)	0.316
Menopausal status	Premenopausal	42	59	1	1	
	Postmenopausal	33	166	3.58 (2.07, 6.17)	2.49 (1.18, 5.23)	0.016**
History of abortion	Yes	10	19	1.67 (0.73, 3.76)	2.16 (0.79, 5.86)	0.130
	No	65	206	1	1	
Menstrual period regularity	Yes	53	188	0.47 (0.25, 0.87)	1.14 (0.51, 2.55)	0.744
	No	22	37	1		
Age at menarche in years	≤12	26	50	1.59 (0.74, 3.43)	1.81 (0.73, 4.49)	0.196
	13–16	35	132	0.81 (0.40, 1.65)	0.77 (0.31, 1.90)	0.573
	≥16	14	43	1	1	
Ever used an oral contraceptive	Yes	44	83	2.42 (1.42, 4.13)	2.74 (1.34, 5.59)	0.005***
	No	31	142	1	1	
Family Hx of cancer	Yes	23	36	2.32 (1.26, 4.25)	2.33 (1.12, 4.82)	0.023***
	No	52	189	1	1	
BMI	Normal	35	142	1	1	
	Underweight	10	26	1.56 (0.68, 3.53)	2.05 (0.77, 5.41)	0.145
	Overweight and/or obesity	30	57	2.13 (1.19, 3.80)	2.29 (1.14, 4.59)	0.020***
Physical activity	Yes	17	67	1	1	
	No	58	158	1.44 (0.78, 2.66)	1.98 (0.89, 4.38)	0.090
Fruit intake per week	≤7	66	185	1	1	
	>7	9	40	0.63 (0.29, 1.37)		
Use of packed food or drinks	Yes	30	68	1.59 (0.89, 2.64)	1.69 (0.84, 3.40)	0.136
	No	45	157	1	1	
Solid oil	Yes	38	76	2.01 (1.18, 3.42)	2.36 (1.20, 4.67)	0.013***
	No	37	149	1	1	

***Significant at a p-value <0.001 and *significant at a p-value <0.05. AOR, adjusted odds ratio; BMI, body mass index; COR, crude odds ratio.

and treatment of BC regardless of whether a woman is using oral contraceptives.

Women's nutritional status significantly impacts BC risk with overweight or obese women having a 2.29-fold greater risk than normal-weight women. This finding is comparable to that of a study conducted in Jordan and two other studies in Ethiopia (8, 30, 31). The possible justification could be unhealthy eating patterns that are marked by high consumption of refined carbohydrates, sugar, and saturated fats (32). This increased risk can be attributed to the higher levels of estrogen produced by adipose tissue and the fact that obese women are more physically inactive, both of which can promote the growth of BC cells.

Furthermore, consuming saturated oil significantly increases BC risk. Women consuming solid oil have 2.36 times greater odds of developing BC than nonusers. This result is in line with a study performed in the USA showing that eating saturated fat increases the risk of developing BC (33). The possible reason could be that saturated fatty acids increase low-density lipoprotein cholesterol, obesity, and free radicals, which increase the risk of BC (34). A meta-analysis revealed that a high-fat diet is a risk factor for BC (35). Another systematic review showed that an unhealthy high-fat diet may contribute to obesity and affect BC (36).

The strengths of this study included the use of an observational study design with a 1:3 case-to-control ratio, which enhances its ability

to identify BC determinants and its validity due to its multicenter nature. The possible study limitations include the small number of patients in the health facility, recall bias, and over- or underreporting of self-reported data on dietary consumption and physical activity.

5 Conclusion

BC is a public health problem both globally and in Ethiopia. This study aimed to identify the determinants of BC. Therefore, postmenopausal status, BMI, family history of cancer, being overweight, using oral contraceptives, and consuming solid oil were identified as risk factors for BC. Therefore, women should adopt healthier lifestyles through healthy nutrition and regular physical exercise, which might contribute to reducing the risk of developing BC in women. In addition, early detection and regular screening are proactive approaches for identifying BC.

Data availability statement

The original contributions presented in the study are included in the article/supplementary material. Further inquiries can be directed to the corresponding authors.

Ethics statement

Ethical clearance was obtained from the Ethical Review Committee of Yanet-Liyana College of Health Science (with Ref # of LHC/YLCHS/OGL/981/15 and Date: 29/05/2023 GC). The studies were conducted in accordance with the local legislation and institutional requirements. The participants provided their written informed consent to participate in this study.

Author contributions

SK: Conceptualization, Data curation, Formal analysis, Funding acquisition, Investigation, Methodology, Project administration, Resources, Software, Supervision, Writing – original draft, Writing – review & editing. TA: Conceptualization, Data curation, Formal analysis, Investigation, Methodology, Project administration, Software, Supervision, Writing – original draft, Writing – review & editing. AM: Data curation, Formal analysis, Investigation, Methodology, Software, Validation, Visualization, Writing – original draft, Writing – review & editing.

Funding

The author(s) declare that no financial support was received for the research, authorship, and/or publication of this article.

Acknowledgments

We would like to extend our sincere gratitude to Yanet-Liyana College of Health Science for their ethical letter provision. We would also like to acknowledge all our data collectors and supervisors who participated in the data collection at the field level. We would like to extend our gratitude to all the study participants for their important insights and contributions in providing information in this research process.

Conflict of interest

The authors declare that the research was conducted in the absence of any commercial or financial relationships that could be construed as a potential conflict of interest.

Publisher's note

References

1. Arnold M, Morgan E, Rumgay H, Mafra A, Singh D, Laversanne M, et al. Current and future burden of breast cancer: Global statistics for 2020 and 2040. *Breast*. (2022) 66:15–23. doi: 10.1016/j.breast.2022.08.010

2. Kashyap D, Pal D, Sharma R, Garg VK, Goel N, Koundal D, et al. Global increase in breast cancer incidence: risk factors and preventive measures. *BioMed Res Int*. (2022) 2022. doi: 10.1155/2022/9605439

3. Sasco AJ. Cancer and globalization. *BioMed Pharmacother*. (2008) 62:110–21. doi: 10.1016/j.biopha.2007.10.015

4. Sung H, Ferlay J, Siegel RL, Laversanne M, Soerjomataram I, Jemal A, et al. Global cancer statistics 2020: GLOBOCAN estimates of incidence and mortality worldwide for 36 cancers in 185 countries. *CA: A Cancer J Clin*. (2021) 71:209–49. doi: 10.3322/caac.21660

5. Nguyen D, Yu J, Reinhold WC, Yang SX. Association of independent prognostic factors and treatment modality with survival and recurrence outcomes in breast cancer. *JAMA Netw Open*. (2020) 3:e207213–e. doi: 10.1001/jamanetworkopen.2020.7213

6. Mekonnen BD. tffBreast self-examination practice and associated factors among female healthcare workers in Ethiopia: a systematic review and meta-analysis. *PloS One*. (2020) 15:e0241961. doi: 10.1371/journal.pone.0241961

7. Bray F, Parkin DM. Cancer in sub-Saharan Africa in 2020: a review of current estimates of the national burden, data gaps, and future needs. *Lancet Oncol*. (2022) 23:719–28. doi: 10.1016/S1470-2045(22)00270-4

8. Tolessa L, Sendo EG, Dinegde NG, Desalew A. Risk factors associated with breast cancer among women in addis ababa, Ethiopia: Unmatched case–control study. *Int J Women's Health*. (2021) 13:101–10. doi: 10.2147/IJWH.S292588

9. Bacha RH, Jabir YN, Asebot AG, Liga AD. Risk factors affecting survival time of breast cancer patients: The case of southwest Ethiopia. *J Res Health Sci*. (2021) 21: e00532. doi: 10.34172/jrhs.2021.65

10. Anderson BO, Abdel-Wahab M, Fidarova E. The Global Breast Cancer Initiative: a strategic collaboration to strengthen health care for noncommunicable diseases. *Lancet Oncol*. (2021) 22(5):578–81. doi: 10.1016/S1470-2045(21)00071-1

11. Bejitual K, Fikre R, Ashegu T, Zenebe A. Determinants of neonatal sepsis among neonates admitted to the neonatal intensive care unit of public hospitals in Hawassa City Administration, Sidama Region, Ethiopia, 2020: an unmatched, case–control study. *BMJ Open*. (2022) 12:e056669. doi: 10.1136/bmjopen-2021-056669

12. Mertens E, Barrenechea-Pulache A, Sagastume D, Vasquez MS, Vandevijvere S, Peñalvo JL. Understanding the contribution of lifestyle in breast cancer risk prediction: a systematic review of models applicable to Europe. *BMC Cancer*. (2023) 23(1):687. doi: 10.1186/s12885-023-11174-w

13. WHO. Breast cancer fact sheet (2021). Available online at: https://www.who.int/news-room/fact-sheets/detail/breast-cancer.

14. Liu H, Shi S, Gao J, Guo J, Li M, Wang L. Analysis of risk factors associated with breast cancer in women: a systematic review and meta-analysis. *Trans Cancer Res*. (2022) 11:1344. doi: 10.21037/tcr

15. Khalis M, Charbotel B, Chajès V, Rinaldi S, Moskal A, Biessy C, et al. Menstrual and reproductive factors and risk of breast cancer: A case–control study in the Fez region, Morocco. *PloS One*. (2018) 13:e0191333. doi: 10.1371/journal.pone.0191333

16. Duche H, Tsegay AT, Tamirat KS. Identifying risk factors of breast cancer among women attending selected hospitals of Addis Ababa city: hospital-based unmatched case–Control study. *Breast Cancer (Dove Med Press)*. (2021) 13:189–97. doi: 10.2147/BCTT.S293867

17. Tolessa L, Sendo EG, Dinegde NG, Desalew A. Risk factors associated with breast cancer among women in Addis Ababa, Ethiopia: unmatched case–Control study. *Int J Womens Health*. (2021) 13:101–10. doi: 10.2147/IJWH.S292588

18. Tekeste Z, Berhe N, Arage M, Degarege A, Melaku YA. Cancer signs and risk factors awareness in Addis Ababa, Ethiopia: a population-based survey. *Infect Agent Cancer*. (2023) 18:1. doi: 10.1186/s13027-022-00477-5

19. Siegel RL, Miller KD, Wagle NS, Jemal A. Cancer statistics, 2023. *CA: Cancer J Clin*. (2023) 73:17–48. doi: 10.3322/caac.21763

20. García-Estévez L, Cortés J, Pérez S, Calvo I, Gallegos I, Moreno-Bueno G. Obesity and breast cancer: a paradoxical and controversial relationship influenced by menopausal status. *Front Oncol*. (2021) 11:705911. doi: 10.3389/fonc.2021.705911

21. Rothschild HT, Abel MK, Patterson A, Goodman K, Shui A, van Baelen K, et al. Obesity and menopausal status impact the features and molecular phenotype of invasive lobular breast cancer. *Breast Cancer Res Treat*. (2022) 191:451–8. doi: 10.1007/s10549-021-06453-8

22. Fakhri N, Chad MA, Lahkim M, Houari A, Dehbi H, Belmouden A, et al. Risk factors for breast cancer in women: an update review. *Med Oncol*. (2022) 39:197. doi: 10.1007/s12032-022-01804-x

23. Zimmerman DW. Teacher's corner: A note on interpretation of the paired-samples t test. *J Educ Behav Stati*. (1997) 22:349–60. doi: 10.3102/10769986022003349

24. Hassen F, Enquselassie F, Ali A, Addissie A, Taye G, Tsegaye A, et al. Association of risk factors and breast cancer among women treated at Tikur Anbessa Specialized Hospital, Addis Ababa, Ethiopia: a case–control study. *BMJ Open*. (2022) 12:e060636. doi: 10.1136/bmjopen-2021-060636

25. Durham DD, Abraham LA, Roberts MC, Khan CP, Smith RA, Kerlikowske K, et al. Breast cancer incidence among women with a family history of breast cancer by relative's age at diagnosis. *Cancer*. (2022) 128:4232–40. doi: 10.1002/cncr.34365

26. Vishwakarma G, Ndetan H, Das DN, Gupta G, Suryavanshi M, Mehta A, et al. Reproductive factors and breast cancer risk: A meta-analysis of case–control studies in Indian women. *South Asian J cancer*. (2019) 8:080–4. doi: 10.4103/sajc.sajc_317_18

27. Dehesh T, Fadaghi S, Seyedi M, Abolhadi E, Ilaghi M, Shams P, et al. The relation between obesity and breast cancer risk in women by considering menstruation status and geographical variations: a systematic review and meta-analysis. *BMC Womens Health*. (2023) 23:392. doi: 10.1186/s12905-023-02543-5

28. Bardaweel SK, Akour AA, Al-Muhaissen S, AlSalamat HA, Ammar K. Oral contraceptive and breast cancer: do benefits outweigh the risks? A case–control study from Jordan. *BMC women's Health*. (2019) 19:1–7. doi: 10.1186/s12905-019-0770-x

29. Das D. Breast cancer: Risk factors and prevention strategies. *World J Biol Pharma Health Sci*. (2022) (12)(3):265280. doi: 10.30574/wjbphs.2022.12.3.0253

30. Ayoub NM, Yaghan RJ, Abdo NM, Matalka II, Akhu-Zaheya LM, Al-Mohtaseb AH. Impact of obesity on clinicopathologic characteristics and disease prognosis in preand postmenopausal breast cancer patients: a retrospective institutional study. *J Obes*. (2019) 2019:1–11. doi: 10.1155/2019/3820759

31. Duche H, Tsegay AT, Tamirat KS. Identifying risk factors for breast cancer among women attending selected hospitals of Addis Ababa city: Hospital-based unmatched case–control study. *Breast Cancer: Targets Ther*. (2021) 13:189–97. doi: 10.2147/BCTT.S293867

32. Seiler A, Chen MA, Brown RL, Fagundes CP. Obesity, dietary factors, nutrition, and breast cancer risk. *Curr Breast Cancer Rep*. (2018) 10:14–27. doi: 10.1007/s12609-018-0264-0

33. Dandamudi A, Tommie J, Nommsen-Rivers L, Couch S. Dietary patterns and breast cancer risk: a systematic review. *Anticancer Res*. (2018) 38:3209–22. doi: 10.21873/anticanres.12586

34. Xia H, Ma S, Wang S, Sun G. Meta-analysis of saturated fatty acid intake and breast cancer risk. *Medicine*. (2015) 94:e2391. doi: 10.1097/MD.0000000000002391

35. Uhomoibhi TO, Okobi TJ, Okobi OE, Koko JO, Uhomoibhi O, Igbinosun OE, et al. High-fat diet as a risk factor for breast cancer: a meta-analysis. *Cureus*. (2022) 14:e32309. doi: 10.7759/cureus.32309

36. Gopinath A, Cheema AH, Chaludiya K, Khalid M, Nwosu M, Agyeman WY, et al. The impact of dietary fat on breast cancer incidence and survival: a systematic review. *Cureus*. (2022) 14:e30003. doi: 10.7759/cureus.30003

frontiers | Frontiers in Oncology

TYPE Clinical Trial
PUBLISHED 18 April 2024
DOI 10.3389/fonc.2024.1354377

OPEN ACCESS

EDITED BY
Sung Gwe Ahn,
Yonsei University Health System,
Republic of Korea

REVIEWED BY
Chang Ik Yoon,
The Catholic University of Korea,
Republic of Korea
Elizabeth Ann Salerno,
Washington University in St. Louis,
United States

*CORRESPONDENCE
Josefine Wolff
josefine.wolff@med.uni-muenchen.de

RECEIVED 12 December 2023
ACCEPTED 04 March 2024
PUBLISHED 18 April 2024

CITATION
Wolff J, Seidel S, Wuelfing P, Lux MP, Eulenburg Cz, Smollich M, Baumann F, Seitz S, Kuemmel S, Thill M, Tio J, Braun M, Hollaender H, Seitz A, Horn F, Harbeck N and Wuerstlein R (2024) App-based support for breast cancer patients to reduce psychological distress during therapy and survivorship – a multicentric randomized controlled trial.
Front. Oncol. 14:1354377.
doi: 10.3389/fonc.2024.1354377

App-based support for breast cancer patients to reduce psychological distress during therapy and survivorship – a multicentric randomized controlled trial

Josefine Wolff[1,2]*, Svenja Seidel[2], Pia Wuelfing[2], Michael Patrick Lux[3], Christine zu Eulenburg[4], Martin Smollich[5], Freerk Baumann[6], Stephan Seitz[7], Sherko Kuemmel[8], Marc Thill[9], Joke Tio[10], Michael Braun[11], Hannah Hollaender[1], Angenla Seitz[2], Felicitas Horn[2], Nadia Harbeck[1] and Rachel Wuerstlein[1]

[1]Breast Center, Department of Gynecology and Obstetrics, and Comprehensive Cancer Center Ludwig-Maximilian University Munich (LMU) University Hospital, Munich, Germany, [2]Department Clinical Research, PINK! Gegen Brustkrebs GmbH, Hamburg, Germany, [3]Department of Gynecology and Obstetrics, Frauenklinik St. Louise and St. Josefs-Krankenhaus, St. Vincenz Klinik GmbH, Paderborn, Germany, [4]Department for Medical Biometry and Epidemiology, University Medical Center Hamburg-Eppendorf, Hamburg, Germany, [5]Institute of Nutritional Medicine, University Hospital Schleswig-Holstein, Luebeck, Germany, [6]Department I of Internal Medicine, University of Cologne, Cologne, Germany, [7]Department of Obstetrics and Gynecology, Caritas Hospital St. Josef, University of Regensburg, Regensburg, Germany, [8]Breast Unit, Kliniken Essen-Mitte, Essen, Germany, [9]Markus Hospital, Breast Center, Frankfurt, Germany, [10]Department of Gynecology and Obstetrics, University Hospital of Münster, Münster, Germany, [11]Department of Gynecology, Breast Center, Red Cross Hospital, Munich, Germany

Introduction: The negative impact of unmanaged psychological distress on quality of life and outcome in breast cancer survivors has been demonstrated. Fortunately, studies indicate that distress can effectively be addressed and even prevented using evidence-based interventions. In Germany prescription-based mobile health apps, known as DiGAs (digital health applications), that are fully reimbursed by health insurances, were introduced in 2020. In this study, the effectiveness of an approved breast cancer DiGA was investigated: The personalized coaching app PINK! Coach supports and accompanies breast cancer patients during therapy and follow-up.

Methods: PINK! Coach was specifically designed for breast cancer (BC) patients from the day of diagnosis to the time of Follow-up (aftercare). The app offers individualized, evidence-based therapy and side-effect management, mindfulness-based stress reduction, nutritional and psychological education, physical activity tracking, and motivational exercises to implement lifestyle changes sustainably in daily routine. A prospective, intraindividual RCT (DRKS00028699) was performed with n = 434 patients recruited in 7 German breast cancer centers from September 2022 until January 2023. Patients with BC were included independent of their stage of diseases, type of therapy and molecular characteristics of the tumor. Patients were randomized into one of two groups: The intervention group got access to PINK! over 12 weeks; the control group served as a waiting-list comparison to "standard of care."

The primary endpoint was psychological distress objectified by means of Patient Health Questionnaire-9 (PHQ-9). Subgroups were defined to investigate the app's effect on several patient groups such as MBC vs. EBC patients, patients on therapy vs. in aftercare, patients who received a chemotherapy vs. patients who did not.

Results: Efficacy analysis of the primary endpoint revealed a significant reduction in psychological distress (least squares estimate -1.62, 95% confidence interval [1.03; 2.21]; p<0.001) among intervention group patients from baseline to T3 vs, control group. Subgroup analysis also suggested improvements across all clinical situations.

Conclusion: Patients with breast cancer suffer from psychological problems including anxiety and depression during and after therapy. Personalized, supportive care with the app PINK! Coach turned out as a promising opportunity to significantly improve psychological distress in a convenient, accessible, and low-threshold manner for breast cancer patients independent of their stage of disease (EBC/MBC), therapy phase (aftercare or therapy) or therapy itself (chemotherapy/other therapy options). The app is routinely available in Germany as a DiGA. Clinical Trial Registration: DRKS Trial Registry (DRKS00028699).

KEYWORDS

breast cancer, psychological distress, app-based coaching, depression, digital intervention, supportive care in cancer

1 Introduction

Breast cancer patients face an increased risk of experiencing psychiatric disorders, including depression and anxiety (1). The link between depression and anxiety status and cancer outcomes has been well investigated. Psychological distress is related to higher cancer-specific mortality and poorer cancer survival in patients with breast cancer (2–4). Both, low levels of psychological distress and low fatigue are independently correlated with longer periods of recurrence-free survival and overall survival (3, 4). In addition, psychological distress is also associated with a lower quality of life and an increased incidence of side effects (5, 6).

Overall, the negative impact of unmanaged psychological distress on breast cancer patients has numerous consequences for those affected, in terms of their treatment outcomes, survival, recurrence, as well as their daily life after acute therapy and long-term psychosocial well-being (3–8). Fortunately, studies indicate that distress can be effectively addressed and even prevented using digital, evidence-based interventions (9–14). Existing data also indicate that psychological interventions have the potential to impact neuroendocrine factors such as cortisol levels, as well as immune function markers, particularly lymphocyte proliferation and the production of TH1 cytokines. Psychological interventions can have a detrimental impact on various biological processes relevant to breast cancer. Initiation and progression of cancer involve a complex series of steps, including environmental exposures, genetic alterations, evasion of apoptosis, cell proliferation, evasion of immune surveillance, angiogenesis, and metastasis. Emerging evidence suggests that psychosocial stress can influence the trajectory of the disease at multiple stages within this process (15–18). Offering digital psychological support to breast cancer patients could have clinically meaningful psychological as well as biological effects.

With an annual incidence of 70.000 new cases in Germany alone, and a substantial number of survivors, the healthcare system is struggling to meet the increasing demand for supportive care and psycho-oncological support during and after initial breast cancer treatment. This challenge is particularly pronounced in rural areas where the access to care is noticeably lower compared to urban regions (19, 20). In acute cases, patients in most clinics have the opportunity to schedule a short-term appointment with a psycho-oncologist. However, psychotherapeutic support during and after therapy comes with long waiting times. Currently, in Germany, patients have to wait around 4 months for an outpatient psychotherapy spot.[1]

To address this gap in healthcare provision and improve support for breast cancer patients and survivors across all stages of treatment,

1 https://www.psychotherapeutenkammer-berlin.de/ 26.07.2023.

digital app-based solutions present a promising and cost-effective opportunity. Research indicates that eHealth tools are emerging as effective platforms for delivering lifestyle interventions during breast cancer care (21, 22). Given the prolonged survival and long-term follow-up required for both early-stage and some metastatic breast cancer patients, studies emphasize the importance of providing evidence-based information on nutritional strategies, incorporating physical activity into daily routines, managing treatment side effects, and offering mental health coaching (23–26).

Due to multimodal therapeutic concepts for BC patients, especially EBC patients, treatments lead to full recovery in more than 70-80%. The burden of survivorship can indeed be overwhelming. Breast cancer survivors face a wide range of physiological and psychosocial challenges, often dealing with late and long-term effects from intensive treatment therapies. Despite these difficulties, breast cancer survivors express a strong desire to actively manage their health. This leads to a wide range of app-based support offerings for breast cancer patients worldwide. Mobile health (mHealth) apps can play a crucial role in addressing this need by providing patients with a dynamic platform to continuously monitor and track symptoms over time. These apps allow survivors to interact with peers for support and discussions on survivorship topics, offer resources for caregivers, send reminders for medication or follow-up appointments, and provide relevant education on managing health concerns during survivorship. Nevertheless, current studies indicate the need of criteria for end users and clinicians to help choose the right apps for better clinical outcomes (27–29).

The PINK! Coach App offers individualized, evidence-based therapy and side-effect management, mindfulness-based stress reduction, nutritional and psychological education, physical activity tracking and motivational exercises to implement lifestyle changes sustainably in daily routine of breast cancer patients. PINK! aims to support patients with breast cancer in every stage of disease and therapy in order to empower patients to take an active role during their therapy and in aftercare independent of factors such as stage of disease, type of therapy, age, place of residence or the clinic the patient is being treated or was treated. Using PINK! offers patients personalized, time- and location-independent coaching (14).

As a DiGA (German: “Digitale Gesundheitsanwendung”, Engl.: “Digital health application”) PINK! Coach is one of 47 prescription-based mobile health apps[2] in Germany that are fully reimbursed by health insurances. To become a DiGA, mHealth applications undergo a rigorous certification process that includes providing scientific evidence of efficacy through clinical trials. Other certification requirements encompass safety, functional capability, quality, interoperability, data protection, and data security. As a result, some of the main barriers to patient adoption, such as high costs, lack of integration with current standards of care, and concerns about quality, are addressed within the German system, thus making it unique from an international perspective (30).

The preceding pilot study with the self-management app PINK! demonstrated effective reduction in psychological distress and fatigue among breast cancer patients and survivors. Our study revealed that participants who had access to the app and received individual coaching for 12 weeks experienced significant improvements in their levels of psychological distress and fatigue symptoms on average. Additionally, the usage of the app also led to an increase in physical activity levels within the 12-week period. Particularly noteworthy were the positive effects observed in participants who extensively utilized the app, defined as those who used it for at least 200 minutes over the 12 weeks (14).

The present study was designed to demonstrate the medical benefits and positive care effects of the app in terms of psychological distress among breast cancer patients in a multicentric setting to substantiate and validate the results of the pilot study. The study design of this research was further specified to investigate more precise insights into the mechanisms of action of the app on all breast cancer patients. Due to the numerous treatment options available for breast cancer, the individual situations of the patients vary significantly. As a result, the app must also be tailored to each individual to provide comprehensive support to all patients. We hypothesized that PINK! Coach empowers breast cancer patients at every stage of the disease to enhance their daily routines and lifestyle, thereby enabling them to live a healthier life in a sustainable manner and consequently reduce psychological distress.

2 Methods

The PINK! Coach App study was approved by the Medical Ethical Committee of the LMU University of Munich, Germany on 21.07.2022 (Reference number: 22-0498) Furthermore, the Medical Ethical Committees of all clinics that participated in this multicenter RCT approved of this study. The trial has been registered prospectively in the DRKS Trial Registry (DRKS00028699).

2.1 Study design

In this multicenter RCT, all breast cancer patients were recruited and randomly assigned to either intervention group (IG) or control (CG). CG served as a waiting list comparison to the “standard of care”. IG immediately received access to PINK! Coach on top of the “standard of care” while CG received access to PINK! Coach after 12 weeks. Given the design of the intervention, participants were not blinded to group assignment. A 1:1 randomization was performed with a computer-generated sequence. The participating investigators were blinded to the group allocation and did not have access to the collected data. Data were collected at baseline (before randomization), after 4 weeks (T1), after 8 weeks (T2) and after 12 weeks (T3) which was the primary endpoint of this study. To investigate long-term effects of the PINK! Coach App, a follow-up 6 and 12 months after baseline is currently being conducted.

2.2 Recruitment and inclusion criteria

Patients were recruited at 7 German Breast cancer Centers with the Breast Center of the LMU University Hospital in Munich as the

2 https://diga.bfarm.de/de/verzeichnis 29.06.2023.

Principal Investigator. Patients had to meet the following inclusion criteria: They had to be at least 18 years old, German-speaking, diagnosed with histologically confirmed breast cancer, own a smartphone, have an email address, and be willing to use an app as a therapy companion. In addition, the diagnosis of the initial occurrence or recurrence should have been made within the past 12 months or up to 12 months after the surgery. Furthermore, patients should either be undergoing therapy for at least 12 weeks or have been discharged to post-treatment follow-up (aftercare) at the time of recruitment. For all patients with metastatic breast cancer (MBC), the therapy status (first-line or second-line) is irrelevant, as all MBC patients were assigned to the treatment group.

Patients were identified, informed and included in the study at all participating breast cancer centers. All patients in this study signed a written informed consent. After baseline documentation and the patients first questionnaire, they were randomized to IG and CG. The following inclusion and exclusion criteria were defined:

- they had to be at least 18 years old,
- German-speaking,
- diagnosed with histologically confirmed breast cancer,
- own a smartphone,
- have an email address.
- and be willing to use an app as a therapy companion.

2.3 Intervention

PINK! Coach was designed specifically for early-stage and metastatic breast cancer (BC) patients from the day of diagnosis to the time of aftercare. The app offers individualized, evidence-based therapy and side-effect management, mindfulness-based stress reduction, nutritional and psychological education, physical activity tracking, and motivational exercises to implement lifestyle changes sustainably in daily routine. PINK! Coach offers multimodal content in 3 categories: nutrition, physical activity, and mental health. Content is provided as articles, videos, podcasts and daily goals to achieve. Those daily goals are steps counts, nutritional habits, physical exercises, MBSR exercises and more. The patients decide themselves if and how many goals they try to achieve each day. The goal is to motivate patients to start changing daily lifestyle habits. All information is evidence-based, validated, and permanently updated based on recent research results and current German Breast Cancer Guidelines (AGO recommendations; S3 guidelines) by the PINK! research expert board. To maintain and strengthen the motivation for change in patients, PINK! Coach incorporates various motivating elements. One element is the automated and pseudo-individualized coaching delivered contextually through push notifications. In order to boost motivation and performance, users also receive success messages upon achieving goals and can continually track their success statistics.

Through an automated chatbot, patients have the opportunity to gather information about the side effects of medication-based tumor therapies (chemotherapy, immunotherapy, antibody therapy, hormone therapy), radiation therapy, and breast cancer surgeries. Assuming that the entered symptoms are related to the side effects of the medications, the chatbot provides recommendations, primarily focusing on self-help tips (i.e., the application of conventional home remedies and behaviors). The symptoms are differentiated according to CTCAE criteria. In case of more severe symptoms the chatbot directly advises contacting the doctor without providing further self-help recommendations. The goal of the chatbot is to provide patients with confidence regarding the occurrence, intensity, and management of side effects, thereby reducing psychological distress.

The personalization of content is achieved through regular check-ups. Initially, these check-ups are requested for download, and then they are repeated at 2-week or 4-week intervals. The check-ups include questions about tumor biology and the status of therapy. Additionally, validated questionnaires about therapy-related side effects and psychological stress are administered. General information such as the individual's professional situation is also taken into account.

As part of the change process, PINK! Coach guides patients into self-observation, where they consciously perceive their nutrition and physical activity. This is done through nutrition and exercise tracking. The results are analyzed and presented on a weekly and monthly basis, making the impact of individual decisions visible for success. Another important aspect is the setting of (intermediate) goals. The patient is supported in selecting possible goals appropriate for the specific time. The course contents build on each other, leading gradually to a successful adaptation of habits. The mental health section includes a 12-week course based on elements of cognitive-behavioral therapy aimed at reducing mental stress, anxiety, and other related effects.

These multimodal features, shown in Figure 1, of the PINK! Coach app aim to individually address the complex interaction of psychological stress, quality of life, side effects, and personal aspects, in order to help each patient to improve their lifestyle in a tailored manner. PINK! Coach was developed by PINK! gegen Brustkrebs GmbH.

2.4 Objective and outcome measures

The primary objective of this study was to test whether using PINK! Coach App over 12 weeks during therapy or in aftercare leads to a significant reduction of psychological distress in patients with early-stage and metastatic breast cancer compared to control group that provided comparison to "standard of care" as waiting list.

The PHQ-9 is a versatile tool used for screening, diagnosing, monitoring, and assessing the severity of depression. It consists of nine items, and the total score is calculated by assigning scores of 0, 1, 2, and 3 to the response categories of "not at all," "several days," "more than half the days," and "nearly every day," respectively. The PHQ-9 total score can range from 0 to 27, obtained by summing up the scores of all nine items. Specific cut-off points are used to classify the severity of depression: scores of 5, 10, 15, and 20 represent mild, moderate, moderately severe, and severe depression, respectively.

10.3389/fonc.2024.1354377

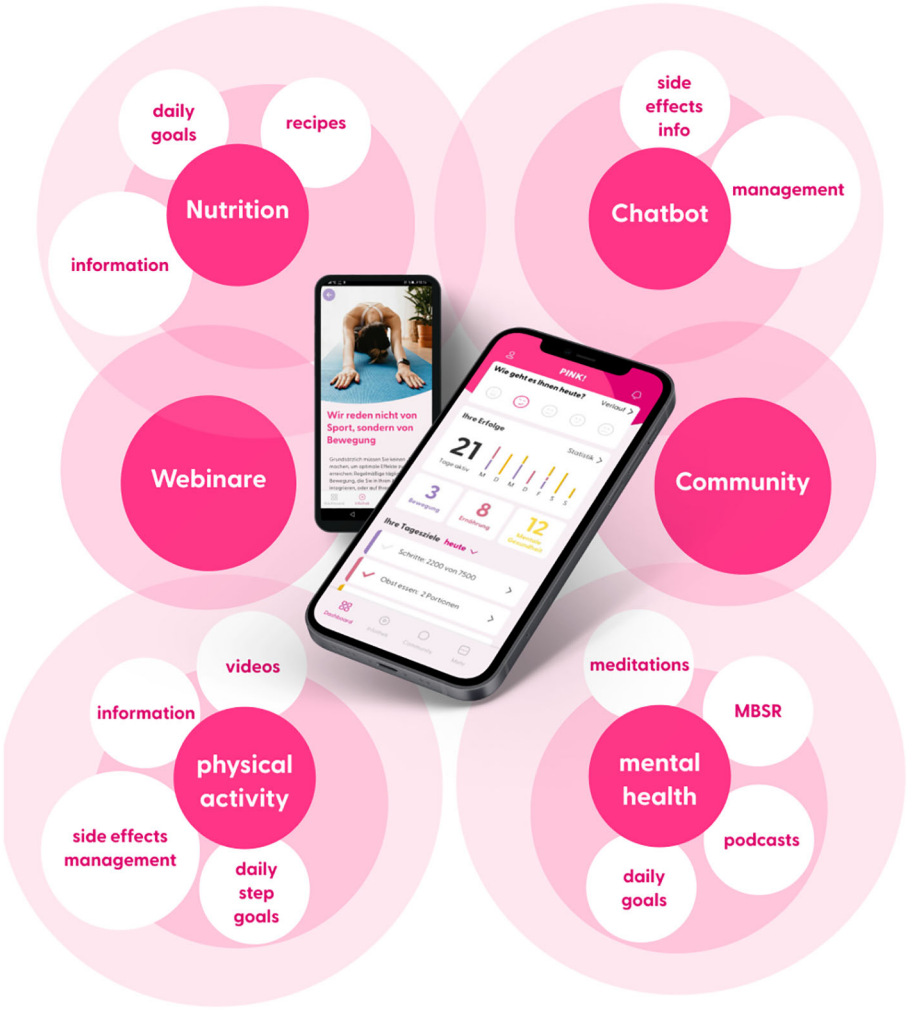

FIGURE 1
PINK! Coach App functionalities.

The total scores of the PHQ-9 allow for the classification of the severity of depression. This helps assess the clinical relevance of changes in the score over a specific period of time. The classification of the severity of the PHQ-9 score thus provides a practical means of evaluating progress or treatment efficacy in depression. The following Table 1 displays the clinical evaluation of the PHQ-9.

The transition to another group can be considered a clinically relevant change and is highly likely to have a noticeable impact on the patient (31).

2.5 Statistical analysis

The Full Analysis Set (FAS) contained both adherent and non-adherent patients, who were randomized and had at least the baseline PHQ-9 assessment. As sensitivity analysis, we analyzed changes in scores for only adherent patients (per protocol) which were all patients that finished all questionnaires (Baseline, T1, T2, and T3). Significance

TABLE 1 Clinical evaluation of PHQ-9 score points in 5 groups of depression symptoms.

Scorepoints PHQ-9	Clinical evaluation
0-4	Minimal or no depression: The patient exhibits only a few depressive symptoms or no depressive symptoms at all.
5-9	Mild depression: The patient exhibits mild depressive symptoms that do not significantly impair daily functioning.
10-14	Moderate depression: The patient exhibits moderate depressive symptoms that may cause some impairment in daily functioning.
15-19	Moderately severe depression: The patient exhibits pronounced depressive symptoms that noticeably impair daily functioning.
>20	Severe depression: The patient exhibits severe depressive symptoms that significantly impair daily functioning and may require intensive treatment.

level was set at $p \leq .05$. The demographic, medical history and outcome variables were described using frequency and descriptive statistics. Analyses were performed using STATA Version 16.0.

The primary endpoint was the difference in changes from baseline in the PHQ-9 total score at T3 (12 weeks). As primary analysis, a linear mixed model (random intercept model) was applied, adjusting for baseline PHQ-9 and therapy status (therapy or aftercare). For sensitivity analysis, different imputation algorithms were used to deal with missing values at post-assessment. Subgroups according to therapy group (therapy or aftercare), chemotherapy (yes or no) and stage (EBC or MBC/recurrent disease) were analyzed similar to the primary analysis.

An analysis of response was applied using a generalized linear mixed model similar to the primary analysis, with response as a dichotomous endpoint. Standardized effect sizes (Cohen's d) were calculated.

The PINK! Coach App study has been approved by the Medical Ethical Committee of the LMU University of Munich, Germany on 21.07.2022 (Reference number: 22-0498) Furthermore, the Medical Ethical Committees of all clinics that participated in this multicenter RCT approved of this study. The trial has been registered prospectively in the DRKS Trial Registry (DRKS00028699).

To assess the clinical relevance of the determined results, an attempt was made to determine the Minimal Clinically Important Difference (MCID) in addition to calculating effect sizes using Cohen's method. The Minimal Clinically Important Difference of the PHQ-9 has not yet been determined for a cohort of breast cancer patients. There are no publications on this topic in the known databases. However, there are publications on the MCID of the PHQ-9 in other patient cohorts with different diagnoses. Therefore, it is currently not possible to directly compare our results with the data published so far. Nevertheless, responder analyses were conducted to assess clinical relevance.

3 Results

From September 2022 until January 2023, a total of 435 patients met the inclusion criteria and signed the informed consent, answered the baseline questionnaire, and were randomized to one of the study groups IG or CG. 191 patients were randomized to the IG, 205 to the CG whereby 298 were in therapy and 98 in aftercare. Over 12 weeks there were 39 dropouts in total, with 21 in the IG and 18 in the CG which corresponds to 9.0% dropout rate. 50.3% of CG and 49.7% of IG received a chemotherapy. Figure 2 displays the recruitment flowchart.

The data show a homogeneous distribution of patients in the IG and CG with respect to the recorded variables. The collective is heterogeneous due to broad inclusion criteria, but the distribution across the study groups is homogeneous.

Table 2 displays the distribution of tumor biological characteristics of the entire collective in the IG and CG as well as in the subgroups of therapy and aftercare patients divided by EBC and MBC. Patients with TNBC (triple-negative breast cancer) or HER2-positive breast cancer are approximately equally distributed across both groups. Patients with hormone receptor-positive tumors are evenly distributed across both groups.

The median age is 52 years. The median age of the IG and CG differs marginally. The variances in both groups are nearly equal.

3.1 PHQ-9 overall IG vs. CG

The primary endpoint was the difference in PHQ-9 reduction at T3 between IG and CG. In the IG, the PHQ-9 total score showed a reduction (delta) from baseline to T3 (12 weeks) of -1.5 score points (least squares estimate difference between IG and CG -1.52; 95% confidence interval (CI) [–1,91, –1,07] The calculation of difference values (Deltas) was not based on the mean values at different time points but rather as the mean of the difference values for each pair of values at the respective time points.

A reduction in the total score is associated with a reduction in psychological distress. The reduction of 1.5 score points corresponds to a moderate relative reduction of 18.8% compared to baseline. The use of the app resulted in a significantly higher reduction compared to the control arm [least squares estimate difference between IG and CG -1.52, 95% confidence interval (CI) (1.03; 2.21); p<0.001] in psychological distress shown in Figure 3. In the CG, a delta of 0 was measured between baseline and T3. Therefore, no reduction or increase in the PHQ-9 total score, indicating consistent psychological distress, was observed in patients without app usage. The intervention group had a slightly higher baseline value of 8.0 compared to the control group (7.5).

The estimates are based on a mixed model for repeated measurements with group assignment (intervention group versus control group), measurement time, the interaction of group * time, baseline PHQ9 score, and the stratification variable "Therapy/aftercare." The patient is included as a random effect in the model. Baseline is defined as time point T0. The least squares mean differences between the intervention and control groups are reported.

The effects of the app were also estimated for pre-specified subgroups using the mixed-effects model. The following forest plot displays the results.

3.2 PHQ-9 subgroup therapy/aftercare

One subgroup analysis of the primary endpoint considered the time point during the course of therapy. Patients were categorized into the "therapy" group (during acute treatment) or the "aftercare" group. The following Figure 4 displays the results of the subgroup analysis.

The subgroup "Intervention Therapy" (IG therapy) presents a delta of -1.4 in the PHQ-9 total score from baseline to T3. This corresponds to a relative reduction of 17.3% compared to baseline and a significantly reduced psychological distress during the observation period (least squares estimate difference between IG and CG -1.67, 95% confidence interval (CI) [1,01, 2,33]; p<0.001). The PHQ-9 baseline value in the therapy group is consistent with the initial level of psychological distress in the entire collective. The "Control group Therapy" (CG therapy) exhibits a slightly lower baseline value and a slight increase in psychological distress over the observation period (delta of 0.4 from baseline to T3).

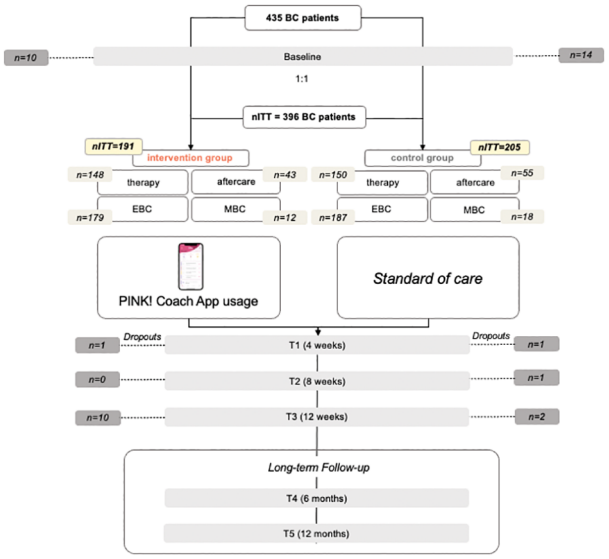

FIGURE 2
Study flow chart with number of patients, EBC/MBC, therapy/aftercare and dropouts.

In the "Intervention aftercare" group (IG aftercare), the psychological distress decreases significantly: the delta of -2.1 (least squares estimate difference between IG and CG -1.12, 95% confidence interval (CI) [−0,04, 2,29]; p<0.001) corresponds to a relative reduction of 27.3% in the PHQ-9 total score from baseline to T3. The PHQ-9 baseline value in the IG aftercare is slightly lower than in the overall collective. Thus, the initial psychological distress in the aftercare patients is lower than that of patients in the acute therapy phase. The "Control group aftercare" also shows a slightly lower PHQ-9 baseline value and a delta of -1.1 from baseline to T3.

Results of a mixed model analysis revealed an estimated effect size of 1.67 in IG therapy with a SE of 0.34 and an effect of 1.65 with SE 0.64 in IG aftercare. P-values were $p_{therapy}$<0.001 and $p_{aftercare}$=0.01. Cohen´s d in IG therapy was -0.54 and in IG aftercare -0.44.

3.3 PHQ-9 subgroups EBC/MBC

Furthermore, a subgroup analysis was conducted in the "EBC" (early breast cancer) and "MBC" (metastatic breast cancer) groups. This is particularly clinically relevant because in the metastatic setting, psychological distress differs from early breast cancer due to the initial condition of an incurable disease, changes in socioeconomic background, the nature, and especially the duration of treatment, as well as the intensity of distress caused by side effects. Results are displayed in Figure 4.

The results show a reduction of -1.5 score points [least squares estimate difference between IG and CG -1.45, 95% confidence interval (CI) (0,87, 2,04); p<0.001] in the PHQ-9 total score in the "Intervention group EBC" (IG EBC). This corresponds to the results of the entire collective. The baseline values of PHQ-9 in EBC

TABLE 2 Patient characteristics ITT collective EBC/MBC.

	Parameter	Value	Intervention	Control	Therapy	aftercare
EBC	*Number of patients*	*n (%)*	182 *(100.0)*	188 *(100.0)*	272 *(100.0)*	98 *(100.0)*
	Median Age		52.0	52.0	52.0	53.0
	HR+ HER2 neg.	*n (%)*	106 *(58.2)*	103 *(54.8)*	139 *(51.1)*	70 *(71.4)*
	HER2 pos.	*n (%)*	40 *(22.0)*	44 *(23.4)*	66 *(24.3)*	18 *(18.4)*
	TNBC	*n (%)*	36 *(19.8)*	41 *(21.8)*	67 *(24.6)*	10 *(10.2)*
	CHT	*%*	*51.2*	*44.9*	*58.3*	*20.9*
MBC	*Number of patients*	*n (%)*	9 *(5.6)*	17 *(9.5)*	26 (8.7)	0 (0.0)
	Median Age		52.5	54.5	52.5	–
	HR+ HER2 neg.	*n (%)*	2 *(22.2)*	2 *(11.8)*	4 *(15.4)*	–
	HER2 pos.	*n (%)*	6 *(66.6)*	12 *(70.6)*	18 *(69.2)*	–
	TNBC	*n (%)*	1 *(11.1)*	3 *(17.6)*	4 *(15.4)*	–
	CHT	*%*	33.3	47.0	42.3	–
Total	*Number of patients*	396 (100.0)				
	Median Age	52.0				
	HR+ HER2 neg.	*n*	209			
	HER2 pos.	*n*	84			
	TNBC	*n*	77			
	CHT	*%*	48.1			

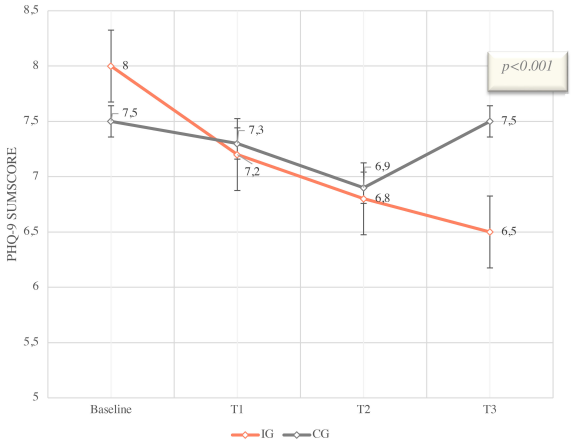

FIGURE 3
PHQ-9 Sumscore means with SD and 95% CI from Baseline (T0) to T3 (12 weeks), IG vs. CG of ITT colletive (n=396).

compared to the overall collective are only marginally different. The level of psychological distress in the EBC collective is consistent with the average baseline distress in the overall collective. Therefore, the level of psychological distress in the EBC collective is equivalent to the average baseline distress in the intervention group.

On the other hand, the "Intervention group MBC" (IG MBC) exhibits a significantly higher baseline value in the PHQ-9 score compared to the overall collective (9.7 vs. 7.9). The delta from baseline to T3 is -1.3 (least squares estimate difference between IG and CG -2.13, 95% confidence interval (CI) [−0,56, 4,82]; p=0.12), corresponding to a relative reduction of 13.4% in the PHQ-9 total score compared to baseline.

The "Control group" in EBC shows a delta of -0.1 from baseline to T3. The "Control group MBC" (CG MBC) however, shows an increase of 0.6 points in the PHQ-9 total score over the observation period. The baseline values of the control groups EBC and MBC differ. The number of MBC patients was n=9 in the intervention group and n=17 in the control group.

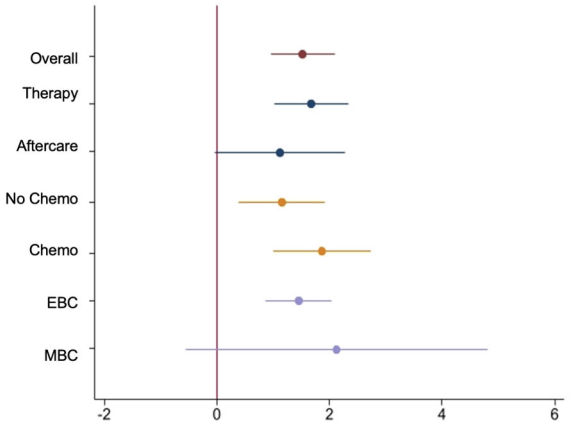

FIGURE 4
Forest-Plot of Least Squares mean difference of mixed model in overall ITT Set and subgroups.

3.4 PHQ-9 subgroups CHT/nCHT

The subgroup "Intervention with chemotherapy" (IG CHT) shows a delta of -1.9 score points from baseline to T3 [least squares estimate difference between IG and CG -1.87, 95% confidence interval (CI) (1,00, 2,7); p<0.001]. The delta, representing the reduction in psychological distress, is even more pronounced in patients undergoing chemotherapy compared to the overall IG (Figure 2). This corresponds to a relative reduction of 22.1% in the PHQ-9 total score compared to baseline. Additionally, the PHQ-9 baseline value in the "Intervention with chemotherapy" subgroup is higher than the average baseline value of the entire collective. The "Control group with chemotherapy" (CG CHT) shows a delta of 0.3 from baseline to T3, indicating consistent psychological distress over the 12-week observation period. The PHQ-9 baseline value is also higher than in the overall collective.

The "Intervention group without chemotherapy" (IG nCHT) shows a delta of -1.3 score points from baseline to T3 (least squares estimate difference between IG and CG -1.15, 95% confidence interval (CI) [0,39, 1,92]; p=0.003). The effect of the app on reducing psychological distress is slightly smaller in patients without chemotherapy compared to those undergoing chemotherapy or the overall collective. The baseline value of 7.5 is also slightly lower than that of the overall intervention group. The "Control group without chemotherapy" (CG nCHT) shows a delta of -0.2 in the PHQ-9 total score from baseline to T3, indicating almost consistent psychological distress. The PHQ-9 baseline value of 7.2 is slightly lower than the value of the overall control group (7.5) and also slightly lower than the value of the intervention group (8.0).

Results of a mixed model analysis revealed an estimated effect size of 1.87 in IG CHT with a SE of 0.44 and an effect of 1.15 with SE 0.39 in the IG nCHT subgroup.

47 out of a total of 191 ITT patients in the intervention group showed a usage time of 0 minutes after 12 weeks. This means that approximately 25% of the patients did not use the app throughout the entire intervention period.

The remaining patients had an average usage time of 466.4 minutes in the first month (baseline to T1), equivalent to around 17 minutes per day. In the second month from T1 to T2, the usage time was 274 minutes, or 10 minutes per day. In the third month from T2 to T3, it was 313 minutes. It appears that about a quarter of the patients did not use the app or used it only briefly. The remaining 75% used the app intensively and throughout the entire intervention period and all elements of the app.

4 Discussion

This multicenter, randomized controlled study with a waitlist control aimed to primarily investigate whether the psychological distress caused by a breast cancer diagnosis, one of the most relevant side effects during treatment and aftercare, could be improved through an app-based coaching program (PINK! Coach).

The study population was representative and adequately reflected the diversity of diagnosis and treatment situations,

including factors such as age, tumor stages, and tumor biological characteristics.

The average age of breast cancer diagnosis is approximately 64 years (7), with one in four affected individuals being younger than 55 years and one in ten being younger than 45 years old. The median age of the patients in the population studied in this study was 52 years, which is lower than the average age of the general breast cancer population. This can be attributed to the fact that the participating study centers are clinically and scientifically specialized certified breast centers located in larger cities, which also offer specific treatment options for younger patients. These centers have an interdisciplinary diagnostic, therapeutic, and supportive network in place to address issues such as fertility preservation, genetic predisposition, etc., and incorporate them directly into the optimal treatment plan. Younger patients are therefore deliberately referred to such centers. The willingness to participate in a clinical study can also be age-dependent. However, the study also included numerous older patients who actively and consistently utilized the intervention throughout the study period.

Approximately 20% of women with breast cancer experience tumor spread and the formation of metastases despite treatment, occurring over months to years. About 7% of women are diagnosed with metastases at the time of their initial breast cancer diagnosis (primary metastatic patients).

In this study, only MBC patients with newly diagnosed metastasis were included. The study population comprises 7% MBC patients, which adequately reflects the clinical reality. The distribution of MBC patients between the intervention and control groups is similar in the full analysis set (ITT).

Regarding tumor biological characteristics (TNM, TNBC/HR +/HER2+/-), the studied population is representative. For example, approximately 15-20% of breast cancer tumors are HER2-positive. In the studied population, 20.2% of patients had a HER2-positive tumor, which aligns with the real-world population of breast cancer patients. In the past, HER2-positive breast cancer tumors were considered as an aggressive tumor type with a poor prognosis. However, the introduction of targeted therapies in form of HER2-directed drugs, has significantly improved therapeutic options (7). From being a negative prognostic factor, HER2 positivity has become a positive predictive factor, indicating response to targeted anti-HER2 therapies. Therefore, patients with HER2-positive tumors now have a good prognosis due to the available therapeutic options. However, the use of anti-HER2 therapies is often associated with substantial side effects, which has implications for psychological distress. In addition, the treatment duration with anti-HER2 therapies is significantly longer, which adds to the burden on patients (7).

The distribution of patients with triple-negative breast cancer (TNBC) and hormone receptor-positive tumors (ER and/or PR positive) is approximately equal between the two study groups (intervention vs. control). The proportion of TNBC patients in the studied population is 20.8%. This proportion aligns with the expected occurrence of TNBCs in this study. The slightly higher percentage and the younger age of the population may be influenced by the nature of the study center. Patients with TNBC are often younger, more willing to travel longer distances to a specialized center and are frequently enrolled in clinical trials. Patients with TNBC have a high psycho-oncological support need because achieving a non-PCR (Pathological Complete Remission) is more common compared to other types of breast cancer. Consequently, treatment approaches often need to be escalated, leading to a longer duration of treatment. Additionally, TNBC is more frequently diagnosed in younger patients, and they often experience greater psychological distress due to their family situation. TNBC is also often associated with genetic factors, which can further increase the burden. Overall, the psychological impact of TNBC can be significant, requiring specialized support and care to address the emotional and mental well-being of patients facing this challenging form of breast cancer (7, 32–34).

The primary endpoint of psychological distress was measured using the validated PHQ-9 questionnaire. The PHQ-9 questionnaire is a commonly used tool for assessing depressive symptoms. It consists of nine questions based on the nine diagnostic criteria for a depressive disorder according to the Diagnostic and Statistical Manual of Mental Disorders (DSM-5) (31).

In the overall full analysis set (FAS) population, a reduction of -1.5 score points (least squares estimate difference between IG and CG -1.52; 95% confidence interval (CI) [–1,91, –1,07] in the PHQ-9 was observed in the intervention group. The estimates are based on a mixed model for repeated measurements with group assignment (intervention group versus control group), measurement time, the interaction of group * time, baseline PHQ9 score, and the stratification variable "Therapy/aftercare." The patient was included as a random effect in the model. Baseline is defined as time point T0. The least squares mean differences between the intervention and control groups were reported. This corresponds to a significant and clinically meaningful reduction ($p<0.001$) compared to the control group.

In the control group, there was no change in the PHQ-9 from baseline to T3. A reduction of 1.5 points in the PHQ-9 score can be interpreted as a slight improvement in depressive symptoms. It is important to note that the clinical relevance of such a change can vary individually and depends on other factors, such as the severity of baseline symptoms, individual patient perception, and daily functioning. In the intervention group, at baseline, 61 out of 170 patients, or 36%, had a PHQ-9 score above 10, indicating moderate to severe depression (31–33).

In clinical studies or research work, statistical methods such as effect estimations from mixed models can be used to assess the clinical relevance of observed changes. In the FAS population, an effect size of 1.52 was found. A reduction of 1.5 points in the PHQ-9 score and an estimated effect size of 1.52 of the mixed model can be considered as a moderate effect size. This result is further supported by the calculated effect size according to Cohen, which is d=0.5 for the entire cohort.

Other studies, even with other DiGAs with psychological endpoints, show similar results in sumscore reduction and cohen´s d (35–37). However, the clinical significance should always be considered in the context of the individual situation and the overall symptomatology. Patients often subjectively perceive the improvement in their mental well-being as highly relevant (9, 10, 33).

Studies that have examined the PHQ-9 questionnaire in breast cancer patients, the extent of depressive symptoms, and the relationship between breast cancer and mental health have provided two important insights: breast cancer patients have an increased prevalence of depression. Studies have shown that breast cancer patients may have an increased risk of experiencing depressive symptoms and depression. The prevalence varies depending on the study, but some studies report rates as high as 40% (compared to 36% in the population).

Furthermore, there is a correlation between psychological distress and different treatment phases as well as the age of breast cancer patients. Various treatment phases such as diagnosis, surgery, chemotherapy, or aftercare care can be associated with an increased risk of depressive symptoms in breast cancer patients.

The data from this study show a higher baseline value of PHQ-9 in the subgroup receiving chemotherapy, as well as a larger reduction over the 12-week period. In comparison, the control group showed no change in the PHQ-9. The subgroup without chemotherapy, however, had a lower baseline value and a slightly smaller delta over 12 weeks. Nevertheless, the data from both subgroups were significant ($p<0.001$) when compared between intervention and control. From a clinical perspective, these results are expected because chemotherapy for the treatment of breast cancer can cause various psychological side effects. These effects can vary individually and depend on several factors such as the type of chemotherapy, dosage, individual tolerability, the patient's psychological condition before treatment, as well as the fact that chemotherapy is indicated – which can trigger anxiety and concerns. However, the data also show that patients who did not receive chemotherapy still experience a similar level of psychological distress as patients who underwent chemotherapy. A cancer diagnosis itself, regardless of the stage and tumor biological characteristics, can profoundly impact one's life.

The intervention with PINK! Coach had significant effects on both groups, which are clinically meaningful. The correct clinical interpretation of alterations on a numerical scale should take into account not just statistical significance but also whether the observed change holds significance for patients. Equivalent changes on a numerical scale might carry distinct clinical importance in various patient populations, such as those differing in age, disease severity, or injury type. Additionally, statistical significance is intertwined with the sample size.

To assess the clinical relevance of the determined results, an attempt was made to determine the Minimal Clinically Important Difference (MCID) in addition to calculating effect sizes using Cohen's method. The Minimal Clinically Important Difference of the PHQ-9 has not yet been determined for a cohort of breast cancer patients. There are no publications on this topic in the known databases. However, there are publications on the MCID of the PHQ-9 in other patient cohorts with different diagnoses. For determining clinical relevance there is currently no established methodological approach. Additionally, there are currently no comparative data from other publications that have investigated the same population with a comparable intervention. Consequently, more research is needed to contextualize the collected data.

In recent years, research has focused on the development of personalized treatment concepts. Therapeutic decisions are mainly based on molecular and histological characteristics of the tumor. The primary goal is to find optimal treatment pathways or tailor treatments specifically to early breast cancer patients (EBC), taking into account long-term toxic side effects and improving quality of life. This has led to a significant de-escalation of therapy and a lower rate of chemotherapy being performed, as observed in the studied population. However, the data also confirm that even without chemotherapy, breast cancer patients experience a high level of psychological distress (38).

Both EBC and MBC patients experience psychological and social distress after diagnosis, during treatment, and in the follow-up period one year after diagnosis. This was confirmed by the data available. The ongoing follow-up (at 6 and 12 months) will provide a more detailed insight.

Another subgroup analysis of the population, divided into "therapy" and "aftercare," reveals similar results. The subgroup "intervention therapy" shows a delta of -1.5 from baseline to T3, which corresponds to a relative reduction of 18.3% compared to baseline. The baseline value is consistent with that of the entire population. The "control group therapy" has a lower baseline value and a delta of 0.3 from baseline to T3, indicating a slight increase in psychological distress. The "intervention aftercare" group shows a delta of -2.1, corresponding to a relative reduction of 34.6% from baseline to T3. For comparison, a two-year treatment with the medication Abemaciclib in patients with hormone receptor-positive high-risk early-stage carcinoma results in a relative risk reduction of 35% in terms of invasive recurrence or distant metastasis - which is generally considered a clinically significant effect. However, comprehensive therapy includes not only efficacy in treating the tumor but also physical and psychological well-being.

The baseline value is lower than that of the entire population. The "control group aftercare" also shows a slightly lower baseline value and a delta of -1.1 from baseline to T3. It was also observed that the intervention in both subgroups led to a significant reduction in psychological distress compared to the control group. These results indicate that the intensity of psychological distress is highly individual but can still be reduced through clinically significant interventions.

The study has reached its primary endpoint after 12 weeks of intervention. The comparison between study groups in the overall population and subgroups are significant. The studied population is comparable to the entire population of breast cancer patients, indicating that PINK! Coach helps all affected individuals in terms of psychological distress. The study data suggests that PINK! Coach can be established as a routine component of breast cancer care and is also accepted by the patients as part of their therapy and/or aftercare.

PINK! Coach is structured in a multimodal manner and provides patients with personalized content based on their information regarding therapy, tumor biology, age, and personal situation. Patients receive daily tasks aimed at sustainably improving their lifestyle regarding nutrition, physical activity and mental health. This

approach is designed to ensure ongoing motivation and empowerment. In terms of results, especially within subgroups, this personalization appears to help many patients in different situations to change their lifestyle. As the emergence of psychological distress is highly individual and complex, it is reasonable to assume that the reduction of this mental burden is also complex and attributable to various functions of the app.

Customization of content and coaching proves effective for all patients across diverse subgroups in a disease as heterogeneous as breast cancer. Educational content reduces fears and enhances self-management, empowering patients to actively participate in their therapy (27–29, 32, 33, 39). Nevertheless, more research is necessary to understand the exact mechanism of action of the app.

The data on dropouts from the study indicate that patients who discontinued their participation mainly did so because they were randomized into the control group but desired immediate use of the app. This highlights the high demand for low-threshold support options that can be easily integrated into daily life and routines. This suggests that the implementation of PINK! Coach in breast cancer care is a promising addition to therapy management and patient support.

Utilization of mobile health (mHealth) applications within clinical environments is increasing. mHealth apps have been employed to enhance preventive measures, enhance early detection, facilitate care management, and provide assistance to both survivors and individuals dealing with chronic conditions. Nevertheless, there exists a scarcity of comprehensive information regarding the effectiveness and practicality of these mHealth apps (40). Considering the increasing number of mHealth apps available to patients and their increasing use in breast cancer care, it is important to understand their effects. Different international studies (26) of the last years showed promising results in patient-doctor communication, therapy management, health-related quality of life, BMI reduction and increasing physical activity as well as stress reduction (41, 42). Nevertheless, there is a lack of compelling data regarding the advantages of mHealth in addressing persistent adverse psychological effects (43). Therefore, long-term data with breast cancer survivors are necessary to investigate whether the effects observed so far endure. To generate long-term data on the positive psychological effects of the PINK! app, a 1-year follow-up has been planned, which will provide insight into the extent to which the observed effects persist.

Nevertheless, mHealth applications hold substantial significance for both developed nations and emerging economies, offering an economical means to extend healthcare access and deliver health-related information on a broader scale (40). In Germany, the highest proportion of patients receiving psycho-oncological care are breast cancer patients (66.7%) (44). With the increasing number of cases and the rising demand for psycho-oncological support for breast cancer patients and survivors, the healthcare system is reaching its capacity limits. The resources at clinics are no longer sufficient to accommodate such a high number of patients requiring long-term psycho-oncological care. As a result, evidence-based mHealth apps aimed at reducing psychological distress also hold significant potential in Germany (22, 30, 45).

5 Conclusion

By personalizing its content, PINK! Coach empowers patients to positively influence their own lifestyle. The individual situation and needs of the patients are taken into account. This allows patients to set individual priorities and engage with aspects that are important to them, impacting their quality of life and mental well-being. The factors influencing the quality of life and mental health of patients in the context of breast cancer diagnosis and treatment are diverse. This is consistent with our observation that various subgroups experience significant benefits from using PINK! Coach.

Data availability statement

The raw data supporting the conclusions of this article will be made available by the authors, without undue reservation.

Ethics statement

The studies involving humans were approved by Medical Ethical Committee of the LMU University of Munich, Germany on 21.07.2022 (Reference number: 22-0498). The studies were conducted in accordance with the local legislation and institutional requirements. The participants provided their written informed consent to participate in this study.

Author contributions

JW: Conceptualization, Formal analysis, Methodology, Visualization, Writing – original draft, Writing – review & editing. SvS: Data curation, Project administration, Software, Writing – review & editing. PW: Conceptualization, Funding acquisition, Methodology, Resources, Supervision, Writing – review & editing. ML: Conceptualization, Investigation, Methodology, Writing – review & editing. CzE: Conceptualization, Data curation, Methodology, Validation, Writing – review & editing. MS: Conceptualization, Methodology, Validation, Writing – review & editing. FB: Conceptualization, Methodology, Writing – review & editing. StS: Conceptualization, Investigation, Writing – review & editing. SK: Investigation, Writing – review & editing. MT: Investigation, Writing – review & editing. JT: Investigation, Writing – review & editing. MB: Investigation, Writing – review & editing. HH: Investigation, Methodology, Writing – review & editing. AS: Project administration, Writing – review & editing. FH: Project administration, Writing – review & editing. NH: Conceptualization, Methodology, Supervision, Writing – review & editing. RW: Conceptualization, Formal analysis, Investigation, Methodology, Project administration, Supervision, Validation, Writing – review & editing, Writing – original draft.

Funding

The author(s) declare financial support was received for the research, authorship, and/or publication of this article. This study was funded by PINK! gegen Brustkrebs GmbH. The funder was not involved in the study design, collection, analysis, interpretation of data, the writing of this article, or the decision to submit it for publication.

Conflict of interest

Authors JW, SvS, PW, AS, and FH were employed by the company PINK!. Authors NH, MS, FB, and RW had a consulting contract with PINK!.

The remaining authors declare that the research was conducted in the absence of any commercial or financial relationships that could be construed as a potential conflict of interest.

Publisher's note

References

1. Tsaras K, Papathanasiou I, Mitsi D, Veneti A, Kelesi M, Zyga S, et al. Assessment of depression and anxiety in breast cancer patients: prevalence and associated factors. *Asian Pac J Cancer Prev APJCP*. (2018) 19:1661–9. doi: 10.22034/APJCP.2018.19.6

2. Wang YH, Li JQ, Shi JF, Que JY, Liu JJLappin, et al. Depression and anxiety in relation to cancer incidence and mortality: a systematic review and meta-analysis of cohort studies. *Mol Psychiatry*. (2020) 25(7):1487–99. doi: 10.1038/s41380-019-0595-x

3. Groenvold M, Petersen MA, Idler E, Bjorner JB, Fayers PM, Mouridsen HT. Psychological distress and fatigue predicted recurrence and survival in primary breast cancer patients. *Breast Cancer Res Treat*. (2007) 105(2):209–19. doi: 10.1007/s10549-006-9447-x

4. Modi ND, Danell NO, Perry RNA, Abuhelwa AY, Rathod A, Badaoui S, et al. Patient-reported outcomes predict survival and adverse events following anticancer treatment initiation in advanced HER2-positive breast cancer. *ESMO Open*. (2022) 7:100475. doi: 10.1016/j.esmoop.2022.100475

5. Phoosuwan N, Lundberg PC. Psychological distress and health-related quality of life among women with breast cancer: a descriptive cross-sectional study. *Supportive Care Cancer*. (2022) 30(4):3177–86. doi: 10.1007/s00520-021-06763-z

6. Zhou K, Bellanger M, Le Lann S, Robert M, Frenel JS, Campone M. The predictive value of patient-reported outcomes on the impact of breast cancer treatment-related quality of life. *Front Oncol*. (2022) 12:925534. doi: 10.3389/fonc.2022.925534

7. Harbeck N, Gnant M. Breast cancer. *Lancet*. (2017) 389(10074):1134–50. doi: 10.1016/S0140-6736(16)31891-8

8. Voigt V, Neufeld F, Kaste J, Bühner M, Sckopke PWuerstlein, et al. Clinically assessed posttraumatic stress in patients with breast cancer during the first year after diagnosis in the prospective, longitudinal, controlled COGNICARES study. *Psychooncology*. (2017) 26(1):74–80. doi: 10.1002/pon.4102

9. Cillessen L, Johannsen M, Speckens AEM, Zachariae R. Mindfulness - based interventions for psychological and physical health outcomes in cancer patients and survivors: a systematic review and meta-analysis of randomized controlled trials. *Psychooncology*. (2019) 28(12):2257–69. doi: 10.1002/pon.5214

10. Matis J, Svetlak M, Slezackova A, Svoboda M, Sumec R. Mindfulness-based programs for cancer patients via eHealth and mHealth: a systematic review and synthesis of quantitative research (preprint) J. *Med Internet Res*. (2020) 22(11): e20709. doi: 10.2196/20709

11. Nissen ER, O'Connor M, Kaldo V, Højris I, Borre M, Zachariae R, et al. Internet-delivered mindfulness-based cognitive therapy for anxiety and depression in cancer survivors: a randomized controlled trial. *Psychooncology*. (2020) 29(1):68–75. doi: 10.1002/pon.5237

12. Piet J, Würtzen H, Zachariae R. The effect of mindfulness-based therapy on symptoms of anxiety and depression in adult cancer patients and survivors: a systematic review and Meta-analysis. *J Consult Clin Psychol*. (2012) 80(6):1007–20. doi: 10.1037/a0028329

13. Drewes C, Kirkovits T, Schiltz D, Schinkoethe T, Haidinger R, Goldmann-Posch U, et al. EHealth acceptance and new media preferences for therapy assistance among breast cancer patients. *JMIR Cancer*. (2016) 2(2):e13. doi: 10.2196/cancer.5711

14. Wolff J, Harbeck N, König A, Ehrl B, Smollich M, Baumann F, et al. Pilotstudie zur App-basierten Therapiebegleitung mit der PINK! App von Brustkrebspatientinnen zur Reduktion der psychischen Belastung und Verbesserung der Lebensqualität. *Senologie*. (2022) 19:43–44. doi: 10.1055/s-0042-1748454

15. McGregor BA, Antoni MH. Psychological intervention and health outcomes among women treated for breast cancer: a review of stress pathways and biological mediators. *Brain Behav Immun*. (2009) 23:159–66. doi: 10.1016/j.bbi.2008.08.002

16. Carlson LE, Speca M, Patel KD, Goodey E. Mindfulness-based stress reduction in relation to quality of life, mood, symptoms of stress, and immune parameters in breast and prostate cancer outpatients. *Psychosomatic Med vol*. (2003) 65:4. doi: 10.1097/01.psy.0000074003.35911.41

17. Black DS, Slavich GM. Mindfulness meditation and the immune system: a systematic review of randomized controlled trials. *Ann New York Acad Sci*. (2016) 1373:13–24. doi: 10.1111/nyas.12998

18. Luecken LJ, Compas BE. Stress, coping, and immune function in breast cancer. *Ann Behav Med*. (2002) 24:336–44. doi: 10.1207/S15324796ABM2404_10

19. Anbari AB, Wanchai A, Graves R. Breast cancer survivorship in rural settings: a systematic review. *Supportive Care Cancer*. (2020) 28:3517–31. doi: 10.1007/s00520-020-05308-0

20. Afshar N, English DR, Milne RL. Rural-urban residence and cancer survival in high-income countries: A systematic review. *Cancer*. (2019) 125(13):2172–84. doi: 10.1002/cncr.32073

21. Hashemi SM, Rafiemanesh H, Aghamohammadi T, Badakhsh M, Amirshahi M, Sari M, et al. Prevalence of anxiety among breast cancer patients: a systematic review and meta-analysis. *Breast Cancer*. (2020) 27(2):166–78. doi: 10.1007/s12282-019-01031-9

22. Doyle-Lindrud S. State of eHealth in Cancer Care: Review of the Benefits and Limitations of eHealth Tools. *Clin J Oncol Nurs*. (2020) 24(3):10–5. doi: 10.1188/20.CJON.S1.10-15

23. De Cicco P, Catani MV, Gasperi V, Sibilano M, Quaglietta M, Savini I. Nutrition and breast cancer: A literature review on prevention, treatment and recurrence. *Nutrients*. (2019) 11(7):1514. doi: 10.3390/nu11071514

24. Friedenreich CM, Morielli AR, Lategan I, Ryder-Burbidge C, Yang L. Physical activity and breast cancer survival-epidemiologic evidence and potential biologic mechanisms. *Curr Nutr Rep*. (2022) 11:717–41. doi: 10.1007/s13668-022-00431-2

25. Aguiñaga S, Ehlers DK, Cosman J, Severson J, Kramer AF, McAuley E. Effects of physical activity on psychological well-being outcomes in breast cancer survivors from prediagnosis to posttreatment survivorship. *Psychooncology*. (2018) 27(8):1987–94. doi: 10.1002/pon.4755

26. Harbeck N, Fasching PA, Wuerstlein R, Degenhardt T, Lüftner D, Kates RE, et al. Significantly longer time to deterioration of quality of life due to CANKADO PRO-React eHealth support in HR+ HER2- metastatic breast cancer patients receiving palbociclib and endocrine therapy: primary outcome analysis of the multicenter randomized AGO-B WSG PreCycle trial. *Ann Oncol*. (2023) 34:660–9. doi: 10.1016/j.annonc.2023.05.003

27. Kapoor A, Nambisan P, Baker E. Mobile applications for breast cancer survivorship and self-management: A systematic review. *Health Inf J*. (2020) 26:2892–905. doi: 10.1177/1460458220950853

28. Yang S, Bui CN, Park K. Mobile health apps for breast cancer: content analysis and quality assessment. *JMIR mHealth uHealth*. (2023) 11:e43522. doi: 10.2196/43522

29. Rincon E, Monteiro-Guerra F, Rivera-Romero O, Dorronzoro-Zubiete E, Sanchez-Bocanegra CL, et al. Mobile phone apps for quality of life and well-being assessment in breast and prostate cancer patients: systematic review. *JMIR mHealth uHealth*. (2017) 5:e187. doi: 10.2196/mhealth.8741

30. Uncovska M, Freitag B, Meister S, Fehring L. Patient acceptance of prescribed and fully reimbursed mHealth apps in Germany: an UTAUT2-based online survey study. *J Med Syst*. (2023) 47:14. doi: 10.1007/s10916-023-01910-x

31. Kroenke K, Spitzer RL, Williams JB. The PHQ-9: validity of a brief depression severity measure. *J Gen Intern Med*. (2001) 16:606–13. doi: 10.1046/j.1525-1497.2001.016009606.x

32. Naik H, Leung B, Laskin J, McDonald M, Srikanthan A, Wu J, et al. Emotional distress and psychosocial needs in patients with breast cancer in British Columbia: younger versus older adults. *Breast Cancer Res Treat*. (2020) 179:471–7. doi: 10.1007/s10549-019-05468-6

33. Campbell-Enns H, Woodgate R. The psychosocial experiences of women with breast cancer across the lifespan: a systematic review protocol. *JBI Database System Rev Implement Rep*. (2015) 13:112–21. doi: 10.11124/jbisrir-2015-1795

34. Hass HG, Seywald M, Wöckel A, Muco B, Tanriverdi M, Stepien J. Psychological distress in breast cancer patients during oncological inpatient rehabilitation: incidence, triggering factors and correlation with treatment-induced side effects. *Arch Gynecol Obstet vol*. (2023) 307:919–25. doi: 10.1007/s00404-022-06657-3

35. Koevoets EW, Schagen SB, de Ruiter MB, Geerlings MI, Witlox L, van der Wall E, et al. Effect of physical exercise on cognitive function after chemotherapy in patients with breast cancer: a randomized controlled trial (PAM study). *Breast Cancer Res: BCR*. (2022) 24:36. doi: 10.1186/s13058-022-01530-2

36. Chow PI, Showalter SL, Gerber M, Kennedy EM, Brenin D, Mohr D, et al. Use of mental health apps by patients with breast cancer in the United States: pilot pre-post study. *JMIR Cancer*. (2020) 6:e16476. doi: 10.2196/16476

37. Shao D, Zhang H, Cui N, Sun J, Li J, Cao F. The efficacy and mechanisms of a guided self-help intervention based on mindfulness in patients with breast cancer: A randomized controlled trial. *Cancer vol*. (2021) 127:1377–86. doi: 10.1002/cncr.33381

38. Gram EG, Manso TFR, Heleno B, Siersma V, Rogvi J, Brandt Brodersen J. The long-term psychosocial consequences of screen-detected ductal carcinoma in situ and invasive breast cancer. *Breast*. (2023) 70:41–8. doi: 10.1016/j.breast.2023.06.003

39. Voigt V, Neufeld F, Kaste J, Bühner M, Sckopke P. Wuerstlein R Clinically assessed posttraumatic stress in patients with breast cancer during the first year after diagnosis in the prospective, longitudinal, controlled COGNICARES study. *Psychooncology*. (2017) 26:74–80. doi: 10.1002/pon.4102

40. Jongerius C, Russo S, Mazzocco K, Pravettoni G. Research-tested mobile apps for breast cancer care: systematic review. *JMIR mHealth uHealth*. (2019) 7:e10930. doi: 10.2196/10930

41. Davis S, Oakley-Girvan I. mHealth education applications along the cancer continuum. *J Cancer Educ*. (2015) 30:388–94. doi: 10.1007/s13187-014-0761-4

42. Bender JL, Yue RYK, To MJ, Deacken L, Jadad AR. A lot of action, but not in the right direction: systematic review and content analysis of smartphone applications for the prevention, detection, and management of cancer. *J Med Internet Res*. (2013) 15: e287. doi: 10.2196/jmir.2661

43. Pope Z, Lee J, Zeng N, Lee H, Gao Z. Feasibility of smartphone application and social media intervention on breast cancer survivors' health outcomes. *Transl Behav Med*. (2018) 9(1):11–22. doi: 10.1093/tbm/iby002

44. Singer S, Dieng S, Wesselmann S. Psycho-oncological care in certified cancer centres–a nationwide analysis in Germany. *Psycho-oncology*. (2013) 22:1435–7. doi: 10.1002/pon.3145

45. Bergelt C, Schölermann C, Hahn I, Weis J, Koch U. Psychoonkologische Versorgung von Brustkrebspatientinnen im Krankenhaus und im ambulanten Sektor" [Psychooncological care for breast cancer patients in hospitals and in the outpatient sector]. *Gesundheitswesen (Bundesverband der Arzte Des Offentlichen Gesundheitsdienstes (Germany))*. (2010) 72:700–6. doi: 10.1055/s-0029-1242771

frontiers | Frontiers in Oncology

TYPE Original Research
PUBLISHED 24 April 2024
DOI 10.3389/fonc.2024.1222698

OPEN ACCESS

EDITED BY
Anika Nagelkerke,
University of Groningen, Netherlands

REVIEWED BY
Xiaohui Liu,
Dalian Medical University, China
Francesco Salvatore,
University of Naples Federico II, Italy

*CORRESPONDENCE
Emma Bolderson
emma.bolderson@qut.edu.au

RECEIVED 15 May 2023
ACCEPTED 28 February 2024
PUBLISHED 24 April 2024

CITATION
Rose M, Burgess JT, Cheong CM, Adams MN, Shahrouzi P, O'Byrne KJ, Richard DJ and Bolderson E (2024) The expression and role of the Lem-D proteins Ankle2, Emerin, Lemd2, and TMPO in triple-negative breast cancer cell growth.
Front. Oncol. 14:1222698.
doi: 10.3389/fonc.2024.1222698

The expression and role of the Lem-D proteins Ankle2, Emerin, Lemd2, and TMPO in triple-negative breast cancer cell growth

Maddison Rose[1], Joshua T. Burgess[1], Chee Man Cheong[1], Mark N. Adams[1], Parastoo Shahrouzi[2], Kenneth J. O'Byrne[1,3], Derek J. Richard[1] and Emma Bolderson[1]*

[1]Cancer and Ageing Research Program, Centre for Genomics and Personalised Health, School of Biomedical Sciences, Translational Research Institute, Queensland University of Technology, Brisbane, QLD, Australia, [2]Department of Medical Genetics, Faculty of Medicine, Institute of Basic Medical Sciences, University of Oslo, Oslo, Norway, [3]Cancer Services, Princess Alexandra Hospital, Brisbane, QLD, Australia

Background: Triple-negative breast cancer (TNBC) is a sub-classification of breast carcinomas, which leads to poor survival outcomes for patients. TNBCs do not possess the hormone receptors that are frequently targeted as a therapeutic in other cancer subtypes and, therefore, chemotherapy remains the standard treatment for TNBC. Nuclear envelope proteins are frequently dysregulated in cancer cells, supporting their potential as novel cancer therapy targets. The Lem-domain (Lem-D) (LAP2, Emerin, MAN1 domain, and Lem-D) proteins are a family of inner nuclear membrane proteins, which share a ~45-residue Lem-D. The Lem-D proteins, including Ankle2, Lemd2, TMPO, and Emerin, have been shown to be associated with many of the hallmarks of cancer. This study aimed to define the association between the Lem-D proteins and TNBC and determine whether these proteins could be promising therapeutic targets.

Methods: GENT2, TCGA, and KM plotter were utilized to investigate the expression and prognostic implications of several Lem-D proteins: Ankle2, TMPO, Emerin, and Lemd2 in publicly available breast cancer patient data. Immunoblotting and immunofluorescent analysis of immortalized non-cancerous breast cells and a panel of TNBC cells were utilized to establish whether protein expression of the Lem-D proteins was significantly altered in TNBC. SiRNA was used to decrease individual Lem-D protein expression, and functional assays, including proliferation assays and apoptosis assays, were conducted.

Results: The Lem-D proteins were generally overexpressed in TNBC patient samples at the mRNA level and showed variable expression at the protein level in TNBC cell lysates. Similarly, protein levels were generally negatively correlated with patient survival outcomes. siRNA-mediated depletion of the individual Lem-D proteins in TNBC cells induced aberrant nuclear morphology, decreased proliferation, and induced cell death. However, minimal effects on nuclear morphology or cell viability were observed following Lem-D depletion in non-cancerous MCF10A cells.

Conclusion: There is evidence to suggest that Ankle2, TMPO, Emerin, and Lemd2 expressions are correlated with breast cancer patient outcomes, but larger patient sample numbers are required to confirm this. siRNA-mediated depletion of these proteins was shown to specifically impair TNBC cell growth, suggesting that the Lem-D proteins may be a specific anti-cancer target.

KEYWORDS

triple negative breast cancer, cancer therapy, Lem-domain proteins, nuclear envelope, inner nuclear membrane

1 Introduction

Triple-negative breast cancers (TNBCs) are a subcategory of breast carcinomas that do not overexpress the human epidermal growth factor receptor 2 (HER2) and lack expression of the estrogen (ER) and progesterone (PR) receptors (1). TNBC is of interest within the scientific community due to the evident discrepancy between survival outcomes for TNBC patients and other breast cancer subtypes.

Specifically, TNBC tumors have been shown to have a significantly earlier and higher rate of recurrence, with recurrence rates peaking at 1–3 years post-therapy (2). The burden of TNBC is emphasized by low 5-year survival rates being 16%, compared with non-TNBC subtypes (3). Despite substantial advances in targeted and personalized cancer therapeutics, chemotherapeutics and surgery remain the primary treatment modalities for TNBC patients due to the lack of hormone receptors on this tumor type (4). Disease reoccurrence, distant metastatic lesions, and acquired resistance are common for TNBC tumors. Therefore, there is evident need for the exploration of novel therapeutic approaches for TNBC to improve patient outcomes.

The nuclear envelope (NE) is a double lipid membrane, originally defined for its role in physically separating the nucleus and cytoplasm within eukaryotic cells (5). This double lipid membrane can be further subcategorized as the inner nuclear membrane (INM) and outer nuclear membrane. There is substantial literature demonstrating that the INM proteins are required to maintain cellular functioning. Dysregulation or mutations of these proteins have been shown to be involved in disease pathophysiology, including cancer and progeria syndromes (4, 6–8).

The INM is host to several proteins, including the Lem (LAP2, Emerin, MAN1 domain, and Lem-D) domain proteins, which share a ~45-residue Lem-domain (Lem-D) that binds to and interacts with the INM protein, Banf1 (9–12). The Lem-D proteins can be further categorized into numerical groups (Groups I–III) based on their membrane topology. Group I proteins, Emerin, Lap2β, Lemd1, and Lap2α, possess nucleoplasmic domains, and a transmembrane domain, except for Lap2α (10–12). Group II proteins, MAN1 and Lemd2, have two transmembrane domains and a winged helix DNA-binding MSC domain (9, 13, 14). Finally, Group III proteins are functionally diverse from the other subgroups, Ankle2 includes an endoplasmic reticulum transmembrane domain and Ankle1 undergoes nucleo-cytoplasmic shuttling (15, 16). Given the Lem-D proteins have broad membrane topology, it is conceivable that this translates to diverse roles in tumorigenesis (13). Collectively, these Lem-D proteins have been shown to participate in each of the hallmarks of cancer: aberrant cell cycle progression, cell migration and invasion, aberrant mitosis, dysregulated DNA repair mechanisms, upregulated proliferation, and dysregulated cell signaling (14–17). Expression of several Lem-D proteins is known to be altered in numerous cancer models, including breast cancer, further supporting a role of the Lem-D proteins in TNBC tumorigenesis (17–20).

Here, we investigate the role of several Lem-D proteins, Ankle2, Emerin, TMPO, and Lemd2, in TNBC tumorigenesis, establishing that depletion of several INM proteins has anti-proliferative effects and induces apoptosis on TNBC cells, supporting the assertion that targeting the Lem-D proteins may be an efficacious strategy to treat TNBC.

2 Methodology and materials

2.1 Reagents

All chemical reagents were purchased from Sigma-Aldrich (Sigma-Aldrich, Saint Louis, MO, USA), unless otherwise stated.

2.2 Antibodies

Antibodies used were as follows: anti-Emerin (5430, Cell Signaling Technology, Danvers, MA, USA 1:500 for IF, 1:1000 for IB), anti-Lemd2 (PA553589, Thermo Fisher Scientific, Waltham MA, USA 1:300 for IF, 1:1000 for IB), anti-Ankle2 (GTX120698, Genetex, Irvine, CA, United States 1:200 for IF, 1:1000 for IB), and anti-TMPO (L3414-.2ML, Sigma-Aldrich, Saint Louis, MO 1:500 for IF, 1:1000 for IB), anti-GAPDH (glyceraldehyde-3-phosphate dehydrogenase) (D16H11, Cell Signaling Technology, 1:4000 for IB), and anti–Gamma-Tubulin (T6557, Sigma-Aldrich, 1:3000 for

IB). Fluorescent secondary antibodies used were Alexa Fluor 488 (Cat# A32766, Molecular Probes, Thermo Fisher Scientific 1:200 for IF) and 594 (Cat# A32754, Molecular Probes, Thermo Fisher Scientific, 1:200 for IF), IRDye® 800CW Donkey anti-Mouse IgG Secondary Antibody (926-32212, LiCor Bioscience, Lincoln, NE, USA), and IRDye® 680RD Donkey anti-Rabbit IgG Secondary Antibody (926-68073, LiCor Bioscience).

2.3 Cell culture

BT549, Hs578T, MDA-MB-231, and MDA-MB-468 cells were utilized as representative TNBC cells. MCF10A cells were used as a non-malignant, breast tissue–derived control. BT549 and Hs578T cells were cultured in RPMI (Thermo Fisher Scientific), and MDA-MB-231 and MDA-MB-468 cells were cultured in DMEM (Thermo Fisher Scientific). All cell lines were obtained from the American Type Culture Collection (ATCC) (Manassas, VA, USA). All cell lines were supplemented with 10% fetal bovine serum (FBS) (Thermo Fisher Scientific). MCF10A cells were maintained in DMEM/F12, supplemented with 20% FBS, 100 ng/mL Cholera Toxin (Sigma-Aldrich) 20ng/mL EGF and 0.01 mg/mL Insulin (Sigma-Aldrich). All cells were cultured at 37°C in an atmosphere of 5% CO_2.

2.4 siRNA transfections

Control (4390843) and INM silencer select siRNAs [Ankle2 (s23124), TMPO (s24159), Emerin (s2245840), and Lemd2 (s48070) siRNAs] were purchased from Thermo Fisher Scientific. RNAiMax (Invitrogen, Waltham, MA, USA) was used to transfect siRNA, as per manufacturer guidelines.

2.5 Immunoblotting

Cells were lysed (lysis buffer: 20 mM HEPES pH 7.5, 250 mM KCl, 5% glycerol, 10 mM MgCl2, 0.5% Triton X-100, protease/phosphatase inhibitor cocktail (Thermo Fisher Scientific), sonicated and cleared by centrifugation. Fifteen microgram of protein was separated on a 4%–12% BIS-TRIS gel (Invitrogen) prior transfer to nitrocellulose membrane. Following transfer the membrane was blocked in Intercept Blocking Buffer (LiCor Bioscience) for 30 min at room temperature. Immunoblotting was carried out with the indicated antibodies (see above for antibody details), incubated with the indicated primary antibodies for 1h at room temperature in phosphate-buffered saline solution (PBS-T), washed 3 times in PBS-T, prior to 1h room temperature incubation in Alexa-conjugated secondary antibodies in PBS-T and washed 3 times in PBS-T at room temperature. Anti-GAPDH or γ-tubulin antibodies were used as a loading control. Immunoblots were imaged using an Odyssey infrared imaging system (LiCor Bioscience).

2.6 Immunofluorescent microscopy

Immunofluorescence was performed as previously (21). Briefly, 5,000 cells/well were seeded in a 96-well plate and allowed to adhere for 24h. Cells were pre-treated with extraction buffer for 5 min to visualize chromatin bound protein, prior to fixation in 4% paraformaldehyde for 20 min at room temperature. Cells were permeabilized for 5 min in 0.2% Triton X-100/PBS prior to blocking for 30 min in 3% bovine serum albumin/PBS. Subsequently, cells were incubated in indicated primary antibodies for 1h at room temperature in PBS, washed 3 times in PBS, prior to 1h room temperature incubation in Alexa-conjugated secondary antibodies in PBS. Cells were then counter-stained in Hoechst 33342 in PBS (1μg/mL) for 5 min at room temperature, washed 3 times in PBS and imaged on a DeltaVision pDV deconvolution microscope with 100×/1.42 oil objective (Applied Precision Inc, Issaquah, WA, USA). ImageJ was utilized to assemble images. High-throughput imaging was performed using the IN Cell Analyzer 6500 Imaging System (GE HealthCare Life Sciences, Arlington Heights, IL, USA). Nuclear, cytoplasmic, and cellular staining intensity was analyzed using the IN Cell Investigator software (GE HealthCare Life Sciences) with a minimum of 200 nuclei quantified/per condition.

2.7 Nuclear envelope localization and morphology quantification

Immunofluorescent staining and imaging were conducted as above. Localization and quantification were performed as previously described (12). Briefly, a minimum of 200 cells/condition were manually determined to have Lem-D proteins localized/not localized to the NE and for their "nuclear roundness" using the nuclear form factor function (form factor = $\frac{4\times\pi\times area}{perimeter^2}$) within the IN Cell Investigator software (GE HealthCare Life Sciences) suite. Nuclear form factor is also defined as the measure of nuclear circularity or as the nuclear contour ratio; this measurement was deemed the most suitable measurement of nuclear circularity as existing literature demonstrates that it reflects the extent of abnormality in multi-lobed nuclei more accurately than other measurements, including solidity or eccentricity (22, 23). As a secondary technique, nuclear roundness was assayed by manually determining cells to have normal/abnormal nuclear morphology.

2.8 Proliferation assay

Seventy-two hours following transfection, 500/cells per well were seeded at sub-confluence into a 96-well plate and allowed to adhere for 24h. Following adhesion, the 96-well plate was placed into an Incucyte S3 Live Cell Imaging System (Essen Bioscience, Ann Arbor, MI, USA) and an unlabeled cellular confluence assay was utilized to determine proliferation rate over a 5-day period. Proliferation curves are representative of results and area under the curve (AUC) graphs represent the mean and S.D. of three independent experiments.

2.9 Apoptosis assay

Cell death was quantified using an Annexin V-FITC apoptosis kit (ALX-850-020-KI02, Enzo Life Sciences, Farmingdale, NY, USA). Five days post-transfection, cells were enzymatically lifted and media containing floating cells was collected. Cells were then resuspended at 1×10^6 cells/mL in 488-conjugated anti-annexin (1:40), containing binding buffer. Cells were incubated for 20 min at room temperature and stained with propidium iodide (1 mg/mL). Cells were assayed using a CytoFLEX Flow Cytometer (Beckman Coulter Life Sciences, Indianapolis, IN, USA), and data were analyzed using FlowJo analysis software.

2.10 Bioinformatics and statistical analysis

Data from the GENT2 database (http://gent2.appex.kr/gent2/) were used to assess Lem-D protein transcript levels across breast cancer stages and histologies compared to surrounding healthy tissue (24). Box plots show median expression levels for each gene of interest with interquartile ranges and notches show the 95% confidence intervals. Significance levels were determined by unpaired Mann–Whitney U tests. Data extracted from the GENT2 database included breast cancer and non-cancerous breast tissues from 72 publicly available datasets (Ankle2: 4293 cancer samples and 92 non-cancerous samples).

Plot functions within the cBioPortal for Cancer Genomics (https://www.cbioportal.org/) were utilized to analyze potential correlations between mRNA expression of genes of interest (n = 312, four Grade I, 38 Grade II, and 270 Grade III samples) based on TNBC tumor grade. Raw TCGA data were obtained via the cBioPortal for Cancer Genomics and compiled in Graph Pad Prism 9.0 and one-way analyses of variance (ANOVAs) were utilized to establish statistical significance.

Kaplan–Meier Plotter database (http://kmplot.com/analysis/index.php?p=service) was used to perform survival analysis for all breast cancer samples based on Lem-D protein mRNA and protein expression levels as described (25). Expression was categorized as high- or low-expressed based on the median mRNA expression within the database. For mRNA analysis, sample sizes were as follows: Lemd2 (Geneprobe set – 2224980, n = 943, low expression = 470, high expression = 473), TMPO (Geneprobe set – 203432, n = 1879, low expression = 940, high expression = 939), Ankle2, (Geneprobe set – 212200, n = 1879, low expression = 947, high expression = 932), and Emerin (Geneprobe set – 209477, n = 1887, low expression = 944, high expression = 935). For protein analysis, the Tang dataset was utilized to analyze the correlation between Lemd2 and TMPO expression and OS (n = 126), and the Liu dataset was used to analyze the correlation between Ankle2 and Emerin expression and OS (n = 65) (26, 27). A log-rank test and Cox proportional hazard analysis were used to determine the statistical significance of survival outcomes.

Unless otherwise stated, data are presented as mean values and error bars represent SD from three biologically independent experiments. Normality was assessed using the Shapiro–Wilk test in Graph Pad Prism. If normality test was passed, statistical analysis was performed using a two-tailed Student's t-test or one-way ANOVAs. If normality test failed, statistical analysis was performed using a Mann–Whitney U test or Kruskal–Wallis H test.

3 Results

3.1 Expression of the Lem-domain proteins in patient samples

To establish whether the expression of the Lem-D proteins was dysregulated in breast cancer, the mRNA fold change of each Lem-D protein was analyzed using the GENT2 dataset (Figures 1A–D) (24). *Ankle2*, *TMPO*, *Emerin*, and *Lemd2* were significantly overexpressed in breast tumor samples, in comparison to adjacent normal tissue. However, for most of the transcripts investigated, the difference in expression was only a 0.1- to 0.3-fold change (Figures 1A–D). Furthermore, expression data for Grades I–III TNBC samples within the TCGA dataset were utilized to establish correlations between tumor stage and expression of Lem-D transcripts (Figures 1E–H). The only datasets that reached statistical significance were the difference in mRNA between Grades II and III TNBC carcinomas. No statistically significant difference was observed between Grades I and II or I and III tumors. Although, it should be noted that the datasets contain less than 10 samples, which could impact the overall significance of the results. Given this dataset did not include values for non-cancerous samples, we were unable to establish the difference in expression of the Lem-D proteins in each grade and non-cancerous tissue.

Kaplan–Meier plots were generated to investigate the level of correlation between Lem-D protein mRNA expression and overall survival (OS), defined as the time from diagnosis to death, in breast cancer patients. Plots were generated utilizing the mRNA genechip data available within the KM plotter online database (Figures 1I–L). Kaplan–Meier survival probabilities are generated at each datapoint based on the number of surviving patients, relative to the number of patients at risk. *TMPO* mRNA expression was negatively correlated with breast cancer patient OS (Figure 1J). *Ankle2* and *EMD* mRNA expressions were also negatively correlated with OS, however, were not statistically significance (Figures 1I, K). In contrast, *Lemd2* expression positively correlated with OS to a level that did not reach statistical significance (Figure 1L). Kaplan–Meier plots were also generated for protein-expression datasets; however, datasets available were of a small size (n = 65 for Ankle2 and Emerin and n = 126 for TMPO and Lemd2). From these datasets, protein expression of the Lem-D proteins showed a negative relationship with OS, reaching statistical significance for Ankle2, EMD, and Lemd2. However, statistical significance was not reached for the correlation between protein expression of TMPO and breast cancer patient OS (Supplementary Figure S1). Together, these analyses suggest that overexpression of the Lem-D proteins is generally associated with lower overall patient survival.

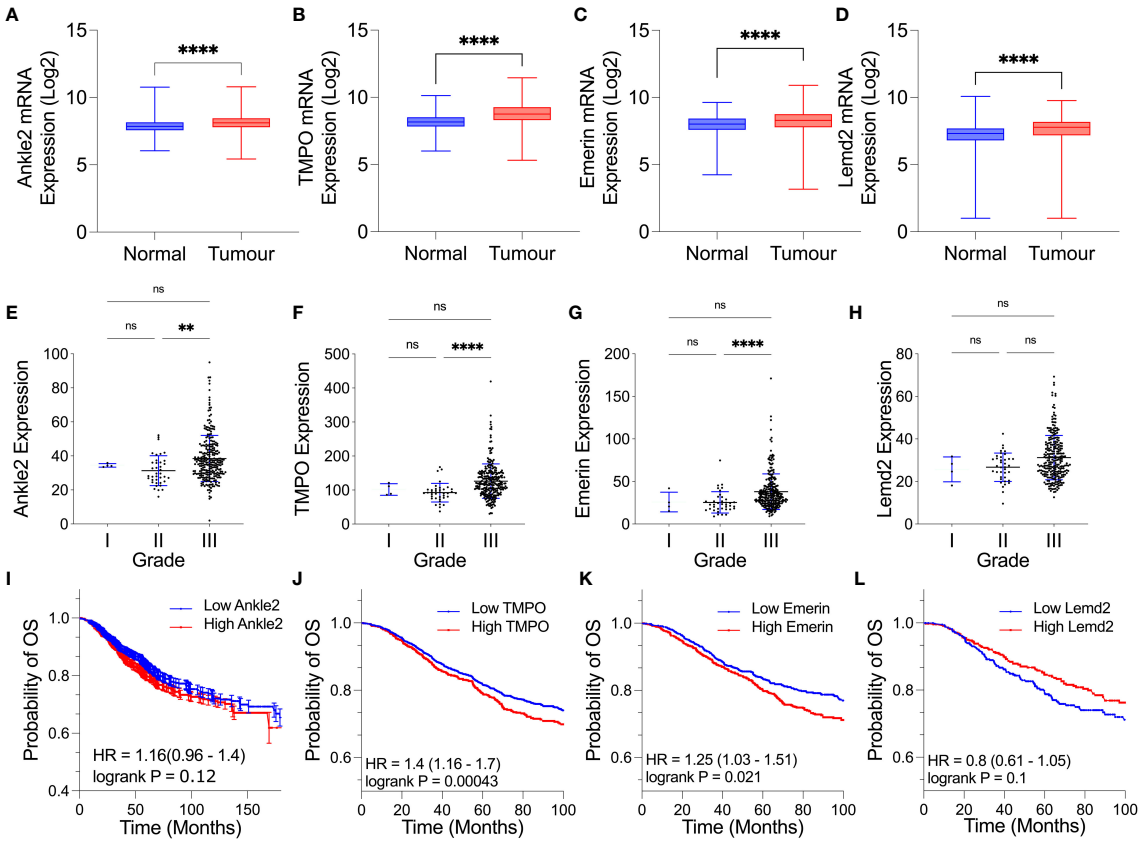

FIGURE 1
Expression of several Lem-D proteins is significantly elevated in TNBC tumor patient samples. **(A–D)** Box plots of Lem-D gene expression comparing normal and breast tumor patient samples utilizing the Gene Expression database of Normal and Tumor tissues 2 (GENT2) database: **(A)** Ankle2 expression, **(B)** TMPO expression, **(C)** Emerin expression, and **(D)** Lemd2 expression. **(E–H)** Graphical representation of expression of the Lem proteins in Stages I, II, and III TNBC patient samples utilizing The Cancer Genetics Atlas (TCGA) database: **(E)** Ankle2 **(F)** TMPO **(G)** Emerin, and **(H)** Lemd2 expressions. **(I–L)** Kaplan–Meier values for Lem-D gene expression in breast cancer patients showed that high mRNA expression of Lem-D genes was associated with a decrease in the probability of patient overall survival. Lem-D mRNA transcript expression was categorized as high or low expressed based on the median mRNA expression within the database. The effect of **(I)** Ankle2, **(J)** TMPO, **(K)** Emerin, and **(L)** Lemd2 mRNA expression on patient overall survival. For **(A–H)**: error bars denote standard deviation of the mean. Statistical significance was calculated using a Kruskal–Wallis test: ****$p < 0.0001$, **$p < 0.0021$. For **(I–L)**: statistical significance was calculated using a log-rank p-test. ns, not significant.

3.2 Expression and localization of the Lem-D proteins in TNBC cells

Given the Lem-D transcripts, *Ankle2*, *TMPO*, *Emerin*, and *Lemd2*, were overexpressed in breast cancer patient samples and overexpression largely associated with poorer patient outcomes, we next investigated whether the Lem-D proteins were similarly overexpressed in TNBC cell lines.

To investigate the expression of the Lem-D proteins in TNBC, immunoblotting was conducted in the representative TNBC cell lines: BT549, Hs578T, MDA-MB-231, and MDA-MB-468, in comparison to epithelial MCF10A cells as a non-cancerous breast tissue cell line. Ankle2 expression was significantly downregulated in the BT549 and Hs578T TNBC cell lines, in comparison to the non-cancerous MCF10A cells (Figures 2A, B). In contrast, Emerin was shown to be over-expressed in one out of four of the TNBC cells, in comparison to MCF10A cells, whereas there were no significant changes in LEMD2 protein levels (Figures 2A, C, D). There are three main isoforms of TMPO, and these were all detected by the TMPO antibody used in this study. While there were no significant changes in TMPOα or β protein levels, TMPOγ was shown to be significantly increased in all four TNBC cell lines tested (Figures 2A, E–G).

Mislocalization of proteins is a well-recognized characteristic of tumor cells (28). Therefore, we next investigated whether localization of the Lem-D proteins was maintained in TNBC cells. Immunofluorescent microscopy of TNBC cells demonstrated that localization of the Lem-D proteins was largely consistent with that of non-cancerous MCF10A cells (Figure 3; Supplementary Figure S2). Across all tumorigenic cell lines, Emerin and TMPO staining maintained clear NE localization, with some nuclear staining, in TNBC and MCF10A cells. Ankle2 staining was predominately NE localized, with minor cytoplasmic staining, likely attributed to endoplasmic reticulum localized Ankle2 (29). Similarly, Lemd2 predominately localized to the NE, with evident cytoplasmic staining in TNBC and MCF10A cells. There was minimal variation between the percent of TNBC and MCF10A cells where the Lem-D proteins did not localize to the NE (Figures 3B–E).

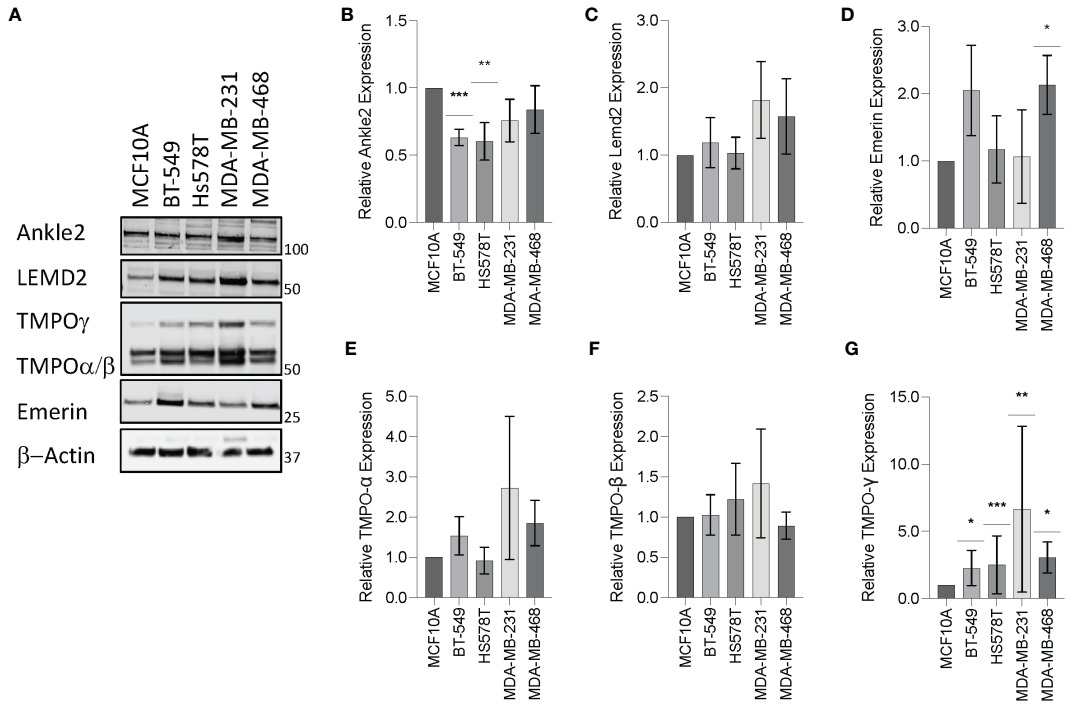

FIGURE 2
Expression of the Lem-domain proteins in TNBC cells. **(A)** Representative Western blot of BT549, Hs578T, MDA-MB-231, and MDA-MB-468 whole cell lysates showing expression of Lemd2, Ankle2, Emerin, and TMPO isoforms in TNBC cell lines, in comparison to the control MCF10A non-cancerous breast tissue cells. β–Actin was utilized as a loading control to allow for standardization via densitometry in ImageJ Software **(B–G)** Graphs represent densitometry analysis of Lem protein expression determined via Western blot analysis in TNBC normalized to non-cancerous MCF10A cells: **(B)** Ankle2 **(C)** Lemd2 **(D)** Emerin, and **(E–G)** TMPOα, β, and γ. Graphed values represent results from three individual repeats and error bars denote standard deviation of the mean. Statistical significance was calculated using an unpaired t-test: ***$p < 0.0002$, **$p < 0.0021$, *$p < 0.0332$.

However, in MDA-MB-468 cells there was a small but significant decrease in the percent of NE localized Lemd2 cells, compared to MCF10As (Figure 3E).

Atypical nuclear morphology is a hallmark of cancer cells and aberration of NE proteins induces abnormal nuclear morphology in cells (7, 30–32). Therefore, we sought to investigate whether Lem-D protein depletion induces abnormal nuclear morphology. Protein expression of Ankle2, Emerin, TMPO, and Lemd2 was depleted via siRNA and confirmed by immunofluorescent microscopy [Supplementary Figure S3 (168h post-transfection), Supplementary Figure S4 (72h post-transfection)]. Nuclear morphology was analyzed via immunofluorescent microscopy and quantified using the form factor analysis of InCarta software and values were verified by visually categorizing nuclei as having abnormal/normal morphology (Figure 4; Supplementary Figure S5). siRNA-mediated depletion of all Lem-D proteins significantly decreased the form factor value at 96h post-transfection of TNBC cells, in comparison to control siRNAs. Furthermore, Lem-D protein depletion did not significantly alter form factor values from respective controls in MCF10A cells (Figure 4). Visual quantification of nuclei as having abnormal/normal morphology supported these findings, demonstrating that siRNA-mediated depletion of Lem-D proteins significantly increased the percent of TNBC cells with abnormal nuclear morphology, but not MCF10A cells (Figure 4; Supplementary Figure S5). Collectively, suggesting a tumor-specific role for the Lem-D in maintaining nuclear morphology.

3.3 Depletion of the Lem-domain proteins inhibits TNBC cell growth

To investigate the role of the Lem-D proteins in TNBC growth, an Incucyte S3 direct cell count proliferation assay was conducted to establish changes in proliferative capacity of TNBC and MCF10A cells following siRNA-mediated depletion of the Lem-D proteins. BT549 and MDA-MB-231 were selected as representative TNBC cell lines.

Ankle2 and Emerin depletion did not significantly impact upon the proliferation of non-cancerous MCF10A cells, as demonstrated by the proliferation graphs and AUC analysis (Figures 5A, D). In contrast, TMPO and Lemd2 depletion had a 20%–30% reduction in MCF10A cell proliferation, as demonstrated via AUC analysis compared to the cells transfected with control siRNA (Figures 5A, D). Lemd2 depletion was shown to decrease the proliferative capacity of the tumorigenic BT549 and MDA-MB-231 cells by ~50%–65%. This suggests some level of tumor specificity, as the anti-proliferative effect of Lemd2 depletion in TNBC cells was twofold to 2.5-fold higher than observed in MCF10A cells. (Figures 5B–F). The marked antiproliferative effect following TMPO depletion in BT549 and MDA-MB-231 cells was similar in MCF10A cells, suggesting that siRNA-mediated depletion of TMPO is not likely to be a targeted mechanism of inhibiting TNBC cell growth. Finally, Ankle2 and Emerin depletion showed similar anti-proliferative outcomes in BT549 and MDA-MB-231 cells, reducing the proliferation rate to ~50% of respective endogenous rates (Figures 5B–F).

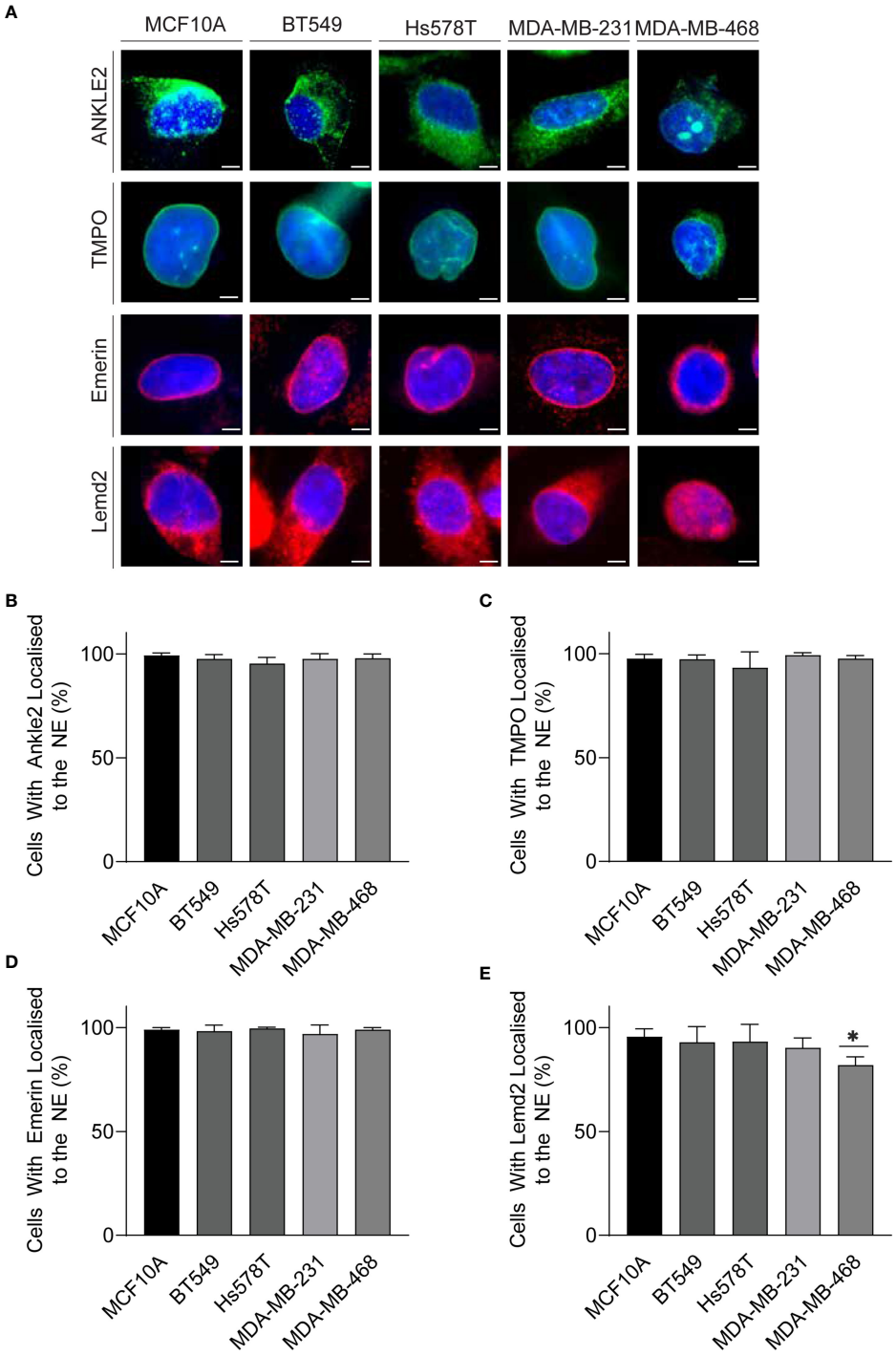

FIGURE 3
The Lem-D proteins are consistently localized in TNBC cells. **(A)** Representative immunofluorescent microscopy images of MCF10A, BT549, Hs578T, MDA-MB-231, and MDA-MB-468 cells. Cells were stained with Ankle2, TMPO, Emerin, and Lemd2 antibodies. Cells were counterstained with Hoechst 33342 (blue). **(B–E)** Quantification of the portion of cells with individual Lem-D proteins localized to the NE. **(B)** Ankle2, **(C)** TMPO, **(D)** Emerin, and **(E)** Lemd2. Quantifications are based on 200 cells/condition in at least three experimentally independent experiments. Error bars denote standard deviation of the mean. Scale bars = 10 μM. Statistical significance was calculated using an unpaired t-test: *$p < 0.0332$.

Given that Lem-D protein depletion was shown to inhibit tumor cell proliferation, we next investigated whether this was due to cell death. An Annexin V/PI apoptosis assay was conducted 5 days post-transfection with the Lem-D and control siRNAs and measured by flow cytometry (Figures 6A–C; Supplementary Figure S6). In MCF10A cells, transfection with the Lem-D siRNAs did not significantly increase cell death, compared to control siRNA (Figure 6A). However, depletion of all Lem-D proteins significantly increased the percentage of early or late-apoptotic cells in the BT549 cell line, in comparison to the control siRNA

10.3389/fonc.2024.1222698

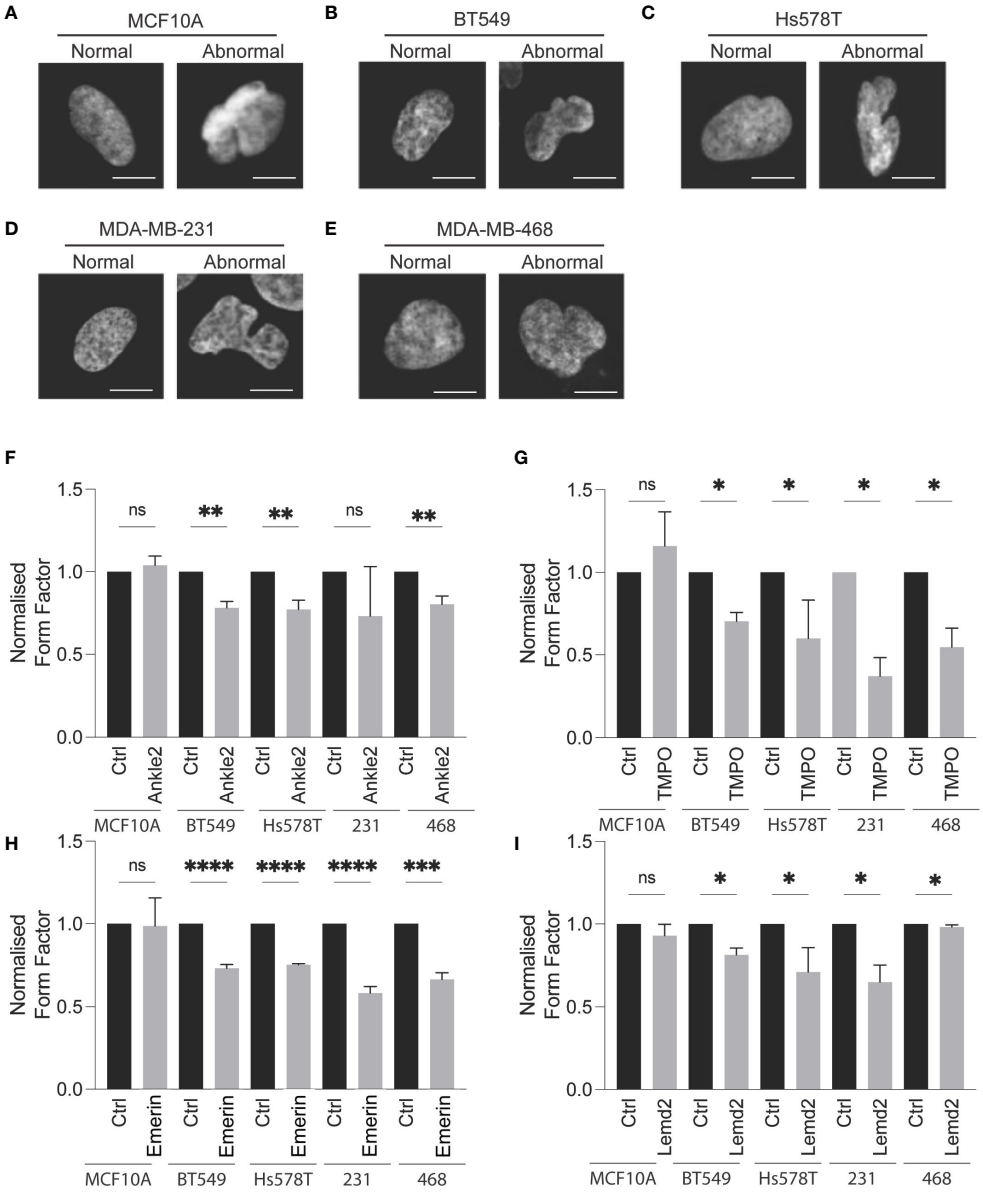

FIGURE 4
siRNA-mediated depletion of the Lem-D proteins induces aberrant NE morphology in TNBC cells. Representative immunofluorescent microscopy images of MCF10A and TNBC cells transfected with control and Lem-domain (Lem-D) protein siRNAs. Cells were stained with Hoechst 33342 to visualize the nucleus. Representative cells categorized to have normal and abnormal nuclear morphology: **(A)** MCF10A **(B)** BT549 **(C)** Hs578T **(D)** MDA-MB-231, and **(E)** MDA-MB-468. Quantification of cells with aberrant nuclear morphology in Control and Lem-D protein siRNA transfected cells. Normalized nuclear form factor values for: **(F)** Ankle2, **(G)** TMPO, **(H)** Emerin, and **(I)** Lemd2 siRNA. Form Factor score of 1 = perfect round nucleus. Quantifications are based on 200 cells/condition in at least three independent experiments. Error bars denote standard deviation of the mean. Statistical significance was calculated using an unpaired t-test: ****$p < 0.0001$, ***$p < 0.0002$, **$p < 0.0021$, *$p < 0.0332$. ns, not significant.

(Figure 6B). Similarly, Lem-D protein depletion in MDA-MB-231 cells significantly increased the percent of apoptotic or necrotic cells, relative to the control (Figure 6C).

4 Discussion

The Lem-D proteins have been shown to be dysregulated in various cancer models and, suppression or silencing of several of these proteins is known to produce anti-proliferative effects in breast, colon, lung, gastric, and cervical cancer models (14, 17, 33–36). Our findings build upon the existing knowledge of the roles of Lem-D proteins in tumor cells and demonstrate the role of several Lem-D proteins: Ankle2, TMPO, Emerin, and Lemd2 in TNBC growth and cell survival. This study provides novel insight into the capacity of this protein family as potentially exploitable as an anti-cancer therapy.

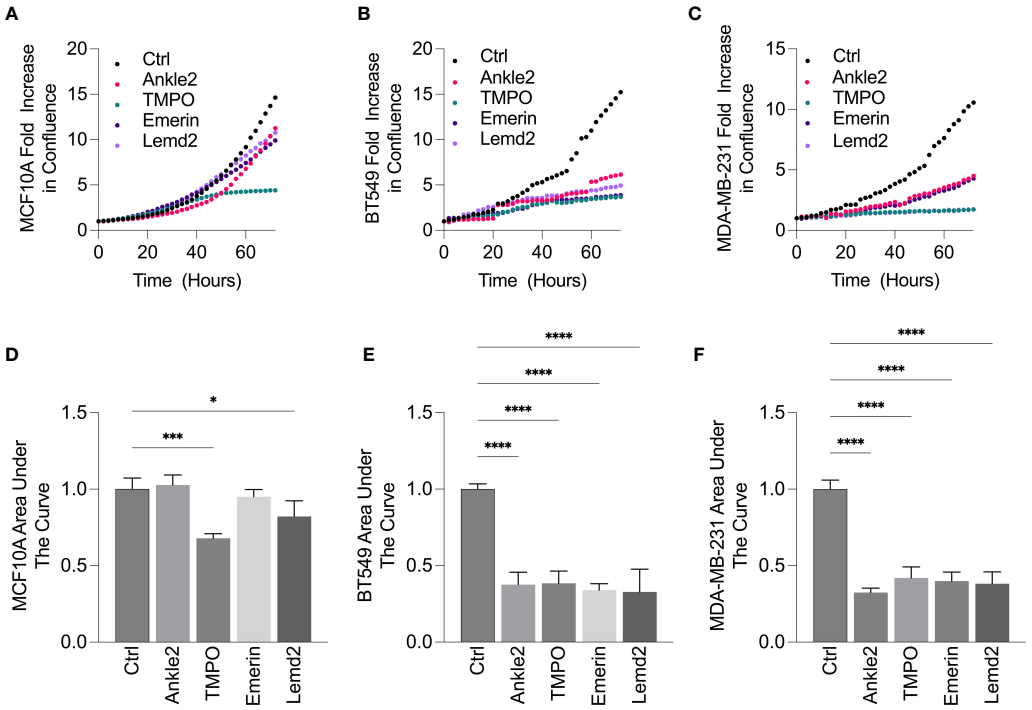

FIGURE 5
siRNA-mediated depletion of Lem-D proteins inhibits TNBC cellular proliferation. **(A–E)**. Representative proliferation curves from 72h post-transfection with Control and individual Lem-D protein siRNAs using the Incucyte S3 live cell imaging system in MCF10A and TNBC cells. **(A)** MCF10A **(B)** BT549 and **(C)** MDA-MB-231. **(D–F)** Relative area under the proliferation curve for **(A–C)** from at least three independent experiments. Error bars denote standard deviation of the mean. Values are normalized back to Control siRNA for respective cell lines. Statistical significance was calculated using an unpaired t-test: ****$p < 0.0001$, ***$p < 0.0002$, *$p < 0.0332$.

4.1 Ankle2 in triple-negative breast cancer

Ankle2 is a Lem-D protein required for maintaining NE structural integrity and has a multifaceted role in post-mitotic nuclear reassembly. Specifically, Ankle2 is essential for preserving appropriate dephosphorylation of Banf1 during mitosis, via both inhibiting the Banf1 phosphorylating kinase, VRK1, and upregulating PP2A-mediated dephosphorylation, to promote chromatin recruitment (37). To understand the role of Ankle2, and the other Lem-D proteins, in breast cancer tumorigenesis, bioinformatic analysis of the GENT2 database was conducted to establish whether mRNA levels of the Lem-D proteins were altered in breast cancer samples, in comparison to non-cancerous tissue adjacent to tumor margins (24). We demonstrated that *Ankle2* transcripts were overexpressed in breast cancer samples, compared to non-cancerous tissue, and the extent of overexpression negatively correlated with breast cancer patient OS.

Despite this initially positive trend, we observed significant downregulation of Ankle2 expression in half of the TNBC cells compared to a non-cancerous control. In contrast to our findings, Ankle2 overexpression has previously been reported in ER-positive breast cancer models, with Ankle2 being identified to have an essential role in promoting ERα DNA-binding and transactivation activity (17). Given that TNBC cells lack the ER receptor, it is conceivable that this may contribute to the lack of Ankle2 overexpression observed in TNBC cells specifically.

Consistent with earlier findings in both mammalian and Drosophila models, we observed Ankle2 localization to the NE and ER in TNBC cells (29). Furthermore, we demonstrated that siRNA-mediated depletion of Ankle2 induced a markedly abnormal nuclear phenotype in TNBC cells, consistent with prior findings in U-2OS osteosarcoma cells and HeLA cervical carcinoma cells (38, 39). Ankle2's role in maintaining nuclear integrity has been previously attributed to the role of Ankle2's phosphorylation status in NE breakdown and reformation (37, 38). Consistent with our observations, Ankle2 depletion by CRISPR/Cas9 technology has been previously shown to impair the mechanical stability of the nucleus and induce chromosomal instability via disrupting the association between Banf1, Lamin A, and Lap2a with the chromosomes following mitosis (39). LEM-4L silencing has been previously shown to disrupt Banf1 dephosphorylation and subsequent post-mitotic NE reformation in *C. elegans* (37). Together, these findings suggest that the abnormal nuclear phenotype observed in TNBC cells following Ankle2 depletion may arise due to ineffective post-mitotic NE reformation. Furthermore, our data demonstrates that siRNA-mediated Ankle2 depletion inhibits cell proliferation and induces cell death in a largely tumor-specific manner. While our investigation is the first to

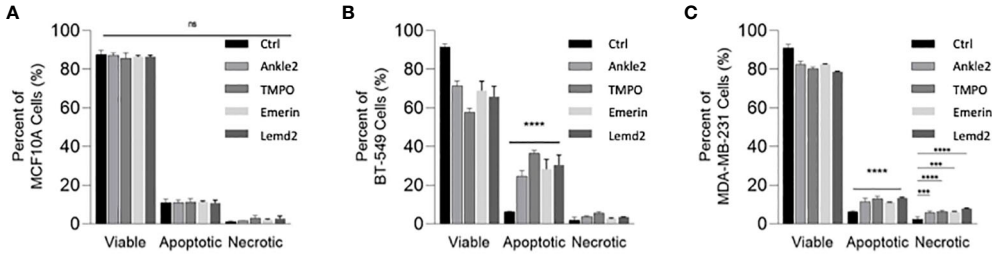

FIGURE 6
siRNA-mediated depletion of the Lem-D proteins induces TNBC cell death. Graphs represent percent of live, apoptotic (early and late apoptotic) and necrotic cells 5 days post-transfection with Control, Ankle2, TMPO, Emerin, and Lemd2 siRNAs **(A)** MCF10A **(B)** BT549 **(C)** MDA-MB-231 cells. Graphed values represent results from three individual repeats and error bars denote standard deviation of the mean. Statistical significance was calculated using an unpaired *t*-test: ****$p < 0.0001$, ***$p < 0.0002$. ns, not significant.

propose a role for Ankle2 TNBC proliferation, previous studies in hormone-positive breast cancer cells and HeLa cells support this observation (17, 39).

Based on the known cellular functions of Ankle2, it can be hypothesized that Ankle2 depletion may impair TNBC proliferation and induce cell death due to the inability to reform the NE following mitosis in the highly mitotic TNBC cells, resulting in mechanically vulnerable cells and potential cell death.

4.2 Emerin in triple-negative breast cancer

Emerin is an inner NE protein known to be involved in maintaining the nuclear morphology of interphase cells and post-mitotic nuclear reformation. We demonstrate *EMD* transcript overexpression in breast cancer patient samples. EMD protein was also increased in two out of four TNBC cell lysates tested, when compared to non-cancerous cell lines. However, previous investigations have produced conflicting results regarding the expression of Emerin protein in breast cancer samples, with one study showing a decrease in Emerin protein levels (40) and one showing an increase in comparison to human primary breast epithelial cells (20). Our findings also demonstrated that *EMD* expression was shown to negatively correlate with patient outcomes suggesting a possible role for Emerin in breast cancer cell growth and proliferation.

Consistent with prior findings in both mammalian cells and *C. elegans*, we observed Emerin localization to the NE in both the MCF10A and TNBC cells (41, 42). Like our Ankle2-related findings, we observed that siRNA-mediated depletion of Emerin induced an abnormal nuclear morphology in TNBC cells. Previous studies have shown that deletion of regions of the *EMD* sequence has been shown to induce improper centromere and tubulin network localization and increase mitotic time (36, 43). Therefore, this suggests that abnormal nuclear morphology may arise following Emerin depletion due to failed or defective mitotic events. The role of Emerin in maintaining appropriate mitotic progression may also contribute to the anti-proliferative effect and cell death observed following Emerin depletion in TNBC cells. Numerous prior investigations have reported a role for Emerin in cellular proliferation, and that siRNA-mediated depletion of Emerin inhibited cellular proliferation through multiple proposed methods (44, 45). However, it has been previously shown that Emerin directly binds beta-catenin, a signaling factor of the Wnt pathway which is commonly dysregulated in tumor cells. Specifically, Emerin null cells have been shown to have suppressed beta-catenin activity and upregulated cellular proliferation (46). GFP-Emerin overexpression has also been shown to decrease tumor size in mice models (47). Collectively, our findings and prior literature indicate that Emerin is likely to have a multifaced role in tumor cell growth and proliferation, which may be impacted by several underlying factors, therefore, indicating the need for further investigation into the underlying role of Emerin in tumor cell growth.

4.3 Lemd2 in triple-negative breast cancer

Lemd2 is an INM protein with a known role in several cellular processes, including nuclear organization. Cellular investigations in HeLa cells and *C. elegans* also suggest a role of Lemd2 in maintaining nuclear morphology due to its interactions with chromatin and the nuclear lamina, with siRNA-mediated depletion of Lemd2 inducing a similar nuclear phenotype to that observed within our own investigations (48, 49).

Unlike the other Lem-D proteins investigation, Lemd2 expression was shown to positively correlate with OS in breast cancer patients. While our study is the first to investigate Lemd2 expression in breast cancer, a previous study has shown Lemd2 overexpression in prostate adenocarcinoma models (16). Furthermore, our findings demonstrated the localization of Lemd2 to the NE and cytosol, which we hypothesized to be lysosomal. This NE localization of Lemd2 is consistent with prior findings in *S. pombe* yeast and multiple human cell lines, including U-2OS and HeLa cells (32, 50). While our investigation was the first to propose the lysosomal localization of Lemd2, Lemd2 has been shown to interact with ESCRT-III, a key protein involved in maintaining the lysosomal membrane (50). Similarly, WT Lemd2 overexpression has been shown to have similar localization in U-2OS cells (51). However, further investigations are required to validate the proposed localization of Lemd2 to the lysosomes.

Additionally, Lemd2 depletion was shown to induce an abnormal nuclear phenotype in the TNBC cell lines but not non-cancerous MCF10A cells. Given that Lemd2 has been previously identified to have essential roles in NE reformation during mitosis, it can be proposed that TNBC cells may exhibit abnormal nuclear morphology following improper NE reformation during mitosis (50).

Our findings also demonstrated that siRNA-mediated depletion of Lemd2 significantly impaired cellular proliferation and induced apoptosis in a TNBC cell–specific manner. While the exact tumor inhibiting mechanism is yet to be established, Lemd2's role in inducing aberrant nuclear morphology and inhibiting the growth of TNBC could be attributed to Lemd2's role in NE rupture repair. Lemd2 is required for the recruitment of ESCRT-III mediated repair machinery to the site of NE ruptures (52). Therefore, given abnormal nuclear morphology and uncontrollable proliferation are pre-existing hall marks of tumor cells, it is conceivable that these collectively result in NE ruptures which are unable to be repaired in Lemd2-deficient cells. Therefore, further inducing aberrant nuclear morphology, inhibiting tumor cell growth, and inducing cell death. However, Lemd2 has also been shown to have multiple other cellular functions, including participation within the MAPK signaling pathway. Therefore, potential change in the activity of these pathways should also be investigated to further elucidate Lemd2's role in tumor cell growth (53).

4.4 TMPO in triple-negative breast cancer

TMPO is alternatively spliced to produce three main isoforms, several of which have been linked to nuclear mechanics and are known to be NE localized (54). The TMPO isoform, TMPOα, has been indicated to have a role in maintaining nuclear organization via stabilizing higher order chromatin organization (55). TMPOβ is also known to participate in nuclear growth in Xenopus *laevis* models, with the treatment of cells with the human TMPOβ fragment 1–187 inducing a dose-dependent formation of scalloped nuclei phenotype, consistent with that observed within our investigations (54). Our data indicate that TMPO may be overexpressed in breast cancer tumors, as demonstrated by patient data and that the TMPOγ isoform protein is significantly increased in TNBC cell lines. Previous investigations have demonstrated TMPO overexpression in multiple tumor cell lines, including breast, colorectal, cervical, and pancreatic cancer models (35, 56–59). Furthermore, we demonstrate that TMPO overexpression may play a role in breast cancer tumor growth pathways, given that mRNA expression was negatively correlated with patient outcomes.

Consistent with earlier findings, we observed compelling NE localization of TMPO (60). Furthermore, siRNA-mediated TMPO depletion was shown to induce aberrant nuclei morphology in TNBC cell lines but not non-cancerous MCF10A cells. Given the recognized cellular functions of TMPO, it can be proposed that TMPO-depleted TNBC cells may exhibit aberrant nuclear morphology due to loss of appropriate chromatin organization or due to improper NE or nucleus formation in post-mitotic cells. TMPO expression has also been shown to inversely correlate with the level of nuclear membrane ruptures and this may play a role in the induction of abnormal nuclei (61).

TMPO expression has previously been shown to correlate with the proliferative capacity in multiple cellular models (62), supporting a role for TMPO in unregulated cancer cell proliferation. Unlike the other Lem-D proteins examined, depletion of TMPO was shown to induce significant anti-proliferative effects in both the TNBC and the non-cancerous MCF10A cells. Consistently, siRNA-mediated depletion of TMPO has previously been shown to induce growth-inhibiting phenotypes, such as reduced proliferation and the induction of apoptosis, in non-cancerous dermal fibroblasts and tumor models (63, 64). TMPO loss in Hutchinson Gilford progeria patient fibroblasts has also been casually linked to a proliferation defect in these cells (65). Previous investigations suggest that the role of TMPO in cell proliferation is likely due to TMPO's role in pRb-mediated cell cycle control. TMPO can directly bind to Rb and is essential for the anchorage of Rb to the nucleus induces E2F activation and downstream gene expression and maintains appropriate cell cycle progression (66). TMPO has also been shown to have a key role in maintaining genomic stability, specifically via chaperoning replication protein A (RPA) to the site of DNA damage (67).

While the mechanism surrounding the lack of cancer specificity effect was not elucidated within our investigation, this does suggest that other Lem-D proteins may be more suited candidates as cancer therapeutics than TMPO, as there may be a heightened risk of toxicity to normal cells with this target.

4.5 Potential shared mechanisms of anti-cancer activity

Annexin V/PI apoptosis assays demonstrated that the extent of cell death did not fully correlate with the anti-proliferative effect induced by Lem-D protein depletion in TNBC cells. For instance, depletion of the Lem-D proteins was shown to reduce the proliferative capacity of MDA-MB-231 cells by >50%; however, only a 15%–20% decrease in viability was reported. Similar discrepancies were observed in BT549 cells following Lem-D protein depletion. It is possible that the anti-proliferative effect is not exclusively induced by cell death or occurs at a later point than the 5-day time point examined, and the true level of cell death is not being fully observed by our assay. Given the Lem-D proteins are known to have diverse functions, the proliferative arrest could be due to mitotic arrest or cellular senescence or quiescence after improper mitotic progression, which is feasible if targeting Lem-D proteins disrupts the reformation of the NE (37, 39, 68, 69). Therefore, future experiments should include investigating the role of these proteins in cell cycle progression, specifically mitosis.

It is evident that the Lem-D proteins have several unique functions in maintaining the NE structural integrity of interphase cells and during mitotic NE breakdown and reformation, with disruption of any of these processes uniquely leading to impaired NE integrity and a subsequent aberrant nuclear phenotype. However, it cannot currently be distinguished whether siRNA-

mediated depletion of the individual Lem-D proteins may also induce aberrant nuclei in TNBC cells via a common mechanism mediated by their universal Lem-D, rather than their cellular functions discussed above.

To date, there have been minimal studies conducted in non-cancerous mammalian cells examining the effect of Lem-D protein depletion on the nuclear morphology of "normal" cells (70). Within our investigations, we have shown that, unlike TNBC cells, depletion of the Lem-D proteins does not significantly alter nuclear morphology in non-cancerous MCF10A cells. While we are unable to establish an exact mechanism by which depletion of the Lem-D proteins induces a tumor-specific outcome, several potential mechanisms should be investigated in further studies. It is well reported that nuclear morphology is frequently altered under endogenous conditions in tumor cells, with nuclear invaginations and folded nuclei being associated with higher malignancy rates and poor patient outcomes (71). Similarly, the criteria for pathological diagnosis of several cancers include the detection of aberrant NE protein expression or morphology (72).

While the localization of the Lem-D proteins is well established in non-diseased mammalian cells and other cancer models, it remains to be established whether this is maintained in TNBC cell lines (39, 49, 55, 73). We demonstrated that localization of Lem-D proteins to the INM is largely maintained in TNBC, and these proteins participate in cellular processes required to preserve TNBC nuclear morphology. While the underlying mechanism of these siRNA-induced aberrant nuclear morphologies was not within the scope of this investigation, several mechanisms have been considered based on known roles of the proteins.

Particularly, it is conceivable that tumor cells have a more prominent change in nuclear morphology following Lem-D protein depletion due to a mechanical vulnerability induced by their pre-existing abnormal nuclear structure, which promotes further distortion of the nucleus following disruption to NE homeostasis. Not only are the Lem-D proteins involved directly in maintaining nuclear morphology due to their NE localization and mitotic roles but they have also been identified as interactors of other proteins involved in maintaining nuclear stability, such as Lamin A/C and Lamin B (15, 73, 74). Expression of these proteins is also frequently mis-localized or decreased in breast cancer, thereby, suggesting that depletion of their Lem-D interactors may further impair the function of these proteins, emphasizing the reduction in nuclear stability induced by their dysregulation.

Our data demonstrate that siRNA-mediated depletion of Ankle2, Emerin, and Lemd2 inhibits cell proliferation in a largely tumor-specific manner in TNBC cells. Further investigations would benefit from the use of a xenograft model to validate the utility of targeting the Lem-D proteins in TNBC.

In conclusion, our works demonstrate the consistent localization of Ankle2, TMPO, Emerin, and Lemd2 to the NE in TNBC cells. siRNA-mediated depletion of these proteins also indicates a tumor-specific role of the Lem-D proteins in maintaining TNBC nuclear morphology. Furthermore, the induction of aberrant nuclei via depletion of these proteins produces an evident anti-proliferative effect and cell death in TNBC cells. Except for TMPO, this phenotype was demonstrated to be predominately tumor specific. Therefore, while further work is needed to elucidate the underlying mechanism by which the Lem-D proteins regulate TNBC growth, our findings provide the first evidence for a dynamic role of the Lem-D proteins in tumorigenesis and the potential for targeting this family as an anti-cancer therapy.

Data availability statement

The original contributions presented in the study are included in the article/Supplementary Material. Further inquiries can be directed to the corresponding author.

Ethics statement

Experimental procedures were approved by the Queensland University of Technology, Human Research Ethics Committee.

Author contributions

EB conceived and directed the project. MR, CC, PS, and JB contributed to the laboratory experiments. All the authors contributed to project design and writing the manuscript. All authors contributed to the article and approved the submitted version.

Funding

The author(s) declare financial support was received for the research, authorship, and/or publication of this article. This project was supported by a grant from the QUT Centre for Genomics and Personalised Health. MR also received a scholarship from the QUT Centre for Genomics and Personalised Health.

Acknowledgments

The authors wish to acknowledge the members of the Cancer and Ageing Research Program at QUT for their scientific insight in respect to this manuscript. We would also like to acknowledge the Translational Research Institute for the exceptional research environment, in particular the Flow Cytometry Core Facility.

Conflict of interest

Authors EB, DR, and KO are founders of Carpe Vitae Pharmaceuticals. EB, KO, and DR are inventors on provisional

patent applications filed by Queensland University of Technology.

The remaining authors declare that the research was conducted in the absence of any commercial or financial relationships that could be construed as a potential conflict of interest.

Publisher's note

All claims expressed in this article are solely those of the authors and do not necessarily represent those of their affiliated organizations, or those of the publisher, the editors and the reviewers. Any product that may be evaluated in this article, or claim that may be made by its manufacturer, is not guaranteed or endorsed by the publisher.

Supplementary material

The Supplementary Material for this article can be found online at: https://www.frontiersin.org/articles/10.3389/fonc.2024.1222698/full#supplementary-material

References

1. Garrido-Castro AC, Lin NU, Polyak K. Insights into molecular classifications of triple-negative breast cancer: improving patient selection for treatment. *Cancer Discovery*. (2019) 9:176–98. doi: 10.1158/2159-8290.CD-18-1177

2. Pogoda K, Niwinska A, Murawska M, Pienkowski T. Analysis of pattern, time and risk factors influencing recurrence in triple-negative breast cancer patients. *Med Oncol*. (2013) 30:388. doi: 10.1007/s12032-012-0388-4

3. Howard FM, Olopade OI. Epidemiology of triple-negative breast cancer: A review. *Cancer J (Sudbury Mass)*. (2021) 27:8–16. doi: 10.1097/ppo.0000000000000500

4. Bellon JR, Burstein HJ, Frank ES, Mittendorf EA, King TA. Multidisciplinary considerations in the treatment of triple-negative breast cancer. *CA Cancer J Clin*. (2020) 70:432–42. doi: 10.3322/caac.21643

5. Brown R. *Observations on the Organs and Mode of Fecundation in Orchideae and Asclepiadeae*. London:Taylor (1833).

6. Chow KH, Factor RE, Ullman KS. The nuclear envelope environment and its cancer connections. *Nat Rev Cancer*. (2012) 12:196–209. doi: 10.1038/nrc3219

7. Paquet N, Box JK, Ashton NW, Suraweera A, Croft LV, Urquhart AJ, et al. Nestor-guillermo progeria syndrome: A biochemical insight into barrier-to-autointegration factor 1, alanine 12 threonine mutation. *BMC Mol Biol*. (2014) 15:27. doi: 10.1186/s12867-014-0027-z

8. Bertrand AT, Brull A, Azibani F, Benarroch L, Chikhaoui K, Stewart CL, et al. Lamin a/C assembly defects in lmna-congenital muscular dystrophy is responsible for the increased severity of the disease compared with emery-dreifuss muscular dystrophy. *Cells*. (2020) 9(4):844. doi: 10.3390/cells9040844

9. Lin F, Blake DL, Callebaut I, Skerjanc IS, Holmer L, McBurney MW, et al. Man1, an inner nuclear membrane protein that shares the lem domain with lamina-associated polypeptide 2 and emerin*. *J Biol Chem*. (2000) 275:4840–7. doi: 10.1074/jbc.275.7.4840

10. Bolderson E, Burgess JT, Li J, Gandhi NS, Boucher D, Croft LV, et al. Barrier-to-autointegration factor 1 (Banf1) regulates poly [Adp-ribose] polymerase 1 (Parp1) activity following oxidative DNA damage. *Nat Commun*. (2019) 10:5501. doi: 10.1038/s41467-019-13167-5

11. Burgess JT, Cheong CM, Suraweera A, Sobanski T, Beard S, Dave K, et al. Barrier-to-autointegration-factor (Banf1) modulates DNA double-strand break repair pathway choice *via* regulation of DNA-dependent kinase (DNA-pk) activity. *Nucleic Acids Res*. (2021) 49:3294–307. doi: 10.1093/nar/gkab110

12. Rose M, Burgess JT, O'Byrne K, Richard DJ, Bolderson E. The role of inner nuclear membrane proteins in tumourigenesis and as potential targets for cancer therapy. *Cancer Metastasis Rev*. (2022) 41:953–63. doi: 10.1007/s10555-022-10065-z

13. Barton LJ, Soshnev AA, Geyer PK. Networking in the nucleus: A spotlight on lem-domain proteins. *Curr Opin Cell Biol*. (2015) 34:1–8. doi: 10.1016/j.ceb.2015.03.005

14. Li D, Wang D, Liu H, Jiang X. Lem domain containing 1 (Lemd1) transcriptionally activated by sry-related high-mobility-group box 4 (Sox4) accelerates the progression of colon cancer by upregulating phosphatidylinositol 3-kinase (Pi3k)/protein kinase B (Akt) signaling pathway. *Bioengineered*. (2022) 13:8087–100. doi: 10.1080/21655979.2022.2047556

15. Naetar N, Korbei B, Kozlov S, Kerenyi MA, Dorner D, Kral R, et al. Loss of nucleoplasmic lap2alpha-lamin a complexes causes erythroid and epidermal progenitor hyperproliferation. *Nat Cell Biol*. (2008) 10:1341–8. doi: 10.1038/ncb1793

16. He T, Zhang Y, Li X, Liu C, Zhu G, Yin X, et al. Collective analysis of the expression and prognosis for lem-domain proteins in prostate cancer. *World J Surg Oncol*. (2022) 20:174. doi: 10.1186/s12957-022-02640-z

17. Gao A, Sun T, Ma G, Cao J, Hu Q, Chen L, et al. Lem4 confers tamoxifen resistance to breast cancer cells by activating cyclin D-cdk4/6-rb and erα Pathway. *Nat Commun*. (2018) 9:4180. doi: 10.1038/s41467-018-06309-8

18. Bardia A, Hurvitz SA, Tolaney SM, Loirat D, Punie K, Oliveira M. Sacituzumab govitecan (Trodelvy) for metastatic triple-negative breast cancer. *Med Lett Drugs Ther*. (2021) 63:e25–e7. doi: 10.1056/NEJMoa2028485

19. Alhudiri IM, Nolan CC, Ellis IO, Elzagheid A, Rakha EA, Green AR, et al. Expression of lamin a/C in early-stage breast cancer and its prognostic value. *Breast Cancer Res Treat*. (2019) 174:661–8. doi: 10.1007/s10549-018-05092-w

20. Capo-chichi CD, Cai KQ, Smedberg J, Ganjei-Azar P, Godwin AK, Xu XX. Loss of a-type lamin expression compromises nuclear envelope integrity in breast cancer. *Chin J Cancer*. (2011) 30:415–25. doi: 10.5732/cjc.010.10566

21. Bolderson E, Tomimatsu N, Richard DJ, Boucher D, Kumar R, Pandita TK, et al. Phosphorylation of exo1 modulates homologous recombination repair of DNA double-strand breaks. *Nucleic Acids Res*. (2010) 38:1821–31. doi: 10.1093/nar/gkp1164

22. Janssen AFJ, Breusegem SY, Larrieu D. Current methods and pipelines for image-based quantitation of nuclear shape and nuclear envelope abnormalities. *Cells*. (2022) 11(3):347. doi: 10.3390/cells11030347

23. Takaki T, Montagner M, Serres MP, Le Berre M, Russell M, Collinson L, et al. Actomyosin drives cancer cell nuclear dysmorphia and threatens genome stability. *Nat Commun*. (2017) 8:16013. doi: 10.1038/ncomms16013

24. Park SJ, Yoon BH, Kim SK, Kim SY. Gent2: an updated gene expression database for normal and tumor tissues. *BMC Med Genomics*. (2019) 12:101. doi: 10.1186/s12920-019-0514-7

25. Lanczky A, Gyorffy B. Web-based survival analysis tool tailored for medical research (Kmplot): development and implementation. *J Med Internet Res*. (2021) 23: e27633. doi: 10.2196/27633

26. Liu NQ, Stingl C, Look MP, Smid M, Braakman RB, De Marchi T, et al. Comparative proteome analysis revealing an 11-protein signature for aggressive triple-negative breast cancer. *J Natl Cancer Inst*. (2014) 106:djt376. doi: 10.1093/jnci/djt376

27. Tang W, Zhou M, Dorsey TH, Prieto DA, Wang XW, Ruppin E, et al. Integrated proteotranscriptomics of breast cancer reveals globally increased protein-mrna concordance associated with subtypes and survival. *Genome Med*. (2018) 10:94. doi: 10.1186/s13073-018-0602-x

28. Xu YY, Yang F, Zhang Y, Shen HB. Bioimaging-based detection of mislocalized proteins in human cancers by semi-supervised learning. *Bioinformatics*. (2015) 31:1111–9. doi: 10.1093/bioinformatics/btu772

29. Link N, Chung H, Jolly A, Withers M, Tepe B, Arenkiel BR, et al. Mutations in ankle2, a zika virus target, disrupt an asymmetric cell division pathway in drosophila neuroblasts to cause microcephaly. *Dev Cell*. (2019) 51:713–29 e6. doi: 10.1016/j.devcel.2019.10.009

30. de Las Heras JI, Schirmer EC. The nuclear envelope and cancer: A diagnostic perspective and historical overview. *Adv Exp Med Biol*. (2014) 773:5–26. doi: 10.1007/978-1-4899-8032-8_1

31. Samwer M, Schneider MWG, Hoefler R, Schmalhorst PS, Jude JG, Zuber J, et al. DNA cross-bridging shapes a single nucleus from a set of mitotic chromosomes. *Cell*. (2017) 170:956–72.e23. doi: 10.1016/j.cell.2017.07.038

32. Kume K, Cantwell H, Burrell A, Nurse P. Nuclear membrane protein lem2 regulates nuclear size through membrane flow. *Nat Commun*. (2019) 10:1871. doi: 10.1038/s41467-019-09623-x

33. Gu M, LaJoie D, Chen OS, von Appen A, Ladinsky MS, Redd MJ, et al. Lem2 recruits chmp7 for escrt-mediated nuclear envelope closure in fission yeast and human cells. *Proc Natl Acad Sci U.S.A*. (2017) 114:E2166–e75. doi: 10.1073/pnas.1613916114

34. Kim HJ, Hwang SH, Han ME, Baek S, Sim HE, Yoon S, et al. Lap2 is widely overexpressed in diverse digestive tract cancers and regulates motility of cancer cells. *PloS One*. (2012) 7:e39482. doi: 10.1371/journal.pone.0039482

35. Parise P, Finocchiaro G, Masciadri B, Quarto M, Francois S, Mancuso F, et al. Lap2alpha expression is controlled by E2f and deregulated in various human tumors. *Cell Cycle*. (2006) 5:1331–41. doi: 10.4161/cc.5.12.2833

36. Dabauvalle MC, Muller E, Ewald A, Kress W, Krohne G, Muller CR. Distribution of emerin during the cell cycle. *Eur J Cell Biol*. (1999) 78:749–56. doi: 10.1016/S0171-9335(99)80043-0

37. Asencio C, Davidson IF, Santarella-Mellwig R, Ly-Hartig TB, Mall M, Wallenfang MR, et al. Coordination of kinase and phosphatase activities by lem4 enables nuclear envelope reassembly during mitosis. *Cell*. (2012) 150:122–35. doi: 10.1016/j.cell.2012.04.043

38. Kaufmann T, Kukolj E, Brachner A, Beltzung E, Bruno M, Kostrhon S, et al. Sirt2 regulates nuclear envelope reassembly through ankle2 deacetylation. *J Cell Sci*. (2016) 129:4607–21. doi: 10.1242/jcs.192633

39. Snyers L, Erhart R, Laffer S, Pusch O, Weipoltshammer K, Schöfer C. Lem4/ankle-2 deficiency impairs post-mitotic re-localization of baf, lap2α and lamina to the nucleus, causes nuclear envelope instability in telophase and leads to hyperploidy in hela cells. *Eur J Cell Biol*. (2018) 97:63–74. doi: 10.1016/j.ejcb.2017.12.001

40. Liddane AG, McNamara CA, Campbell MC, Mercier I, Holaska JM. Defects in emerin–nucleoskeleton binding disrupt nuclear structure and promote breast cancer cell motility and metastasis. *Mol Cancer Res*. (2021) 19:1196–207. doi: 10.1158/1541-7786.Mcr-20-0413

41. Buchwalter A, Schulte R, Tsai H, Capitanio J, Hetzer M. Selective clearance of the inner nuclear membrane protein emerin by vesicular transport during er stress. *Elife*. (2019) 8. doi: 10.7554/eLife.49796

42. Lee KK, Gruenbaum Y, Spann P, Liu J, Wilson KLC. Elegans nuclear envelope proteins emerin, man1, lamin, and nucleoporins reveal unique timing of nuclear envelope breakdown during mitosis. *Mol Biol Cell*. (2000) 11:3089–99. doi: 10.1091/mbc.11.9.3089

43. Dubinska-Magiera M, Koziol K, Machowska M, Piekarowicz K, Filipczak D, Rzepecki R. Emerin is required for proper nucleus reassembly after mitosis: implications for new pathogenetic mechanisms for laminopathies detected in edmd1 patients. *Cells*. (2019) 8(3):240. doi: 10.3390/cells8030240

44. Lee B, Lee S, Lee Y, Park Y, Shim J. Emerin represses stat3 signaling through nuclear membrane-based spatial control. *Int J Mol Sci*. (2021) 22:6669. doi: 10.3390/ijms22136669

45. Lee B, Lee T-H, Shim J. Emerin suppresses notch signaling by restricting the notch intracellular domain to the nuclear membrane. *Biochim Biophys Acta Mol Cell Res*. (2016) 1864:303–13. doi: 10.1016/j.bbamcr.2016.11.013

46. Markiewicz E, Tilgner K, Barker N, van de Wetering M, Clevers H, Dorobek M, et al. The inner nuclear membrane protein emerin regulates beta-catenin activity by restricting its accumulation in the nucleus. *EMBO J*. (2006) 25:3275–85. doi: 10.1038/sj.emboj.7601230

47. Liddane AG, McNamara CA, Campbell MC, Mercier I, Holaska JM. Defects in emerin-nucleoskeleton binding disrupt nuclear structure and promote breast cancer cell motility and metastasis. *Mol Cancer Res*. (2021) 19:1196–207. doi: 10.1158/1541-7786.MCR-20-0413

48. Liu J, Lee K, Segura-Totten M, Neufeld E, Wilson K, Gruenbaum Y. Man1 and emerin have overlapping function(S) essential for chromosome segregation and cell division in caenorhabditis elegans. *Proc Natl Acad Sci United States America*. (2003) 100:4598–603. doi: 10.1073/pnas.0730821100

49. Ulbert S, Antonin W, Platani M, Mattaj IW. The inner nuclear membrane protein lem2 is critical for normal nuclear envelope morphology. *FEBS Lett*. (2006) 580:6435–41. doi: 10.1016/j.febslet.2006.10.060

50. von Appen A, LaJoie D, Johnson IE, Trnka MJ, Pick SM, Burlingame AL, et al. Lem2 phase separation promotes escrt-mediated nuclear envelope reformation. *Nature*. (2020) 582:115–8. doi: 10.1038/s41586-020-2232-x

51. Marbach F, Rustad CF, Riess A, Đukić D, Hsieh T-C, Jobani I, et al. The discovery of a lemd2-associated nuclear envelopathy with early progeroid appearance suggests advanced applications for ai-driven facial phenotyping. *Am J Hum Genet*. (2019) 104:749–57. doi: 10.1016/j.ajhg.2019.02.021

52. Denais C, Gilbert RM, Isermann P, McGregor AL, Mt L, Weigelin B, et al. Nuclear envelope rupture and repair during cancer cell migration. *Sci (New York NY)*. (2016) 352:353–8. doi: 10.1126/science.aad7297

53. Caravia XM, Ramirez-Martinez A, Gan P, Wang F, McAnally JR, Xu L, et al. Loss of function of the nuclear envelope protein lemd2 causes DNA damage-dependent cardiomyopathy. *J Clin Invest*. (2022) 132(22):e158897. doi: 10.1172/JCI158897

54. Dechat T, Vlcek S, Foisner R. Review: lamina-associated polypeptide 2 isoforms and related proteins in cell cycle-dependent nuclear structure dynamics. *J Struct Biol*. (2000) 129:335–45. doi: 10.1006/jsbi.2000.4212

55. Gesson K, Vidak S, Foisner R. Lamina-associated polypeptide (Lap)2α and nucleoplasmic lamins in adult stem cell regulation and disease. *Semin Cell Dev Biol*. (2014) 29:116–24. doi: 10.1016/j.semcdb.2013.12.009

56. Rosty C, Sheffer M, Tsafrir D, Stransky N, Tsafrir I, Peter M, et al. Identification of a proliferation gene cluster associated with hpv E6/E7 expression level and viral DNA load in invasive cervical carcinoma. *Oncogene*. (2005) 24:7094–104. doi: 10.1038/sj.onc.1208854

57. Futschik M, Jeffs A, Pattison S, Kasabov N, Sullivan M, Merrie A, et al. Gene expression profiling of metastatic and nonmetastatic colorectal cancer cell lines. *Genome Lett*. (2002) 1:26–34. doi: 10.3892/or.2021.7961

58. Buterin T, Koch C, Naegeli H. Convergent transcriptional profiles induced by endogenous estrogen and distinct xenoestrogens in breast cancer cells. *Carcinogenesis*. (2006) 27:1567–78. doi: 10.1093/carcin/bgi339

59. Ohuchida K, Mizumoto K, Ishikawa N, Fujii K, Konomi H, Nagai E, et al. The role of S100a6 in pancreatic cancer development and its clinical implication as a diagnostic marker and therapeutic target. *Clin Cancer Res*. (2005) 11:7785–93. doi: 10.1158/1078-0432.Ccr-05-0714

60. Harris CA, Andryuk PJ, Cline SW, Mathew S, Siekierka JJ, Goldstein G. Structure and mapping of the human thymopoietin (Tmpo) gene and relationship of human tmpo B to rat lamin-associated polypeptide 2. *Genomics*. (1995) 28:198–205. doi: 10.1006/geno.1995.1131

61. Chen NY, Kim PH, Tu Y, Yang Y, Heizer PJ, Young SG, et al. Increased expression of lap2β Eliminates nuclear membrane ruptures in nuclear lamin–deficient neurons and fibroblasts. *Proc Natl Acad Sci*. (2021) 118:e2107770118. doi: 10.1073/pnas.2107770118

62. Gotic I, Schmidt WM, Biadasiewicz K, Leschnik M, Spilka R, Braun J, et al. Loss of lap2 alpha delays satellite cell differentiation and affects postnatal fiber-type determination. *Stem Cells*. (2010) 28:480–8. doi: 10.1002/stem.292

63. Pekovic V, Harborth J, Broers JL, Ramaekers FC, van Engelen B, Lammens M, et al. Nucleoplasmic lap2alpha-lamin a complexes are required to maintain a proliferative state in human fibroblasts. *J Cell Biol*. (2007) 176:163–72. doi: 10.1083/jcb.200606139

64. Zhang L, Wang G, Chen S, Ding J, Ju S, Cao H, et al. Depletion of thymopoietin inhibits proliferation and induces cell cycle arrest/apoptosis in glioblastoma cells. *World J Surg Oncol*. (2016) 14:267. doi: 10.1186/s12957-016-1018-y

65. Vidak S, Kubben N, Dechat T, Foisner R. Proliferation of progeria cells is enhanced by lamina-associated polypeptide 2α (Lap2α) through expression of extracellular matrix proteins. *Genes Dev*. (2015) 29:2022–36. doi: 10.1101/gad.263939.115

66. Markiewicz E, Dechat T, Foisner R, Quinlan RA, Hutchison CJ. Lamin a/C binding protein lap2alpha is required for nuclear anchorage of retinoblastoma protein. *Mol Biol Cell*. (2002) 13:4401–13. doi: 10.1091/mbc.e02-07-0450

67. Bao K, Zhang Q, Liu S, Song N, Guo Q, Liu L, et al. Lap2α Preserves genome integrity through assisting rpa deposition on damaged chromatin. *Genome Biol*. (2022) 23:64. doi: 10.1186/s13059-022-02638-6

68. Barkan R, Zahand AJ, Sharabi K, Lamm AT, Feinstein N, Haithcock E, et al. Ce-emerin and lem-2: essential roles in caenorhabditis elegans development, muscle function, and mitosis. *Mol Biol Cell*. (2012) 23:543–52. doi: 10.1091/mbc.E11-06-0505

69. Peter M, Nakagawa J, Doree M, Labbe JC, Nigg EA. *In vitro* disassembly of the nuclear lamina and M phase-specific phosphorylation of lamins by cdc2 kinase. *Cell*. (1990) 61:591–602. doi: 10.1016/0092-8674(90)90471-p

70. Flores LF, Tader BR, Tolosa EJ, Sigafoos AN, Marks DL, Fernandez-Zapico ME. Nuclear dynamics and chromatin structure: implications for pancreatic cancer. *Cells*. (2021) 10(10):2624. doi: 10.3390/cells10102624

71. Zeng Y, Zhuang Y, Vinod B, Guo X, Mitra A, Chen P, et al. Guiding irregular nuclear morphology on nanopillar arrays for Malignancy differentiation in tumor cells. *Nano Lett*. (2022) 22:7724–33. doi: 10.1021/acs.nanolett.2c01849

72. Fischer AH. The diagnostic pathology of the nuclear envelope in human cancers. *Adv Exp Med Biol*. (2014) 773:49–75. doi: 10.1007/978-1-4899-8032-8_3

73. Brachner A, Reipert S, Foisner R, Gotzmann J. Lem2 is a novel man1-related inner nuclear membrane protein associated with a-type lamins. *J Cell Sci*. (2005) 118:5797–810. doi: 10.1242/jcs.02701

74. Wazir U, Ahmed MH, Bridger JM, Harvey A, Jiang WG, Sharma AK, et al. The clinicopathological significance of lamin a/C, lamin B1 and lamin B receptor mrna expression in human breast cancer. *Cell Mol Biol Lett*. (2013) 18:595–611. doi: 10.2478/s11658-013-0109-9

frontiers | Frontiers in Oncology

TYPE Original Research
PUBLISHED 24 May 2024
DOI 10.3389/fonc.2024.1297074

OPEN ACCESS

EDITED BY
Sharon R. Pine,
University of Colorado Anschutz Medical Campus, United States

REVIEWED BY
Luigi Losco,
University of Salerno, Italy
Federico Camilli,
University of Perugia, Italy
Professor Areerat Suputtitada, M.D., Chulalongkorn University, Thailand

*CORRESPONDENCE
Gamze Ünver
gamze.unver@ksbu.edu.tr

RECEIVED 19 September 2023
ACCEPTED 01 May 2024
PUBLISHED 24 May 2024

CITATION
Kavak SK and Ünver G (2024) Effect of complex decongestive therapy on frailty and quality of life in women with breast cancer-related lymphedema: the before-and-after treatment study.
Front. Oncol. 14:1297074.
doi: 10.3389/fonc.2024.1297074

Effect of complex decongestive therapy on frailty and quality of life in women with breast cancer-related lymphedema: the before-and-after treatment study

Songül Keskin Kavak[1] and Gamze Ünver[2]*

[1]Physical Therapy and Rehabilitation Clinic, Ankara Dr. Abdurrahman Yurtaslan Oncology Training and Research Hospital, Ankara, Türkiye, [2]Nursing Department, Faculty of Health Science, Kutahya Health Sciences University, Kutahya, Türkiye

Objective: To investigate the impact of Complex Decongestive Therapy (CDT) on the severity of frailty and quality of life in individuals suffering from postmastectomy lymphedema syndrome.

Methods: Participants who met the inclusion criteria were informed about CDT and informed consent was obtained. Edmonton Frailty Scale (EFS), extremity volüme (EV), lymphedema stage(LS), EQ-5D General Quality of Life Scale (EQ-5D-5L), and Quick Disabilities of Arm, Shoulder, and Hand (DASH) scores were evaluated by the same physician before and after treatment. A total of 15 sessions of CDT were performed for 3 weeks, five days a week. During the treatment period, hospitalized patients received guidance from a nurse on protecting the affected arm in their daily routine.

Results: Eighty patients with breast cancer-related lymphedema who met the inclusion criteria were included in the study. Following a period of 3 weeks of practice and training, the specialist physician conducted the final evaluation and assessments. All patients showed a statistically significant reduction in EV, and regression in LS, EFS, and Quick DASH score ($p<0.001$). Statistically significant improvement was also observed in quality of life and general health status. ($p<0.001$).

Conclusion: The application of 15 sessions of CDT and educational interventions to women with postmastectomy lymphedema syndrome due to breast cancer yielded positive outcomes. This approach led to an enhancement in patients' functional capacity, improving their quality of life and a subsequent reduction in the severity of frailty.

KEYWORDS

lymphedema, complex decongestive therapy, breast cancer, frailty, quality of life

Introduction

Breast cancer is indeed a significant global health concern, ranking as the most common cancer among women worldwide. According to the 2020 GLOBOCAN data, it represents 11.7% of all cancer incidence in women, highlighting its widespread impact on female populations globally (1).

Breast cancer-related lymphedema (BCRL) is a chronic and progressive complication associated with treatments such as lymph node dissection, surgery, or radiation therapy for breast cancer. This condition involves the accumulation of protein-rich fluid in the interstitial spaces and results from the disruption of normal lymphatic drainage (2). Incidence rates for BCRL can vary widely, but estimates suggest that approximately 30% of women diagnosed with breast cancer may develop BCRL (3). Early detection and the implementation of appropriate management strategies are crucial in enhancing the quality of life for individuals affected by BCRL.

Frailty is characterized as a prominent geriatric syndrome arising from the progressive decline in physiological reserves within the neuromuscular, metabolic, and immune systems with advancing age (4). Predominant symptoms encompass weight loss, weakness, fatigue, and reduced mobility, whereas notable observations entail sarcopenia, osteopenia, malnutrition, compromised balance, and coordination, as well as deceleration in walking speed (5). Challenges in assessing frailty within the clinical routine of breast cancer patients are well recognized (6). Illustratively, in a study investigating the impact of pre-chemotherapy inflammation on post-chemotherapy frailty in breast cancer patients, it was observed that elevated levels of inflammatory cytokines before chemotherapy correlated with subsequent frailty following chemotherapy (7). Literature studies have provided substantiation to the notion that factors inducing immobilization, such as lymphedema, sarcopenia, and osteopenia, contribute to the heightened severity of frailty after breast cancer treatments (including surgery, chemotherapy, radiotherapy, and hormone therapy) (8, 9).

Research findings indicate that patients experiencing BCRL often encounter challenges such as restricted range of motion, joint stiffness, and a sense of apprehension towards movement, all of which contribute to a state of immobilization (10). Contemporary research has demonstrated that the asymmetrical increase in volume resulting from upper extremity lymphedema significantly impacts postural stability. This phenomenon can disrupt the swing phase of gait, leading to a compromised sense of balance and coordination. Consequently, these factors collectively contribute to a reduced quality of life for individuals experiencing such conditions (11).

The physical therapy intervention for individuals with lymphedema is rooted in the principles of Complete Decongestive Therapy (CDT), encompassing several core components. These components entail diligent skin care, the application of manual lymphatic drainage, the utilization of bandaging techniques, and the incorporation of specific exercises. This comprehensive approach aims to alleviate the symptoms and manage the progression of lymphedema, ultimately improving the overall well-being of affected individuals (12). Lymphedema, once established, lacks a complete curative solution. If left untreated, it can result in progressive extremity volume enlargement, subsequently fostering a chronic inflammatory state and culminating in fibrotic changes. Consequently, the imperative for efficacious lymphedema management remains pivotal to mitigate these undesirable outcomes and enhance the overall quality of life for affected individuals (13).

A recently published study presented a new perspective on the treatment of lymphedema after breast cancer surgery. In the protocol presented in the study; Patients with breast cancer-related lymphedema were treated with CDT for at least 3 months, and surgical treatment was selected for those who did not show significant improvement. After surgery, all patients received 6 months of postoperative CDT consisting of continuous multilayer bandage compression therapy and multiple weekly MLD sessions. Patients were then switched to single-layer compression garments while weekly MLD sessions were gradually reduced and discontinued (14).

In one study, frailty in breast cancer patients aged 50 years and older was assessed using a modified frailty score derived from self-reported assessments and was associated with increased frailty during treatment and up to 6 months after treatment (15).

In the realm of breast cancer treatment research, while there exist studies scrutinizing the ramifications of frailty throughout the therapeutic journey, a notable absence persists in terms of inquiries into the impact of comprehensive decompression therapy on frailty severity and quality of life in individuals afflicted by lymphedema stemming from breast cancer surgery (16).

The primary objective of our study is to ascertain the influence of CDT on the severity of frailty and quality of life in patients afflicted with BCRL. We also aim to provide valuable information on patient management and therapeutic interventions that may benefit health practitioners and medical staff responsible for the care and treatment of lymphedema.

Methods

Study cohorts

The study enrolled female participants who had experienced BCRL, manifesting as unilateral upper extremity swelling, edema, stiffness, and restricted movement. These individuals had previously undergone breast cancer treatment, including surgery, chemotherapy, and radiotherapy. They presented at the oncological rehabilitation outpatient clinic and demonstrated adequate cognitive function(assessed by a physician)to comprehend the conducted tests. Exclusion criteria encompassed subjects with visual impairments, vestibular balance challenges, a history of stroke, prior orthopedic or neurological disorders, deep vein thrombosis, or skin infections such as erysipelas or cellulitis.

Power analysis

Power Analysis Power analysis is used in medical research to determine the smallest sample size required to detect a clinically

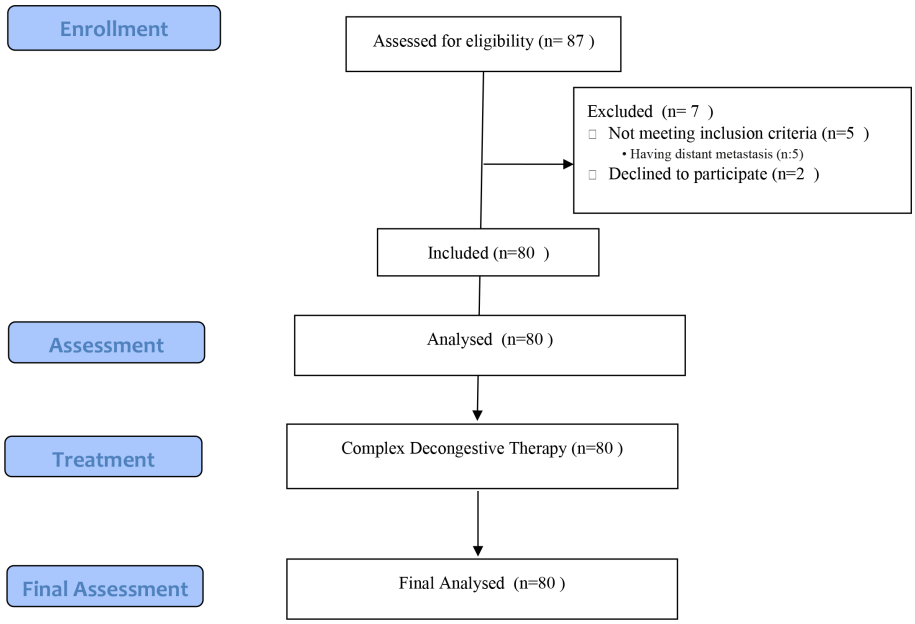

FIGURE 1
Flow chart of the study.

significant effect at a given statistical significance level. We used to posthoc power analysis program. According to the posthoc power analysis performed using the G*Power 3.1.9.2 program. The G Power analysis used a pre-determined effect size (Cohen's d) value of 0.5. The alpha level (Type I error) was set at 0.05, and the power level was set at 0.95. Given that a balanced sample size was used in the study, 80 patients were selected. the actual power was found to be 0.984 with a 5% margin of error.

Data collection tools

The international society of lymphology scale

The International Society of Lymphology scale is utilized for staging lymphedema, and each patient is assessed based on the following stages (17):

- Stage 0: This signifies a subclinical state where there is no apparent swelling despite impairments in lymph transport.
- Stage 1: There is an early onset of the condition with a visible accumulation of protein-rich tissue fluid. The swelling may exhibit pitting, meaning that pressing with the thumb causes an indentation that persists for some time. The swelling subsides with elevation of the affected limb.
- Stage 2: Increase in swelling that does not subside with elevation. Initially, pitting is evident, but over time, the tissue undergoes further proliferation and hardening, making pitting more difficult to induce.
- Stage 3: Tissues become harder (more fibrotic), and pitting is absent. There is a potential for further enlargement of the lymphedema, sometimes reaching extreme proportions. Additionally, skin changes such as thickening, hyperpigmentation, increased (deepened) skin folds, fat deposits, and warty overgrowths are present.

Quick DASH (Disabilities of Arm, Shoulder and Hand)

The Quick-DASH is a concise adaptation of the Arm, Shoulder, and Hand Disability Questionnaire, aimed at evaluating limitations in activity and participation related to upper extremity conditions. Consisting of 11 questions, the scale assesses challenges individuals face during their daily activities. Each response is ranked on a Likert scale from 1 to 5, reflecting varying degrees of difficulty. The scale underwent a validity and reliability study in the Turkish context in 2011, demonstrating its robustness and appropriateness for assessing such impairments (18).

Edmonton frailty scale

The Edmonton Frailty Scale (EFS), initially developed by Rolfson et al. (19) at the University of Alberta, Canada, to assess frailty in elderly populations, underwent a Turkish validity and reliability study conducted by Aygör in 2013. The scale encompasses 9 dimensions associated with frailty, as recognized in the Comprehensive Geriatric Evaluation framework. These dimensions encompass cognitive status, general health status, functional independence, social support, medication use, nutrition, mood, continence, and functional status. The scale comprises a total of 11 items. Cognitive status is evaluated using the 'clock test,' while functional performance is assessed through the 'Timed Get Up and Go test'. The scale includes 11 items covering the 9 frailty dimensions. The overall score, derived from summing up the scores of all 11 items, is employed

for scale evaluation. Scores can range from 0 (lowest) to 17 (highest), with an increasing total score indicating heightened frailty severity. The internal consistency of the "Edmonton Frailty Scale" was assessed by Aygör, yielding a Cronbach's alpha coefficient of 0.75. In this present study, the Cronbach's alpha coefficient for the EFS was calculated to be 0.771 (19, 20)

EQ-5D-5L (EQ-5D general quality of life scale)

The EQ-5D-5L general quality of life scale, developed by the EuroQol group in collaboration with the Western European Quality of Life Research Society in 1987, comprises two main components. The first component is the health profile for the day, encompassing five sub-dimensions: mobility, self-care, usual activities, pain/discomfort, and anxiety/depression. Each sub-dimension offers respondents five response options: "no problem," "slight problem," "moderate problem," "severe problem," and "extreme problem." The second component involves a visual analog scale, wherein individuals assign a value between 0 and 100 to depict their current health status on a thermometer-like scale. Quality of life scores ranging from 0 to 100 are obtained from the VAS section, with higher scores indicating a more favorable perception of health. The study utilized the Turkish version of the scale, which has been translated into 171 languages by the EuroQol group. Although the scale lacks a Cronbach's alpha value calculated by EuroQol, international studies have consistently reported Cronbach's alpha values exceeding 0.80 (21).

Research practice

In our study, eligible patients received comprehensive information regarding the proposed CDT, and their informed consent was obtained. These patients underwent an initial assessment conducted by a specialized physician. A total of 15 CDT sessions were subsequently administered, spanning a 3-week duration with sessions conducted on 5 days per week. In our center, CDT was applied as a treatment modality including manual lymph drainage (MLD), multilayer bandaging, compression garment, diaphragmatic and aerobic exercise, and skin care.

MLD was applied to all patients every morning. The neck and shoulder collectors were drained. The contralateral axillary lymph nodes were stimulated. The lymph class was directed from the diseased side to the unaffected side via an anterior axillo-axillary anastomosis. On the diseased side, the inguinal lymph nodes were stimulated and the lymphatic fluid was diverted from the upper quadrant to the lymph nodes on the same side via the axillo-inguinal anastomosis. This redirected lymphatic fluid from the congested area to the area with adequate lymphatic flow.

Multilayer bandaging was applied daily after MLD. It was started distally with the shortest length bandages. It was progressed by stretching in a proximal direction. After treatment, each patient wore a stage 2 upper limb compression garment. Diaphragmatic and aerobic exercise combinations consist of resistance and breathing exercises. These exercises increase sympathetic activity and cause contraction of smooth muscle in the lymphatic vessels. They increase intra-abdominal pressure. This creates a pumping effect in the thoracic duct. These effects increase lymphatic absorption. It also increases the conversion of lymphatic fluid into free circulation.

Neutral PH skin creams were used for skin care. After bathing, the skin was thoroughly dried between the fingers and moisturized with odor-free natural products.

During the treatment period, patients who were hospitalized or under medical care were provided with guidance from a nurse on appropriate measures to safeguard their lymphedema-affected arms during their daily activities. Following three weeks of practice and guidance, a final evaluation was carried out, and the relevant assessment scales were completed by the attending physician (Figure 1).

Analysis

The data analysis was conducted using IBM SPSS Statistics version 23 (IBM Corp., Released 2017). The normal distribution of the data was assessed using the Shapiro-Wilk test. Categorical data were presented as frequencies and percentages. For comparing dependent data that did not follow a normal distribution, the Wilcoxon Signed Ranks Test (Z*-table value) was employed. The Mann-Whitney U test (Z**-table value) was utilized to compare independent data sets that lacked a normal distribution. To compare measurement values across three or more independent groups without a normal distribution, the Kruskal-Wallis H test (X2-table value) was applied. A statistically significant threshold was defined as $p < 0.05$.

Ethics committee approval

Individuals who fulfilled the eligibility criteria and sought care at the Health Sciences University Oncological Physical Medicine and Rehabilitation Department outpatient clinics were considered for participation in the study. Those who satisfied the inclusion and exclusion criteria expressed their willingness to partake, and provided written informed consent, adhering to the ethical principles outlined in the Helsinki Declaration, were enrolled in the study.

Ethical approval for this study was obtained from the Oncology Training and Research Hospital Clinical Research Ethics Committee (decision no: 2022-11/2113, date: 09.11.2022). Written informed consent was obtained from all patients after providing them with detailed information about the study.

Results

The mean age of the participants was 65.42 ± 4.12 years. The majority of the participants were married (71.3%). Approximately 20% of the participants had a master's degree or higher and a significant proportion were housewives. The mean body mass index (BMI) of the participants was 30.27 ± 4.45 kg/m^2, indicating that they were significantly above the recommended weight range (classified as obese). Other sociodemographic characteristics of the patients are given in Table 1.

The average duration of lymphedema in the patients was found to be 24.86 ± 27.10 months. Among the participants, 32.5% had

hypertension and 26.3% had diabetes mellitus. All participants had undergone a consistent cancer treatment process. Notably, 100% of the patients reported experiencing symptoms of increased warmth and swelling in their extremities, with the majority (91.3%) also experiencing tension-related symptoms (Table 2).

The mean scores on the various scales were compared between the patients before and after the treatment. In comparison to the initial assessment, post-treatment evaluations revealed a reduction in extremity volüme (11), a decrease in lymphedema stage (15), an improvement in quality of life(Quick DASH), a decrease in frailty (EFS), a reduction in activity participation restrictions, and an enhancement in general health status(HSA) among the patients (Table 3).

Among the different occupational groups, civil servants and retired patients experienced greater improvements in EFS, Quick DASH, and HSA compared to housewives. (p=0.001, p=0.001, p=0.034 respectively) In terms of marital status, married patients showed more pronounced improvements in HSA than single patients. (p=0.023) Moreover, patients without any chronic diseases exhibited more significant enhancements in EFS and EV. (p=0.014, p=0.001, respectively) (Table 4).

TABLE 1 Sociodemographic characteristics of the patients at baseline.

(N=80)		
Median age (range) — yr		65 (59 - 77)
Age group — no. (%)		
<65 yr		31 (38.75)
≥65 yr		49 (60)
Mean Height ± S.D.(range) — cm		159.75 ± 5.73 (144 - 169)
Mean Weight ± S.D.(range) — kg		77.01 ± 10.40 (56 - 103)
Mean BMI ± S.D.(range) — kg/m^2		30.27 ± 4.45 (20.57 - 44.44)
Comorbidity— no. (%)		
Hypertension		18 (22.5)
Diabetes Mellitus		7 (8.75)
Hypothroidi		3 (3.75)
Asthma		8 (10)
Lymphedema Stages		
Stage 1		10 (12.5)
Stage 2		41 (51.25)
Stage 3		29 (36.25)
Duration of Lymphedema, Mean± S.D.(range) — month		
Marital status— no. (%)	Married	57 (71.3)
	Single	23 (28.8)
Educational status— no. (%)	Literate	11 (13.8)
	Primary education	46 (57.5)
	Secondary education	7 (8.8)
	Bachelor and above	16 (20.0)
Profession— no. (%)	Housewife	62 (77.5)
	Civil Servant/ Retired	17 (21.3)
	Teacher	1 (1.3)
Smoking History— no. (%)	Current	34 (42.5)
	Never	46 (57.5)

BMI, Body Mass Index; S.D., Standard Deviation; cm, centimeters; kg, kilograms; yr, year.

Discussion

Our study showed remarkable results in patients with BCRL undergoing CDT, demonstrating a reduction in limb volume, regression of LS, improvement in quality of life, reduction of frailty, alleviation of activity limitations, and an overall improvement in general health status.

Existing literature highlights that breast cancer patients often encounter physical and psychological challenges, exacerbated by the severity of lymphedema, leading to a negative impact on their overall quality of life (22, 23). For instance, Orhan et al. demonstrated in their study involving 83 breast cancer patients that quality of life and upper extremity functional status were more adversely affected in cases of severe lymphedema compared to milder instances. However, the overall population exhibited only a weak correlation between lymphedema severity and quality of life

TABLE 2 Findings regarding the health status of the patients.

Chronic disease — no. (%)	Hypertension	26 (32.5)
	DM	21 (26.3)
	Thyroid	8 (10)
	Asthma	5 (6.2)
	None	20 (25)
Cancer treatment process— no. (%)	Surgery	80 (100)
	Chemotherapy	80 (100)
	Radiotherapy	80 (100)
	Hormone therapy	80 (100)
Other symptoms in extremity— no. (%)	Tension	73 (91.3)
	Temperature rise	80 (100)
	Inflatable	80 (100)
	Pain	61 (76.3)
	Lethargy	45 (56.3)
	Feeling of heaviness	58 (72.5)
Mean Lymphedema time ± S.D.(range) — months		24.86 ± 27.10(1 - 96)

DM, Diabetes Mellitus; S.D., Standard Deviation.

TABLE 3 Comparison of the scales used in the research before and after.

	Before CDT	After CDT	p**	Z*
Extremity volume, Mean ± S.D. (range) — ml	680.5 (442.25-884)	287 (187-385.25)	**<0.001**	-7.772
Lymphedema stage Median. (range)	2 (2-3)	1 (1-1)	**<0.001**	-7.534
EQ-5D-5L,Mean± S.D. (range)	9 (7.25-10.75)	5 (5-6)	**<0.001**	-7.512
EFS, Mean± S.D. (range)	9 (4-13)	6.5 (3-9.75)	**<0.001**	-5.452
Quick DASH, Mean± S.D. (range)	56.81 (34.65- 72.72)	15.90 (6.81-22.72)	**<0.001**	-7.773
HSA, Mean± S.D. (range)	50 (40-57.5)	90 (80-90)	**<0.001**	7.850

Z*, Wilcoxon Signed Ranks Test; CDT, Complex Decongestive Therapy; ml, Milliliters; DASH, Disabilities of Arm, Shoulder and Hand; EFS, The Edmonton Frailty Scale; EQ-5D-5L, EQ-5D General Quality of Life Scale; HSA, Health status assessment. **p<0,05.

(24). In line with retrospective findings by Samancı et al., breast cancer patients receiving CDT over 15-30 sessions experienced a significant reduction in lymphedema volüme (25). In our study, statistically significant regression was also observed after 15 sessions of CDT.

In the study by Özcan et al., the group of patients who received CDT showed a reduction in lymphoedema volume, relief from pain and heaviness, and improvement in shoulder mobility. Functional capacity and quality of life were also improved in the study participants (26). Koul and colleagues carried out a lymphedema management approach that involved manual lymph drainage, complex decongestion therapy, and a home program with simple lymphatic drainage and exercise training. It is worth noting that the home program resulted in a 24% reduction in the cases studied by (27). In another study, patients with BCRL were divided into two groups conventional treatment and CDT, and significant improvement was observed in the health-related quality of life of patients after CDT (28). Our study was similarly consistent with the existing literature emphasizing that CDT contributes to improved quality of life.

Indeed, weight gain and obesity have been recognized as contributors to an elevated risk of lymphedema development

TABLE 4 Comparison of some sociodemographic characteristics of the patients and their post-treatment scale scores.

		EFS	LS	EQ-5D-5L	Quick DASH	HSA	EV
		Median (Q1-Q3)					
Profession	Housewife [1]	7 (5-11)	1 (1-1)	5 (5-7)	19.3 (9.1-27.3)	80 (80 -90)	311 (206.3-394.3)
	Civil Servant/ Retired[2]	4 (1-7)	1 (1-1)	5 (5-5)	6.8 (–15.9)	80 (80 -85)	187 (175.5-381.5)
	Teacher [3]	–	1 (1-1)	5 (5-5)	-	90 (90 -90)	244 (244-244)
X^{2*}		14.904	3.706	4.199	13.494	6.767	3.327
p**		**0.001**	0.151	0.123	**0.001**	**0.034**	0.189
Marital Status	Married	6 (3.5-9)	1 (1-1)	5 (5-6)	15.5 (6.8-27.27)	90 (80 -90)	287 (187-354.5)
	Single	8 (1-10)	1 (1-1)	5 (5-7)	15.9 (6.8-20.45)	80 (80 -90)	330 (187-432)
Z*		0.091	-0.635	-0.048	-1.312	-2.277	0.584
p		0.928	0.525	0.962	0.190	**0.023**	0.584
Chronical Disease	Yes	7 (4.25-11)	1 (1-1)	5 (5-6)	15.9 (9.7-27.27)	80 (80 -90)	312 (222-420)
	No	4.5 (1-8.75)	1 (1-1)	5 (5-6.5)	10.22 (–20.45)	80 (80 -90)	189 (166-246)
Z*		-2.453	-0.577	-1.174	-2.290	-1.648	-3.248
p**		**0.014**	0.056	0.24	0.022	0.099	**0.001**

X^{2*}, Kruskal-Wallis H test; Z*, Wilcoxon Signed Ranks Test; CDT, Complex Decongestive Therapy; ml, Milliliters; DASH, Disabilities of Arm, Shoulder and Hand; EFS, The Edmonton Frailty Scale; EQ-5D-5L, The 5-level EQ-5D version; EV, Extremity volume; HSA, Health status assessment; LS, Lymphedema stage. **p<0,05.

(29). Despite observing elevated body mass indexes among the women in our study, it is noteworthy that the outcomes of complex decongestion therapy were not adversely impacted.

The emergence of frailty is influenced by factors such as sarcopenia, chronic illnesses, immune function alterations, and neuroendocrine system changes (30). In our study, where 75% of participants had chronic conditions and the mean age was 65, these elements likely contributed to the observed frailty severity.

Our study exhibited significant changes in the QUICK DASH scores and health status evaluations of the patients after the intervention. These results align with Devoogdt et al., who reported that 31% of breast cancer-treated patients experienced impaired shoulder mobility, and 51% faced limitations in their daily activities (31). The study found that women who self-reported symptoms of lymphedema had a significant higher score on the Disabilities of Arm, Shoulder, and Hand questionnaire (mean difference 23.4, 95% confidence interval 19.3–27.5). This higher score indicates that these women experienced more significant activity limitations and participation restrictions compared to those without lymphedema symptoms (32). Considering our study's outcomes, the observed increase in QUICK DASH scores and improved functional capacities of patients suggest a potential enhancement in quality of life and a reduction in frailty severity.

Limitations of the study

This study has several limitations. Firstly, there is no control group, the small sample size is a notable limitation, which can impact the generalizability of the findings to a larger population. Additionally, the lack of long-term follow-up limits the ability to assess the sustained effects of complex decongestive therapy. The method of assigning participants to treatment groups based on the day of the week they attended the clinic may introduce biases, and the absence of random assignment could be a potential limitation.

Conclusion

In conclusion, the administration of 15 sessions of CDT along with educational interventions for breast cancer patients with BCRL resulted in improved functional capacity, subsequently enhancing their quality of life and thereby mitigating the severity of frailty. Future research should focus on evaluating the outcomes of a unified treatment plan in a larger and more diverse population to enhance the generalizability of the results.

Data availability statement

The original contributions presented in the study are included in the article/supplementary material. Further inquiries can be directed to the corresponding author.

Ethics statement

The studies involving humans were approved by ANKARA ONCOLOGY RESEARCH AND TRAINING HOSPITAL. The studies were conducted in accordance with the local legislation and institutional requirements. The participants provided their written informed consent to participate in this study.

Author contributions

SK: Writing – review & editing, Project administration, Funding acquisition, Supervision, Investigation, Formal analysis, Data curation. GÜ: Resources, Writing – review & editing, Writing – original draft, Methodology, Formal analysis.

Funding

The author(s) declare that no financial support was received for the research, authorship, and/or publication of this article.

Conflict of interest

The authors declare that the research was conducted in the absence of any commercial or financial relationships that could be construed as a potential conflict of interest.

Publisher's note

References

1. Sung H, Ferlay J, Siegel RL, Laversanne M, Soerjomataram I, Jemal A, et al. Global cancer statistics 2020: GLOBOCAN estimates of incidence and mortality worldwide for 36 cancers in 185 countries. *CA Cancer J Clin*. (2021) 71:209–49. doi: 10.3322/caac.21660

2. Document C. The diagnosis and treatment of peripheral lymphedema: 2020 consensus document of the international society of lymphology. *Lymphology*. (2020) 53 (1):3–19. doi: 10.2458/lymph.4649

3. Muñoz-Alcaraz MN, Jiménez-Vílchez AJ, Pérula-De Torres LÁ, Serrano-Merino J, García-Bustillo Á, Pardo-Hernández R, et al. Effect of conservative rehabilitation interventions on health-related quality of life in women with upper limb lymphedema secondary to breast cancer: A systematic review. *Healthcare*. (2023) 11:2568. doi: 10.3390/healthcare11182568

4. Özdemir S, Öztürk ZA, Türkbeyler İH, Şirin F, Göl M. Geriatrik hastalarda farkli ölçekler kullanilarak kirilganlik prevalansinin belirlenmesi. *Kahramanmaraş Sütçü İmam Üniversitesi Tıp Fakültesi Dergisi*. (2017) 12(3):1–5. doi: 10.17517/ksutfd.338266

5. Fairhall N, Aggar C, Kurrle SE, Sherrington C, Lord S, Lockwood K, et al. Frailty intervention trial (FIT). *BMC Geriatrics*. (2008) 8:27. doi: 10.1186/1471-2318-8-27

6. Jauhari Y, Gannon MR, Dodwell D, Horgan K, Tsang C, Clements K, et al. Addressing frailty in patients with breast cancer: A review of the literature. *Eur J Surg Oncol*. (2020) 46:24–32. doi: 10.1016/j.ejso.2019.08.011

7. Gilmore N, Kadambi S, Lei L, Loh KP, Mohamed M, Magnuson A, et al. Associations of inflammation with frailty in patients with breast cancer aged 50 and over receiving chemotherapy. *J Geriatr Oncol*. (2020) 11:423–30. doi: 10.1016/j.jgo.2019.04.001

8. Suskin J, Shapiro CL. Osteoporosis and musculoskeletal complications related to therapy of breast cancer. *Gland Surgery*. (2018) 7:411–23. doi: 10.21037/gs

9. Vehmanen LK, Elomaa I, Blomqvist CP, Saarto T. The effect of ovarian dysfunction on bone mineral density in breast cancer patients 10 years after adjuvant chemotherapy. *Acta Oncologica*. (2014) 53:75–9. doi: 10.3109/0284186X.2013.792992

10. Can AG, Can SS, Ekşioğlu E, Çakcı FA. Is kinesiophobia associated with lymphedema, upper extremity function, and psychological morbidity in breast cancer survivors? *Turkish J Phys Med Rehabil*. (2019) 65:139. doi: 10.5606/tftrd.2019.2585

11. Cuviena CF, Perez CS, Nardo VC, Siqueira das Neves LM, Rangon FB, Guirro ECO. Influence of age and lymphedema on the postural balance of women undergoing breast cancer treatment. *J Bodyw Mov Ther*. (2021) 27:307–13. doi: 10.1016/j.jbmt.2021.02.024

12. Tambour M, Tange B, Christensen R, Gram B. Effect of physical therapy on breast cancer related lymphedema: protocol for a multicenter, randomized, single-blind, equivalence trial. *BMC Cancer*. (2014) 14:239. doi: 10.1186/1471-2407-14-239

13. Bennett JA, Winters-Stone KM, Dobek J, Nail LM. Frailty in older breast cancer survivors: age, prevalence, and associated factors. *Oncol Nurs Forum*. (2013) 40:E126–E34. doi: 10.1188/13.ONF.E126-E134

14. Ciudad P, Bolletta A, Kaciulyte J, Losco L, Manrique OJ, Cigna E, et al. The breast cancer-related lymphedema multidisciplinary approach: Algorithm for conservative and multimodal surgical treatment. *Microsurgery*. (2023) 43:427–36. doi: 10.1002/micr.30990

15. Magnuson A, Lei L, Gilmore N, Kleckner AS, Lin FV, Ferguson R, et al. Longitudinal relationship between frailty and cognition in patients 50 years and older with breast cancer. *J Am Geriatrics Society*. (2019) 67:928–36. doi: 10.1111/jgs.15934

16. Uslu A, Canbolat O. Relationship between frailty and fatigue in older cancer patients. *Semin Oncol Nurs*. (2021) 37:151179. doi: 10.1016/j.soncn.2021.151179

17. Witte MH, Bernas MJ. Evolution of the 2020 international society of lymphology consensus document parallels advances in lymphology: an historical perspective. *Lymphology*. (2020) 53:1–2. doi: 10.2458/lymph.4650

18. Koldas Dogan S, Ay S, Evcik D, Baser O. Adaptation of Turkish version of the questionnaire Quick Disability of the Arm, Shoulder, and Hand (Quick DASH) in patients with carpal tunnel syndrome. *Clin Rheumatol*. (2011) 30:185–91. doi: 10.1007/s10067-010-1470-y

19. Rolfson DB, Majumdar SR, Tsuyuki RT, Tahir A, Rockwood K. Validity and reliability of the edmonton frail scale. *Age Ageing*. (2006) 35(5):526–9. doi: 10.1093/ageing/afl041

20. Aygör H. Edmonton Kırılganlık Ölçeği'nin Türk toplumu için geçerlik ve güvenirliğinin incelenmesi: Ege Üniversitesi (2013).

21. van Reenen M, Janssen B. EQ-5D-5L user guide: basic information on how to use the EQ-5D-5L instrument. *Rotterdam: EuroQol Res Foundation*. (2015) 9.

22. Abu-Helalah M, Al-Hanaqta M, Alshraideh H, Abdulbaqi N, Hijazeen J. Quality of life and psychological well-being of breast cancer survivors in Jordan. *Asian Pacific J Cancer Prev*. (2014) 15:5927–36. doi: 10.7314/APJCP.2014.15.14.5927

23. Galiano-Castillo N, Ariza-García A, Cantarero-Villanueva I, Fernández-Lao C, Díaz-Rodríguez L, Arroyo-Morales M. Depressed mood in breast cancer survivors: associations with physical activity, cancer-related fatigue, quality of life, and fitness level. *Eur J Oncol Nurs*. (2014) 18:206–10. doi: 10.1016/j.ejon.2013.10.008

24. Orhan C, Özgül S, Nakip G, Baran E, Üzelpasaci E, Çinar GN, et al. Meme kanseri tedavisiyle ilişkili lenfödemi olan hastalarda lenfödem şiddetinin yaşam kalitesi, üst ekstremite fonksiyonu ve fiziksel aktivite düzeyi üzerindeki etkileri. *Anadolu Kliniği Tıp Bilimleri Dergisi*. (2019) 24:189–98. doi: 10.21673/anadoluklin.554019

25. Samancı N, Karataş Ö, Samur A, Çipli A, Balcı N. Efficacy of complex decongestive therapy on breast cancer-related lymphedema: a cross-sectional study. *J Surg Med*. (2019) 3(4):300–3. doi: 10.28982/josam.551125

26. Sezgin Ozcan D, Dalyan M, Unsal Delialioglu S, Duzlu U, Polat CS, Koseoglu BF. Complex decongestive therapy enhances upper limb functions in patients with breast cancer-related lymphedema. *Lymphat Res Biol*. (2018) 16:446–52. doi: 10.1089/lrb.2017.0061

27. Koul R, Dufan T, Russell C, Guenther W, Nugent Z, Sun X, et al. Efficacy of complete decongestive therapy and manual lymphatic drainage on treatment-related lymphedema in breast cancer. *Int J Radiat Oncol Biol Phys*. (2007) 67:841–6. doi: 10.1016/j.ijrobp.2006.09.024

28. Melam GR, Buragadda S, Alhusaini AA, Arora N. Effect of complete decongestive therapy and home program on health- related quality of life in post mastectomy lymphedema patients. *BMC Women's Health*. (2016) 16(23):1–9. doi: 10.1186/s12905-016-0303-9

29. Sudduth CL, Greene AK. Current overview of obesity-induced lymphedema. *Advances in wound care*. (2022) 11(7):392–8. doi: 10.1089/wound.2020.1337

30. Kapucu ss. Kırılgan yaşlı ve hemşirelik bakımı. *Osmangazi J Med*. (2017) 39:122–9. doi: 10.20515/otd.288967

31. Devoogdt N, Christiaens MR, Geraerts I, Truijen S, Smeets A, Leunen K, et al. Effect of manual lymph drainage in addition to guidelines and exercise therapy on arm lymphoedema related to breast cancer: randomised controlled trial. *BMJ*. (2011) 343:d5326–d. doi: 10.1136/bmj.d5326

32. Dawes D, Meterissian S, Goldberg M, Mayo N. Impact of lymphoedema on arm function and health-related quality of life in women following breast cancer surgery. *J Rehabil Med*. (2008) 40:651–8. doi: 10.2340/16501977-0232

frontiers | Frontiers in Oncology

TYPE Original Research
PUBLISHED 26 June 2024
DOI 10.3389/fonc.2024.1347166

OPEN ACCESS

EDITED BY
Sharon R. Pine,
University of Colorado Anschutz Medical Campus, United States

REVIEWED BY
Ossama Tawfik,
Saint Luke's Health System, United States
Alisson Clemenceau,
Yale University, United States

*CORRESPONDENCE
Hossein Schandiz
hschandiz@gmail.com

†These authors have contributed equally to this work and share last authorship

RECEIVED 30 November 2023
ACCEPTED 04 June 2024
PUBLISHED 26 June 2024

CITATION
Schandiz H, Farkas L, Park D, Liu Y, Andersen SN, Geisler J and Sauer T (2024) Low progesterone receptor levels in high-grade DCIS correlate with HER2 upregulation and the presence of invasive components. *Front. Oncol.* 14:1347166. doi: 10.3389/fonc.2024.1347166

Low progesterone receptor levels in high-grade DCIS correlate with HER2 upregulation and the presence of invasive components

Hossein Schandiz[1,2*], Lorant Farkas[2,3], Daehoon Park[3], Yan Liu[2,4], Solveig N. Andersen[2], Jürgen Geisler[1,2†] and Torill Sauer[2†]

[1]Department of Oncology, Akershus University Hospital (AHUS), Lorenskog, Norway, [2]Institute of Clinical Medicine, Faculty of Medicine, University of Oslo, Oslo, Norway, [3]Department of Pathology, Oslo University Hospital, Oslo, Norway, [4]Department of Clinical Molecular Biology (EpiGen), Akershus University Hospital (AHUS), Lorenskog, Norway

Objective: In this study, we investigated pivotal molecular markers in human high-grade breast ductal carcinoma *in situ* (DCIS). Expression status of estrogen receptor (ER), progesterone receptor (PR), and human epidermal growth receptor 2 (HER2) was measured among various subtypes (Luminal (Lum) A, LumB HER2$^-$, LumB HER2$^+$, HER2-enriched and triple-negative).

Methods: In total, 357 DCIS cases were classified into respective subtypes, according to the 2013 St. Gallen guidelines. Each subtype was categorized into three subcategories: "Pure" (those without an invasive component), "W/invasive" (those with an invasive component), and "All" (the entire group of the given subtype). ER and PR expression were registered as intervals. Equivocal HER2 immunohistochemistry (IHC) cases (2+) were further investigated using dual-color *in situ* hybridization.

Results: The majority of patients (71%) were over the age of 50. We discovered no significant differences in the proportion of age between the "Pure" and "W/invasive" groups. There was no significant difference in ER/PR expression between "Pure" luminal subtypes of DCIS and "W/invasive" cases. We compared the HER2 IHC scores of "0", "1+", and "2+" among LumA and LumB HER2 subtypes and identified no statistically significant differences between "Pure" and "W/invasive" (p = 0.603). ER and PR expression ≥ 50% cutoff value was present in > 90% of all LumA cases. The incidences of cases with ER expression at cutoff values of < 10% and ≥ 50% in LumA were significantly different compared to other luminal subtypes (p < 0.0001). The proportion of cases with PR expression < 20% showed significant differences in the various luminal subtypes. In luminal B subtypes, low PR expression (< 20%) was significantly associated with both strong HER2 expression (3+) and the presence of an invasive component (p = 0.0001 and p = 0.0365, respectively).

Conclusions: ER and PR expression at ≥ 50% cutoff values were found in more than 90% of LumA cases. Samples with ER < 10% and ≥ 50% in LumA were

significantly different compared to other luminal subtypes ($p < 0.0001$). Low PR expression in high-grade DCIS was strongly associated with HER2 overexpression (3+) and an invasive component ($p = 0.0001$ and $p = 0.0365$, respectively).

KEYWORDS

ductal carcinoma *in situ*, invasive breast carcinoma, molecular subtypes, precision medicine, immunohistochemistry, hormone receptors, HER2, *in situ* hybridization

Introduction

Breast ductal carcinoma *in situ* (DCIS), a precancerous lesion that is considered to be a precursor of invasive breast carcinoma (IBC), is a frequent finding during modern breast cancer diagnostics after mammography screening was implemented (1). In industrialized countries, the incidence of DCIS is approximately 20%–25% of all malignant lesions detected in national screening programs (1, 2). Only a proportion of these lesions eventually transform into IBC. If left untreated, it is predicted that 8%–17.6% of DCIS cases may progress to IBC after 10 years, and in some studies, this percentage has been as high as 20%–30% (3). Many of these lesions are small when detected and guidelines for *in situ* lesions recommend either surgery alone or surgery followed by radiation as the usual treatment options. Treatment of DCIS is still exclusively determined by the extent and histological grade of the lesion (4). Our overall aim is to identify distinct subtypes of DCIS lesions that often progress to IBC, or not, to pave the way toward precision medicine for patients diagnosed with DCIS. We hypothesize that selected patients at high risk for the development of invasive cancers may require intensified, tailored, and targeted treatment, possibly including immunotherapy (e.g., anti-PD-1/PD-L1 (5, 6)) and anti-human epidermal growth factor receptor 2 (HER2) therapy, as offered to patients diagnosed with IBC (7–10). We believe that changing the current guidelines may not only have beneficial impacts on patients, avoiding under- and overtreatment, but also the health system will be able to better allocate funding to patients diagnosed with high-grade DCIS. To date, the utility of immunohistochemistry (IHC) markers has not been established in DCIS diagnostics, in contrast to IBC, where the hormone receptors (HRs) for estrogen (ER) and progesterone (PR), HER2, and Ki67 proliferation index are all deciding on a complex treatment algorithm. DCIS of the breast is a heterogeneous entity with nuclear atypia varying from mild to pronounced with various distinct growth patterns. We regularly confirm the presence of IHC-stained DCIS as part of the routine diagnosis of IBC but do not take much notice of it since these findings currently have no impact on therapy. Few studies have evaluated these markers in DCIS according to their molecular subtypes (11–13). In a previous study of high-grade breast DCIS, we reported the distribution of molecular subtypes. LumA and luminal B HER2-negative (LumB HER2$^-$) cases together comprised 50.4%, luminal B HER2-positive (LumB HER2$^+$) comprised 22.1%, HER2-enriched comprised 21.8%, and triple-negative (TPN) subtype comprised 5.6% of cases. We also identified the HER2-enriched subtype as a high-risk entity because it was significantly correlated with the presence of an invasive component (14, 15). This study aimed to investigate the pivotal and well-established molecular breast cancer markers, ER, PR, and HER2, in the respective subtypes of human high-grade DCIS, aiming to identify those DCIS lesions that most probably will progress to IBC.

Abbreviations: DCIS, ductal carcinoma *in situ*; BC, invasive breast carcinoma; IHC, immunohistochemistry; ER, estrogen receptor; PR, progesterone receptor; HER2, human epidermal growth factor receptor 2; Ki67, proliferation index; HR, hormone receptor; dc-SISH, dual-color silver-enhanced *in situ* hybridization; FFPE, formalin-fixed paraffin-embedded.

Materials and methods

Our study material consisted of formalin-fixed and paraffin-embedded (FFPE) histopathological specimens from the consecutive patient cohort stored in the diagnostic archive at Akershus University Hospital, Norway. Collected between 1996 and 2018, these samples represented 494 female patients diagnosed with DCIS of the breast. Experienced breast pathologists actively graded the histopathological specimens using the Van Nuys classification system (15, 16). To our knowledge, this is the largest DCIS biobank that has been approved for cancer research purposes in Europe. We chose to focus on and investigate grade 3 (high-grade) DCIS cases because these lesions are thought to have the highest risk of recurrence and progression to IBC (16–19). A total of 357 high-grade DCIS cases were submitted to IHC analysis, stained for ER, PR, HER2, and Ki67, and subjected to further studies. These were classified into their respective subtypes in accordance with the 2013 St. Gallen International Consensus Conference Guidelines, currently established for molecular subtyping of IBC lesions (15). Briefly, according to this classification (20), the LumA subtype was defined when ER was positive (≥ 1%) and/or PR was ≥ 20%, HER2$^-$, and Ki67 index was < 20%. LumB HER2$^-$ was defined as ER that was positive, HER2$^-$, and Ki67 index expression was ≥ 20%, or when ER was ≥ 1%, Ki67 was ≥ 20% or PR expression was < 20%, and HER2 was negative. LumB HER2$^+$ was defined when ER and/or PR were

positive and HER2$^+$ and Ki67 were at any value. HER2-enriched was defined as ER and PR negativity, HER2 positivity, and any Ki67 value. TPN was defined when ER, PR, and HER2 were negative and Ki67 was at any value. The general definitions of the molecular subtypes in IBC, according to IHC surrogate markers, are provided in Supplementary Table S1 (21–23). All procedures have been described in detail in our previous study (15). Each subtype was sorted into three subcategories: "Pure" (n = 306) meaning those without an invasive component; "W/invasive" (n = 51) meaning those with an invasive component; and "All" (n = 357) meaning the entire group of the given subtype. We decided to split the patients based on age (younger than 50 and older than 50), taking into account other studies that looked at the incidence and mortality rate of DCIS (2, 24).

Immunohistochemistry and dual-color silver-enhanced *in situ* hybridization

IHC staining for ER, PR, HER2, and Ki67 was performed using a Dako Autostainer (Agilent). Antigen retrieval was achieved in a PT-Link station by immersion in EnVision™ FLEX Target Retrieval Solution at a high pH (K8004, Agilent) and heating at 97°C for 20 min. Endogenous peroxidase activity was quenched by incubating the slides in the EnVision™ FLEX peroxidase blocking reagent (K8000, Agilent) for 5 min. For HER2 IHC, nonspecific staining was inhibited by an animal-free blocking solution 1× (No. 15019) for 30 min. Primary antibodies Ki67 (1:200), ER (1:50), and PR (1:100) were diluted in EnVision™ FLEX Antibody Diluent (K8006, Agilent); antibody HER2 (1:200) was diluted in SignalStain® Antibody Diluent (No. 8112, Cell Signaling), and slides were incubated with primary antibodies for 20–60 min at room temperature. For ER and PR IHC, rabbit (K800921–2, Agilent) and mouse (K800221–2, Agilent) linkers were added for 15 min for signal amplification after incubation with the primary antibody. This was followed by incubation with the ready-to-use secondary buffered solution (k8002, EnVision FLEX/HRP, Agilent) for 20 min. The sections were reacted with 3.30-diamino-benzidine tetrahydrochloride (DAB) solution for 10 min and counterstained with hematoxylin (link) (k8008, Agilent) for 5 min. In each run, a positive tissue control with invasive mammary carcinoma was included. Details of the antibody clones, staining, and dilutions are described in Table 1. The ER and PR IHC positivity was defined as ≥ 1% positive tumor (DCIS) cells in accordance with the updated guidelines of the American Society of Clinical Oncology (ASCO) and College of American Pathologists (CAP) (25) developed for IBC. We chose to divide the ER into the following intervals: < 1%, 1%–10%, > 10%–50%, and > 50%–100%, and PR in < 1%, 1%–20%, > 20%–50%, and > 50%–100%, based on St. Gallen 2013 and numerous other studies that examined the prognostic and predictive values in different HRs cutoff points (20, 26, 27). Ki67% IHC was estimated, by counting 200 DCIS cells in two separate hotspot foci, and the ratios were calculated and recorded as continuous values, rather than categorical values. Ki67 cutoff threshold was set at 20%, in accordance with the 2013 St. Gallen Recommendations (28) established for IBC. Three breast pathologists interpreted the IHC analysis in ER, PR, HER2, and Ki67. HER2 IHC was scored based on ASCO/CAP guidelines, as in routine diagnostics for IBC (29, 30). Briefly, HER2 was scored "0" when IHC staining was absent or membrane staining was weak and pale in ≤ 10% of DCIS cells. HER2 was considered "1+" when partial and incomplete membrane staining also showed a faint intensity within > 10% of the DCIS cells, and HER2 that was scored as "3+" showed strong and complete positive membrane staining in > 10% of DCIS cells. HER2 was identified as "2+" when the membrane was stained faint to moderately complete in > 10% of DCIS cells or strongly and completely in ≤ 10% of DCIS cells, which was considered equivocal and was subjected to further dual-color silver-enhanced *in situ* hybridization (dc-SISH) analysis performed on a Ventana BenchMark (Roche Diagnostics, Switzerland) machine using the fully automated Ultra-IHC/ISH Staining Module (31) with CC2 as a buffer. The dc-SISH results were interpreted in accordance with the ASCO/CAP comprehensive guidelines and algorithms established for IBC (32). We did not observe any changes in the quality or intensity of ER, PR, Ki67, HER2 IHC, or HER2 SISH, regardless of when the sample was taken.

Statistical analysis

GraphPad Prism version 9.4 was used for the statistical calculations. We applied different tests to calculate statistical significance, ensuring they were conducted only when appropriate. Pearson's Chi-square (χ^2) or Fisher's exact tests were used to calculate p-values when comparing two proportions, using the contingency table. Statistical significance was set *a priori* at $p < 0.05$.

Results

Hormone receptor status

The majority of patients (71%) were older than 50 years (Supplementary Figures S1A, B; Table 2). There were no significant

TABLE 1 Details of antibodies' clone, staining, and dilutions.

Antibody	Clone	Staining	Reference ID	Vendor	Dilution
Anti-Ki67	MIB-1	Nuclear	M724001–2	Agilent (USA)	1:200
Anti-human estrogen receptor α	EP1	Nuclear	M364301–2	Agilent (USA)	1:50
Anti-human progesterone receptor	PR 636	Nuclear	M356901–2	Agilent (USA)	1:100
Anti-HER2/ErbB2	D8F12	Membrane	#4290	Cell Signaling (USA)	1:200

TABLE 2 Distribution of age ⩽ 50 years is demonstrated among all subtypes that are further subcategorized in "Pure" and "W/invasive", respectively.

Age (years)	LumA "Pure" (n = 110)	LumB HER2$^-$ "Pure" (n = 48)	LumB HER2$^+$ "Pure" (n = 70)	HER2-enriched "Pure" (n = 60)	TPN "Pure" (n = 18)
< 50	34%	31%	31%	23%	6%
≥ 50	66%	69%	69%	77%	94%
Age (years)	**LumA "W/invasive"** (n = 17)	**LumB HER2$^-$ "W/invasive"** (n = 5)	**LumB HER2$^+$ "W/invasive"** (n = 9)	**HER2-enriched "W/invasive"** (n = 18)	**TPN "W/invasive"** (n = 2)
< 50	35%	20%	56%	22%	50%
≥ 50	65%	80%	44%	78%	50%

differences in the proportion of age in the "Pure" (n = 306) versus "W/invasive" (n = 51) groups. Of "All" cases, 98% of the LumA subtype showed an ER ≥ 50%. PR expression ≥ 50% was found in 91% of cases in this subtype. In general, the expression of PR was slightly lower than that of ER in the LumA subtype. Details of ER and PR expression in luminal subtypes (LumA, LumB HER2$^-$, and LumB HER2$^+$) according to 2013 St. Gallen consensus meeting guidelines are shown in Figures 1A-F; Supplementary Table S2. The incidence of ER-positive cases at a cutoff of < 10% in the LumA subtype was significantly lower than that in the LumB HER2$^-$ and LumB HER2$^+$ subtypes (p < 0.0001, chi-square) (Figure 2A). In contrast, there was a statistically significant increase in ER expression at a cutoff of ≥ 50% in the LumA compared to the latter subtypes (p < 0.0001, chi-square) (Figure 2B). The proportion of PR-positive cases at a cutoff of < 20% showed significant differences in luminal subtypes between the LumA, LumB HER2$^-$, and LumB HER2$^+$ subtypes (3%, 47%, and 44%, respectively) (p < 0.0001, Chi-square) (Figure 2C). There was also a significantly higher proportion of patients with a PR ≥ 50% among the LumA subtype (p < 0.0001, Chi-square) (Figure 2D). We demonstrated that low PR expression (< 20%) was significantly associated with a concurrent invasive component (p = 0.0365, Fisher's exact test) (Figure 3A). We observed no significant differences in ER expression (< 1%, 1%–10%, > 10%–50%, > 50%–100%) and PR expression (< 1%, 1%–20%, > 20%–50%, > 50%–100%)

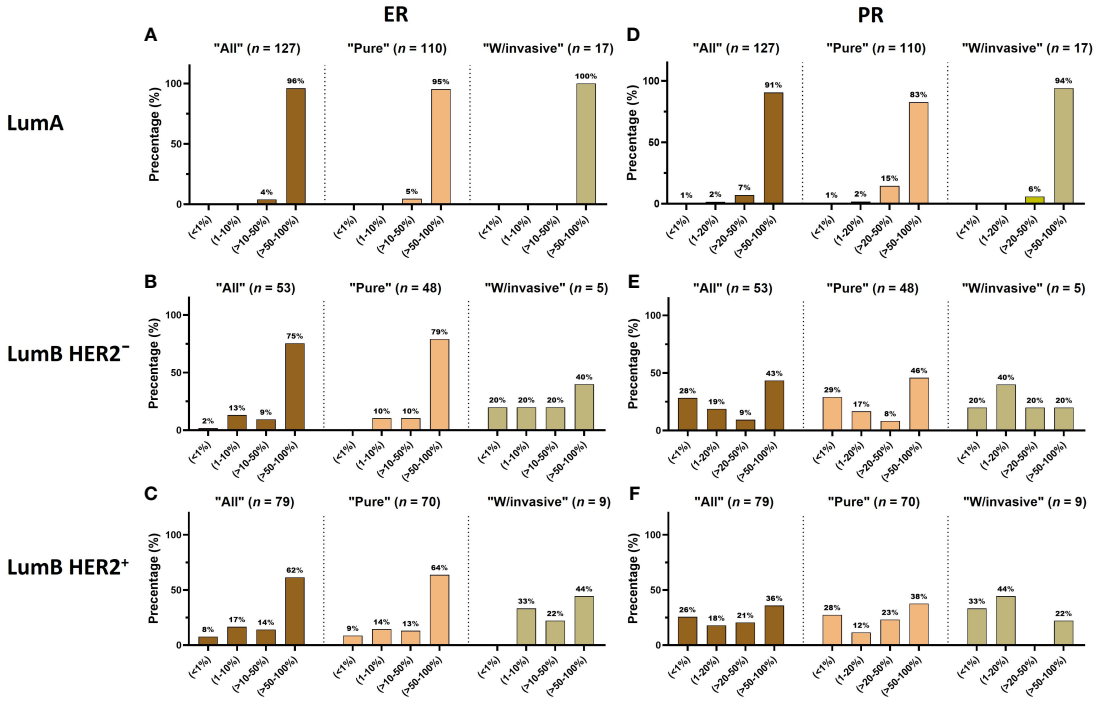

FIGURE 1
(A–F) The distribution of ER and PR expression is displayed in each luminal subtype (LumA, LumB HER2$^-$ and LumB HER2$^+$). Each subtype is further subcategorized into "All", "Pure", and "W/invasive", respectively.

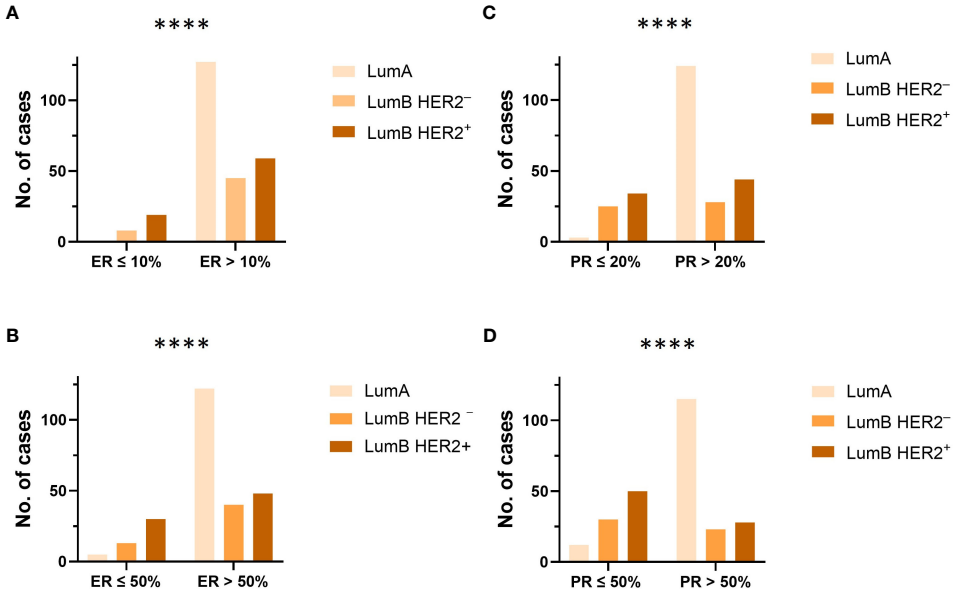

FIGURE 2
(A, B) The proportion and distribution of ER at cutoff values of 10% and 50%, were compared between each luminal subtype (LumA, LumB HER2⁻ and LumB HER2⁺), respectively. ****p-value < 0.0001, Chi-square test. **(C, D)** The proportion and distribution of PR at cutoff values of 20% and 50%, were compared between each luminal subtype (LumA, LumB HER2⁻, and LumB HER2⁺), respectively. ****p-value < 0.0001, Chi-square test.

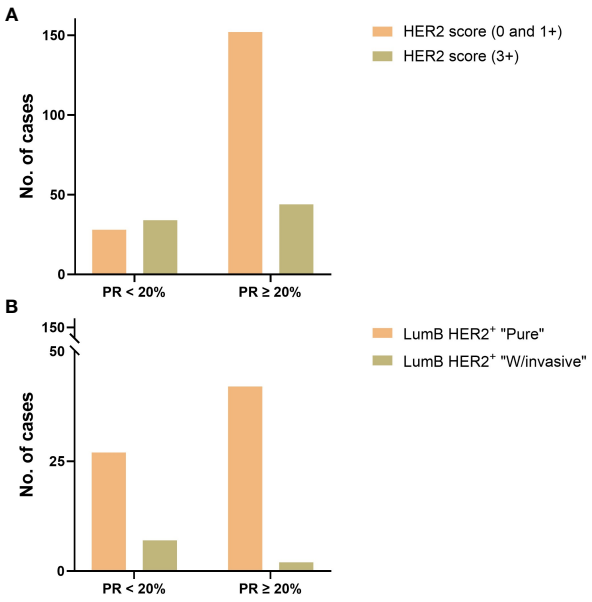

FIGURE 3
(A) PR expression status with a cutoff value of 20% was compared to HER2 IHC scores ("0", "1+", and "3+") in luminal B subtypes and showed a significant difference (p-value = 0.0001, Fisher's exact test) in favor of those with HER2 IHC score 3+. **(B)** PR expression status with a cutoff value of 20% in the LumB HER2+ subtype was compared in the "Pure" vs. "W/invasive" subcategories and showed a significant difference (p-value = 0.0365, Fisher's exact test) in favor of the "W/invasive" component.

between luminal subtypes in "Pure" cases of high-grade DCIS and those "W/invasive" components.

HER2 status

The distribution of HER2 IHC scores showed the proportions for score 0 as 41%; score 1+ as 13%; score 2+ as 4%; and score 3+ as 42%. Of the LumA cases, 96% were HER2⁻, with an IHC score of 0 or 1+ (Table 3). We compared the HER2 IHC 0, 1+, and 2+ scores among LumA and LumB HER2⁻ subtypes and did not find statistically significant differences when the "Pure" and "W/invasive" were compared (p = 0.603, Chi-square). We found a significant association between HER2 overexpression (score 3+) and low PR expression (< 20%) in the luminal B subtypes (p = 0.0001, Fisher's exact test) (Figure 3B). A total of 16 cases were HER2 IHC equivocal (2+ score) and subjected to HER2 dc-SISH analysis. Five cases belonged to LumA, one to LumB HER2⁻, seven to LumB HER2⁺, and one to HER2-enriched, whereas two samples belonged to the TPN subtype. Nonamplified cases had a mean of 3.1 HER2 gene signals and 2.3 chromosome 17 (CEP17) signals. Amplification by dc-SISH was observed in 50% of cases. The LumB HER2⁺ subtype accounted for 88% of all dc-SISH amplification cases. Figures 4A-F display dc-SISH staining in selected cases, from nonamplification to high amplification (clusters). Details of the dc-SISH findings, HER2 gene, and centromeric probe for CEP17 count and ratios are summarized in Table 4.

TABLE 3 HER2 IHC expression is displayed according to the molecular subtypes.

Subtypes	0 (*n* = 147; 41%)	1+ (*n* = 45; 13%)	2+ (*n* = 16; 4%)	3+ (*n* = 149; 42%)	Subtotal (*n* = 357; 100%)
LumA (*n* = 127)	97 (76%)	25 (20%)	5 (4%)		*n* = 127
"Pure" (*n* = 110)	85 (77%)	20 (18%)	5 (5%)		
"W/invasive" (*n* = 17)	12 (70%)	5 (30%)			
LumB HER2$^-$ (*n* = 53)	37 (70%)	15 (28%)	1 (2%)		*n* = 53
"Pure" (*n* = 48)	34 (71%)	13 (27%)	1 (2%)		
"W/invasive" (*n* = 5)	3 (60%)	2 (40%)			
LumB HER2$^+$ (*n* = 79)			7 (9%)	72 (91%)	*n* = 79
"Pure" (*n* = 70)			6 (9%)	64 (91%)	
"W/invasive" (*n* = 9)			1 (11%)	8 (89%)	
HER2-enriched (*n* = 78)			1 (1%)	77 (99%)	*n* = 78
"Pure" (*n* = 60)			1 (2%)	59 (98%)	
"W/invasive" (*n* = 18)				18 (100%)	
TPN (*n* = 20)	13 (65%)	5 (25%)	2 (10%)		*n* = 20
"Pure" (*n* = 18)	12 (67%)	4 (22%)	2 (11%)		
"W/invasive" (*n* = 2)	1 (50%)	1 (50%)			

The number (n) of HER2 IHC score ("0", "1+", "2+", and "3+") is given for each respective subtype. The proportion of the HER2 IHC score is given within each subtype.

Discussion

ER regulates PR expression in human breast tissue; thus, the latter hormone receptor is a clinical prognostic marker of ER action (33, 34). Therefore, low PR expression may indicate low or fading ER expression. Overall, our results demonstrated considerable heterogeneity in high-grade DCIS. High ER and PR expression were significantly more prevalent in the LumA subtype than in the LumB HER2$^-$ and LumB HER2$^+$ subtypes. In contrast, low ER and PR expression were more common in the latter two subtypes ($p <$ 0.0001, Chi-square). Our results are consistent with those made in IBC (23). Furthermore, we found that low PR expression was significantly associated with HER2 overexpression (IHC score 3+) in both luminal B subtypes and in those with an invasive component (p = 0.0001 and p = 0.0365, respectively; Fisher's exact test). These findings indicate that low PR expression in DCIS is an independent marker for progression to IBC and upregulation of the HER2 gene, with poor outcomes in patients diagnosed with IBC (35–39). Konecny et al. (40) identified an inverse relationship between HR levels and HER2 gene amplification in a large number of human breast cancer tissues. Huang HJ et al. investigated the relationship between age, HRs, and HER2 status in female patients with invasive breast cancer (41). They found that the relationship between HRs and HER2 expression varied with patient age, with a negative correlation primarily observed in patients aged > 45 years. This is an intriguing finding given that the majority (71%) of patients in our study material were over the age of 50 years (Supplementary Figures S1A, B). Shah et al. (42) reported a significant difference between age and ER/PR expression, although they did not identify any significant variation between age and HER2 overexpression. In our earlier study, we identified that HER2 overexpression in cases classified as the HER2-enriched subtype was concurrent with early morphological invasive growth in high-grade DCIS (15). HER2 gene amplification in IBC is an independent poor prognostic factor (43, 44). The prognostic and predictive roles of PR in IBC have been reported by others in some previous studies (35, 36, 45–47). However, while drugs that target ER are common therapeutic tools for the treatment of patients diagnosed with IBC (48), an effective drug targeting PR has not yet been approved for the treatment of these patients (35). Further studies are necessary to investigate whether, in diagnosing IBC and DCIS, PR can possibly be a reliable and reproducible prognostic and predictive marker in selected patients. Our results showed that HER2 expression varied greatly, with no significant differences between the LumA and LumB HER2$^-$ subtypes (Table 3). The LumB HER2$^+$ subtype had the highest number of equivocal (IHC 2+ score) lesions (7 of 16) and harbored an IHC 3+ score in 72 of 149 (48%) cases. The HER2-enriched subtype was uniform and had a strong IHC 3+ score in all except one case, whereas the LumB HER2$^+$ subtype was quite heterogeneous, showing cluster amplification as well as polysomy and aneusomy with varying HER2 ratios, consistent with a lower grade of HER2 gene amplification. Our findings show that LumB subtypes are a heterogeneous family that displays a biological continuum of alterations in growth pattern, HR, and HER2 expression. Bediaga et al. (49) demonstrated that, in IBC, the LumB HER2 subtypes (HER2$^+$ and HER2$^-$) had both low and high DNA methylation categories, resulting in different epigenetic and clinical features. The high DNA methylation subgroup

10.3389/fonc.2024.1347166

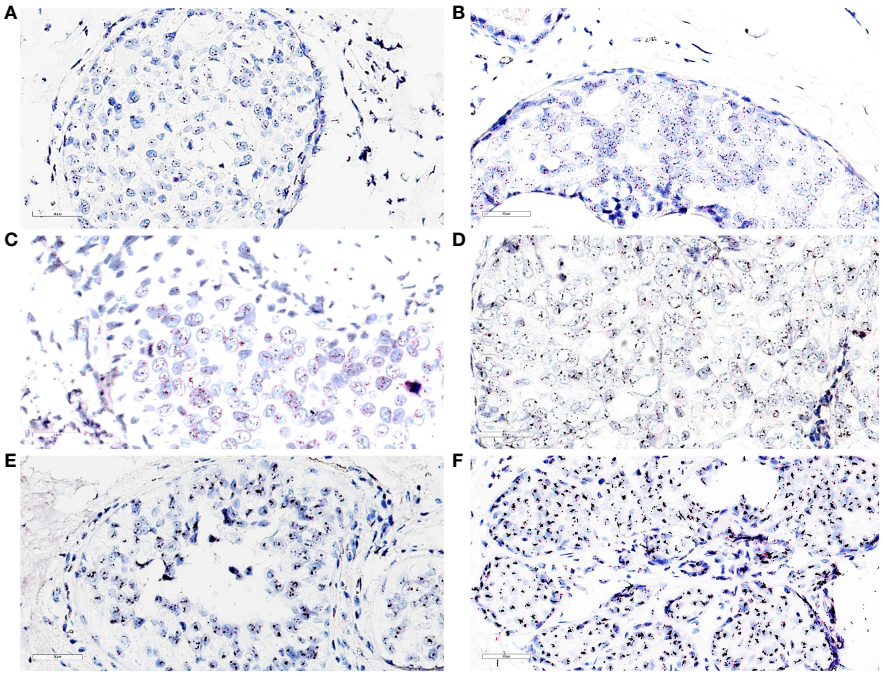

FIGURE 4
(A) dc-SISH of HER2 (black signals) and CEP17 (red signals) displaying nonamplification (disomy). HER2/CEP17 was equal to 1.25 (2.75/2.2); ×40 magnification. **(B)** dc-SISH of HER2 (black signals) and CEP17 (red signals) displaying a heterogenous nonamplification with two to four HER2 and CEP17 signals. HER2/CEP17 was equal to 1.16 (3.43/2.95); ×40 magnification. **(C)** dc-SISH of HER2 (black signals) and CEP17 (red signals) displaying tetrasomy nonamplification. HER2/CEP17 was equal to 1.16 (4.65/4.0); ×40 magnification. **(D)** dc-SISH of HER2 (black signals) and CEP17 (red signals) displaying amplification. HER2/CEP17 was equal to 4.67 (7.7/1.65); ×40 magnification. **(E)** dc-SISH of HER2 (black signals) and CEP17 (red signals) displaying HER2/CEP17 high amplification (cluster); ×40 magnification. **(F)** dc-SISH of HER2 (black signals) and CEP17 (red signals) displaying HER2/CEP17 high amplification (cluster) with retrograde lobular cancerization (*cancerization* of lobules) growth pattern; ×40 magnification.

TABLE 4 The details of dc-SISH analyses on HER2 2+ (IHC) samples.

Subtype	HER2 signals	CEP17 signals	HER2-CEP17 ratio	Amplified?
LumA	3.2	2.45	1.3	No
LumA	2.14	1.64	1.3	No
LumA	2.0	2.0	1.0	No
LumA	2.9	2.25	1.29	No
LumA	3.95	3.2	1.23	No
LumB HER2$^-$	3.43	2.95	1.16	No
LumB HER2$^+$	Clusters			Yes
LumB HER2$^+$	Clusters			Yes
LumB HER2$^+$	Clusters			Yes
LumB HER2$^+$	Clusters			Yes
LumB HER2$^+$	7.7	1.6	4.7	Yes
LumB HER2$^+$	7.5	1.7	4.4	Yes
LumB HER2$^+$	10.7	2.6	4.1	Yes
HER2-enriched	8.2	1.5	5.5	Yes
TPN	4.6	4.0	1.1	No
TPN	2.7	2.2	1.2	No

corresponded to the LumB HER2$^+$ subtype, whereas the low DNA methylation group clustered with the LumA subtype. Our results also support this finding since only the present cutoff value for the Ki67 proliferation index determines whether a DCIS sample that is HR-positive and HER2$^-$, is categorized as LumA or LumB HER2$^-$. In the context of IBC, these cutoff values have been subject to discussions and changes in numerous studies (28, 50, 51). We investigated ER and PR expression in DCIS with various cutoff values and did not demonstrate any statistically significant differences between cases classified as "Pure" with those classified as "W/invasive".

Strengths and limitations of the study

To our knowledge, this study material is the largest DCIS biobank that has been approved for cancer research purposes in Norway. It is a large collection of tissue material that represents a 22-year period and was obtained during the initial diagnosis. All samples were assessed and rated by qualified mammary pathologists. IHC analyses were performed in a single pathology department in accordance with national standards and recommendations.

Limitations of the study

Pathologists and clinicians are aware of the challenges associated with the Ki67 IHC assessment, which can lead to differences in the results of analyses within and between departments of pathology.

Conclusions

The majority of patients (71%) in our material study were over 50 years old. IHC analysis of ER and PR revealed a spectrum from low to high expression within the DCIS LumA and LumB subtypes, with the former displaying significantly higher expression than the latter ($p < 0.0001$). According to our results, the LumB subtypes are a diverse group that exhibits a biological continuum of changes in HR, growth pattern, and HER2 amplification. In this study, we demonstrated that low PR in high-grade DCIS was linked to concurrent HER2 overexpression as well as the coexistence of an invasive component in the luminal B subtypes ($p = 0.0001$ and $p = 0.0365$, respectively). PR and HER2 may have the potential to be incorporated into diagnostic tools as robust and reproducible prognostic and predictive markers for distinguishing high-risk *in situ* lesions that progress to IBC. The results of this study may contribute to the identification of high-risk patients with DCIS potentially in need of systemic adjuvant therapy. This question has to be addressed in clinical trials.

Data availability statement

The datasets for this article are not publicly available due to concerns regarding participant/patient anonymity. Requests to access the datasets should be directed to the corresponding author.

Ethics statement

The studies involving humans were approved by Regional Committee for Medical and Health Research Ethics (REK). The studies were conducted in accordance with the local legislation and institutional requirements. Written informed consent for participation was not required from the participants or the participants' legal guardians/next of kin because all living patients received an information letter in which the purpose of the project was described. The text of the information letter was approved by the Regional Committee for Medical and Health Research Ethics (REK) (case Nos. 29299 and 307976). A prepaid return envelope was enclosed in the letters patients received, in addition to a sheet to sign and return if they objected. If they agreed, they would not need to undertake any action. We received reservations from ten patients; consequently, their cases were excluded from further examinations.

Author contributions

HS: Conceptualization, Data curation, Formal analysis, Investigation, Methodology, Project administration, Resources, Software, Validation, Visualization, Writing – original draft, Writing – review & editing. LF: Conceptualization, Methodology, Supervision, Validation, Writing – review & editing. DP: Formal analysis, Validation, Writing – review & editing. YL: Visualization, Writing – review & editing. SA: Formal analysis, Methodology, Writing – review & editing. JG: Conceptualization, Formal analysis, Funding acquisition, Methodology, Project administration, Resources, Supervision, Validation, Visualization, Writing – review & editing. TS: Conceptualization, Data curation, Formal analysis, Investigation, Project administration, Supervision, Validation, Visualization, Writing – review & editing.

Funding

The author(s) declare financial support was received for the research, authorship, and/or publication of this article. Akershus University Hospital in Norway generously provided open-access funding. We extend our sincere appreciation to the National Network for Breast Cancer Research in Norway, Akershus University Hospital, Division of Medicine, and the University of Oslo, Faculty of Medicine (JG), for their valuable research support.

Conflict of interest

The authors declare that the research was conducted in the absence of any commercial or financial relationships that could be construed as a potential conflict of interest.

Publisher's note

All claims expressed in this article are solely those of the authors and do not necessarily represent those of their affiliated organizations, or those of the publisher, the editors and the reviewers. Any product that may be evaluated in this article, or claim that may be made by its manufacturer, is not guaranteed or endorsed by the publisher.

Supplementary material

The Supplementary Material for this article can be found online at: https://www.frontiersin.org/articles/10.3389/fonc.2024.1347166/full#supplementary-material

References

1. Ponti A, Lynge E, James T, Májek O, von Euler-Chelpin M, Anttila A, et al. International variation in management of screen-detected ductal carcinoma in *situ* of the breast. *Eur J Cancer (Oxford England: 1990)*. (2014) 50:2695–704. doi: 10.1016/j.ejca.2014.07.019

2. Elin Wølner Bjørnson ÅSH, Hofvind S. *Breast Screen Norway: 25years of organized screening*. Oslo: Cancer Registry of Norway (2022). Available at: https://www.kreftregisteret.no/globalassets/mammografiprogrammet/rapporter-og-publikasjoner/2022–25-arsrapport_webversjon.pdf.

3. Ryser MD, Weaver DL, Zhao F, Worni M, Grimm LJ, Gulati R, et al. Cancer outcomes in DCIS patients without locoregional treatment. *J Natl Cancer Instit*. (2019) 111:952–60. doi: 10.1093/jnci/djy220

4. Parker S. Clinical guidelines for the management of breast cancer (2019). Available online at: https://www.england.nhs.uk/mids-east/wp-content/uploads/sites/7/2018/02/guidelines-for-the-management-of-breast-cancer-v1.pdf.

5. Ubago JM, Blanco LZ, Shen T, Siziopikou KP. The PD-1/PD-L1 axis in HER2+ Ductal carcinoma *in situ* (DCIS) of the breast. *Am J Clin pathol*. (2019) 152:169–76. doi: 10.1093/ajcp/aqz020

6. Wang X, Liu Y. PD-L1 expression in tumor infiltrated lymphocytes predicts survival in triple-negative breast cancer. *Pathol Res practice*. (2020) 216:152802. doi: 10.1016/j.prp.2019.152802

7. Mercogliano MF, Bruni S, Mauro FL, Schillaci R. Emerging targeted therapies for HER2-positive breast cancer. *Cancers (Basel)*. (2023) 15(7):1987. doi: 10.3390/cancers15071987

8. Montagna E, Colleoni M. Hormonal treatment combined with targeted therapies in endocrine-responsive and HER2-positive metastatic breast cancer. *Ther Adv Med Oncol*. (2019) 11:1758835919894105. doi: 10.1177/1758835919894105

9. Hua X, Bi XW, Zhao JL, Shi YX, Lin Y, Wu ZY, et al. Trastuzumab plus endocrine therapy or chemotherapy as first-line treatment for patients with hormone receptor-positive and HER2-positive metastatic breast cancer (SYSUCC-002). *Clin Cancer Res*. (2022) 28:637–45. doi: 10.1158/1078-0432.CCR-21-3435

10. Iqbal N, Iqbal N. Human epidermal growth factor receptor 2 (HER2) in cancers: overexpression and therapeutic implications. *Mol Biol Int*. (2014) 2014:852748. doi: 10.1155/2014/852748

11. Davis JE, Nemesure B, Mehmood S, Nayi V, Burke S, Brzostek SR, et al. Her2 and ki67 biomarkers predict recurrence of ductal carcinoma in situ. *Appl Immunohistochem Mol Morphol*. (2016) 24:20–5. doi: 10.1097/PAI.0000000000000223

12. Fulawka L, Blaszczyk J, Tabakov M, Halon A. Assessment of Ki-67 proliferation index with deep learning in DCIS (ductal carcinoma in *situ*). *Sci Rep*. (2022) 12:3166. doi: 10.1038/s41598-022-06555-3

13. Petrone I, Resende, Rodrigues F, Valverde Fernandes P, Abdelhay E. Immunohistochemical biomarkers in ductal carcinoma *in situ*. *Open J Pathol*. (2020) 10:129–46. doi: 10.4236/ojpathology.2020.104013

14. Schandiz H, Park D, Kaiser YL, Lyngra M, Talleraas IS, Geisler J, et al. Abstract A015: A novel diagnostics approach to Ductal Carcinoma *In Situ* (DCIS) with potential impact on the therapeutic algorithms. *Cancer Prev Res*. (2022) 15(12_Supplement_1): A015. doi: 10.1158/1940–6215.DCIS22-A015

15. Schandiz H, Park D, Kaiser YL, Lyngra M, Talleraas IS, Geisler J, et al. Subtypes of high-grade breast ductal carcinoma in *situ* (DCIS): incidence and potential clinical impact. *Breast Cancer Res Treat*. (2023) 201:329–38. doi: 10.1007/s10549-023-07016-9

16. Silverstein MJ, Poller DN, Waisman JR, Colburn WJ, Barth A, Gierson ED, et al. Prognostic classification of breast ductal carcinoma-in-situ. *Lancet*. (1995) 345 (8958):1154–7. doi: 10.1016/S0140-6736(95)90982-6

17. Maxwell AJ, Clements K, Hilton B, Dodwell DJ, Evans A, Kearins O, et al. Risk factors for the development of invasive cancer in unresected ductal carcinoma in situ. *Eur J Surg Oncol*. (2018) 44:429–35. doi: 10.1016/j.ejso.2017.12.007

18. Jones JL. Overdiagnosis and overtreatment of breast cancer: Progression of ductal carcinoma in *situ*: the pathological perspective. *Breast Cancer Res*. (2006) 8:204. doi: 10.1186/bcr1397

19. Hoffman AW, Ibarra-Drendall C, Espina V, Liotta L, Seewaldt V. Ductal carcinoma *in situ*: challenges, opportunities, and uncharted waters. *Am Soc Clin Oncol Educ book*. 2012:40–4. doi: 10.14694/EdBook_AM.2012.32.228

20. Goldhirsch A, Winer EP, Coates AS, Gelber RD, Piccart-Gebhart M, Thürlimann B, et al. Personalizing the treatment of women with early breast cancer: highlights of the St Gallen International Expert Consensus on the Primary Therapy of Early Breast Cancer 2013. *Ann Oncol*. (2013) 24:2206–23. doi: 10.1093/annonc/mdt303

21. Maisonneuve P, Disalvatore D, Rotmensz N, Curigliano G, Colleoni M, Dellapasqua S, et al. Proposed new clinicopathological surrogate definitions of luminal A and luminal B (HER2-negative) intrinsic breast cancer subtypes. *Breast Cancer res: BCR*. (2014) 16:R65. doi: 10.1186/bcr3679

22. Sali AP, Sharma N, Verma A, Beke A, Shet T, Patil A, et al. Identification of luminal subtypes of breast carcinoma using surrogate immunohistochemical markers and ascertaining their prognostic relevance. *Clin Breast Cancer*. (2020) 20:382–9. doi: 10.1016/j.clbc.2020.03.012

23. Orrantia-Borunda E A-NP, Acuña-Aguilar LE, Gómez-Valles FO, Ramírez-Valdespino CA. Subtypes of Breast Cancer. In: *Breast Cancer*. Exon Publications, Brisbane, Australia (2022).

24. Roca-Barceló A, Viñas G, Pla H, Carbó A, Comas R, Izquierdo Á, et al. Mortality of women with ductal carcinoma in *situ* of the breast: a population-based study from the Girona province, Spain (1994–2013). *Clin Trans Oncol*. (2019) 21:891–9. doi: 10.1007/s12094-018-1994-1

25. Allison KH, Hammond MEH, Dowsett M, McKernin SE, Carey LA, Fitzgibbons PL, et al. Estrogen and progesterone receptor testing in breast cancer: ASCO/CAP guideline update. *J Clin Oncol*. (2020) 38:1346–66. doi: 10.1200/JCO.19.02309

26. Yu KD, Cai YW, Wu SY, Shui RH, Shao ZM. Estrogen receptor-low breast cancer: Biology chaos and treatment paradox. *Cancer Commun (Lond)*. (2021) 41:968–80. doi: 10.1002/cac2.12191

27. Viale G, Regan MM, Maiorano E, Mastropasqua MG, Dell'Orto P, Rasmussen BB, et al. Prognostic and predictive value of centrally reviewed expression of estrogen and progesterone receptors in a randomized trial comparing letrozole and tamoxifen adjuvant therapy for postmenopausal early breast cancer: BIG 1–98. *J Clin Oncol*. (2007) 25:3846–52. doi: 10.1200/JCO.2007.11.9453

28. Harbeck N, Thomssen C, Gnant M. St. Gallen 2013: brief preliminary summary of the consensus discussion. *Breast Care (Basel)*. (2013) 8:102–9. doi: 10.1159/000351193

29. Wolff AC, Hammond MEH, Allison KH, Harvey BE, Mangu PB, Bartlett JMS, et al. Human epidermal growth factor receptor 2 testing in breast cancer: american society of clinical oncology/college of american pathologists clinical practice guideline focused update. *Arch Pathol Lab Med*. (2018) 142:1364–82. doi: 10.5858/arpa.2018-0902-SA

30. Wolff AC, Somerfield MR, Dowsett M, Hammond MEH, Hayes DF, McShane LM, et al. Human epidermal growth factor receptor 2 testing in breast cancer: American society of clinical oncology-college of American pathologists guideline update. *J Clin Oncol*. (2023) 41(22):3867-3872. doi: 10.1200/JCO.22.02864

31. VENTANA HER2 Dual ISH DNA Probe Cocktail: Roche (2020). Available online at: https://diagnostics.roche.com/content/dam/diagnostics/us/en/LandingPages/her2-dual-ish/VENTANA-HER2-Dual-ISH-Method-Sheet.pdf.

32. HER2 Breast Cancer Testing Guideline Update Algorithms: American Society of Clinical Oncology (ASCO) & The College of American Pathologists (CAP) (2023). Available online at: https://documents.cap.org/documents/her2_breast_update_algorithms_2023.pdf.

33. Hicks DG, Lester SC. Hormone Receptors (ER/PR). In: Hicks DG, Lester SC, editors. *Diagnostic Pathology: Breast, 2nd ed*. Elsevier, Philadelphia (2016) 430–9.

34. Diep CH, Ahrendt H, Lange CA. Progesterone induces progesterone receptor gene (PGR) expression via rapid activation of protein kinase pathways required for cooperative estrogen receptor alpha (ER) and progesterone receptor (PR) genomic action at ER/PR target genes. *Steroids*. (2016) 114:48–58. doi: 10.1016/j.steroids.2016.09.004

35. Ono M, Tsuda H, Yoshida M, Shimizu C, Kinoshita T, Tamura K. Prognostic significance of progesterone receptor expression in estrogen-receptor positive, HER2-negative, node-negative invasive breast cancer with a low ki-67 labeling index. *Clin Breast Cancer*. (2017) 17:41–7. doi: 10.1016/j.clbc.2016.06.012

36. Purdie CA, Quinlan P, Jordan LB, Ashfield A, Ogston S, Dewar JA, et al. Progesterone receptor expression is an independent prognostic variable in early breast cancer: a population-based study. *Br J Cancer*. (2014) 110:565–72. doi: 10.1038/bjc.2013.756

37. Paakkola NM, Karakatsanis A, Mauri D, Foukakis T, Valachis A. The prognostic and predictive impact of low estrogen receptor expression in early breast cancer: a systematic review and meta-analysis. *ESMO Open*. (2021) 6:100289. doi: 10.1016/j.esmoop.2021.100289

38. Slamon DJ, Clark GM, Wong SG, Levin WJ, Ullrich A, McGuire WL. Human breast cancer: correlation of relapse and survival with amplification of the HER-2/neu oncogene. *Science*. (1987) 235:177–82. doi: 10.1126/science.3798106

39. Ross JS, Fletcher JA. The HER-2/neu oncogene in breast cancer: prognostic factor, predictive factor, and target for therapy. *Stem Cells*. (1998) 16:413–28. doi: 10.1002/stem.160413

40. Konecny G, Pauletti G, Pegram M, Untch M, Dandekar S, Aguilar Z, et al. Quantitative association between HER-2/neu and steroid hormone receptors in hormone receptor-positive primary breast cancer. *JNCI: J Natl Cancer Instit*. (2003) 95:142–53. doi: 10.1093/jnci/95.2.142

41. Huang HJ, Neven P, Drijkoningen M, Paridaens R, Wildiers H, Van Limbergen E, et al. Hormone receptors do not predict the HER2/neu status in all age groups of women with an operable breast cancer. *Ann Oncol*. (2005) 16:1755–61. doi: 10.1093/annonc/mdi364

42. Shah A, Haider G, Abro N, Bhutto S, Baqai TI, Akhtar S, et al. Correlation between age and hormone receptor status in women with breast cancer. *Cureus*. (2022) 14:e21652. doi: 10.7759/cureus.21652

43. Wang J, Xu B. Targeted therapeutic options and future perspectives for HER2-positive breast cancer. *Signal Transduct Target Ther*. (2019) 4:34. doi: 10.1038/s41392-019-0069-2

44. Luo C, Zhong X, Wang Z, Wang Y, Wang Y, He P, et al. Prognostic nomogram for patients with non-metastatic HER2 positive breast cancer in a prospective cohort. *Int J Biol Mark*. (2019) 34:41–6. doi: 10.1177/1724600818824786

45. Cao SS, Lu CT. Recent perspectives of breast cancer prognosis and predictive factors. *Oncol Lett*. (2016) 12:3674–8. doi: 10.3892/ol.2016.5149

46. Nicolini A, Ferrari P, Duffy MJ. Prognostic and predictive biomarkers in breast cancer: Past, present and future. *Semin Cancer Biol*. (2018) 52:56–73. doi: 10.1016/j.semcancer.2017.08.010

47. Badowska-Kozakiewicz AM, Patera J, Sobol M, Przybylski J. The role of oestrogen and progesterone receptors in breast cancer - immunohistochemical evaluation of oestrogen and progesterone receptor expression in invasive breast cancer in women. *Contemp Oncol (Pozn)*. (2015) 19:220–5. doi: 10.5114/wo.2015.51826

48. Patel R, Klein P, Tiersten A, Sparano JA. An emerging generation of endocrine therapies in breast cancer: a clinical perspective. *NPJ Breast Cancer*. (2023) 9:20. doi: 10.1038/s41523-023-00523-4

49. Bediaga NG, Beristain E, Calvo B, Viguri MA, Gutierrez-Corres B, Rezola R, et al. Luminal B breast cancer subtype displays a dicotomic epigenetic pattern. *SpringerPlus*. (2016) 5:623. doi: 10.1186/s40064-016-2235-0

50. Focke CM, van Diest PJ, Decker T. St Gallen 2015 subtyping of luminal breast cancers: impact of different Ki67-based proliferation assessment methods. *Breast Cancer Res Treat*. (2016) 159:257–63. doi: 10.1007/s10549-016-3950-5

51. Gnant M, Harbeck N, Thomssen C. St. Gallen 2011: summary of the consensus discussion. *Breast Care (Basel)*. (2011) 6:136–41. doi: 10.1159/000328054

frontiers | Frontiers in Oncology

TYPE Original Research
PUBLISHED 17 July 2024
DOI 10.3389/fonc.2024.1342439

OPEN ACCESS

EDITED BY
Anika Nagelkerke,
University of Groningen, Netherlands

REVIEWED BY
Mohamed Emam Sobeih,
Cairo University, Egypt
Lyana Setiawan,
Darmais National Cancer Hospital, Indonesia
Noorwati Sutandyo,
Dharmais Hospital National Cancer Center, Indonesia

*CORRESPONDENCE
Qiongle Peng
pengxiaoman@ujs.edu.cn
Xiaoling Ren
xiaochuju@qq.com

RECEIVED 21 November 2023
ACCEPTED 18 June 2024
PUBLISHED 17 July 2024

CITATION
Peng Q, Zhu J and Ren X (2024) Thromboelastogram and coagulation function index: relevance for female breast cancer.
Front. Oncol. 14:1342439.
doi: 10.3389/fonc.2024.1342439

Thromboelastogram and coagulation function index: relevance for female breast cancer

Qiongle Peng[1*], Jinmei Zhu[2] and Xiaoling Ren[3*]

[1]Department of Blood Transfusion, Affiliated Hospital of Jiangsu University, Zhenjiang, China, [2]School of Medicine, Jiangsu University, Zhenjiang, China, [3]Department of Medical Laboratory, Wuxi Traditional Chinese Medicine Hospital, Wuxi, China

Introduction: Screening and postoperative intervention of breast tumors are critical for the effective diagnosis and treatment of disease development, and reliable diagnostic/screening methods become a key link.

Objective: Thromboelastogram (TEG), routine platelet (PLT) count, and the coagulation function indicators in patients with different breast diseases were determined and analyzed to explore their predictive value in secondary bleeding disorders.

Methods: A total of 131 patients with breast diseases, admitted to Jiangsu University Affiliated Hospital from January 2019 to December 2022, were selected as the research subjects. The detection items were analyzed using the receiver operating curve (ROC) after grouping for secondary bleeding disorders of patients with breast cancer.

Results: The reaction (*R*) and the coagulation (*K*) times were lower in the malignant breast disease group, while the coagulation angle (α), maximum amplitude (MA), coagulation index (CI), fibrinogen (FIB), and D-dimer (D-D) were higher than those in the benign breast disease group. The *t*-tests proved that the MA and FIB values were statistically significant ($p < 0.05$) in the benign and malignant breast disease groups. The *R* and *K* in patients with breast diseases were positively correlated with the activated partial thromboplastin time (aPTT) and D-D, but were negatively correlated with PLT. The α angle was negatively correlated with aPTT and D-D, but was positively correlated with PLT. The MA for PLT function was positively correlated with FIB and PLT. CI was negatively correlated with aPTT, thrombin time (TT), and D-D, but was positively correlated with PLT. ROC curve analysis showed that the CI and α angle had a significant predictive value, whereas the correlation of the other indicators was relatively low.

Abbreviations: aPTT, activated partial thromboplastin time; CI, coagulation index; D-D, D-dimer; FIB, fibrinogen; K, coagulation time; MA, maximum amplitude; PLT, platelet count; PT, prothrombin time; R, reaction time; ROC, receiver operating characteristic; TT, thrombin time; TEG, thromboelastogram; α, coagulation angle.

Conclusion: Coagulation tests showed significant differences in patients with breast cancer, differing from those with benign breast diseases. TEG combined with conventional coagulation indicators is potentially valuable for the prediction of secondary bleeding disorders in patients with breast cancer.

KEYWORDS

thromboelastogram, coagulation function, breast cancer, hemorrhagic diseases, hypercoagulability

1 Introduction

Thromboembolic and hemorrhagic diseases caused by coagulation are some of the important causes of death in patients with malignant tumors. Armand Trousseau first described the connection between blood clots and cancer in 1865 (1). Since then, more research has discovered that patients with tumors are prone to developing hypercoagulable blood, and multiple studies support the interaction between tumor cells and the coagulation system in various ways (2). Cancer cells in the blood of patients with malignant tumors coagulate with other cells or with cancer cells themselves to form a thrombus, called cancer-related thrombus (cancer-associated thrombosis, CAT), which is one of the serious complications in patients with malignant tumors, and the fatality rate is high (3). Patients with malignant tumors are prone to venous thromboembolism (VTE) under a hypercoagulable state (4). A study on patients with colorectal cancer showed that the incidence of postoperative VTE in patients with malignant tumors is higher and lasts for more than 1 month, which is related to their hypercoagulable state (5). The incidence of cerebral venous thrombosis and visceral venous thrombosis (splanchnic vein thrombosis, SVT) is particularly high in patients with myeloproliferative tumors (myeloproliferative neoplasm, MPN) (6), despite the mechanisms of hematological malignancy differing from those of breast cancer (7). SVT includes Budd–Chiari syndrome and portal vein thrombosis (8). In addition, transitional thrombophlebitis, arterial thrombosis, disseminated intravascular coagulation (DIC), and non-bacterial thrombotic endocarditis (NBTE) have all been classified as complications of a hypercoagulable state in patients with malignant tumors (9). These studies provided proof of the complex relationship between blood hypercoagulability and various tumor diseases, with heavy family burden and economic challenges.

At present, research on the potential mechanisms of blood hypercoagulability in patients with malignant tumors mainly reflects the following aspects: a) tumor cells release procoagulant substances (10); b) the interaction between tumor cells and the fibrinolytic system (11, 12); c) tumor cell-mediated platelet (PLT) activation (2, 13); d) tumor-related complement activation (14, 15); e) genetic factors (16, 17); and f) clinical factors (18, 19). Increasing research on epidemiological and biological issues has presented the correlation between blood hypercoagulability and thrombosis, although the exploration of its mechanism is still on the way (20–22). For instance, circulating tumor cells are associated with an increased risk of VTE in patients with metastatic breast cancer (23). The dissemination of tumor-derived microvesicles promotes hypercoagulability and increased PLT activation (24). Intrinsic heparin plays an important role in balancing the blood flow patency and thrombosis (25). In cancer therapy, preoperative irradiation produces lesions triggering both bleeding and thrombosis, and most chemotherapeutic protocols affect PLT synthesis (20).

More studies have shown that the blood of patients with malignant tumors is in a state of hypercoagulability (26). The monitoring of the blood hypercoagulable state coupled with disease diagnosis generally involves clinical and laboratory examinations. In addition, the expert experience system based on histological examination and pathological analysis provides evidence for the preliminary diagnosis and further assessment of a disease (27). Laboratory thromboelastogram (TEG) (28, 29) and the blood coagulation function indices (20) indicate that patients with malignant tumors go through a state of blood hypercoagulability, which is significant for nonsurgical cancer therapy and preoperative irradiation. The TEG parameters of patients with tumors deviate from the normal value, and the blood is in a state of hypercoagulability (26). In the histological, anatomical observation of patients with malignant tumors, the thrombus of PLTs and the fibrin in blood vessels increased abnormally, and the immunohistochemistry of fibrin around tumor cells showed an increase of coagulation products, namely, PLT clot and fibrin (29). Immunohistochemical analysis is of value in the auxiliary diagnosis of malignant tumors, showing that histological examination provides evidence of a blood hypercoagulable state in clinical diagnosis (30). In terms of pharmacology, anticoagulants or anti-PLT drugs for patients with malignant tumors are useful for anticoagulation factors (31), indicating the blood hypercoagulable state in these patients, and effective intervention can assist the treatment. Clinical studies of several patients with MPN have shown that oral anticoagulants could reduce tumor metastasis and improve prognosis. The recurrence rate of VTE is fairly low, and there is no complication of massive hemorrhage (32).

Breast cancer is the most common malignant tumor endangering women's health (33), and it is of great significance to

explore the changes in coagulation function in patients with breast cancer. The hypercoagulable state of blood is closely associated with breast cancer-related thrombus and directly affects the results of breast tumor screening, risk assessment, hospitalization and hospitalization prevention, and other medical interventions. In biomedicine, breast cancer relates to complex systemic factors in many aspects, including clinical factors, genetic inheritance, coagulant substance, PLT activation, and tumor-associated complement (Figure 1). In this sense, cancer-related thrombosis has become an important basis for the prediction and clinical analysis of breast cancer (3). A number of blood parameters related to transfusion technology [e.g., TEG (34), routine blood test (35), and PLT count (36)] are important in providing effective information during the whole procedure of medical interventions, including tumor screening (37), risk assessment (38), and inpatient (39) and outpatient prevention (40). Research shows that venous thrombosis is one of the common causes of death in patients with breast cancer (41). TEG, as a laboratory indicator reflecting the dynamic changes of blood coagulation, presents an important guiding value for comprehensive analysis in combination with conventional indicators of coagulation function. The positive and negative predictive values can be determined using TEG for bleeding and thrombosis (42). Therefore, in this study, we examined and analyzed the changes in TEG, PLT count, and coagulation function in patients with breast cancer and in those with benign breast diseases. We assessed the risk of patients with breast cancer suffering from blood disorders by conducting a correlation analysis. It is hoped that the results of this study guide the prevention of such complications for the preliminary detection of breast cancer in clinical procedures.

2 Materials and methods

2.1 Samples

A total of 131 patients with breast diseases were gathered remotely from clinical facilities admitted to the Affiliated Hospital of Jiangsu University from January 2019 to December 2022 as the research subjects. These patients were aged 25–88 years and with complete case data. The exclusion criteria were serious heart failure, liver and kidney diseases, and blood system diseases, as well as the use of medication within a week that affects the coagulation function, such as anticoagulants and procoagulants (Table 1). According to the pathological diagnosis, patients with breast tumors were divided into two groups, including 53 cases of malignant breast cancer and 67 cases of benign breast tumor. After determining the TEG parameters, PLT count, and the

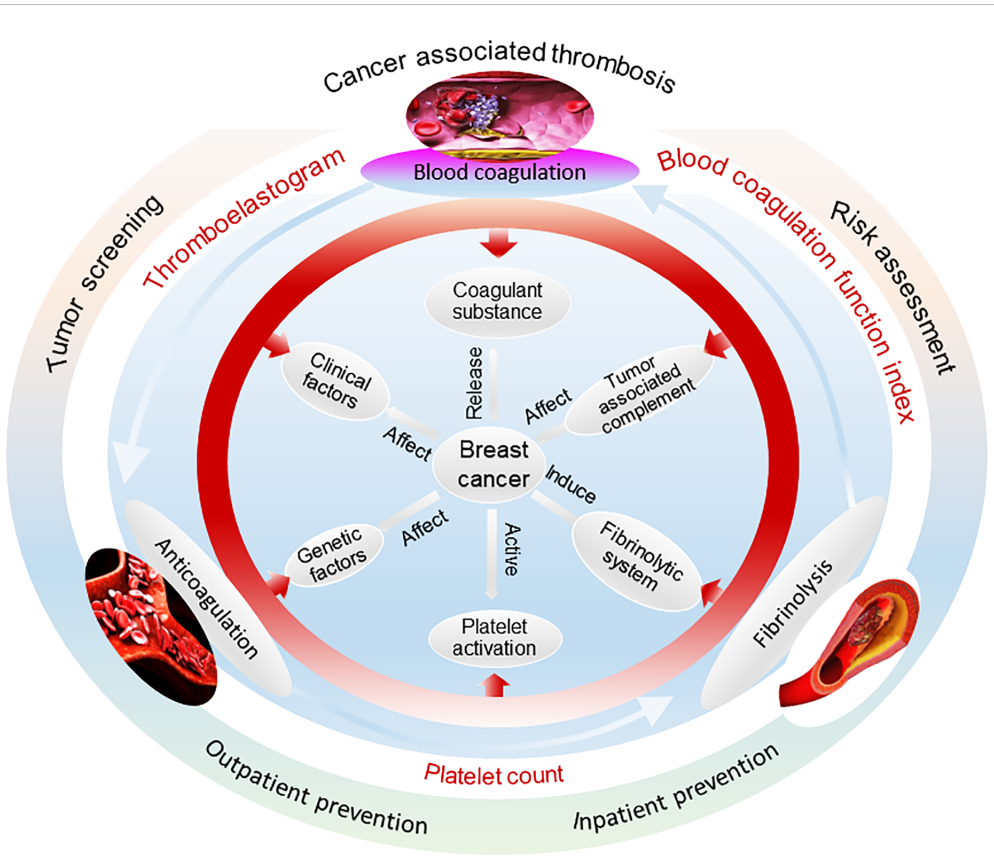

FIGURE 1
Mechanisms of the occurrence and development of breast cancer that relate to many factors from various aspects. Cancer-related thrombosis has become an important basis for breast cancer prediction and clinical analysis. Blood parameters of the thromboelastogram and routine blood and platelet count are important in providing effective information for medical interventions such as tumor screening, risk assessment, and inpatient and outpatient prevention.

TABLE 1 Inclusion and exclusion criteria during sample collection for this research.

Item	Discrimination	Inclusion	Exclusion
Breast disease	Pathological diagnosis	Yes	No
Age (years)	25–88	Yes	No
Gender	Women	Yes	No
Case data	Complete	Yes	No
Intravenous catheterization	Within a week	No	Yes
Anticoagulants	Within a week	No	Yes
Coagulants	Within a week	No	Yes
Cardiac insufficiency	With	No	Yes
Liver and kidney diseases	With	No	Yes
Hematological diseases	With	No	Yes

coagulation function indicators, the two groups were compared for differences in each indicator. Furthermore, patients with breast cancer were divided into the secondary bleeding disorder group (nine cases) and the non-secondary bleeding disorder group (44 cases) according to their clinical manifestations. The receiver operating characteristic (ROC) curve was used to analyze the diagnostic value of the above detection items for the secondary bleeding disorder of patients with breast cancer.

2.2 Examination methods

2.2.1 Routine coagulation determination

The fasting venous blood of patients was collected in the morning. These samples were placed into a sodium citrate anticoagulant tube, fully mixed, centrifuged at 3,000 rpm for 15 min to separate plasma, and assessed within 2 h. The instrument used was a Sysmex CS-5100 fully automatic blood coagulation analyzer, which utilizes coagulation tests to determine the prothrombin time (PT), activated partial thromboplastin time (aPTT), thrombin time (TT), and fibrinogen (FIB). Immunoturbidimetry was used to determine the D-dimer (D-D). Routine coagulation function indices such as the PT and aPTT were also measured based on plasma (43).

2.2.2 Platelet count determination

The fasting venous blood of patients was also collected in the morning and placed into an EDTA anticoagulant tube, fully mixed, and examined within 2 h. The instrument used was a Sysmex XE-2100 fully automatic blood cell analyzer.

2.2.3 Thromboelastography determination

The fasting venous blood of patients was further collected in the morning and placed into a sodium citrate anticoagulant tube, fully mixed, and examined within 2 h. The instrument used was Haemonetics TEG 5000 (Haemoscope Corporation®, Niles, IL, USA), while the supporting kit was the activation coagulation detection kit (coagulation method) (TEG Hemostasis System Kaolin, Haemonetics Corp., Braintree, MA, USA). An activated coagulation detection reagent is a standardized reagent that includes kaolin, mixed phospholipids, and buffer stabilizers, which can detect coagulation disorders related to the intrinsic and extrinsic coagulation pathways. Kaolin activators are similar to diatomaceous earth, but are not easily affected by aprotinin. In this study, the kaolin reagent was firstly restored to room temperature and then 1.0 mL of a blood sample was added to the reagent. The tube was gently inverted and mixed five times, and 20 µL of 0.2 mol/L calcium chloride was added to the preheated reaction cup of the TEG instrument. Subsequently, 340 µL of the sample was drawn and mixed with kaolin in the reaction cup. The cup slot was moved up and the tests started.

2.3 Statistical analysis

Statistical descriptions of the routine coagulation function indicators (i.e., the PLT count and TEG parameters) in patients with benign and malignant breast diseases were determined. The data were normalized during the clustering analysis. After excluding data related to a number of complex cases of non-tumor diseases, the dataset (n = 120) is presented in Supplementary Table S1 following a preliminary normalization treatment.

SPSS 25.0 statistical software was used to conduct general descriptive statistics on various indicators in the benign breast and malignant disease groups. A t-test was used to examine differences in the coagulation-related indices between the breast cancer group and the benign breast disease group, and the test values were statistically significant ($p < 0.05$). Correlation analysis was also performed on various indicators, such as the TEG, PLT count, and coagulation function in patients with breast diseases using Pearson's correlation coefficient. The ROC curve was used to analyze the predictive value of TEG, routine PLT test, and coagulation function for the secondary hemorrhagic disease of patients with breast cancer.

3 Results

3.1 Descriptive statistics

The descriptive statistics of the routine coagulation function indicators, PLT count, and the TEG parameters in patients with benign (B) and malignant (M) breast diseases, are shown in Table 2. The timeline of the TEG curve from left to right can be divided into three stages: 1) from the activation of the coagulation factor to fibrin formation; 2) fibrin formation, PLT aggregation, and blood clot formation; and 3) fibrinolysis. Among the TEG parameters, the mean values of reaction time (R) and coagulation time (K) in the malignant breast disease group were lower than those in the benign breast disease group. These indicate the patients' hypercoagulability or hyperfibrinolysis with

TABLE 2 Results of the routine coagulation function indicators, platelet count, and thromboelastogram (TEG) indices and variations.

Item	Tumor	Normal	Mean	SD	Min.	Max.
R (min)	B	5–10	6.01	1.38	2.9	10.6
	M		5.80	1.57	3.2	10.5
K (min)	B	1–3	1.62	0.56	0.8	4.1
	M		1.51	0.48	0.9	2.9
α (deg)	B	53–72	67.05	6.10	41.4	78.4
	M		68.18	6.49	52.3	78.5
MA (mm)	B	50–70	61.78	9.00	−2.6	73.7
	M		64.74	4.47	56.1	75.5
CI (a.u.)	B	−3 to 3	0.50	1.93	−7.2	3.8
	M		0.95	2.02	−3.9	3.9
PT (s)	B	9–13	10.84	0.69	8.9	12.7
	M		11.05	0.79	9.7	13.0
aPTT (s)	B	23.3–32.5	26.17	2.32	21.4	35.6
	M		26.05	1.99	22.2	30.8
TT (s)	B	14–21	17.17	1.03	14.7	20.7
	M		17.23	0.96	14.6	19.1
FIB (g/L)	B	2–4	2.97	0.73	1.909	5.493
	M		3.50	1.10	2.044	7.590
D-D (mg/L)	B	<0.55	0.50	0.46	0.10	2.11
	M		1.56	4.75	0.10	26.70
PLT ($\times 10^9$/L)	B	100–350	228.14	80.27	70	480
	M		236.36	65.95	116	401

R, reaction time; K, coagulation time; α, coagulation angle; MA, maximum amplitude; CI, coagulation index; PT, prothrombin time; aPTT, activated partial thromboplastin time; TT, thrombin time; FIB, fibrinogen; D-D, D-dimer; PLT, platelets; B, benign; M, malignant.

consideration of the coagulation factor function (*R*), FIB function [*K* and the coagulation angle (α)], and PLT function (maximum amplitude, MA) in the whole blood. Of these parameters, *R* has indicative effects in the clinical evaluation of blood coagulation function, the guidance of component transfusion, and the prediction of thrombus/bleeding and medication risks.

The histograms for the group data distribution after processing for normalization and statistics are presented in Figure 2. There were significant differences in the statistical characteristics of the histograms among patients with benign and malignant breast tumors in some indices of the TEG atlas [e.g., *R*, *K*, and the coagulation index (CI)]. For patients with benign breast tumors, the *R* value had a higher frequency in the range 3.2–9.04, indicating that this value is not sensitive to the clinical reference of patients with benign breast tumors. On the other hand, for patients with malignant tumors, the *R* value was concentrated in the range 4.28–8.48, and the distribution density at both ends was low. Both malignant and benign breast tumors tend to obey normal distribution. Nevertheless, in comparison, the expected value of a malignant tumor was smaller ($\mu \approx 5.8$) and the mean variance was larger ($\sigma \approx 1.57$). For patients with benign breast tumors, the *K* value was highly concentrated in the range 1.16–1.74, and its distribution on both sides was more uniform, tending to obey a normal distribution. The expected value μ was approximately 1.62, while the mean variance σ was approximately 0.56. For malignant breast tumors, the expected value μ was reduced to 1.51, while the mean variance σ was approximately 0.48.

The mean values of the α angle, MA, and CI were higher in the malignant breast disease group. Of the coagulation function indicators, the mean values of aPTT and PLT in the malignant breast disease group were lower than those in the benign breast disease group. The histograms for the different variable distributions of patients with benign/malignant breast tumors are presented and compared in Figure 3. The mean values of PT, TT, FIB, and D-D were higher in the group of benign breast diseases. Comparison of the blood routine parameters revealed differences in the statistical characteristics of the histograms between benign and malignant breast tumors, particularly in PT and aPTT. The PT values of benign tumors were highly concentrated in the range 10.2–12.7, while those of malignant breast tumors were more widely distributed in the range 9.7–11.9. The expected PT value of malignant tumors is offset by 0.2 to the right, indicating an increased probability of anticoagulants in the blood. In addition, the expected value of FIB in the blood of patients with malignant breast tumors increased from 2.98 to 3.5. The FIB in the blood of patients with malignant tumors was significant, indicating an increased risk of cardiovascular disease.

3.2 Disparity level

Disparity level testing was conducted for the routine coagulation function indicators, PLT count, and the TEG parameters in patients with benign and malignant breast diseases. A *t*-test was used to examine differences in the routine coagulation function indicators, PLT count, and the TEG parameters in patients with benign and malignant breast diseases (Table 3).

Differences in the routine coagulation function indicators, PLT count, and the TEG parameters were analyzed in patients with benign and malignant breast diseases. The statistical *t*-values and *p*-values of D-D were obtained without assuming equal variance conditions, while the *t*-values and *p*-values of the other indicators were obtained under assumption of equal variance conditions. Correlation analysis of the routine coagulation function indicators, PLT count, and TEG parameters was conducted in patients with breast diseases. The results of the homogeneity of variance showed that PT and D-D were statistically significant ($p < 0.05$). The results of normal fitting showed that the expected value of D-D in malignant breast tumors increased by 200%. D-D is generally prone to increase after thrombosis, which is an important molecular marker for its diagnosis.

Increased values are common in deep venous thrombosis, pulmonary embolism, myocardial infarction, and hyperfibrinolysis secondary to DIC. The *t*-test for the MA value and the FIB index in the benign and malignant breast disease groups showed $p < 0.05$, with significant difference between the two groups. However, the *t*-test for

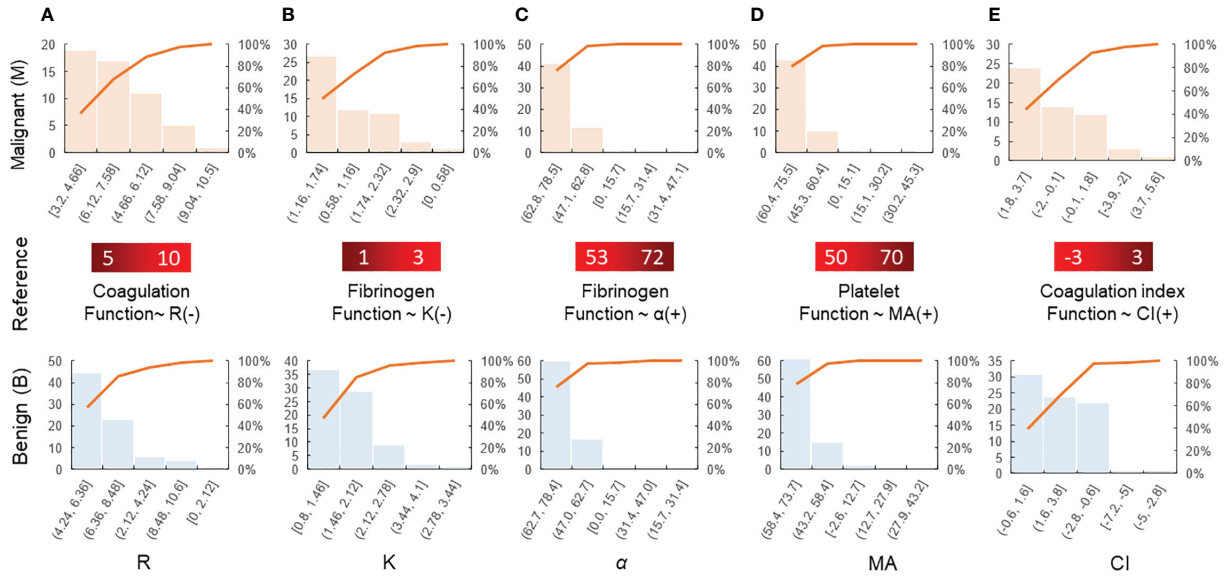

FIGURE 2
Histogram of various parameters derived from the thromboelastography maps of patients with benign/malignant breast tumors: **(A)** R, **(B)** K, **(C)** α, **(D)** MA, and **(E)** CI. The coagulation factor activity R (2–8min) reflects the function of clotting factors. Both K and α-angle reflect the function of fibrinogen. MA reflects the function of platelets. CI, coagulation composite index, is of great significance for the clinical prediction of thrombosis and bleeding. The blood sample is in a hypercoagulable state when CI>3, and the blood sample is in a hypocoagulable state when CI is less than −3.

the other indicators showed $p > 0.05$, and the differences were not statistically significant. Furthermore, the box–whisker plots of the various blood transfusion indices of patients with benign/malignant breast tumors were compared (Figure 4), which were in accordance with the results of the *t*-tests.

3.3 Correlation analysis

Correlation analysis of the given parameters is of clinical significance. In the determination of the TEG map parameters and the four coagulation tests, it was found that they are mostly

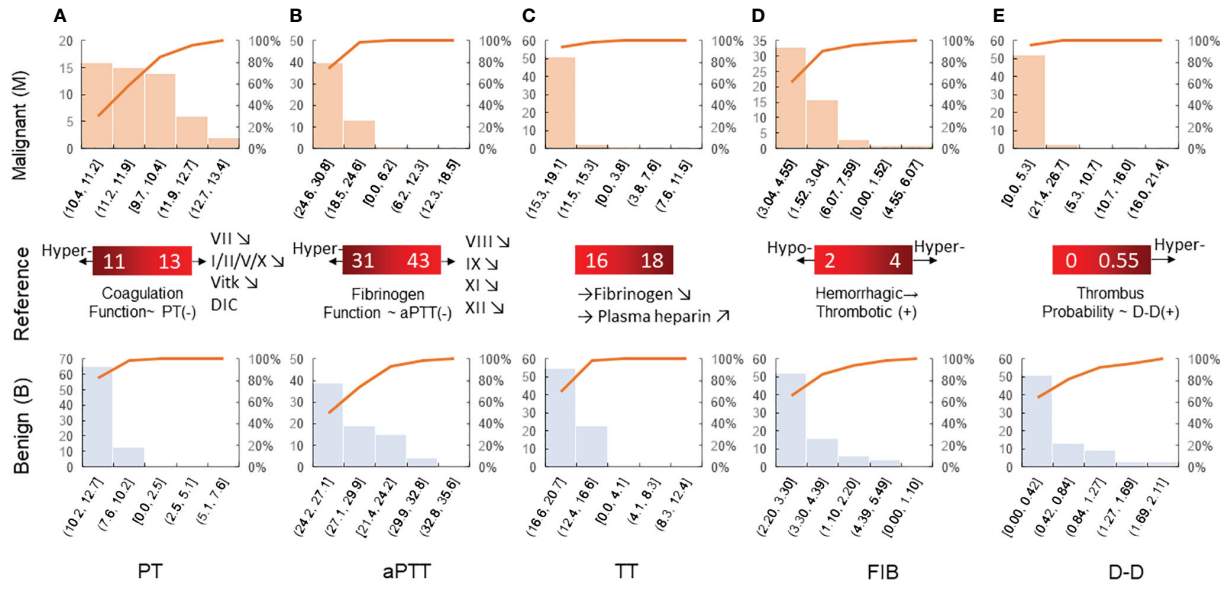

FIGURE 3
Histogram of blood routine coagulation indexes of patients with benign/malignant breast tumors: **(A)** PT, **(B)** aPTT, **(C)** TT, **(D)** FIB, and **(E)** D-D. Prothrombin time is the extrinsic coagulation pathway to reflect the extrinsic coagulation function. aPTT suggests the abnormal intrinsic coagulation factor and the screening test reflects the intrinsic coagulation pathway. Thrombin time is the required time for plasma coagulation after the standardized thrombin solution. Fibrinogen is the detection of plasma fibrinogen, and its increase is seen in thrombotic diseases and conversely in hemorrhagic diseases.

10.3389/fonc.2024.1342439

TABLE 3 Differences in the routine coagulation function indicators.

Parameter	Homogeneity of variance		*t*-test	
	F	*p*	*t*	*p*
R	1.502	0.223	0.818	0.415
K	0.214	0.645	1.209	0.229
α	0.745	0.390	−1.015	0.312
MA	1.517	0.220	−2.206	0.029*
CI	0.671	0.414	−1.299	0.196
PT	3.097	0.081	−1.556	0.122
aPTT	0.245	0.622	0.291	0.771
TT	0.187	0.666	−0.332	0.740
FIB	2.134	0.146	−3.256	0.001*
D-D	10.348	0.002*	−1.608	0.114
PLT	1.058	0.306	−0.617	0.538

R, reaction time; K, coagulation time; α, coagulation angle; MA, maximum amplitude; CI, coagulation index; PT, prothrombin time; aPTT, activated partial thromboplastin time; TT, thrombin time; FIB, fibrinogen; D-D, D-dimer; PLT, platelets.
* read the statistical significance ($p<0.05$).

prone to present variation trends in the blood coagulation state. Pearson's correlation coefficient was used to analyze the correlation between TEG, routine PLT, and the coagulation function indicators in patients with breast diseases. The results of the correlation analysis of the medical function indicators and/or the parameters in patients with breast diseases are shown in Table 4.

3.4 Sensitivity and specificity

The ROC curve or sensitivity curve is the core index of the performance evaluation of medical diagnostic tests and predictive models. Through analysis of the results of the disease group and the control group, the upper and lower limits, the group distance, and the cutoff points of the measured values were determined. A cumulative frequency distribution table was listed according to the selected group spacing interval. The true positive rate (TPR; sensitivity), the specificity, and the false-positive rate (FPR; 1 – specificity) of all cutoff points were calculated and plotted as the ROC curves. The abscissa and ordinate of the ROC curve were the non-specificity and sensitivity, respectively. The sensitivity and the specificity of the routine coagulation function indicators and the TEG parameters in detecting secondary bleeding disorders in patients with breast cancer were analyzed. The ROC curve was used to analyze the predictive value of TEG, routine PLT, and coagulation function indicators for secondary bleeding disorder in patients with breast cancer.

The ROC curve can be used for threshold selection and model comparison; however, due to the limited number of samples, the ROC curves were not smooth but stepped. A change in the FPR (1 – Sp) and the TPR (Se) requires at least one sample to change. The area under the ROC curve (AUC) can be used for model comparison. Among the TEG parameters in the ROC curve

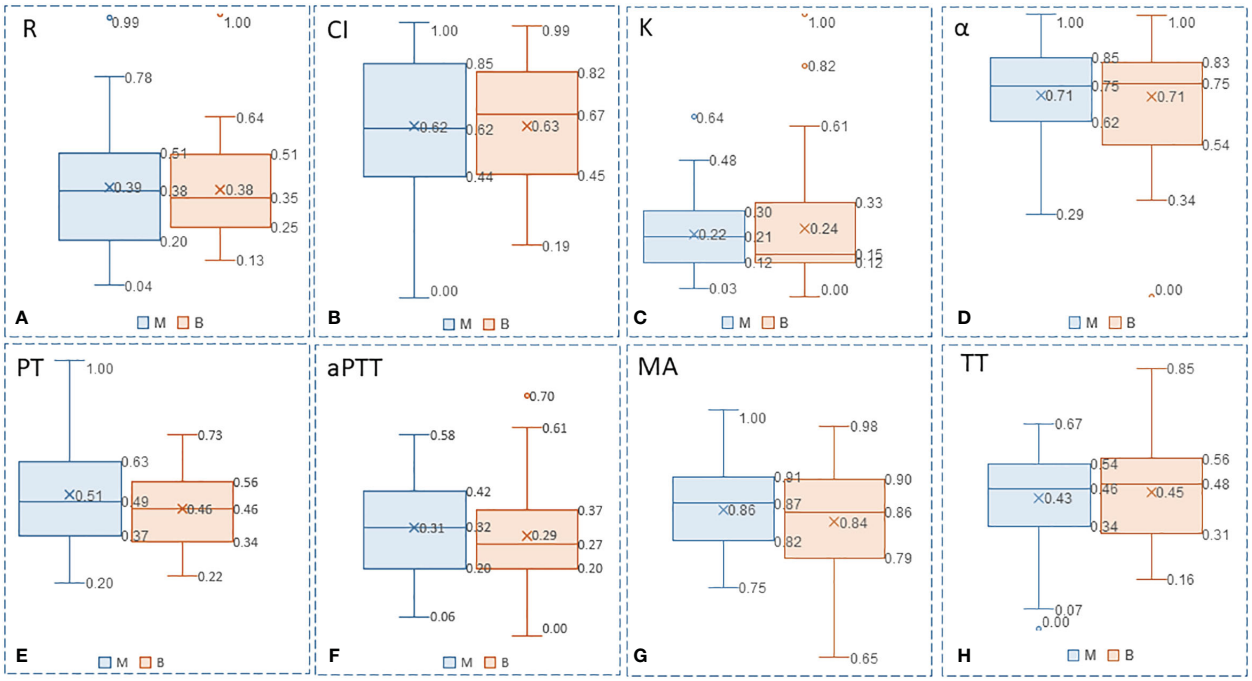

FIGURE 4
Box-whisker plots of the various blood transfusion indexes of patients with benign/malignant breast tumors: **(A)** R, **(B)** CI, **(C)** K, **(D)** α, **(E)** PT, **(F)** aPTT, **(G)** MA, and **(H)** TT. Five variables (Upper limit, RO 75% quantile, median, Rd 25% quantile, lower limit) were presented to construct box-whisker plots. The plots show the average level, degree of fluctuation, and outliers, and the width of the box reflects the degree of fluctuation of the data to some extent.

TABLE 4 Correlation analysis of the routine coagulation data and TEG parameters.

		R	*K*	*α*	MA	CI
PT	*r*	−0.060	−0.016	0.016	0.082	0.077
	p	0.495	0.853	0.858	0.350	0.382
aPTT	*r*	0.208	0.250	−0.232	−0.116	−0.281
	p	0.017*	0.004**	0.008**	0.188	0.001**
TT	*r*	0.137	0.066	−0.056	−0.094	−0.115
	p	0.118	0.451	0.526	0.288	0.193
FIB	*r*	0.021	−0.080	−0.035	0.210	0.077
	p	0.809	0.365	0.689	0.016	0.386
D-D	*r*	0.210	0.266	−0.279	−0.085	−0.249
	p	0.016*	0.002**	0.001**	0.332	0.004**
PLT	*r*	−0.195	−0.341	0.320	0.279	0.336
	p	0.025*	0.000**	0.000**	0.001**	0.000**

R was positively correlated with aPTT and D-D, but was negatively correlated with PLT. K was positively correlated with aPTT and D-D, but was negatively correlated with PLT. The α angle was negatively correlated with aPTT and D-D, but was positively correlated with PLT. MA was positively correlated with FIB and PLT. CI was negatively correlated with aPTT, TT, and D-D, but was positively correlated with PLT.

R, reaction time; K, coagulation time; α, coagulation angle; MA, maximum amplitude; CI, coagulation index; PT, prothrombin time; aPTT, activated partial thromboplastin time; TT, thrombin time; FIB, fibrinogen; D-D, D-dimer; PLT, platelets.

*p < 0.05 (double tail); **p < 0.01 (single tail).

(Figure 5), CI and the α angle showed significant predictive value for classification (AUC > 0.8) for detecting secondary bleeding disorders in patients with breast cancer. The diagnostic value of the other indices was fairly low (AUC < 0.7).

The ROC curve of the coagulation function indicators and PLT is shown in Figure 6. The indices of aPTT, TT, PT, and DD were not in line with the actual scenario (AUC < 0.5), whereas PLT was not significant (AUC < 0.7) in detecting secondary bleeding disorders in patients with breast cancer. For the results of the coagulation function indicators and PLT, the correlation between each indicator and secondary bleeding disorder was not significant for the detection of bleeding disorders.

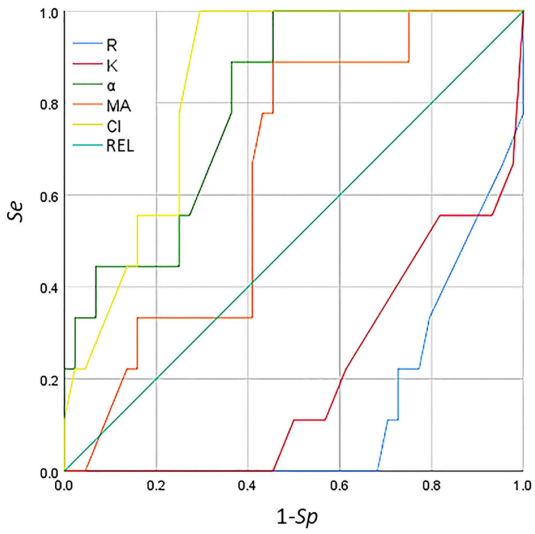

FIGURE 5
Receiver operating characteristic (ROC) curve analysis of the thromboelastogram (TEG) parameters for the detection of secondary bleeding disorders in patients with breast cancer.

4 Discussion

4.1 Parameters in the thromboelastogram

Different from the conventional coagulation function index, a thromboelastogram can reflect the dynamic process of coagulation, including PLT aggregation (44), coagulation factor initiation (45), fibrin formation, and fibrinolysis (46). The clinical significance is not limited to thrombotic disease (47), thrombocytopenia, coagulation factor deficiency diseases, and hyperfibrinolytic disease. A series of parameters are derived and presented following TEG (48). The *R* value indicates the time required for the initiation of clotting and the formation of initial fibrin clots. In the TEG test, the intrinsic coagulation factors and anticoagulants affect the *R* value (49). With the continuous activation of the coagulation cascade reaction, the strength of blood clotting continuously increases. The *K* value refers to the time from the formation of the initial fibrin clot to a certain strength of blood clotting. This value is related to the PLT concentration and function, the extrinsic coagulation factor, thrombin, FIB, and hematocrit (46). An increase in *K* indicates that the function of FIB in the whole blood of the patient is insufficient, while a decrease in *K* indicates a hyperfunction of FIB. The α angle reflects the rate of clot formation, specifically the rate of fibrin formation and the cross-linking of fibrin and PLTs (50). The effect of the α angle is consistent with the reciprocal of *K* and is affected by the same factors. An increased α angle is related to an increased FIB function in the whole blood of patients, while a decreased α angle is related to insufficient FIB function (51). MA indicates the maximum clotting strength, while the PLT concentration function, the FIB concentration, and the PLT–FIB interaction all determine the clotting strength and the influence of PLTs (52). An increased MA indicates an increased PLT function in the whole blood of a patient, while a decreased MA indicates a decreased PLT function. The end of the clotting process is followed by the fibrinolysis process (53).

TEG tests can indicate various diseases related to perioperative bleeding of unknown origin, suspicion of hyperfibrinolysis, monitoring of FIB replacement, thrombocytopenia, and disorders of polymerization (54). The tests derive a series of parameters by combining relevant software processing in the TEG maps. The *R* value represents the time required for the initiation of coagulation and the formation of initial fibrin clots (55). The intrinsic coagulation factors and anticoagulants influence the *R* value, with an increased *R* indicating a low coagulation state, such as an increased coagulation factor activity and the use of anticoagulants (56). A reduced *R* indicates no fibrinolysis and that the blood is in a hypercoagulable state, such as a decrease in the coagulation factor activity for the PLT-rich plasma and in patients with chronic dissection (57). As the coagulation cascade reaction is continuously activated, the strength of

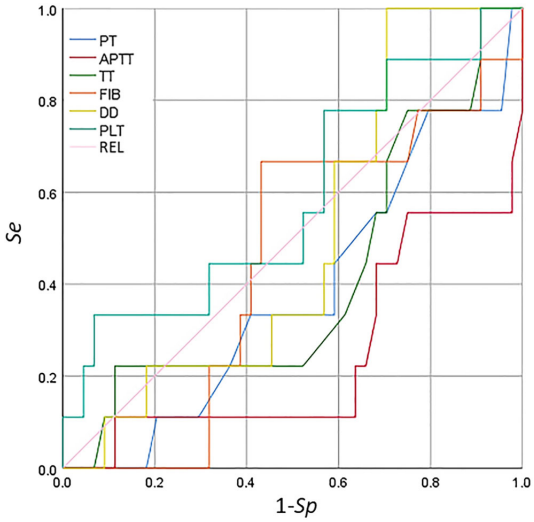

FIGURE 6
Receiver operating characteristic (ROC) curve analysis of the coagulation function indicators and platelet count for the detection of secondary bleeding disorders in patients with breast cancer.

blood clotting continues to increase (58). MA represents the maximum clotting strength reached by a blood clot. The PLT concentration and function, the FIB concentration, and the interaction of PLTs with FIB all determine the strength of blood clotting, with the influence of PLTs being major (59).

4.2 Blood coagulation function index

The coagulation indicators, including *R*, *K*, MA, and CI, are correlated with a diagnosis of thrombosis or embolism. In particular, decreased *R* and *K* values and increased α angle, MA, and CI indicate that the blood is prone to be in a hypercoagulable state. An increase in FIB and D-D is also closely related to a high coagulation state. Linkins and Lapner summarized the general characteristics of D-D detection, discussed the concept of increasing the threshold of D-D for the diagnosis of VTE according to prior probability and age, and provided a clinical point of view on the role of D-D detection in the diagnosis and prognosis of VTE (60). In the descriptive statistics of the routine coagulation function indicators, PLT count, and the TEG parameters in patients with benign and malignant breast diseases, the mean values of *R* and *K* in the malignant breast disease group were lower than those in the benign breast disease group, but the mean values of the α angle, MA, CI, FIB, and D-D were higher than those in the benign breast disease group. The results of the test of differences in the routine coagulation function indicators, PLT count, and the TEG parameters in patients with benign and malignant breast diseases showed that the *t*-test for MA and FIB in both benign and malignant breast disease groups was $p < 0.05$, indicating significant difference between the two groups. The indicators in patients with malignant breast diseases pointed to hypercoagulability, which differed somewhat from those in patients with benign breast diseases (61). Moreover, at 90% confidence interval, the FIB test had a $p < 0.1$, while the *p*-values of CI, D-D, PLT, and the other indicators tested for $p > 0.1$ were very close to 0.1. Correlation analysis of the routine coagulation function indicators, PLT count, and the TEG parameters in patients with breast diseases showed that the *R* value was positively correlated with aPTT and D-D, but was negatively correlated with PLT. The *K* value was positively correlated with aPTT and D-D, but was negatively correlated with PLT. The α angle was negatively correlated with aPTT and D-D, but was positively correlated with PLT. The MA was positively correlated with FIB and PLT. The CI was negatively correlated with aPTT, TT, and D-D, but was positively correlated with PLT. The correlation analysis between *R* and APTT (or PT) showed a higher response degree of kaolin-activated coagulation for intrinsic coagulation pathways than that of extrinsic coagulation pathways. PLT was negatively correlated with *R* and *K*, as well as the α angle. There was a positive correlation between the α angle, MA, and CI, indicating consistency between the TEG examination and the PLT count. The PLT concentration and function, the FIB concentration, and the interaction between PLTs and FIB all determine the strength of blood clotting. MA was positively correlated with FIB and PLT, which is consistent with this conclusion. ROC curve analysis of the predictive value of TEG, routine PLT, and the coagulation function indicators for secondary bleeding disorders in patients with breast cancer showed that CI and the α angle had predictive value. The CI and the α angle were obtained from the TEG testing parameters, indicating that TEG testing has significant predictive value for secondary bleeding disorders in patients with breast cancer. TEG detection for breast cancer patients is on the way, accompanied by routine coagulation assessment to prevent bleeding disease.

4.3 Blood hypercoagulability

The formation of blood hypercoagulability in patients with breast cancer increases the risk of thrombosis and hemorrhagic disease and promotes the occurrence and development of tumors. In addition, this hypercoagulable state supports tumor immune escape and interferes with immunotherapy. Blood hypercoagulability can be measured using various indices (e.g., CI, *R*, *K*, MA, PT, TT, aPTT, FIB, and D-D), despite these indices having clear differences among them when referring to normal ranges. Thromboelastographic detection should be carried out at the same time as routine coagulation function assessment in patients with breast cancer, which provides an important basis for rational clinical treatment. There is increasing research on the correlation between routine coagulation function indicator assessment and thromboelastographic detection in tumor diseases. More and more attention will be paid to thromboelastographic detection, and it will also continue to improve and develop. Combined with the assessment of routine coagulation function indicators, enough theoretical references have become more available to provide the basis for the auxiliary diagnosis and prevention of malignant tumors and their secondary diseases.

Despite the reduced *R* and K values in the malignant breast disease group, there was a significant difference in the MA and FIB between the benign and malignant breast disease groups in the current study. This suggests that PLT function and FIB are sensitive to the occurrence and development of breast tumors. There was no significant difference

in the other indices ($p > 0.05$). In comparison, the mean values of α, MA, CI, FIB, and D-D in the malignant breast disease group were higher than those in the benign breast disease group. Despite the D-D levels increasing in almost all cases of acute thromboembolism, D-D can be detected at low levels in healthy individuals due to the conversion of small amounts of FIB into fibrin physiologically, which also increases with age (60). LY30 and LY60 represent the strength of blood clotting at 30 and 60 min after the beginning of fibrinolysis, respectively, reflecting the speed of clot dissolution (62), despite the no clear variation between LY30 and LY60 in our study. An increase in these values indicates hyperfibrinolysis, while a decrease indicates a weakened fibrinolysis (63). As discussed above, the controlling and/or regulatory factors of blood hypercoagulability are complex, and our current research found statistical correlations between them. In this study, the mean value of CI was within the normal range, despite a variation between 0.5 and 0.95 for the patients with benign and malignant breast tumors.

5 Conclusion

Female patients with breast cancer are more prone to complications with blood hypercoagulable state than those with benign breast diseases. The combination of thromboelastography tracing and routine blood coagulation indices might have a more guiding role in the treatment and prediction of secondary bleeding disorders in patients with breast cancer. The *R* and *K* values in the malignant breast disease group were lower than those in the benign breast disease group; however, the α angle, MA, CI, FIB, and D-D in the malignant breast disease group were higher than those in the benign breast disease group. The CI, α angle, and MA of TEG might predict secondary bleeding disorders in patients with breast cancer.

Data availability statement

The original contributions presented in the study are included in the article/Supplementary Material. Further inquiries can be directed to the corresponding authors.

Ethics statement

The studies involving humans were approved by Ethics Committee of Drug Clinical Trials in Affiliated Hospital of Jiangsu University. The studies were conducted in accordance with the local legislation and institutional requirements. The participants provided their written informed consent to participate in this study.

Author contributions

QP: Conceptualization, Funding acquisition, Investigation, Methodology, Project administration, Supervision, Writing – original draft, Writing – review & editing. JZ: Formal analysis, Software, Visualization, Writing – original draft. XR: Resources, Validation, Writing – review & editing.

Funding

The author(s) declare financial support was received for the research, authorship, and/or publication of this article. This research was funded by the Science and Technology program (no. jdfyRC2017003) and "Beigu Talent" Youth Program (no. BGYCB202203) of the Affiliated Hospital of Jiangsu University, Medical Teaching and Research Collaborative Project (JDYY2023004) of Jiangsu University, and Jiangsu Society of Blood Transfusion (no. JS2022036).

Conflict of interest

The authors declare that the research was conducted in the absence of any commercial or financial relationships that could be construed as a potential conflict of interest.

Publisher's note

Supplementary material

The Supplementary Material for this article can be found online at: https://www.frontiersin.org/articles/10.3389/fonc.2024.1342439/full#supplementary-material

References

1. Jarcho S. Armand trousseau: Lecture on angina pectoris. *Am J Cardiol*. (1959) 3:558–64. doi: 10.1016/0002-9149(59)90379-0

2. Ward MP, Kane LE, Norris LA, Mohamed BM, Kelly T, Bates M, et al. Platelets, immune cells and the coagulation cascade; friend or foe of the circulating tumour cell? *Mol Cancer*. (2021) 20:59. doi: 10.1186/s12943-021-01347-1

3. Khorana AA, Mackman N, Falanga A, Pabinger I, Noble S, Ageno W, et al. Cancer-associated venous thromboembolism. *Nat Rev Dis Primers*. (2022) 8:11. doi: 10.1038/s41572-022-00336-y

4. Olson MC, Lubner MG, Menias CO, Mellnick VM, Mankowski Gettle L, Kim DH, et al. Venous thrombosis and hypercoagulability in the abdomen and pelvis: Causes and imaging findings. *RadioGraphics*. (2020) 40:190097. doi: 10.1148/rg.2020190097

5. Khan F, Tritschler T, Kahn SR, Rodger MA. Venous thromboembolism. *Lancet*. (2021) 398:64–77. doi: 10.1016/S0140-6736(20)32658-1

6. Tremblay D, Yacoub A, Hoffman R. Overview of myeloproliferative neoplasms: History, pathogenesis, diagnostic criteria, and complications. *Hematology/Oncol Clinics*. (2021) 35:159–76. doi: 10.1016/j.hoc.2020.12.001

7. Chen L, Kong X, Yan C, Fang Y, Wang J. The research progress on the prognostic value of the common hematological parameters in peripheral venous blood in breast cancer. *OncoTargets Ther*. (2020) 13:1397–412. doi: 10.2147/OTT.S227171

8. Riva N, Donadini MP, Dentali F, Squizzato A, Ageno W. Clinical approach to splanchnic vein thrombosis: Risk factors and treatment. *Thromb Res*. (2012) 130:S1–3. doi: 10.1016/j.thromres.2012.08.259

9. Asopa S, Patel A, Khan OA, Sharma R, Ohri SK. Non-bacterial thrombotic endocarditis. *Eur J Cardio-Thoracic Surg*. (2007) 32:696–701. doi: 10.1016/j.ejcts.2007.07.029

10. Kobayashi S, Koizume S, Takahashi T, Ueno M, Oishi R, Nagashima S, et al. Tissue factor and its procoagulant activity on cancer-associated thromboembolism in pancreatic cancer. *Cancer Sci*. (2021) 112:4679–91. doi: 10.1111/cas.15106

11. Moik F, Ay C. Hemostasis and cancer: Impact of haemostatic biomarkers for the prediction of clinical outcomes in patients with cancer. *J Thromb Haemostasis*. (2022) 20:2733–45. doi: 10.1111/jth.15880

12. Buller HR, Van Doormaal FF, Van Sluis GL, Kamphuisen PW. Cancer and thrombosis: from molecular mechanisms to clinical presentations. *J Thromb Haemostasis*. (2007) 5:246–54. doi: 10.1111/j.1538-7836.2007.02497.x

13. Caine GJ, Nadar SK, Li GYH, Stonelake PS, Blann AD. Platelet adhesion in breast cancer: development and application of a novel assay. *Blood Coagulation Fibrinolysis*. (2004) 15:513–8. doi: 10.1097/00001721-200408000-00012

14. Singh AK, Malviya R. Coagulation and inflammation in cancer: Limitations and prospects for treatment. *Biochim Biophys Acta (BBA) - Rev Cancer*. (2022) 1877:188727. doi: 10.1016/j.bbcan.2022.188727

15. Magrini E, Minute L, Dambra M, Garlanda C. Complement activation in cancer: Effects on tumor-associated myeloid cells and immunosuppression. *Semin Immunol*. (2022) 60:101642. doi: 10.1016/j.smim.2022.101642

16. Tawil N, Rak J. Blood coagulation and cancer genes. *Best Pract Res Clin Haematol*. (2022) 35:101349. doi: 10.1016/j.beha.2022.101349

17. Garnier D, Magnus N, D'Asti E, Hashemi M, Meehan B, Milsom C, et al. Genetic pathways linking hemostasis and cancer. *Thromb Res*. (2012) 129:S22–9. doi: 10.1016/S0049-3848(12)70012-9

18. Watson NW, Shatzel JJ, Al-Samkari H. Cyclin-dependent kinase 4/6 inhibitor-associated thromboembolism: a critical evaluation of the current evidence. *J Thromb Haemostasis*. (2023) 21:758–70. doi: 10.1016/j.jtha.2022.12.001

19. Falanga A, Marchetti M, Vignoli A. Coagulation and cancer: biological and clinical aspects. *J Thromb Haemostasis*. (2013) 11:223–33. doi: 10.1111/jth.12075

20. Kvolik S, Jukic M, Matijevic M, Marjanovic K, Glavas-Obrovac L. An overview of coagulation disorders in cancer patients. *Surg Oncol*. (2010) 19:e33–46. doi: 10.1016/j.suronc.2009.03.008

21. Guglietta S, Rescigno M. Hypercoagulation and complement: Connected players in tumor development and metastases. *Semin Immunol*. (2016) 28:578–86. doi: 10.1016/j.smim.2016.10.011

22. Nasser NJ, Fox J, Agbarya A. Potential mechanisms of cancer-related hypercoagulability. *In: Cancers*. (2020). doi: 10.3390/cancers12030566

23. Kirwan CC, Descamps T, Castle J. Circulating tumour cells and hypercoagulability: a lethal relationship in metastatic breast cancer. *Clin Trans Oncol*. (2020) 22:870–7. doi: 10.1007/s12094-019-02197-6

24. Campello E, Ilich A, Simioni P, Key NS. The relationship between pancreatic cancer and hypercoagulability: a comprehensive review on epidemiological and biological issues. *Br J Cancer*. (2019) 121:359–71. doi: 10.1038/s41416-019-0510-x

25. Watson C, Saaid H, Vedula V, Cardenas JC, Henke PK, Nicoud F, et al. Venous Thromboembolism: Review of clinical challenges, biology, assessment, treatment, and modeling. *Ann Biomed Eng*. (2024) 52:467–86. doi: 10.1007/s10439-023-03390-z

26. Sabharwal S, Jalloh HB, Levin AS, Morris CD. What proportion of patients with musculoskeletal tumors demonstrate thromboelastographic markers of hypercoagulability? *A pilot study Clin Orthopaedics Related Research®*. (2023) 481:553–61. doi: 10.1097/CORR.0000000000002314

27. Krithiga R, Geetha P. Breast cancer detection, segmentation and classification on histopathology images analysis: A systematic review. *Arch Comput Methods Eng*. (2021) 28:2607–19. doi: 10.1007/s11831-020-09470-w

28. Quarterman C, Shaw M, Johnson I, Agarwal S. Intra- and inter-centre standardisation of thromboelastography (TEG®). *Anaesthesia*. (2014) 69:883–90. doi: 10.1111/anae.12748

29. Ahmadi SE, Shabannezhad A, Kahrizi A, Akbar A, Safdari SM, Hoseinnezhad T, et al. Tissue factor (coagulation factor III): a potential double-edge molecule to be targeted and re-targeted toward cancer. *biomark Res*. (2023) 11:60. doi: 10.1186/s40364-023-00504-6

30. Peng Y, Butt YM, Chen B, Zhang X, Tang P. Update on immunohistochemical analysis in breast lesions. *Arch Pathol Lab Med*. (2017) 141:1033–51. doi: 10.5858/arpa.2016-0482-RA

31. Floyd CN, Ferro A. Indications for anticoagulant and antiplatelet combined therapy. *BMJ*. (2017) 359:j3782. doi: 10.1136/bmj.j3782

32. Doyle A, Breen K, McLornan DP, Radia D, Hunt BJ, Ling G, et al. Outcomes of patients receiving direct oral anticoagulants for myeloproliferative neoplasm associated venous thromboembolism. *Blood*. (2019) 134:4183. doi: 10.1182/blood-2019-128170

33. Chen W, Zheng R, Baade PD, Zhang S, Zeng H, Bray F, et al. Cancer statistics in China, 2015. *CA-A Cancer J Clin*. (2016) 66:115–32. doi: 10.3322/caac.21338

34. Fainchtein K, Tera Y, Kearn N, Noureldin A, Othman M. Hypercoagulability and thrombosis risk in prostate cancer: The role of thromboelastography. *Semin Thromb Hemost*. (2022) 49:111–8. doi: 10.1055/s-0042-1758116

35. Huang B, Wu F-C, Wang W-D, Shao B-Q, Wang X-M, Lin Y-M, et al. The prognosis of breast cancer patients with bone metastasis could be potentially estimated based on blood routine test and biochemical examination at admission. *Ann Med*. (2023) 55:2231342. doi: 10.1080/07853890.2023.2231342

36. Li S, Lu Z, Wu S, Chu T, Li B, Qi F, et al. The dynamic role of platelets in cancer progression and their therapeutic implications. *Nat Rev Cancer*. (2024) 24:72–87. doi: 10.1038/s41568-023-00639-6

37. P. a. Ding J, Sun C, Chen S, Yang P, Tian Y, Zhou Q, et al. Zhao: Combined systemic inflammatory immunity index and prognostic nutritional index scores as a screening marker for sarcopenia in patients with locally advanced gastric cancer. *Front Nutr*. (2022) 9:981533. doi: 10.3389/fnut.2022.981533

38. Liu S, Zhao Q, Huang F, Yang Q, Wang Y, Wang H, et al. Exposure to melamine and its derivatives in Chinese adults: The cumulative risk assessment and the effect on routine blood parameters. *Ecotoxicol Environ Saf*. (2022) 241:113714. doi: 10.1016/j.ecoenv.2022.113714

39. Chen Z, Sun T, Yang Z, Zheng Y, Yu R, Wu X, et al. Monitoring treatment efficacy and resistance in breast cancer patients *via* circulating tumor DNA genomic profiling. *Mol Genet Genomic Med*. (2020) 8:e1079. doi: 10.1002/mgg3.1079

40. Isiksacan Z, D'Alessandro A, Wolf SM, McKenna DH, Tessier SN, Kucukal E, et al. Assessment of stored red blood cells through lab-on-a-chip technologies for precision transfusion medicine. *Proc Natl Acad Sci*. (2023) 120:e2115616120. doi: 10.1073/pnas.2115616120

41. Agnelli G. Venous thromboembolism and gancer: a two-way clinical association. *Thromb Haemost*. (1997) 78:117–20. doi: 10.1055/s-0038-1657512

42. Wang Z, Li J, Cao Q, Wang L, Shan F, Zhang H. Comparison between thromboelastography and conventional coagulation tests in surgical patients with localized prostate cancer. *Clin Appl Thrombosis/Hemostasis*. (2017) 24:755–63. doi: 10.1177/1076029617724229

43. Ramanujam V, DiMaria S, Varma V. Thromboelastography in the perioperative period: A literature review. *Cureus*. (2023) 15:e39407. doi: 10.7759/cureus.39407

44. Bochsen L, Wiinberg B, Kjelgaard-Hansen M, Steinbrüchel DA, Johansson PI. Evaluation of the TEG® platelet mapping™ assay in blood donors. *Thromb J*. (2007) 5:3. doi: 10.1186/1477-9560-5-3

45. Karon BS. Why is everyone so excited about thromboelastrography (TEG)? *Clinica Chimica Acta*. (2014) 436:143–8. doi: 10.1016/j.cca.2014.05.013

46. Zeng Z, Fagnon M, Nallan Chakravarthula T, Alves NJ. Fibrin clot formation under diverse clotting conditions: Comparing turbidimetry and thromboelastography. *Thromb Res*. (2020) 187:48–55. doi: 10.1016/j.thromres.2020.01.001

47. Mao C, Xiong Y, Fan C. Comparison between thromboelastography and conventional coagulation assays in patients with deep vein thrombosis. *Clinica Chimica Acta*. (2021) 520:208–13. doi: 10.1016/j.cca.2021.06.019

48. Hartmann J, Dias JD, Pivalizza EG, Garcia-Tsao G. Thromboelastography-guided therapy enhances patient blood management in cirrhotic patients: A Meta-analysis based on randomized controlled trials. *Semin Thromb Hemost*. (2023) 49:162–72. doi: 10.1055/s-0042-1753530

49. Shamseddeen H, Patidar KR, Ghabril M, Desai AP, Nephew L, Kuehl S, et al. Features of blood clotting on thromboelastography in hospitalized patients with cirrhosis. *Am J Med*. (2020) 133:1479–1487.e2. doi: 10.1016/j.amjmed.2020.04.029

50. Litvinov RI, Weisel JW. Fibrin mechanical properties and their structural origins. *Matrix Biol*. (2017) 60-61:110–23. doi: 10.1016/j.matbio.2016.08.003

51. Ariëns RAS. Fibrin(ogen) and thrombotic disease. *J Thromb Haemostasis*. (2013) 11:294–305. doi: 10.1111/jth.12229

52. Moore HB, Moore EE, Chapman MP, Gonzalez E, Slaughter AL, Morton AP, et al. Viscoelastic measurements of platelet function, not fibrinogen function, predicts sensitivity to tissue-type plasminogen activator in trauma patients. *J Thromb Haemostasis*. (2015) 13:1878–87. doi: 10.1111/jth.13067

53. Paniccia R, Priora R, Alessandrello Liotta A, Abbate R. Platelet function tests: a comparative review. *Vasc Health Risk Manage*. (2015) 11:133–48. doi: 10.2147/VHRM.S44469

54. Lang T, v. M. Depka: Possibilities and limitations of thromboelastometry/thromboelastography. *Hamostaseologie*. (2006) 26:S21–9. doi: 10.1055/s-0037-1617078

55. Goncalves JPN, de Waal GM, Page MJ, Venter C, Roberts T, Holst F, et al. The value of detecting pathological changes during clot formation in early disease treatment-naïve breast cancer patients. *Microsc Microanalysis*. (2021) 27:425–36. doi: 10.1017/S1431927621000015

56. Konstantinidi A, Sokou R, Parastatidou S, Lampropoulou K, Katsaras G, Boutsikou T, et al. Clinical application of thromboelastography/thromboelastometry (TEG/TEM) in the neonatal population: A narrative review. *Semin Thromb Hemost*. (2019) 45:449–57. doi: 10.1055/s-0039-1692210

57. Everts P, Onishi K, Jayaram P, Lana JF, Mautner K. Platelet-rich plasma: New performance understandings and therapeutic considerations in 2020. *In: Int J Mol Sci*. (2020). doi: 10.3390/ijms21207794

58. Diamond SL. Systems biology of coagulation. *J Thromb Haemostasis*. (2013) 11:224–32. doi: 10.1111/jth.12220

59. Kattula S, Byrnes JR, Wolberg AS. Fibrinogen and fibrin in hemostasis and thrombosis. *Arterioscler Thrombosis Vasc Biol*. (2017) 37:e13–21. doi: 10.1161/ATVBAHA.117.308564

60. Linkins LA, Takach Lapner S. Review of D-dimer testing: Good, bad, and ugly. *Int J Lab Hematol*. (2017) 39:98–103. doi: 10.1111/ijlh.12665

61. Gotta J, Gruenewald LD, Eichler K, Martin SS, Mahmoudi S, Booz C, et al. Unveiling the diagnostic enigma of D-dimer testing in cancer patients: Current evidence and areas of application. *Eur J Clin Invest*. (2023) 53:e14060. doi: 10.1111/eci.14060

62. Morrow GB, Feller T, McQuilten Z, Wake E, Ariëns RAS, Winearls J, et al. Cryoprecipitate transfusion in trauma patients attenuates hyperfibrinolysis and restores normal clot structure and stability: Results from a laboratory sub-study of the FEISTY trial. *Crit Care*. (2022) 26:290. doi: 10.1186/s13054-022-04167-x

63. Fan D, Ouyang Z, Ying Y, Huang S, Tao P, Pan X, et al. Thromboelastography for the prevention of perioperative venous thromboembolism in orthopedics. *Clin Appl Thrombosis/Hemostasis*. (2022) 28:10760296221077975. doi: 10.1177/10760296221077975

frontiers | Frontiers in Oncology

TYPE Original Research
PUBLISHED 23 July 2024
DOI 10.3389/fonc.2024.1337194

OPEN ACCESS

EDITED BY
Anika Nagelkerke,
University of Groningen, Netherlands

REVIEWED BY
Rebekah Young,
The Ohio State University, United States
Jana Fox,
Albert Einstein College of Medicine,
United States

*CORRESPONDENCE
Xiangpan Li
rm001227@whu.edu.cn

†These authors have contributed equally to this work

RECEIVED 12 November 2023
ACCEPTED 10 July 2024
PUBLISHED 23 July 2024

CITATION
Zhao F, Yang D, Lan Y and Li X (2024) Management and outcomes of breast cancer patients with radiotherapy interruption. *Front. Oncol.* 14:1337194. doi: 10.3389/fonc.2024.1337194

Management and outcomes of breast cancer patients with radiotherapy interruption

Fangrui Zhao[1†], Dashuai Yang[2†], Yanfang Lan[1†] and Xiangpan Li[1*]

[1]Department of Oncology, Renmin Hospital of Wuhan University, Wuhan, Hubei, China, [2]Department of Hepatobiliary Surgery, Renmin Hospital of Wuhan University, Wuhan, Hubei, China

Background: Many cancer patients have not received timely treatment or even had treatment interruptions due to the COVID-19 pandemic. The objective of this investigation was to evaluate whether the prognosis of patients with breast cancer after surgery was affected by any interruptions in radiotherapy.

Methods: The healthcare documents for breast cancer patients experiencing radiotherapy interruption after surgery, including treatment-related characteristics, and time of interruption, type of disease progression, and survival status, were collected between January and April 2020 during the Wuhan blockade.

Results: The final number of patients included was 148, and neither the Kaplan-Meier (KM) survival curve nor the cross-tabulation analysis found statistical significance. Cox regression analysis also did not identify risk factors associated with PFS.

Conclusions: The prognosis of patients with postoperative breast cancer may not be significantly impacted by the interruption of radiotherapy, given its integration with additional treatments like targeted and endocrine therapies.

KEYWORDS

breast cancer, radiotherapy, interruption, COVID-19, prognosis

Abbreviations: ER, estrogen receptor; PR, progesterone receptor; HER2, human epidermal growth factor receptor 2; VEGF, vascular endothelial growth factor; COVID-19, coronavirus disease 2019; OS, overall survival; PFS, progression-free survival; RTI, radiotherapy interrupted; non-RTI, non-radiotherapy interrupted; PSM, propensity score matching.

Background

Breast cancer has become more prevalent than lung cancer, ranking as the fifth most common type of cancer and the fifth leading cause of cancer-related fatalities globally (1). According to statistics, approximately 2.3 million people will be diagnosed with breast cancer in 2020, and 685,000 people will die from breast cancer (2). The incidence of breast cancer is projected to reach 4.4 million cases by 2070 (3). Breast cancer accounts for approximately 24.5% of all cancer cases in women, making it the leading cause of global cancer-related deaths, representing approximately 15.5%. It ranks first in most countries in the world in terms of incidence and mortality in 2020 (1).

The classification of breast cancer is primarily based on the presence or absence of estrogen receptor (ER), progesterone receptor (PR), and human epidermal growth factor receptor 2 (HER2), reflecting its diverse nature. These distinct subtypes exhibit variations in etiology and prognostic outcomes (4). The most prevalent subtype of breast cancer is characterized by being estrogen receptor (ER) and/or progesterone receptor (PR) positive while lacking human epidermal growth factor receptor 2 (HER2), accounting for approximately 73% of all breast cancers (5).

The selection of the treatment protocol should rely on the patient's molecular profile. The treatment strategies vary depending on the stage of breast cancer. Surgical management of ductual carcinoma *in situ* includes breast conserving surgery (lumpectomy), often followed by radiotherapy, or mastectomy, after which radiotherapy is not indicated, aside from rare cases of positive margin when re-resection cannot be done. When ER is positive, endocrine therapy may also be an option. Depending on its biological profile, invasive ductal carcinoma may require endocrine therapy, targeted agents, immunotherapy, and/or chemotherapy, in the neoadjuvant or adjuvant setting (6). Triple-negative breast cancer almost always is an indication for chemotherapy, as it is typically the most aggressive subtype of breast cancer.

Radiotherapy has become an essential part of breast cancer treatment. Postoperative radiation therapy has the potential to eliminate any remaining tumor cells, leading to enhanced control rates of both local (primary site) and/or regional (axillary nodal basin) diseases (7, 8) and minimizing the need for extensive surgical procedures (9–11). It has been shown that the 10-year local recurrence rate and distant metastasis rate were reduced by approximately 16% and the risk of death by approximately 4% in female patients with negative lymph nodes after breast-conserving surgery who received radiotherapy (8). Patients who have experienced a recurrence of breast cancer in the same area can also achieve favorable outcomes through re-administration of radiotherapy (12–14). Studies have demonstrated that reirradiation can lead to high rates of local control, ranging from 43% to 96%, and varying complete response rates between 41% and 71% (14).

Coronavirus disease 2019 (COVID-19) emerged in December 2019, and the World Health Organization declared that it reached pandemic status on 11 March 2020 (15, 16). Due to the highly infectious nature of the virus, isolation and reduction in crowd gathering became the mainstream response until new treatments and vaccines were available (17). The outbreak of COVID-19 not only led to the suspension of many social events and closure of public facilities but also had a dramatic impact on healthcare services (18). Many cancer patients progressed or even died due to delayed diagnosis, untimely treatment, or even interruption (19, 20). Radiotherapy is a crucial component in the management of breast cancer, and it remains to be studied whether interruption of radiotherapy due to an epidemic outbreak can cause disease progression.

Methods

Patients

Clinical data of all breast cancer patients who received radiotherapy (interrupted or uninterrupted) at 10 hospitals in Hubei province since the outbreak of the new crown epidemic (January–April 2020) were collected. The inclusion criteria were as follows: 1) patients with pathological diagnosis of invasive breast cancer and 2) patients who had undergone surgery and postoperative radiotherapy. The breast cancer patients included in this study were treated with regional nodal irradiation (RNI) in addition to breast/chest wall irradiation for node-positive patients. In addition, patients who were node-negative but clinically assessed as high risk were also treated with RNI.

Demographic, clinical, and treatment information was retrieved from each hospital's medical records and filing system.

Statistical analysis

The overall survival (OS) was defined as the duration from the initiation of radiotherapy following breast cancer surgery until death resulting from any cause, while progression-free survival (PFS) referred to the period from the commencement of radiotherapy after breast cancer surgery until disease progression. Patients were continuously monitored for tumor progression and survival data until their last follow-up in March 2023. Radiotherapy interruption was defined as a situation in which the treatment plan has to be temporarily suspended for some reason during the course of radiotherapy. Included patients were divided into two groups based on whether or not the interruption lasted more than 7 days, i.e., radiotherapy interrupted (RTI) and non-radiotherapy interrupted (non-RTI), using propensity score matching (PSM) to adjust for potential baseline confounders (demographic data, clinical characteristics, and treatment) to make the two groups comparable. The analysis of categorical variables involved the use of cross-tabulation and chi-square tests, while survival data estimation was conducted using Kaplan–Meier curves and log-rank tests. Cox regression analysis was employed to identify and evaluate risk factors associated with progression-free survival (PFS). Statistical significance was determined based on two-tailed p-values <0.05. All statistical analyses were performed using SPSS 24.0 (SPSS Inc., Chicago, USA).

10.3389/fonc.2024.1337194

Results

Radiotherapy interruption did not cause survival difference

We collected data related to radiotherapy for breast cancer patients in 10 hospitals in Hubei province, and all patients were women. The total number of patients included through PSM was 148, with 74 patients in each of the RTI and non-RTI groups. The details of the included patients are shown in Table 1. The reason for the interruption of radiotherapy is mainly due to the COVID-19 outbreak, which has caused regional lockdown and prevented patients from travelling normally. The average age of individuals in the RTI group was recorded as 48 years, while those in the non-RTI group had an average age of 50 years. The proportion of patients ≤50 years old was the same in both groups. In the RTI group, 18% of patients were clinically staged as stage I, 43% as stage II, and 38% as stage III. In the non-RTI group, the proportions of patients clinically staged as stage I, stage II, and stage III were 12%, 42%, and 45%, respectively. Only a small proportion of included patients received neoadjuvant chemotherapy (RTI, 27%; non-RTI, 14%), targeted therapy (RTI, 23%; non-RTI, 27%), and endocrine therapy (RTI, 36%; non-RTI, 34%). However, the use of neoadjuvant chemotherapy was almost twice as high in the RTI (vs. non-RTI) group.

TABLE 1 Baseline characteristics of postoperative breast cancer patients.

	Group			
	Non-RTI		RTI	
Median age (years old)	48		50	
Age				
≤50	43	58%	43	58%
>50	31	42%	31	42%
TNM				
I	13	18%	9	12%
II	32	43%	31	42%
III	28	38%	33	45%
IV	1	1%	1	1%
Neoadjuvant chemotherapy				
No	54	73%	64	86%
Yes	20	27%	10	14%
Adjuvant chemotherapy				
No	30	41%	20	27%
Yes	44	59%	54	73%
Targeted therapy				
No	57	77%	54	73%
Yes	17	23%	20	27%
Endocrinotherapy				
No	47	64%	49	66%
Yes	27	36%	25	34%
Continued				
No	—		23	31%
Yes	—		51	69%

In the RTI group, 59% of patients received adjuvant chemotherapy, while in the non-RTI group, this percentage was higher at 73%. The median duration of follow-up (calculated from the commencement of radiotherapy until the most recent contact) was 37.3 months (ranging from 1.3 months to 46.2 months). Figure 1 illustrates that there was no disparity in survival between the two groups due to the interruption of radiotherapy (p=0.733), and Figure 2 further confirms that radiotherapy interruption did not affect PFS in patients after breast cancer surgery (p=0.722). In addition, the 3-year PFS rates were comparable between the two groups, with percentages of 91.9% and 90.5%, respectively.

In the non-RTI group, two patients died and four patients progressed. In contrast, in the RTI group, no patients died. Of these seven patients, only one patient did not choose to return to thehospital for further radiotherapy after the interruption of radiotherapy.

No discernible risk factors associated with PFS were identified

In the RTI cohort, a majority of patients (69%) opted for hospital readmission to continue their radiotherapy treatment,

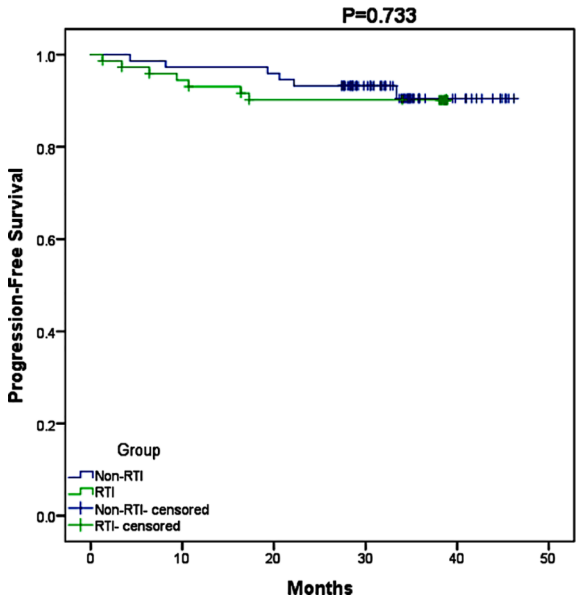

FIGURE 1
Kaplan-Meier survival curve of PFS between RTI and non-RTI.

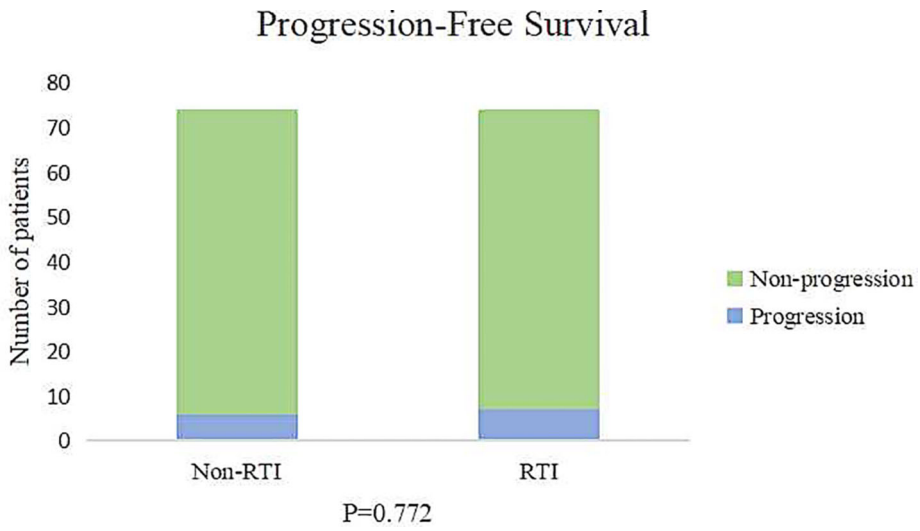

FIGURE 2
The impact of RTI on disease progression.

TABLE 2 Multivariate Cox proportional hazards regression model analysis of PFS in RTI.

Groups	p	Exp(B)	95.0% CI	
Age				
≤50				
>50	0.736	1.375	0.216	8.772
TNM	0.203			
I				
II	0.337	0.222	0.01	4.79
III	0.724	0.632	0.05	8.053
IV	0.233	8.838	0.247	316.82
Neoadjuvant chemotherapy				
No				
Yes	0.474	3.391	0.119	96.236
Adjuvant chemotherapy				
No				
Yes	0.346	4.753	0.186	121.373
Targeted therapy				
No				
Yes	0.955	0.948	0.15	5.981
Endocrinotherapy				
No				
Yes	0.428	0.406	0.044	3.772
Continued				
No				
Yes	0.461	2.368	0.239	23.487

with a median RTI of 78 days (ranging from 7 days to 155 days). Cox risk regression models suggested that clinical stage, neoadjuvant chemotherapy, adjuvant chemotherapy, targeted therapy, endocrine therapy, and return to continued treatment were not factors in the difference in survival (p>0.05) (Table 2). The KM survival curve further demonstrated that there was no difference in prognosis between patients who continued to return to radiotherapy and those who abandoned continuing radiotherapy (p=0.306) (Figure 3). Although there was a noticeable decrease in the 3-year PFS rate for patients who received continued radiotherapy (88.2%) compared to those who did not (95.7%), statistical analysis did not reveal any significant difference between the two groups (p=0.562) (Figure 4).

Discussion

Radiotherapy is typically recommended after lumpectomy for most patients with invasive breast cancer, stages I–III, and after mastectomy for women with T4 disease and/or lymph node metastases. The integration of these treatments optimizes disease management at the local level, resulting in favorable survival outcomes (21). In the last decades, radiotherapy techniques have been greatly improved (22), and the incidence of radiotherapy-induced cardiopulmonary toxicity has improved (23).

The primary mechanism of radiotherapy is to eliminate cancerous cells by causing irreversible harm to the genetic material and membranes of these cells (24). Ionizing radiation stimulates the generation of reactive oxygen species (ROS) through the breakdown of cellular components. Direct damage to DNA occurs as a result of ionizing radiation, while ROS induce DNA cross-linking, base or sugar impairment, and single- and double-strand breaks (DSBs) (25).

However, due to the COVID-19 pandemic, Wuhan went into lockdown, which also led to interruptions in breast cancer patients

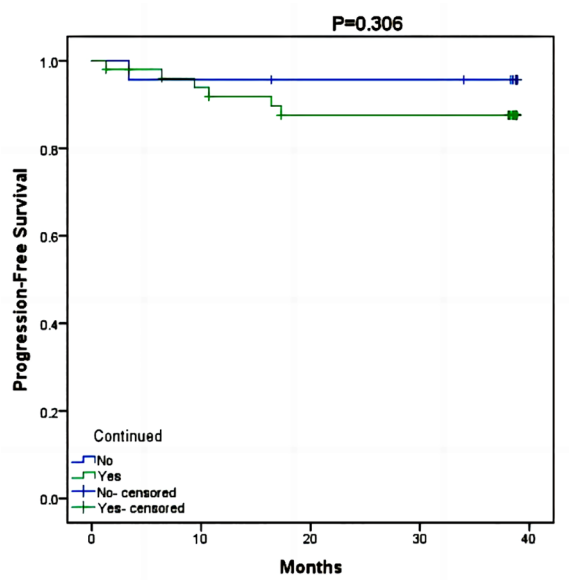

FIGURE 3
Kaplan-Meier survival curve of PFS between patients who continued radiotherapy and those who did not.

undergoing radiotherapy, with interruptions ranging from 6 to 155 days. In rapidly proliferating cancers, prolonging the duration of radiotherapy leads to a decrease in tumor control (26). This loss of tumor control may be related to the accelerated proliferation (repopulation) of tumor cells that survive the interruption period (27, 28). In nasopharyngeal carcinoma, radiotherapy interruptions of just more than 7 days can adversely affect patient prognosis (29, 30), and in head and neck cancers (31). However, Richard et al. noted that breast cancer patients who underwent surgery within 90 days of diagnosis and radiotherapy within 365 days did not have as great an impact on prognosis as expected (32). The impact on survival after patients with breast cancer experiencing interruption in the course of radiotherapy is, as yet, unknown.

In theory, it appears possible to evaluate the influence of radiotherapy interruption on the prognosis of breast cancer through assessing the duration for tumor cells to multiply. In practice, however, tumors initially grow at a parabolic exponential growth rate, and then, the expansion rate begins to decrease and plateau, which is related to limitations in blood supply, growth space, and nutrition, and the chaotic growth pattern of the tumor itself (32, 33). The nonlinear growth kinetic pattern of the tumor results in a tumor multiplication time that is not constant (32, 34, 35), which also causes the assessment to become unreliable. Second, the overall duration of the tumor's existence remains indeterminable, further leading to uncertainty in the relationship between tumor multiplication time and the prognostic impact of interrupted radiotherapy (32).

The findings of this investigation indicate that the discontinuation of radiotherapy appeared to have minimal impact on individuals diagnosed with breast cancer. First, all of the patients underwent surgery, which removed the vast majority of the tumor cells, and most of the patients were treated with chemotherapy. Paclitaxel induces tumor cell aggregation in G2 and M phases to promote cell death. Although concurrent chemotherapy is not often used in the treatment of breast cancer, its synergistic effect in radiotherapy is undeniable. It has been demonstrated that the combination of a low dosage of paclitaxel effectively reduces the proliferation and survival of cancer cells when subjected to fractionated radiotherapy in lung cancer (36). Radiation exerts its effects during the G1/S and G2/M stages, while paclitaxel induces the accumulation of tumor cells in the G2 and M phases. The growth delay observed when combining paclitaxel with fractionated radiotherapy is attributed to the obstruction of various stages within the cell cycle (36, 37). Paclitaxel has been found to enhance the sensitivity of breast cancer cells to radiation by improving tumor interstitial pressure and oxygenation and promoting apoptosis (37).

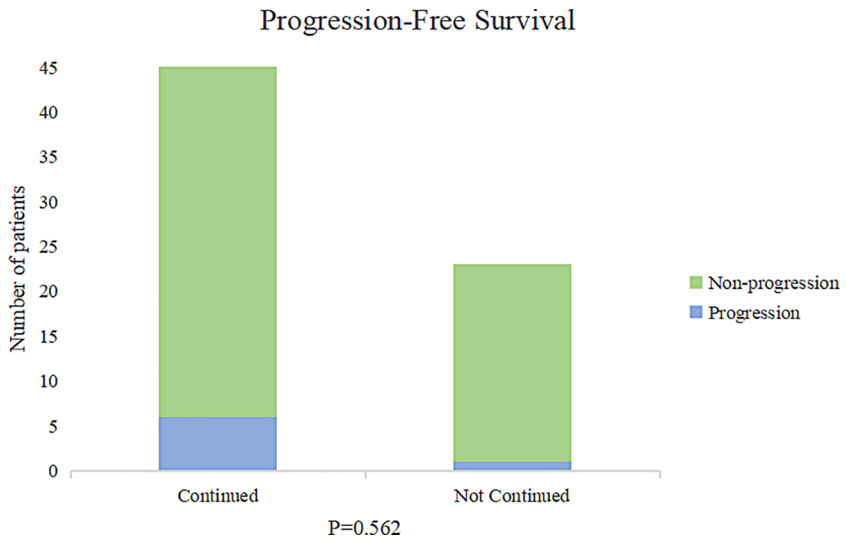

FIGURE 4
Effect of continuation of radiotherapy after RTI on disease progression.

Furthermore, radiosensitivity in breast cancer can be increased through the use of alkylating agents like cisplatin (38) and antimetabolites such as capecitabine (39).

Patients who are HER2+ and/or ER and/or PR positive may undergo adjuvant HER2-targeted therapy and/or endocrine therapy concurrently with radiotherapy (21). The majority of patients in this study underwent endocrine therapy and/or targeted therapy, which may further compensate for the effect of radiotherapy interruption. Endocrine therapy is the cornerstone of hormone-responsive breast cancer treatment, and commonly used agents include aromatase inhibitors or tamoxifen (40). Combining RT with aromatase inhibitors or tamoxifen enhances radiosensitivity and apoptosis (41) and promotes tumor volume reduction (42, 43). Wang et al. conducted a study that discovered that the combination of endocrine therapy and RT resulted in cell redistribution within the G1 phase, leading to a significant decrease in the proportion of breast cancer cells arrested in the G2 and S phases compared to RT alone. Furthermore, an increase in cell cycle arrest was observed, along with a reduction in the regulation of DNA-PKcs, a protein involved in non-homologous repair, and RAD51, a protein involved in homologous recombination repair (44). Therefore, endocrine therapy can be used as a radiosensitizer for hormone receptor-positive breast cancer cells and can be performed in parallel with RT (45, 46).

The limitations of this study were as follows: 1) the sample size was limited, and only postoperative breast cancer patients were included in the study; 2) the duration of follow-up was insufficient, potentially leading to undetected recurrence and metastasis of tumors, necessitating further observation; 3) differences in survival would take many more years to detect, but this is most likely limited by the sample size of this study and the length of follow-up.

Conclusions

The period of the COVID-19 pandemic and the implementation of a lockdown in Wuhan from 23 January to 8 April 2020 provided an exceptional opportunity to assess the impact of contemporary interruptions in radiotherapy. This study offered the most comprehensive follow-up to date for evaluating outcomes associated with interruption of radiotherapy. The results of the study analysis suggest that radiotherapy interruption did not have an impact on the short-term outcomes of postoperative breast cancer patients, which could be due in part to the combination with other treatment modalities. However, what a great risk reduction tool radiation is in the adjuvant (post-op) setting in breast cancer. Therefore, the importance of timely action should not be undermined when RTI happens.

Data availability statement

The raw data supporting the conclusions of this article will be made available by the authors, without undue reservation.

Ethics statement

The studies involving humans were approved by The Ethics Committee of Renmin Hospital of Wuhan University. The studies were conducted in accordance with the local legislation and institutional requirements. Written informed consent for participation was not required from the participants or the participants' legal guardians/next of kin because this was a retrospective study, so informed consent was not required.

Author contributions

FZ: Software, Writing – original draft. DY: Formal analysis, Methodology, Writing – original draft. YL: Conceptualization, Data curation, Writing – review & editing. XL: Writing – review & editing.

Funding

The author(s) declare financial support was received for the research, authorship, and/or publication of this article. This research was supported by Renmin Hospital of Wuhan University Cross-Innovation Talent Project (JCRCWL-2022–003).

Conflict of interest

The authors declare that the research was conducted in the absence of any commercial or financial relationships that could be construed as a potential conflict of interest.

Publisher's note

References

1. Lei S, Zheng R, Zhang S, Wang S, Chen R, Sun K, et al. Global patterns of breast cancer incidence and mortality: A population-based cancer registry data analysis from 2000 to 2020. *Cancer Commun (Lond)*. (2021) 41:1183–94. doi: 10.1002/cac2.12207

2. Sung H, Ferlay J, Siegel RL, Laversanne M, Soerjomataram I, Jemal A, et al. Global cancer statistics 2020: GLOBOCAN estimates of incidence and mortality worldwide for 36 cancers in 185 countries. *CA Cancer J Clin*. (2021) 71:209–49. doi: 10.3322/caac.21660

3. Soerjomataram I, Bray F. Planning for tomorrow: global cancer incidence and the role of prevention 2020-2070. *Nat Rev Clin Oncol*. (2021) 18:663–72. doi: 10.1038/s41571-021-00514-z

4. McCarthy AM, Friebel-Klingner T, Ehsan S, He W, Welch M, Chen J, et al. Relationship of established risk factors with breast cancer subtypes. *Cancer Med*. (2021) 10:6456–67. doi: 10.1002/cam4.4158

5. Howlader N, Altekruse SF, Li CI, Chen VW, Clarke CA, Ries LA, et al. US incidence of breast cancer subtypes defined by joint hormone receptor and HER2 status. *J Natl Cancer Inst*. (2014) 106(5):dju055. doi: 10.1093/jnci/dju055

6. Trayes KP, Cokenakes SEH. Breast cancer treatment. *Am Fam Physician*. (2021) 104:171–8.

7. Ebctcg, McGale P, Taylor C, Correa C, Cutter D, Duane F, et al. Effect of radiotherapy after mastectomy and axillary surgery on 10-year recurrence and 20-year breast cancer mortality: meta-analysis of individual patient data for 8135 women in 22 randomised trials. *Lancet*. (2014) 383:2127–35. doi: 10.1016/S0140-6736(14)60488-8

8. G. Early Breast Cancer Trialists' Collaborative, Darby S, McGale P, Correa C, Taylor C, Arriagada R, et al. Effect of radiotherapy after breast-conserving surgery on 10-year recurrence and 15-year breast cancer death: meta-analysis of individual patient data for 10,801 women in 17 randomised trials. *Lancet*. (2011) 378:1707–16. doi: 10.1016/S0140-6736(11)61629-2

9. Giuliano AE, Hunt KK, Ballman KV, Beitsch PD, Whitworth PW, Blumencranz PW, et al. Axillary dissection vs no axillary dissection in women with invasive breast cancer and sentinel node metastasis: a randomized clinical trial. *JAMA*. (2011) 305:569–75. doi: 10.1001/jama.2011.90

10. Fisher B, Anderson S, Bryant J, Margolese RG, Deutsch M, Fisher ER, et al. Twenty-year follow-up of a randomized trial comparing total mastectomy, lumpectomy, and lumpectomy plus irradiation for the treatment of invasive breast cancer. *N Engl J Med*. (2002) 347:1233–41. doi: 10.1056/NEJMoa022152

11. Van de Steene J, Soete G, Storme G. Adjuvant radiotherapy for breast cancer significantly improves overall survival: the missing link. *Radiotherapy Oncol*. (2000) 55:263–72. doi: 10.1016/S0167-8140(00)00204-8

12. Fattahi S, Ahmed SK, Park SS, Petersen IA, Shumway DA, Stish BJ, et al. Reirradiation for locoregional recurrent breast cancer. *Adv Radiat Oncol*. (2021) 6:100640. doi: 10.1016/j.adro.2020.100640

13. Merino T, Tran WT, Czarnota GJ. Re-irradiation for locally recurrent refractory breast cancer. *Oncotarget*. (2015) 6:35051–62. doi: 10.18632/oncotarget.v6i33

14. Marta GN, Hijal T, de Andrade Carvalho H. Reirradiation for locally recurrent breast cancer. *Breast*. (2017) 33:159–65. doi: 10.1016/j.breast.2017.03.008

15. Li Q, Guan X, Wu P, Wang X, Zhou L, Tong Y, et al. Early transmission dynamics in wuhan, China, of novel coronavirus-infected pneumonia. *N Engl J Med*. (2020) 382:1199–207. doi: 10.1056/NEJMoa2001316

16. W.H. Organization. Coronavirus disease (COVID-19) pandemic . Available online at: https://www.euro.who.int/en/health-topics/health-emergencies/coronavirus-covid-19/novel-coronavirus-2019-ncov.

17. Gandhi M, Yokoe DS, Havlir DV. Asymptomatic transmission, the achilles' Heel of current strategies to control covid-19. *N Engl J Med*. (2020) 382:2158–60. doi: 10.1056/NEJMe2009758

18. Peng SM, Yang KC, Chan WP, Wang YW, Lin LJ, Yen AM, et al. Impact of the COVID-19 pandemic on a population-based breast cancer screening program. *Cancer*. (2020) 126:5202–5. doi: 10.1002/cncr.33180

19. Spicer J, Chamberlain C, Papa S. Provision of cancer care during the COVID-19 pandemic. *Nat Rev Clin Oncol*. (2020) 17:329–31. doi: 10.1038/s41571-020-0370-6

20. Liang W, Guan W, Chen R, Wang W, Li J, Xu K, et al. Cancer patients in SARS-CoV-2 infection: a nationwide analysis in China. *Lancet Oncol*. (2020) 21:335–7. doi: 10.1016/S1470-2045(20)30096-6

21. Gradishar WJ, Moran MS, Abraham J, Aft R, Agnese D, Allison KH, et al. Breast cancer, version 3.2022, NCCN clinical practice guidelines in oncology. *J Natl Compr Canc Netw*. (2022) 20:691–722. doi: 10.6004/jnccn.2022.0030

22. Shah C, Al-Hilli Z, Vicini F. Advances in breast cancer radiotherapy: implications for current and future practice. *JCO Oncol Pract*. (2021) 17:697–706. doi: 10.1200/OP.21.00635

23. Darby SC, Ewertz M, McGale P, Bennet AM, Blom-Goldman U, Bronnum D, et al. Risk of ischemic heart disease in women after radiotherapy for breast cancer. *N Engl J Med*. (2013) 368:987–98. doi: 10.1056/NEJMoa1209825

24. Delaney G, Jacob S, Featherstone C, Barton M. The role of radiotherapy in cancer treatment: estimating optimal utilization from a review of evidence-based clinical guidelines. *Cancer*. (2005) 104:1129–37. doi: 10.1002/cncr.21324

25. Helleday T, Petermann E, Lundin C, Hodgson B, Sharma RA. DNA repair pathways as targets for cancer therapy. *Nat Rev Cancer*. (2008) 8:193–204. doi: 10.1038/nrc2342

26. Hendry JH, Bentzen SM, Dale RG, Fowler JF, Wheldon TE, Jones B, et al. A modelled comparison of the effects of using different ways to compensate for missed treatment days in radiotherapy. *Clin Oncol (R Coll Radiol)*. (1996) 8:297–307. doi: 10.1016/S0936-6555(05)80715-0

27. Hermens AF, Barendsen GW. Changes of cell proliferation characteristics in a rat rhabdomyosarcoma before and after x-irradiation. *Eur J Cancer (1965)*. (1969) 5:173–89. doi: 10.1016/0014-2964(69)90065-6

28. Thames HD Jr., Peters LJ, Withers HR, Fletcher GH. Accelerated fractionation vs hyperfractionation: rationales for several treatments per day. *Int J Radiat Oncol Biol Phys*. (1983) 9:127–38. doi: 10.1016/0360-3016(83)90089-5

29. Zhao F, Yang D, Li X. Effect of radiotherapy interruption on nasopharyngeal cancer. *Front Oncol*. (2023) 13:1114652. doi: 10.3389/fonc.2023.1114652

30. Yao JJ, Zhang F, Gao TS, Zhang WJ, Lawrence WR, Zhu BT, et al. Survival impact of radiotherapy interruption in nasopharyngeal carcinoma in the intensity-modulated radiotherapy era: A big-data intelligence platform-based analysis. *Radiother Oncol*. (2019) 132:178–87. doi: 10.1016/j.radonc.2018.10.018

31. Bese NS, Hendry J, Jeremic B. Effects of prolongation of overall treatment time due to unplanned interruptions during radiotherapy of different tumor sites and practical methods for compensation. *Int J Radiat Oncol Biol Phys*. (2007) 68:654–61. doi: 10.1016/j.ijrobp.2007.03.010

32. Bleicher RJ. Timing and delays in breast cancer evaluation and treatment. *Ann Surg Oncol*. (2018) 25:2829–38. doi: 10.1245/s10434-018-6615-2

33. Laird AK. Dynamics of tumour growth: comparison of growth rates and extrapolation of growth curve to one cell. *Br J Cancer*. (1965) 19:278–91. doi: 10.1038/bjc.1965.32

34. Pearlman AW. Breast cancer–influence of growth rate on prognosis and treatment evaluation: a study based on mastectomy scar recurrences. *Cancer*. (1976) 38:1826–33. doi: 10.1002/(ISSN)1097-0142

35. Tilanus-Linthorst MM, Kriege M, Boetes C, Hop WC, Obdeijn IM, Oosterwijk JC, et al. Hereditary breast cancer growth rates and its impact on screening policy. *Eur J Cancer (Oxford Engl 1990)*. (2005) 41:1610–7. doi: 10.1016/j.ejca.2005.02.034

36. van Rijn J, van den Berg J, Meijer OW. Proliferation and clonal survival of human lung cancer cells treated with fractionated irradiation in combination with paclitaxel. *Int J Radiat oncology biology Phys*. (1995) 33:635–9. doi: 10.1016/0360-3016(95)00216-L

37. Golden EB, Formenti SC, Schiff PB. Taxanes as radiosensitizers. *Anticancer Drugs*. (2014) 25:502–11. doi: 10.1097/CAD.0000000000000055

38. Cui L, Her S, Dunne M, Borst GR, De Souza R, Bristow RG, et al. Significant radiation enhancement effects by gold nanoparticles in combination with cisplatin in triple negative breast cancer cells and tumor xenografts. *Radiat Res*. (2017) 187:147–60. doi: 10.1667/RR14578.1

39. Sherry AD, Mayer IA, Ayala-Peacock DN, Abramson VG, Rexer BN, Chakravarthy AB. Combining adjuvant radiotherapy with capecitabine in chemotherapy-resistant breast cancer: feasibility, safety, and toxicity. *Clin Breast Cancer*. (2020) 20:344–352.e1. doi: 10.1016/j.clbc.2020.02.010

40. Rutqvist LE. Adjuvant endocrine therapy. *Best Pract Res Clin Endocrinol Metab*. (2004) 18:81–95. doi: 10.1016/S1521-690X(03)00046-0

41. Zeng ZJ, Li JH, Zhang YJ, Zhao ST. Optimal combination of radiotherapy and endocrine drugs in breast cancer treatment. *Cancer Radiother*. (2013) 17:208–14. doi: 10.1016/j.canrad.2013.01.014

42. Kantorowitz DA, Thompson HJ, Furmanski P. Effect of conjoint administration of tamoxifen and high-dose radiation on the development of mammary carcinoma. *Int J Radiat oncology biology Phys*. (1993) 26:89–94. doi: 10.1016/0360-3016(93)90177-W

43. Wazer DE, Tercilla OF, Lin PS, Schmidt-Ullrich R. Modulation in the radiosensitivity of MCF-7 human breast carcinoma cells by 17B-estradiol and tamoxifen. *Br J Radiol*. (1989) 62:1079–83. doi: 10.1259/0007-1285-62-744-1079

44. Wang J, Yang Q, Haffty BG, Li X, Moran MS. Fulvestrant radiosensitizes human estrogen receptor-positive breast cancer cells. *Biochem Biophys Res Commun*. (2013) 431:146–51. doi: 10.1016/j.bbrc.2013.01.006

45. Azria D, Belkacemi Y, Romieu G, Gourgou S, Gutowski M, Zaman K, et al. Concurrent or sequential adjuvant letrozole and radiotherapy after conservative surgery for early-stage breast cancer (CO-HO-RT): a phase 2 randomised trial. *Lancet Oncol*. (2010) 11:258–65. doi: 10.1016/S1470-2045(10)70013-9

46. Ishitobi M, Shiba M, Nakayama T, Motomura K, Koyama H, Nishiyama K, et al. Treatment sequence of aromatase inhibitors and radiotherapy and long-term outcomes of breast cancer patients. *Anticancer Res*. (2014) 34:4311–4.

Frontiers in Oncology

Advances knowledge of carcinogenesis and tumor progression for better treatment and management

The third most-cited oncology journal, which highlights research in carcinogenesis and tumor progression, bridging the gap between basic research and applications to imrpove diagnosis, therapeutics and management strategies.

Discover the latest Research Topics

See more →

Frontiers

Avenue du Tribunal-Fédéral 34
1005 Lausanne, Switzerland
frontiersin.org

Contact us

+41 (0)21 510 17 00
frontiersin.org/about/contact